Report on environmental risk assessment and mitigation strategies

Work Package 7

Deliverable – D7.3

Report on environmental risk assessment and mitigation strategies

Work Package 7

Deliverable – D7.3

Version: final

Work package 7

29 June 2020

Website: http://www.gemex-h2020.eu

The GEMex project is supported by the European Union's Horizon 2020 programme for Research and Innovation under grant agreement No 727550 and the Mexican Energy Sustainability Fund CONACYT-SENER, project 2015-04-268074

Authors

Chapter 1: TNO: Elisabeth Peters, ENEA: Massimo Angelone, OGS: Mariangela Guidarelli

Chapter 2: ENEA: Massimo Angelone, Fabio Spaziani, Vladimiro Verrubbi

Chapter 3: TNO: Thibault Candela, Elisabeth Peters, Jan Diederik van Wees

Chapter 4: ENEA: Giovanni Bongiovanni, Massimo Angelone, Vladimiro Verrubbi

Chapter 5: OGS: Mariangela Guidarelli and Enrico Priolo

Table of Contents

List of figures

List of tables

Executive summary

In this work, environmental concerns relating to a potential EGS development at the site of Acoculco (Mexico) are evaluated and potential mitigation measures discussed. This work is done in the framework of Task 7.3 of the GEMex project. The concerns that are addressed here are related to possible pollution of soil, water and aquifers and induced seismicity. For the latter, different aspects are investigated: potential for induced seismicity, impact of the shallow subsurface on ground motion resulting from induced seismicity, micro-seismic monitoring design and traffic light systems for mitigation.

Geochemical characterization of soil and water has been carried out with the aim to study the potential influence of the geothermal exploitation on these environmental matrices and the potential effects on human health. Concerning the waters, the results have evidenced, for some major and trace elements, concentrations sensibly higher for drinking waters than the guideline values defined by international organizations (WHO, EPA, EU) and Mexican legislation. The water chemistry depends greatly on seasonality: dry periods are characterized by enrichment in some elements while in the wet ones the dilution due to rainfall prevails. Some elements, especially arsenic, reach concentrations in waters that might pose serious problems for the animal's health themselves and for that of the consumers since farming is a key activity in the area. The soil geochemistry evidences that minor and trace elements show a large concentration range related to the wide compositional heterogeneity which is typical of the geothermal area's rocks. This applies mainly for S and As, while the Mn variability range can be related to the redox conditions' changes.

Potential for induced seismicity was analysed during stimulation (GEMex D7.2) and production (GEMex D7.1). The results show that the risk for induced seismicity during stimulation appears to be small given the current information on stress and fault orientation. Different scenarios were run with varying stress regimes and fault orientations, but all simulated events were smaller than -0.5. This seems to be in line with the low level of seismicity observed during micro-seismic monitoring (Mexican GEMex PT5.2). During geothermal production, the injection of large amounts of cold water shows a larger impact.

The impact of the subsurface characteristics on ground motion was studied for two site specific seismic events, one from induced seismicity and one of tectonic origin. It is observed that there are similarities in the measured ground motion characteristics and in the effects on the built environment, that can be related to the presence of lateral discontinuities in the geology. Based on the insights gained from this analysis, the aspects of the Acoculco geology that can amplify the superficial motion are investigated. Because the amplitude and frequency content of the observed micro-seismic data is limited, only tentative conclusions can be reached, which show that locally generated earthquakes can travel through discontinuous media rich in faults with relevant lateral discontinuities that can modify the seismic field in the sense of producing refractions/reflections capable to shift the frequency content of seismic motion to higher frequencies and then to higher peak values. In some of the station sites, the possibility of stratigraphic amplification of seismic motion is apparent.

Finally an extensive literature review is presented on micro-seismic monitoring and traffic light systems for EGS development. Based on the literature review, a set of recommendations for micro-seismic monitoring network design is presented, which includes technical details and suggestions for supplementary monitoring options such as monitoring in a deep borehole and geodetic measurements. Experience with and recommendations for EGS management procedures conclude the report, with special attention to risk-based traffic light systems and public outreach.

1 Introduction

Authors: Elisabeth Peters, Massimo Angelone, Mariangela Guidarelli

In this report the results are presented of task 7.3 of the GEMex project. The goal of this task is to evaluate environmental concerns related to a potential EGS development at the site of Acoculco (Mexico). This site has been identified by Comisión Federal de Electricidad (CFE) as a potential site for EGS development and is studied extensively in GEMex. Enhanced Geothermal System (EGS) techniques are used to create permeability in hot, dry and impermeable formations by creating new fractures or, more frequently, by enhancing and connecting existing fractures. These fractures act as heat exchangers and heat up cold water, which is injected and circulated to produce electricity at the surface. Both during the stimulation which is required to create an EGS and during the production phase, risks to the environment can occur.

The environmental impact and emission of a geothermal power plant are generally lower than from a conventional electricity generation plant. In a typical geothermal power plant, potential risks can arise from several factors as those reported below:

- gaseous emissions
- induced landslides
- induced seismicity
- land subsidence
- natural hydrothermal manifestations disturbance
- natural landscape changes
- noise pollution
- water pollution and use
- wildlife habitat and vegetation disturbance

For EGS, the environmental impacts of the geothermal exploitation are considered of the same order of magnitude or, sometimes, lower. Nevertheless, in some cases and in particular situations, the utilization of this resource can lead to adverse effects on the environment. Proper understanding of the risks, monitoring and implementation of mitigating measures can significantly reduce the risk to the environment. We have evaluated two types of environmental concerns: potential threats to water and soil and induced seismicity. The main focus has been on induced seismicity.

With respect to potential threats to water and soil, which is documented in Chapter 2, the focus is on the description the current, natural state: the base line. Understanding the natural variability in the chemical composition is required to monitor for changes due to geothermal production. Secondly, the goal is to identify the potential vulnerability of resources such as aquifer, surface and soils.

Induced seismicity can be a major threat to geothermal development, in particular for developments in hard rock formations with high temperature and near urban environments. In addition, the potential for seismicity becomes an environmental factor for determining the economics of EGS project development and its public acceptance. Three aspects of induced seismicity are investigated:

- In Ch. 3, it is investigated whether the stress conditions and faults in the Acoculco area, are susceptible to induced seismicity. The analysis is based on results from D7.1 and D7.2 in which induced seismicity is estimated both during potential hydraulic stimulation and in the production phase.

- Ch. 4 investigates whether the subsurface in the Acoculco area contains heterogeneities which impact ground surface motion and how this affects micro-seismic monitoring.
- Finally, in Ch. 5 general recommendations for micro-seismic monitoring and traffic light systems during stimulation and production are presented based on literature review.

2 Geochemical assessment of soils and waters in the Acoculco geothermal area

Authors: Massimo Angelone, Fabio Spaziani, Vladimiro Verrubbi

2.1 Introduction

The Acoculco geothermal area is located in the northwest range of the state of Puebla in the eastern part of the Mexican volcanic belt. The geological data document three distinct volcanic periods that led to the formation of the Tulancingo caldera occurred about 2.7 million years ago and, subsequently, of that of Acoculco, which was developed inside in more recent times being about one million years younger. The area occupied by the Acoculco caldera is about 255 km^2 and geological data indicate that the volcanic activity ended about 0.24 million years ago. The main studies on this region have shown that the formation of volcano-tectonic structures is connected to the rise of massive magmatic masses along a system of regional faults with N-W and N-E directions. (López-Hernández and Castillo-Hernández, 1997; López-Hernández et al., 2009). For a more detailed description of the geo-vulcanological features of this region we suggest the specialized literature and to the recent work reported in the GEMex project deliverables (in particular D3.1 and D4.1).

A complex faults system characterizes the geothermal area of Acoculco where heterogeneous permeability conditions greatly influence the geothermal fluid fluxes. As reported by Pfeiffer et al. (2014): "The absence of water reservoir at depth is attributed to the low permeability of the wall-rock. The upper 800 m rock layer is intensely hydrothermally altered and probably impedes the recharge of the system by meteoric waters". Previously, Canet et al. (2010) identified two major zones of alteration. A shallow one, extending to 500-600 m depth with ammonium-argillic alteration of the volcanic rocks indicating temperatures > 200 °C, and a deeper one down to ~1000 m depth with an alteration assemblage of epidote–calcite–chlorite suggesting temperatures of ~240 °C. Surficial rocks are characterized by a widespread silicic alteration, whilst advanced argillic alteration occurs principally near the gas manifestations of Los Azufres and Alcaparrosa. See also Canet et al., 2015a, 2015b; López-Hernández et al., 2009).

Evidence indicates that the deep hydrothermal system does not influence the surface waters circulation but mainly the water chemistry because waters acidity is related to H_2S oxidation. H_2S is present in the hydrothermal gas after dissolution in shallow meteoric aquifers or superficial meteoric waters. (Pfeiffer et al., 2014). According to López-Hernández et al (2009): "springs might be a mixture of deep geothermal fluids and shallow waters. Water isotopic data do not differ from meteoric value, although important dilution with shallow meteoric water could mask the deep signature".

Geochemical data indicate that the hydrothermal system, associated with the evolution of the caldera, is currently not active but there is some evidence for a hidden hydrothermal system. In fact, around EAC-1 and EAC-2 wells, the meteoric waters mix with the hydrothermal fluids and the temperatures are generally below 30°C, while, at about 2 km of depth, temperatures are close to about 300°C. Hot springs are present in Chignahuapan, a settlement 20 km from Acoculco.

In this area rainfall is high. In fact, the annual average calculated over an interval of 20 years in the closest meteorological station is 727 mm. As a consequence, a significant volume of meteoric waters is available and, promoted by the high rocks cracking, interact with the deeper geothermal fluids which are also characterized by an acidic chemism as a consequence of the interaction between meteoric water and H_2S of geothermal origin.

From a hydrological point of view, the Acoculco region can be considered as a watershed between two basins. The largest is a closed type basin and occupies an area of about 2800 km^2 extending to NW and with a flow direction to NW. The second, classified as an open basin, covers an area of about 1610 km^2 and has a flow direction from NE. In both areas there are no permanent waterways but they are temporary in relation to the characteristics of the climatic season. The same occurs for the superficial water that can be temporary, more or less numerous and with an extremely variable extension depending on the intensity and distribution of the rainfall.

From the above it is evident that the chemistry of surface waters depends greatly on the geo-lithological characteristics and climatic conditions. At Acoculco, the influence of geothermal fluids is proved by the high presence of anions, especially chlorides and sulphates. In some cases, abnormal nitrate concentrations exceeding the legal limits for drinking waters were measured in surface water samples.

It should be remembered that, in this environmental settings, significant variations in the concentration levels of potential pollutants can be linked to both dilution and concentration factors due to variations in the amount of rainfall. Another complexity factor that influences data interpretation is the poor reproducibility of the samples due to the seasonal and spatial variability of the sampling sites depending on shallow water and related soils extension.

Considering that geothermal activity influences the geochemical behavior both of soils and waters, a characterization of these environmental matrices was therefore conducted. The aim of such approach, was to evaluate any potential risk on the environment as a whole and, then, on human health, as a consequence of the geothermal exploitation.

Another purpose is to provide a baseline that, through the introduction of geochemical methodologies, will permit to identify, quantify and predict the possible impact of geothermal activities on the environment.

2.2 Geopedological setting

The following information has been collected from various sources such as Bautista et al., (2019), and from INEGI (Instituto Nacional de Estadística y Geografía) website (INEGI, 1997).

In the Acoculco region conifers and oaks are the prevailing plants with large patches of herbaceous vegetation. As for conifers tree communities are similar to those typical of temperate and semi-cold regions characterized by different humidity regimes. In the region is present also a variety of vegetation introduced as a result of human activities. Agriculture is the main economic activity followed by pastoralism INEGI 2014, which is strongly linked to the rainfall regime and the water retention capacity of soils.

From a pedological point of view, as reported by INEGI 2014, seven pedological units have been described in the study area characterized by the presence of superficial horizons rich in organic substance with fine to medium textures and with clay accumulations in the underlying horizons. The most common soils are Andosols and Lovisols distributed on the 48 and 45% of the territory, respectively. Instead, the soils classified as Phaeozems and Vertisols are present for a 3% each of the region land.

Since the soil properties strongly influence trace elements mobility, here below we report a brief soil description that differentiate the main pedological units outcropping in the Acoculco area.

The Andosols, whose parent material is made up of volcanic rocks, are generally characterized by a base saturation > 50% while the textural class, permeability and water retention capacity are generally classified as medium and the nutrient retention capacity ranges from medium to high. Within the andosols pedological units' differences in some characteristics are also reported such as the presence of relatively thick superficial horizons. a darker coloring, a lower bases saturation and a medium to high organic substance content.

The Lovisols are characterized, in depth, by strong accumulations of clay which is characterized by a high activity and strong base saturation.

The Phaeozems have a high bases saturation, are rich in organic substance and are characterized by dark to very dark colouring and by strong clay mobilization that accumulates in the deeper horizons. The presence of a compact horizon below 100 cm of depth is another typical character of these soils that also exhibit a low permeability and an affinity to retain water and nutrients.

The Vertisols show a widespread occurrence of cracks produced by the clay expansion and contraction in relation to wet and dry seasons turnover. A reddish-brown horizon, at a depth of about 50 cm, is typical of these soils, whose cement is made up of silica of secondary origin; moreover, the good surface texture promotes low permeability, aeration and a high retention capacity for water and nutrients.

2.3 Acoculco shallow waters

The data discussed in this deliverable were collected during the field campaign of the GEMex project by the participants of WP 4.3 (Geochemical characterization and origin of cold and thermal fluids). The working group included both Mexican and European partners, and researchers from CICESE (Center for Scientific Research and Higher Education at Ensenada). Unfortunately, due to unexpectedly long period required to carry out the field operations and for the full activity's coordination between the working groups, the data here discussed were provided with great delay. Moreover, the dataset was lacking for some variables, and others were provided missing or incomplete. Consequently, it was not feasible to carry out some data processing methods normally performed on this type of matrix. For example, due to the incompleteness of anions data, including the total lack of data relating to HCO3-, it was not possible to determine the hydrogeochemical facies.

For the reasons described above, in order to obtain a homogeneous dataset for statistical processing, only the variables common to all samples were considered. For instance, data relating to Sr, B, etc., have been excluded as they have not been provided for the entire series of samples.

A total of 49 water samples were analysed: 26 collected in the wet season and 23 in the dry season. General statistics are reported in Table 2-1 and Table 2-2 for the wet and dry seasons, respectively. The complete list of the samples is reported in Appendix 1 and 2.

The dry season waters display higher values concerning some physical parameters, for example in the case of the electrical conductivity (mean 207 and 519 µS/cm, respectively for wet and dry season). Besides, the concentration levels for some elements are higher than Mexican and internationally (WHO, EPA and EU) admitted limits that, for an appropriate comparison, we have reported in Table 2-3 and Table 2-4.

In particular, environmental concerns arise for Al whose concentration levels reach, in the dry season, values up to 160 times the legal reference limit for Mexico drinking waters while, in the wet season, this value is reduced to 85 times. In the dry season arsenic exhibits a maximum level of 1.91 mg/L which is about 200 times the guideline value. This element also seems to be affected by seasonality, since in the dry season the maximum concentration value is about three times the one measured in the wet season.

High concentrations have been found also for Na and Zn, mainly in the dry season, with a maximum value of 674 and 0.64 mg/L, respectively.

The pH, another parameter that influences the mobility of the elements, shows values that are below the guidelines for drinking waters. In both seasons the pH ranges are enough similar, with a minimum of around 3.4 (clearly lower than the guideline value of 6.5) and a maximum between 7 and 8.

Table 2-5, Table 2-6 and Table 2-7 show the correlation coefficients values among all the variables for the surface waters calculated separately for each season and for the whole dataset. The Spearman's correlation has been applied instead of the more classic Pearson as the data is not normally distributed. As a first approximation, wet season samples evidence a major number of significant correlations among the variables. Concerning the chemical-physical parameters, it is evident the poor correlation between the EC and all the other variables. In the wet season, pH shows negative correlation with some variables (such as Al, Zn and Co), while the temperature is strongly positively correlated with Fe, Mg and K.

As easily predictable, among the major elements, Al and Fe are those that exhibit the greatest number of significant correlations as they are the main constituents of both minerals of primary and secondary formation. Among the minor elements, Zn is the one with the most significant correlations with all other variables, especially in the wet season, in particular with Ni ($r = 0.93$), Co ($r = 0.92$) and Mn ($r = 0.86$). A remarkable correlation has also been found between Pb and Cr ($r = 0.83$).

The outcome that the total number of significant correlations among the dry season water variables is lower, is probably related to the strong rain seasonality. In fact, in the wet season, the rainwater promotes the solubilisation and subsequent leaching, from volcanic rocks' minerals and hydrothermal deposits, of those elements with higher mobility. Instead, throughout the dry season, the ionic species display a reduced mobility owing to the prevalence of absorption phenomena and the lack of water continuity between the free pores of the embedding rocks. This evidence is further confirmed by the Cluster Analysis calculated for both seasons (Figure 2-1 and Figure 2-2). In fact, in the diagram related to the wet season there are smaller distances between the variables and the clusters.

In order to discuss the high number of measured variables on the whole, a multivariate statistics approach, PCA (Principal Component Analysis), was also applied.

Regarding the wet season (Figure 2-3), PCA highlights four groups (A, B, C, D):

- Group A brings together the waters characterized by the highest concentrations in Fe, Al, Ni and Zn.
- Group B, represented by a single sample, is distinguished by the highest concentrations of Pb, V, Cr, U and Cu. All the samples taken in 2015 fall in the above-mentioned groups.
- Group C stands out for the highest concentrations in major elements as Ca, Mg, Na, K and, among minor elements, in As.
- In the last group D, clearly separated on the graph from the others, the samples characterized by the lowest pH values are merged.

As for the dry season (Figure 2-4), the PCA analysis differentiates three groups (E, F, G):

- Group E is characterized by the highest absolute concentrations in Fe, Pb, Ni, Co and Zn.

- The F group is distinguished by the highest concentrations in Na, K and, above all As. In fact, the sampling points correspond with an active hydrothermal area, characterized by continuous fluid emission and by the deposition of salts, sulphates and carbonates.
- Lastly, in group G the samples characterized by intermediate concentration levels between the two extremes E and F are included.

The data discussed up to now show that the concentrations of some elements in the waters outcropping in Acoculco are quite high as they are directly related to the emissions of geothermal fluids. These levels, in many cases, exceed both the Mexican and the international guidelines (WHO, EPA, EU) for drinking water (tables 3a and 3b). In particular, we point out, the extremely anomalous values found for As and Al. In addition, values above the guideline limits also occur for Cd, Na and pH. This last parameter is to be considered of major importance, since the acidic character of the system affects the mobility of the elements as it promotes the release of ionic species in solution.

As a general consideration, in the dry season the waters are characterized by a slight enrichment in some elements while in the wet season the effect of dilution by rainfall prevails.

Since pastoralism is widespread in the area, particular attention must be paid monitoring the quality of the water utilized to water the animals. The concentration levels of some elements and, in particular of As, are such as to pose serious problems for the animal's health themselves and for that of the consumers. A continuous quality control management of these products should be considered in order to obtain the highest quality of the products and the end user guarantee.

Table 2-1. General statistic for the water sampled in the wet season

	EC	pH	T	Al	Ca	Fe	K	Mg	Mn	Na	As	Cd	Co	Cr	Cu	Ni	Pb	Sb	U	V	Zn
	µS/cm		°C	mg/L	mg/L	mg/L	mg/L	mg/L	mg/L	mg/L	µg/L	µg/L	µg/L	µg/L	µg/L	µg/L	µg/L	µg/L	µg/L	µg/L	µg/L
Samples	26	26	26	26	26	26	26	26	26	26	26	26	26	26	26	26	26	26	26	26	26
Min	11.1	3.4	12.9	0.03	0.69	0.05	0.17	0.17	0.01	0.57	0.10	.001	0.09	0.02	0.03	0.01	0.01	0.01	0.01	0.02	0.10
Max	786	7.3	27.2	17.4	48.2	40.0	32.4	13.2	2.38	68.8	651	1.45	11.8	7.29	13.7	9.53	2.39	14.7	0.22	9.05	224
Mean	207	5.2	18.1	5.70	18.4	3.62	5.81	4.47	0.63	12.4	61.5	0.11	2.88	0.61	3.84	2.80	0.33	3.41	0.04	0.96	66.0
Std. dev	216	1.2	3.48	6.52	16.9	7.86	6.89	4.10	0.74	14.9	138	0.29	3.51	1.40	4.19	2.89	0.54	4.87	0.04	2.03	71.1
Median	128	5.0	17.4	2.49	11.4	1.51	3.75	3.07	0.25	8.54	9.92	0.02	1.41	0.27	2.03	1.97	0.12	1.00	0.03	0.28	26.3
Co. var	104	23.4	19.3	114	91.8	217	119	91.7	119	120	225	259	122	228	109	103	165	143	106	212	108

Table 2-2. General statistic for the water sampled in the dry season

	EC	pH	T	Al	Ca	Fe	K	Mg	Mn	Na	As	Cd	Co	Cr	Cu	Ni	Pb	Sb	U	V	Zn
	µS/cm		°C	mg/L	mg/L	mg/L	mg/L	mg/L	mg/L	mg/L	µg/L	µg/L	µg/L	µg/L	µg/L	µg/L	µg/L	µg/L	µg/L	µg/L	µg/L
Samples	23	23	23	23	23	23	23	23	23	23	23	23	23	23	23	23	23	23	23	23	23
Min	2.80	3.4	9.8	.0015	1.98	0.03	0.42	0.60	.003	2.34	0.10	.001	.0006	.001	0.03	0.01	.0004	0.01	.01	0.0005	0.10
Max	1556	7.9	28.2	31.7	67.3	17.9	35.1	19.2	5.02	674	1933	7.34	30.7	4.27	27.2	25.0	0.82	19.9	0.34	4.52	638
Mean	519	5.2	20.6	3.11	31.6	3.17	10.8	8.16	0.82	56.3	226	0.85	4.74	0.46	4.98	4.33	0.23	2.01	0.08	0.76	78.6
Std. dev	398	1.4	5.5	7.05	19.3	4.52	10.3	5.28	1.07	137	499	1.81	8.58	0.87	5.91	6.28	0.23	4.18	0.10	0.98	144
Median	475	4.7	20.3	0.17	29.0	2.02	8.03	7.00	0.75	21.1	7.64	0.09	0.60	0.23	3.56	2.38	0.17	0.96	0.03	0.42	30.9
Co. var	76.8	27.5	26.8	226	61.2	143	94.8	64.7	130	243	221	212	181	188	119	145	100	208	128	130	184

Table 2-3. Admitted limits for some elements in drinking water in Mexico. NOM-127-SSA1-1994 (Concentration as mg/L)

Parameter	Ref. Value	Parameter	Ref. Value
Al	0.20	F^-	1.50
As	0.01	Mn	0.15
Ba	0.70	Hg	0.001
Cd	0.05	NO_3^-	10
Cl^-	250	NO_2^-	0.05
Cu	2.00	NH_4^+	0.50
Fe	0.30	pH	6.5-8.5
Pb	0.01	Na	200
SO_4^{2-}	400	Zn	5

Table 2-4. WHO, EPA and E.U. guidelines concentrations for drinking waters (Concentrations as mg/L; EC as µS/cm)

Parameter	WHO	EPA	EU
Al	0.20	0.05-0.2	0.2
As	0.01	0.01	0.01
Cd	0.003	0.005	0.005
Cr tot	0.005	0.1	0.005
Cu	2.0	1.0	2.0
Fe	--	0.3	0.2
Mn	0.05	0.05	0.05
Na	200	--	200
Pb	0.01	0.015	0.01
Zn	3.0	5.0	--
pH	6.5-8.5	--	6.5-8.5
EC	2500	--	2500

Table 2-5. Correlation matrix for all water (dry and wet season)

	EC	pH	T	Al	Ca	Fe	K	Mg	Mn	Na	As	Cd	Co	Cr	Cu	Ni	Pb	Sb	U	V	Zn
EC	1.00																				
pH	-0.05	1.00																			
T	-0.06	-0.25	1.00																		
Al	0.02	-0.43	0.04	1.00																	
Ca	0.21	-0.12	0.36	0.40	1.00																
Fe	-0.08	-0.58	0.26	0.65	0.39	1.00															
K	0.09	-0.17	0.41	0.34	0.82	0.45	1.00														
Mg	0.20	-0.13	0.36	0.47	0.96	0.46	0.82	1.00													
Mn	0.04	-0.48	0.25	0.63	0.70	0.73	0.65	0.74	1.00												
Na	0.17	-0.08	0.34	0.27	0.83	0.34	0.90	0.84	0.58	1.00											
As	0.02	0.04	0.31	0.19	0.52	0.30	0.67	0.49	0.46	0.56	1.00										
Cd	0.17	-0.17	-0.15	0.27	0.44	0.26	0.39	0.44	0.40	0.44	-0.03	1.00									
Co	0.06	-0.61	0.04	0.69	0.45	0.75	0.41	0.49	0.81	0.35	0.14	0.44	1.00								
Cr	0.06	-0.28	0.18	0.54	0.45	0.64	0.41	0.44	0.41	0.40	0.18	0.33	0.45	1.00							
Cu	0.32	-0.07	-0.10	0.30	0.26	0.21	0.16	0.26	0.10	0.27	-0.22	0.50	0.33	0.63	1.00						
Ni	0.15	-0.50	0.22	0.65	0.58	0.68	0.47	0.61	0.70	0.43	0.11	0.46	0.87	0.55	0.46	1.00					
Pb	0.19	-0.23	-0.01	0.44	0.35	0.56	0.34	0.38	0.34	0.35	0.10	0.48	0.45	0.82	0.70	0.53	1.00				
Sb	0.29	0.21	-0.39	0.06	0.08	-0.12	0.03	0.03	-0.09	0.01	-0.03	0.48	0.10	0.04	0.44	0.07	0.30	1.00			
U	0.24	-0.13	0.09	0.28	0.23	0.18	0.12	0.25	0.00	0.23	-0.28	0.26	0.31	0.55	0.79	0.51	0.57	0.19	1.00		
V	0.01	-0.24	0.51	0.38	0.51	0.60	0.55	0.58	0.39	0.45	0.34	0.17	0.39	0.61	0.28	0.51	0.51	-0.04	0.45	1.00	
Zn	0.19	-0.51	0.08	0.67	0.62	0.72	0.53	0.60	0.79	0.43	0.25	0.44	0.85	0.63	0.42	0.86	0.59	0.13	0.32	0.38	1.00

Table 2-6. Correlation matrix for waters collected during the dry season

	EC	pH	T	Al	Ca	Fe	K	Mg	Mn	Na	As	Cd	Co	Cr	Cu	Ni	Pb	Sb	U	V	Zn
EC	1.00																				
pH	-0.04	1.00																			
T	-0.12	-0.26	1.00																		
Al	0.30	-0.14	-0.20	1.00																	
Ca	0.21	0.22	-0.03	0.50	1.00																
Fe	0.05	-0.63	-0.14	0.47	0.13	1.00															
K	0.18	0.21	0.13	0.29	0.65	0.15	1.00														
Mg	0.20	0.18	-0.12	0.66	0.88	0.27	0.63	1.00													
Mn	0.05	-0.39	-0.16	0.65	0.52	0.79	0.46	0.67	1.00												
Na	0.14	0.37	0.00	0.41	0.68	0.05	0.87	0.70	0.35	1.00											
As	-0.01	0.13	0.14	0.25	0.65	0.18	0.92	0.54	0.47	0.76	1.00										
Cd	0.02	0.02	-0.56	0.40	0.28	0.27	0.21	0.33	0.35	0.31	0.20	1.00									
Co	0.06	-0.55	-0.30	0.60	0.20	0.82	0.15	0.36	0.75	0.18	0.13	0.43	1.00								
Cr	0.23	-0.03	-0.22	0.23	0.37	0.49	0.16	0.29	0.40	0.15	0.14	0.24	0.35	1.00							
Cu	0.41	0.19	-0.30	0.23	0.29	0.08	0.11	0.26	0.04	0.30	-0.09	0.42	0.34	0.53	1.00						
Ni	0.09	-0.41	-0.21	0.52	0.25	0.67	0.09	0.32	0.52	0.14	0.03	0.35	0.82	0.44	0.53	1.00					
Pb	0.30	-0.09	-0.37	0.44	0.46	0.56	0.31	0.51	0.53	0.38	0.18	0.55	0.60	0.79	0.64	0.65	1.00				
Sb	0.31	0.23	-0.44	0.35	0.52	-0.01	0.41	0.41	0.13	0.58	0.36	0.69	0.27	0.17	0.57	0.30	0.51	1.00			
U	0.28	-0.04	0.08	0.11	0.12	-0.01	-0.09	0.16	-0.12	0.16	-0.28	0.03	0.28	0.26	0.74	0.51	0.37	0.22	1.00		
V	0.00	-0.39	0.41	0.09	0.16	0.37	0.27	0.25	0.25	0.14	0.23	0.05	0.33	0.23	0.09	0.35	0.29	-0.07	0.35	1.00	
Zn	0.25	-0.36	-0.31	0.53	0.47	0.75	0.29	0.47	0.75	0.23	0.25	0.42	0.80	0.64	0.46	0.79	0.79	0.34	0.22	0.17	1.00

Table 2-7. Correlation matrix for waters collected during the wet season

	EC	pH	T	Al	Ca	Fe	K	Mg	Mn	Na	As	Cd	Co	Cr	Cu	Ni	Pb	Sb	U	V	Zn
EC	1.00																				
pH	-0.02	1.00																			
T	-0.11	-0.30	1.00																		
Al	-0.11	-0.71	0.57	1.00																	
Ca	0.09	-0.48	0.67	0.66	1.00																
Fe	-0.13	-0.57	0.76	0.86	0.67	1.00															
K	-0.06	-0.55	0.70	0.68	0.90	0.72	1.00														
Mg	0.08	-0.47	0.71	0.69	0.99	0.72	0.91	1.00													
Mn	0.14	-0.61	0.67	0.67	0.89	0.66	0.80	0.86	1.00												
Na	-0.10	-0.58	0.63	0.57	0.89	0.67	0.89	0.88	0.82	1.00											
As	0.26	-0.10	0.51	0.23	0.43	0.48	0.43	0.48	0.48	0.45	1.00										
Cd	0.14	-0.52	0.27	0.48	0.54	0.38	0.49	0.52	0.51	0.42	-0.30	1.00									
Co	0.18	-0.69	0.55	0.82	0.86	0.69	0.75	0.85	0.90	0.71	0.27	0.65	1.00								
Cr	-0.09	-0.51	0.49	0.77	0.52	0.81	0.56	0.57	0.41	0.55	0.15	0.47	0.55	1.00							
Cu	0.15	-0.29	0.03	0.35	0.21	0.33	0.16	0.22	0.10	0.20	-0.33	0.55	0.31	0.70	1.00						
Ni	0.17	-0.59	0.64	0.85	0.84	0.74	0.75	0.84	0.84	0.67	0.25	0.64	0.96	0.62	0.37	1.00					
Pb	0.04	-0.39	0.29	0.54	0.22	0.61	0.27	0.28	0.20	0.27	0.03	0.44	0.31	0.83	0.72	0.39	1.00				
Sb	0.49	0.27	-0.37	-0.29	-0.21	-0.29	-0.27	-0.21	-0.30	-0.40	-0.41	0.30	-0.12	-0.02	0.43	-0.11	0.10	1.00			
U	0.02	-0.36	0.17	0.57	0.29	0.49	0.28	0.32	0.12	0.29	-0.21	0.52	0.37	0.80	0.80	0.48	0.76	0.14	1.00		
V	-0.17	-0.23	0.53	0.68	0.57	0.76	0.60	0.66	0.33	0.50	0.34	0.26	0.48	0.81	0.41	0.55	0.58	-0.07	0.60	1.00	
Zn	0.24	-0.70	0.63	0.82	0.84	0.74	0.80	0.83	0.86	0.70	0.33	0.60	0.92	0.62	0.36	0.93	0.43	-0.10	0.42	0.49	1.00

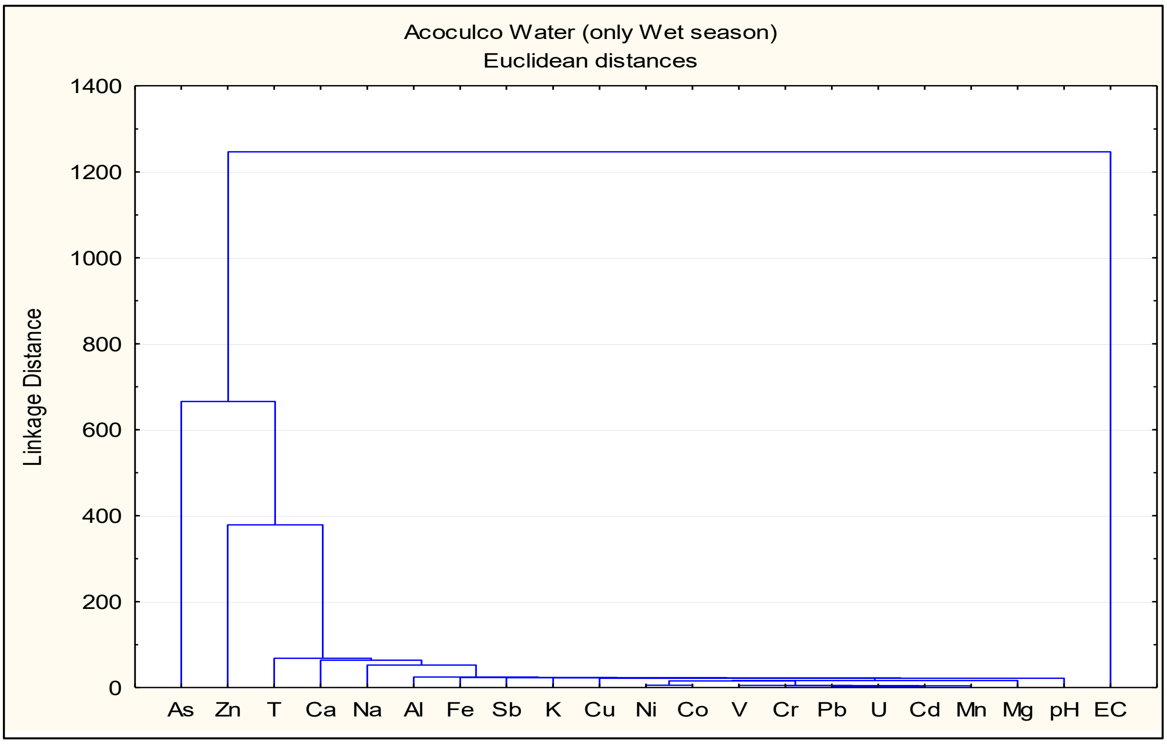

Figure 2-1. Cluster analysis for water samples (wet season)

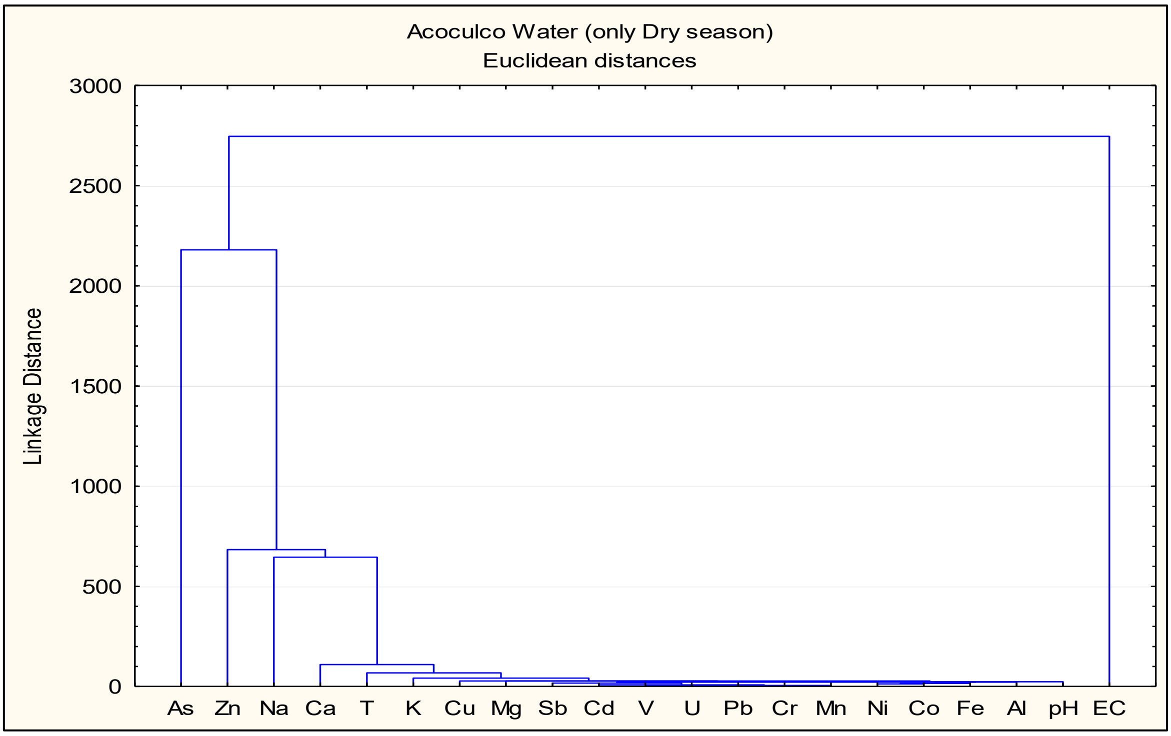

Figure 2-2. Cluster analysis for water samples (dry season)

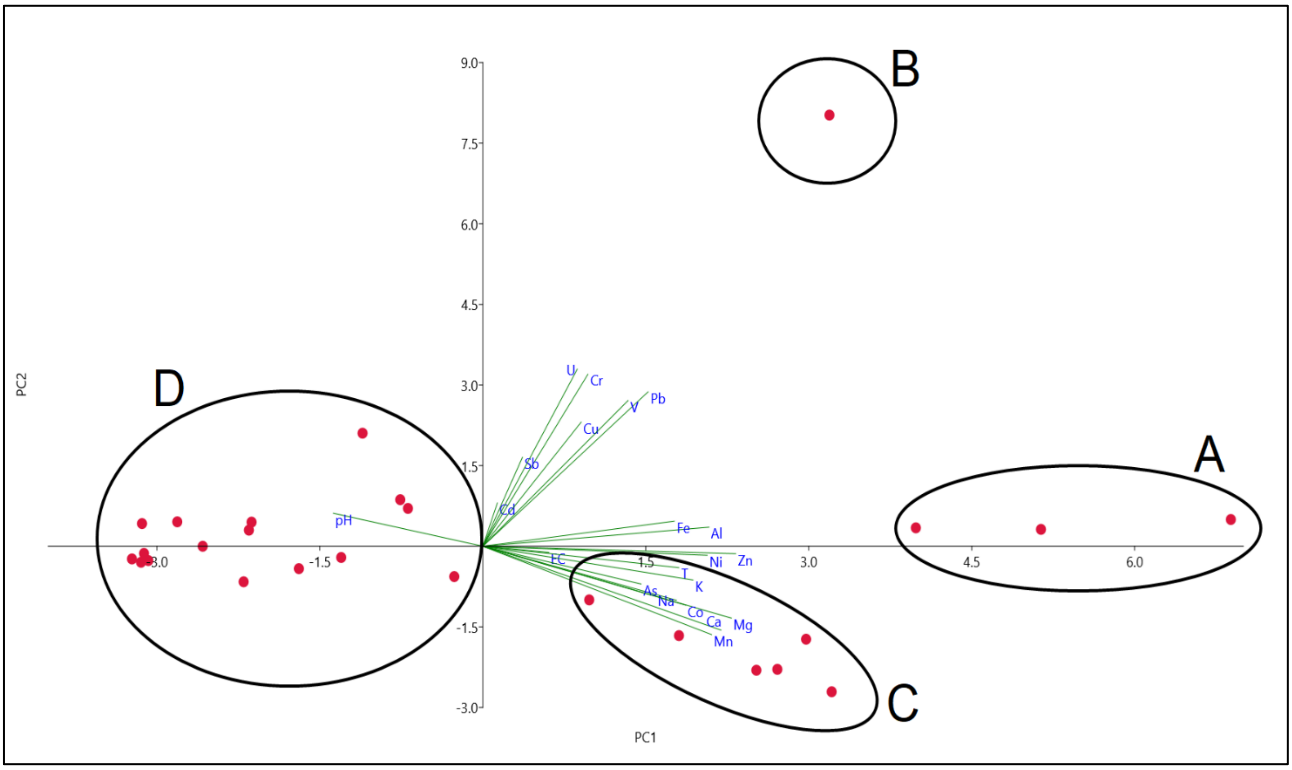

Figure 2-3. PCA for water samples (wet season)

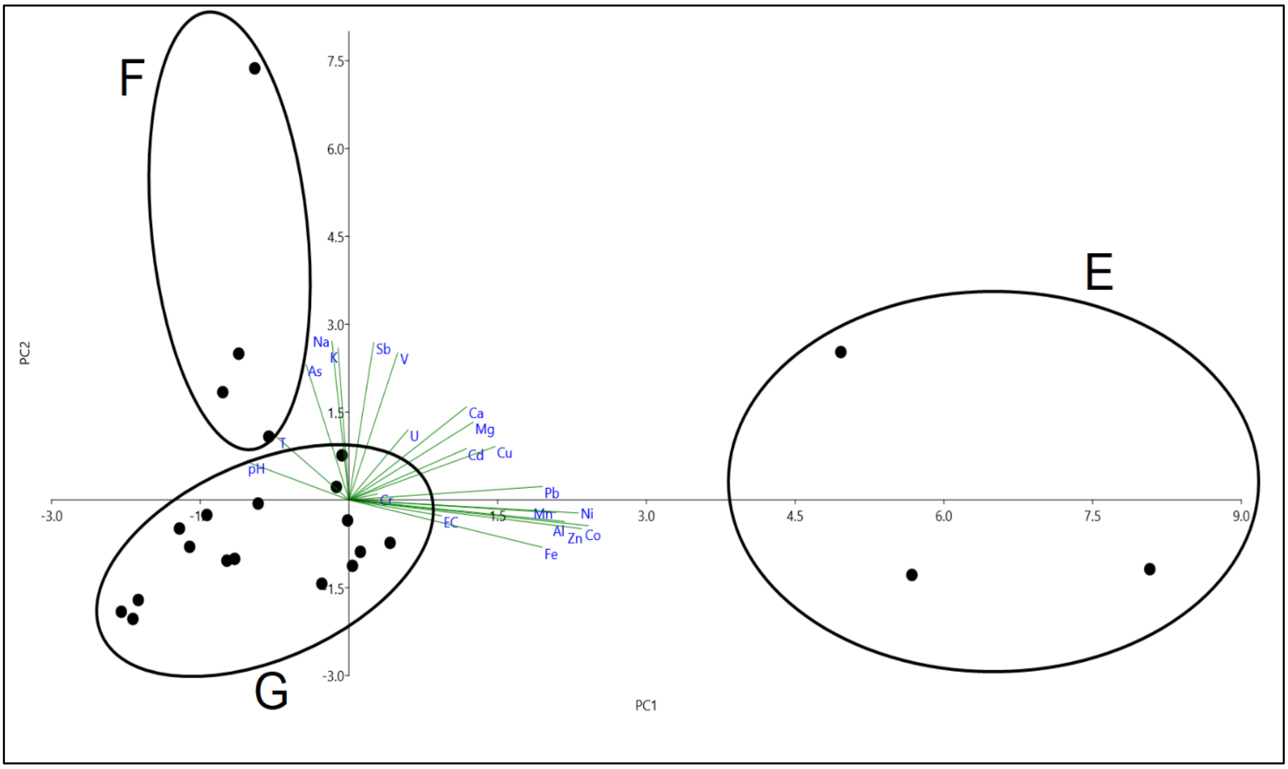

Figure 2-4. PCA for water samples (dry season)

2.4 Acoculco geothermal soils

In the Acoculco area 18 soils were sampled from 2015 to 2018, in different seasons, for a total of 60 samples split between superficial (0-10 cm), intermediate (10-20 cm) and deep (sampling interval from 20 to 30 and from 30 to 40 cm). As in the case of water, the samples were collected directly during the campaign activities of the GEMex project by a team of Mexican and European colleagues and researcher from CICESE, whom we thank for their active collaboration. The new data used and discussed in this document have been produced mainly by colleagues from CICESE. The methodologies applied for soil sampling, the laboratory procedures and the final analysis of major and trace elements were also carried out by the colleagues of CICESE and by the team of experts who collaborated in Mexican GEMex Work Package 9 (see Appendix 3 for details on analysis procedure).

As explained above, the soils were collected at intervals of 10 cm deep starting from the surface. The maximum depth reached has always been 40 cm, obtaining a maximum of four samples for each sampling point. Unfortunately, additional pedological information such as the soil taxonomic classification, number, type and horizons description, grain size analysis, content in organic substance etc., has not been provided with the geochemical data. This will entail an interpretative limit on the final data discussion and for an exhaustive characterization of the area.

The complete list of the samples is reported in Appendix 4, 5, 6 and 7, while the general statistics data for major and trace elements have been reported in Table 2-8 and Table 2-9.

Table 2-8. General statistics for major elements in Acoculco soils

	Al %w	Ca %w	Fe %w	K %w	Mg %w	Na %w	P %w	S %w	Si %w	Ti %w	Zr %w
Samples	60	60	60	60	60	60	60	60	59	60	59
Min	2.86	0.14	0.77	0.43	0.08	0.10	0.02	0.01	20.60	0.40	0.001
Max	10.80	5.72	9.51	2.24	0.63	1.05	0.37	14.70	33.80	1.24	0.37
Mean	7.79	0.99	4.59	1.34	0.20	0.54	0.10	1.69	26.84	0.78	0.17
Stand. dev	1.43	0.75	2.62	0.43	0.11	0.21	0.06	3.41	2.95	0.20	0.08
Median	7.98	1.03	3.67	1.30	0.19	0.53	0.10	0.19	26.40	0.79	0.17
Coeff. var	18.34	75.73	57.14	32.46	56.01	38.40	59.09	201.67	10.99	25.88	47.04

Table 2-9. General statistics for trace elements in Acoculco soils

	As	Ba	Cl	Cr	Mn	Ni	Rb	V	Zn
Samples	52	59	53	49	60	55	60	32	55
Min	0.80	387.00	66.90	0.84	12.70	15.1	12.00	73.50	24.9
Max	2200	4200	251	96.20	3000	212	1200	238	180
Mean	309	1420	140	56.25	401	73.13	141	152	111
Stand. dev	498	881	37.81	22.42	558	43.85	159	44.80	47.07
Median	29.55	1200	137	54.50	136	71	110	156	122
Coeff. var	161	62.02	27.02	39.86	139	59.97	113	29.53	42.59

From these tables it is evident, for some elements, a wide concentration range mainly ascribed to the considerable spatial and compositional heterogeneity typical of the geothermal areas. In fact, they are characterized by a large dispersion of emission points. The faults and the associated fractures are not always active; they are fragmented and undergo recurrent sealing processes due to precipitation and/or clay formation by mineralized solutions transported with hydrothermal fluids. These occurrences are also fostered by the high temperatures that characterize these environments. Besides, the same physical-chemical processes can lead to structural alterations in minerals that can change their original permeability. The consequence is the wide compositional, structural and textural variability developed by the soils, which is evident also on samples collected at short distance from each other.

In particular, as emerges from the summary statistics the greater variability, as expected, is observed for S and As, elements typically associated with geothermal systems. For Mn, which is the third element in decreasing order in the value of the coefficient of variation, the broad variability is probably associated with the space-time alternation of the redox systems, typical of the geothermal environment.

Concerning Rb, the wide range of variability depends instead on the geochemical characteristics of this element, which, as is known, lead to its enrichment in the hydrothermal fluids. In fact, Rb is geochemically classified as an incompatible element, as it hardly tends to enter the structure of newly formed minerals, and is usually associated with oxidizing environments.

The correlation matrix between the variables (Table 2-10) confirms the existence of the strong chemical-physical inhomogeneity of this environment. In fact, the number of significant correlations is rather small. Among the elements most associated with the hydro-thermalism, the correlation between As/S, with a value of $r = 0.82$, stands out. Among the metals, the greatest correlation is shown for the Fe/V ($r = 0.85$) and Fe/Zn ($r = 0.81$) pairs. A good correlation was also obtained for the pair of variables Rb/Mn ($r = 0.81$). This last correspondence appears to be hard to explain, considering the different geochemical character that characterizes these chemical species.

The pairs of variables V/Zn ($r = 0.76$) and Fe/Zn ($r = 0.80$) are also well correlated. Instead, the good correlation found between Ca/Zn ($r = 0.75$) is probably related to the similarity between the ionic rays of the two elements. This led them to be associated in some phases of magmatic differentiation and, consequently, to be present in the final volcanic emissions.

Table 2-10. Correlation matrix for major and trace elements for all soils in Acoculco geothermal area.

	Al	Ca	Fe	K	Mg	Na	P	S	Si	Ti	Zr	As	Ba	Cl	Cr	Mn	Ni	Rb	V	Zn
Al	1.00																			
Ca	0.23	1.00																		
Fe	0.45	0.72	1.00																	
K	-0.02	-0.43	-0.37	1.00																
Mg	0.34	0.31	0.39	-0.38	1.00															
Na	0.20	0.16	0.04	0.66	-0.24	1.00														
P	0.17	0.04	0.09	0.03	0.09	-0.06	1.00													
S	-0.21	-0.60	-0.64	0.37	-0.07	-0.10	0.53	1.00												
Si	-0.09	-0.23	-0.41	0.36	-0.46	0.34	-0.16	0.02	1.00											
Ti	0.36	0.22	0.53	-0.26	0.45	-0.19	0.16	-0.11	-0.27	1.00										
Zr	-0.33	-0.74	-0.74	0.43	-0.39	-0.12	-0.08	0.49	0.37	-0.28	1.00									
As	-0.28	-0.66	-0.64	0.41	-0.22	-0.15	0.06	0.82	0.07	-0.35	0.54	1.00								
Ba	-0.45	-0.64	-0.67	0.48	-0.59	-0.06	0.19	0.65	0.42	-0.35	0.69	0.68	1.00							
Cl	-0.06	0.27	0.17	-0.23	-0.14	-0.12	0.56	0.11	0.01	0.10	-0.14	-0.15	0.13	1.00						
Cr	0.02	0.57	0.54	-0.46	0.23	0.02	-0.25	-0.64	-0.21	0.19	-0.48	-0.70	-0.65	0.003	1.00					
Mn	0.01	0.18	0.27	-0.22	0.35	-0.18	-0.09	-0.27	-0.25	-0.05	-0.27	-0.30	-0.21	0.03	0.05	1.00				
Ni	-0.16	0.20	0.01	-0.03	-0.12	0.15	-0.37	-0.14	-0.01	0.11	0.04	-0.01	-0.08	-0.17	0.25	-0.51	1.00			
Rb	0.08	0.08	0.20	-0.12	0.39	-0.21	0.01	-0.20	-0.23	-0.01	-0.17	-0.25	-0.22	-0.02	0.04	0.81	-0.63	1.00		
V	0.60	0.41	0.85	0.02	0.37	0.21	0.32	-0.22	-0.31	0.70	-0.46	-0.42	-0.54	0.05	0.27	-0.24	0.12	-0.20	1.00	
Zn	0.44	0.75	0.80	-0.34	0.22	0.08	0.35	-0.44	-0.43	0.25	-0.69	-0.56	-0.60	0.32	0.35	0.19	-0.07	0.18	0.76	1.00

An additional tool widely used to better understand the links between the variables is the Principal Components Analysis (PCA). For the Acoculco soils the PCA (Figure 2-5) highlights, first of all, a wide samples dispersion. However, a more in-depth evaluation allows us to distinguish four groups, which has been indicated with the letters A, B, C, and D:

- Group A, essentially, includes the soils belonging to the series A15Ac4 and A15Ac5, which are the samples most enriched in Al, Fe, V and Zn.
- Group B contains the samples characterized by the highest concentrations of Ca, Mg and Mn.
- Group C holds, mainly, samples of the series B15Ac1b and B15Ac1c; it is strongly affected by the elements associated to geothermal activity such as, for example, arsenic and sulphur.
- Finally, belong to group D, a set of variables that are characterized by a wide dispersion in the PCA graph. This group includes soils with the highest concentrations of Na, K, Si, Ba and Zr.

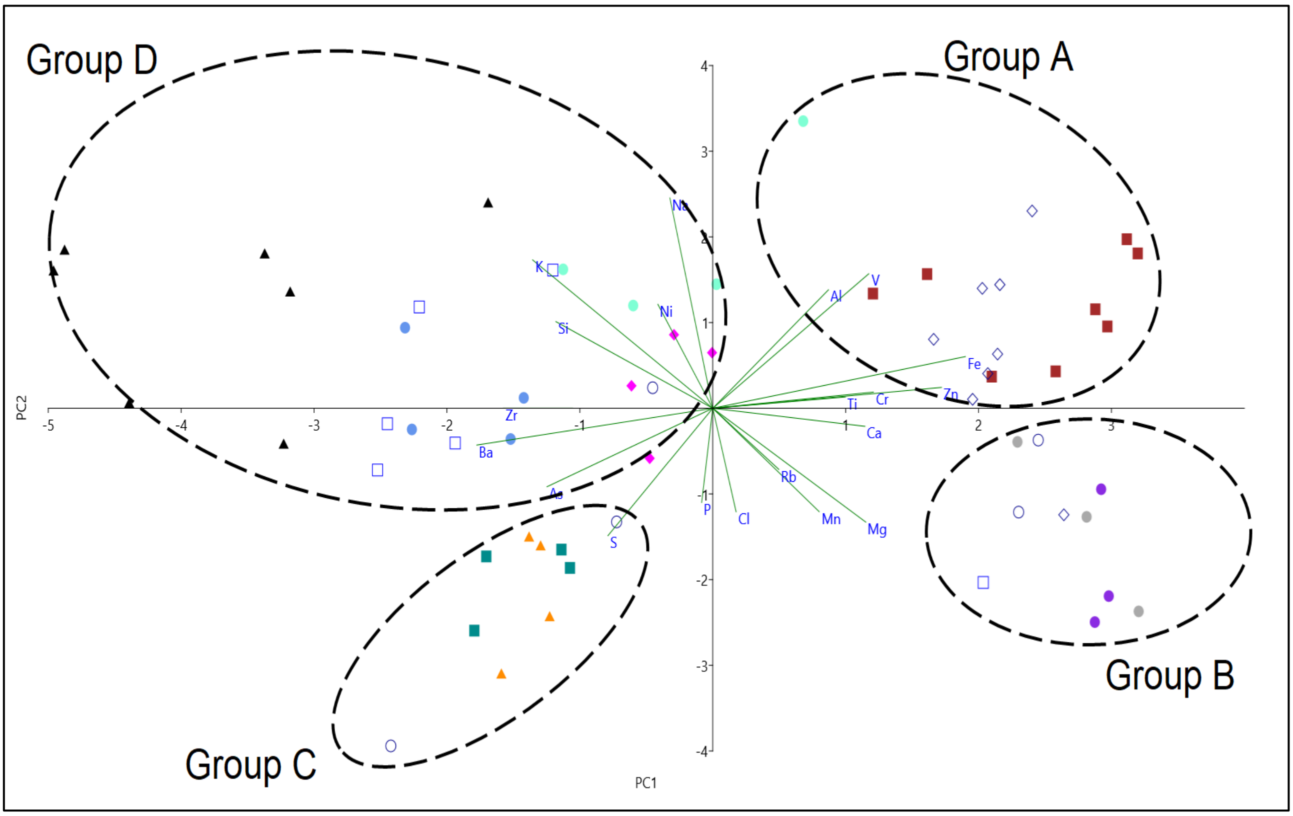

Figure 2-5. PCA for all Acoculco soil samples.

The Cluster Analysis (Figure 2-6) shows that Ba, and, to a lesser extent, also As, are the elements characterized by a marked distance compared to the other geochemical parameters. This probably depends on the Ba greater geochemical mobility triggered by the particular redox conditions.

The concentration levels for some trace elements do not show any particular concern. Arsenic is an exception (0.80-2200; mean 309 mg/kg), almost always above the typical values found in natural soils. Such levels, may entail a hazard, in terms of its enrichment in local water and agriculture products. Among the heavy metals, Zn (mean 111 mg/kg), exceeds world natural soils typical values. Levels of attention also stand out for Ni (15.1-212; mean 73 mg/kg) and, to a lesser extent, for Cr (0.84-96; mean 56 mg/kg), since 200 and 100 mg/kg are respectively suggested as excessive levels for world soils.

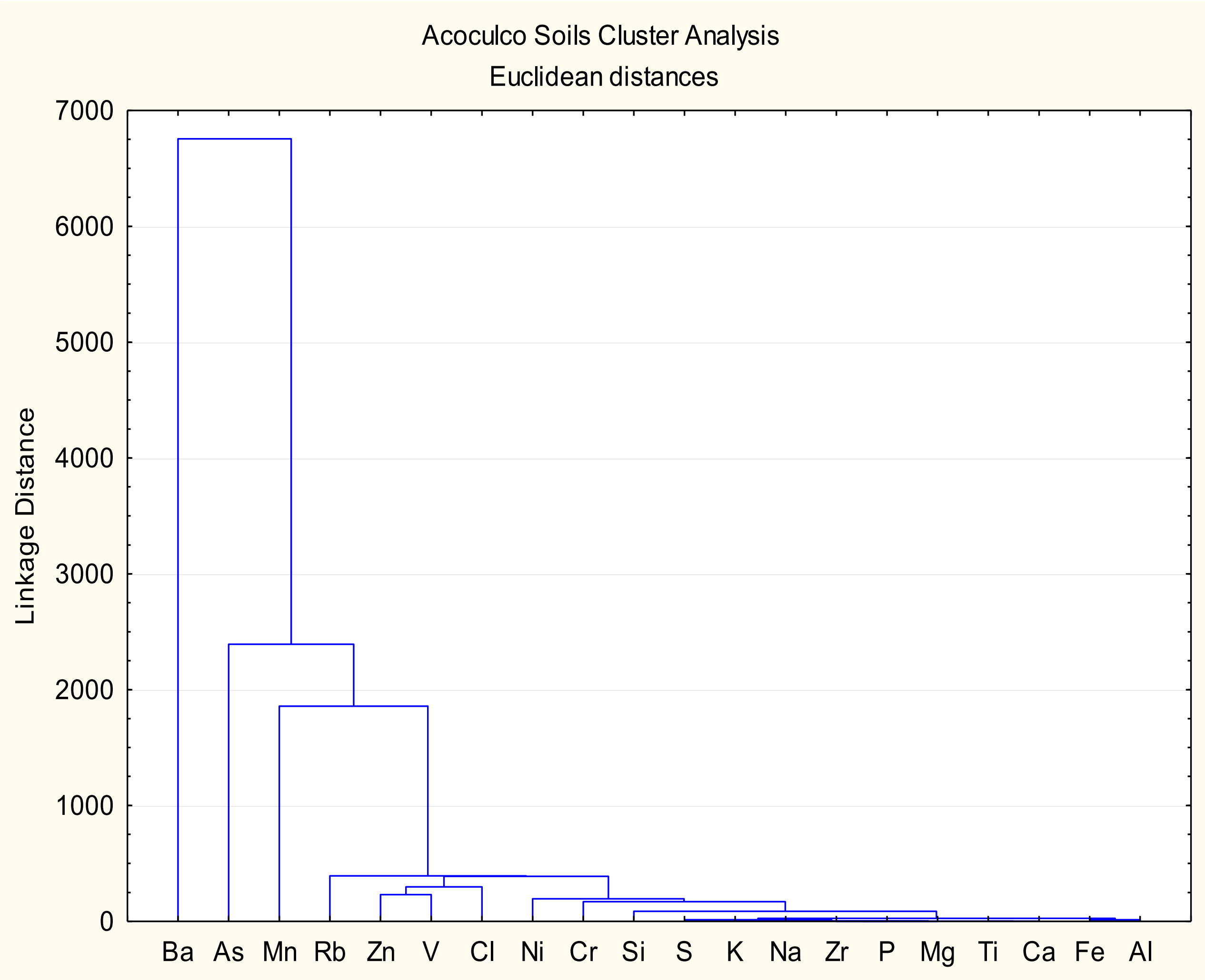

Figure 2-6. Cluster analysis applied to all Acoculco soils for major and trace elements

2.5 Conclusions

On behalf of the GEMex project, a geochemical study on major and minor elements in selected shallow waters and soils in the surrounding of the Acoculco geothermal area has been carried out to characterize the baseline in terms of the geochemical setting of the area and to evaluate the behavior of the elements that can arise environmental concerns and impact on the local population.

This aspect is of particularly importance especially for high temperature reservoirs (>230°C) as Acoculco is. In fact, high temperatures geothermal fluids are characterized by high levels of dissolved minerals. Then, an excessive levels of pollutants as: arsenic, mercury, boron etc., are carried in the liquid stream, poisoning waters and soils. Wells casing breaks and runoff are the reasons way the liquid streaming can be introduced in the environment.

The results obtained on waters, revealed concentration for some elements, both major and minor ones, higher than the guideline values defined by international organizations (WHO, EPA, EU) and Mexican legislation for drinking waters. The geothermal activity and the rain seasonality seem to primarily affect the chemistry of the waters. In the dry season, the waters are characterized by enrichment in some elements, while in the wet season the effect of dilution by rainfall prevails.

Since farming is a key activity in the area, particular attention must be paid in monitoring the quality of the water utilized for cultivation and animal feeding. Some elements, especially As, reach concentrations that might pose serious problems for the animal's health themselves and for that of the consumers, since amounts up to 651 (wet season) and 1933 µg/L (dry season) were found. Al and Fe reached values up of 17.4 and 40.0 mg/L in the wet season and 31.7 and 17.9 mg/L in the dry season. Even if these elements may not be necessarily toxic, they can affect the quality of farming products.

The soil geochemistry evidences that minor and trace elements show a large concentration range related to the wide compositional heterogeneity which is typical of the geothermal areas. This applies mainly to S and As, while the Mn variability can be related to the redox conditions' changes.

The correlation matrix calculated for all the variables shows high r values especially for some pairs of elements associated with hydro-thermalism as As/S (r=0.82). Among the metals the greatest correlation is for Fe/V (r=0.85) and Fe/Zn (r=0.81) as far V/Zn (r=0.76) and Fe/Zn (r=0.80). The correlation between Ca and Zn (r=0.75) is the consequence of the ionic rays' similarity which leads them to participate in the same geochemical processes.

The PCA (Principal Component Analysis) evidences a wide samples dispersion and discriminates four groups: Group A includes the samples most enriched in Al, Fe, V and Zn; Group B contains samples with the highest concentrations of Ca, Mg and Mn; Group C holds the samples most strongly conditioned by geothermal activity as evidenced by the presence of elements such as As and S; finally, group D includes a set of samples characterized by a wide dispersion in the PCA graph (this group includes soils with the highest concentrations of Na, K, Si, Ba and Zr).

The Cluster Analysis also shows that Ba, in particular and, to a lesser extent, As, are the elements characterized by a marked distance with respect to the other geochemical parameters. This probably depends on the Ba greater geochemical mobility triggered by the particular redox conditions.

As final remarks, in Acoculco geothermal area the concentration levels in soils for some trace elements do not show any particular concern. Arsenic is an exception (0.80-2200; mean 309 mg/kg), almost always above the typical values found in natural soils. Such levels may entail a hazard, in terms of its enrichment in local water and agriculture products. Among the heavy metals, Zn (mean 111 mg/kg) exceeds world natural soils typical values. Levels of attention also stand out for Ni (15.1-212; mean 73 mg/kg) and, to a lesser extent, for Cr (0.84-96; mean 56 mg/kg), since 200 and 100 mg/kg are respectively suggested, considering the data from world soils, as "excessive levels". However, the identification of elements with excessive levels does not always denote an immediate danger to the environment as the possible mobilization and consequent danger depends on the occurrence of aspects such as:

- abrupt changes in soil gas emission,
- changes in the temperature and redox potential.

All contribute to mobilization or re-mobilization of heavy metals from soil to water and vice versa, inducing a potential risk for the environment and population.

If any geochemical conditions that can promote the element mobility take place, these "excessive levels" would not necessarily represent a real hazard. However, this requires continuous control of the waters and soils chemical-physical properties through scheduled environmental monitoring campaigns.

Further information relating to the mobility of trace elements in a geothermal environment can be found in Deliverable 8.4 and, in particular, in the section: Potentially Harmful Elements (PHE) mobility assessment in geothermal soils.

2.6 References Chapter 2

Bautista F., Ihl, T., Bedolla-Ochoa C. (2019). La edafodiversidad y su distribución espacial en Michoacán. En: La biodiversidad en Michoacán.Estudio de Estado 2, vol. I. CONABIO, México, pp. XX-XX. https://www.researchgate.net/publication/255686037_La_edafodiversidad_y_su_distribucion_espacial_en_Michoacan

Blair N. Dickie and Katherine M. Luketina (2005). Sustainable Management of Geothermal Resources in the Waikato Region, New Zealand. Proceedings World Geothermal Congress Antalya, Turkey, 24-29 April 2005.

Canet C., Arana L., González-Partida E., Pi T., Prol-Ledesma RM., Franco S.I., Villanueva-Estrada RE., Camprubí A., Ramírez-Silva G., López-Hernández A. (2010). A statistics-based method for the short-wave infrared spectral analysis of altered rocks: An example from the Acoculco Caldera, Eastern Trans-Mexican Volcanic Belt. Journal of Geochemical Exploration 105, 1–10.

Canet C., Hernández-Cruz B., Jiménez-Franco A., Pi T., Peláez B, Villanueva-Estrada R.E., Alfonso P., González-Partida E., Salinas S. (2015).Combining ammonium mapping and short-wave infrared (SWIR)reflectance spectroscopy to constrain a model of hydrothermalalteration for the Acoculco geothermal zone, Eastern Mexico. Geothermics 53 (2015) 154–165

EPA: https://www.epa.gov/dwstandardsregulations

EU's drinking water standards, 1998. Council Directive 98/83/EC on the quality of water intented for human consumption. Adopted by the Council, on 3 November 1998.

FAO. 2009. Guía para la descripción de suelos. Cuarta edición. Traducido y adaptado al castellano por Ronald Vargas Rojas. Proyecto FAO-SWALIM. Nairobi. Kenia- Universidad Mayor San Simón. Bolivia.

GEMex Work Package 4, Deliverable 4.3 (2019). Lelli M., Cuevas Villanueva R.A. Final report on geochemical characterization and origin of cold and thermal fluids. Task 4.3. http://www.gemex-h2020.eu
INEGI: https://www.inegi.org

INEGI, 1997 Características edafológicas, fisiográficas, climáticas e hidrográficas de Méxicohttps://www.rua.unam.mx/portal/recursos/ficha/18641/caracteristicas-edafologicas-fisiograficas-climaticas-e-hidrograficas-de-mexico

INEGI. (2014). Diccionario de Datos Edafológicos escala 1: 250.000. versión III. México.
IUSS Working Group WRB (2015). Base referencial mundial del recurso suelo 2014. Actualización 2015. Sistema internacional de clasificación de suelos para la nomenclatura de suelos y la creación de leyendas de mapas de suelos. Informes sobre recursos mundiales de suelos 106. FAO. Roma.

Liua W., Ramirez A. (2017) State of the art review of the environmental assessment and risks of underground geo-energy resources exploitation. Renewable and Sustainable Energy Reviews 76 (2017) 628–644

Lopez-Hernandez, A., Castillo-Hernandez D., (1997). Exploratory Drilling at Acoculco, Puebla, México: A Hydrothermal System With Only Nonthermal Manifestation. Geotherm. Res. Council Trans., 21, 429-433.

López-Hernández, A., García-Estrada, G., Aguirre-Díaz, G., González-Partida, E., Palma-Guzmán, H., Quijano-León, J. (2009). Hydrothermal activity in the Tulancingo-Acoculco Caldera Complex, central Mexico: exploratory studies. Geothermics 38, 279–293.

M.I.T Massachusetts Institute of Technology (2006). The future of geothermal Energy. Impact of enhanced geothermal Systems (EGS) on the United States in the 21st Century.

http://geothermal.inel.gov/

http://www1.eere.energy.gov/geothermal/egs_technology.html

Norma Oficial Mexicana (1994). NOM-127-SSA1-1994. "Salud Ambiental. Agua Para Uso Y Consumo Humano–Limites Permisibles De Calidad Y Tratamientos A Que Debe Someterse El Agua Para Su Potabilización".

L. Peiffer , R. Bernard-Romero, A.Mazot , Y.A. Taran, M. Guevara, E. Santoyo (2014): Fluid geochemistry and soil gas fluxes (CO_2–CH_4–H_2S) at a promissory Hot Dry Rock Geothermal System: The Acoculco caldera, Mexico

Quinto A., Santoyo E. Torres V., Gonzales E., Castillo D. (1995). Estudio geoquímico-ambiental de los efluentes naturales producidos en la zona geotérmica de Acoculco. Puebla. Ingeniería Hidráulica en México. Vol. X. Núm. 3. p. 21-27. septiembre-diciembre de 1995.

Water Research Center: https://water-research.net/index.php/standards/secondary-standards

3 Potential induced seismicity during stimulation and production at Acoculco site

Authors: Thibault Candela, Elisabeth Peters, Jan Diederik van Wees

3.1 Structural setting

The potential EGS site is located in the Acoculco caldera which is part of the Trans Mexican Volcanic Belt (TMVB). The site is characterised by two fault orientations: NW-SE and NE-SW. The NW-SE striking faults are oblique to strike-slip faults and the NE-SW striking faults are oblique to normal faults (Figure 3-1). See for example GEMex D7.1 (Peters et al., 2020) or D7.2 (Hofmann et al., 2020) for more information on the structural setting and stress conditions.

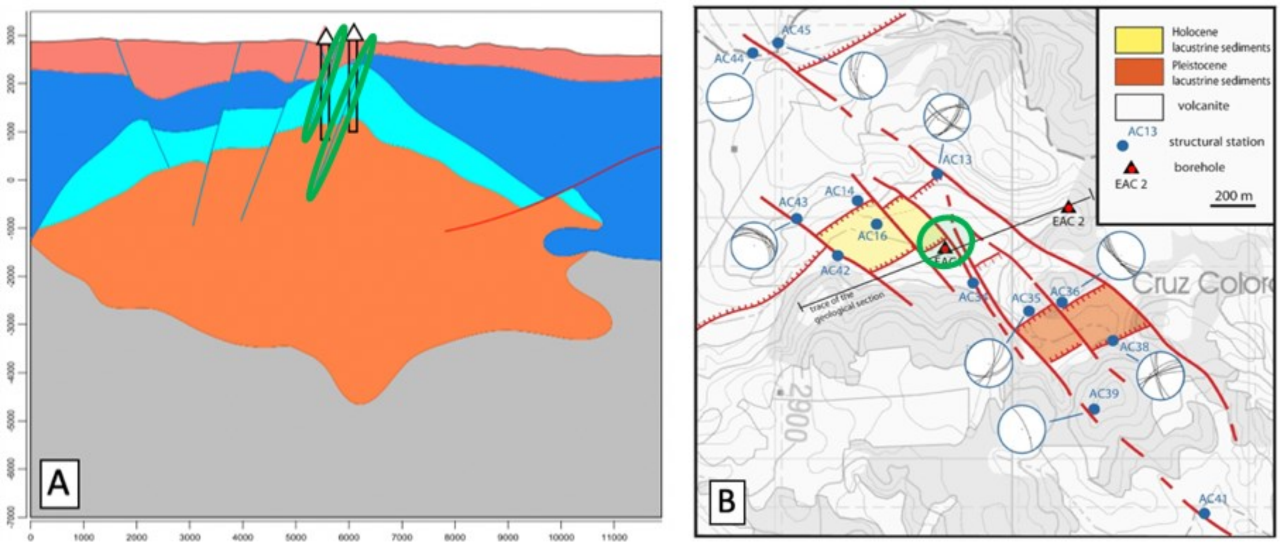

Figure 3-1. Fault zones marked green on the geological cross-section (A) and the closest fault intersection zone marked green on the structural geological top-view map (B) are potential stimulation targets (adapted from Kruszewski et al. submitted).

Deformation

Within the GEMex project also InSAR (Interferometric Synthetic Aperture Radar) and GPS data was analysed to detect deformation at the surface (Békési et al., 2019, GEMex D5.7). The InSAR data from Acoculco did not result in a reliable deformation signal, probably due to vegetation cover and presumably very small deformation. The regional analysis of the GPS data showed horizontal displacement in NW-SE direction of up 3 cm, indicating a tectonically active region.

3.2 Micro-seismic base line monitoring

Important information for the evaluation of risk for induced seismicity is the natural tectonic seismicity. Pre-GEMex monitoring of seismicity in the Acoculco Caldera is limited. A preliminary study with 6 seismic stations showed very limited local natural seismicity (Jousset et al., 2019 GEMex D5.3).

Within the Mexican GEMex project, monitoring of the natural seismicity has taken place in the period May 2018 to July 2019. In total 18 stations were used (Figure 3-2). The design of the monitoring network is described by Hernández et al. (2020). The analysis of the data is not completed at this point, but the preliminary analysis showed 33 local seismic events (Figure 3-3) with a magnitude of up to 3 (Figueroa et al., 2019). The area monitored using the stations is considerably larger than the area included in the local geological model (Figure 3-3), which covers an area of 10 x 8.5 km. In this area only one event was observed.

3.3 Induced seismicity risk

Geothermal development of the Acoculco Geothermal field requires stimulation. In GEMex, various scenarios for stimulation and Enhanced Geothermal System (EGS) production development have been considered, which have been described extensively in deliverables D7.2 (Hofmann et al, 2020) and D7.1 (Peters et al., 2020) respectively. In these reports the potential for induced seismicity was analysed as well, however not yet in a combined perspective and implications for monitoring needs and in the context of (base line) monitoring findings.

To this end, we summarize here the findings of D7.1 and D7.2 for induced seismicity and its implications. D7.2 shows that the risk for induced seismicity during stimulation appears to be small, given the current information on stress and fault orientation. Different scenarios were run with varying stress regimes and fault orientations, but all simulated events were smaller than -0.5. This seems to be in line with the low level of seismicity observed during micro-seismic monitoring (Figueroa et al., 2019 and previous section). During production, the injection of large amounts of cold water shows a larger impact, as simulated in D7.1. The cooling due to injection causes significant stress changes which can cause a 1000-fold rise in natural seismicity rates in local fault structures (D7.1, Figure 3-4, Figure 3-5 and Figure 3-6).

Adopting a base line seismicity rate of 1 yr^{-1} for the area of the local geological model (10 x 8.5 km; see section 3.2), the estimated background seismicity rate for the sub-area of the EGS production would be about 0.01 event yr^{-1}, for events with magnitude $Mw>0$. In D7.1 induced seismicity event catalogues due to fluid flow and cooling have been modelled for EGS production systems for both strike slip and normal slip fault orientation. The interaction with different in-situ stress conditions for strike slip and normal slip fault orientations gives markedly different response in induced seismicity: in a strike slip fault setting induced seismicity is more moderate compared to normal faulting (Figure 3-4, Figure 3-5 and Figure 3-6). Simulations for induced seismicity catalogues indicated that for a strike slip fault orientation the maximum magnitude may be lower than M=3, whereas for a normal fault orientation maximum possible magnitudes can rise to M=4.5. It should be noted that the modelled catalogues assume a specific seismic hazard model, which is subject to discussion (see D7.1) and can be modelled also in a more heuristic way calibrated by data being gathered during stimulation and production (see chapter 4).

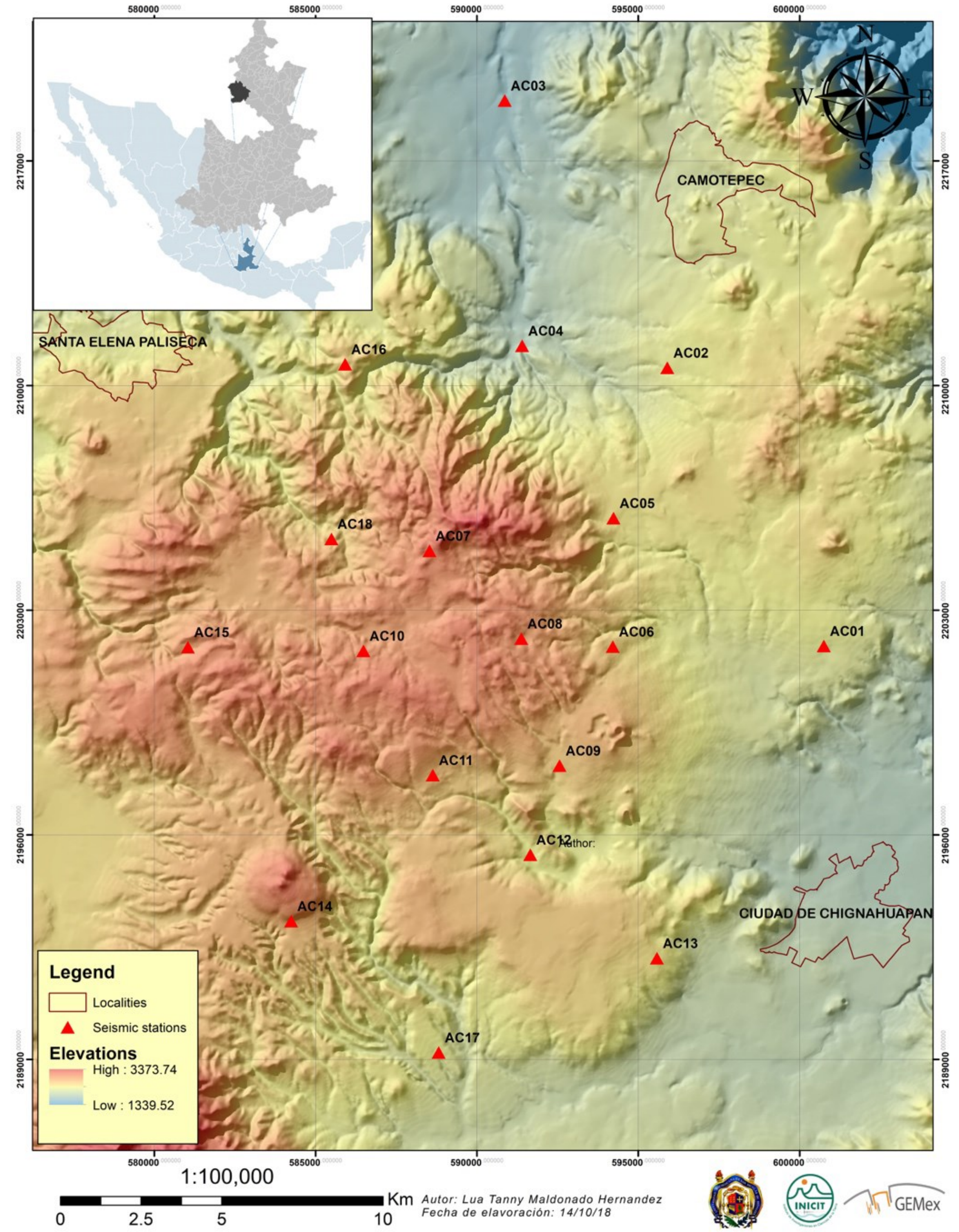

Figure 3-2. Network deployment of the seismic stations. stations shown as red triangle. The wells EAC-1 and EAC-2 are located between AC07 and AC08. Source: Figueroa et al, 2019.

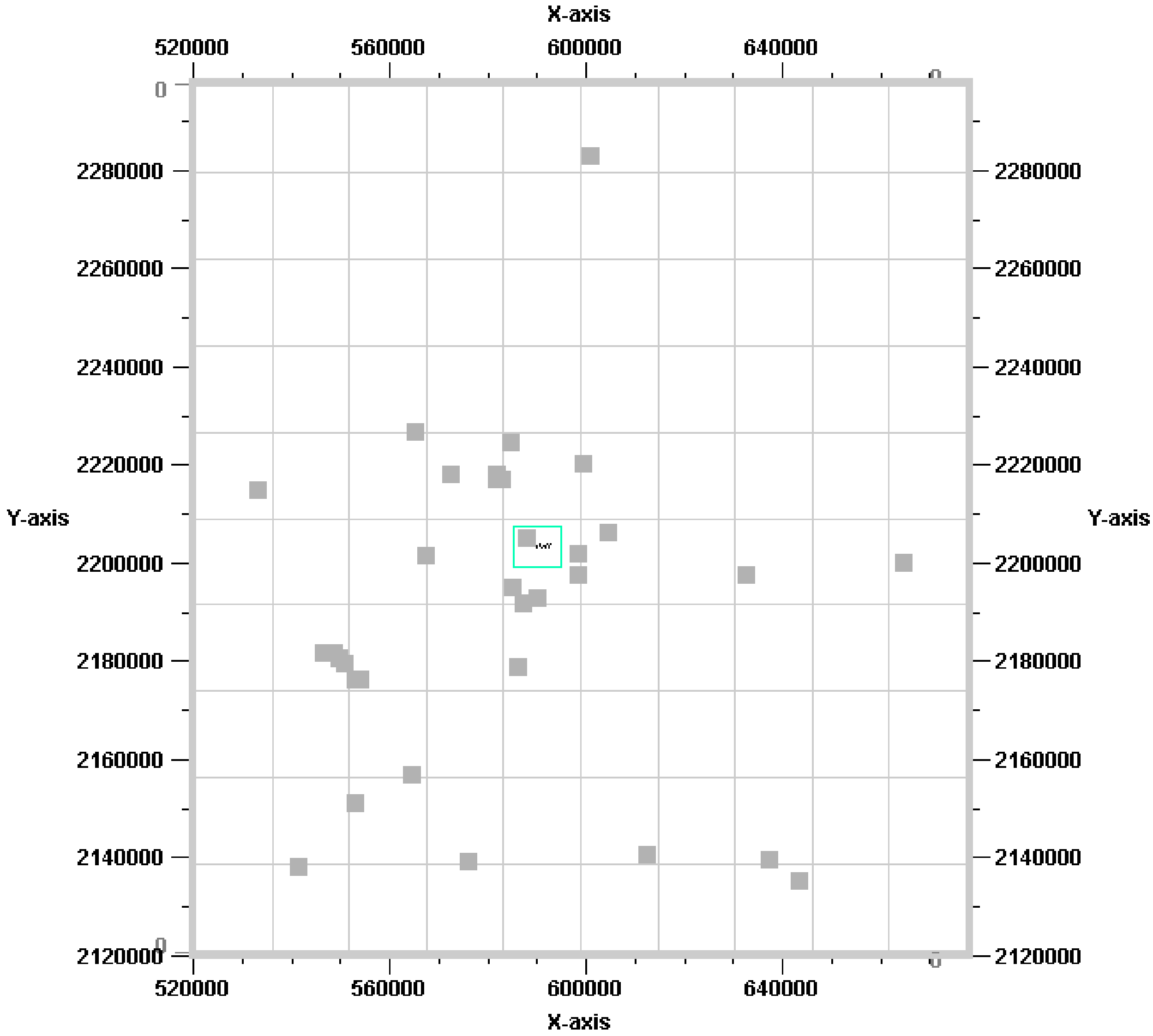

Figure 3-3. Locations of observed micro-seismic events from (Figueroa et al, 2019) in the period May 2018 to July 2019. Rectangle indicates the area of the local geological model.

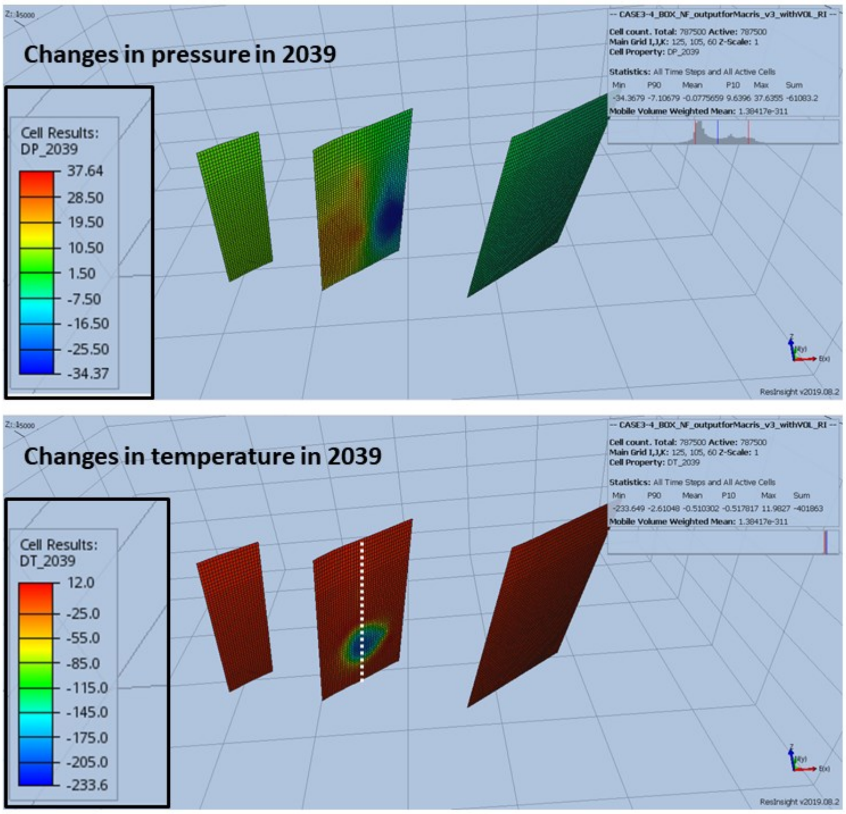

Figure 3-4. Normal-slip fault model: changes in fault pressure (up) and temperature (down). The sub-vertical dashed white line indicates the pillar where the changes in Coulomb stress, pressure, temperature are presented in Figure 3-5.

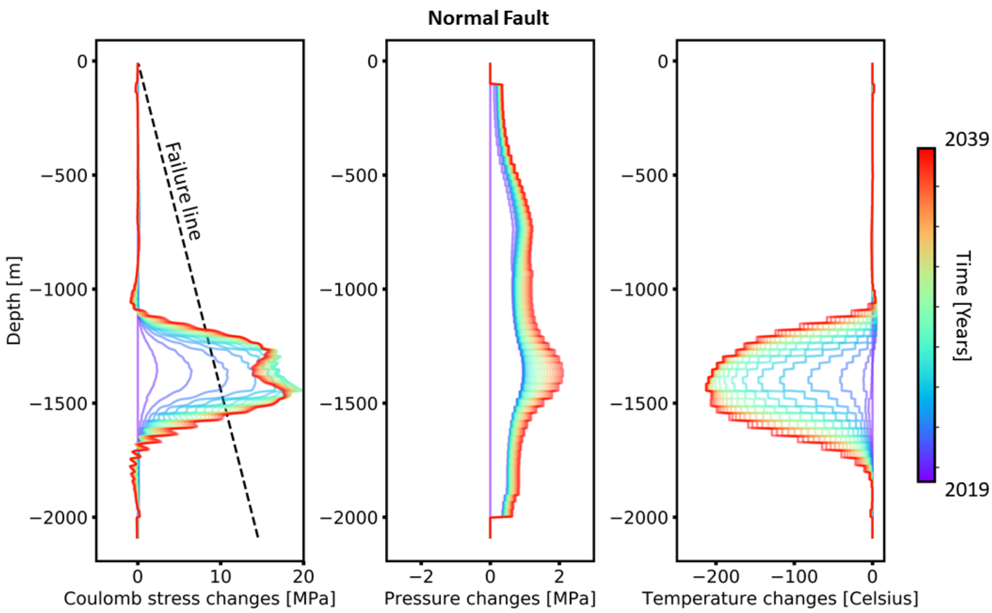

Figure 3-5. Normal-slip fault model: temporal evolution of Coulomb stress, pressure, temperature changes along the pillar presented in Figure 3-4.

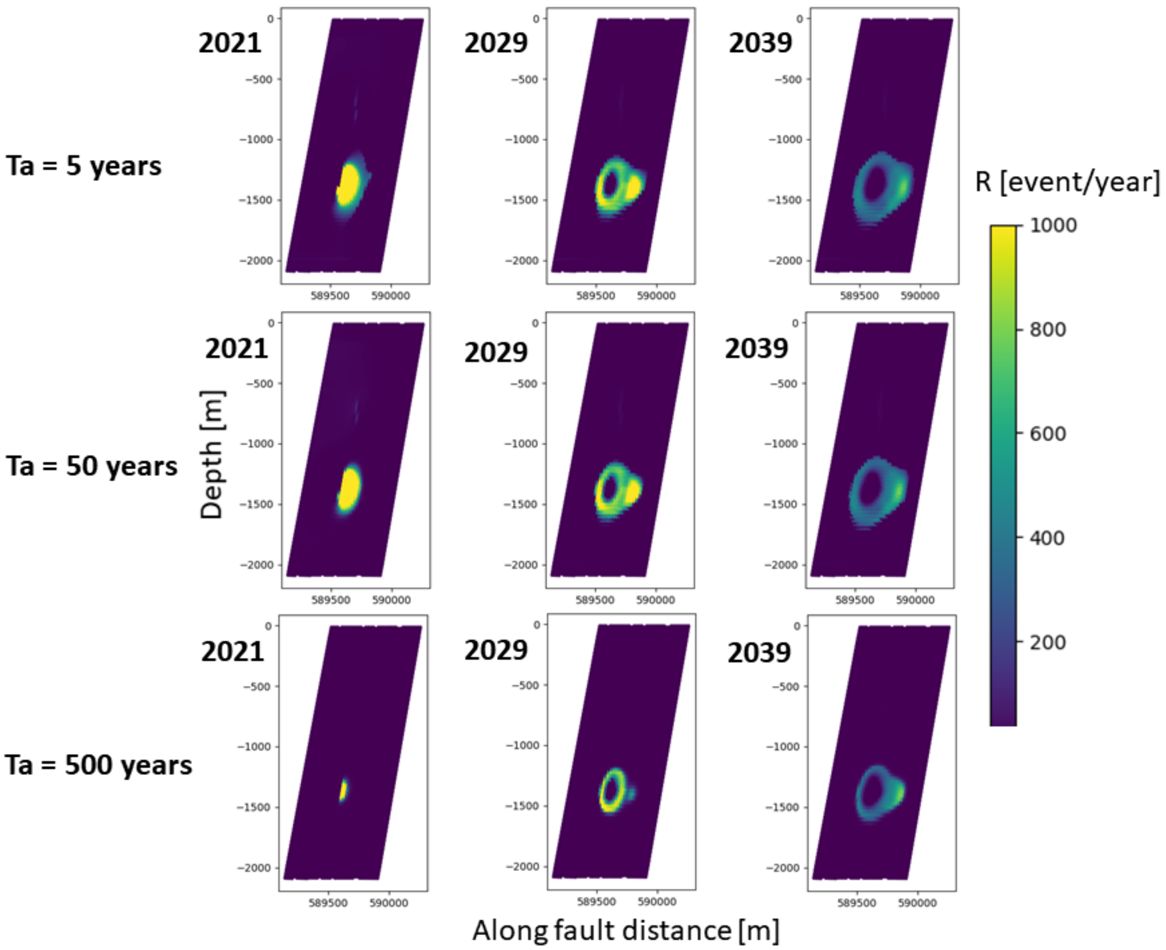

Figure 3-6. Normal-slip fault model: spatio-temporal evolution of relative seismicity rate R. When the change in Coulomb stress is positive, the fault is following a destabilizing stress path and can eventually reach the failure line. T_a is the characteristic time delay for the earthquake nucleation process.

3.4 References Chapter 3

Békési, E., Fokker, P.A.,Limberger, J., Bonté, D., Páll Hersir, G., Ágústsdóttir, T., Garcia, O., Muñiz Jauregui, A.,Ávila Olivera., J.A., Garduño-Monroy, V.H., Van Wees, J.D., 2019. InSAR and GPS of the Acoculco and Los Humeros geothermal fields. GEMex deliverable D5.7.

Figueroa, A., Perton, M., Calo, M. and V. Márquez. 2019. Reporte técnico con la revisión de la actividad sísmica natural y/o antropogénica detectada en Acoculco. Mexican GEMex Etapa6 PT5.2 Seismic.

Hernández, A.L., Calò, M., Figueroa, A., Mendiola, L.E. 2020. Informe técnico studio de optimización de redes sísmicas y detección de sismicidad inducida geothérmico de Acoculco. English translation “Set up of an optimized seismic monitoring system for the Acoculco injection test” by Hernández, A.L., Figueroa-Soto, A., Caló, M. GEMex report.

Hofmann, H., F. Parisio, B. Lepillier, T. Candela, E. Peters, M. Kruszewski and L. Weydt. 2020. Report on optimised stimulation scenario for Acoculco. GEmex deliverable D7.2.

Jousset, Ph., K. Agustsson, E. Barison, G. Böhm, M. Caló, I. G. Chavarria, B. Farina, E. Gaucher, Ka. Loer, J. Martins, M. Perton, F. Poletto, E. Saenger, A. Figueroa Soto, T. Toledo, A. Verdel and C. Werner, 2019. Seismic structures of the Acoculco and Los Humeros geothermal fields. GEMex deliverable D5.3.

Peters, E., T. Candela, B. Lepillier, H. Hofmann, P. Deb, M. Kruszewski, W. Wheeler, E. Bastesen, E. Trumpy, L. Weydt, K. Bär, I. Sass, J. D. van Wees. 2020. Report on model of potential drill target and proposed drill path. GEMex Deliverable D7.1.

4 Seismic hazard monitoring and risk mitigation in EGS (Acoculco)

Authors: Giovanni Bongiovanni, Massimo Angelone, Vladimiro Verrubbi

In literature two very complete approaches for assessing induced seismicity can be found. The first one (National research Council, 2013), comprises all the possible source of induced seismicity and treats the problem in a common general way. It underlines that while a probabilistic hazard analysis should be advisable, there are intrinsic difficulties in collecting and assembling statistical data on different wells at different depths and mainly in different geological environment. The proposal is then to study each single well with an appropriate mix of statistical and analytical approaches.

For EGS this study adopts the seven-step procedure of the USA Department of Energy (Majer et al., 2012), the second complete approach:
Step 1 Perform a preliminary screening evaluation.
Step 2 Implement an outreach and communication program.
Step 3 Review and select criteria for ground vibration and noise.
Step 4 Establish seismic monitoring.
Step 5 Quantify the hazard from natural and induced seismic events.
Step 6 Characterize the risk of induced seismic events.
Step 7 Develop risk-based mitigation plan.

The steps 4 and 5 have been largely discussed in chapter 3 of this report. This chapter focusses mainly on step 6 in particular in view of the understanding the characteristics of seismic hazards and appropriate seismic monitoring and risk mitigation for Acoculco. To this end, this chapter is structured as follows, first we introduce in section 4.1 generic aspects of seismic hazard assessment and its implications for EGS seismic hazard monitoring through a "traffic light" approach . Subsequently, we highlight the importance of understanding the structural and stratigraphic framework in site response for induced and natural seismic events by comparing the Basel induced event and an Italian tectonic event in sections 4.2, and next consider key aspects of the Acoculco setting of relevance for seismic response in section 4.3. In sections 4.4 and 4.5 we subsequently highlight the importance of the site characteristics for seismic hazard, vulnerability and risk in Acoculco and provide a more site specific seismic risk and monitoring analysis for the geothermal site in Acoculco in section 4.6.

4.1 Introduction

Following some strong earthquakes such as Friuli 1976, Irpinia 1980, Molise 2002, Emilia 2012, Umbria-Marche 1997 (all in Italy), Mexico City 1985, Kobe 1992 (Japan), Izmit 1999 (Turkey), researches on the dynamic behaviour of lands and their spatial problems had a strong scientific interest and development in the last forty years.

The problems inherent to the different effect produced on the terrain shaking by the same seismic event, which could have had very different consequences even between contiguous areas (distances of less than hundreds of meters), have long been known by scientists since they were firstly observed after Messina (1908) and San Francisco (1957) earthquakes. However, there has been a return of scientific interest in this topic only since the second half of the eighties of the past century. This new interest in this issue was to the need to expand the scientific bases necessary to implement building safety and reduce the seismic risk to the population in urban areas developed in tectonically active areas.

In this context the main problem is to deepen the knowledge of the causes responsible for the variations of the superficial seismic wave in terms of amplitude, frequency and length. It is quite clear that a greater understanding of the phenomenon would have positive implications in territorial planning and in the management of emergencies related to seismic effects. Furthermore, integrating the cognitive framework of the territory with hazard analysis would allow a better definition of risk analysis and mitigation activities.

The permanent deformations that occur in outcropping formations can also be traced back to the effects of seismic action, while the main and frequent associated geological phenomena are: landslides (Wasowski et al., 2011; Romeo, 2000), land liquefaction (Seed and Idriss 1982) and differential failure and dislocation along fault planes.

This list of occurrences is often a direct consequence of the seismic activity and provides a warning concerning the complexity of this issue and the involved dynamics. As a consequence, arise also the need for a specific data acquirement for each class of effects, bearing in mind that all information necessary to characterize a given area are site specific depending on the geological, geotechnical and geophysical features of the site under examination.

In this type of activity, the first aspect that must be carefully considered concerns the collection and storage of the available data obtained from previous surveys. Their analysis and interpretation will allow us to highlight any temporal or spatial data gaps in case to plan any further investigations.

In the first phase of the study it will be very important to acquire the most up-to-date and detailed basic cartography of the study area, preferably at 1: 5000 or 1: 10000, model scale and in digital format too.

With regard to thematic cartography it will be necessary to acquire or produce "ex novo" the topographic, geological, lithological, geotechnical and geomorphological maps together to the landslides map. Furthermore, all the data acquired through previous survey campaigns or obtained with the new studies will be reported in a specific GIS database which will represent the new reference for the territory. In this digital form it will be very easy constantly update information for each variable considered.

Starting from the calculation of the seismic wave amplifications, the essential data will be acquired through drill and geophysical surveys (Geoelectric, Seismic refraction, Down Hole, Cross Hole, Masw: Multichannel Analysis of Surface Waves, Environmental Noise Measurements, etc.). Other information will come from the geotechnical and geo-mechanical surveys and from the digital land model.

With these data it will be possible to reconstruct the site morphology and lithostratigraphy. Furthermore, it will be possible to ascertain the depth and the seismic bedrock trend as well as its deepness morphology, the measurement of the fundamental vibration period, the velocity profile of the waves Vs.

An important effect/phenomenon to consider is the possible occurrence of soil liquefaction. To test this contingency, it will be necessary to evaluate the susceptibility of the soil itself. Other information, deemed necessary, includes data on the characteristics of the aquifer, its depth and spatial variations as well as a good knowledge of the global site's hydrogeology. Other information must contain data concerning the behaviour of the terrain under cyclic loading that we can achieve by cyclical triaxial measurements or resonance column. Besides, supplementary information will be got from the characterization of the granulometric curve of the shallow formations and their expected shaking behaviour on the surface.

Another important parameter to be considered is the slope instability evaluation. This data can be obtained defining both the topographic profile and the landslide model.

All this information will be reported in the digital cartographic map that will allow us to split the territory into sub-areas characterized by a similar seismic response. This in order to identify the areas that evidence the greatest risk where to actuate all the actions necessary to mitigate the possible effects produced by the seismic shaking.

Since many years it has been recognized that pumping fluids into or out of the Earth has the potential to cause seismic events that can be felt and eventually produce damage to artefacts. Historically, induced seismicity has occurred in many different energy and industrial applications (reservoir impoundment, mining, construction, waste disposal, and oil and gas production, geothermal energy extraction). The largest magnitudes of induced earthquakes have been attributed to reservoir impoundment and hydrocarbon extraction, but the direct connection between human activities and seismicity is debatable. Reservoir impoundment probably originated the Koyna earthquake (India 1967, M=6.5), and the Aswan earthquake (Egypt 1981, M=5.6). Hydrocarbon extraction, as triggering, has been associated to Coalinga earthquake (CA, USA 1983, M=6.5) and Wittier Narrows earthquake (CA USA 1987, M=6) and to the exceptional seismic sequence, because the region was considered aseismic, in Gazil (Uzbekistan) with a M=7 earthquake in April 1976 followed by a M=7 earthquake in May 1976 and another M=7 earthquake in 1984. The consequences of these events were relevant in terms of injuries and damages. In the field of geothermal energy extraction, the three most relevant seismic event recorded and investigated are Basel (Switzerland 2006 M=3.4), Cooper Basin (Australia 2003 M=3.7) and Geysers (CA USA 1982 M=4.6), the more recent M=5.0 earthquake at Geysers (2016) should be considered too. Cooper Basin is in a remote area and there is very little concern about. The event of 1982, as well as those of magnitude above 3, caused non-structural damages; it is relevant to note that one event of M=3.03 gave an unexpected acceleration of 21% g at Anderson Springs at 1.2 miles from the epicentre. The event in Basel produced small non-structural damages, strong community concern and stopped the geothermal extraction activities; the recorded PGA, at less than 1 Km from the epicentre, is 6% g. Some characteristics of the Basel site and of the seismic sequence will be considered, since the site is an EGS (Enhanced Geothermal System).

Another aspect considered by this study is the regulation of fluid injection for EGS if induced seismicity is observed to be caused by the proposed stimulation (hydraulic fracturing) operation. The Bureau of Land Management (BLM) procedure is adopted; this includes the use of a “traffic light” system that allows hydraulic fracturing to proceed as planned (green light) if it does not result in an intensity of ground motion in excess of Mercalli IV “light” shaking (an acceleration of less than 3.9%g), as recorded by an instrument located at the site of public concern. However, if ground motion accelerations in the range of 3.9%g to 9.2%g are repeatedly recorded, equivalent to Mercalli V “moderate” shaking, then the hydraulic fracturing operation is required to be scaled back (yellow light) to reduce the potential for a further occurrence of such events. Finally, if the operation results in producing a recorded acceleration of greater than 9.2%g, resulting in “strong” Mercalli VI or greater shaking, then the active hydraulic fracturing operation is to immediately cease (red light). For the Basel sequence the operation of fluid injection is presented as related to the magnitude of the seismic events, and the peak acceleration in the range of yellow light, ~ 6% g, was after the stopping of the operations. *The rate of injection (quantity of liquid over time) was gradually increased until, on the sixth day, the maximum rate was reached. Shortly after, an earthquake with a local magnitude of 2.6 occurred, whereupon the rate of injection was first decreased and then stopped altogether a few hours later. Approximately five hours after that, an earthquake with a local magnitude of 3.4 (moment magnitude 3.1) occurred. Having an intensity of V ("moderate" on the Mercalli scale), it was felt over a wide area and caused minor damage. Three more quakes with local magnitudes of higher than 3.0 ensued, the last occurring in February 2007.* This fact associated with the reported PGA 21% g for a M=3 earthquake at Geysers suggest that **the threshold for the traffic light should be tailored to each specific site**.

4.2 Comparison of some aspects of Basel induced earthquake and an Italian tectonic event.

Ripperger et al. (2009) in a detailed study of the earthquake records during the 2006 Basel seismic induced sequence, analysed the records obtained from the stations as reported in Figure 4-1. The epicentre of the earthquake was between stations Sbaf and Otter. Among other findings, the authors make a 3-D simulation incorporating the geophysical 3-D model of the Basel region, and compare the response spectra of the synthetic signal to those of the recorded ones for two stations, Figure 4-2. It is apparent the mismatch for short periods. In the analysis the authors associate this fact both to closeness to faults and/or surface geology.

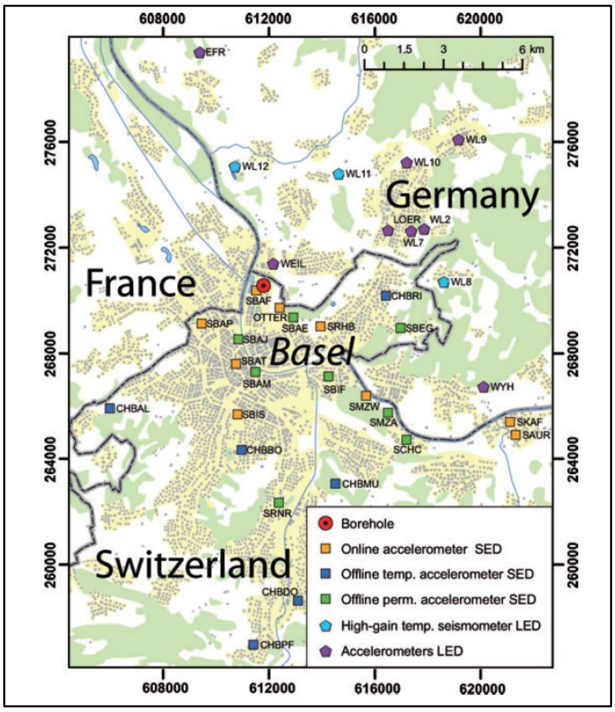

Figure 4-1: Seismic stations location map in Basel.

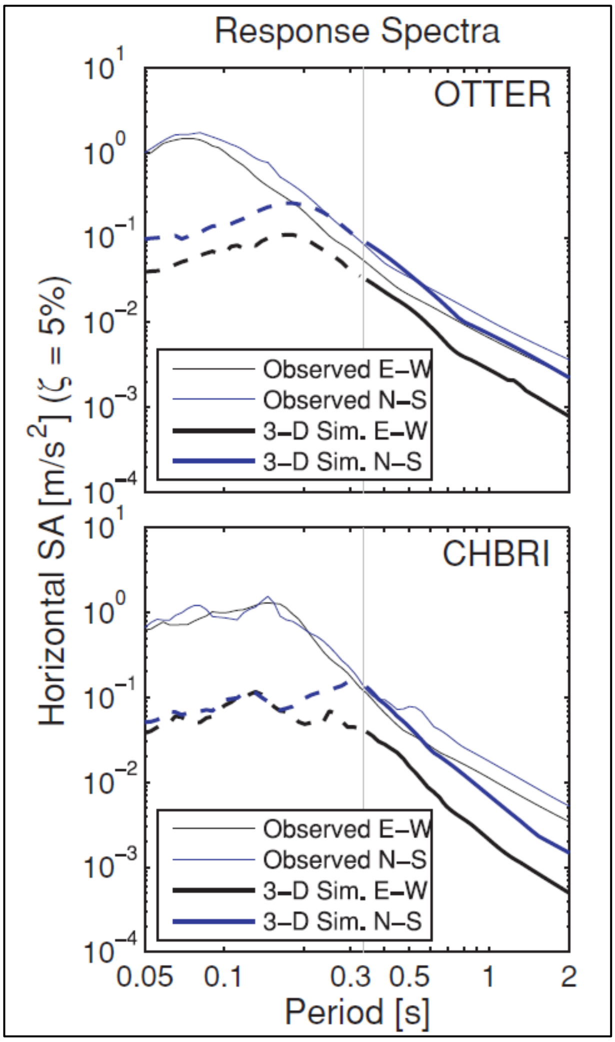

Figure 4-2: Response spectra comparison of the recorded and synthetic data for Basel earthquake.

On October 31, 2002 an earthquake, M=5.4 M_W=5.7, struck a southern Italy area giving damage focused in a small village, San Giuliano di Puglia. Strong damage differences occurred inside the village within few hundred meters, Figure 4-3. No seismic instrumentation was present in the village. The geology of this area is described as in Figure 4-4.

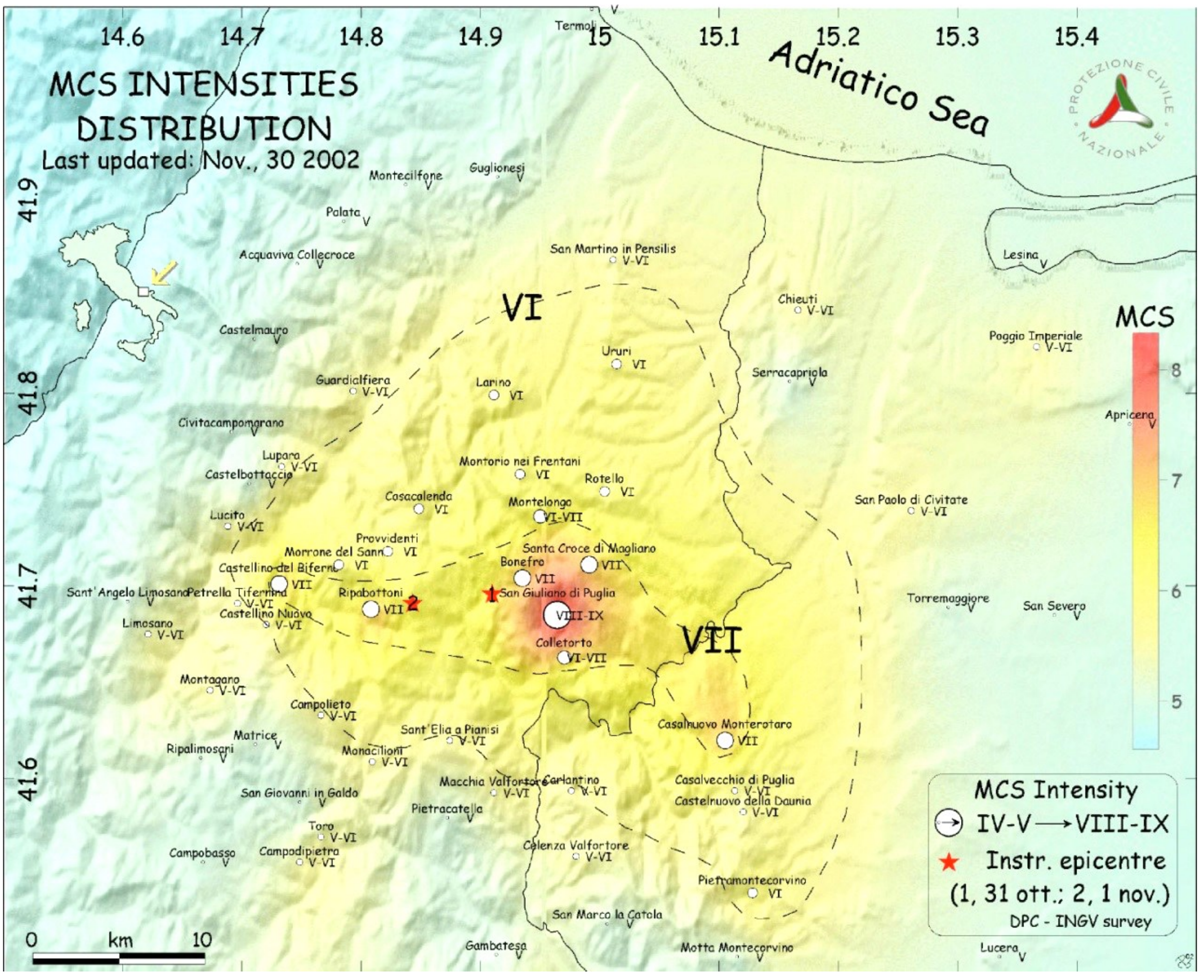

Figure 4-3: Macro seismicity intensities map (MCS) for San Giuliano area, Italy. (Baranello et al., 2003)

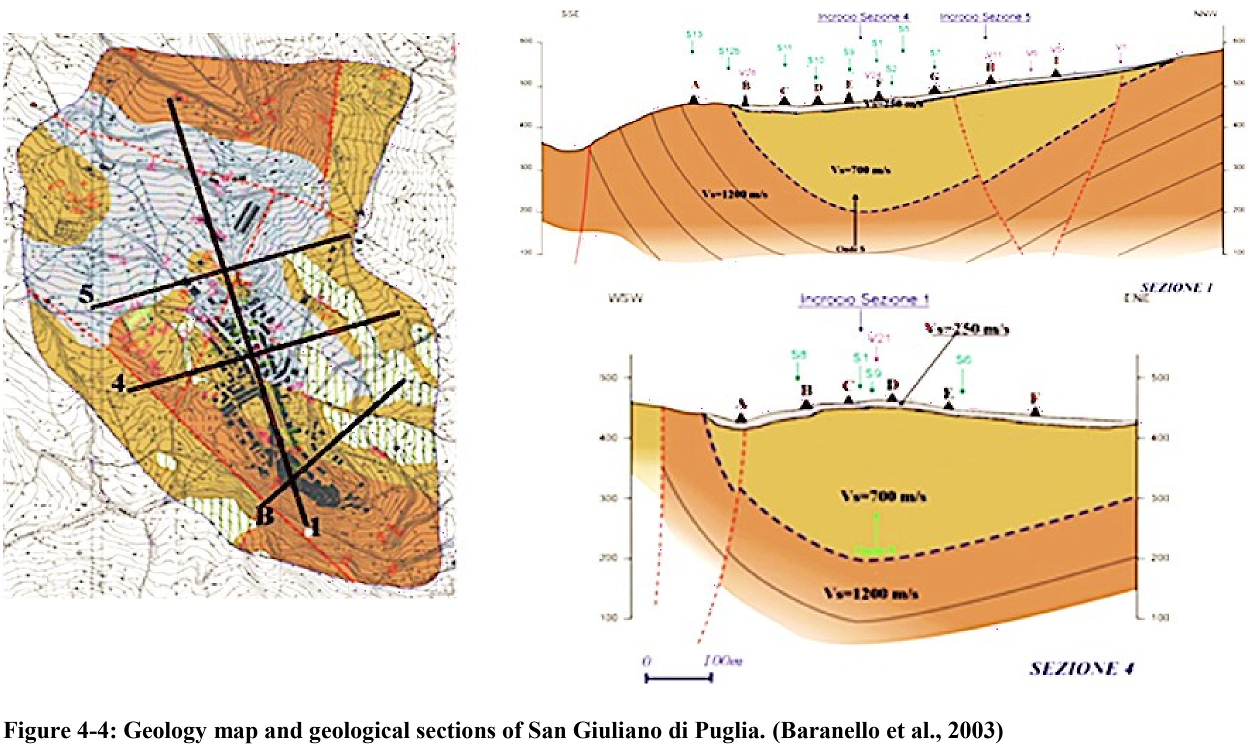

Figure 4-4: Geology map and geological sections of San Giuliano di Puglia. (Baranello et al., 2003)

Next a local accelerometric network was installed as in Figure 4-5 and some related information are reported in Table 4-1. Very detailed studies (Caputo et al., 2007) permitted to assess the most realistic geology resulting in Figure 4-6, where a fault system was identified. This fault system includes the transversal fault lines within the village previously supposed as gravitative discontinuities, Figure 4-7.

Figure 4-5: Accelerometric stations location in San Giuliano di Puglia.

Table 4-1: Accelerometric stations data for San Giuliano di Puglia area.

Station	**Location**
SGSC Clay close to flysch	Surface
SGSC Clay close to flysch	-30 m
SGPA Clay	Surface
SGPA Clay	-56 m
SGMA Flysch	-10 m

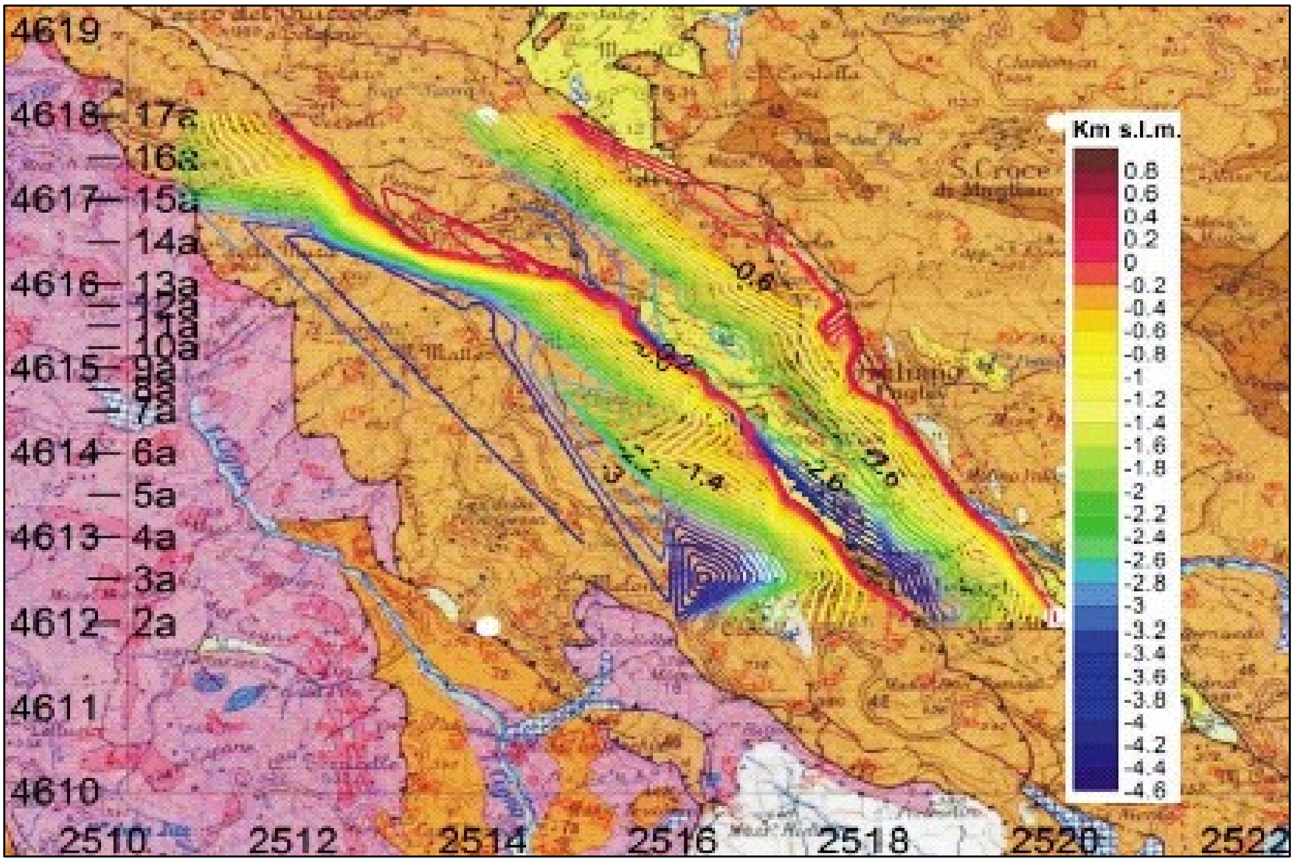

Figure 4-6: San Giuliano di Puglia (Central Italy) updated geological map after the seismic study.

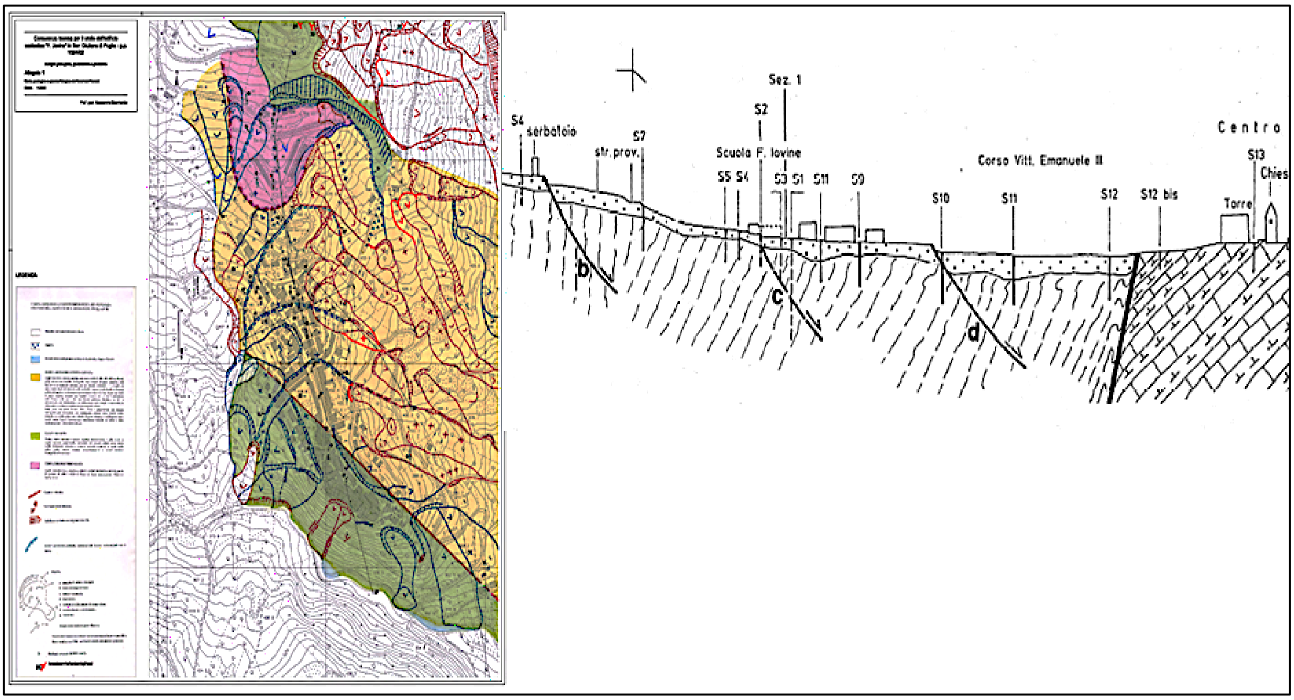

Figure 4-7: Old hypothesis of the local geology. Station SGMA is close to line c.

The accelerometric network has recorded several events, the most relevant of which is summarized in Figure 4-8 by comparing the Fourier spectra (Sanò et al., 2015).

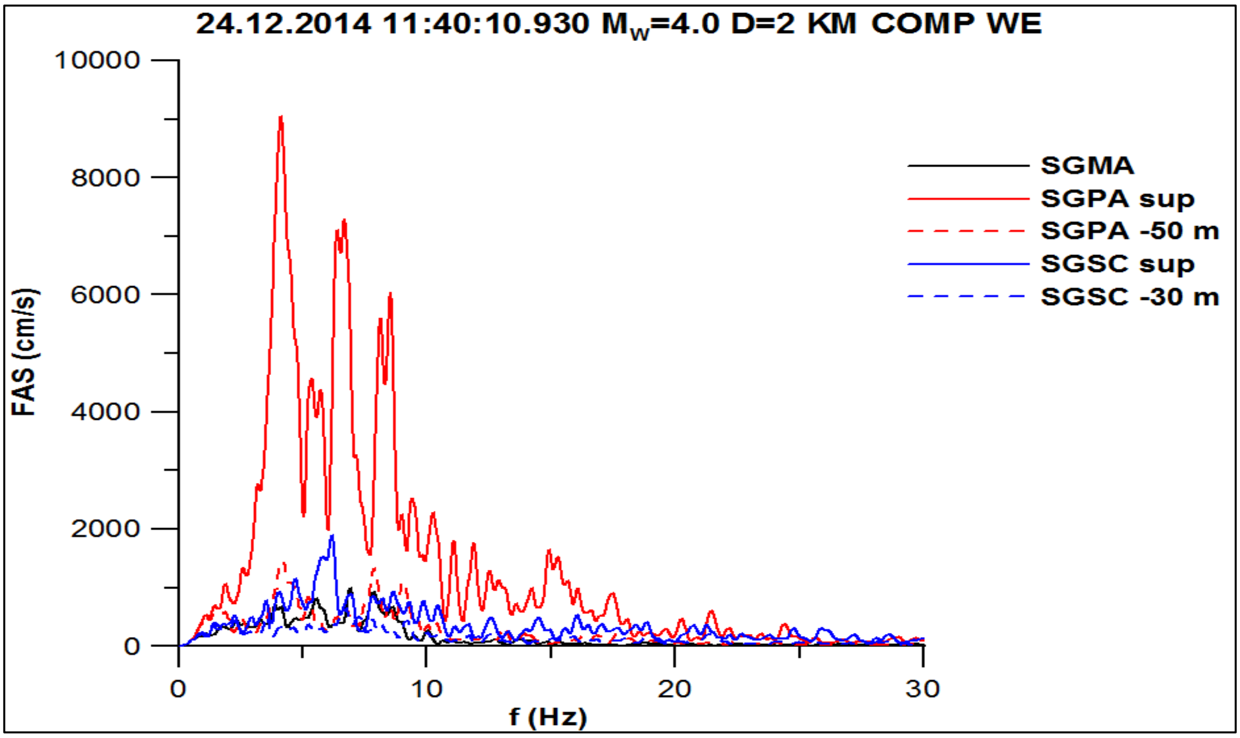

Figure 4-8: Synthesis of the recorded earthquake.

From this figure it is evident the exceptional amplification at station SGPA. Site response has been modeled with a boundary element program (2D) and the comparison in terms of response spectra at the station SGPA is presented in Figure 4-9.

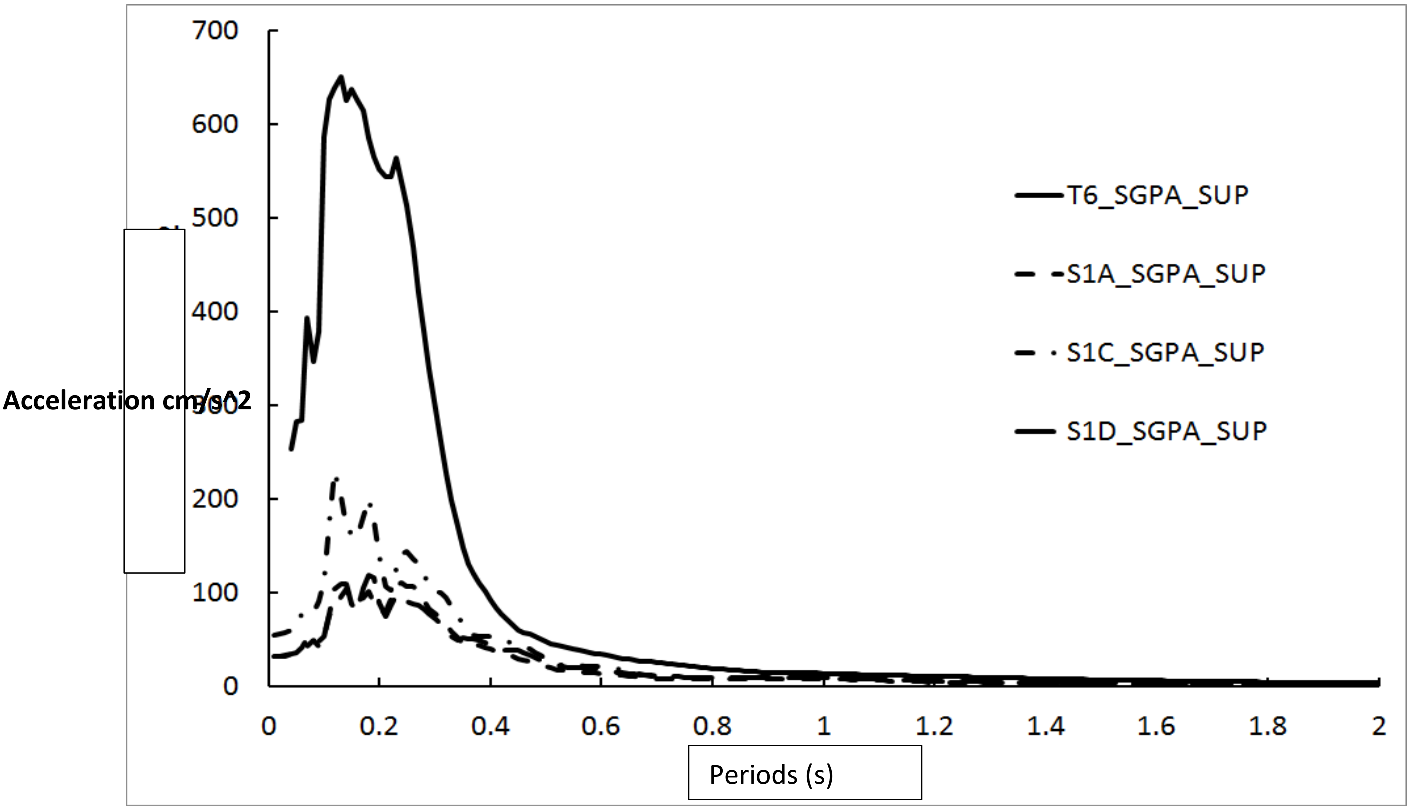

Figure 4-9: Comparison between response spectra of the recorded signal and of synthetic ones.

T6_SGPA_SUP is the response spectrum of the component recorded acceleration, the others correspond to different model parameters. At the date state of knowledge, the only cause of the response at SGPA is the presence of the lateral discontinuity represented by the very close fault line.

Similarity in the frequency content anomaly between this event and the one presented for Basel is to be considered to assess amplification effects in areas where lateral discontinuities are present.

4.3 Some consideration on Acoculco site.

The activity related to this deliverable started with great delay owing to missing authorizations for the seismic network deployment to the site. Data is still being collected and only partial analysis can therefore be made for Acoculco.

The Acoculco caldera cover an area of about 290 Km^2 and, according to (Avellan et al., 2018) has an asymmetric structure. The caldera belongs to the NE side of the Trans- Mexican Volcanic Belt (TMVB) a volcanic arc which is developing along the E-W direction for about 1000 km, Figure 4-10.

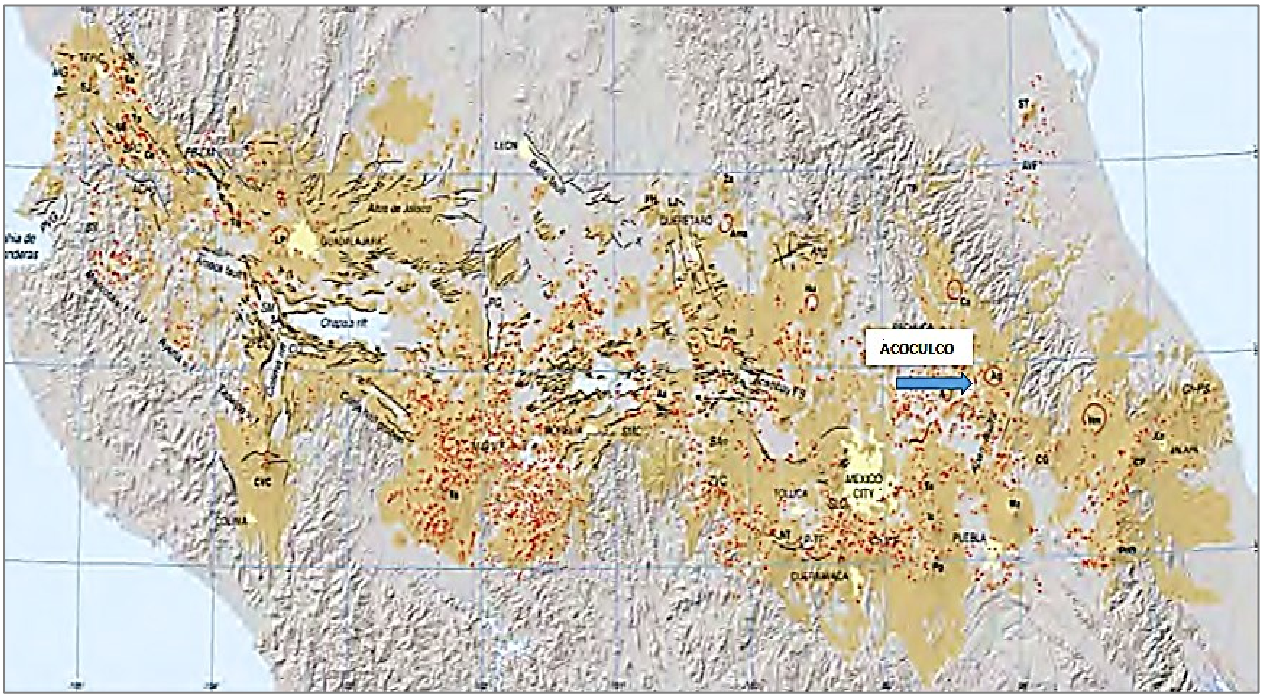

Figure 4-10: Location of Acoculco geothermal area in the Trans Mexican Volcanic Belt (TMVB).

The epicentre of earthquakes observed on the TMVB from 1858 to 2012, Figure 4-11, and the uniform hazard map of central Mexico for a return period of 500 years, Figure 4-12, show that the region of Acoculco is interested by low to moderate seismicity and it appears compulsory to install a regional seismic network to be able to discriminate the existing natural seismicity, including seismic sources, from the expected future induced seismicity.

Local geology is characterized by the presence of the caldera and a fault system, Figure 4-13, and by strong lateral discontinuities due both to the faults and to the strong differences in the stratigraphy for the two existing wells. This condition suggests the possibility of amplification of the seismic waves similar to those shown for the Basel 2006 sequence.

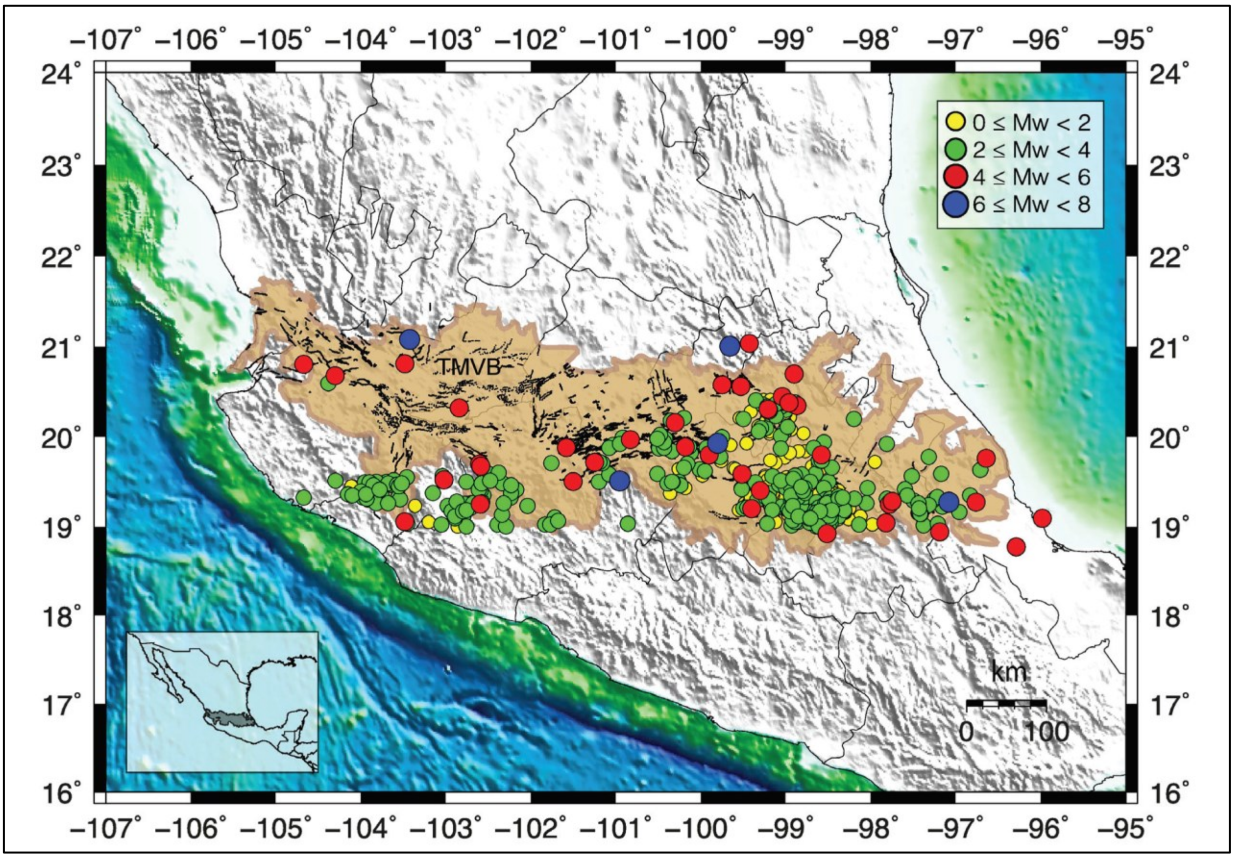

Figure 4-11: Historical earthquakes location in TMVB

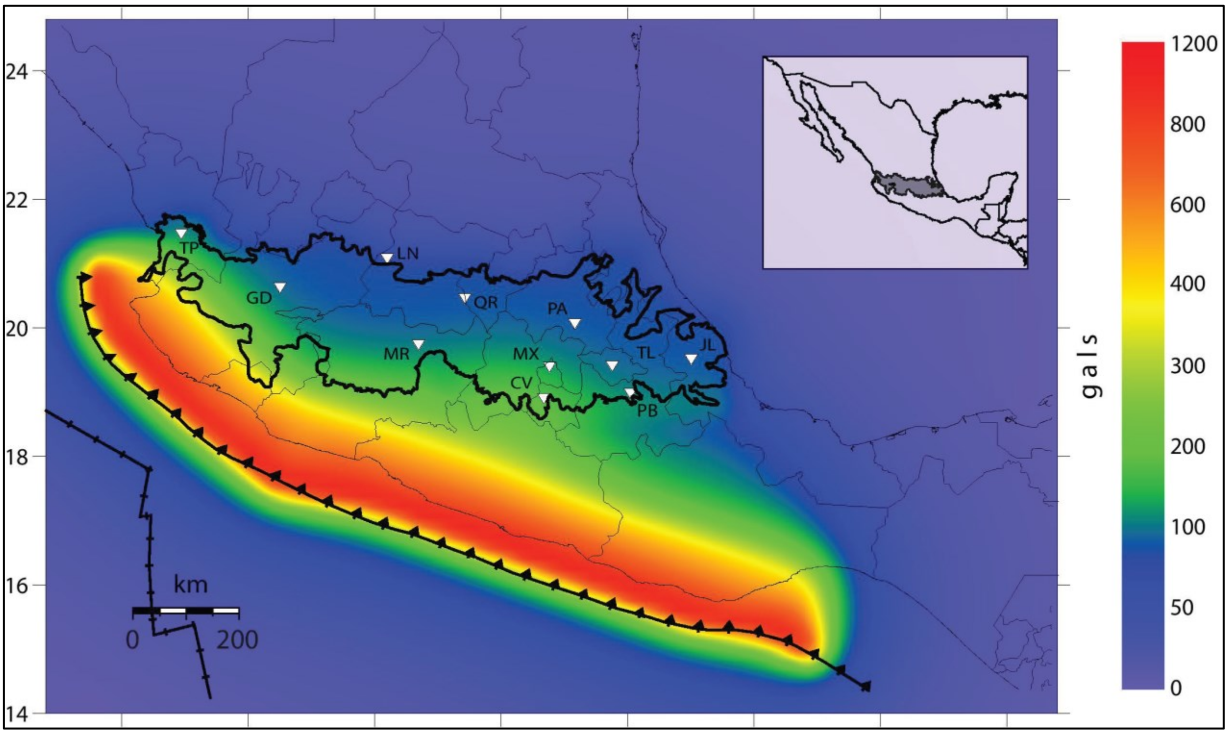

Figure 4-12: Uniform hazard map of central (Mexico). Source: Bayona Viveros J.A., Suarez G., Ordaz M. (2017).

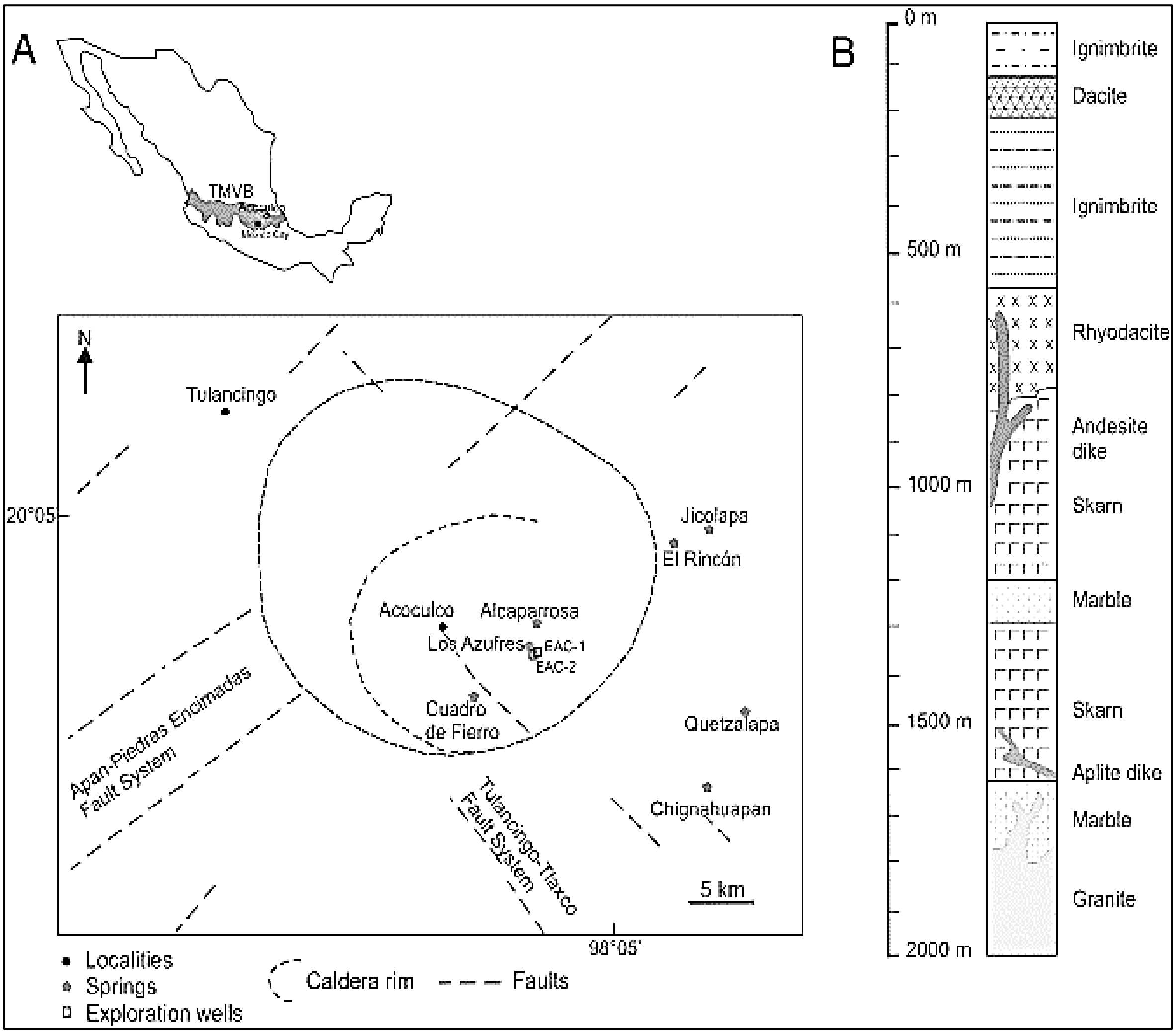

Figure 4-13: Fault system pattern and stratigraphy in Acoculco, from Peiffer et al., 2015.

The studies on this area date back to the mid-eighties of the last century when there was evidence of a remarkable geothermal potential as a consequence of a continuous sequence of volcanic activity starting from the Miocene as confirmed by the geochronological data, dating back to about 12.7 MA the oldest volcanism. The same chronological data suggest that the Acoculco Caldera was formed about 3 MA. From this time the area has been characterized by a continuous volcanic activity subdivided, in turn, into three stages called, starting from the oldest to the most recent: early post caldera volcanism, late post caldera volcanism and extra caldera volcanism. These events have had a fairly similar duration of about 1M years. The most recent extra-caldera activity has been dated to about 60,000 years from the present emitting lavas and producing volcanic cones of basaltic-andesitic composition.

In all the intermediate periods an intense volcanic activity characterized the region, alternating explosive and effusive products with the emission of pyroclastic materials characterized by an extremely variable composition including, for the sake of simplification, basaltic and andesitic rocks up to terms of differentiation with predominant silica rich materials as those of the rhyolite suite including magmas, domes, pyroclastic effusion, etc.

For a detailed and up-to-date discussion on the geo-volcanological features of the Acoculco geothermal area and for further and complete information concerning the succession of volcanic events, see more specific works such as Avellan et al., (2019) and references herein and the recent Deliverables D 5.3 and D 6.1 made on behalf of the GEMex project to which this document belongs too.

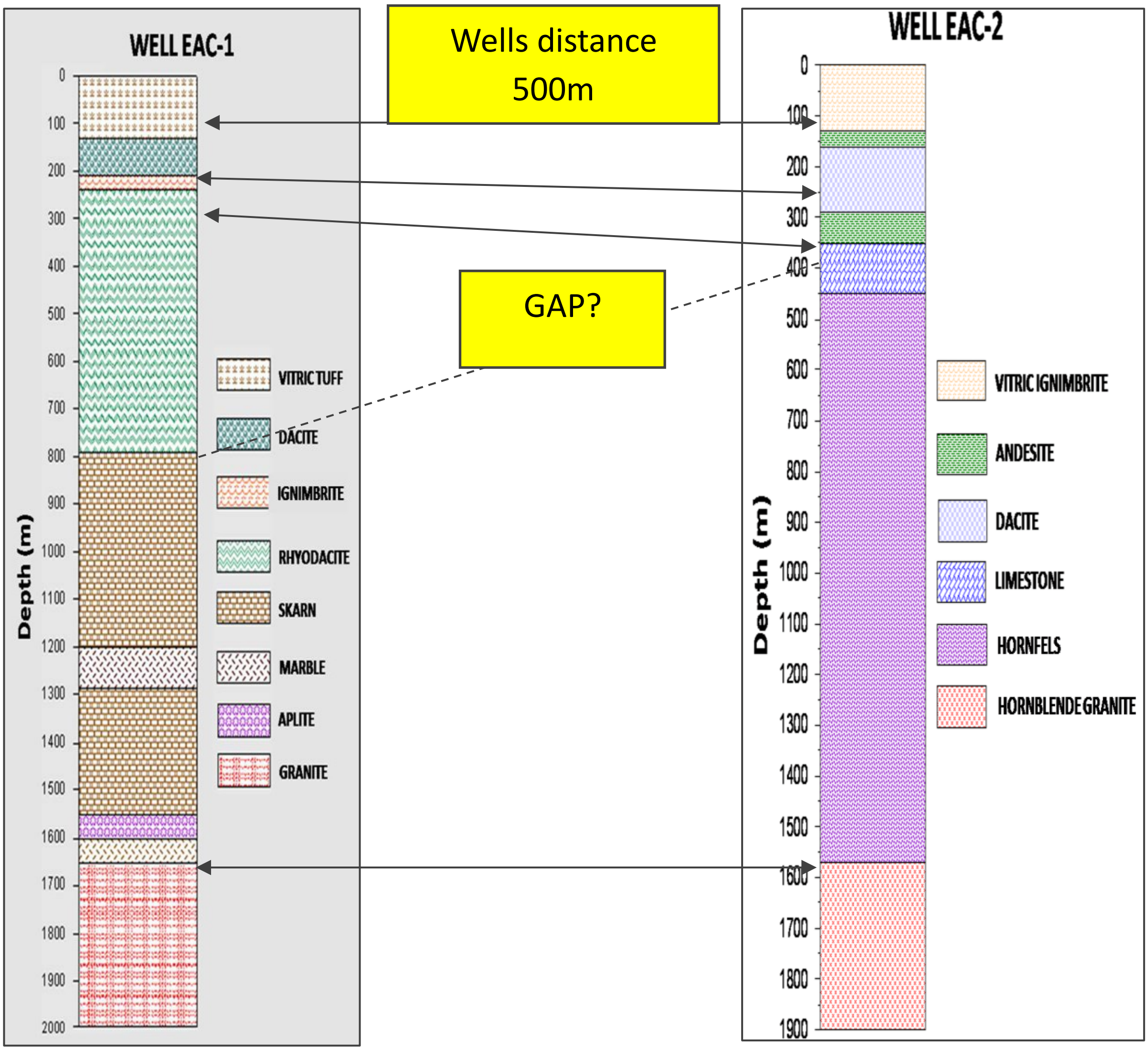

Figure 4-14: Acoculco stratigraphic log for EAC-1 and EAC-2 wells. Source Arce et al., 2015 Evidences of stratigraphy differences in wells EAC-1 and EAC-2 in Acoculco.

For the activities related to induced seismicity, for easily understandable reasons, detailed knowledge of the stratigraphy is of great importance.

Unfortunately, an analysis of the existing scientific production has allowed a partial stratigraphical reenactments because the interest has been mainly directed to the reconstruction of volcanic and petrological events according to the characterization of the geothermal field. In addition, the great spatial variability and depositional heterogeneity, typical in the volcanic environment, is an additional limit which greatly hinders the stratigraphic reconstruction.

The reference stratigraphy for Acoculco geothermal area has been based, for many years, on data achieved from two wells drilled up to the depth of 2000 m by the Mexican electricity company named C.F.E. (FEDERAL ELECTRICITY COMMISSION). These wells are identified with the acronym EAC -1 and EAC-2, and were drilled, respectively, in 1994 and 2008 (Figure 4-14 and Figure 4-15). They are located at a distance of about 500 and at about 2000 meters of depth a temperature > 300 ° C have been measured. According to Giordano et al., 2014, the wells stratigraphy evidence a strong tectonic activity and basement fragmentation. Based on geochemical and geophysical considerations, the Acoculco geothermal system has been classified as Hot Dry Rock.

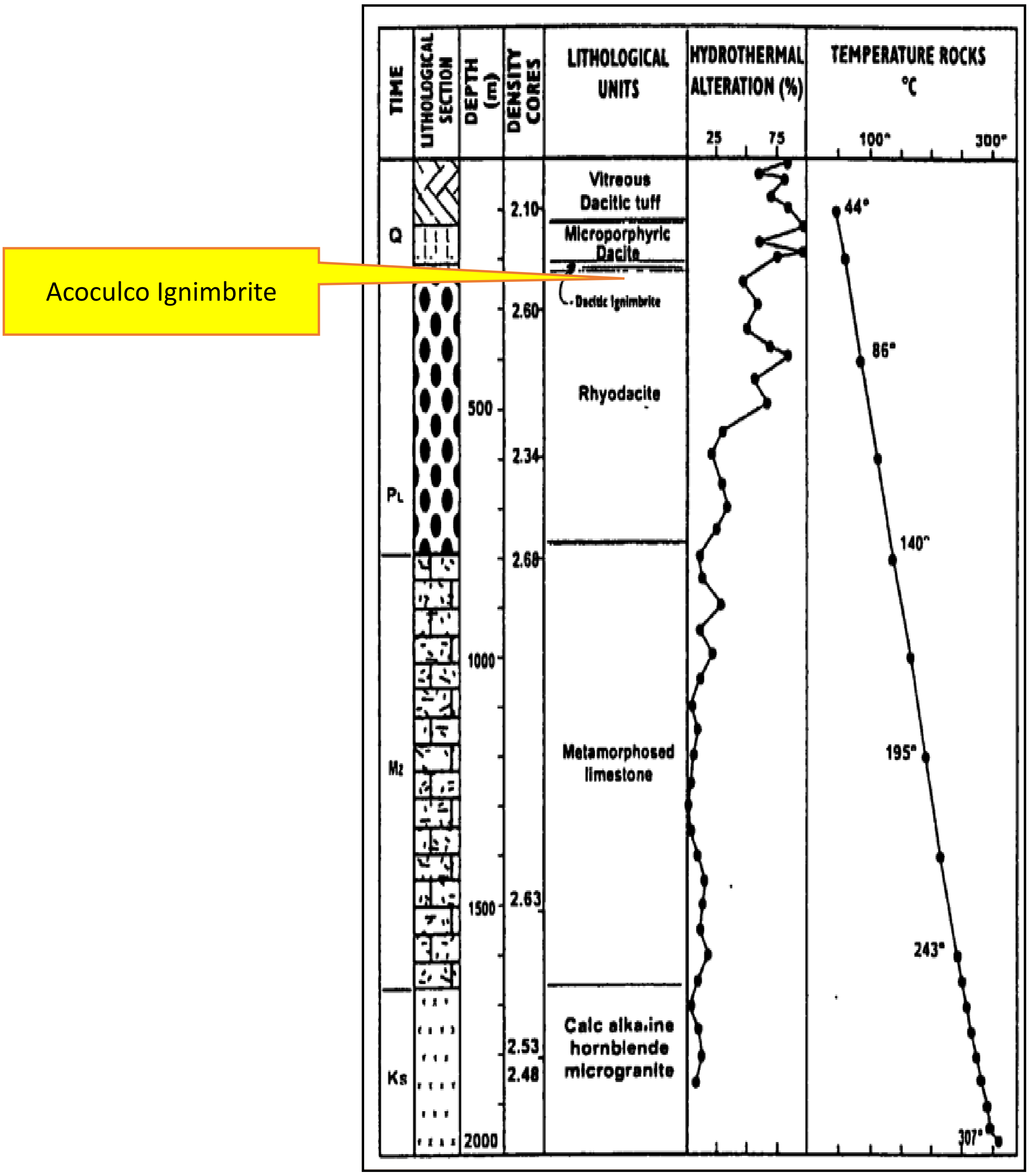

Figure 4-15: Drilling data for EAC-1 well. From Lopez-Hernandez and Castillo-Hernandez, 1997

Unfortunately, for the reason reported before, the stratigraphic detail obtained with these surveys, especially in the depth range from 100-200 m, does not reach the necessary detail for an in-depth study of induced seismicity. In fact, it is not possible to associate differences in seismic waves speeds with the layers thickness and the geological characteristics (composition, texture, etc.) of the volcanic deposits. In addition, shallow non-homogeneous lake sediments are widely scattered in the region often intermixed with volcanic materials and characterized, in turn, by extremely variable thicknesses ranging from a few decimeters to a few meters.

Moreover, stratigraphy also shows the presence of heterogeneous volcanic material with great differences in chemical composition, lithology and mechanical properties as lava flows, dikes, pyroclastites, etc. To make more difficult this picture changes in seismic waves velocity can be also ascribed at the severe rocks hydrothermal alteration responsible for changes in the rock's mechanical properties (Lopez-Hernandez and Castillo-Hernandez, 1997).

An additional difficulty is related to the presence of scattered alluvial and lacustrine deposits interspersed with volcanic rocks. Unfortunately, this spatial and compositional heterogeneity do not permit us to reconstruct an accurate stratigraphy with the available information. The presence on the surface of lacustrine/alluvial sediments (Figure 4-16) indicates the possibility of stratigraphic amplification of seismic motion.

Stratigraphic amplification of seismic motion is related to the presence of softer superficial soil layers laying over harder, *i.e.* lower V_S velocities versus higher, typical of alluvial deposits, from a few meters up to several ten meters. If the ratio between the harder and the softer soils velocities is high enough the natural frequencies of the softer soils can be excited and then amplify the incoming motion at those frequencies. Consequently, if the structures built over those soils have natural frequencies close to those of the soil, they could be driven to large self-excitation and be seriously damaged. Besides the caldera sediments, the alluvial deposits in the Acoculco area have been reconstructed from literature data as reported in Figure 4-16, together with inhabited places.

Though not very close to the geothermal site, the city of Tulacingo shows the presence of both the possible source of amplification of the seismic motion, Figure 4-16, Figure 4-17 and Figure 4-18, since it is located along the Tulacingo fault and founded on holocenic silty sand.

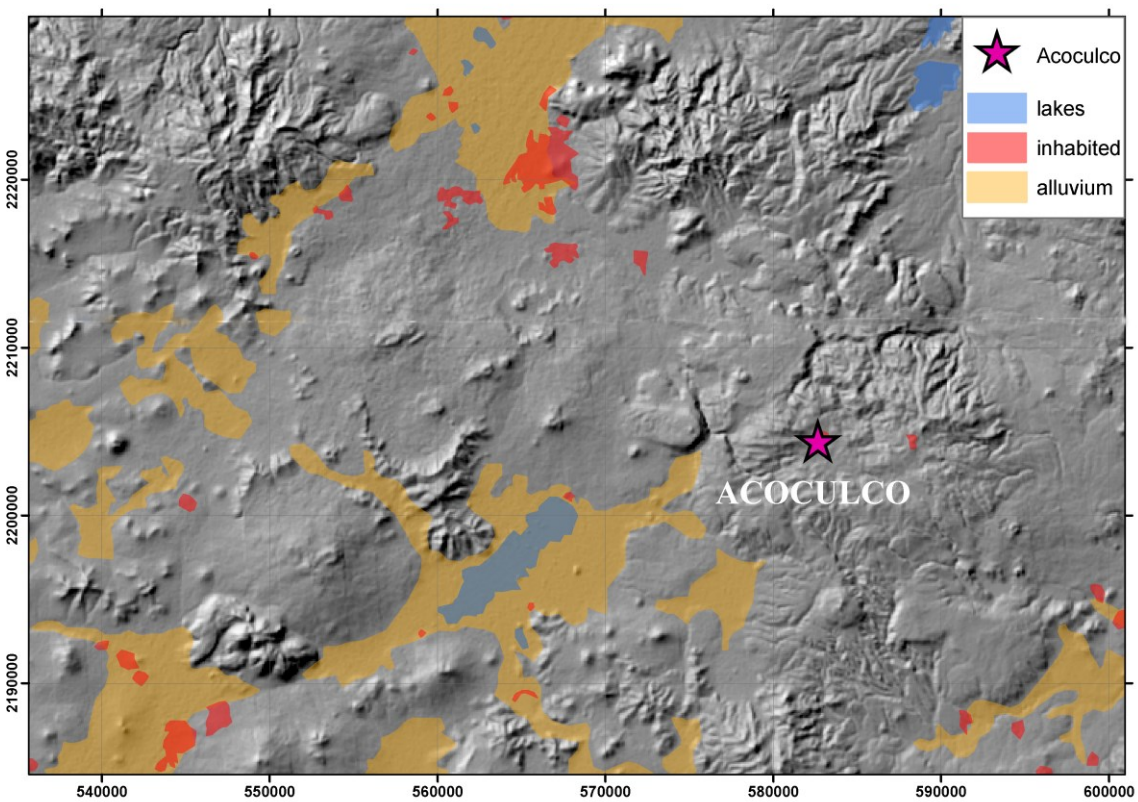

Figure 4-16: Alluvium sediments pattern and inhabited places distribution around Acoculco geothermal area.

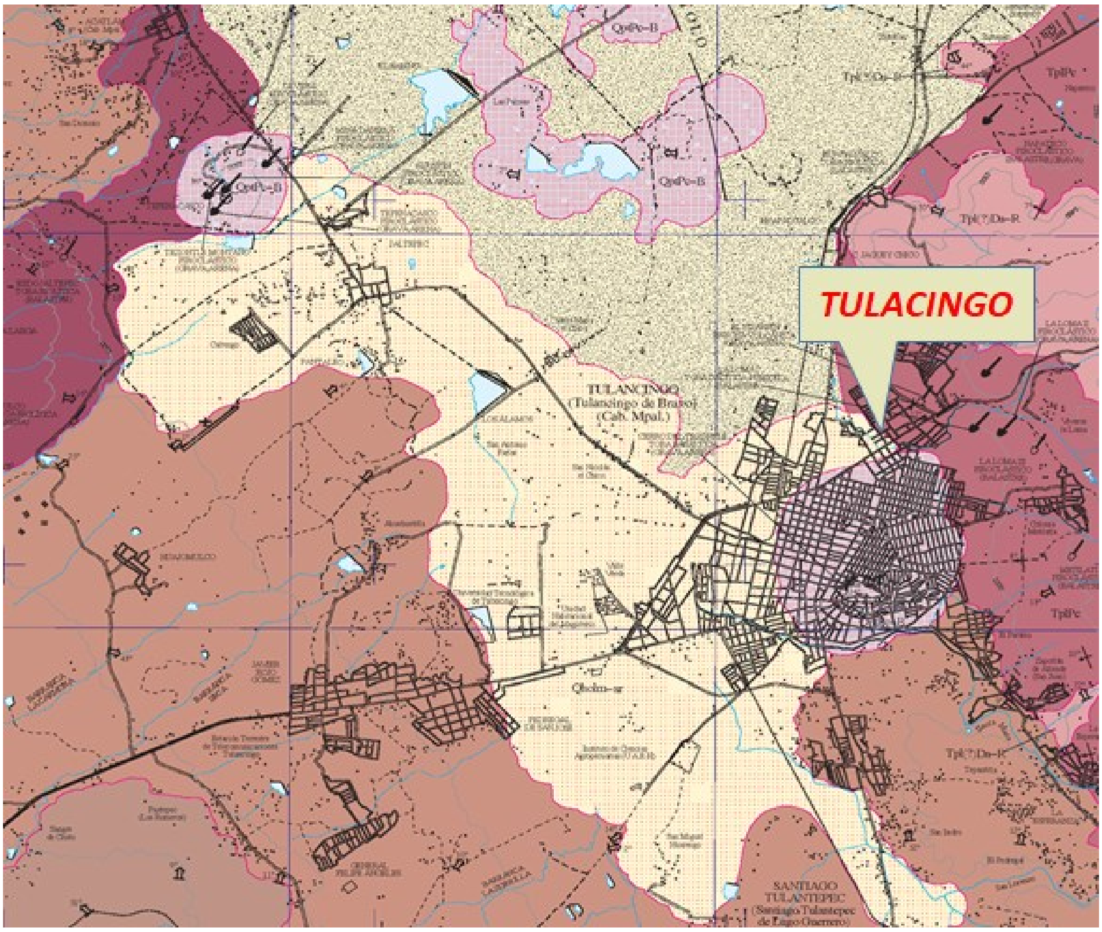

Figure 4-17: Map evidencing the relation between Tulacingo city location, the Tulacingo fault and the soft alluvial soils deposits.

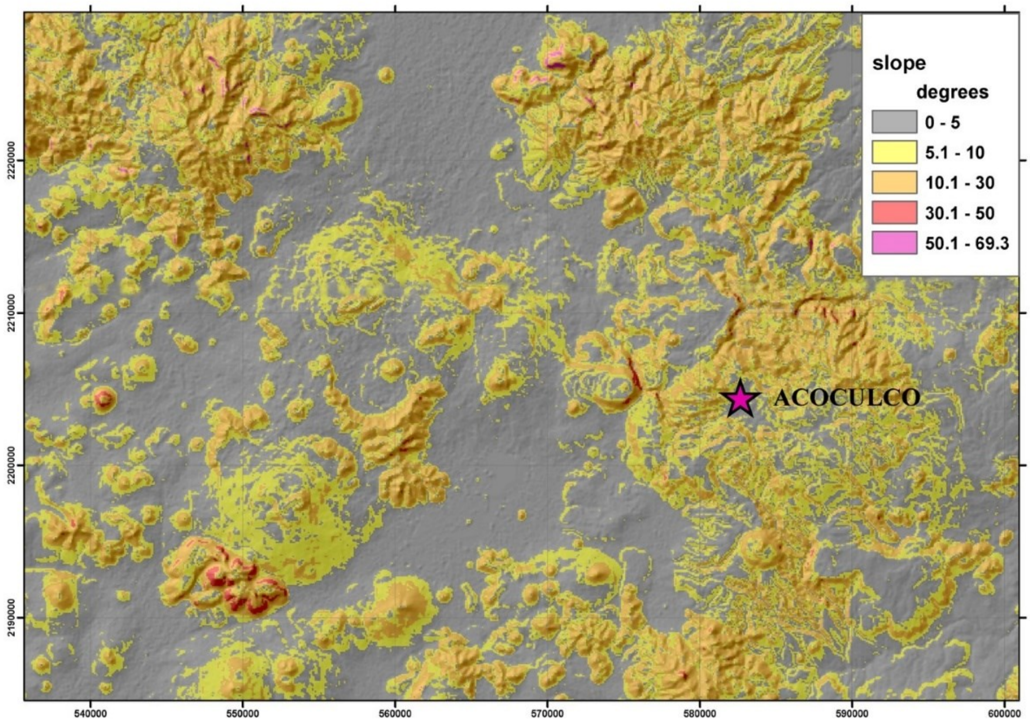

Figure 4-18: Morphological map evidencing the main slope patterns in the Acoculco area

The stratigraphic complexity of the area is evident by analyzing Table 4-2 obtained by retrieving literature data from some research and environmental activities performed by local authorities.

Table 4-2: Stratigraphical reconstruction of the recent intracalderic deposits in the Tulancingo-Acoculco area evidencing thepresence of lacustrine deposits.

	Thickness m	**Status**	**Lithology**	**Notes**
Top Intracalderic deposits	50 max	*Xahualalulco (20-25m)* *El Manzanito (29)m*	Lacustrine Sediments	Heterogeneous weathered volcanic rocks. Clay and silt beds (2-5cm)
UNIT 7	30-40		Pumice and andesitic ashes	
UNIT 6	12,5-20		Lapilli deposits, ashes, glass	Massive deposits andesitic composition
UNIT 5	40		Mainly pumice in ash matrix	0,60 andesite and ash levels inside
UNIT 4	4,5		Glass ashes, pumice, lithics	2,8m: white stratified ash level
UNIT 3	20		Ashes deposits	Andesitic, lithic inside
UNIT 2	30		Volcanic ashes, mainly basaltic and andesitic	0,40 m ash; 0,02-0,20 m scoria; 27,0 m pumice; 13,0 m pyroclastic/lapilli
UNIT 1	12,5	*Old Ignimbrite* *EAC1-well*	'Massive' Ignimbrite Breccia	Inside content: 0,9 m rhyolitic pumice 2,5 m white ashes
Total thickness (min-max)	**230,5** (190-240)			
Los Laurels Basaltic Andesite	**Thickness 30 m**			
Rhyolitic lava and dome	**Thickness 200 m**			
Dacite Cruz Colorada	**Thickness 80 m**			

Sources: Garcia-Palomo et al., 2002; Lopez-Hernandez et al., 2009; Lopez-Hernandez and Castillo-Hernandes., 1997; Peiffer et al., 2014; Atlas des riesgos del Municipio de Zacatlan, Puebla 2012: Estratigrafia volcanica asociada al sistema Tulancingo-Acoculco.

4.4 Hazard, vulnerability and risk

It is well known that risk is the logical intersection between hazard and vulnerability, being hazard the occurrence of something that can cause harm and vulnerability the predisposition to suffer damage from the hazard. Both hazard and vulnerability can be described and quantified in different ways according to the specific involved subjects. In the case under exam, the hazard is a seismic event induced by the activities of geothermal energy extraction and the subject whose vulnerability to be considered are the structures and peoples in the area where the seismic event acts.

In EGS the seismicity is induced by the fluid injection mainly by increasing the pore pressure, earthquake generation and its magnitude depend also on the mechanical and geometrical properties of the rocks, including closeness to faults that, on turn, could be activated and generate earthquakes. From the event magnitude the expected motion at a specific site can be estimated by GMPEs (Ground Motion Prediction Equations). Very roughly this is the chain to estimate seismic hazard.

Seismic vulnerability of existing structure can be estimated or calculated, given the hazard, by assigning it to a specific vulnerability class, *e.g.* by using the European Macroseismic Scale, EMS, or by a complete engineering approach, modelling, etc.

The main reference document (NAS 2013, Majer et al., 2012) suggest a general approach to be tailored to the site under consideration. According to this presentation two aspects on which the magnitude of the expected hazard depend strongly are the stratigraphic amplification and lateral discontinuities that could greatly enhance the seismic motion at the surface in amplitude and shift the frequency content of this motion from the one predicted by GMPEs.

4.5 Discussion

While for geothermal energy extraction, as well as for induced seismicity evaluation, the characterization of the deep geology is relevant, the seismic wave propagation is affected by the path to the surface and by the geometric and mechanical properties of probably present softer soil layers at the surface itself. According to Figure 4-19 the path to surface include several faults that can modify the seismic field.

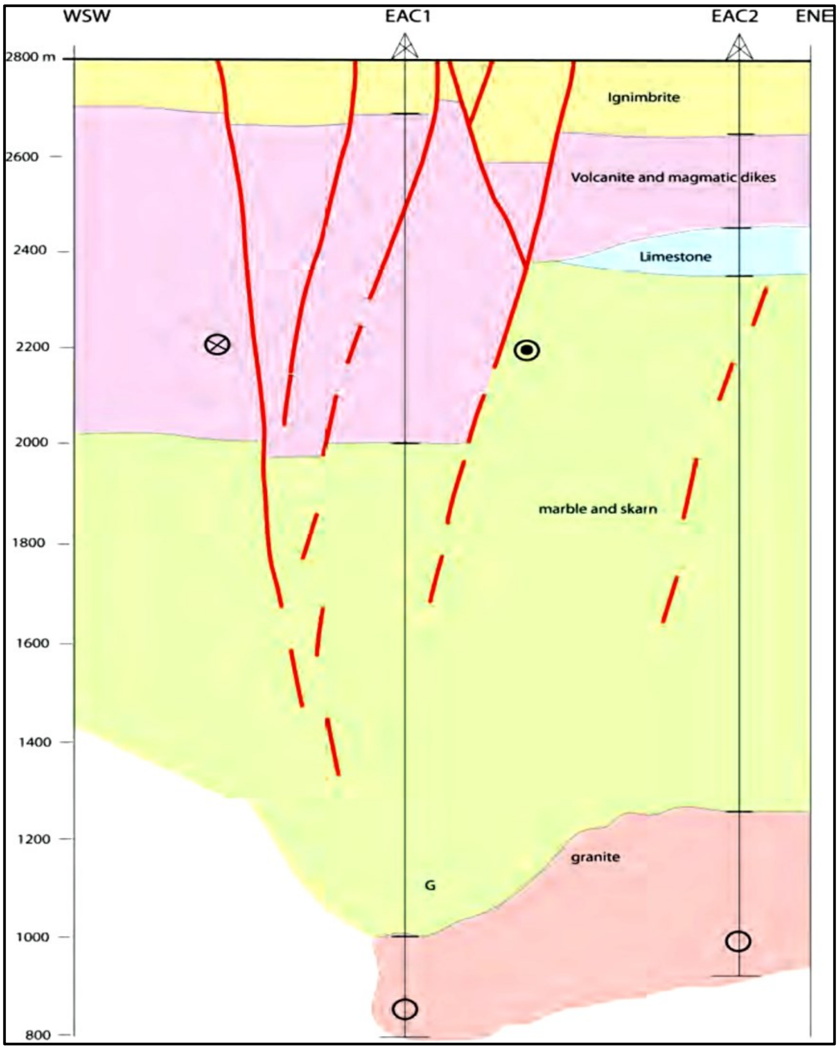

Figure 4-19: Acoculco geologic cross section along the existing EAC-1 and EAC-2 wells (GEMex Deliverable D4.1; Peiffer et al., 2014).

The most direct way to evaluate the influence of the geology along the path is through recording real earthquakes and comparing the data to those estimated from GMPEs.

Detailed knowledge of geometric and mechanical properties of the superficial deposits should be known to estimate their influence of the expected ground motion.

The final recommendation is synthetized in the following points:

1. Produce a detailed geologic map of the superficial deposits.
2. Perform an ambient noise measurement campaign on the relevant sites selected by point 1, with particular regard to the presence of vulnerable structure and/or facilities.
3. Deploy a permanent seismic network, possibly associating seismometers and accelerometers, for earthquake localization purposes, and specific station close to vulnerable structures and/or facilities.

4.6 Some aspects of seismic risk in Acoculco geothermal site

In this section some data provided by Marco Calò, UNAM, will be presented and analyzed. The data consist in continuous recording, 10 days, 16 of 18 stations, missing AC12 and AC14, deployed in the Acoculco area, Figure 4-20. Data are analyzed as they are, without any processing.

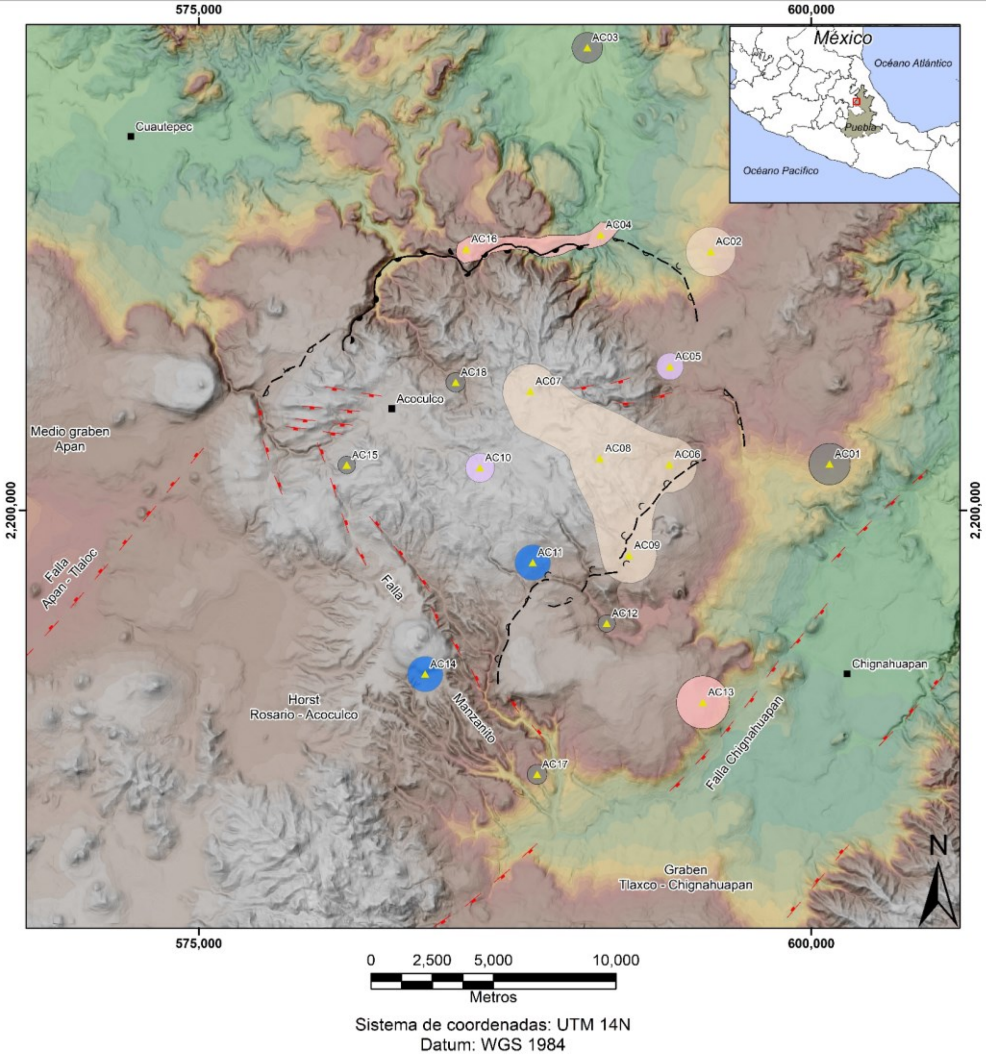

Figure 4-20: Seismic stations' location in Acoculco geothermal site.

After preliminary visual examination of the data, it has been chosen to consider, individually, two days, 80 and 87, for which it seems that there is only noise and the seismic events present in the records of the days 81 82 83 85 and 86. The mean Fourier spectra and spectral ratios, HVSR, for the two days, are computed over time window of 5 minutes due to the relevant presence of very low frequencies, while for earthquakes are computed over the whole length. Spectra have been smoothed with a moving triangular function 1 Hz long.

The figures of time histories, spectra and spectral ratios are presented in the following Appendix:

Appendix 4-A Day 080 Spectra and Spectral Ratios
Appendix 4-B Day 087 Spectra and Spectral Ratios
Appendix 4-C Day 081, Earthquake
Appendix 4-D Day 082, Earthquake
Appendix 4-E Day 083, earthquake

Appendix 4-F Day 085, earthquake
Appendix 4-G Day 086, earthquake
Appendix 4-H Day 086 Spectra
Appendix 4-I Day 086 Spectral Ratios

Looking at the time histories it is observed that the amplitudes of the records with only noise are very low, an example is in Figure 4-21 and a detail in Figure 4-22.

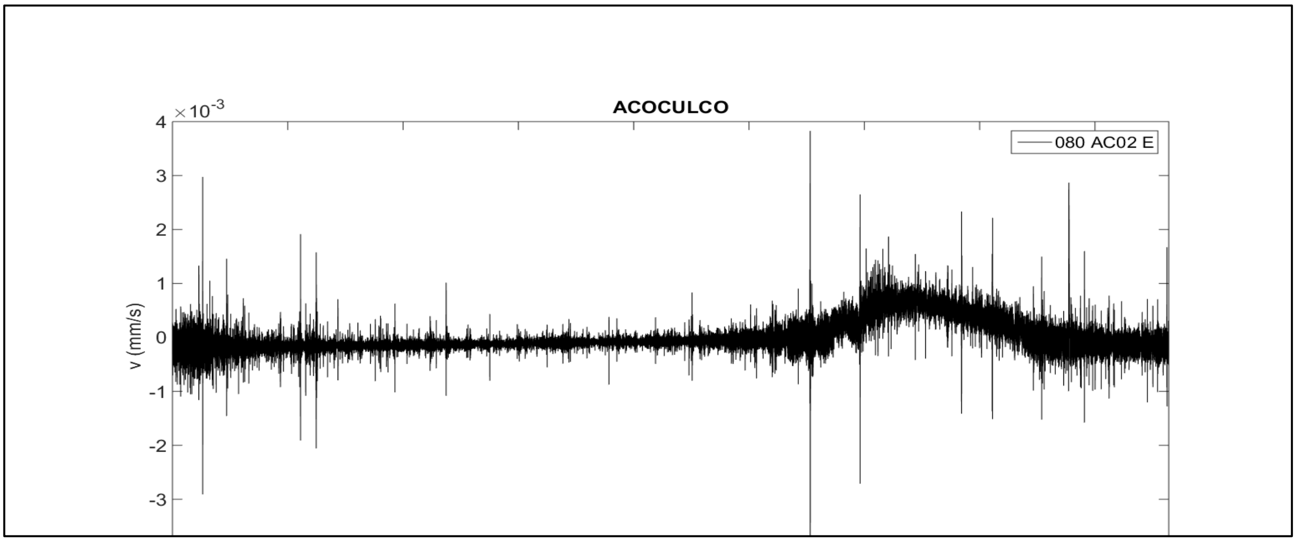

Figure 4-21: Example of 24 hours record

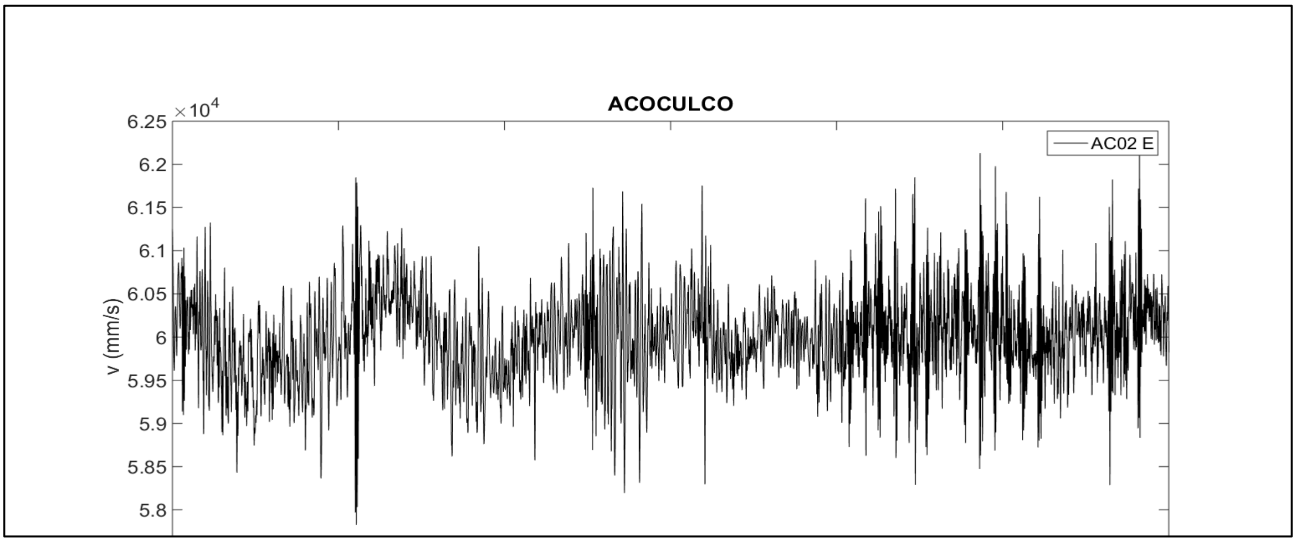

Figure 4-22: Figure 4-21 enlargement detail

The Fourier spectra, Figure 4-23, show that soil motion is dominated by very low frequency centered at 0.13 Hz, 7.6 s, that is to be attributed to ocean waves propagation.

The wavelength is probably too long to interest the eventually present soil deposits that could give stratigraphic amplification of the motion.

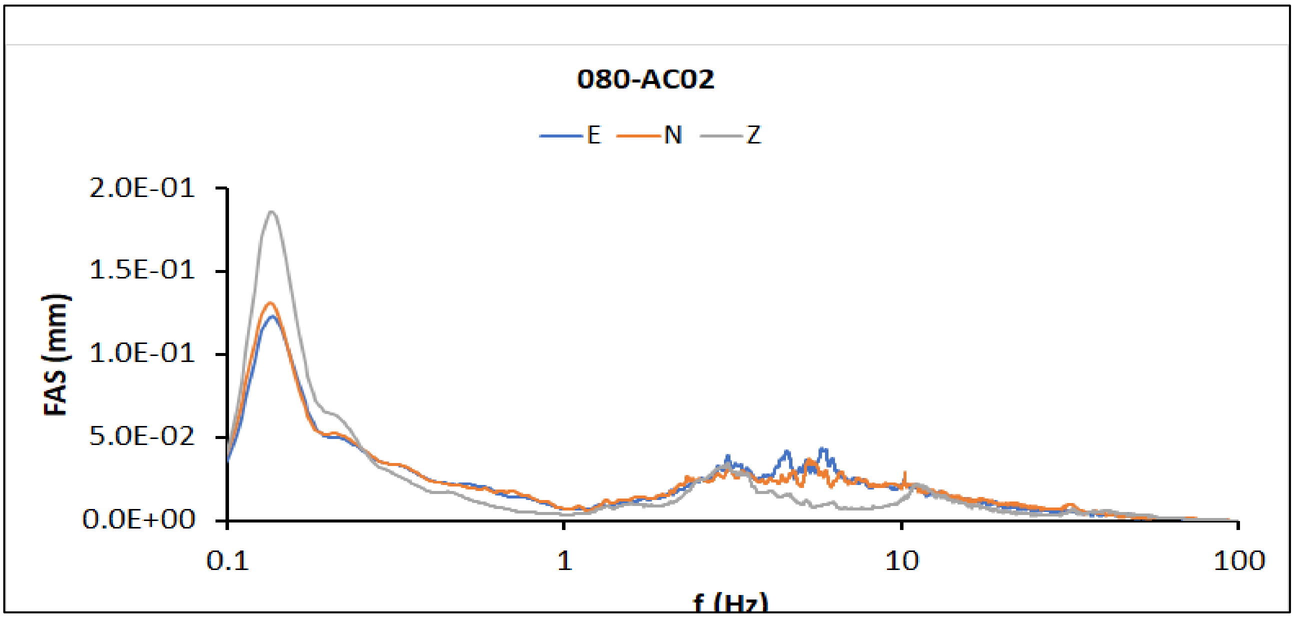

Figure 4-23: Example of Fourier spectra

The other frequency content, Figure 4-24, exhibits a shape, one or more frequencies surmounted by a ripple, that recall the shape expected when echoes, or reflections, are present. Several tests to evaluate the distance of the reflecting surfaces in terms of time did not give reliable results.

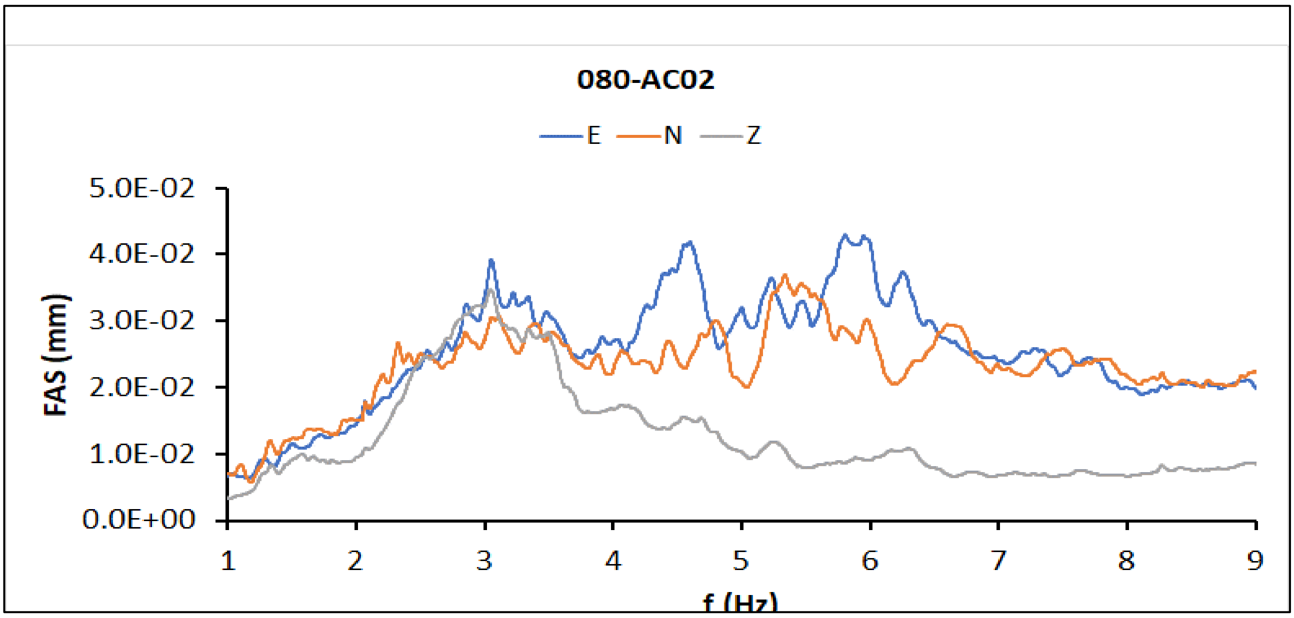

Figure 4-24: Example of other frequency content

In this condition the use of the HVSR technique could not give useful information on the presence of motion amplification due to soil deposits. Nonetheless, the technique has been applied with the aim of verifying if and how the spectral ratios depart from expected presence of one or few peaks corresponding to the presence of soil deposits.

Figure 4-25 is an example of ratio. It is apparent that the ratio exceeds the standard value 2 for a range of frequencies, 4-9 Hz, that does not justify the attribution of this effect to stratigraphic amplification. The smaller peak, centered at 0.76 Hz, could be related to local effect, although the detail of the spectra doesn't exhibit any peak close to that frequency (Figure 4-26) and geological confirmation is needed.

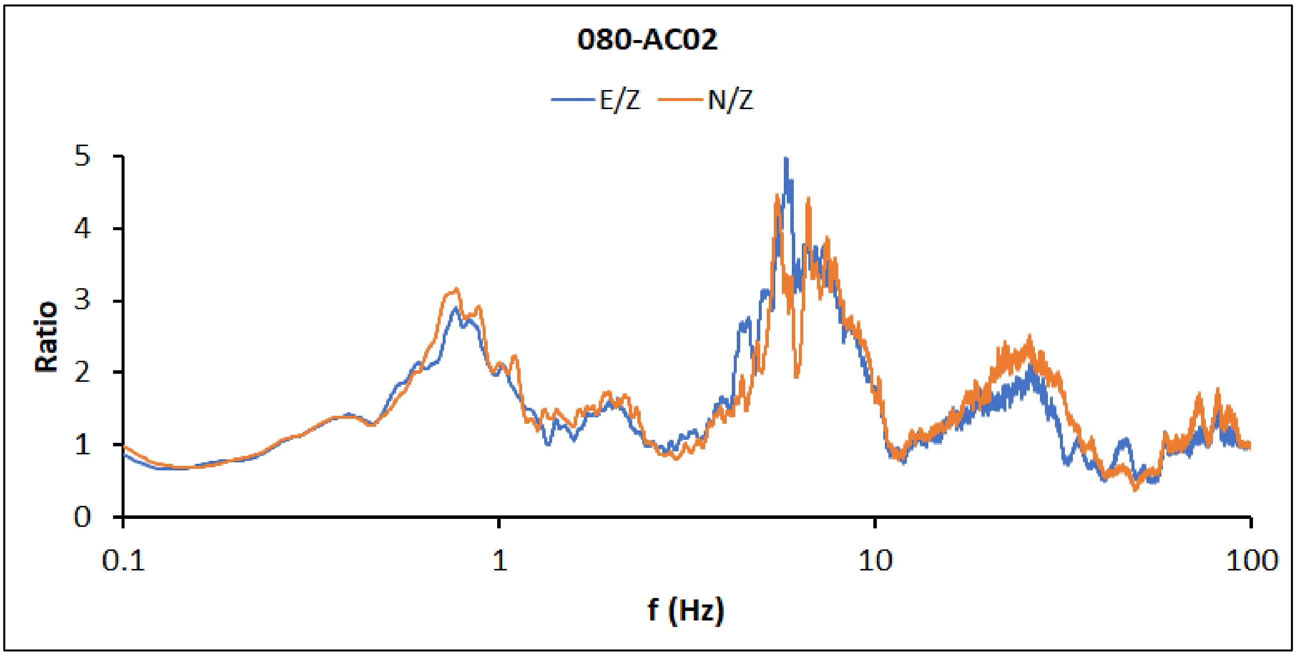

Figure 4-25: Example of HVSR

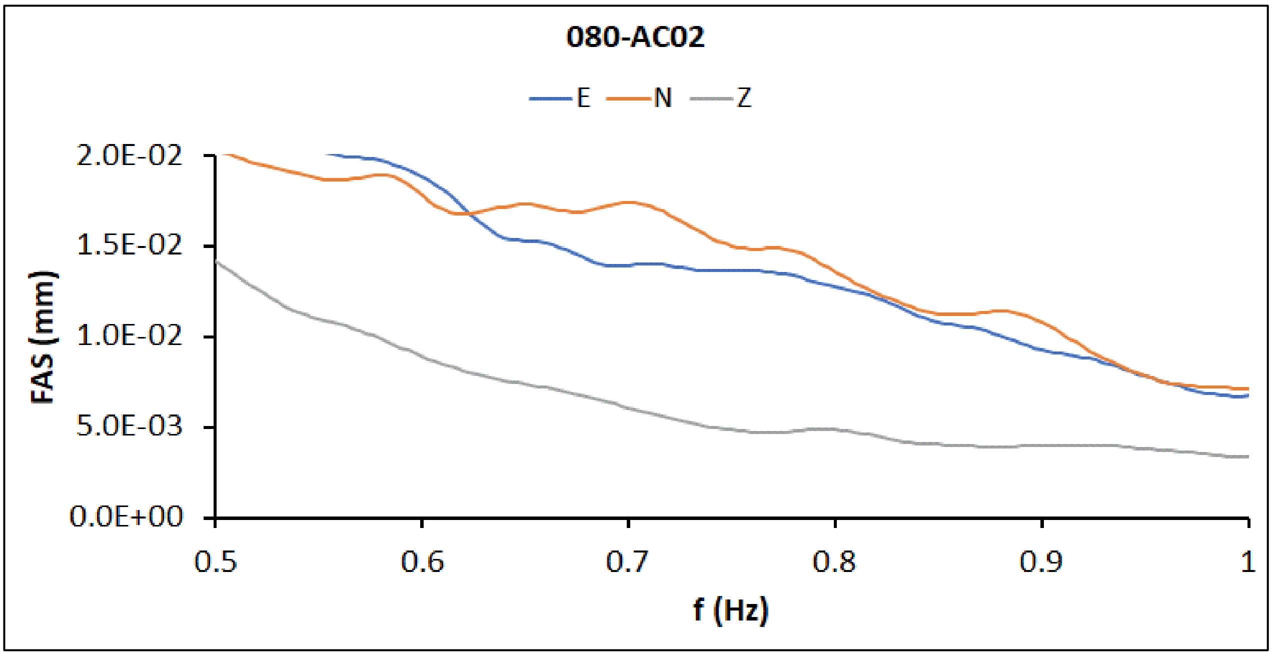

Figure 4-26: Detail of Fourier spectra

The recorded earthquakes have amplitudes higher than the other records, Figure 4-27, but the overall behavior is similar, Figure 4-28 and Figure 4-29, including the limited frequency range. The possible effect of echoes, reflection, is not visible. The shape of the spectral ratios is like that of the previous records. For this earthquake the detail of Fourier spectra shows the presence of peaks around the 0.76 Hz frequency, Figure 4-30. Another aspect of the ratio is the wide range of frequencies, 15-30 Hz, whose amplitude is above 2. Considering this as "amplification" due to reflections we should expect higher peak values in the time histories. This feature is present in several stations.

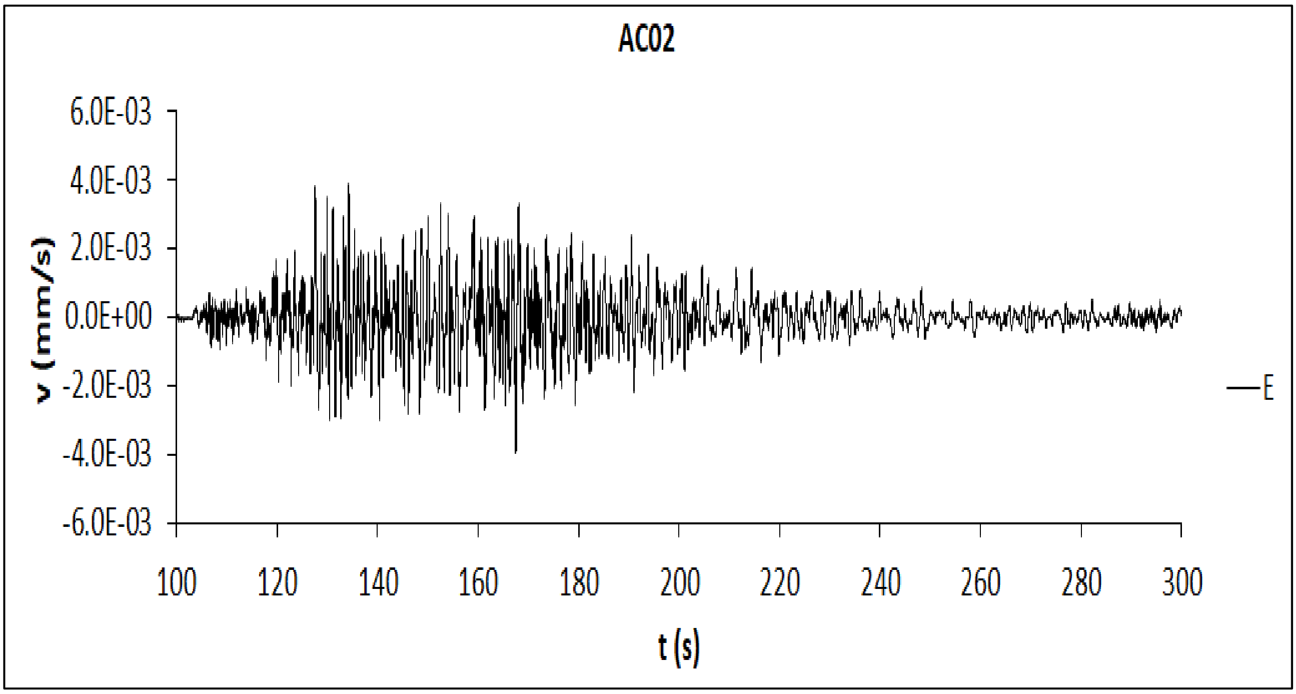

Figure 4-27: Example of recorded earthquake

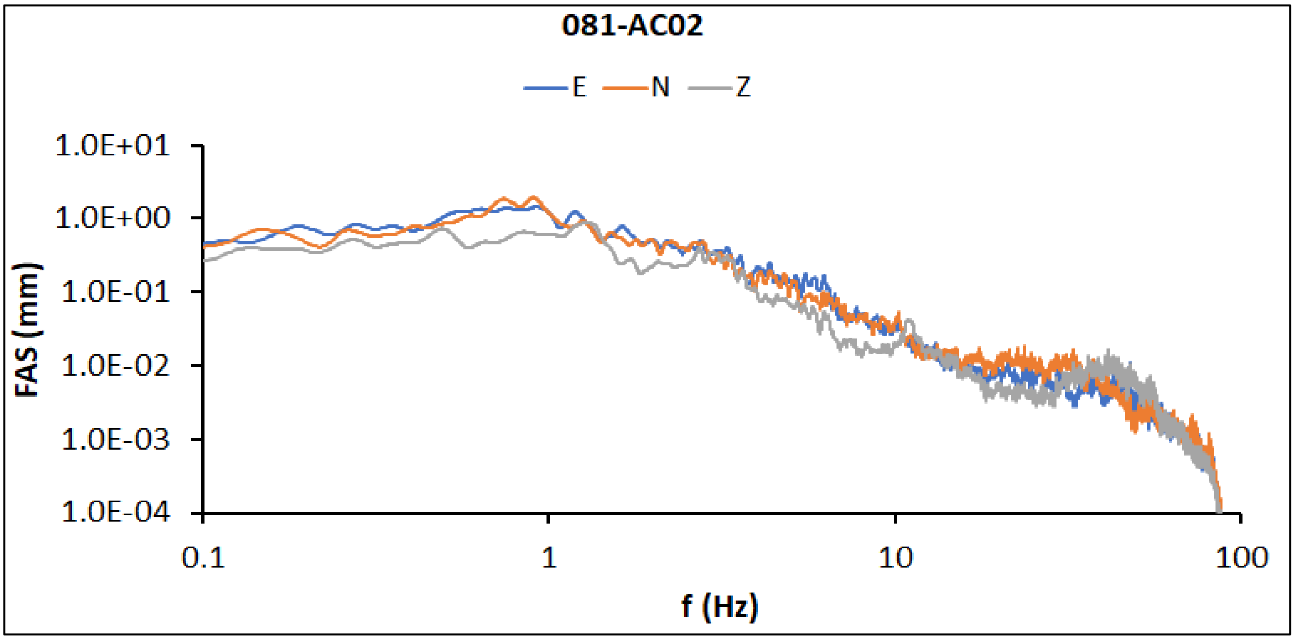

Figure 4-28: Example of earthquake spectra

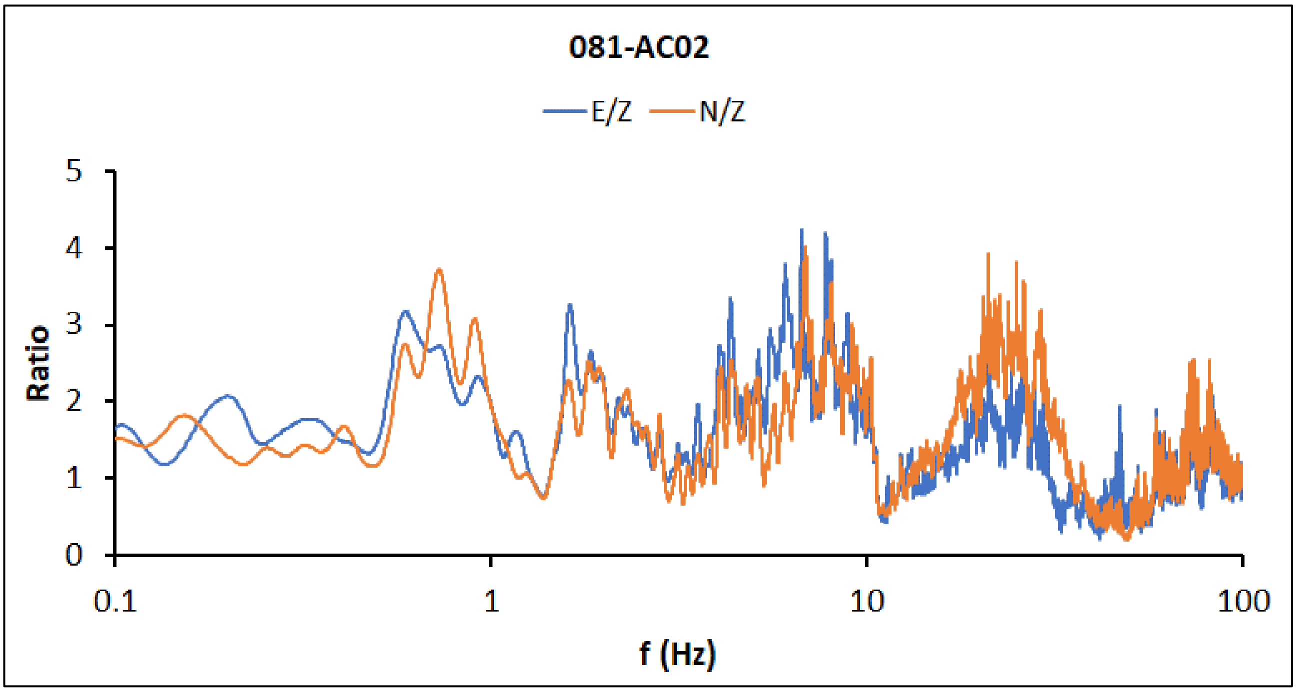

Figure 4-29: Example of earthquake spectral ratios

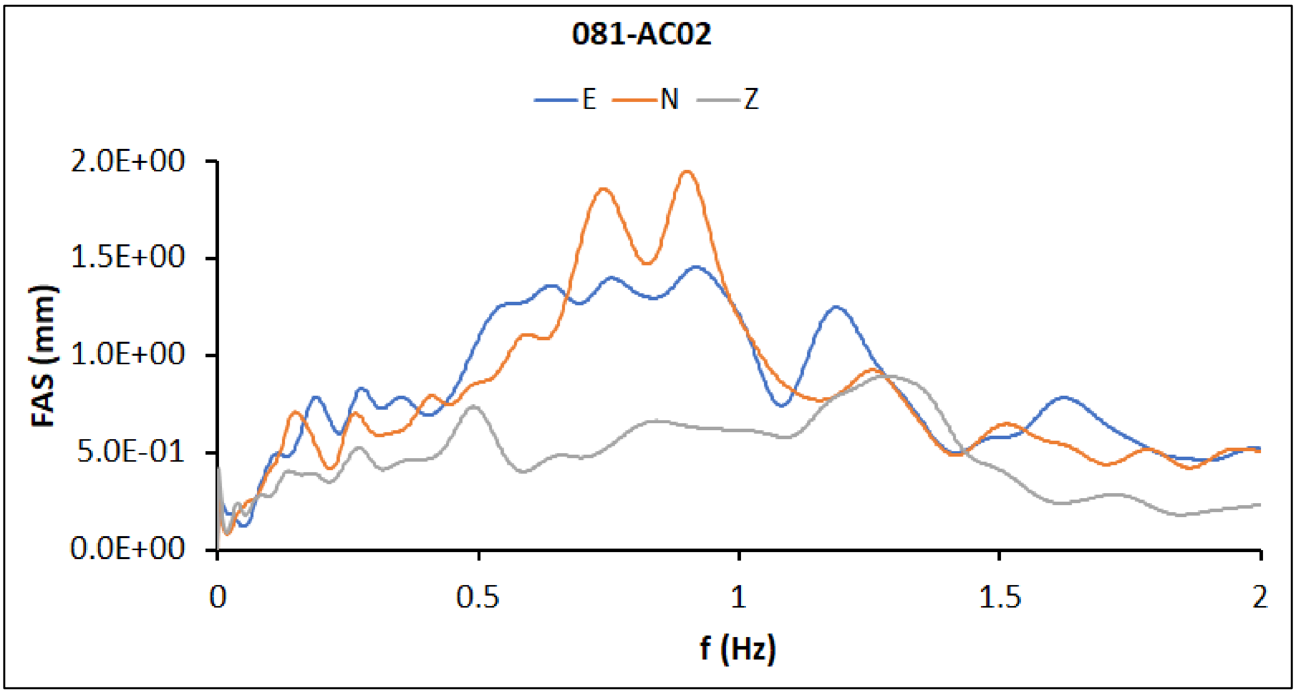

Figure 4-30: Detail of Fourier spectra

For some stations vertical Fourier spectrum is higher than the horizontal ones in the high frequency range, from 10 Hz, Figure 4-31 and Figure 4-32. Beyond the individuation of the geological and mechanical explanation, this fact could contribute in giving a certain relevance to the vertical component of the seismic motion, especially in conjunction with the exposed structures and/or equipment.

In Appendix H and I the comparison of the spectra and of the spectral ratios, noise and earthquakes, for each station are presented. The overall shapes is similar but it is apparent that the earthquakes records carry more information than noise, even if they come from far events.

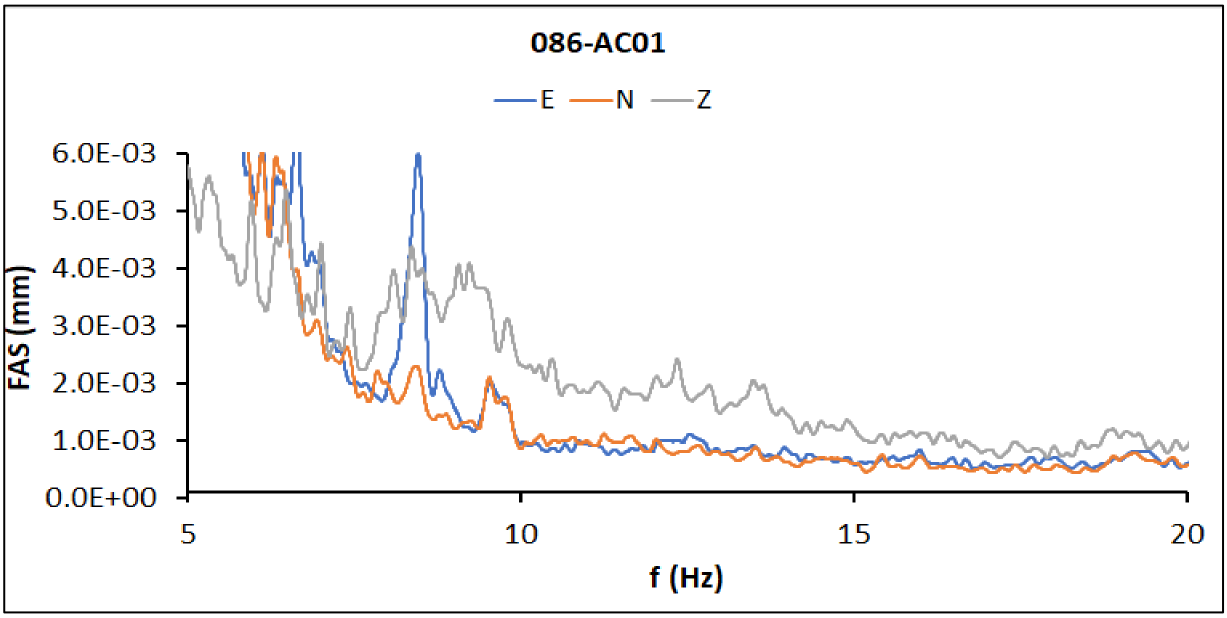

Figure 4-31: Detail of Fourier spectra

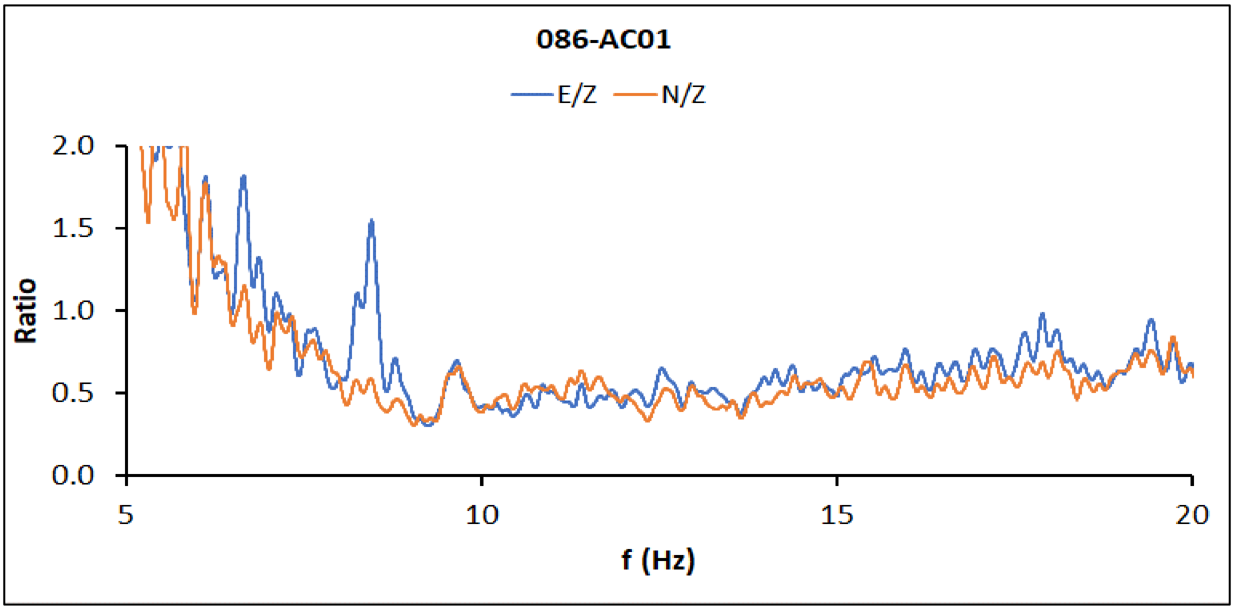

Figure 4-32: Detail of spectral ratios

4.7 Conclusions

The observation can be synthesized as follow:

1. Amplitude of the motion is very low, both for noise and earthquakes
2. The frequency content is limited, very limited for noise
3. Because of points 1 and 2 it is possible that local soil effects could not have been activated

4. Fourier spectra of the noise records show the possibility that complex reflection are present, as expected from the geology of the site.
5. Use of HVSR technique show that amplification of the horizontal motion occurs mainly in wide frequency range, at frequencies up to 30 Hz, so that it cannot be attributed to the presence of surface soil layer/s. In some cases, narrow peaks that could be attributed to stratigraphic effects are present, but peaks in the horizontal components are not apparent.
6. For some stations, vertical spectra are higher than the horizontal ones in the high portion of the spectra.

The ensemble of these observation together with the update geologic knowledge of the area, Deliverable 3.2, lead to the following consequences:

1. Locally generated earthquakes travel through discontinuous media rich of faults with relevant lateral discontinuities that can modify the seismic field in the sense of producing refractions/reflections capable to shift the frequency content of seismic motion to higher frequencies and then to higher peak values.
2. In some of the station sites it is apparent the possibility of stratigraphic amplification of seismic motion.

Defining a path to characterize seismic hazard

The dense seismic network to be installed in Acoculco, as that in Los Humeros, should give information also on the variability of the seismic motion along the surface and should take in account the local geology and the closeness to faults. Installation of downhole instrumentation is strongly advised especially in proximity of faults.

4.8 References Chapter 4

AA.VV. (2010) Microzonazione sismica per la ricostruzione dell'area aquilana, L'Aquila, DPC Regione Abruzzo, 2010.

Arce JL., Layer P., Martinez I., Salinas J.I., Macias-Romo M.C., Morales-Casique E., Benowitz J., Escolero ., Nenhardt N. (2015). Boletín de la Sociedad Geológica Mexicana Volumen 67, n.2, p. 123-143. http://dx.doi.org/10.18268/BSGM2015v67n2a1

Avellán D.R., Macías J.L., Layer P.W., Cisneros G., Sánchez-Núñez J.M., Gómez-Vasconcelos M.G., Pola A., Sosa-Ceballos G., García-Tenorio F., Reyes Agustín G., Osorio-Ocampo S., García-Sánchez L., Mendiola I.F., Marti J., López-Loera H., Benowitz J. (2018): Geology of the late Pliocene – Pleistocene Acoculco caldera complex, eastern Trans-Mexican Volcanic Belt (México), Journal of Maps, Vol. 15, NO. 2,8-18.

Baranello S., Bernabini M., Dolce M., Pappone G., Rosskopf C., Sanò T., Cara P. L., De Nardis R., Di Pasquale G., Goretti A., Gorini A., Lembo P., Marcucci S., Marsan P., Martini M. G., Naso G. (2003). Rapporto finale sulla Microzonazione Sismica del centro abitato di San Giuliano di Puglia. Dipartimento di Protezione Civile, Roma.

Bayona Viveros J.A., Suarez G., Ordaz M. (2017). A probabilistic seismic hazard assessment of the Trans-Mexican Volcanic Belt, Mexico based on historical and instrumentally recorded seismicity" Geofísica Internacional. 56-1: 87-101.

Brambati A., Carulli G. B., Cucchi F., Faccioli E., Onofri R., Stefanini S. e Ulcigrai F. (1980). Studio di microzonazione sismica nell'area di Tarcento (Friuli). Ed. Cluet.

Caputo E., Klin P., Palmieri F. e Priolo E. (2007). Modello geologico-strutturale e geofisico di San Giuliano di Puglia. In: Pacor F., Lovati S., Rovelli A., Caserta A., Nieto D., Böhm G., Priolo E., Klin P., Laurenzano G., Palmieri F., Marello L., Piscitelli S., Mucciarelli M., Strollo A., Gallipoli M. R., Caputo E., Pelli F., Silvestri F., Puglia R., Maugeri M., Grasso S., Eva C. e Ferretti G. (2007). Task 3 Deliverable D9-D10-D11. Risposta sismica locale a San Giuliano di Puglia (CB) e in alcuni Comuni confinanti. Rapporto di Ricerca del Progetto INGV-S3. http://esse3.mi.ingv.it/

Cara F., Rovelli A., Di Giulio G., Marra F., Braun T., Cultrera G., Azzara R., Boschi E. (2005). The role of site effects on the intensity anomaly of San Giuliano di Puglia inferred from aftershocks of the Molise, central southern Italy, sequence. November 2002. Bulletin of the Seismological Society of America, 95: 1457-1468.

Celebi M., Prince J., Dietel C., Onate M., Chávez-García F.J. (1987). The culprit in Mexico City - Amplification of motions. Earthquake Spectra, vol. 3, n. 2.

Ergin, M., Özalaybey S.; Aktar A., Yalçin M.N. (2004). "Site amplification at Avcilar, Istanbul" (PDF). Tectonophysics. 391 (14): 335. Bibcode: 2004Tectp.391.335E. doi:10.1016/j.tecto.2004.07.021.

Gallipoli M. R., Mucciarelli M., Gallicchio S., Tropeano M. e Lizza C. (2004). Horizontal to Vertical Spectral Ratio (HVSR) measurements in the area damaged by the 2002 Molise, Italy, earthquake. Earthquake Spectra, vol. 20, n. S1, pp. S81–S93.

García-Palomo, A., Macías, J.L., Tolson, J.G., Valdez, G.,Mora, J.C., (2002). Volcanic stratigraphy and geological evolition of the Apan region, east central sector of the Trans-Mexica Volcanic Belt. Geofisica International, 41, 133-150.

GEMex WP 4.2 – Final report on active geothermal systems: Los Humeros and Acoculco Deliverable D 4.1

Giaccio B., Ciancia S., Messina P., Pizzi A., Saroli M., Sposato A., Cittadini A., Di Donato V., Esposito P. e Galadini F. (2004). Caratteristiche geologico-geomorfologiche ed effetti di sito a San Giuliano di Puglia (CB) e in altri abitati colpiti dalla sequenza sismica dell'ottobre-novembre 2002. Il Quaternario, 17(1), Ed. Aiqua, p. 83-99.

Giordano G., Calzolari G., Lucci F., (2014). Regional Structural and tectonic synthesis of the Acoculco and Los Humeros Geothermal field. GEMex WP3, Draft version June 14, 2014.

Gizzi, F.T., Potenza, M.R. & Zotta. (2012). 23 November 1980 Irpinia–Basilicata earthquake (Southern Italy): towards a full knowledge of the seismic effects C. Bull Earthquake Eng. 10:1109. https://doi.org/10.1007/s10518-012-9353-z

Idriss I. M., Bolton Seed H. (1968) An analysis of ground motions during the 1957 San Francisco earthquake. In «Bulletin of the Seismological Society of America», 58 (6), pp. 2013-2032.

Lopez-Hernandez A., Garcia Estrada G., Aguirre-Dioaz G., Gonzalez-Partida E., Palma-Guzman H., Quijano-Leon J.L. (2009). Hydrothermal activity in the Tulancingo–Acoculco Caldera Complex, central Mexico: Exploratory studies. Geothermics 38, 279–293.

Lopez-Hernandez, A., Castillo-Hernandez D., (1997). Exploratory Drilling at Acoculco, Puebla,México: A Hidrothermal System With Only NonthermalManifestation. Geotherm. Res. Council Trans., 21, 429-433.

Majer E., Nelson J., Robertson-Tait A., Savy J., Wong I. (2012). Protocol for Addressing Induced Seismicity Associated with Enhanced Geothermal Systems" U.S. Department of Energy, Energy Efficiency & Renewable Energy, Geothermal Technologies Program 2012. DOE/EE-0662

Martelli L., Calabrese L., Ercolessi G., Severi P., Tarabusi G., Pileggi D., Rosselli S., Minarelli L., Pergalani F., Compagnoni M., Vannucchi G., Madiai C., Facciorusso J., Fioravante V., Giretti D., Mucciarelli M., Priolo E., Laurenzano G. (2014). Cartografia speditiva dell'amplificazione e del rischio di liquefazione nelle aree epicentrali del terremoto dell'Emilia 2012 (ML=5.9). Atti del 32° convegno GNGTS 2013.

National Research Council. 2013. Induced Seismicity Potential in Energy Technologies. Washington, DC: The National Academies Press. https://doi.org/10.17226/13355.

Peiffer et al., 2014; Atlas de Riesgos del Municipio de Zacatlan, Puebla, 2012. Estratigrafia volcanica asociada al sistema Tulancingo-Acoculco.

Peiffer, L., C. Wanner, and L. Pan (2015), Numerical modeling of cold magmatic CO2 flux measurements for the exploration of hidden geothermal systems, J. Geophys. Res. Solid Earth, 120,

Ripperger J., Kästli P., Fäh D., Giardini D. (2009) Ground motion and macro seismic intensities of a seismic event related to geothermal reservoir stimulation below the city of Basel—observations and modelling". Geophys. J. Int. (2009) 179, 1757–1771.

Ripperger J., Kästli P., Fäh D., Giardini D. (2009). "Ground motion and macroseismic intensities of a seismic event related to geothermal reservoir stimulation below the city of Basel—observations and modelling" Geophys. J. Int. 179, 1757–1771.

Roman J.C., Sosa Juarico M.A., 2012; Atlas de Riesgos del Municipio de Zacatlan, Puebla, Estratigrafia volcanica asociada al sistema Tulancingo-Acoculco. https://zacatlan.gob.mx/articulo11/1/politicas/Atlas_de_Riesgo_Zacatlan.pdf

Romeo R. W. (2000) - Seismically induced landslide displacement: a predictive model. Engineering geology, 58, 337-351.

Sanò T., Bongiovanni G., Clemente P., Rinaldis D. (2015). "Modellazione dei Fenomeni di Amplificazione Locale Basata su Registrazioni Accelerometriche al Sito" Convegno Anidis, L'Aquila 2015.

Sanò, T. (1999). Local amplification effects during the 1997 Umbria-Marche earthquake" Int. Conference on Earthquake hazard and risk in the Mediterranean region, N.E. University North Cyprus, 18-22 October.

Seed H.B., IDRISS I.M. (1982) Ground motions and soil liquefaction during earthquakes. Earthquake Engineering Research Institute, Berkeley, California, 134 pp.

Siro L. (1983). Indagini di microzonazione sismica. Intervento urgente in 39 centri abitati della Campania e Basilicata colpiti dal terremoto del 23 Novembre 1980. CNR-PFG, Pubbl. 492.

Varnes, D.J. (1984) - Hazard Zonation: A Review of Principal and Practice. Commission of Landslide of IAEG, UNESCO. Natural Hazades, N. 3, 61p.

Wasowski J, Lee C, Keefer D. 2011. Toward the next generation of research on earthquake-induced landslides: Current issues and future challenges. Engineering Geology 122, 1-8.

5 Passive seismic micro-seismicity monitoring design and traffic light recommendations for EGS

Authors: Mariangela Guidarelli and Enrico Priolo

5.1 Introduction

An increasing number of countries are taking interest in geothermal energy because it is a commercially proven form of energy that can contribute to reduce pollutant emissions and slow down the climate change. Considering that one of the major concerns is the increasing emission of greenhouse gases into the atmosphere and the global warming, geothermal energy can play an important role in the mitigation of climate change. Geothermal energy can be classified as a renewable source of energy, environmentally-friendly and sustainable as it can be maintained for long time.

As easily accessible geothermal systems are becoming increasingly scarce, the future of geothermal energy may be represented by the development of so-called supercritical systems and, more importantly, Enhanced Geothermal Systems (EGS) (MIT, 2006).

When hot rock formations have insufficient or little natural permeability, this must be enhanced to enable commercial development. The “enhancement” is performed by engineering the reservoirs through hydraulic fracturing. An EGS system will extract geothermal energy from subsurface rocks creating or accessing a system of fractures through which water can be circulated, heated by the rocks, and pumped/returned back to the surface in production wells. The reservoir may be fractured using high-pressure fluid injection into the subsurface under carefully controlled conditions, to open existing fractures or create new ones and therefore increase permeability. Increased permeability allows fluid to circulate throughout the now-fractured rock and to transport heat to the surface where electricity can be generated (MIT et al., 2006). EGS are less dependent on site-specific hydro-geological conditions than conventional hydro-thermal systems, therefore they have the potential to produce large amounts of electricity almost anywhere in the world.

Although geothermal energy represents an important resource of clean energy, it is not free of possible drawbacks, since the stimulation of a reservoir for an EGS is usually associated with induced seismicity and increased seismic risk (e.g. Giardini, 2009). Therefore, seismic events occurring due to the water injection have to be well recorded and monitored. To mitigate the seismic risk of a damaging event, an appropriate monitoring system needs to be in place for each individual experiment. It is critical that the policy makers and the general community be assured that geothermal technologies will be engineered to minimize induced seismicity risks to acceptable levels.

The GEMex project is a complementary effort of a European and a Mexican consortium on unconventional geothermal systems, i.e. EGS and high-temperature geothermal fields with supercritical conditions (Jolie et al., 2018). One of the objectives of the project is the concept development for exploitation and utilization of geothermal fields, with investigation on optimum stimulation and operation procedures for safe and economic exploitation with control of undesired effects. This includes the passive seismic micro-seismicity monitoring design and traffic light recommendations for EGS.

In this report, we will review the international experiences on passive seismic micro-seismicity monitoring at EGS sites and the existing procedures and protocols for managing induced seismicity. Based on the review of the selected international experiences we have produced a list of recommendations for the seismic monitoring of induced seismicity and mitigation of related hazard.

5.1.1 Short description of EGS systems

MIT (2006) defines EGS as engineered reservoirs designed to economically extract heat from low permeability formations. In places where fractures are not naturally occurring, new ones need to be created or existing ones reactivated. Giardini (2009) provides an exhaustive overview of the issues related to geothermal quake risks. EGS have evolved from the hot dry rock projects realized for the first time at Fenton Hill in 1977 by a team from Los Alamos National Laboratories (Cummings and Morris 1979; Tester et al. 1989).

A brief description of EGS system is provided by Giardini (2009). An EGS involves drilling a hole at least 3 kilometres deep into a layer of non-porous rock where temperatures are higher than 100 °C. Fluids are pumped under high pressure into the rock (a process called stimulation), which induces it to fracture, generating micro-earthquakes, thereby increasing its permeability and creating a reservoir for the fluid. Generating fractures in the target rock mass simultaneously causes micro-seismicity through the fracturing process, defining the paths of the fluids to flow through and heat up. The spatial distribution of the micro-earthquakes provides important clues about the volume and orientation of the fractured rock at depth. Once a sufficiently large reservoir (volume >1 km^3) has developed, a second well is typically drilled into the stimulated volume. Water then flows between the two wells; hot water is extracted from the production borehole and engineered to an energy resource.

The drawback is that such enhanced geothermal systems can induce earthquakes. The initial stimulation creates micro-earthquakes that might be felt at the surface or even produce damage. And the pressurized water forced into the rock could interact with existing deep faults, generating potentially large quakes. The probability of this occurrence is not large, but needs to be considered and evaluated. Highly sensitive seismic monitoring techniques are routinely applied at EGS sites to map the spatial and temporal development of the stimulated volume and to characterize the geothermal reservoir (e.g. Wohlenberg & Keppler 1987; Haering et al. 2008).

5.1.2 Induced seismicity: an overview

Seismicity induced by industrial activities has gained the attention of the general public in recent years because of the deep socio-economic implications. The number of the underground industrial operations in or close to densely populated areas has increased in the last decades, therefore the number of felt earthquakes that are suspected to be caused by human activities has also increased (Giardini, 2009). The number of recognized weak events has also significantly increased, as an effect of the development of new seismic monitoring networks in areas where industrial activities are located worldwide.

There are a number of human activities that have been proposed to induce earthquakes; such activities include the impoundments of water reservoirs, erecting tall buildings, coastal engineering, quarrying, extraction of groundwater, coal, minerals, gas, oil and geothermal fluids, excavation of tunnels, and adding material to the subsurface by allowing abandoned mines to flood and injecting fluid for waste disposal, enhanced oil recovery, hydrofracturing, gas storage and carbon sequestration, nuclear explosions. Assessment of the link between such processes and induced earthquakes is not new and the first well known case of induced seismicity is the case of waste-water disposal at the Rocky Mountains arsenal in the late 1960s (Healy et al. 1968).

The Human-induced Earthquake Database, HiQuake, is a comprehensive record of earthquake sequences supposed to be induced by anthropogenic activity. It reports over 700 cases, spanning the period 1868–2016 (Foulger et al., 2017). In general, induced seismicity is commonly characterized by a large number of small magnitude earthquakes that persist during fluid injection/withdrawal, in some cases even significantly after the end of the activity.

A number of mechanisms can be responsible of induced seismicity, as: stress perturbations produced by underground industrial activities, when proximal to seismogenic structures; massive injection/extraction of fluids in/from reservoir that induces relevant changes in its internal pressure; sudden, large temperature variations that perturb in-situ stress conditions; high-pressure fluid injection, used to create new fractures, may trigger existing silent faults; massive fluid injection at depth and consequent pore pressure diffusion may change the frictional condition on existing faults and lead them to rupture even with relevant delay and at large distance from the injection wells (Grigoli et al., 2017). In recent years the impact of such mechanisms on seismicity has been largely studied from a physical point of view, and several models have been proposed (Shapiro, 2015; Doglioni, 2018). In any case, anthropogenic seismicity remains difficult to forecast and manage (Petersen et al., 2016).

It is important to note that the public perception of induced seismicity is closely linked to the presence or not of the man, and it depends on the geographical region where it occurs. In tectonically active regions, induced seismicity is better tolerated, even when it can be distinguished from natural seismicity, as the population regularly experience small earthquakes and buildings are generally designed taking into account the seismic hazard of the area. On the other hand, people living in relative stable tectonic regions with low seismicity rates may never have felt an earthquake before, and their reaction to felt induced seismicity may relatively larger.

In the recent years, several cases of induced seismicity have caused great concern and protests among local population (e.g. Basel (CH), Groningen (NL), Blackpool (UK)), emphasizing the outstanding importance of making the activity accepted by the population and implementing real strategies of monitoring, access to quantitative data, and public information. Those issues explain the increased involvement of both the scientific community, public administrations and industry to develop monitoring guidelines and establish effective operational protocols to mitigate the risk associated with induced seismicity (Grigoli et al., 2017), while maintaining an acceptable level of economic convenience for industry.

Induced seismicity has successfully been dealt with in many different environments ranging from a variety of injection and engineering applications including waste and water disposal, mining, oil and gas, reservoir impoundment (Majer et al., 2007).

Many studies have pointed out the key-role played by micro-seismic monitoring plays in better understanding the physical mechanisms governing induced seismicity. It is also the fundamental tool used by decision makers to decide whether to stop, decrease, or continue the industrial operations being monitored (Foulger et al., 2017, Grigoli et al., 2017). An overview of the situation about monitoring, discrimination and management of induced seismicity has been recently presented by Grigoli et al. (2017). The authors emphasize that, in order to ensure an optimal monitoring of induced seismicity, two features should be carefully implemented, i.e. (1) the design and deployment of a dense micro-seismic monitoring network and (2) the use of sophisticated near real-time data analysis procedures. Technical specifications of a micro-seismic network to ensure desired monitoring conditions are still debated. In the last years, different network design and optimization methods for micro-seismic monitoring have been proposed, and their use is slowly becoming a common practice, though not yet standardized.

Examples of industrial sites monitored by a dedicated micro-seismic network in Europe are: Groningen (Netherlands, (Dost et al., 2012)), Basel (Switzerland (Kraft and Deichmann, 2014)), Collalto (Italy (Priolo et al., 2015)), and St. Gallen ((Switzerland (Edwards et al., 2015)), where the presence of dedicated networks, equipped with different instrument types including broadband seismic stations, borehole sensors, and accelerometers, guarantee optimal monitoring conditions.

Both the United States and the European Union have no federal laws or regulations specifically related to induced seismicity (Trutnevyte and Wiemer, 2017). Decisional protocols are closely related to the activity being monitored and, in particular, to the regulations of the country (or state for the United States) where industrial activity is carried out. Thus, they may not be transferable to other situations. Many U.S. states require seismic monitoring for wastewater disposal facilities and hydraulic fracturing operations; suspension of the injection after the occurrence of events with magnitude larger than some given threshold; the introduction of Traffic Light Systems. In Canada (Alberta) a three-stage traffic light protocol was introduced to prevent the occurrence of induced seismicity (Schultz et al., 2017). Only a few European countries have specific recommendations and guidelines for seismic monitoring of induced seismicity (among these, the Netherlands, Germany, UK, and Italy) but only few of them have been converted into regulations.

The most widely used tool so far for hazard and risk management and mitigation, and an integral part of protocols or best practice recommendations is the so-called traffic light system (Bommer et al., 2006). The classical traffic-light system uses a three-stage (or in some cases four) action plan that governs the injection/extraction of fluids: (1) Normal, continued as planned (green); (2) Caution, proceeds with caution, possibly at reduced rates (amber); (3) Stop, injection/extraction is suspended (red). In order to determine the transition between two levels, a combination of observations is used; these are typically the measured local (or moment) magnitude and some ground motion parameter (e.g., peak ground velocity). The current traffic light systems are defined ad hoc and thresholds for different stages are mainly chosen on the basis of expert judgment. Recently, Wiemer et al. (2014) introduced the “Adaptive Traffic Light Systems” or ATLS, which is currently in test phase.

5.1.3 EGS and micro-seismicity

Injection or extraction of fluids from geothermal reservoirs can change reservoir pressures and temperatures sufficiently to perturb in-situ stress conditions and cause or trigger seismicity (Cladouhos et al., 2010, Giardini, 2009). For this reason, the most problematic side-effect of EGSs is the potential to generate earthquakes, which may compromise the further development of the project.

Most of the studies on induced seismicity assume that all induced seismic activity is undesirable and then focuses on the question of whether or not an activity carries a risk of triggering seismic events. In the case of EGSs, the aim is to generate seismic events in order to enhance the permeability of the reservoir fracture system, therefore the question is how can it be ensured that the stimulation activities will generate only micro-seismic events, small enough not to produce ground motions that exceed the specified thresholds (Bommer et al., 2006).

Induced seismicity in geothermal settings has been documented in areas such as Indonesia , the Philippines, Japan, Kenya, North and South America, Australia and New Zealand for over 40 years (Zang et al. (2014) and references therein). In Europe, an early description of industrial exploitation of geothermal resources was published by Batchelor and Garnish (1990). Recently, Evans et al. (2012) compiled a survey of induced seismicity responses to fluid injection in European geothermal and CO_2 reservoirs.

Annually, thousands of seismic events are generated during exploitation of geothermal fields, however these events are below local magnitude ML = 2, and below the detection threshold of communities in most cases (e.g., Evans et al., 2012). Geothermal sites in the Rhine Graben near Basel (Deichmann and Giardini, 2009), Landau (Grünthal, 2014) and Soultz-sous-Forêts (Dorbath et al., 2009), however, have experienced ML > 2.5

events due to EGS activities. Although this seismicity has been short-lived it has attracted public concern due to its proximity to populated areas (Kraft et al., 2009).

Majer et al. (2007) reported that *'...To date, the maximum observed earthquakes attributed to EGS operations have been magnitude 3.0 to 3.7 and the largest geothermal injection-related event was magnitude 4.6*'. Later, Majer et al. (2012) also stated that, for EGS, earthquakes are typically smaller than M 3.5 (M representing the momentum magnitude in this context). No cases are known to date where geothermal-induced seismicity has caused structural damage, because, in general, the seismic events are of small magnitude (< M 4.0) (Majer et al., 2016). Baria et al. (2006) and Majer et al. (2007) noted that there is no evidence that induced seismicity has caused significant structural damage at the majority of operating hydrothermal fields around the world. In 2016 a Mw 5.5 earthquake occurred near the Pohang geothermal plant, that apparently contradicts the former conclusions about geothermal induces seismicity.

The International Energy Agency (IEA) identified induced seismicity as an important issue for EGS development in 2004 and brought together scientists and engineers at three international workshops between February 2005 and February 2006. Important outputs from these gatherings were a Protocol for Induced Seismicity Associated with Enhanced Geothermal Systems (Majer, 2009), along with a published paper Induced Seismicity Associated with Enhanced Geothermal Systems (Majer, et al., 2007). It was concluded that EGS-induced seismicity need not pose any threat to the development of geothermal resources if community issues are properly handled and the operators understand the underlying mechanisms causing the seismicity and develop procedures for mitigating any adverse effects. In fact, induced seismicity by itself provides benefits because it can be used as a monitoring tool to understand the effectiveness of the EGS operations and shed light on the mechanics of the reservoir.

According to Zang et al. (2014), thousands of seismic events are generated during exploitation of geothermal fields annually, although in most cases these events are below local magnitude M L = 2, and below the detection threshold of communities (e.g., Evans et al., 2012). Geothermal sites in the Rhine Graben near Basel (Deichmann and Giardini, 2009), Landau (Grünthal, 2014), Soultz-sous-Forêts (Dorbath et al., 2009) and Cooper Basin (Baisch et al., 2006), however, have experienced M L > 2.5 events due to EGS activities. Although this seismicity has been short lived it has attracted public concern due to its proximity to populated areas (Kraft et al., 2009). The recent example of the deep geothermal well near Helsinki (Finland) shows that high-precision, near–real-time monitoring and analysis of seismic data feeding a traffic light system allows safe stimulation of the world's deepest EGS project so far and maintaining event magnitudes during stimulation below a critical threshold (Kwiatek et al., 2019).

5.2 Use of seismic monitoring to reduce seismic hazard

As pointed out in the previous paragraph, induced seismicity in EGS technology is a necessary consequence of fluid injection because it is related to the increase of rock permeability. Monitoring of induced seismicity is necessary in order to both obtain detailed information about reservoirs and fracture systems and to mitigate risks related to induced earthquakes.

Micro-seismic monitoring has become an indispensable technology for the acceptance of EGS developments as it is the case for other applications of hydraulic fracturing and high-pressure water circulation (e.g. the exploitation of unconventional oil and gas resources).

Recent publicity about induced seismicity at several geothermal sites points out the need to address and mitigate any potential problems that induced seismicity may cause in geothermal projects (Majer et al. 2007). It is crucial that policy makers and general community are convinced that geothermal technologies relying on fluid injections will be engineered to minimize induced seismicity risk, ensuring the resource is developed in a safe and cost-effective manner.

A committee appointed by the U.S. National Research Council in 2013 produced a report that summarizes the state of the art about the potential for induced seismicity related to energy development (National Research Council, 2013). The proposed action to deal with induced seismicity is the development of a “best practices” protocol specific to each energy technology. The aim of such protocols is to diminish the possibility of a felt seismic event from occurring and to mitigate the effects of an event if one should occur. A “traffic light” control system within a protocol can be established to respond to an instance of induced seismicity, allowing for low levels of seismicity, but adding monitoring and mitigation requirements, including the requirement to modify or even cease operations if seismic events are of sufficient intensity result in a significant concern to public health and safety. The ultimate success of such a protocol is fundamentally tied to the strength of the collaborative relationships and dialogue among operators, regulators, the research community, and the public.

5.2.1 Existing procedures and protocols

5.2.1.1 Berlin, El Salvador (Bommer et al.2006)

Bommer et al., (2006) proposed the development of a “traffic light” system for monitoring and controlling induced seismic hazard for a hot fractured rock geothermal project in Central America (El Salvador).

The basis of the “traffic light” is a set of physical thresholds that define the limits for human disturbance and damage to vulnerable houses. Thresholds are usually defined in terms of peak ground velocity (PGV), and their values are inferred from recommendations for tolerable vibration levels due to blasting and pile driving, and from correlations between PGV and macro-seismic intensity. The thresholds are converted, via locally derived attenuation equations, into equivalent magnitudes for shallow events (i.e. at depth of 2 km), which is where the induced seismicity is expected to occur. The frequency of events is defined by a recurrence relationship. The system was implemented in almost real time through the deployment of an array of sensitive seismographs around the fracture stimulation well, allowing rapid determination of hypocentral locations and magnitude. A small number of accelerographs were also installed to enable measurement of the induced ground motions. The “traffic light” system devised by Bommer et al. (2006) requires a seismic monitoring system that allows real-time monitoring and processing of the recorded seismicity so that the “traffic light” program could be executed automatically at specified time intervals, reading the event catalogue for a specified number of days up to the time of execution.

5.2.1.2 TLS probabilistic improvement (Bachmann et al., 2011)

Bachmann et al. (2011) tried to improve the “traffic light” alarm system by introducing a probability-statistical forecast models and then translate the forecast to seismic hazard in terms of probabilities of exceeding a ground motion intensity level.

5.2.1.3 Adaptive TLS (Mignan et al., 2017)

Mignan et al., 2017, proposed, as a complementary approach, an adaptive traffic light system (ATLS) that is function of a statistical model of induced seismicity. It offers an actuarial judgement of the risk, which is based on a mapping between earthquake magnitude and risk. Using data from six underground reservoir stimulation experiments, mostly from Enhanced Geothermal Systems, they illustrate how such a data-driven adaptive forecasting system could guarantee a risk-based safety target.

5.2.1.4 The IEA protocol (Majer et al., 2009, 2012, 2016)

The International Energy Agency (IEA) Implementing Agreement for a Cooperative Programme on Geothermal Energy Research and Technology provides an important framework for wide-ranging international co-operation about geothermal energy issues.

The IEA identified induced seismicity as an important issue for EGS development in 2004, and brought together scientists and engineers at three international workshops between February 2005 and February 2006. Important outputs from these gatherings were a Protocol for Induced Seismicity Associated with Enhanced Geothermal Systems, along with a published paper Induced Seismicity Associated with Enhanced Geothermal Systems (Majer, et al., 2007).

Emphasizing the possible impact but also the utility of induced seismicity, the U.S. Department of Energy (DOE) in 2004 promoted an international activity to develop a Protocol to address both technical recommendations and public acceptance issues about EGS-induced seismicity. This resulted in an International Energy Agency (IEA) Protocol (Majer et al., 2009), followed by an updated Protocol in 2012 (Majer et al., 2012), and in a "Best Practices" document (Majer et al., 2016).

The main points that characterize these documents are listed below, and can be summarized into seven steps that an EGS developer should follow in order to handle induced seismicity, implement an outreach campaign, and cooperate with regulatory authorities and local groups (Table 5-1).

Table 5-1: Suggested steps that a EGS developer should follow to address induced seismicity issues, implement an outreach campaign and cooperate with regulatory authorities and local groups, as defined by Majer et al. (2012).

Main steps in addressing induced seismicity
1. Perform a preliminary screening evaluation
2. Implement an outreach and communication program
3. Identify criteria for ground vibration and noise
4. Establish seismic monitoring
5. Quantify the hazard from natural and induced seismic events
6. Characterize the risk from induced seismic events
7. Develop risk-based mitigation plans

An important step in understanding the potential for induced seismicity, as well as in providing data for the EGS design, is to identify past and present natural seismicity. These data will be needed for the induced seismicity hazard and risk analysis, as well as for understanding current stress/faults/fracture patterns. In areas of high natural/background seismicity, it may be undesirable to consider developing an EGS project. Background seismicity data will be needed at both regional and local scale. An estimate of probabilistic seismic hazard can be taken from existing hazard maps. However, adjustments should be made to include natural seismic events as small as moment magnitude M 3.5, if possible. This will create a baseline that can differentiate natural risk from that induced by the EGS, where earthquakes are typically smaller than M 3.5.

For the seismic monitoring, the protocol recommends using seismicity data, ground motion recordings, and updating or installing a local network as soon as possible. The basic information required will be: (1) location and time of the events; (2) magnitude of the events; (3) focal mechanisms; (4) rate of seismicity (Gutenberg-

Richter recurrence parameters); (5) data provided in real time once the EGS project begins stimulation and production.

One of the main elements in forecasting the level of induced seismicity is that of determining the baseline level of seismic activity that exists before the project starts. The amount of available seismic data will vary depending on the project location; in many areas, it is likely that the available baseline data will come from regional seismic monitoring (with interdistance between seismic monitoring stations in the order of tens of kilometers, if not more). Current experience indicates that geothermal projects (particularly EGS projects) require a high sensitivity to seismicity at low magnitude thresholds (magnitude 0 to 1 range) to enable active seismic structures to be properly identified.

The local seismic monitoring should be performed before, during, and after the injection activity in order to validate the engineering design of the injection in terms of fluid movement directions, and to guide the operators with respect to optimal injection volumes and rates, as well as any necessary mitigation actions. Background and local monitoring will also separate any natural seismicity from induced seismicity, providing protection to the operators against specious claims and ensuring that local vibration regulations are being followed. It is also important to make the results of the local monitoring available to the public as soon as possible, especially during initial and ongoing injections that are designed to "create the reservoir." The monitoring should be maintained at a comprehensive level throughout the whole life of the project, and possibly for a further period of some years. If, however, the rate and level of seismicity decrease significantly during the project, consideration can be given to discontinuing the monitoring sooner, i.e. few months after the project ends.

The seismic array must be designed in light of the known background seismicity, as well as the total extent and desired size of the EGS reservoir. In general, an array of seismic sensors should have enough elements to provide location accuracy of 100 to 200 m in the horizontal direction and 500 m in depth. A typical EGS area with a 5 km diameter would preferably have at a minimum an 8-element array of seismic stations covering the 5 km area and a portion of the area outside of the target area, especially if nearby faults and /or public assets may be affected. Also, it will probably be necessary to detect and reliably locate events down to M 0.0 or less.

Experience to date indicates the need for reliably detecting seismicity from M -1.0 up to M 4.0+ range. If the instrumentation can detect and locate M -1.0 events, it is obvious that it can also detect and locate the larger events, but "clipped data" in the upper magnitude ranges must be avoided. Thus, attention must be paid to the dynamic ranges of the sensors, as well as to the digitizing and recording electronics. Also, attention must be paid to the digitization rates of the data, i.e., for small arrays, timing to the millisecond may be necessary to accurately locate the events, as well as to prevent data aliasing. Therefore, the electronics should digitize at a rate of at least 500 samples/sec., obtaining 24-bit resolution from sensors with 120 dB of dynamic range. In addition, the data must be time stamped, with a common time base as it is collected.

Accurate velocity models (3-D) are also needed to correct for wave path effects as well as any temporal changes in velocity structure as the reservoir evolves. Note also that as the EGS operation proceeds, it may be necessary to add and/or move stations to adequately monitor the evolving seismicity.

Once data collection starts, the usual procedure is to collect the data at a central point and have software in place to detect events of interest. For regulatory compliance, operational understanding, and public communication, real time analysis will be needed. It will be necessary to have initial real-time locations and magnitudes of events posted to a publicly available web site.

More sophisticated analysis such as advanced location schemes (double difference locations, tomographic analysis for improved velocity models, moment tensor analysis and joint inversions, etc.) will probably be needed in the operational phases of the project, but are unlikely to be needed during the background monitoring phase. Procedures for almost all those methods are available in the public domain.

The local micro-seismic monitoring should include by integrated by accelerometers in order to record ground shaking that can be felt by population or the vibration of some sensitive structures.

An important point in dealing with induced seismicity is the development of risk-based mitigation plans. If the level of seismic impacts becomes unacceptable, direct mitigation measures are needed to further control the seismicity. A "traffic light" system can allow operations to continue as is (GREEN), or require changes in the operations to reduce the seismic impact (AMBER), or require a suspension of operations (RED) to allow time for further analysis. Indirect mitigation may include community support and compensation.

5.2.1.5 The GEISER Project (GEISER, 2013)

The GEISER (Geothermal Engineering Integrating Mitigation of Induced Seismicity in Reservoirs) project started at the beginning of the year 2010 after successful contract negotiations with the European Commission. The project addressed several of the major challenges the development of geothermal energy is facing, including the mitigation of induced seismicity to an acceptable level. The outcome of the project are: guidelines for the assessment of the seismic hazard associated to induced earthquakes; guidelines for licensing and site development for local authorities and industry; strategies for the mitigation of induced seismicity; and, guidelines for the optimisation of a monitoring network and a real-time monitoring system to help authorities and operators minimize the seismic hazard and manage the risks during operations and production.

The seismic monitoring strategies suggested by GEISER (2013) are explained in the following paragraphs. For the basic seismic monitoring, the GEISER guidelines claim that the recommended data quality is explicitly related to the human perception threshold for vibrations: for transient signals in the frequency range from 5-40 Hz the perception threshold is around 0.3 mm/s. The goal is to reliably identify the onset time of a signal with a peak ground velocity of one order of magnitude below the perception threshold (i.e. a factor in the order of 0.1). If the noise level is too high at the surface, a solution may be to place sensors in boreholes, or to suppress the noise using array technology. To reliably record both P- and S-wave motion the vibration should be measured in three independent directions with known orientations. The sensors should at least be sensitive to vibrations in the frequency range of 5-40 Hz. The timing of the recordings should be synchronized to universal time (UTC), e.g. by GPS.

A basic seismic monitoring network should be in operation for the full lifetime of the EGS project including lead-in and lead-out times. The lead-in is important for the determination of noise levels and assessment of natural seismicity. A lead-in of 6 months or longer is recommended. The lead-out is important to capture any trailing induced seismicity until stabilization of the reservoir. The spatial distribution of the monitoring network should cover the vertical surface projection of the reservoir (or perturbed volume) as well as known or presumed seismogenic faults in its vicinity. The contour of the projection must be extended outward by a distance on the order of the depth of the reservoir. The errors in the event locations should be within, say, ±500 m horizontal and ±2000 m vertical.

All data should be continuously recorded, transmitted to a data centre, and stored for possible future reference. The data should be directly available to a monitoring authority such as a national seismological service. The data should preferably be supplemented by and integrated in existing seismic networks in the direct vicinity.

It is recommended that all data be made publicly available in case the induced seismicity exceeds anticipated levels.

For reservoir seismic monitoring the emphasis is on micro-seismic events that remain well below a perception threshold opposite to the case of classical seismic monitoring. Tremors with magnitude -2 and upwards should be detected throughout the reservoir volume. The critical phase for the reservoir monitoring is the stimulation phase. In practice, it is difficult to achieve an optimal network layout, and the desired detection levels are achievable only using downhole multicomponent measurements close to reservoir depth. However, absolute event location errors in the order of ±100 m horizontal and ±200 m vertical should be feasible.

Background seismicity should be monitored prior to any stimulation activity to define a baseline to evaluate changes in the seismicity rate during stimulation. In the absence of induced seismicity, ambient seismic vibrations can help in determining structural features and temporal changes in reservoir properties.

Local geological structures and seismic velocities should be mapped during the first stimulation phase of a geothermal reservoir. Fracture mapping is recommended down to the reservoir depth. As in the stimulation phase new fractures are created, careful seismic monitoring is needed to maintain control of this permeability-enhancing process. Continuous monitoring of induced seismicity is required from the beginning of the stimulation experiment to detect runaway fracturing, also along buried faults.

5.2.1.6 Swiss guidelines (Wiemer et al., 2017)

Wiemer et al. (2017) suggested the guidelines for seismic monitoring of EGS in Switzerland. With these guidelines, the Swiss Seismological Service (SED) aims to establish a common minimum standard for seismic monitoring of deep geothermal projects in Switzerland that bear the potential of induced seismicity. In project phases that imply increased seismic hazard (e.g. reservoir stimulation), geothermal projects need to establish mitigation strategies, that is, a Traffic Light System (TLS).

According to the Swiss guidelines, for the determination of source parameters, at least four continuously recording stations must be placed around a geothermal system, aiming for a completeness of ML ≥ 1.0. The completeness level to be achieved should be modelled as part of the network design, using realistic assumptions about the noise conditions at the recording sites. The epicentral distance to the expected source region should be about two times the planed geothermal operation depth but less than 10 km. Azimuth gaps of more than 120° between the stations should be avoided. One of the stations should be placed in the centre of the network, close to the expected source region. The recording sites should be chosen in such a way that the measurement accuracy required are fulfilled. The central station should in addition be equipped with an accelerometer that allows recording strong ground motions up to 1 g. The network should be extended by a sufficient number of stations to ensure a completeness level of ML 0.5 with automatic detection algorithms. The monitoring network should ensure a location accuracy of ± 0.5 km horizontally and ± 2.0 km in depth in the expected source region and its direct periphery (within 5 km) for seismic events down to the completeness level.

A notification and alarming system should be set up that provides real-time information on automatically detected and located earthquakes and subsequent manual refinements to the operators and involved cantonal and federal authorities. Notifications and alarms should be sent via SMS, email, and published on a dedicated project page on the internet in quasi-real-time. The guidelines also recommend publishing earthquake catalogues and epicentre maps in near real-time on the internet. Seismic waveform data should be opened to research at least after three years in central databases. Such an open data policy will allow transparency, verification and the application of advanced analysis methods.

5.2.1.7 Australian guidelines (Hunt and Morelli, 2006; Morelli, 2009)

These guidelines suggest that a seismic hazard control system based on a 'traffic light system' similar to that used at the Berlin field in El Salvador (Bommer et al., 2006) be implemented at all future geothermal operations. This would be of particular importance during the initial fluid injection phases of any new project. The idea is that injection volumes should be reduced if ground motion levels and events magnitudes are raised beyond a predetermined level. The seismic monitoring should start well before the start of stimulation operations to get baseline information. The 'traffic light system' should be based on these background levels, and when a background level is approached (amber) the injected fluid volume should be reduced and proceed at a reduced rate.

Strong motion accelerometers, or acceleration measuring geophones, should also be deployed together with the seismometric stations. These should be deployed both downhole and at, or near, surface, to record stronger events that are otherwise clipped by the seismometers. Strong motion accelerometers should also be installed on or near infrastructure determined to be most at risk from a seismic event in the area, so that the measurements can be used for comparison with any thresholds set for strong ground motion (in terms of SRSA, PGA or PGV) as part of the seismic risk management process.

5.3 Seismic monitoring management in EGS sites: review of international experiences

This chapter reports a systematic review of some selected the EGS projects worldwide, based on the information available in the public domain as proposed by (Breede et al, 2013; Breede et al., 2015) and integrated with new ongoing projects.

Selected case studies are: Fenton Hill (New Mexico, USA), Rosemanowes (Cornwall, UK), Hijiori (Japan), Soultz-sous-Forêts (France), Cooper Basin (Australia), Basel (Switzerland), Landau (Germany), Berlín (El Salvador), Pohang (South Korea), Helsinki (Finland).

5.3.1 Summary of EGS projects

Table 5-2:Seismicity of 31 EGS projects as identified by Breede et al. (2013), Breede et al. (2015) (see references therein). The last two cases (shaded rows) are taken from Kim et al. (2018) and Kwiatek et al. (2019).

Project	Start date	Location	Current status	Seismicity
Le Mayet	1978	France	Concluded	Micro-seismicity, not felt on surface
Genesys Hannover	2009	Germany	Under development	Micro-seismicity ($M \leq 1.8$)
Groß Schönebeck	2000	Germany	Under development	Negligible (-1.8 $M \leq -1.0$)
Mauerstetten	2011	Germany	Under development	Unknown
St. Gallen	2009	Switzerland	Production test interrupted	$M \leq 3.5$
Newberry	2010	USA	Under development	Micro-seismicity

Northwest Geysers	2009	USA	Under development	Micro-seismicity (0.9 M ≤ 2.87)
Paralana	2005	Australia	Under development	Micro-seismicity M ≤ 2.6
Bruchsal	1983	Germany	Ongoing	Micro-seismicity
Landau	2003	Germany	Ongoing	Micro-seismicity (M ≤ 2.7), felt by residents
Insheim	2007	Germany	Ongoing	Micro-seismicity M ≤ 2.4
Neustadt-Glewe	1984	Germany	Ongoing	Unknown
Unterhaching	2004	Germany	Ongoing	Unknown
Soultz-sous-Forêts	1987	France	Ongoing	Micro-seismicity (−2 ≤ M ≤ 2.9)
Bouillante	1963/1996	France (Guadeloupe)	Ongoing	Micro-seismicity
Altheim	1989	Austria	Ongoing	Unknown
Lardarello	1970	Italy	Ongoing	M ≤ 3.0
Coso	2002	USA	Ongoing	M ≤ 2.8
Desert Peak	2002	USA	Ongoing	Micro-seismicity: −0.03 ≤ M ≤ 1.7
Berlín	2001	El Salvador	Ongoing	M ≤ 4.4
Cooper Basin	2003	Australia	Abandoned	M ≤ 3.7
Hijiori	1985	Japan	Abandoned	Micro-seismicity
Falkenberg	1977	Germany	Concluded	Micro-seismicity
Genesys Horstberg	2003	Germany	Concluded	No measured event
Fjällbacka	1984	Sweden	Concluded	Micro-seismicity
Rosemanowes	1977	UK	Concluded	M ≤ 3.1
Fenton Hill	1974	USA	Concluded	Micro-seismicity
Ogachi	1989	Japan	Concluded	Micro-seismicity
Bad Urach	1977	Germany	Abandoned	Micro-seismicity
Basel	1996	Switzerland	Abandoned	Frequent earthquakes (including M = 3.4)
Pohang	2012 (Kim et al., 2018)	South Korea	Suspended	Mw 5.5 Pohang earthquake (Lin et al., 2019)
Helsinki	2015 (Kwiatek et al., 2019)	Finland	Under development	Micro-seismicity M ≤ 2.4 (Kwiatek et al., 2019)

5.3.2 Selected cases

5.3.2.1 Fenton Hill

Start date : 1974 (MIT, 2006)
Location : USA
Status : Concluded
Induced Seismicity : Micro-seismicity (Brown, 1995)

Description

The Fenton Hill project was the first attempt to extract geothermal energy from hot dry rocks (HDR) with low permeability in the history of EGS (MIT, 2006). It was initially totally funded by the U.S. government, but later involved active collaborations with Great Britain, France, Germany, and Japan under an International Energy Agency agreement. The Fenton Hill site is characterized by a high-temperature-gradient in a large volume of uniform, low-permeability, crystalline basement rock. It is located on the margin of a hydrothermal system in the Valles Caldera region of New Mexico, not far from the Los Alamos National Laboratory where the project was conceived. The Fenton Hill experience demonstrated the technical feasibility of the HDR concept by 1980, but none of the testing carried out yielded all the performance characteristics required for a commercial-sized system (Brown, 2009; MIT, 2006).

The program was divided into two major phases. Phase I (1974 – 1980), focused on a 3 km deep reservoir with a temperature of about 200°C. Phase II (1979-1995) penetrated into a deeper (4.4 km), hotter (300°C) reservoir. Two separate, confined HDR reservoirs were created by hydraulic fracturing and were flow-tested for almost a year each. Thermal power production ranged from 4 MW for extended routine production intervals to as high as 10 MW for a 30-day period. The testing proved beyond any doubt that it was technically feasible to recover useful amounts of thermal energy from HDR.

During the latter phases of work at Fenton Hill, support for the work had declined to the point where it was not possible to maintain sufficient technical staff to perform continuous flow testing of the reservoir – nor was it possible to perform the necessary re-drilling and wellbore repairs to upgrade the downhole connections to the large fractured system that had been created. With prospects for continued funding very low, all field experiments at the Fenton Hill site were terminated by 2000, after which the site was decommissioned (MIT, 2006)

Natural seismicity

Although New Mexico is over 1000 kilometres from the nearest plate tectonic boundary, it is a moderately seismically active region, with earthquakes occurring in most parts of the state. The Socorro area has been the most active earthquake region of New Mexico during the last past 150 years, and the largest earthquakes in New Mexico's record history occurred in 1906 (Pursley et al., 2013).

Before the beginning of the project, the fault structure and earthquake history of the Fenton Hill area was investigated. It was assessed potential earthquake hazards associated with hydraulic fracturing operations. This analysis led to several conclusions: 1) the level of seismic activity in the region surrounding Fenton Hill was very low, 2) hydraulic fracturing experiments in this area would involve very little seismic risk from natural faults, and 3) such experiments were not likely to activate any of the known faults in the area—including the closest and most recent one in Virgin Canyon (Slemmons, 1975).

Monitoring of induced seismicity

The experiment carried out at Fenton Hill, New Mexico, in December, 1983 provided an opportunity to evaluate the usefulness of monitoring micro-seismicity induced by fluid injection in crystalline rock. Seismic monitoring instrumentation consisted of two types: one, triaxial geophone packages in deep boreholes as close as 100 m to the induced events; the other, vertical component packages in shallow boreholes at distances up to 3.5 km. All seismic data were recorded on analogue tape and selected events were digitized during the experiment. A total of 805 events were reliably located. Seismic monitoring of a massive hydraulic injection into crystalline rock at depths of 3.5 km was able to determine both the large-scale features of the fluid system created, as well as resolving features with dimensions of a few tens of metres. The zone of seismicity appeared to contain the volume of rock in which the major fluid paths are located. (House, 1987).

Protocols

No known protocols. U.S. Department of Energy stated to monitor subsidence, seismicity and quality of water at geothermal sites.

Public reaction

Not available.

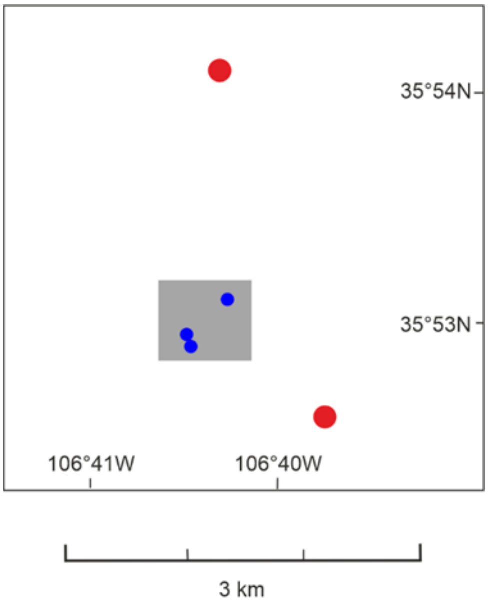

Figure 5-1: Map view of Fenton Hill site and stations used to locate induced micro-seismicity. Red circles: location of two shallow vertical component instruments in correspondence of wells GT-1 and PC-1. Blue triangles: deep borehole three-component seism instruments located in correspondence of wells EE-1, EE-3 and GT-2B. Grey rectangle: Fenton Hill site. Modified from House (1987).

5.3.2.2 Rosemanowes

Start date : 1977 (MIT, 2006)

Location : United Kingdom

Status : Concluded

Induced Seismicity : Micro-seismicity with Mmax 1.9 (Bromley and Mayer 2012)

Description

As a result of experience during Phase I at Fenton Hill, the Camborne School of Mines undertook an experimental HDR project at Rosemanowes, near Penryn in Cornwall (U.K.) in granite rocks. The project was funded by the U.K. Department of Energy and by the European Commission. It started in 1977 and ended in

1992. Three wells were drilled and several stimulation/circulation experiments were undertaken. The temperature was restricted deliberately to below 100°C, to minimize instrumentation problems. This project was never intended as an energy producer but was conceived as a large-scale rock mechanics experiment about the stimulation of fracture networks. The site was chosen because of its clearly defined vertical jointing, high-temperature gradients between 30-40°C/km and its strike-slip tectonic regime (Ledésert & Hébert, 2012).
The Rosemanowes HDR project was active between 1978 and 1991, and culminated in the development and operation of a circulation system at a depth of ~2 km within the granite, which extends to the ground surface. Initially, two wells were drilled to 2050 m and stimulated with a variety of methods, including gel and water injections.

Natural seismicity

The area has low natural seismic hazard. The nearest events of note, which include a M L 3.5 event that occurred in 1981, are clustered near the town of Constantine, some 6 km south of the site (Turbitt et al., 1987). The seismicity of Cornwall and Devon is well investigated. By comparison with average British seismicity, that of Cornwall and Devon can be described as moderately active, rather shallow, and with a fairly low maximum magnitude. There seems to be a correspondence between the more seismically active areas of the two counties and the distribution of larger E-W trending faults (Musson, 2000).
The first, and largest (ML 2.0), earthquake to be detected on the BGS network occurred on July 12th 1987 (Turbitt et al., 1987). Four other events in the BGS catalogue (BGS, 1991) are thought to be linked to the project. In total two geothermal energy related earthquakes exceeded ML 1.5.

Monitoring of induced seismicity

At Rosemanowes the seismicity was monitored using a network of vertical-component-only and 3-component accelerometers cemented in boreholes up to 300 m deep (Baria et al. 1984). Fluid injection in the first two wells was accompanied by thousands of earthquakes (Baria et al., 1985): , the maximum magnitudes during stimulation were very low, 0.16 and − 0.2. The first, and largest (ML 2.0), earthquake to be detected on the BGS network occurred on July 12th 1987 (Turbitt et al., 1987). A further four events in the BGS catalogue are to be linked to the project. Most of the seismic events were not felt by the local population or the on-site project staff (Turbitt et al., 1987), but the ML 2.0 1987 event was mildly felt by the local population within a few kilometres of the site.

Protocols

Not available.

Public reactions

Although seismic events were felt around the Rosemanowes area during reservoir stimulation, there were no complaints, possibly as a result of early public education initiatives (Bromley and Majer, 2000).

5.3.2.3 Hijiori

Start date : 1985 (Sasaki, 1998)

Location : Japan

Status : Abandoned

Induced seismicity : Micro-seismicity (Sasaki, 1998)

Description

Since 1985, the New Energy and Industrial Technology Development Organization (NEDO) has been conducting research to develop elementary technologies for hot dry rock (HDR) geothermal energy extraction at Hijiori, Yamagata Prefecture, Japan (Sasaki, 1998 and references therein). From 1981 to 1986, NEDO participated in a joint research effort in the development of geothermal energy through stimulation of low permeability rock at Fenton Hill, New Mexico. This was carried out with the United States and West Germany under an implementation agreement of the International Energy Agency (IEA). Based on this research, NEDO conducted studies in Hijiori to determine whether the technology developed at Fenton Hill could be adapted to the geological conditions found in Japan. The Hijiori site is in Yamagata Prefecture, on the Japanese island of Honshu. The project site was located on the southern edge of Hijiori caldera.

Two injection wells and two production wells were drilled into granodiorite to extract heat from two artificially created reservoirs at depths of around 1,800 m and 2,200 m where temperatures were measured at 230 degree C and 270 degree C, respectively. The location was chosen to take advantage of the high temperature gradient in this area of recent volcanic activity.

Natural seismicity

Most of microearthquakes occur along the deeper portion of the main thrust zone beneath the Pacific Ocean. In northeaster Japan, the Pacific plate is subducting beneath the North American– Okhotsk plate at the Japan Trench at a rate of ~80 mm/yr. The level of seismicity is very high around the plate boundary, both within the subducting slab and in the shallow part of the overriding continental plate.

Monitoring of induced seismicity

A ten-station seismic network deployed at the edge and outside of Hijiori caldera monitored induced seismic events or acoustic emissions related to the stimulation experiments. A borehole seismic network was constructed, consisting of 10 stations deployed in a circle at a radius of 1.5 to 3 km around the injection and production wells (Sasaki and Kaieda, 2002). To reduce noise and improve detection of high-frequency signals, seismometers were cemented in the boreholes at depths ranging from 50 m to 150 m. The seismometers used were three-component geophones with a natural frequency of 5 Hz.

The seismic activity was very low for about 4 hours after the beginning of the stimulation. Several hundreds of micro-events with magnitude smaller than -1.0 were observed, with maximum magnitude of 0.3. A total of 107 micro-earthquake events were located.

Protocols

Not available.

Public reactions

Not available.

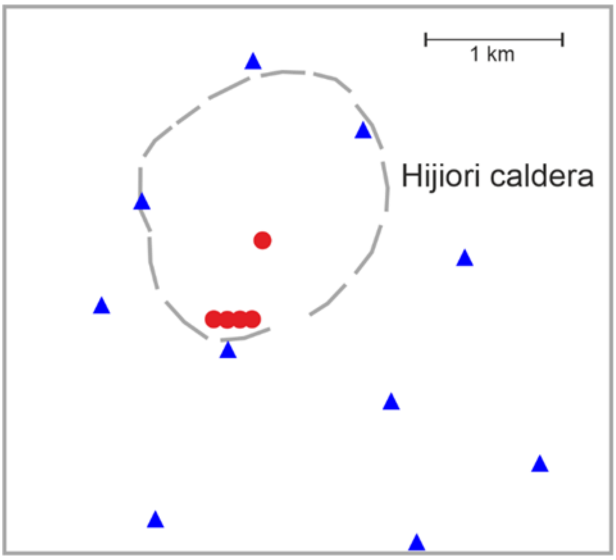

Figure 5-2:Map view of Hijiori site. Red circles: the four wells as injection and production wells in the experiments. Blue triangles: borehole seismic instruments. Grey dashed line: Hijiori caldera rim.

5.3.2.4 Soultz-Sous-Forêts

Start date : 1987 (Majer et al., 2007)
Location : France
Status : ongoing
Induced seismicity : Micro-seismicity (M = −2 to 2.9) (Genter 2012)

Description

Research at the European Hot Dry Rock (HDR) site at Soultz-sous-Forêts started in 1987, following the encouragement by the European Commission to pool France's limited available funds to form a coordinated multinational team. The main task was to develop the technology needed to access the vast HDR energy resource at the site, about 50 km north of Strasbourg, in Alsace (France), in the northern part of the Upper Rhine Graben (Majer et al., 2007). Seismic events with magnitudes greater than 2 occurred during the shut-in phase. Although minor damages were caused by this EGS project, it did generate concern among the local population.

The development of the project site began in 1987 with the drilling of a 2 km deep well to explore the granitic basement below 1.4 km. Subsequently, a doublet system was firstly developed and circulated at 3.0–3.5 km depth in 1992–1997, and it was followed by a triplet at 4.5–5.0 km depth developed and tested between 1998 and 2009.

Five circulation tests performed in 2005, 2008 (twice), 2009 and 2010 offered the opportunity to observe the occurrence of microearthquakes. Long-term circulation of the deep system with power production commenced in 2010 (Genter et al., 2010). After 20 years of research and development on the geothermal reservoir, a 1.5 MWe power plant has been designed, built and tested at the EGS site of Soultz-sous-Forêts.

Natural Seismicity

The site is located in a zone of minor natural earthquake hazard, as defined by the seismic risk authority in France. The Upper Rhine Graben region, where the EGS project is located, features low-to-moderate seismic hazard. In 1954 a series of events with magnitudes up to ML 4.8 and intensities up to Intensity VI on the European Macro-seismic Scale (EMS-98) occurred 10–20 km southeast of Soultz, towards Seltz/Wissenbourg (Helm, 1996).

Monitoring of induced seismicity

For each stimulation test, the induced micro-seismic activity was monitored by a surface seismological network managed by the Ecole et Observatoire des Sciences de la Terre from the Strasbourg University. In 2000, 18 temporary seismological stations, composed of one component and three components sensors were set up. In 2003, a permanent network was deployed, and is still in operation around Soultz-sous-Forêts to continuously monitor the seismic activity. For the 2003 stimulation, the permanent network was integrated by 14 temporary three-component stations, to form a more comprehensive network. For 2004 and 2005, only four additional three-component temporary stations were installed (Charléty et al., 2007).

The Soultz seismic network is composed of short-period (1 Hz) seismometers, one or three components, deployed at surface. Signals are digitized on site by 15-bit GEOSTAR data loggers and sampled at 150 Hz. The signals are then transmitted to a central site via a radio link where samples are synchronized with an external time receiver. Waveforms from the telemetered stations are currently acquired in real-time via queries and supported by a SeisComp3 server. This server, located at University of Strasbourg and dedicated to geothermal projects in the Rhine Graben, performs both real-time processing of the data and their archiving (Maurer et al., 2015).

The five circulation tests performed in the period 2005-2010 offered the opportunity to observe the occurrence of microearthquakes. Among them, earthquakes of magnitude ranging between 2 and a maximum of 2.3 occurred, which were likely to be felt by the population (Cuenot et al., 2011). The largest induced events in the Soultz reservoir appear to be associated with a fault system that intersects the injection wells (Dorbath et al., 2009). Interestingly, all wells at Soultz were intersected by numerous fracture zones that were critically stressed for the most part (Evans, 2005). These were seismically active during the injections, but most events were too small to be felt. The faults are distinguished in Soultz as larger structures that have accommodated greater offset.

Protocols

Not available

Public reactions

The largest events were M1.9 during the initial stimulation and M2.9 during deeper stimulation. Although no structural damage was caused, public complaints led to restrictions on subsequent stimulation options. A possible consequence is that some wells do not have good hydraulic connection with other wells. Better public education about the project at an earlier stage might have been beneficial (Bromley and Majer, 2000).

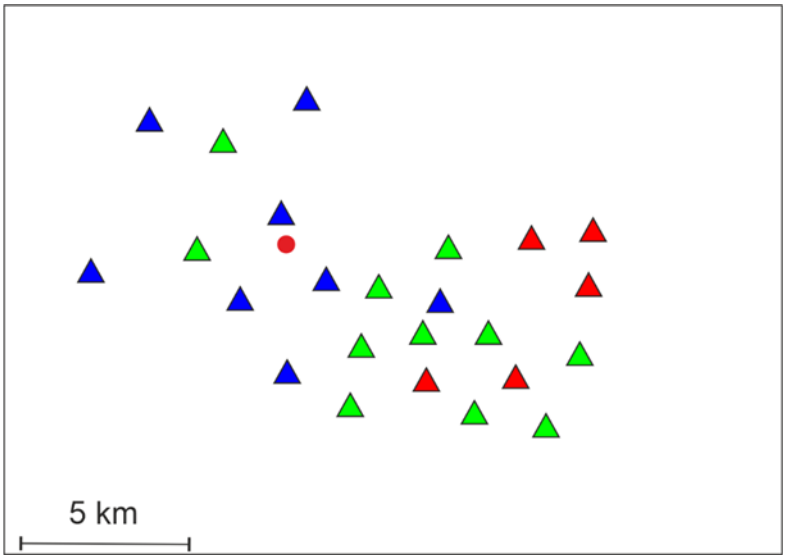

Figure 5-3:Monitoring seismic network at Soultz in 2017 (Mignon et al., 2017). Blue triangles: Soultz permanent network. Red triangles: Rittershoffen project permanent network, Green triangles: real-time temporary seismic network installed specifically for the starting of the exploitation operations. Red dot: location of the Soultz project. Modified from Mignon et al. (2017).

5.3.2.5 Basel

Start date : 1996 (Giardini, 2009)

Location : Switzerland

Status : abandoned due to induced seismicity

Induced seismicity : M ≤ 3.4 (Haring et al., 2008)

Description

The Basel Deep Heat Mining project (Häring et al., 2008) aimed to become one of the first commercial power plants based on the EGS technology. It was planned to enhance reservoir permeability at about 4 – 5 km depth in the crystalline basement by injecting fluid at high pressure over a time period of more than two weeks. A seismic monitoring system was installed along with a hazard and risk management scheme (“traffic light” system following Bommer et al., 2006).

The Basel project in Switzerland experienced induced seismic events - some exceeding 3.0 in magnitude - associated with water injection and hydraulic fracturing, that has caused light damages in Basel and wide concern among the public. This led to the suspension of the EGS project (Giardini 2009).

Natural seismicity

Basel is located in a high-stress region associated with the largest and most destructive earthquake in the history of Switzerland; in 1356 the city was in fact largely destroyed by an earthquake of magnitude 6.5 or greater (Giardini et al., 2004). Within a 10-km radius around the city of Basel, 15 events with ML ≥ 2 and 10 events with 1 ≤ ML ≤ 2 have occurred since 1975.

Monitoring of induced seismicity

The micro-seismic monitoring network array was carefully designed using numeric modelling techniques. The objective was to achieve an optimal balance between network sensitivity, network resolution, operational reliability and financial constraints. The implemented monitoring network comprises an array of six borehole stations (Haring et al., 2008) ranging from 320 m to 2745 m depth. Each seismic monitoring station is equipped with a downhole three-component geophone designed to withstand temperatures of up to 125°C and pressures of up to 345bar in long-term operation. The hydraulic stimulation of the Basel EGS was one of the most densely monitored deep fluid injection in the world.

Bachmann et al. (2011) analysed the monitoring completeness and bulk statistical parameters of the recorded earthquake sequences. The seismicity recorded during and after the stimulation of the Basel EGS is one of the best monitored sequences of its kind. Their analysis of the monitoring completeness as a function of time shows that Mc(t) varies between 0.5 and 0.9. The absolute location error of a single event estimated from the result of the location algorithm is about 1 km for the epicentre coordinates and 1.2 km for the focal depth (Deichmann & Giardini, 2009).

The main stimulation started on 2 December 2006, when a total of 11,566 m3 of water was injected. The gradual increase in flow rate and wellhead pressure was accompanied by a steady increase in seismicity, both in terms of event rates and magnitudes. The early morning of 8 December, after water had been injected at maximum rates in excess of 50 l/s and at wellhead pressures of up to 29.6 MPa for about 16 hours (Häring et al. 2008), a magnitude ML 2.6 event occurred within the reservoir. This exceeded the safety threshold for continued stimulation, so that injection was stopped prematurely. In the afternoon and evening of the same day, two additional events of magnitude ML 2.7 and 3.4 occurred within the same source volume. The maximum recorded PGV value in the vicinity of the well was 9.3 mm/s. As this value exceeded the “red” TLS threshold, that was set at 5 mm/s, the pumping activity was suspended. The “red” threshold of the ground motion was exceeded at three other monitoring stations too. In the following days about one third of the injected water volume flowed back out of the well (Häring et al. 2008). Though the seismic activity declined rapidly thereafter, even more than two years later sporadic micro-seismicity was being detected in the stimulated rock volume by the downhole-instruments.

Protocols

The Basel Deep Heat Mining project adopted the general framework of the “traffic light” system used at Berlín, but, in light of the sensitivities at Basel, used very low thresholds for ground motion; for example, “red” (i.e. suspension of fluid injection) was defined by a PGV threshold of 60 mm/s in Berlín, whereas this threshold was set as 5 mm/s (or a magnitude of 2.9) in Basel (Majer et al., 2007).

Public reactions

The induced earthquakes occurred in Basel caused aversion against the project among the population and media which then led to the temporal suspension of the experiment. In 2009, the project was fully cancelled as a consequence of a comprehensive risk study (Baisch et al., 2009b).

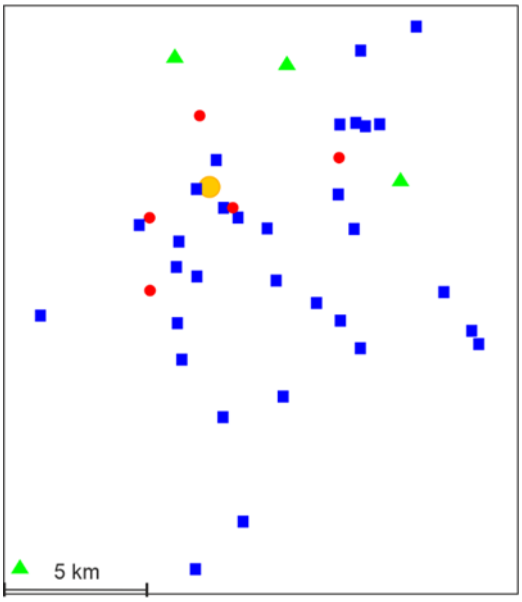

Figure 5-4:Seismic stations in Basel and surroundings during the stimulation in December 2006 and for about six months thereafter (from Deichmann and Giardini, 2009). Red dots: borehole sensors. Blue squares: accelerometers. Green triangles: accelerometers. Orange circle: location of the injection well. Modified from Deichmann and Giardini (2009).

5.3.2.6 Berlín

Start date : 2001 (Bommer et al., 2006)
Location : El Salvador
Status : ongoing
Induced seismicity : ≤4.4 M (Bommer et al. 2006)

Description

In 2003 hydraulic stimulations were carried out in a geothermal field in eastern El Salvador, Central America, as part of a project to explore the feasibility of commercial hot fractured rock energy generation. The proponents developed and implemented a procedure for managing injection-induced seismicity that involves simple criteria to determine whether injection should continue. The HFR project at Berlín presented an unusual problem, in terms of induced ground shaking. El Salvador is in a region of very high seismic activity, affected by two principal sources of earthquakes: the subduction of the Cocos Plate beneath the Caribbean Plate in the Middle America Trench, producing Benioff-Wadati zones, and shallow crustal events associated to the chain of Quaternary volcanoes (Bommer et al., 2006).

The Berlín geothermal field, located on the flanks of the dormant volcano Cerro Tecapa (last eruption thought to have been in 1878), was developed in the 1990s and the current 66 MWe (i.e., MW of electricity, the actual useful output) of installed power plant capacity was brought on stream by CEL (Comisión Hidroeléctrica del Rio Lempa), the state electricity company, between 1992 and 2000. Currently, 54 MWe are being generated from 8 production wells with the fluid exhausted from the power plant–water at 183°C–being disposed of via a reinjection system comprised of 10 injection wells. Depths of the field's wells range from about 700 m for some of the shallow injection wells down to some 2500 m for the deeper production and injection wells.

Natural seismicity

El Salvador is a region of very high seismic activity, affected by two principal sources of earthquakes: the subduction of the Cocos plate beneath the Caribbean plate in the Middle America Trench, producing Benioff–Wadati zones, and shallow crustal events coincident with the chain of Quaternary volcanoes (e.g., Dewey et al., 2004). Large-magnitude earthquakes in the subduction zone tend to cause moderately intense shaking across large parts of southern El Salvador, the most recent example of such an event being the Mw 7.7

earthquake of 13 January 2001. The upper crustal earthquakes are limited to smaller magnitudes, the Mw 6.6 event of 13 February 2001 being representative of the maximum size of these earthquakes.
Berlín is also located in a seismically active region, so it is difficult to differentiate between natural and induced or triggered seismic events. Seismicity in the reservoir increased after the occurrence of two large nearby tectonic earthquakes in early 2001. Fractures within the Berlin reservoir apparently have a poor capacity to accumulate large amounts of stress; therefore, strain energy is released frequently through natural swarms of low-magnitude events. However, some micro-seismicity is spatially correlated to areas of pressure and temperature change, in both production and injection areas, although there is no clear correlation in timing found between the monthly seismicity data and the monthly mass injected or extracted (Bromley and Majer, 2012).

Monitoring

Part of the geothermal field development activities has been the installation of a surface seismic monitoring array–the Berlín Surface Seismic Network (BSSN)– which was brought into use in 1996 to monitor seismicity in and around the field. At Berlín, the monitoring of the HFR project involved two separate instrumental arrays. A seismograph network was installed around the geothermal field with the primary purpose of detecting micro-seismic activity as a means of monitoring fracture propagation. However, the seismograph monitoring system also permitted almost real-time calculation of hypocentres and magnitudes, from which median estimates of PGV at the surface could be obtained. A small network of strong motion accelerographs was also installed at key locations in order to provide instrumental verification of the actual PGV levels. Following a design study to determine the array configuration which would optimize the accuracy with which events in the region of interest could be located, the final decision to install a network comprising six monitoring sites centred on the injector well. At five of the monitoring sites new shallow boreholes were drilled for the deployment of the sensors. At the sixth site, sensors were deployed in an existing unproductive geothermal well. Two geophone packages were deployed in each borehole, one shallow (~ 10 m in the newly drilled boreholes and ~ 435 m in the legacy well) and one deep (~ 100 m in the newly drilled boreholes and ~ 540 m in the legacy well). This provided additional redundancy in the system and resulted in the use of two distinct types of sensors—low frequency (4.5 Hz) fixed geophones in the shallower section of the wells and higher frequency (30 Hz) geophones with magnetic orientation sensors for use at the bottom of the well—giving a broader frequency bandwidth coverage for the network as a whole. The system started to acquire data on 30 October 2002. The period of background monitoring before the start of stimulation operations provided the opportunity to tune the system parameters to optimize the performance of the system to trigger and record as many genuine local events as possible.
The purpose of the strong-motion network was to provide PGV values for the "traffic light" system and to have independent verification of the system. The strongest recorded motion was produced by a ML 4.4 event on 16 September 2003, during an interval between pumping episodes.

Protocols

The Berlín case history is an example of a project with a built-in warning system for monitoring, quantifying and controlling the risk associated with induced seismicity. Thresholds of tolerable ground motion were inferred from guidelines and regulations on tolerable levels of vibration and from correlations between instrumental strong-motion parameters and intensity, considering the vulnerability of the exposed housing stock. The thresholds were defined in terms of peak ground velocity (PGV) and incorporated into a "traffic light" system that also took account of the frequency of occurrence of the induced earthquakes. The system was implemented through a dedicated seismograph array and locally derived predictive equations for PGV. The "traffic light" was used as a decision-making tool regarding the duration and intensity of pumping levels during the hydraulic stimulations. The system was supplemented by a small number of accelerographs and re-calibrated using records obtained during the rock fracturing.
The limits of the "traffic light" system were defined according to the following criteria:

- Red: The lower magnitude bound of the red zone corresponds to the level of ground shaking at which damage to buildings in the area is expected to set in. Injection is suspended immediately.
- Amber: The amber zone is defined by ground-motion levels at which people would be aware of the seismic activity associated with the hydraulic stimulation, but damage would be unlikely. Pumping proceeds with caution, possibly at reduced flow rates, and observations are intensified.
- Green: The green zone is characterized by levels of ground motion that are either below the threshold of general detectability or, at higher ground-motion levels, at occurrence rates lower than the already-established background activity level in the area. Injection operations proceed as planned.

Public reaction

Not available.

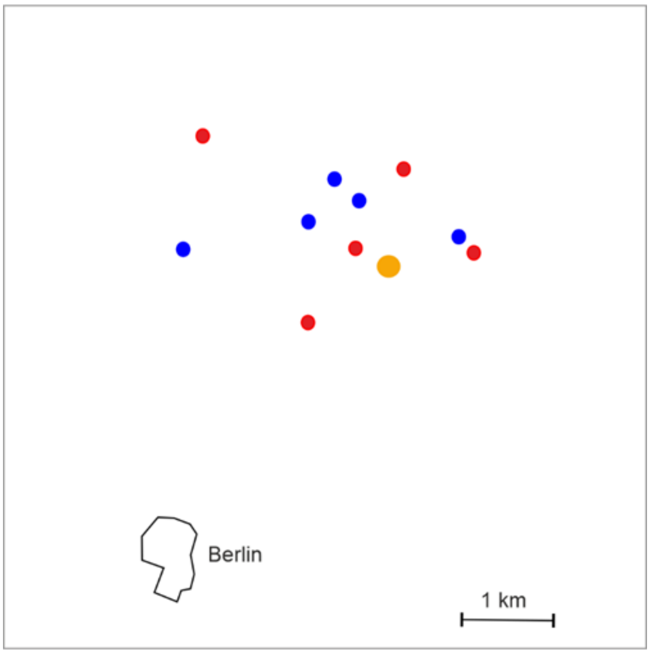

Figure 5-5:Map of the Berlín geothermal field and surrounding area. Red dots: seismographs. Blue dots: accelerographs. Orange circle: Location of the power plant. Modified from Bommer et al. (2006).

5.3.2.7 Cooper Basin

Start date : 2003 (Baisch et al., 2006)

Location : Australia

Status : closed

Induced seismicity : M ≤ 3.7 (Majer et al., 2007)

Description

Cooper Basin is an example of a new project with the potential for massive injection. Test injections have triggered seismic events with magnitude above 3.0. The project was, however, in a remote area, and there was little or no community concern.

The Cooper Basin geothermal field is located in the northeast of South Australia near the Queensland border. Geothermal exploration started in 2002, and to date six deep wells have been drilled into the granite to a depth level of 3629–4852 m. Four of these wells are located in the Habanero field, the other two wells are at distances of 9 and 18 km, respectively, in the Jolokia and Savina fields. Several hydraulic stimulations were conducted to enhance the hydraulic conductivity in the subsurface. Stimulation activities in the Habanero field were accompanied by pronounced seismic activity occurring on a single, sub horizontal fault, which existed prior to geothermal exploration (Baisch et al., 2006, 2009a).

Natural seismicity

The region has a history of low level of seismic activity.

Monitoring of induced seismicity

Seismic monitoring equipment was initially installed at so-called Habanero plant for the 2003 stimulation. It was an analogue system and only recorded for the length of the stimulation.

The monitoring array was a local eight-station network of three-component geophones in boreholes between 88 and 1793 m depth. The recording system was a 16-bit, 5 kHz system in triggered mode (Asanuma et al., 2005a). During the 2005 EGS stimulation, the Habanero seismic network consisted of eight three-component borehole seismic stations equipped with SMART24 24-bit digitizers recording continuously at either 500 Hz or 1000 Hz. Between 08 August 2005 and 12 August 2005, the sample rate was set to 1000 Hz. After 13 August 2005, the sample rate was set for 500 Hz. The deepest seismometer was deployed at the centre of the network at a depth of 1783 m with respect to the wellhead. The remaining seismometers were installed between 79 – 370 m in two roughly concentric circles around the reservoir. Seismic signals were picked up by the deep detector (at 1700 m depth) and in most cases also by the near-surface stations, with clear onsets of P and S waves. Asanuma et al. (2005) recorded 32,000 triggers, with 11,724 of them located in 3D space and time on site during the stimulations.

During the combined 2005 stimulation of the Habanero 1 and Habanero 2 wells, approximately 16,000 micro-seismic events were detected (Baisch et al., 2009a). Of these events, only 8886 microearthquakes were of sufficient quality for hypocentre determination (Baisch et al., 2009a). The 2005 Habanero 2 stimulation lasted 12 days between 9 - 20 August. The 2005 Habanero 1 stimulation lasted 9 days.

In 2010 the monitoring seismic network was extended (Baisch et al., 2015). Stimulation activities were monitored with a 17-element station network consisting of three-component 4.5 Hz geophones deployed in boreholes at depth levels of approximately 100 m. Two additional surface stations were operated with three-component 1 Hz seismometers. Each seismic station was equipped with a three-channel 24-bit digitizer recording continuously at a sampling rate of 500 Hz. Continuous waveform recordings were stored locally on a hard disk, and the seven live stations additionally transmitted data by a wireless local area network to the central data acquisition office. During the 8-day stimulation period, a total of 73 events were detected. Event magnitudes determined relative to the magnitude scale described by Baisch et al. (2009a) range between ML −1.4 and 1.0. Another 139 events occurred within the following six months, with the strongest event (ML 1.6) occurring 127 days after the injection was terminated.

Protocols

Guidelines suggested by recent studies conducted on the induced seismicity risks related to engineered geothermal system operations in South Australia (Hunt and Morelli, 2006; Morelli, 2009).

Public reactions

In terms of public acceptance, the site is remote, with few inhabitants in the vicinity; thus, there is little cause for concern as regards the possible effects of induced seismicity.

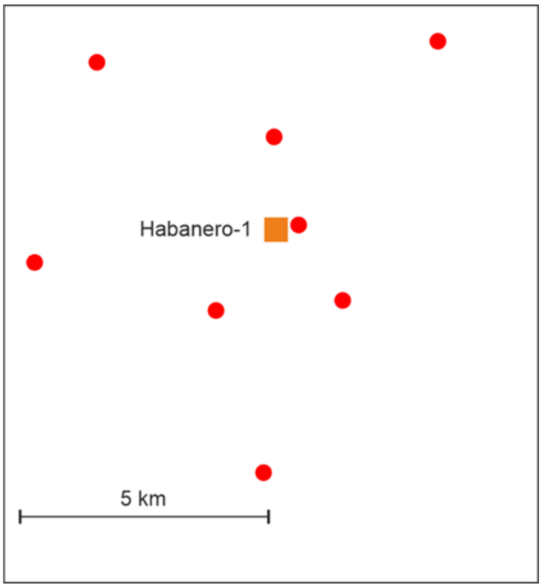

Figure 5-6: Location of Cooper Basin and of the seismic stations at the site. Red dots: seismic stations. Orange square: Habanero-1 well. Modified from Majer et al. (2007).

5.3.2.8 Landau

Start date : 2003 (Majer et al., 2007)

Location : Germany

Status : ongoing

Induced seismicity : Micro-seismicity (M ≤ 2.7) (Bönnemann et al., 2010)

Description

The Landau project is the first EGS project in a town in Germany, which is facing similar problems to Basel. Seismic events of 2.7 in magnitude took place in 2009, which resulted in a temporary suspension of the operations. As a consequence of these events, water has to be reinjected at a reduced pressure to avoid induced seismicity, resulting in reduced power generation.

A combined heat and power plant at Landau, in the Rhine Graben, started production of hot water for district heating and power generation in late 2007 (Baumgärtner et al., 2010, Schellschmidt et al., 2010). Injection occurred into lower units of a sedimentary sequence and granitic basement. The two wells were drilled to about 3.3 km depth; one was naturally permeable (intersected a fault) and the other was stimulated using high pressure injection (190 L/s at 13.5 MPa). After 2 years of operations, the project came under review in September 2009, as the consequence of local seismicity (Baisch et al., 2010); plant operation was resumed in November 2009 with the maximum injection pressure lowered to 4.5 MPa in order to limit the potential for induced seismicity.

Natural Seismicity

The region has low-to-moderate natural seismic activity with historical events that produced maximum intensities of up to Io VII–VIII on the European Macroseismic Scale. An event with an estimated maximum intensity of VII occurred some 10 km to the south of Landau, near Kandel in 1903 (Ahorner et al., 1970b).

Monitoring of induced seismicity

In the region around Landau and Insheim the recording of continuous data evolved since the start-up of the Landau geothermal project in 2007. Although up to 50 stations have been recording simultaneously since then, the availability of data is partly restricted. After the ML 2.7 Landau event in 2009, additional stations were installed by Bestec/GEO-X GmbH, Deutsche MontanTechnologie GmbH (DMT GmbH), and the local earthquake monitoring agency.

There were no felt seismic events from the 2007 stimulation. Six micro-earthquakes ranging in magnitude from 1.6 to 1.9 were located by a regional seismic network in the Landau area between February 2008 and May 2009, although their depth was poorly constrained. Two earthquakes (M2.4 and 2.7) were felt by the local population in August 2009, although no significant damage occurred. The latter, along with several other smaller events, occurred on 15th August, shortly after plant operation was halted for maintenance. It was located 1.5 - 2 km north of the plant at 2.3 - 3.3 km depth, so there was initially some uncertainty as to whether it was induced or natural. Owing to this seismicity, the project came under review in September 2009 (Baisch et al., 2010), and plant operation was resumed in November 2009 with the maximum injection pressure lowered to 4.5 MPa in order to limit the potential for induced seismicity.

Protocols

Not available.

Public reactions

After 2 years of operation, the project came under review in September 2009 as the result of local seismicity (Baisch et al., 2010). Two earthquakes (M2.4 and 2.7) were felt by the local population in August 2009, although no significant damage occurred. The latter, along with several other smaller events, occurred on 15th August, shortly after plant operation was halted for maintenance. It was located 1.5 - 2 km north of the plant at 2.3 - 3.3 km depth, so there was initially some uncertainty as to whether it was induced or natural. Plant operation was resumed in November 2009 with the maximum injection pressure lowered to 4.5 MPa in order to limit the potential for induced seismicity.

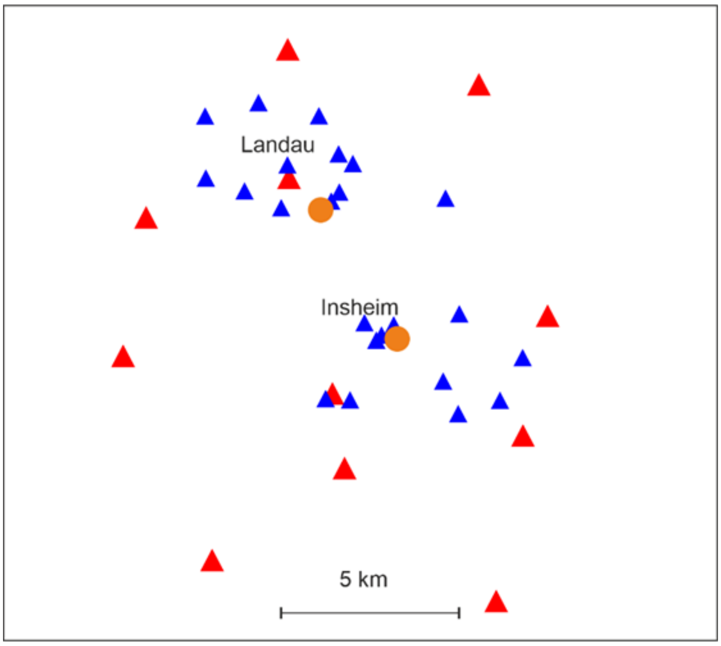

Figure 5-7:Map of seismic network at Landau geothermal site and at the nearby Insheim site. Red triangles: temporary network operated by BGR (Federal Institute for Geosciences and Natural Resources). Blue triangles: industrial networks. Orange circles: geothermal power plants.

5.3.2.9 Pohang

Start date : 2012 (Kim et al., 2018)

Location : South Korea

Status : suspended

Induced seismicity : Pohang earthquake, MW=5.5

Description

The Pohang EGS project was intended to demonstrate the potential of geothermal energy production in a ∼4 km deep granitic reservoir overlain by Cretaceous volcanic and sedimentary rocks, Tertiary volcanic and sedimentary rocks, and Quaternary sediments. The Pohang area is one of the highest heat-flow areas in Korea and has been the focus of dedicated geothermal research since 2003 (Lee et al., 2010). In the project, two geothermal wells, PX-1 and PX-2, with a depth of over 4 km were drilled to expedite water circulation through hot dry rock characterized by artificially enhanced permeability induced by hydraulic stimulation (Kim et al., 2018; Hofmann et al., 2019). Through these geothermal wells, the EGS project team conducted five hydraulic stimulation experiments (Kim et al., 2018). The Pohang earthquake occurred approximately 2 months after the completion of the final hydraulic stimulation experiment (i.e., 18 September 2017).

Natural seismicity

No earthquakes with M L > 2.0 were recorded within 10 km of the Pohang EGS site between 1978 and 2015; a total of six earthquakes with ML 1.2 to 1.9 were detected in the area between 2006 and 2015. Hydraulic injection by the Pohang enhanced geothermal systems has been suspected to trigger the 2017 MW 5.5 Pohang earthquake in South Korea. The last stimulation experiment in the EGS was conducted only 2 months before the disaster, which has led to this suspicion. The earthquake was the most damaging and the second-largest in magnitude in South Korea since the first seismograph was installed in 1905. The earthquake injured 90 people, and the estimated property damage was US$ 52 million. This earthquake was preceded by the MW 5.5 Gyeongju event of 12 September 2016, which occurred ~30 km farther south on a major right-lateral fault, the Yangsan fault, which continues northward through the Pohang area.

Monitoring

A first temporary network deployed as a part of the EGS project, consisting of various instruments: (1) Eleven surface velocity seismometers; (2) nine borehole seismometers installed at depths between 100 and 150 m; (3) a borehole geophone array deployed at depths between 1360 and 1520 m, with an interstation distance of 10 m (17 sensors), which operated for 1 month from July 2017; (4) a vertical seismic profile installed at depths between 1350 and 1550 m, which partly operated during the first, second, and third stimulations (from 27 January 2016 to 2 February 2016, from 24 December 2016 to 11 January 2017, and on 5 April 2017); and, (5) a surface and borehole seismometer installed at a depth of approximately 2300 m. A second temporary network installed after the third stimulation (Kim et al., 2018), which consisted of eight short-period velocity seismometers located within 3 km of the mainshock epicentre.

Protocols

Prior to the drilling, an extensive program of geophysical site characterization was undertaken by the Korea Institute of Geoscience and Mineral Resources (KIGAM) (Korean Government Commission, 2019).

Several institutions from Korea and other countries were active in different capacities in the monitoring and analysis of the seismicity in Pohang. This complicated the exchange and analysis of data and samples.

To manage the potential for inducing unwanted earthquakes, the Pohang EGS project team monitored seismicity during injection and adjusted operations when specific magnitude thresholds were exceeded.

Public reactions

As a consequence of the earthquake, the Pohang enhanced geothermal systems project was suspended, and the Korean Government commissioned the Geological Society of Korea to produce an evaluation report. An Overseas Research Advisory Committee (ORAC) was formed.

According to Lee et al. (2019), the Pohang earthquake provides unequivocal evidence that EGS stimulation can trigger large earthquakes that rupture beyond the stimulated volume and disproves the hypothesis that the maximum earthquake magnitude is governed by the volume of injected fluids. Because that hypothesis tacitly underpins hazard-based methods used for managing induced seismicity, those methods must be revised and based on considerations of risk.

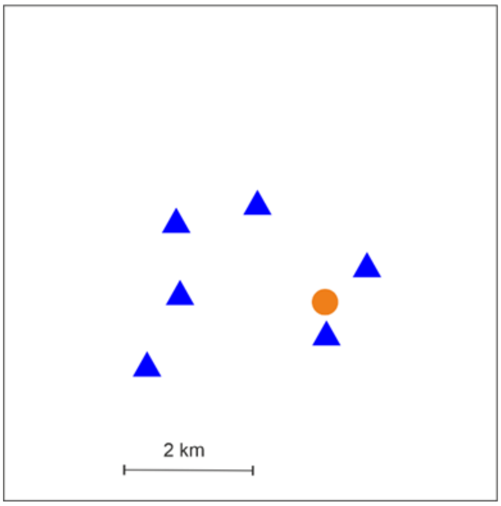

Figure 5-8:Map of the seismic network at the Pohang site. Blue triangles: temporary seismic instruments. Orange dot: Pohang EGS site.

5.3.2.10 Helsinki

Start date: 2015 drilling started (Kwiatek et al., 2019). Construction of the plant is estimated to be finished in 2020.

Location : Finland

Status : Under development

Induced seismicity: micro-seismicity, with M_{max} 2.4 (Kwiatek et al., 2019)

Description

This St1 Deep Heat Oy energy-company joint pilot project is located in the Helsinki metropolitan area, on the urban campus of Aalto University.

A 6.4-km measured depth (MD) stimulation well, OTN-3, and a 3.3-km observation well, OTN-2, were drilled not only using down-the-hole air and water hammer methods but also using rotary methods for steering purposes. Both wells are entirely located in crystalline Precambrian basement rocks consisting of granites, pegmatites, gneisses, and amphibolites. The last 1000 m of OTN-3 was drilled inclined at 42° to the northeast (NE), left uncased, and completed with a five-stage stimulation assembly. OTN-2 was drilled vertically, 10 m offset from OTN-3.

This example shows that high-precision, near–real-time monitoring and analysis of seismic data feeding a traffic light system (TLS) allowed safe stimulation of the world's deepest EGS project so far.

Natural seismicity

The closest event with claims of building damage in recent years was a MW 2.4 event in 2011, located 50 km to the NE from the project site. Two detected microearthquakes were reported to have occurred within 2 km of the drill site in 2011. These were MW 1.7 and 1.4 events and were placed at a depth of 1 km by the Helsinki area network. Both borehole array and satellite network were operating intermittently since 2016, detecting no locatable micro-seismicity at depth close to the inclined deeper section of the OTN-3 well.

Monitoring

Induced seismicity was monitored by a three-component seismic network, with all stations telemetered to the project site. The key element was a 12-level vertical array of three-component seismometers placed at depths of 2.20 to 2.65 km in the OTN-2 well. This array was complemented by an additional 12-station satellite network with seismometers installed in 0.3- to 1.15-km-deep wells at 0.6- to 8.2-km lateral offsets. In addition, a 14-station strong-motion sensor network was placed at nearby critical infrastructure sites. The objective of the borehole array and satellite network was to provide accurate induced-earthquake hypocentre locations and magnitudes for both industrial (stimulation of a permeable fracture network) and regulatory (TLS) purposes. The strong-motion network was aimed at providing direct evidence of potentially damaging shaking.

Protocols

A MW 2.0 event was prescribed by local authorities as the upper limit to the earthquake that could be induced at the depth of the stimulation. This limit was based on the expected peak ground velocity (PGV) at the surface from such an earthquake—a limit substantially below local building codes. Exceeding MW 2.0 (red TLS conditions) would trigger the shut-in of the well, and no further injection would be allowed without new approvals from Finnish authorities. This challenging prescribed limit accounted for potential nuisance effects to the local population and existence of sensitive instrumentation and supercomputing facilities near the St1 project site. Larger events with M W ≥ 1.3 (amber TLS conditions) needed to be reported to local authorities within 20 min, but they were allowed without further consultation.

Public reaction

Not available.

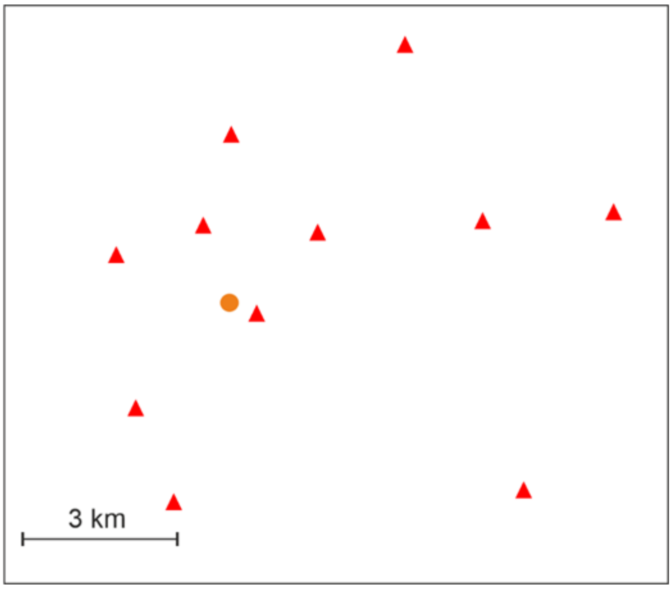

Figure 5-9:Location of St1 Deep Heat Oy project site and the seismic network used to monitor the stimulation campaign. Red triangles: seismic stations. Orange circle: geothermal site.

5.4 Guidelines and decisional protocols

The overall aim of this task is to provide suggestions for the seismic monitoring system, operational procedures, and decision protocols to be adopted at the new EGS site to achieve the following goals:

- mitigation of the induced seismicity hazard,
- optimal exploitation of the resource,
- improvement of the overall safety of the industrial activity.

Based on the review of the selected international experiences and on the studies performed in WP5 we propose some recommendations for the design and use of passive seismic micro-seismicity monitoring and EGS management procedures (e.g. traffic light procedures).During the stimulation phases of EGS projects, seismicity data are needed to understand the potential for induced seismicity and prevent the occurrence of large events, as well as assess the effectiveness of the stimulation to enhance the permeability of the reservoir.

To gain this insight it is necessary to develop a dedicated seismic monitoring system that is intended to accurately map the seismicity in the EGS reservoir and around it, and calibrate geomechanical and statistical seismological models.

A preliminary step is that of identifying the past and current natural seismicity. These data will be needed for the induced seismicity hazard and risk analysis, as well as for understanding current stress/faults/fracture patterns. To this aim, the seismic monitoring network should be in operation at least one year (possibly, even more) before the beginning of the stimulations.

An estimate of probabilistic seismic hazard can be taken from existing hazard maps. However, adjustments should be made to include natural seismic events as small as moment magnitude M 3.5, or less if possible. Low magnitude events are needed to complete the Gutenberg-Richter statistics. This will create a base-line that can differentiate natural risk from the risk induced by the EGS, where earthquakes are typically smaller than M 3.5.

The maximum magnitude/ground motion acceptable from induced seismicity depends on the local situation and should be carefully determined together with local authorities.

5.4.1 Design of the Monitoring System

The suggested network requirements comply with those included in the existing protocols and guidelines to address the induced seismicity possibly caused by EGS, i.e.: International Energy Agency (IEA) Protocol (Majer et al., 2012); GEISER Project Final Reports (GEISER, 2013); guidelines for seismic monitoring of EGS in Switzerland (Wiemer et al., 2017); guidelines for seismic monitoring in Australia (Hunt and Morelli, 2006; Morelli, 2009).

The seismic network should be made of:

1) a network of sensitive seismographs around the fracture stimulation well to allow rapid and accurate determination of hypocentral locations and magnitudes;
2) a set of accelerographs mainly in correspondence of civil infrastructures/buildings for measuring the ground motion.

The seismic monitoring system should be able to provide accurate location and origin time of micro-events, their magnitude and, possibly, their focal mechanisms. In order to identify fractures and stressed faults properly, the network should be highly sensitive to micro-seismicity, with magnitude completeness possibly approaching 0, and in any case < 1.

More specifically, the seismic network should ensure a location accuracy of ± 0.5 km horizontally and less than ± 2.0 km in depth in the expected source volume and its direct periphery, within at least 5 km distance or a distance not less than the well depth. The network geometry should be designed in order to include properly any known background seismicity or seismogenic faults close to the external boundaries. Note also that it may be necessary to adapt the network by adding/moving some stations to adequately cover the evolving seismicity as the EGS operation proceeds.

Considering the temporary network deployed for the GEMex project and the results of the analysis of the collected data we suggest the following technical specifications. For the surface network, a total of 20-25 stations, of which 10-12 within 4-5 km from the reservoir, and 10-12 in the range 5-20 km. About one third/one half of the stations should be equipped with broadband seismometers. Shallow borehole deployment (i.e. some tens of meters) is suggested, depending on the local noise level. We remind that the background noise analysis (PPSD) obtained by WP5 can be used to this aim. We suggest to equip at least one deep well with some three-component linear arrays in order to complement the surface acquisition. The number of accelerometers must be evaluated on the basis of the strategic sites to be monitored. We suggest indicatively to deploy at least 20-25 instruments.

For regulatory compliance, operational understanding, and public communication, real time analysis will be needed. Therefore, the network should be equipped with real-time communication devices so to allow a prompt event detection. All data should be continuously acquired, transmitted to a data centre, and archived for possible future use. The data should be directly available to a monitoring authority such as a national seismological service.

It is recommended that all continuous waveform data be made freely available. We also suggest to publish on a web site real-time locations and magnitudes for events which exceed a given threshold of magnitude or ground motion. For those events, selected waveforms could be made available. Seismic waveform data in central databases should be opened to research as soon as possible and indicatively after no longer than three years. Such an open data policy will allow transparency, verification, and application of advanced analysis methods.

More sophisticated analyses such as advanced location schemes or source parameter determination (e.g. double difference or waveform-based locations, tomographic analysis for improved velocity models, moment tensor analysis and joint inversions, etc.) should be implemented at a later stage, once the amount of earthquake data will allow such kind of analyses.

The monitoring system should be equipped with an automatic notification and alarming service to operators and involved authorities.

Seismic monitoring should start well before the beginning of the exploitation activity possibly with the final network settlement, in order to provide a homogenous framework for estimating both the seismicity baseline and overall sensitivity and performance.

Since fluid injection activities can induce surface deformation even in the order of some centimetres, we suggest to monitor those phenomena in order to both provide important information on the sub-surface processes and estimate the possibly damaging effects at surface. For this reason, we suggest to integrate the seismic monitoring with geodetic monitoring. The geodetic monitoring should use few permanent, continuous GPS stations (e.g. 3-4, with interdistance of 15-20 km) and DINSAR analysis with spatial and time resolution indicatively of 40-80 m and 7-15 days, respectively. Data should be analysed indicatively on a three-month basis, at least during the first years of activity.

Taking into account such guidelines as discussed in this section, the design of the seismic network at Acoculco for monitoring of the injection test planned in the Mexican GEMex has been optimised by Mexican WP 5.2 (Maldonado Hernández,, 2020; Esquivel Mendiola, 2020; López Hernández et al., 2020). For the optimisation, the background noise levels from the micro-seismic baseline monitoring (Mexican GEMex WP5, see also Chapter 3.2) and the structural settings of the area were taken into account. At least 9 of the 18 stations will be equipped with a real time transmitting system.

5.4.2 Operational Procedures

We recommend to develop a risk-based mitigation plan. In general, direct mitigation measures must be adopted in order to reduce the seismicity if the level of seismic impact becomes unacceptable for the population or the seismological parameters indicate a possible evolution toward larger events or fault triggering.

The “traffic light” system (TLS) as devised by Bommer et al. (2006) is the only operational model currently adopted for EGS activities. It is defined by three operational levels, each associated to a colour and a type of intervention, and it requires a real-time seismic monitoring, with a processing that runs continuously, so to feed the TLS itself. The first level is the “green” and it corresponds to regular operations; the second one is “amber”, and it requires changes in the operations to reduce the seismic impact; the third one is “red”, and it corresponds to suspension of operations. Each level (i.e. colour) is defined by thresholds associated to a number of selected parameters, a task that must be performed specifically for each project (i.e. when to stop, when to reduce injection, etc.). In practice, the three colours are associated to a set of increasing thresholds, which correspond to the effect of the ground motion, or its impact, in a range that goes from human perception to the damage to buildings. The parameter usually adopted for defining the ground motion effects is the peak ground velocity (PGV).

Thresholds are first inferred from some engineering recommendations and correlations between PGV and macro-seismic intensity. Then, they are converted, via locally derived attenuation equations, into equivalent magnitudes for events occurring within the expected depth range. The TLS also includes the assumption of a frequency-magnitude relationship.

One of the major shortcomings of the basic TLS approach is that it does not address the issue of seismicity that occurs after the suspension of the pumping operation. The recent (2017) M_W5.5 earthquake in Pohang (e.g. Ellsworth et al., 2019) represents a relevant case-history of this kind of failure. In fact, while the TLS triggered a number of times, leading to several temporary reductions of the fluid injection, it was ineffective to prevent the triggering of a larger, existing, local fault. The gained experience leads us to state the following further suggestions.

First, it is important a careful mapping of existing local fault zones. These zones should be described (e.g. by seismic data, stress regime and orientation measurements, …) in order to define the main fault parameters (e.g. geometry, faulting style, …) and the prevailing stress regime, to be used as an input for assessing the earthquake triggering potential. Particular emphasis should be driven to identify faults which are susceptible to slip in the prevailing stress regime owing to the fluid/pressure diffusion. Any anomalies during deep-well drilling, as a significant loss of heavy drilling mud, may highlight the presence of fault zones.

Second, adopt near real-time analysis procedures within the monitoring system. Procedures should be focused to obtaining accurate hypocentres and source parameters (whenever possible) and documenting the evolution of the seismicity, rather than to the narrow focus of switching the TLS levels. The quantitative information needed to update models and feed decisions should be available within a few days (if not hours), as a variation of the seismological parameters shows up.

A TLS-approach aimed at keeping induced seismicity below a threshold magnitude (e.g., M 2 or 2.5) is not enough, since it is not able to address the potential for a larger earthquake triggered by the injected fluid diffusion on existing faults. Some statistical seismological parameters should be implemented into the automatic TLS (e.g. rate-number of events, Gutenberg Richter’s a and b coefficients), besides the classical used parameters (i.e. earthquake magnitude and ground motion parameters, as PGV). Mw magnitude calculation is recommended.

Third, some advanced analyses should be implemented in order to evaluate the spatial-temporal evolution of seismicity, such as spatial clustering along possible fault planes or diffusion at large distance from the injection wells, especially toward some known fault zones. Physical and statistical models of induced and triggered seismicity need to be developed to cover adequately the possibility that pressure perturbations induced on a fault may trigger run-away events of large magnitudes. These models will be calibrated according to the local situation.

Together with a TLS decision tree prescribing the course of action after the exceedance of some predefined thresholds, the near–real-time earthquake information has to be used by the TLS operator to provide feedback to the stimulation engineers, who can control the pumping rates and well head pressures. The original stimulation strategy can therefore be modified, in response to the occurrence of enhanced seismic activity and after the improved understanding of the reservoir seismic response. For example, Kwiatek et al. (2019) claim that the procedure adopted during the stimulation of a 6.1-km-deep geothermal well near Helsinki (Finland) avoided the nucleation of a project-stopping magnitude MW 2.0 induced earthquake (the limit set by local authorities). Their approach, based on a high-precision, near–real-time monitoring and analysis of seismic data feeding a traffic light system (TLS), allowed a safe stimulation of the world's deepest EGS project so far.

Finally, it would be desirable that EGS and related stimulation activities use a risk-based TLS that adapts to evolving hazards such as fault activation from multiple stimulations. The hypothesis that the maximum earthquake magnitude is governed only by the volume of injected fluids cannot be assumed for risk-evaluation. Hazard-based methods must be revised accordingly, because the largest the volume injected and the extension of the affected volume, the largest is the possibility to intersect existing faults.

However, considering the objective difficulty in implementing a risk-driven approach as well as most of the analysis described above within an automatic, adaptive TLS, we suggest that all TLS-related task be constantly monitored and supervised by a board of experts. In this respect, we suggest the adoption of the "Consensus Meeting of Experts (CMoE)" approach for both supervising the TLS behaviour and, if needed, taking non-automatic decisions. The automatic TLS (though improved through only some of the above specified features) may also be used as a trigger for starting specific analysis and activating the CMoE for specific needs.

It is really important to take into account the seismic risk properly. A risk-based framework for making operational decisions should be used and updated as new knowledge is acquired. Seismic risk scenarios should be developed to evaluate the possible consequences and to identify risk mitigation measures. An independent oversight committee or authority (perhaps the CMoE itself) should be established to provide assurance that all aspects of the project plan, protocols, and standards are designed and conducted to this aim. In Pohang EGS project, operational decision making was internal to the project team, and that proved to be a weak strategy.

Strategies and tools for monitoring, mitigating, and communicating the risk of induced seismicity should be established together with responsible authorities. The project team and the scientific institutions involved should engage in comprehensive and ongoing efforts to monitor, analyse, and understand the evolving seismic hazard. They should prioritize an open-access policy and clear channels of communication to maximize their contribution to the mitigation of seismic risk and to update information to the public authorities on the changing seismic risk conditions.

5.5 References Chapter 5

Asanuma, H., Nozaki, H., Niitsuma, H., and Wyborn, D., 2005. Interpretation of microseismic events with larger magnitude collected at Cooper Basin, Australia, Geoth. Res. T., 29, 87–91.

Bachmann, C.E., Wiemer, S., Woessner, J. and Hainzl, S., 2011. Statistical analysis of the induced Basel 2006 earthquake sequence: introducing a probability-based monitoring approach for Enhanced Geothermal Systems. Geophys. J. Int., 186(2), 793–807, doi: 10.1111/j.1365-246X.2011.05068.x.

Baisch, S., Weidler, R., Vörös, R., Wyborn, D., and DeGraaf, L., 2006. Induced seismicity during the stimulation of a geothermal HFR reservoir in the Cooper Basin (Australia), Bull. Seismol. Soc. Am. 96, no. 6, 2242–2256.

Baisch, S., Vörös, R., Weidler, R. and Wyborn, D., 2009a. Investigation of fault mechanisms during geothermal reservoir stimulation experiments in the Cooper Basin (Australia), Bull. Seismol. Soc. Am. 99, no. 1, 148–158.

Baisch, S., Carbon, D., Dannwolf, U., Delacou, B., Devaux, M., Dunand, F., Jung, R., Koller, M., Martin, C., Sartori, M., Secanell, R. and Vörös, R., 2009b. Deep Heat Mining Basel - Seismic Risk Analysis - SERIANEX - Abstract.

Baisch, S., Vörös, R., Rothert, E., Stang, H., Jung, R. and Schellschmidt, R., 2010. A numerical model for fluid injection induced seismicity at Soultz-sous-Forêts, Int. J. Rock Mech. Min. Sci. 47, 405–413.

Baisch, S., Rothert, E., Stang, H., Vörös, R., Koch, C. and McMahon, A., 2015. Continued Geothermal Reservoir Stimulation Experiments in the Cooper Basin (Australia). Bull. Seismol. Soc. Am., 105(1), 198–209. doi: https://doi.org/10.1785/0120140208.

Baria, R., Hearn, K., Lanyon, G., & Batchelor, A., 1984. Camborne School of Mines geothermal energy project, microseismic results, Tech. rep., Camborne School of Mines.

Batchelor, A. S., Baria, R. and Hearn, K., 1983. Monitoring the effect of hydraulic stimulation by microseismic event location: a case study." SPE 58 th Ann. Tech. Conf ., San Francisco, Calif., USA, Oct. (SPE 12109).

Batchelor, A.S. and Garnish, J.D., 1990. The industrial exploitation of geothermal resources in Europe. Tectonophysics 178, 269–276.

BGS (1991). SW England seismic monitoring for the HDR Geothermal programme (1989-September 1991). British geological Survey Global Seismology Report No WL/91/36.

Bommer, J.J., Oates, S., Cepeda, J.M., Lindholm, C., Bird, J., Torres, R., Marroquín, G., Rivas, J., 2006. Control of hazard due to seismicity induced by a hot fractured rock geothermal project, Eng. Geol., 83, 287–306.

Bönnemann, C., Schmidt, B., Ritter, J., Gestermann, N., Plenefisch, T. and Wegler, U., 2010. Das seismische Ereignis bei Landau vom 15 August 2009 (The seismic event near Landau of 15th August 2010). Final report by the expert panel on seismic risk associated with hydrothermal geothermal plants, Landesamt für Geologie und Bergbau of Rheinland-Pfalz (Regional authority for geology and mines of Rheinland-Pfalz), 54 pp.

Breede, K., Dzebisashvili, K., Liu, X. and Falcone, G., 2013. Overcoming challenges in the classification of deep geothermal potential, Geotherm Energ., 1, doi:10.1186/2195-9706-1-4, 2013.

Breede, K., Dzebisashvili, K. and Falcone, G., 2015. A systematic review of enhanced (or engineered) geothermal systems: past, present and future, Geotherm Energ., 3, 19–39, doi:10.5194/gtes-3-19-2015.

Bromley, C.J. and Mongillo, M.A., 2008. Geothermal energy from fractured reservoirs - dealing with induced seismicity. In: IEA OPEN Energy Technology Bulletin, Issue No. 48. IEA., http://www.iea.org/impagr/cip/pdf/Issue48Geothermal.pdf.

Bromley, C.J. and Majer, E.L., 2012. Geothermal Induced Seismicity - Risks and Rewards, in: Proceedings of New Zealand Geothermal Workshop. Auckland, New Zealand.

Bromley, C., 2012. Geothermal induced seismicity: summary of international experience. Oral presentation presented at IEA-GIA Environmental Mitigation Workshop 2012, Taupo, 15–16 June 2012.

Brown, D., 1995. The US Hot Dry Rock program - 20 years of experience in reservoir testing. Paper presented at world geothermal congress 1995, Firenze, 18–31 May 1995.

Brown, D., 2009. Hot Dry Rock Geothermal Energy: important lessons from Fenton Hill. Paper presented at thirty-fourth workshop on geothermal reservoir engineering, Stanford University, Stanford, 9–11 Feb 2009.

Charléty, J., Cuenot, N., Dorbath, L., Dorbath, C., Haessler, H. and Frogneux, M., 2007. Large earthquakes during hydraulic stimulations at the geothermal site of Soultz-sous-Forêts, International Journal of Rock Mechanics & Mining Sciences, 44, 1091-1105.

Cladouhos, T., Petty, S., Foulger, G., Julian, B. and Fehler, M., 2010. Injection induced seismicity and geothermal energy, Geothermal Resources Council Transactions, 34, 1213-1220.

Cuenot, N., Frogneux, M., Dorbath, C. and Calo', M., 2011. Induced microseismic activity during recent circulation tests at the EGS site of Soultz-sous-Forêts (France), Proceedings, 36th Workshop on Geothermal Reservoir Engineering, Stanford University, Stanford, California, USA.

Cummings RG, Morris GE (1979) Economic modeling of electricity production from Hot Dry Rock geothermal reservoirs: methodology and analysis. EA-630, Research Project 1017 LASL (LA-7888-HDR). OSTI Information Bridge., http://www.osti.gov/bridge/servlets/purl/5716131-wg4gUV/native/5716131.pdf. Accessed 31 May 2013

Deichmann, N., and Giardini, D., 2009. Earthquakes induced by the stimulation of an enhanced geothermal system below Basel (Switzerland): Seismological Research Letters, 80, 784–798, doi: 10.1785/gssrl.80.5.784.

Dewey, J.W., White, R.A. and Hernandez, D.A., 2004. Seismicity and tectonics of El Salvador. In: Rose, P., et al. (Eds.), Natural Hazards in El Salvador. Geological Society of America Special Paper 375, pp. 363–378.

Doglioni, C., 2018. A classification of induced seismicity. Geoscience Frontiers, 9, 1903-1909.

Dorbath, L., Cuenot, N., Genter, A. and Frogneux, M., 2009. Seismic response of the fractured and faulted granite of Soultz-sous-Forêt (France) to 5 km deep massive water injections, Geophys. J. Int. 177, no. 2, 653–675.

Dost, B., Goutbeek, F., van Eck, T. and Kraaijpoel, D., 2012. Monitoring induced seismicity in the North of the Netherlands: Status report 2010, KNMI Sci. Rep. WR 2012-03, Royal Netherlands Meteorol. Inst. (KNMI), De Bilt, Netherlands.

Edwards, B., Kraft, T., Cauzzi, C., Kaestli, P. and Wiemer, S., 2015. Seismic monitoring and analysis of deep geothermal projects in St. Gallen and Basel, Switzerland, Geophys. J. Int., 201(2), 1020–1037.

Ellsworth, W.L., Giardini, D., Townend, J., Ge, S. and Shimamoto, T., 2019. Triggering of the Pohang, Korea, Earthquake (MW 5.5) by enhanced geothermal system stimulation. Seismological Research Letters, 90(5), 1844–1858.

Esquivel Mendiola, L.I., 2020. Optimización de redes de monitoreo sísmico aplicado a campos geotérmicos, Master thesis, Posgrado en Ciencia de la Tierra, Instituto de Geofísica de la UNAM.

Evans, K., Zappone, A., Kraft, T., Deichmann, N. and Moia, F., 2012. A survey of the induced seismic responses to fluid injection in geothermal and CO 2 reservoirs in Europe, Geothermics 41, 30–54, doi:10.1016/j.geothermics.2011.08.002.

Foulger, G.F., Wilson, M.P., Gluyas, J.G., Julian, B.R. and Davies, R.J., 2017. Global review of human-induced earthquakes Earth-Sci. Rev., 178, pp. 438-514.

GEISER, 2013. Geothermal Engineering Integrating Mitigation of Induced Seismicity in Reservoirs, Final Reports. 2013. Available from: http://www.geiser-fp7.fr/ReferenceDocuments/Pages/ReferenceDocuments.aspx.

Genter, A., Cuenot, N., Goerke, X., Bernd, M., and Sanjuan, B., 2010. Status of the Soultz geothermal project during exploitation between 2010 and 2012. 37th Workshop on Geothermal Reservoir Engineering, Stanford University, California, USA, Jan 2012, Stanford, United States. SGP-TR-194, 12 p., 2012.

Giardini, D., Wiemer, S., Fäh, D., Deichmann, N., 2004. Seismic Hazard Assessment of Switzerland. Swiss Seimological Service, ETH Zürich, Switzerland, 82 pp.

Giardini, D., 2009. Geothermal quake risks must be faced, Nature, 461, 848–849.

Gibowicz, S.J., Kijko, A., 1994. An Introduction to Mining Seismology. Academic Press, San Diego, California.

Grigoli, F., Cesca, S., Priolo, E., Rinaldi, A.P., Clinton, J.F., Stabile, T.A., Dost, B., Garcia Fernandez, M., Wiemer, S., and Dahm, T., 2017. Current challenges in monitoring, discrimination, and management of induced industrial activities: a European Perspective, Rev. Geophys., **55**, doi:10.1002/2016RG000542.

Grigoli, F., Cesca, S., Rinaldi, A.P., Manconi, A., López-Comino, J.A., Clinton, J.F., Westway, R., Cauzzi, C., Dahm, T. and Wiemer, S., 2018. The November 2017 M W 5.5 Pohang earthquake: A possible case of induced seismicity in South Korea. Science, 360(6392), 1003–1006. https://doi.org/10.1126/science.aat2010.

Grünthal, G., 2014. Induced seismicity related to geothermal projects versus natural tectonic earthquakes and other types of induced seismic events in Central Europe. Geothermics 52, 22–35.

Häering, M.O., Schanz, U., Ladner, F. and Dyer, B.C., 2008. Characterisation of the Basel 1 enhanced geothermal system, Geothermics, 37(5), 469–495.

Healy, J.H., Rubey, W.W., Griggs, D.T. and Raleigh, C.B.,1968. The Denver earthquakes. Science, v. 161, p. 1301-1310.

Helm, J., 1996. The natural seismic hazard and induced seismicity of the European HDR (Hot Dry Rock) geothermal energy project at Soultz-sous-Forêts (Bas-Rhin, France), PhD thesis. Univ. Louis Pasteur, Strasbourg, France.

House, L., 1987. Locating microearthquakes induced by hydraulic fracturing in crystalline rock, Geophys.Res.Lett., 14(9), 919-921.

Hunt, S.P., and Morelli, C.P., 2006. Cooper Basin HDR Seismic Hazard Evaluation: Predictive modelling of local stress changes due to HFR geothermal energy operations in South Australia.

Jolie, E., Bruhn, D., López Hernández, A., Liotta, D., Garduño-Monroy, V.H., Lelli, M., Hersir, G.P., Arango-Galván, C., Bonté, D., Calcagno, P., Deb, P., Clauser, C., Peters, E., Hernández Ochoa, A.F., Huenges, E., González Acevedo, Z.I., Kieling, K., Trumpy, E., Vargas, J., Gutiérrez-Negrín, L.C., Aragón-Aguilar, A., Halldórsdóttir, S., González Partida, E., van Wees, J.D., Ramírez Montes, M.A., Diez León, H.D. and the GEMex team, 2018. GEMex – A Mexican-European Research Cooperation on Development of Superhot and Engineered Geothermal Systems, February 2018 Conference: 3rd Workshop on Geothermal Reservoir Engineering, StanfordAt: Stanford University, Stanford, California, February 12-14, 2018.

Kim, K.-H., Ree, J.-H., Kim, Y., Kim, S., Kang, S. Y. and Seo, W., 2018. Assessing whether the 2017 M W 5.4 Pohang earthquake in South Korea was an induced event. Science, 360(6392), 1007–1009. https://doi.org/10.1126/science.aat6081.

Korean Government Commission (2019). Summary report of the Korean Government Commission on relations between the 2017 Pohang Earthquake and EGS Project, Geological Society of Korea, Seoul, South Korea, doi: 10.22719/KETEP-20183010111860.

Kraft, T., Mai, P.M., Wiemer, S., Deichmann, N., Ripperger, J., Kästli, P., Bachmann, C., Fäh, D., Wössner, J. and Giardini, D., 2009. Enhanced geothermal systems in urban areas: Lessons learned from the 2006 Basel ml 3.4 earthquake, EOS, 32(90), 273–274.

Kraft, T., and N. Deichmann, 2014. High-precision relocation and focal mechanism of the injection-induced seismicity at the Basel EGS, Geothermics, 52, 59–73.

Kwiatek G., Saarno, T., Ader, T., Bluemle, F., Bohnhoff, M., Chendorain, M., Dresen, G., Heikkinen, P., Kukkonen, I., Leary, P., Leonhardt, M., Malin, P., Martínez-Garzón, P., Passmore, K., Passmore, P., Valenzuela, S., Wollin, C., 2019. Controlling fluid-induced seismicity during a 6.1-km-deep geothermal stimulation in Finland. Sci. Adv. 5, eaav7224.

Ledésert, B., and Hébert, R.L., 2012. The Soultz-sous-Forêts' Enhanced Geothermal System: A Granitic Basement Used as a Heat Exchanger to Produce Electricity. In J. Mitrovic (Ed.), Heat Exchangers -Basics Design Applications.INTECH Open Access Publisher.

López Hernández, A., Figueroa-Soto, A., Calò, M., 2020. Set up of an optimized seismic monitoring system for the Acoculco injection test, short report. GEMex PT1 "Gestión Técnica" and PT5.2 "Sísmica", stage 6.

Majer E., Baria, R., Stark, M., Oates, S., Bommer, J., Smith, B. and Asanuma, H., 2007. Induced seismicity associated with enhanced geothermal systems, Geothermics 36:185–222.

Majer, E., Baria, R. and Stark, M., 2009. Protocol for induced seismicity associated with Enhanced Geothermal Systems. Report produced in Task D Annex I (9 April 2008), International Energy Agency-Geothermal Implementing Agreement.

Majer, E., Nelson, J.T., Robertson-Tait, A., Savy, J. and Wong, I., 2012. Protocol for addressing induced seismicity associated with Enhanced Geothermal Systems, DOE/EE-0662, 45 p.

Majer, E., Nelson, J., Robertson-Tait, A., Savy, J. and Wong, I., 2016, Best Practices for Addressing Induced Seismicity Associated with Enhanced Geothermal Systems (EGS).

Maldonado Hernández, L.T., 2020. Exploración sísmica de la caldera de Acoculco, Puebla, Master thesis, Programa de Maestría en Geociencias y Planificación del Territorio, Instituto de Investigaciones en Ciencias de la Tierra, UMSNH.

Maurer, V., Cuenot, N., Gaucher, E., Grunberg, M., Vergne, J., Wodling, H., Lehujeur, M., Schmittbuhl, J., 2015. Seismic Monitoring of the Rittershoffen EGS Project (Alsace, France), Proceedings World Geothermal Congress 2015 Melbourne, Australia, 19-25 April 2015.

Mignan, A., Broccardo, M., Wiemer, S. and Giardini, D., 2017. Induced seismicity closed-form traffic light system for actuarial decision-making during deep fluid injections. Sci Rep 7, 13607. https://doi.org/10.1038/s41598-017-13585-9.

MIT group: Tester, J.W., Anderson, B.J., Batchelor, A.S., Blackwell, D.D., DiPippo, R., Drake, E.M., Garnish, J., Livesay, B., Moore, M.C., Nichols, K., Petty, S., Toksöz, M.N., Veatch, R.W. Jr, 2006. The Future of geothermal energy - impact of enhanced geothermal systems on the United States in the 21st Century. US Department of Energy, Washington, D.C.

Morelli, C.P., 2009. Analysis and Management of Seismic Risks Associated with Engineered Geothermal System Operations in South Australia. Report Book 2009/11, Petroleum and Geothermal Group, Department of Primary Industries and Resources South Australia, Adelaide. http://www.pir.sa.gov.au/__data/assets/pdf_file/0018/113616/rb2009_11_www.pdf.

Musson, R.M.W, 2000. The seismicity of Cornwall and Devon Geoscience in South-West England, 10, pp. 34-36.

National Research Council (NRC), 2013. Induced Seismicity Potential in Energy Technologies, Natl. Acad. Press, Washington, D. C., doi:10.17226/13355.

Petersen, M.D., Mueller, C.S., Moschetti, M.P., Hoover, S.M., Llenos, A.L., Ellsworth, W.L. and Rukstales, K.S., 2016. Seismic-hazard forecast for 2016 including induced and natural earthquakes in the Central and Eastern United States, Seismol. Res. Lett., 87(6), 1327–1341.

Priolo, E., Romanelli, M., Plasencia Linares, M.P., Garbin, M., Peruzza, L., Romano, M.A., Marotta, P., Bernardi, P., Moratto L., Zuliani, D. and Fabris, P., 2015. Seismic monitoring of an underground natural gas storage facility: The Collalto Seismic Network, Seismol. Res. Lett., 86(1), 109–123, doi:10.1785/0220140087.

Pursley, J., Bilek, S.L. and Ruhl, C., 2013. Earthquake catalogs for New Mexico and bordering areas: 2005-2009, New Mexico Geology, v. 35, no. 1, 3-12.

Sasaki, S., 1998. Characteristics of microseismic events induced during hydraulic fracturing experiments at the Hijiori hot dry rock geothermal energy site, Yamagata, Japan. Tectonophysics, 289:171–188.

Sasaki, S. and Kaieda, H., 2002. Determination of Stress State from Focal Mechanisms of Microseismic Events Induced During Hydraulic Injection at the Hijiori Hot Dry Rock Site. Pure appl. geophys. 159, 489–516. https://doi.org/10.1007/PL00001262

Shapiro, S. A., 2015. Fluid-Induced Seismicity, Cambridge University Press, Cambridge, U. K.

Slemmons, D.B., 1975. "Fault activity and seismicity near the Los Alamos Scientific Laboratory Geothermal Test Site, Jemez Mountains, New Mexico," Los Alamos Scientific Laboratory report LA-59-11-MS, Los Alamos, New Mexico (1975).

Tester, J.W., Brown, D.W. and Potter, R.M., 1989. Hot dry rock geothermal energy - a new energy agenda for the 21st century. Los Alamos National Laboratory report LA-11514-MS. US Department of Energy, Washington D.C.

Trutnevyte, E. and Wiemer, S., 2017. Tailor-made risk governance for induced seismicity of geothermal energy projects: An application to Switzerland, Geothermics, 65, 295–312.

Turbitt, T., Walker, A.B. and Browitt, C.W.A., 1987. Perceptible Hydrofracture Seismic Events Caused by the Hot-dry-rock Geothermal Project in Cornwall (G. S. R. Group, Trans.). British Geological Survey.

Wiemer, S., Kraft, T. and Landtwing, D., 2014. Seismic risk, in Energy from the Earth: Deep geothermal as a resource for the future? TA Swiss Geothermal Project Final Report, edited by S. Hirschberg, S. Wiemer, and P. Burgherr, pp. 263–295, Paul Scherrer Inst., Villigen, Switz.

Wiemer, S., Kraft, T., Trutnevyte, E. and Roth, P., 2017. "Good Practice" Guide for Managing Induced Seismicity in Deep Geothermal Energy Projects in Switzerland, Swiss Seismological Service, https://archive-ouverte.unige.ch/unige:101570.

Wilson, M.P., Davies , R.J., Foulger, G.R., Julian, B.R., Styles, P., Gluyas, J.G., and Almond, S., 2015. Anthropogenic earthquakes in the UK: A national baseline prior to shale exploitation, Marine and Petroleum Geology, 68, 1-17.

Wohlenberg, J. and Keppler, H., 1987. Monitoring and interpretation of seismic observations in hot dry rock geothermal energy systems, Geothermics, 16(4), 441–445.

Acknowledgements

This publication is part of a project that received funding by the European Union's Horizon 2020 research and innovation programme under grant agreement number 727550 and the Mexican Energy Sustainability Fund CONACYT-SENER, project 2015-04-268074.

We acknowledge the Comisión Federal de Electricidad (CFE) for kindly providing the data. We also acknowledge all our European and Mexican colleagues within GEMex for their help and collaboration. A particular acknowledgement is for Ruth Alfaro and Zayre Ivonne González Acevedo from CICESE, Mexico and Matteo Lelli from CNR, Italy for their field work relating to soils and water sampling analysis and comments to the document. Also Angel Figueroa (CONACyT) and Marco Caló (UNAM) are gratefully acknowledged for sharing the micro-seismic monitoring data.

The content of this report reflects only the authors' view. The Innovation and Networks Executive Agency (INEA) is not responsible for any use that may be made of the information it contains.

Appendices Chapter 2

Appendix 1 Main chemical parameter in Acoculco waters (DRY Season)

	Coordinates		EC	pH	Eh	T °C	SO_4^{2-}	NO_3^-	Cl^-	F^-	NO_2^-	NO_3^-	PO_4^{3-}
	X	Y	µS/cm		mV		mg/L	mg/L	mg/L	mg/L	mg/L	mg/L	mg/L
A15Ac1a	589559	2203112	508	4.68	-111	21.5	292.6	7.14	7.14				
A15Ac1b	589559	2203142	503	5.03	33	27.2	559.0	683.23	683.23	8.33			
A15Ac2	589574	2203136	900	6.11	-163	28.2	81.8	4.00	4.00				
A15Ac3	589585	2203137	506	3.75	139	25.1	4.0						
A15Ac4	589544	2203149	473	4.29	-48	28	28.0						
A15Ac5	590181	2203216	218	6.6	-3	24.2	75.7	3.00	3.00				
A16Ac1	589493	2203092	464	7.94	183	15	184.2				0.019	0	0.25
A16Ac3	587900	2202616	427	4.71	312	12.9	188.6	8.00	8.00		0.00	0.012	2.27
A16Ac4	589991	2202767	1132	3.54	446	14.9	549.2	7.22	7.22	0.6	0.00	4.6	2.18
A16Ac6	588198	2202767	844	3.93	346	16.7	354.8	15.1	15.1		0.01	0	0.81
A16Ac8	589020	2202923	947	7.33	186	9.8	392.5	22.48	22.48		0.043	0	0.44
A16Ac10	587929	2202635	475	4.44	336	17.5	201.7	9.00	9.00		0.039	0	0.48
A16Ac12	588273	2202643	573	6.93	120	16.9	234.2	15.24	15.24		0.031	0	0.51
A16Ac17	589594	2203113	862	6.64	-115	20.3	175.2	15.23	15.23		0.008	10.5	1.09
A17Ac5	589602	2203178	694	3.65	218.2	21.5	238.1	8.10	8.10	0.5	0.004	8.3	0.19
A17Ac13	587892	2202614	469	3.94	200.3	18.8	155.3	4.29	4.29	0.3	0.003	0	0.13
A17Ac15	587540	2202383	355	6.56	49.7	11.9	79.5	2.64	2.64	0.21	0.001	0	0.07
A18AC06.1	589565	2203206	1556	4.20		24.3					1.00	0.7	0.05
A18AC06.2	589565	2203173	4.01	3.48		20.00					14.00	1.5	0
A18AC06.3	589587	2203122	5.38	6.49		25.00					24.00	0.2	0.01
A18AC06.4	589578	2203124	5.54	3.42		28.00					0.00	0.5	0.01
A18AC06.5	589555	2203144	7.02	6.38		26.2					6.00	0.5	0.15
A18AC07	589862	2204531	2.80	6.41		19.1					4.00	0.6	0.00

Appendix 1. Main chemical parameter in Acoculco waters (DRY Season). Data from CICESE

Appendix 2 Main chemical parameter in Acoculco waters (WET Season)

	Coordinates		EC	pH	Eh	T °C	SO_4^{2-}	NO_3^-	Cl^-	F^-	NO_2^-	NO_3^-	PO_4^{3-}
	X	Y	µS/cm		mV		mg/L	mg/L	mg/L	mg/L	mg/L	mg/L	mg/L
B15Ac1	589584	2203111	483	4.17	39	18.8							
B15Ac2	589572	2203134	407	5.94	-71	27.2							
B15Ac3	589600	2203113	535	3.54	462	19.3							
B15Ac10	589862	2204423	102	5.76	80	21							
B16Ac1	589493	2203092	253	6.72	94	14.9	62.58	1.73	1.73				
B16Ac3	587900	2202616	134	6.16	97	13.5	14.79	0.47	0.47				
B16Ac5	588198	2202767	171	4.95	135	12.9	58.28	1.32	1.32				
B16Ac6	591376	2203010	539	4.96	9	17.2	77.5	1.38	1.38				
B16Ac7	589020	2202923	786	6.38	-94	20.3	77.75	4.39	4.39				
B16Ac9	587929	2202635	60	6.74	20	16.3							
B16Ac10	589473	2204381	59	6.65	72	17.9	0.79						
B16Ac11	588273	2202643	351	4.20	416	14.9	109.91	1.39	1.39				
B16Ac16	589594	2203113	11	6.65	154	13.4	7.77	2.25	2.25				
B17Ac4	587890	2202682	121	7.33	-36.7	17.2					0.009	2.2	
B17Ac5	587928	2202680	159	5.89	42	17.1					0.003	0.7	
B17Ac14	589438	2204384	52	6.32	18.4	16.1					0.004	7.5	0.06
B17Ac15	589894	2204401	237	3.63	164.9	15.1					0.002	7.5	0.1
B17Ac16	589588	2203113	519	3.51	173.1	17.5					0.014	14.2	0.16
B17Ac17	590159	2203210	253	6.00	35.3	14.8					0.001	7.2	0.09
B18AC06-1	589566	2203169	14	4.8		22.7	47		0.01				
B18AC06-2	589596	2203136	28	3.4		21.2	86	1.10	0.02		52	1.10	
B18AC06-3	589587	2203120	25	3.9		21	98						
B18AC06-4	589572	2203121	26	4.5		21	126				48		
B18AC06-5	589557	2203141	32	5.1		24	106	0.40			62	0.40	
B18AC07	589886	2204541	14	4.5		18	40	0.00			40		
B18AC08	589919	2204273	16	3.8		16.8	43	0.70	0.07		16	0.70	0.14

Appendix 2. Main chemical parameter in Acoculco waters (WET Season). Data from CICESE

Appendix 3 Analysis procedure for soil samples

Information from Zayre Ivonne González Acevedo (CICESE)
For soil analysis, all samples were freeze-dried during 72 h (LABCONCO model 7751020). Soil samples after drying, were milled in agate containers with agate mill balls to obtain particle diameters less than 2 mm. Analysis of X-ray Fluorescence was carried out with 9 g of sample and 1 g agglutinant, pressed at 10 t during 90 s to produce tablets of 4 cm diameter and 8 mm of thickness. The agglutinant was measured as blank. Prepared tablets of soil were analyzed during 35 min with an equipment of X-ray Fluorescence S8 Tiger from Bruker, of 4 MW and crystals of XS-5S, PET and LiF200. Analyses were performed in the Laboratory of Rock Analyses of the CeMIE-Geo facility in Ensenada BC, Mexico. To control accuracy, the sample analysis was performed together with the reference material: Metals in Soils (Sigma Aldrich) prepared and analyzed under the same conditions as soil samples, with recoveries between 95-105%.

Appendix 4 Major elements concentration levels in Acoculco soils (WET Season)

	Coordinates		Depth	Al	Ca	Fe	K	Mg	Na	P	S	Si	Ti	Zr
	X	Y	cm						%w					
B15Ac1a1	589584	2203111	-10	8.15	0.21	3.57	1.55	0.27	0.33	0.0903	1.00	26.30	1.02	0.25
B15Ac1a2			-20	8.50	0.21	3.03	1.61	0.28	0.34	0.0841	0.99	26.90	1.05	0.27
B15Ac1a3			-30	8.26	0.22	1.58	1.79	0.18	0.48	0.0687	0.78	28.00	0.84	0.30
B15Ac1a4			-40	8.39	0.21	1.50	1.83	0.16	0.52	0.0752	1.24	28.10	0.82	0.30
B15Ac1b1	589552	2203122	-10	7.47	0.82	2.88	1.21	0.18	0.41	0.2000	5.47	24.80	0.62	0.14
B15Ac1b2			-20	7.66	1.03	3.45	1.36	0.21	0.46	0.2300	5.40	27.30	0.68	0.14
B15Ac1b3			-30	7.67	0.76	2.50	1.50	0.20	0.51	0.1600	5.64	26.20	0.68	0.19
B15Ac1b4			-40	7.75	0.76	2.47	1.56	0.18	0.53	0.1700	5.25	26.30	0.62	0.17
B15Ac1c1	589575	2203162	-10	8.03	0.39	1.95	1.26	0.20	0.38	0.1300	14.70	24.00	0.62	0.17
B15Ac1c2			-20	8.06	0.41	1.97	1.25	0.22	0.35	0.1300	14.40	24.70	0.64	0.17
B15Ac1c3			-30	7.67	0.38	1.81	1.27	0.20	0.37	0.1200	11.90	23.90	0.64	0.18
B15Ac1c4			-40	7.29	0.50	2.03	1.43	0.20	0.42	0.1100	11.10	24.70	0.66	0.20
B15Ac3a1	589600	2203113	-10	8.23	1.05	2.76	1.70	0.12	0.76	0.1500	0.14	26.80	0.59	0.16
B15Ac3a2			-20	7.69	0.91	5.62	1.76	0.11	0.72	0.1600	0.14	26.40	0.52	0.18
B15Ac3a3			-30	7.06	0.79	2.84	1.53	0.08	0.58	0.1000	0.08	26.50	0.47	0.20
B15Ac3a4			-40	7.33	1.16	3.35	0.76	0.09	0.26	0.0766	0.05	30.90	0.46	0.21
B15Ac3b1	589601	2203150	-10	7.21	1.20	3.77	1.73	0.13	0.81	0.0498	0.03	32.60	0.53	0.11
B15Ac3b2			-20	7.31	1.25	4.86	1.94	0.14	1.02	0.0398	0.03	32.20	0.59	0.11
B15Ac3b3			-30	8.63	1.03	6.34	1.77	0.12	0.93	0.0381	0.03	26.40	0.67	0.13
B15Ac3b4			-40	9.93	0.67	9.22	2.09	0.11	1.02	0.0589	0.03	26.00	0.68	0.19
B15Ac10a1	589862	2204423	-10	10.10	1.39	6.38	0.72	0.45	0.40	0.0336	0.02	27.00	0.70	0.16
B15Ac10a2			-20	9.64	1.12	6.28	0.56	0.57	0.22	0.0225	0.01	21.90	0.64	0.16
B15Ac10a3			-30	5.41	1.17	6.52	0.57	0.63	0.19	0.0192	0.01	22.70	0.68	0.17
B15Ac10b1	589884	2204415	-10	9.19	1.83	6.40	0.75	0.32	0.58	0.1800	0.19	28.50	0.88	0.17
B15Ac10b2			-20	5.30	1.41	6.55	0.73	0.44	0.40	0.0455	0.03	25.80	0.73	0.02
B15Ac10b3			-30	6.20	1.22	6.59	0.63	0.57	0.27	0.0291	0.01	24.40	0.72	0.02

Appendix 3. Major elements concentration levels in Acoculco soils (WET Season). Data from CICESE.

Appendix 5 Major elements concentration levels in Acoculco soils (DRY Season)

	Coordinates		Depth	Al	Ca	Fe	K	Mg	Na	P	S	Si	Ti	Zr
	X	Y							%w					
A15Ac1a1	589559	2203112	-10	5.58	0.41	0.81	2.24	0.080	0.84	0.068	2.130	31.80	0.40	0.21
A15Ac1a2			-20	5.80	0.46	1.23	2.16	0.110	0.79	0.049	1.990	30.40	0.52	0.21
A15Ac1a3			-30	6.74	0.57	1.87	1.99	0.140	0.74	0.056	3.080	27.90	0.65	0.23
A15Ac1a4			-40	7.42	0.74	2.80	1.73	0.190	0.62	0.064	4.380	24.60	0.82	0.25
A15Ac1b1	589559	2203142	-10	10.00	0.34	0.77	1.36	0.230	1.05	0.088	0.810	30.80	0.42	0.00
A15Ac1b2			-20	7.12	0.42	0.97	1.80	0.130	0.52	0.066	1.010	28.60	0.80	0.35
A15Ac1b3			-30	7.11	0.40	0.84	1.94	0.130	0.56	0.069	1.030	29.70	0.85	0.37
A15Ac3a1	589585	2203137	-10	5.87	1.05	2.01	1.53	0.086	0.68	0.042	0.052	33.80	0.45	0.24
A15Ac3a2			-20	7.06	0.79	2.84	1.53	0.079	0.58	0.100	0.083	26.50	0.47	0.20
A15Ac3b1	589591	2203120	-10	6.40	5.72	3.02	0.99	0.180	0.33	0.180	0.850	23.20	0.71	0.13
A15Ac3b2			-20	7.97	0.56	2.00	0.89	0.100	0.27	0.110	0.410	30.90	0.70	0.19
A15Ac3b3			-30	7.98	0.76	2.00	1.18	0.120	0.35	0.092	0.410	29.40	0.83	0.19
A15Ac3b4			-40	7.43	0.80	2.11	1.02	0.110	0.34	0.085	0.380	31.60	0.77	0.21
A15Ac4a1	589544	2203149	-10	10.80	1.05	9.51	1.30	0.210	0.53	0.100	0.056	25.50	1.10	0.13
A15Ac4a2			-20	10.20	1.23	8.48	1.15	0.210	0.53	0.110	0.056	25.00	1.08	0.00
A15Ac4a3			-30	9.65	1.24	8.38	1.02	0.190	0.52	0.110	0.071	25.10	1.02	0.10
A15Ac4a4			-40	9.49	1.22	8.24	0.97	0.190	0.48	0.110	0.053	24.80	0.94	0.10
A15Ac4b1	589521	2203125	-10	9.28	1.13	7.96	1.31	0.190	0.56	0.160	0.079	26.70	1.02	0.10
A15Ac4b2			-20	8.68	1.24	7.03	0.87	0.180	0.44	0.100	0.064	25.80	0.90	0.09
A15Ac4b3			-30	7.74	1.33	6.01	1.07	0.190	0.63	0.051	0.041	30.10	0.98	0.09
A15Ac4b4			-40	8.50	1.36	6.16	1.06	0.200	0.74	0.031	0.049	26.50	0.98	0.09
A15Ac5a1	590181	2203216	-10	9.00	1.34	8.89	1.79	0.230	0.72	0.140	0.180	26.00	1.01	0.11
A15Ac5a2			-20	8.20	1.56	7.06	1.16	0.220	0.53	0.140	0.150	24.40	0.91	0.18
A15Ac5a3			-30	8.19	1.34	7.81	1.45	0.210	0.63	0.130	0.120	24.20	0.93	0.09
A15Ac5a4			-40	8.31	1.46	7.20	1.29	0.220	0.58	0.130	0.130	25.00	0.92	0.17
A15Ac5b1	590205	2203237	-10	7.86	1.14	6.69	1.12	0.200	0.53	0.120	0.230	23.10	0.86	0.08
A15Ac5b2			-20	8.30	1.29	8.06	1.27	0.210	0.56	0.130	0.290		0.93	0.08
A15Ac5b3			-30	8.11	1.52	7.77	1.26	0.220	0.54	0.120	0.210	23.50	0.95	0.08
A15Ac5b4			-40	8.13	1.28	6.88	1.39	0.220	0.63	0.120	0.180	24.30	0.90	0.08
A15Ac6a1	589451	2204396	-10	8.22	1.38	6.43	1.08	0.230	0.66	0.080	0.080	29.80	1.01	0.09
A15Ac6a4			-20	5.48	0.75	6.31	0.43	0.120	0.30	0.030	0.040	20.60	1.10	0.13
A18Ac8a1	590106	2204867	-10	8.53	0.61	2.83	2.00	0.213	0.71	0.255	1.210	28.50	1.02	0.18
A18Ac8a4			-40	5.18	0.53	2.44	1.06	0.223	0.38	0.111	1.930	23.70	1.24	0.34
A18Ac8b1	590106	2204867	-10	2.86	0.14	5.98	0.94	0.146	0.10	0.367	1.010	32.20	0.96	0.20

Appendix 4. Major elements concentration levels in Acoculco soils (DRY Season). Data from CICESE.

Appendix 6 Minor elements concentration levels in Acoculco soils (WET Season)

	Coordinates		As	Ba	Cl	Cr	Cu	Mn	Ni	Rb	Se	V	Zn
	X	Y						mg/Kg					
B15Ac1a1	589584	2203111	346	1600	95.8	0.837	47.8	136	22.3	221	<DL	161	34.7
B15Ac1a2			349	1600	82.5	39.4	46.5	135	<DL	238	<DL	<DL	29.6
B15Ac1a3			415	1300	<DL	10.6	40.2	116	22.2	224	<DL	102	0
B15Ac1a4			399	1600	91.1	<DL	39.4	122	<DL	219	<DL	<DL	35.7
B15Ac1b1	589552	2203122	1200	1900	187	19.1	52.9	651	30.2	142	55.4	74.2	139
B15Ac1b2			1700	2100	205	32.8	57.6	777	32.3	149	43.8	<DL	135
B15Ac1b3			1000	2200	175	<DL	45.2	561	15.1	171	77.8	<DL	110
B15Ac1b4			1100	2100	186	43.1	48.6	544	27.5	188	57.9	<DL	128
B15Ac1c1	589575	2203162	489	1400	137	23.8	47.4	268	32.8	136	21.2	103	107
B15Ac1c2			498	1200	89.4	<DL	45.3	272	21.5	137	16	<DL	93.4
B15Ac1c3			417	1500	91	<DL	46.6	239	19.1	140	<DL	<DL	94.8
B15Ac1c4			472	1500	<DL	40.8	43.9	259	25.8	176	<DL	<DL	62.6
B15Ac3a1	589600	2203113	26	1400	<DL	43	54.4	305	34.7	208	<DL	<DL	160
B15Ac3a2			22.1	1400	154	<DL	51.5	354	33.5	258	<DL	<DL	151
B15Ac3a3			29.9	<DL	135	59.9	55.8	476	42.6	294	<DL	<DL	130
B15Ac3a4			13.1	1400	148	49.3	55.8	607	35.8	96.5	<DL	<DL	134
B15Ac3b1	589601	2203150	14.1	1400	170	61.4	54.7	780	39.8	171	<DL	<DL	103
B15Ac3b2			<DL	1200	100	50.5	45.1	908	29.7	180	<DL	96.9	99.2
B15Ac3b3			15.7	1400	102	48.6	39.3	1100	42.9	178	<DL	105	121
B15Ac3b4			29.1	1200	109	53.6	43	552	49.6	96.5	<DL	188	139
B15Ac10a1	589862	2204423	<DL	615	<DL	88.8	69.9	1900	75.1	214	<DL	157	130
B15Ac10a2			<DL	387	126	66.3	64.3	1400	80.5	254	<DL	123	133
B15Ac10a3			13.3	715	103	93.5	72.3	917	88.9	266	<DL	132	140
B15Ac10b1	589884	2204415	13.1	771	149	52.4	84.1	1100	71	151	<DL	160	165
B15Ac10b2			14.7	592	66.9	91.1	64.9	1100	56.8	229	<DL	141	122
B15Ac10b3			<DL	741	<DL	78.3	61.9	1500	77.4	230	<DL	154	122

Appendix 5 Minor elements concentration levels in Acoculco soils (WET Season). Data from CICESE. DL= detection limit.

Appendix 7 Minor elements concentration levels in Acoculco soils (DRY Season)

	Coordinates		Depth	As	Ba	Cl	Cr	Cu	Mn	Ni	Rb	Se	V	Zn
	X	Y	cm						mg/Kg					
A15Ac1a1	589559	2203112	-10	714	4200	110			23.3	138	34.5	85		54.9
A15Ac1a2			-20	1400	3800	107	48.5		30.1	172	23.6	161		30.9
A15Ac1a3			-30	1400	3400				29.1	124	28.3	348	73.5	49.8
A15Ac1a4			-40	2200	1900	133	43.1		36.6	128	26.7	345	118	49.3
A15Ac1b1	589559	2203142	-10	104	713	98.8		3.99	16.6		12			24.9
A15Ac1b2			-20	313	2000	111			27	162	25.1			35.2
A15Ac1b3			-30	209	1900	102			26.5	175	26			33.9
A15Ac3a1	589585	2203137	-10		1100	164	59.4		19.7	74.1	30			88.5
A15Ac3a2			-20	29.9	1400	135	59.9		25.2	212	42.6			130
A15Ac3b1	589591	2203120	-10		1300	251	82.5		12.7	92.2	39.9			130
A15Ac3b2			-20	326	2300	151	34.3		22.9	78.3	34.3			59.6
A15Ac3b3			-30	220	2800	146	22.6		32.7	121	38.4		116	53.6
A15Ac3b4			-40	172	3300	203	44		31.1	102	30.9		114	59.4
A15Ac4a1	589544	2203149	-10	23.3	541	143	71.2		35.9	79.2	68.3		217	163
A15Ac4a2			-20	24.9	758	122	35		41.8	80.7	82.3		232	168
A15Ac4a3			-30	19.5	675	167	72.4		34.3	61	72.2		196	165
A15Ac4a4			-40	19.5	1200	192	71.8		35.4	63	69.9		184	158
A15Ac4b1	589521	2203125	-10	21	872	136	85.3		34.4	0.0	73.2		211	180
A15Ac4b2			-20	24.9	783	137	62.4		29.7	69.2	72.9		161	155
A15Ac4b3			-30	22.3	825	109	69.5		30.6	80.2	58.1		151	129
A15Ac4b4			-40		560	115	86.7		29.6	108	59.2		149	117
A15Ac5a1	590181	2203216	-10	29.2	760	160	52		33.3	84.3	68.8		238	169
A15Ac5a2			-20	24.8	900	141	94.9		28.3	86.6	76.4			164
A15Ac5a3			-30	21.9	809	132			34.3	102	67.7		190	155
A15Ac5a4			-40	21	897	141	54.5		37.8	81.5	75.1		170	165
A15Ac5b1	590205	2203237	-10	22.1	667	149	58.6		27	97.7	73.3		188	156
A15Ac5b2			-20	30.4	751	121	52.9		33.5	104	68.5		195	174
A15Ac5b3			-30	23.5	870	167	49.6	63.8	3000	65.9	182	30.1		
A15Ac5b4			-40	17.1	721	155	71.6	67.9	880	63.8	198	14.2		
A15Ac6a1	589451	2204396	-10	0.8	700	155	77.8	66.3	772	65.5	1200			
A15Ac6a4			-20	21.4	866		96.2	52.5	799	89.9	122			
A18Ac8a1	590106	2204867	-10	13.4	1400	191	60	53.1	221	31.5	179			102
A18Ac8a4			-20		943	149	27.3	52.8	311		133		162	96.5
A18Ac8b1	590106	2204867	-10	46.7	3950	221	64.9	202	197	22.5	97.7		92.2	42.8

Appendix 6. Minor elements concentration levels in Acoculco soils (DRY Season). Data from CICESE.

Appendices Chapter 4

Appendix 4-A Day 080 Spectra and Spectral Ratios

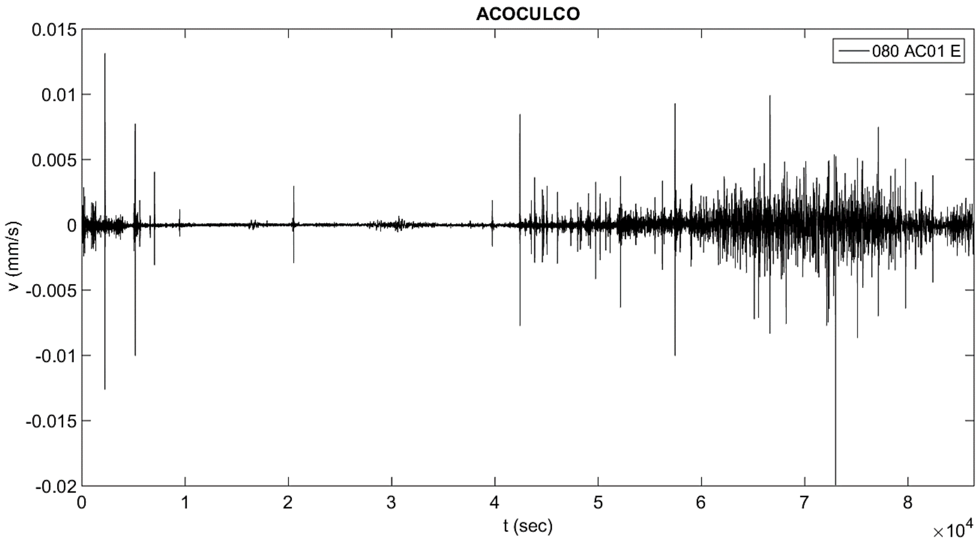

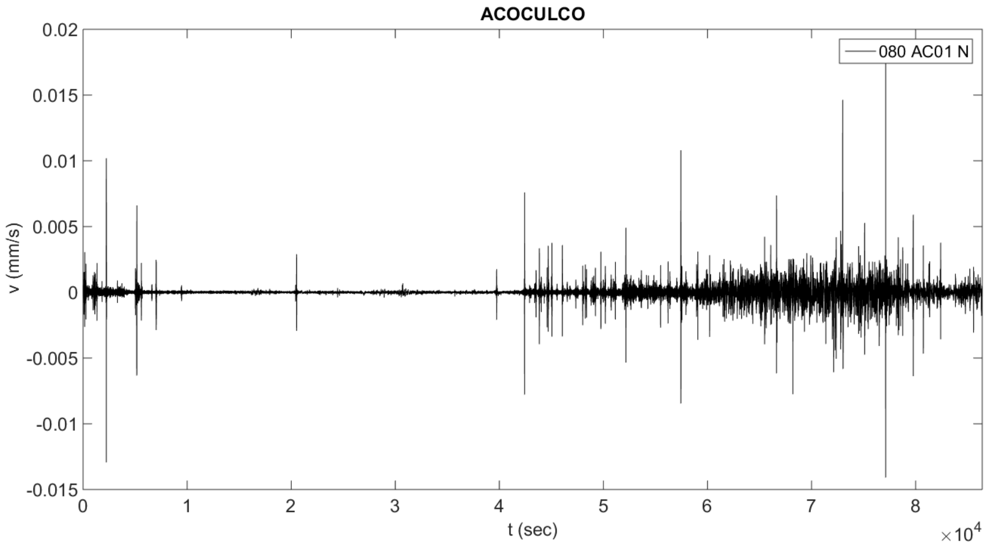

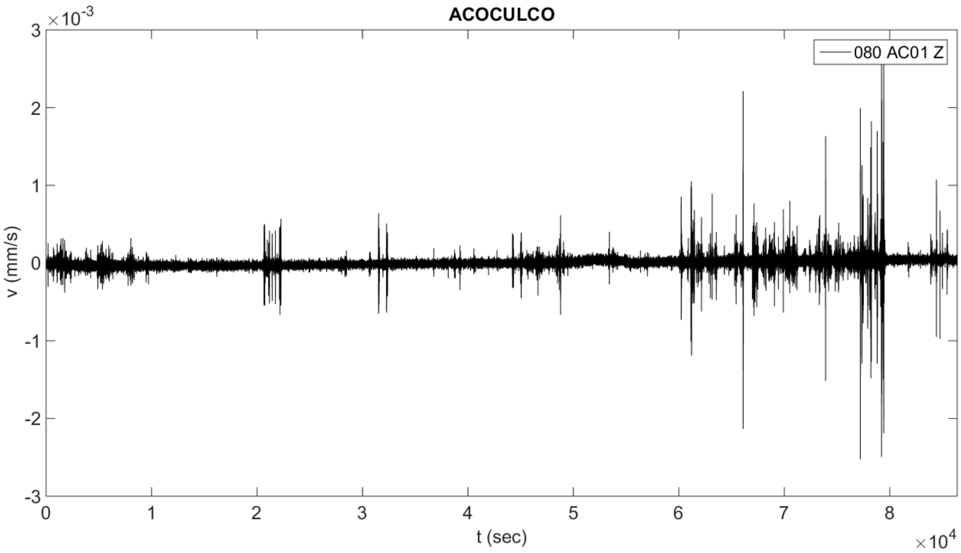

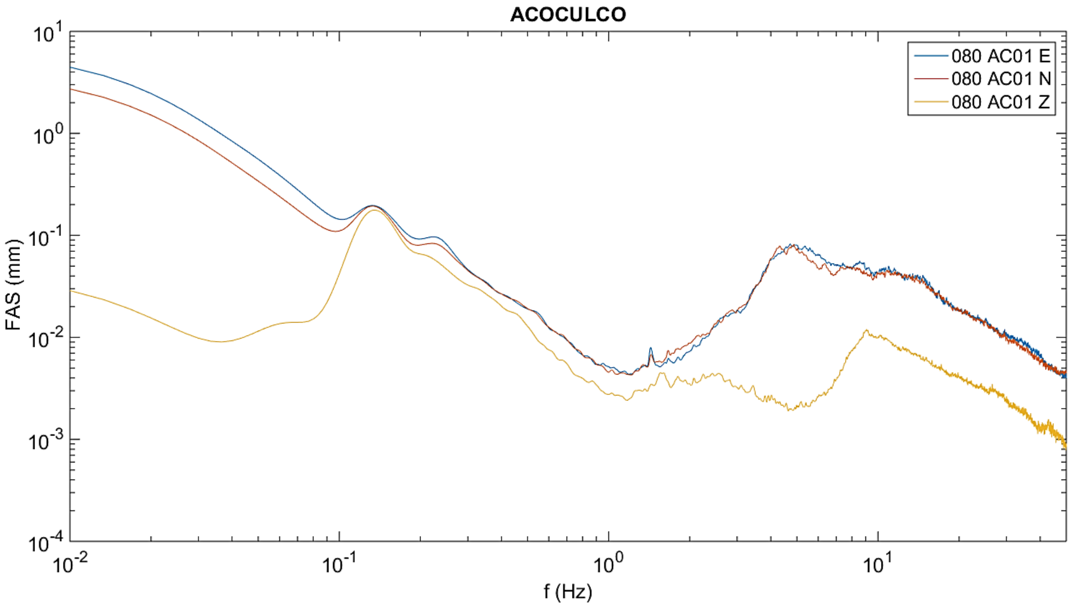
ACOCULCO
080 AC01 E
080 AC01 N
080 AC01 Z
FAS (mm)
f (Hz)

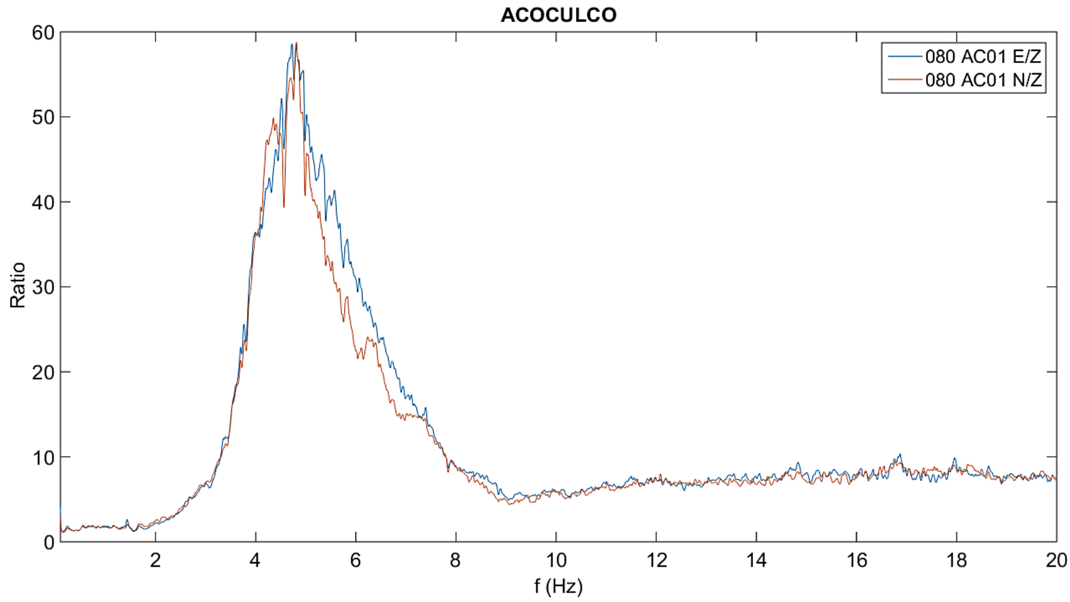
ACOCULCO
080 AC01 E/Z
080 AC01 N/Z
Ratio
f (Hz)

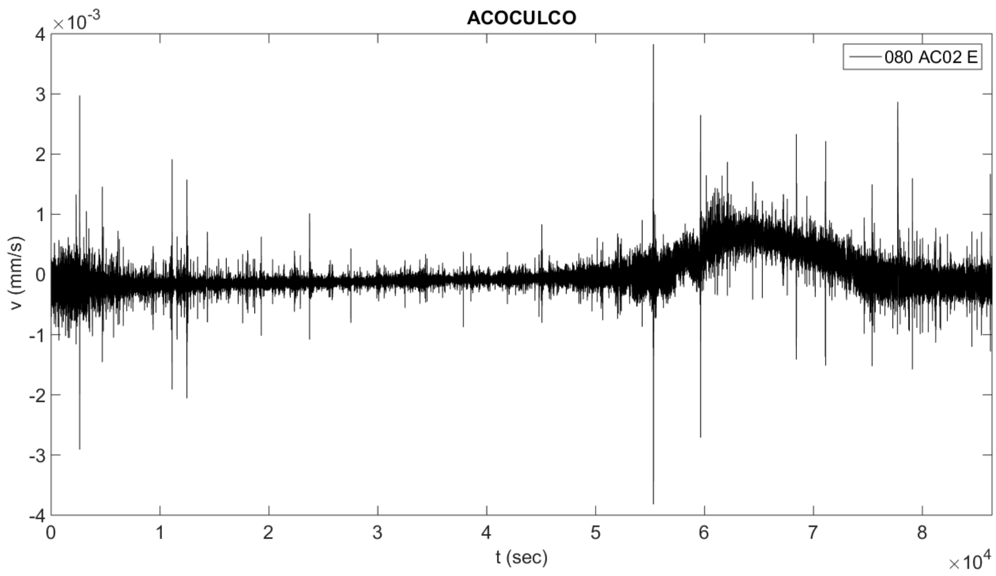
ACOCULCO
080 AC02 E
v (mm/s)
t (sec)
×10^-3
×10^4

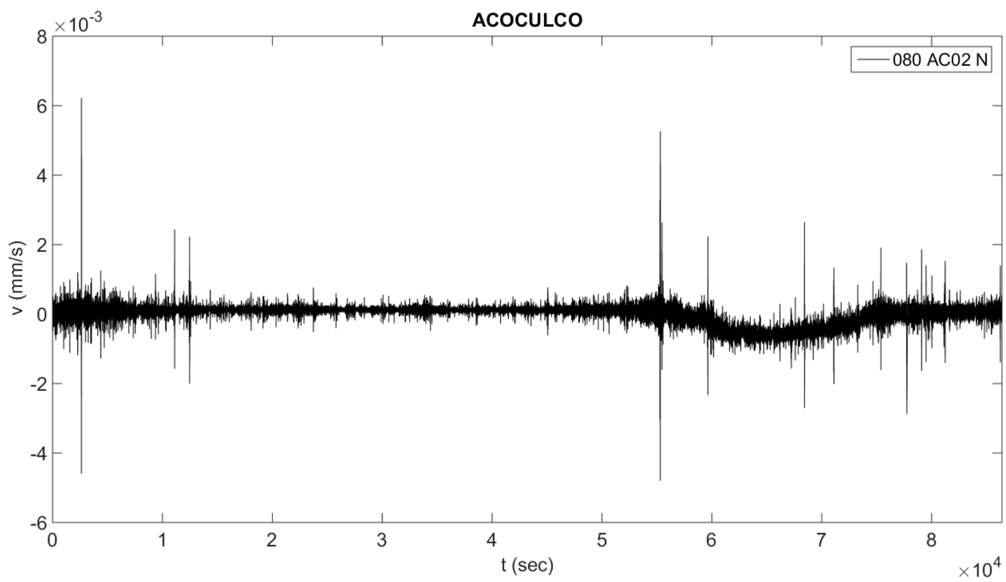
ACOCULCO
080 AC02 N
v (mm/s)
t (sec)
×10^-3
×10^4

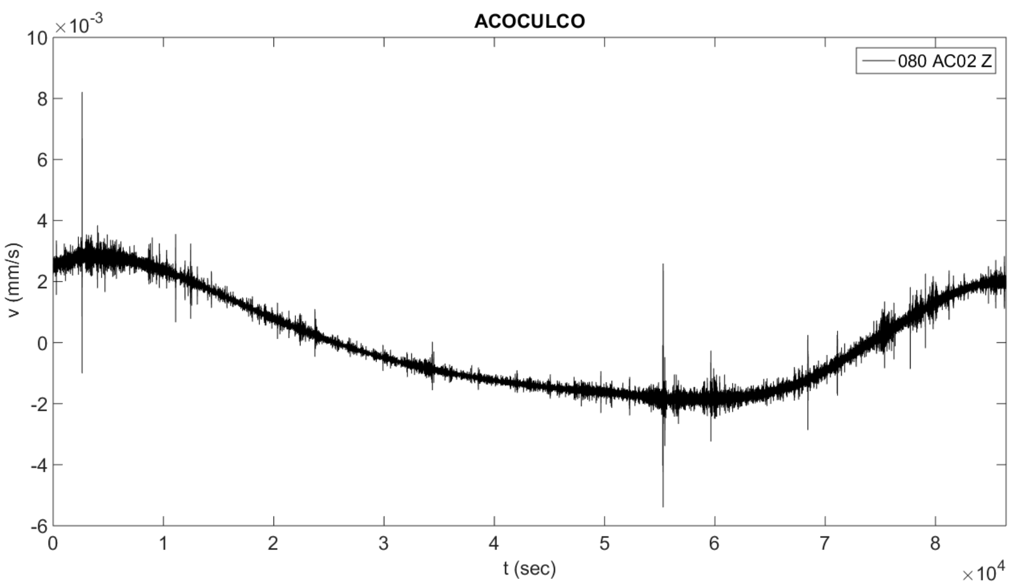
ACOCULCO
080 AC02 Z
v (mm/s)
t (sec)
×10^-3
×10^4

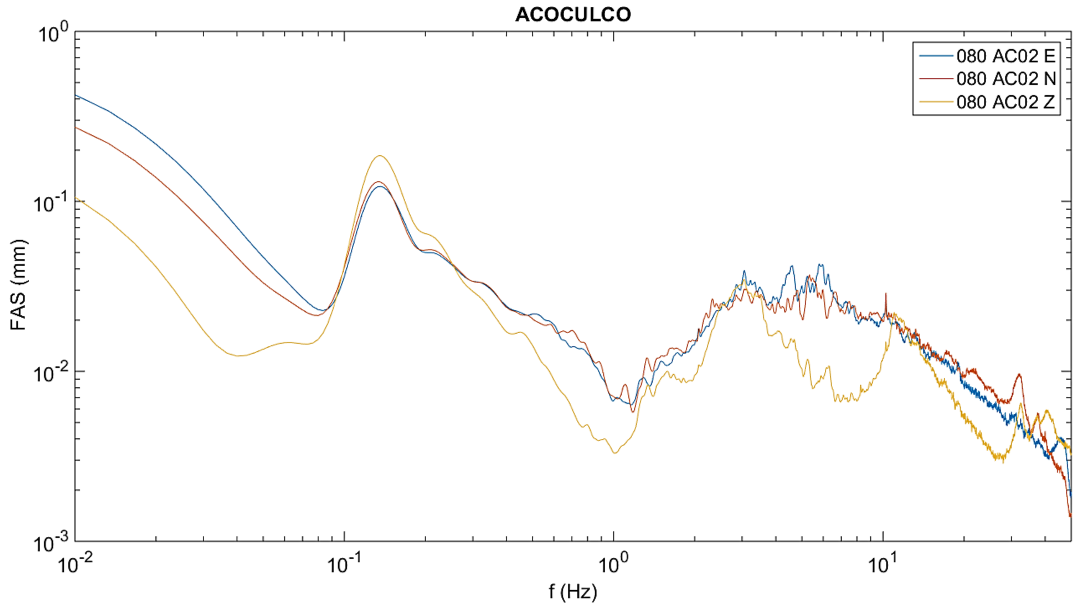
ACOCULCO
080 AC02 E
080 AC02 N
080 AC02 Z
FAS (mm)
f (Hz)

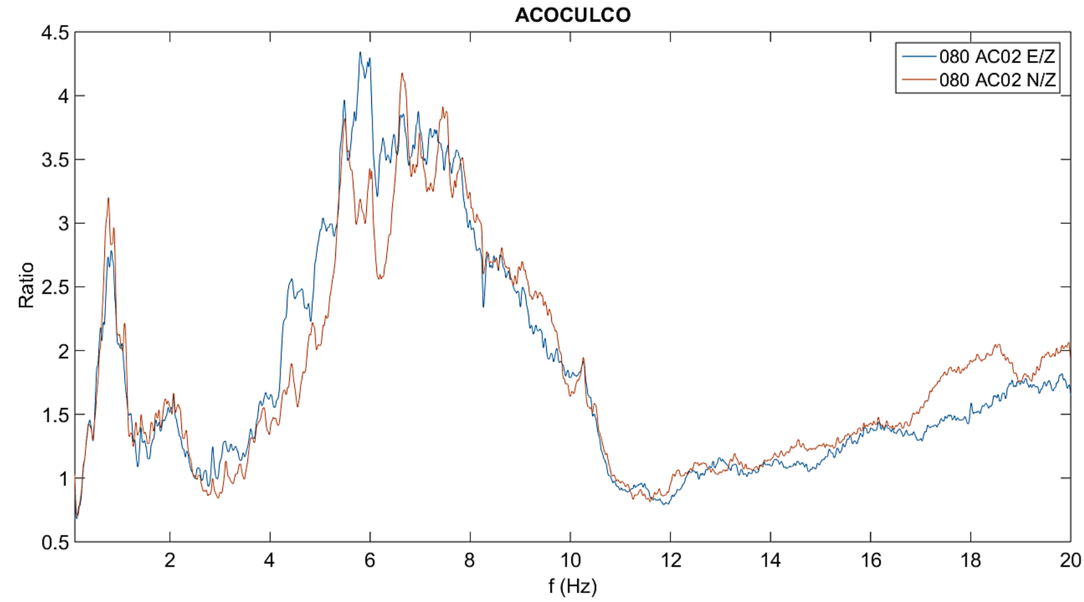
ACOCULCO
080 AC02 E/Z
080 AC02 N/Z
Ratio
f (Hz)

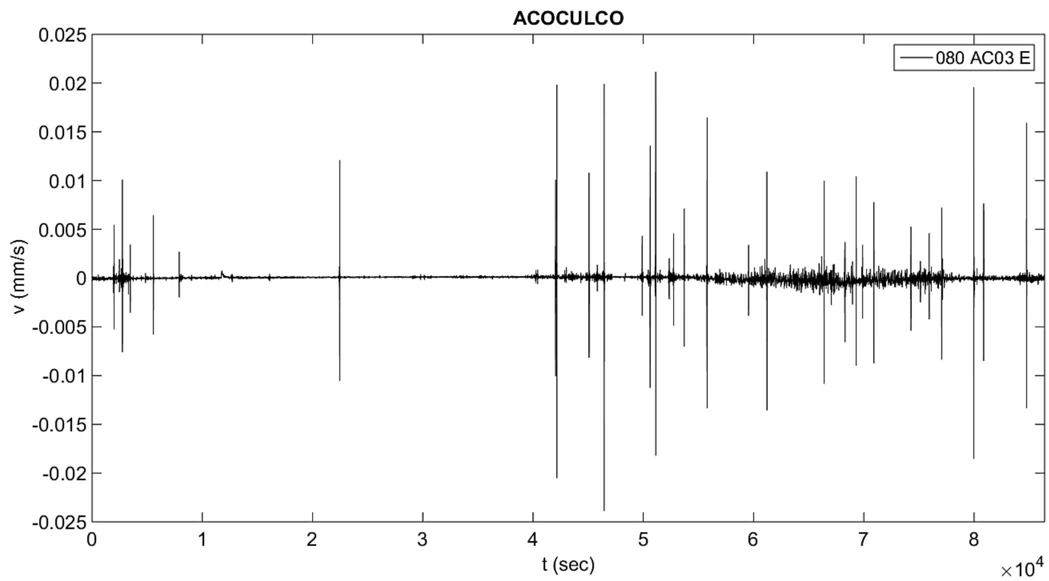
ACOCULCO
080 AC03 E
v (mm/s)
t (sec)
0.025
0.02
0.015
0.01
0.005
0
-0.005
-0.01
-0.015
-0.02
-0.025
0
1
2
3
4
5
6
7
8
$\times 10^4$

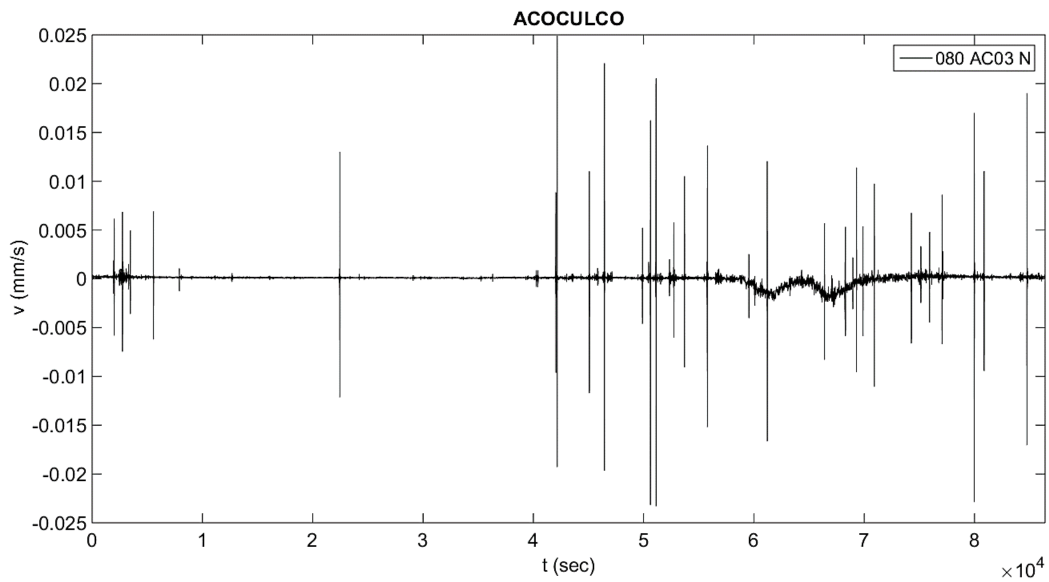
ACOCULCO
080 AC03 N
v (mm/s)
t (sec)
0.025
0.02
0.015
0.01
0.005
0
-0.005
-0.01
-0.015
-0.02
-0.025
0
1
2
3
4
5
6
7
8
$\times 10^4$

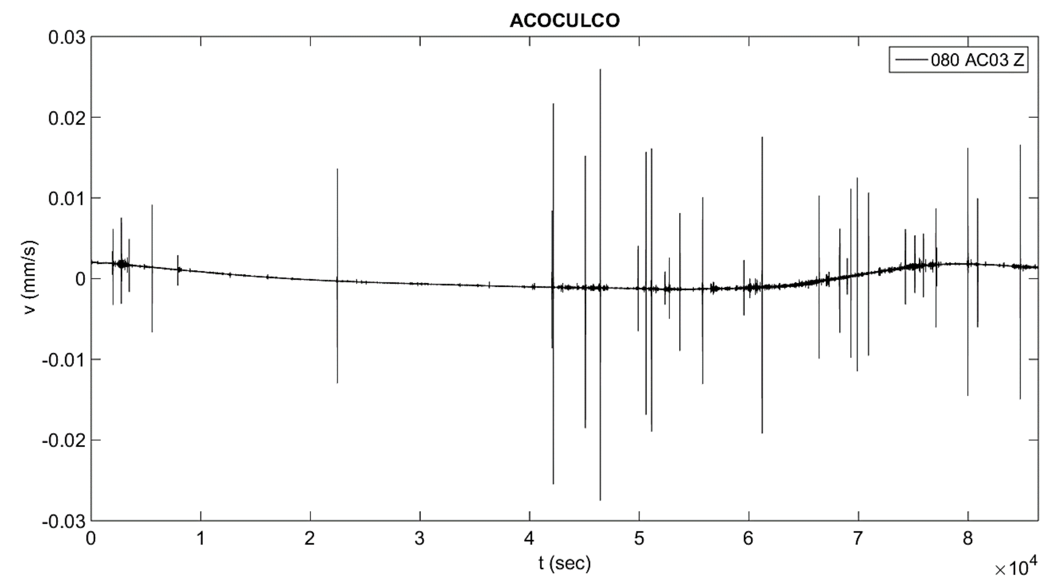
ACOCULCO
080 AC03 Z
v (mm/s)
t (sec)
0.03
0.02
0.01
0
-0.01
-0.02
-0.03
0
1
2
3
4
5
6
7
8
$\times 10^4$

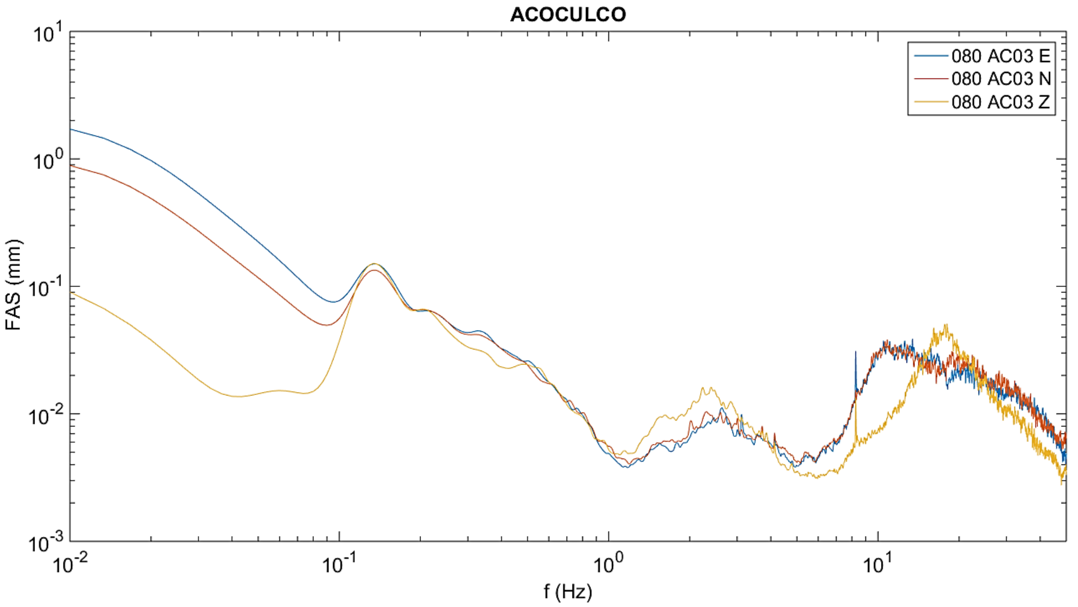
ACOCULCO
080 AC03 E
080 AC03 N
080 AC03 Z
FAS (mm)
f (Hz)

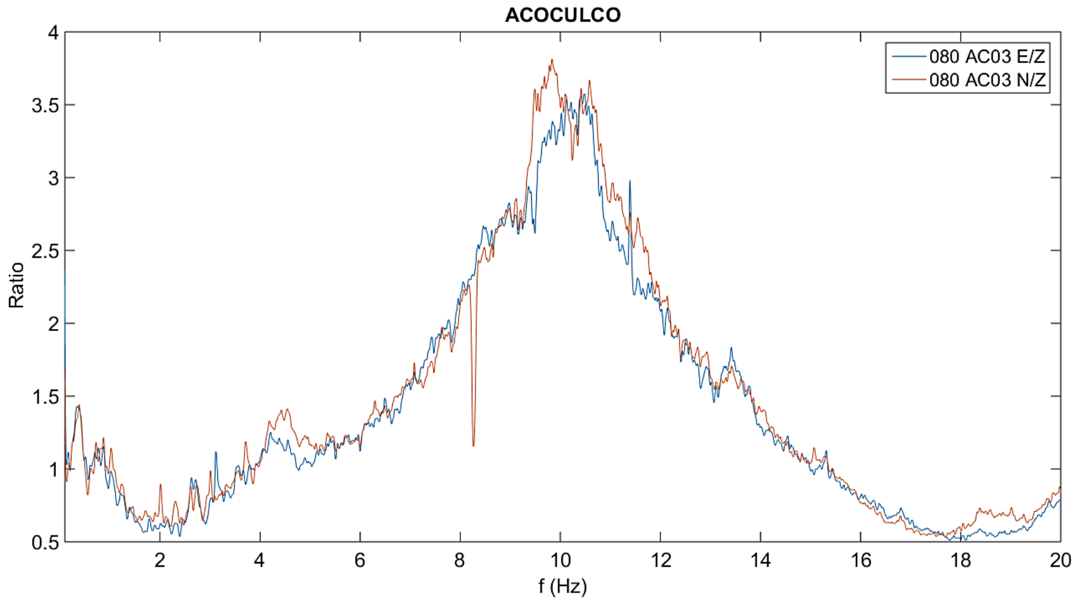
ACOCULCO
080 AC03 E/Z
080 AC03 N/Z
Ratio
f (Hz)

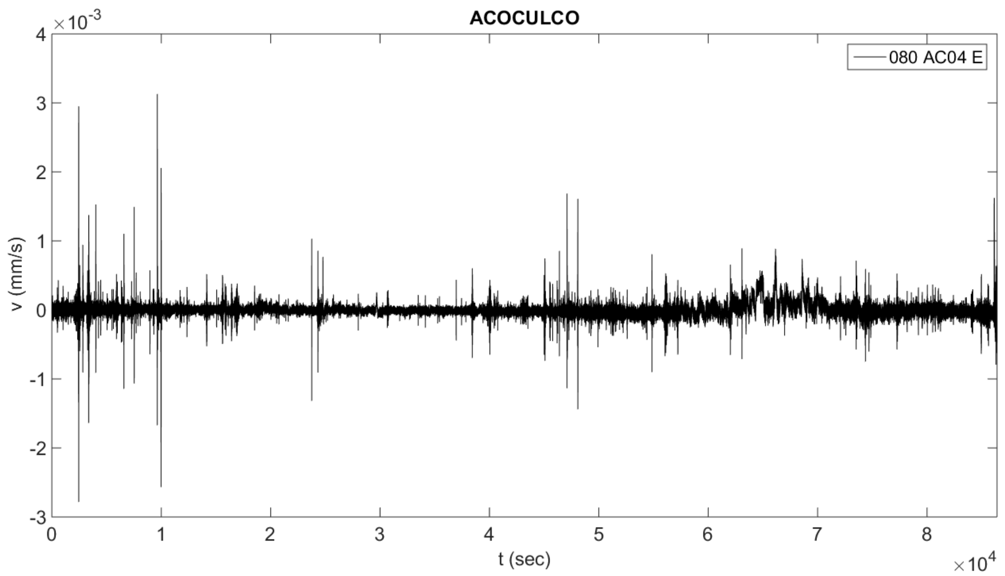
ACOCULCO
×10-3
080 AC04 E
v (mm/s)
t (sec)
×10^4

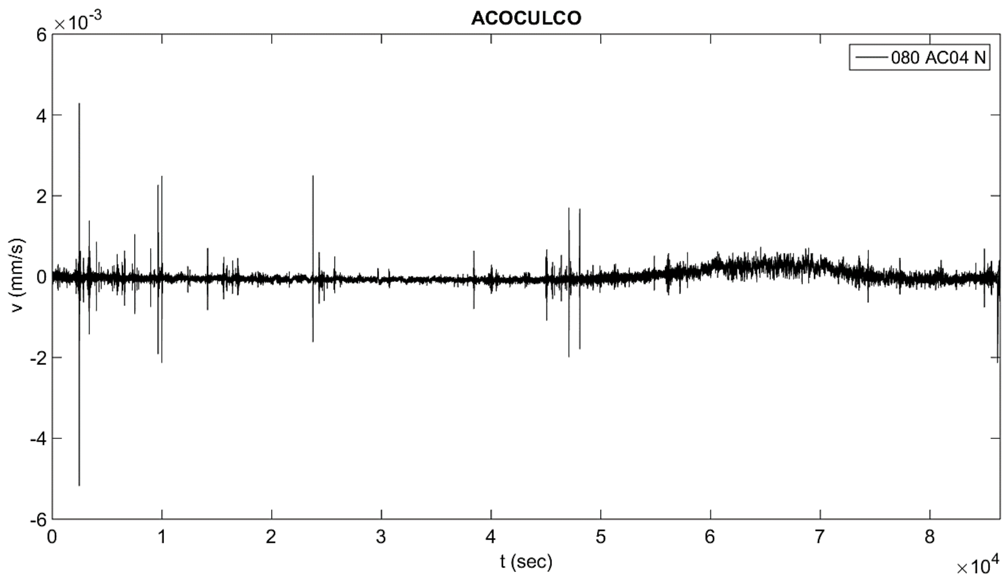
ACOCULCO
×10-3
080 AC04 N
v (mm/s)
t (sec)
×10^4

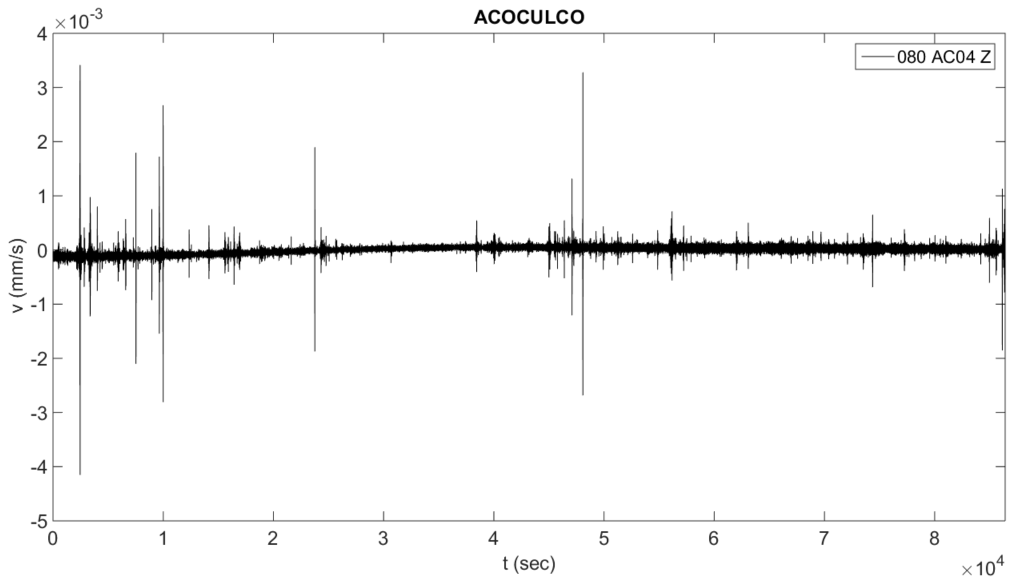
ACOCULCO
×10-3
080 AC04 Z
v (mm/s)
t (sec)
×10^4

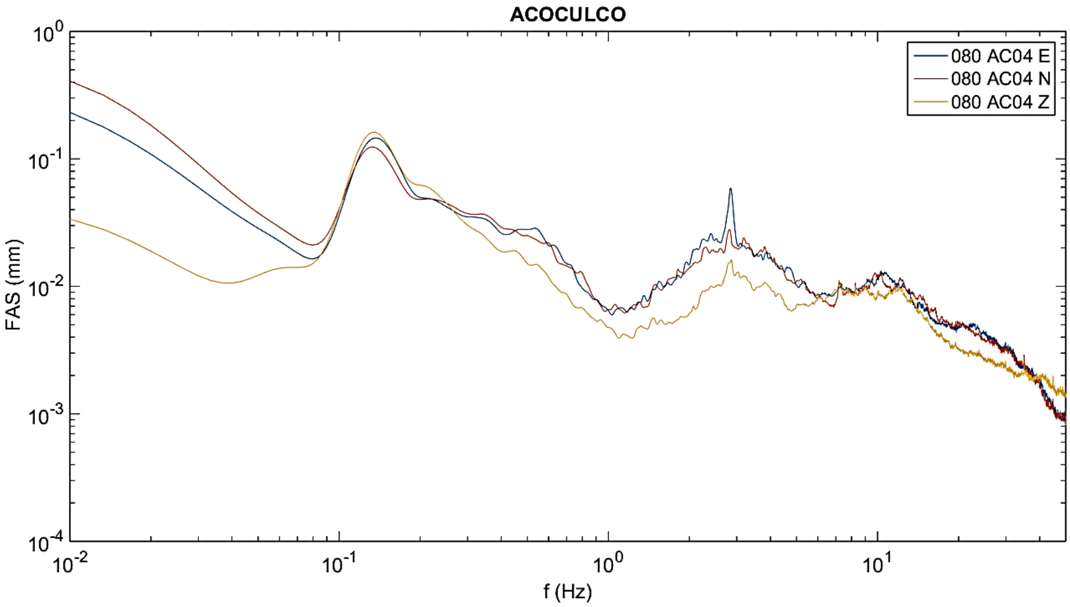
ACOCULCO
080 AC04 E
080 AC04 N
080 AC04 Z
FAS (mm)
f (Hz)

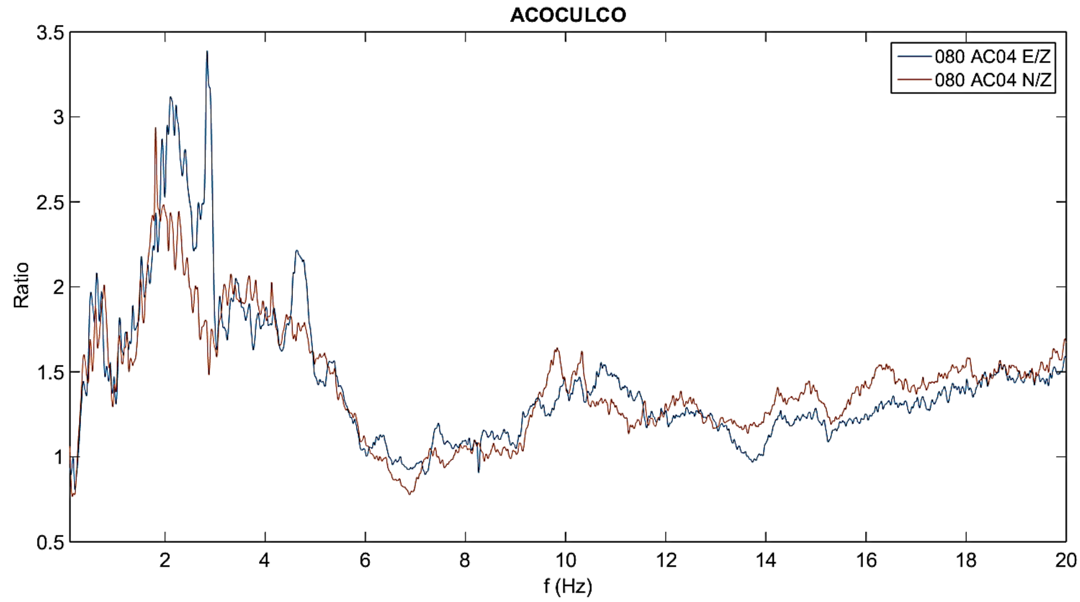
ACOCULCO
080 AC04 E/Z
080 AC04 N/Z
Ratio
f (Hz)

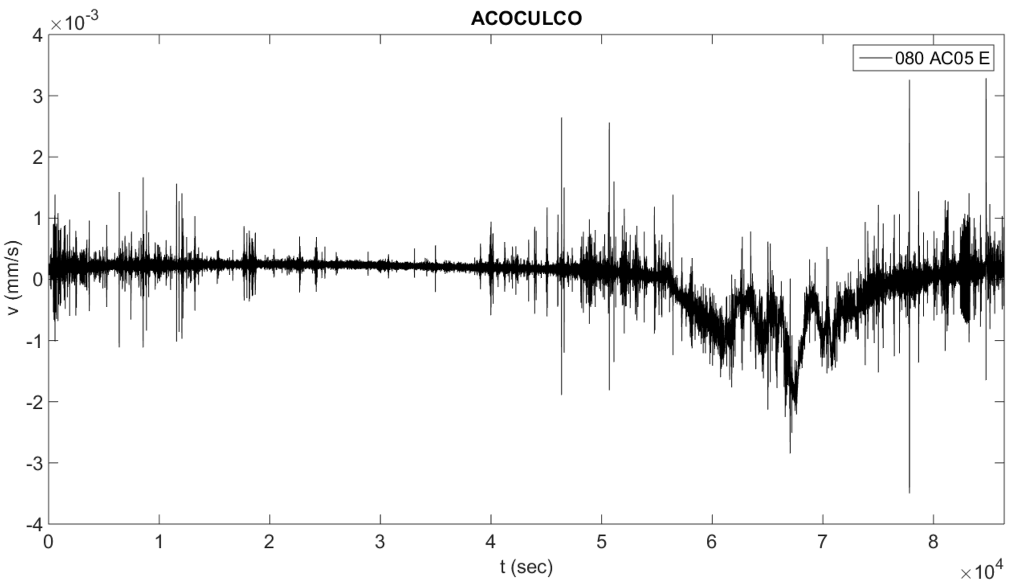
ACOCULCO
×10-3
080 AC05 E
v (mm/s)
t (sec)
×104

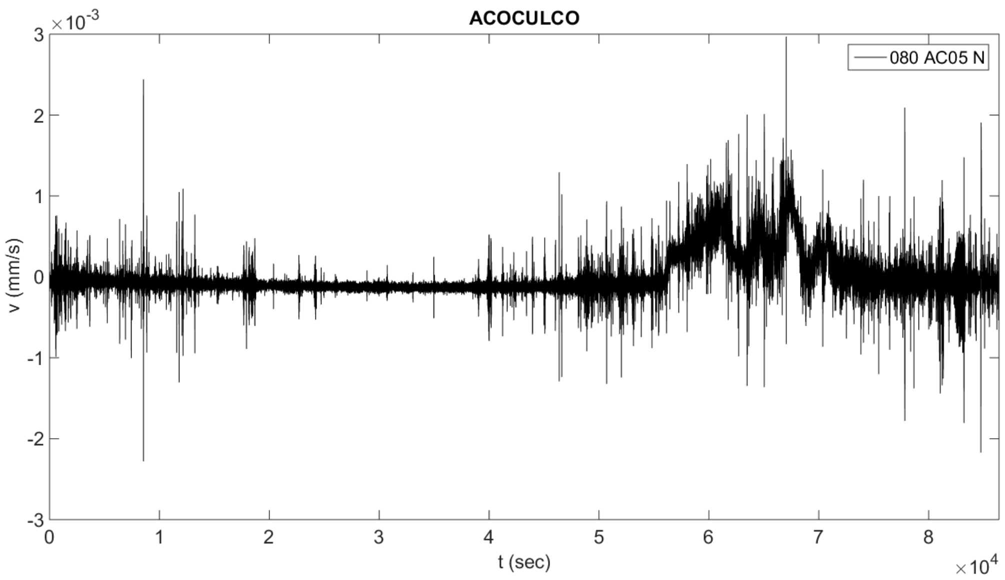
ACOCULCO
×10-3
080 AC05 N
v (mm/s)
t (sec)
×104

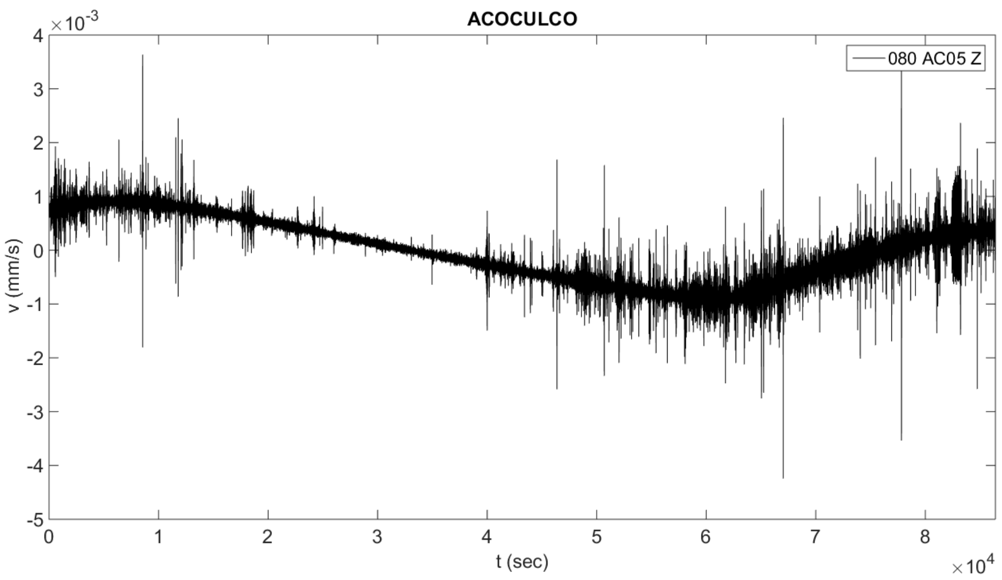
ACOCULCO
×10-3
080 AC05 Z
v (mm/s)
t (sec)
×104

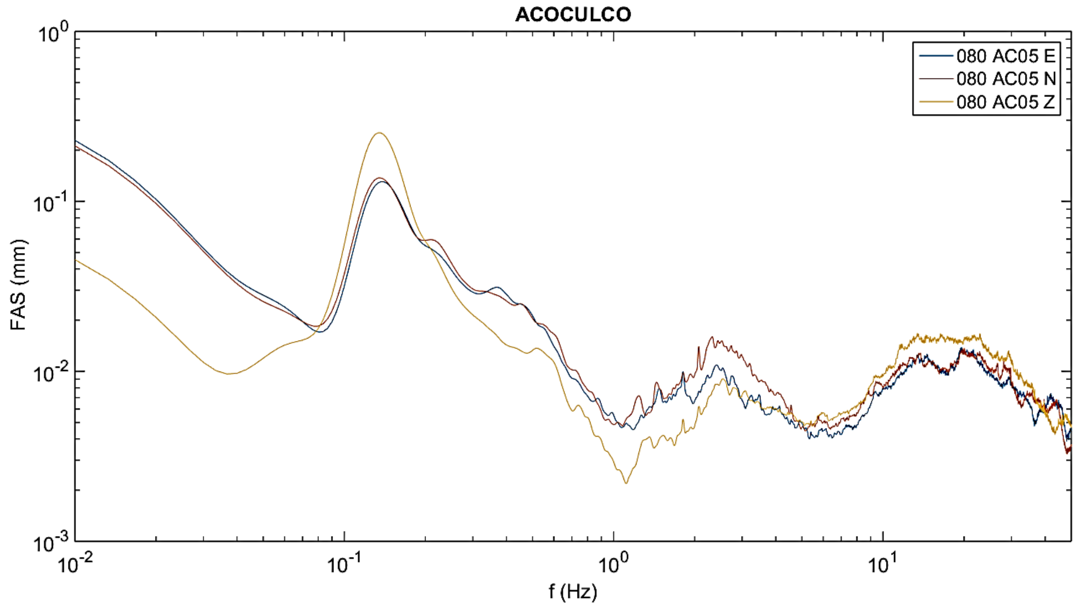
ACOCULCO
080 AC05 E
080 AC05 N
080 AC05 Z
FAS (mm)
f (Hz)

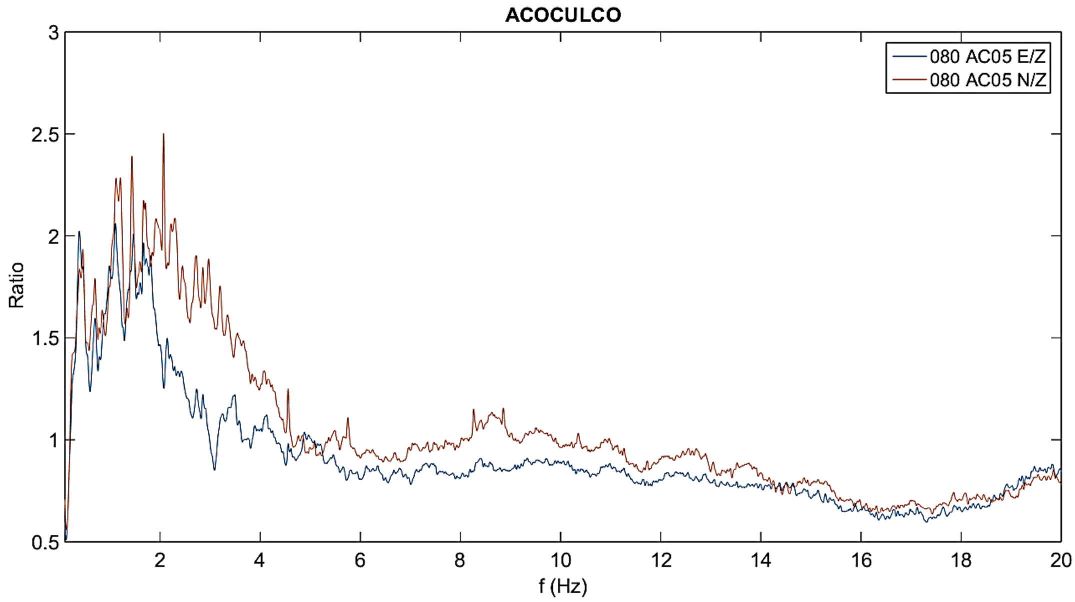
ACOCULCO
080 AC05 E/Z
080 AC05 N/Z
Ratio
f (Hz)

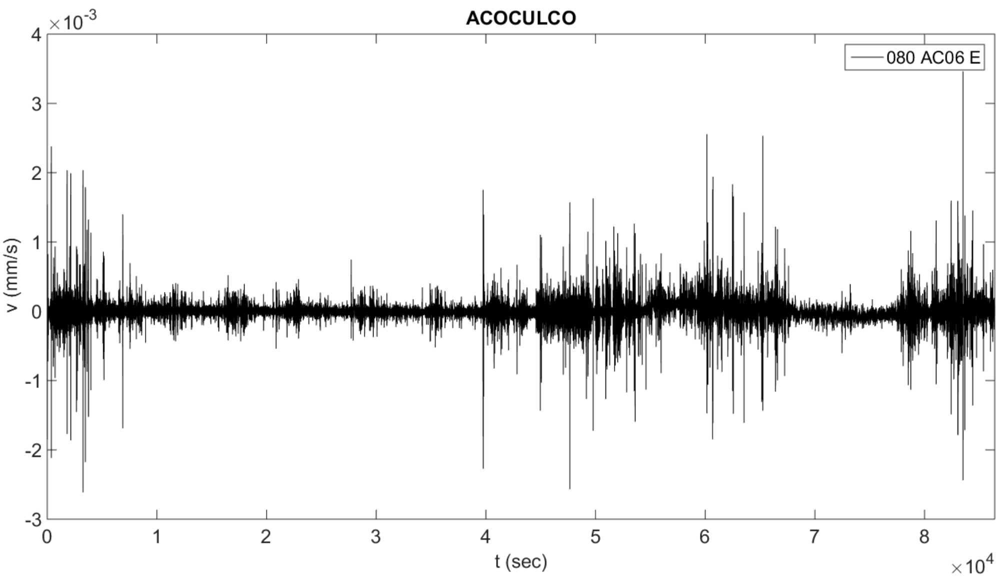
ACOCULCO
080 AC06 E
v (mm/s)
t (sec)
×10^-3
×10^4

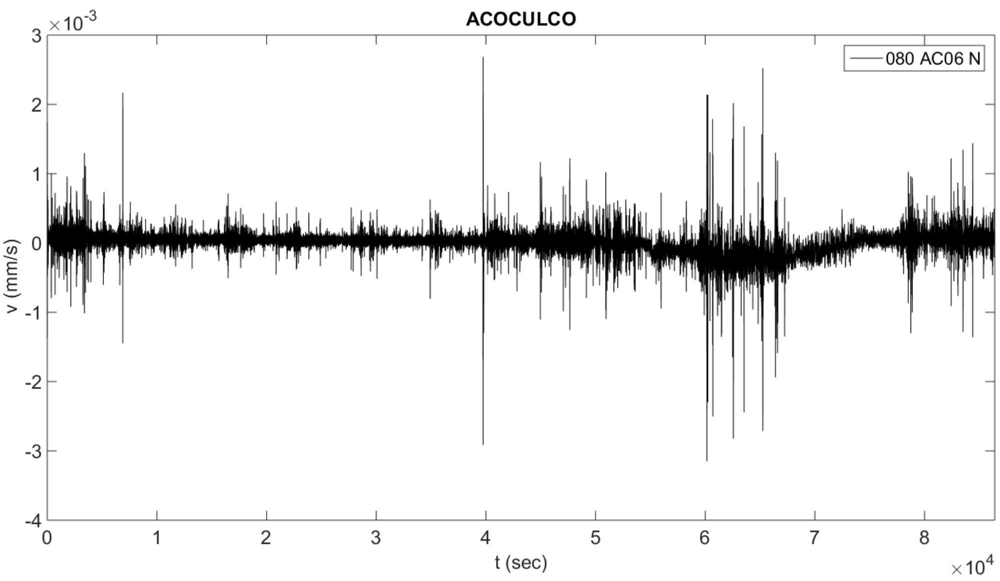
ACOCULCO
080 AC06 N
v (mm/s)
t (sec)
×10^-3
×10^4

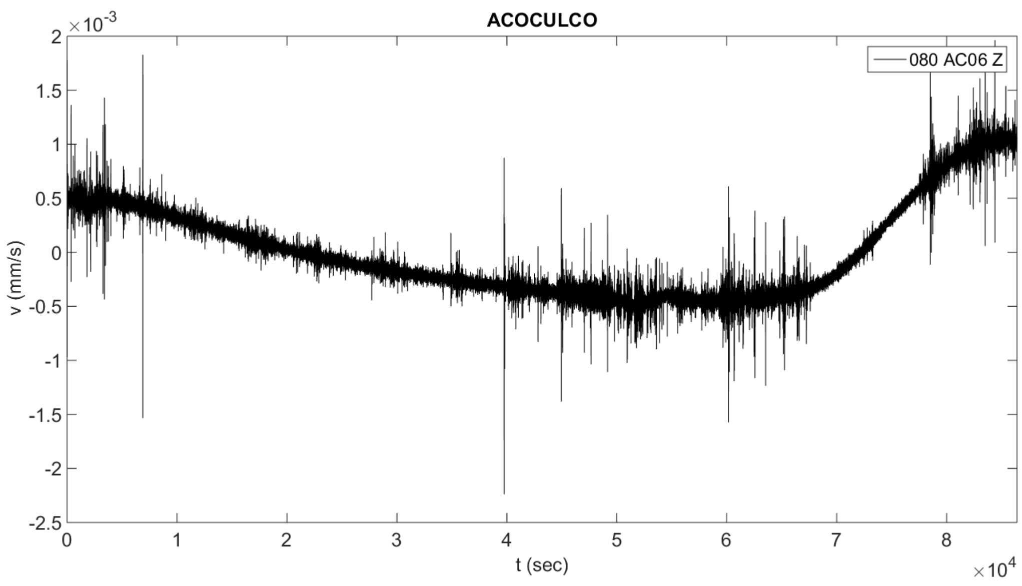
ACOCULCO
080 AC06 Z
v (mm/s)
t (sec)
×10^-3
×10^4

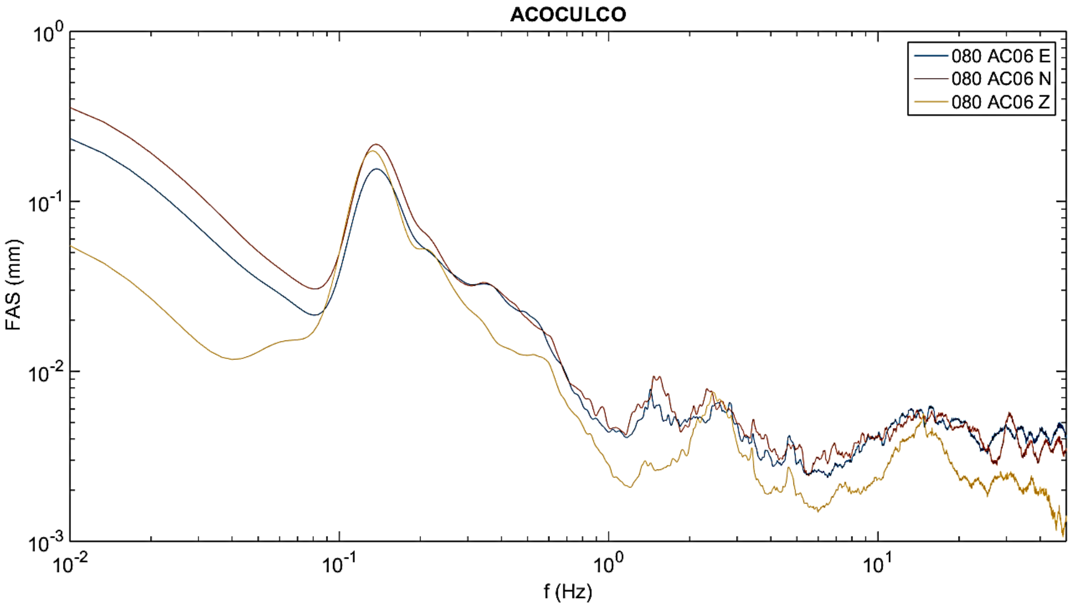

ACOCULCO
080 AC06 E
080 AC06 N
080 AC06 Z
FAS (mm)
f (Hz)

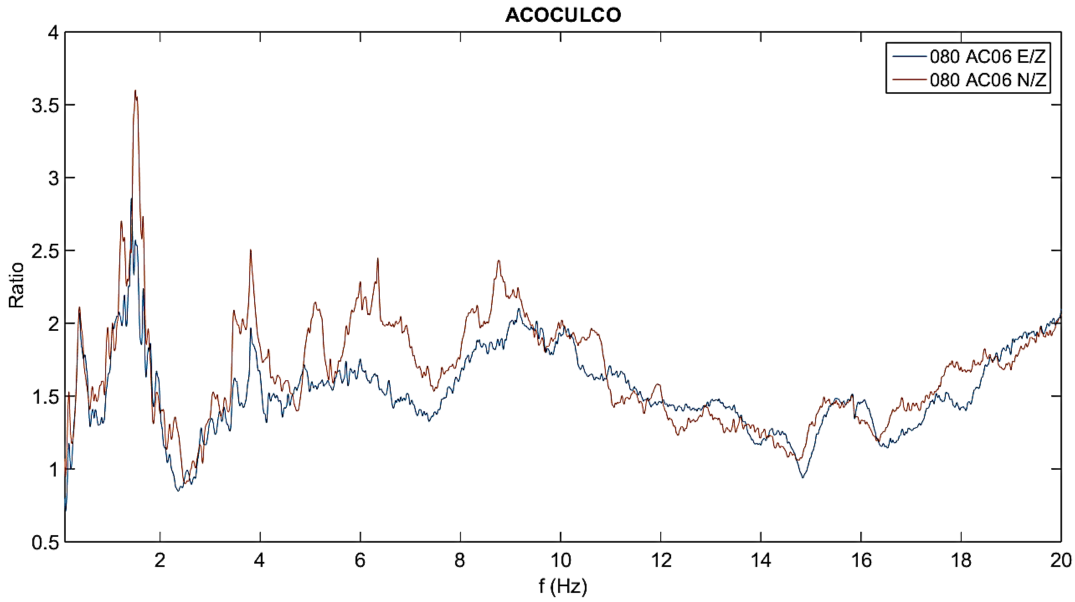

ACOCULCO
080 AC06 E/Z
080 AC06 N/Z
Ratio
f (Hz)

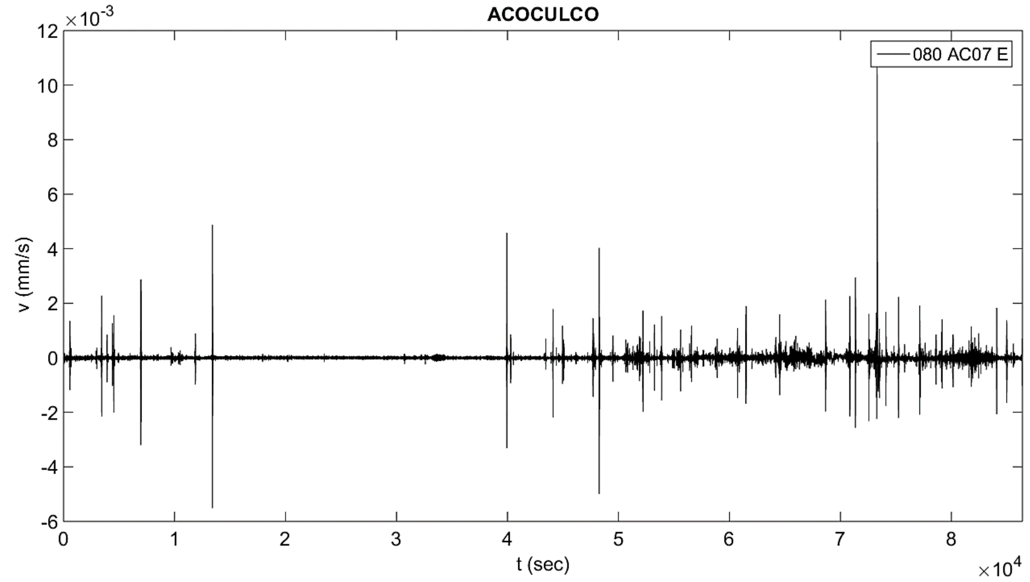
ACOCULCO
×10^-3
080 AC07 E
v (mm/s)
t (sec)
×10^4

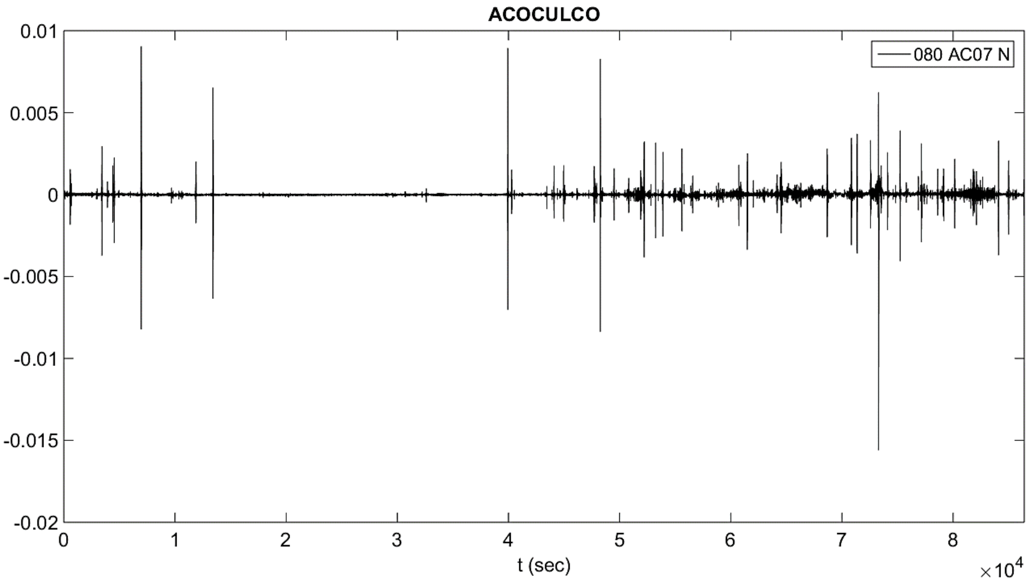
ACOCULCO
080 AC07 N
v (mm/s)
t (sec)
×10^4

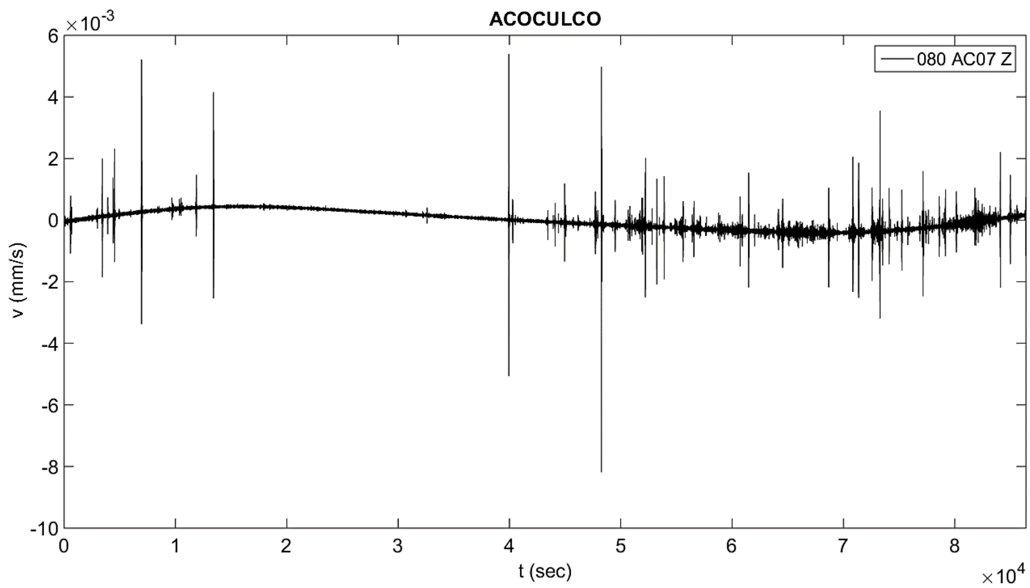
ACOCULCO
×10^-3
080 AC07 Z
v (mm/s)
t (sec)
×10^4

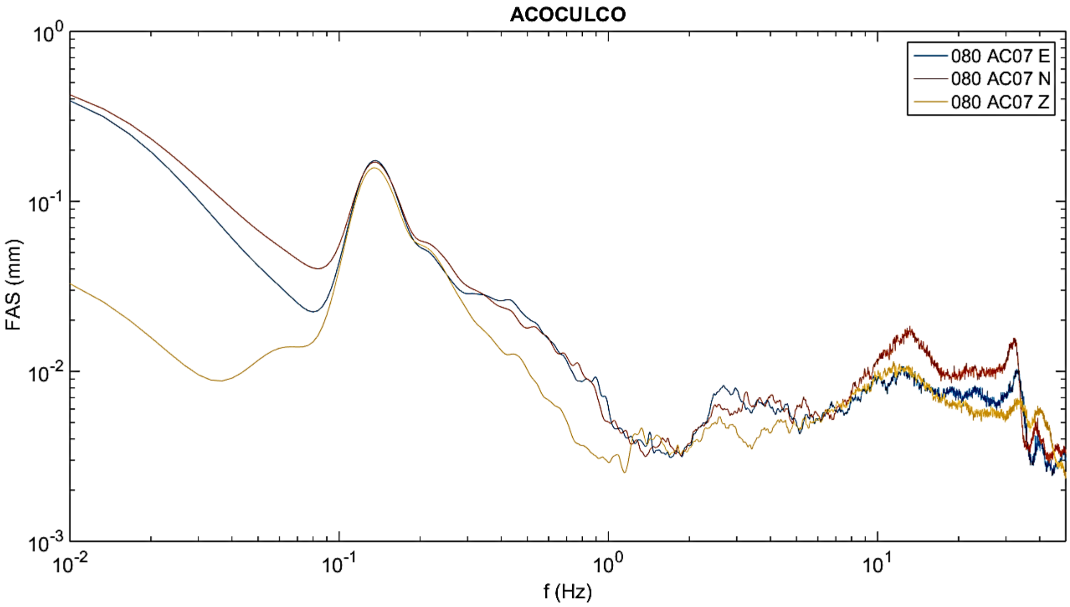
ACOCULCO
080 AC07 E
080 AC07 N
080 AC07 Z
FAS (mm)
f (Hz)

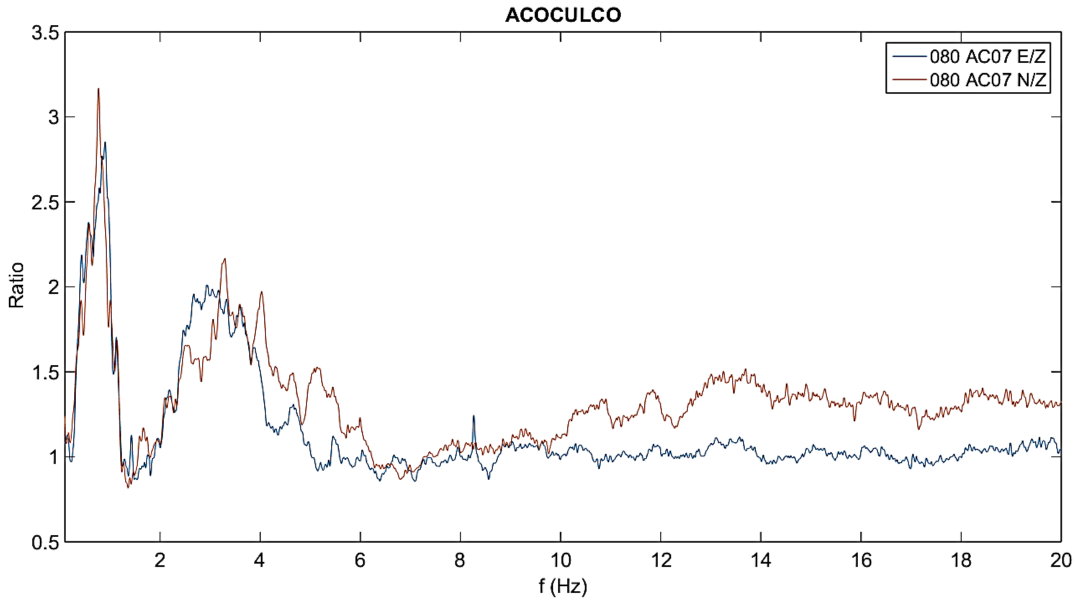
ACOCULCO
080 AC07 E/Z
080 AC07 N/Z
Ratio
f (Hz)

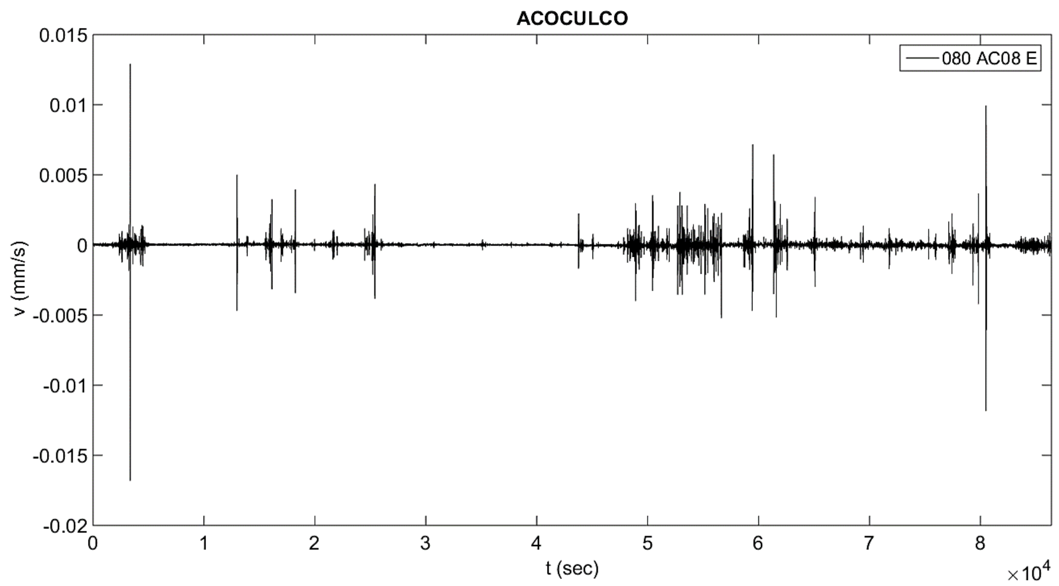
ACOCULCO
080 AC08 E
v (mm/s)
t (sec)
×10^4

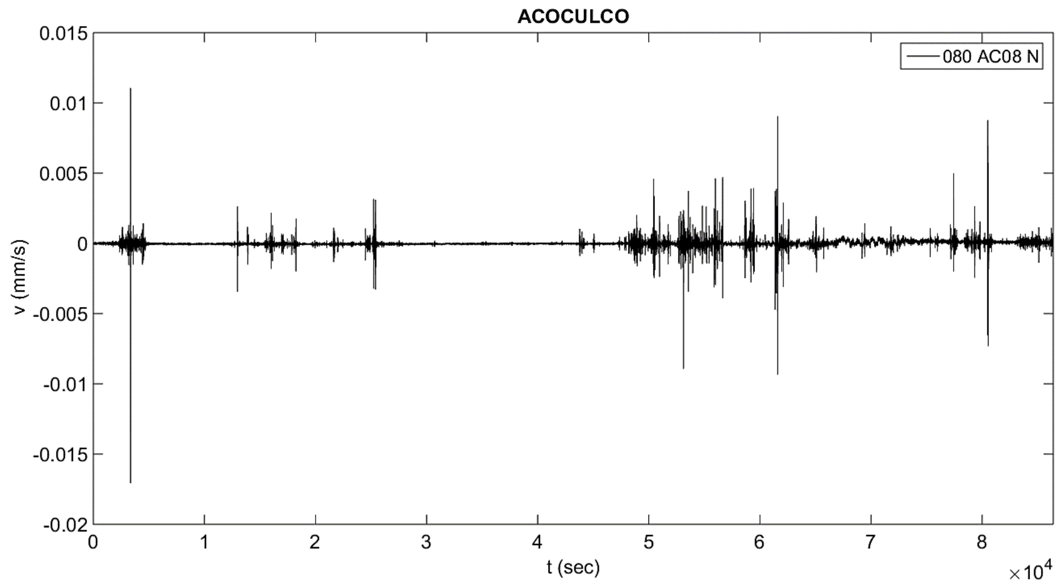
ACOCULCO
080 AC08 N
v (mm/s)
t (sec)
×10^4

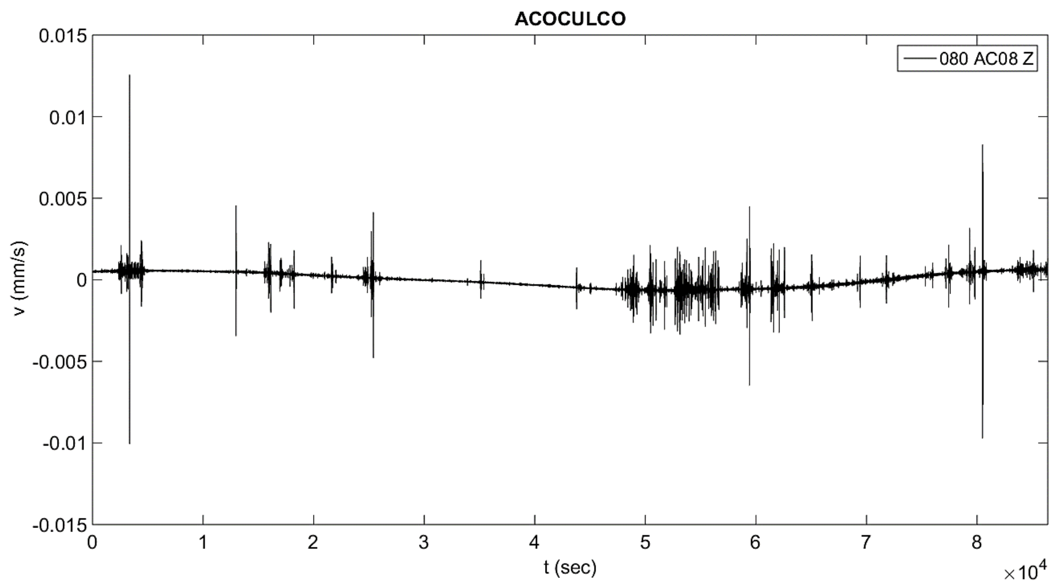
ACOCULCO
080 AC08 Z
v (mm/s)
t (sec)
×10^4

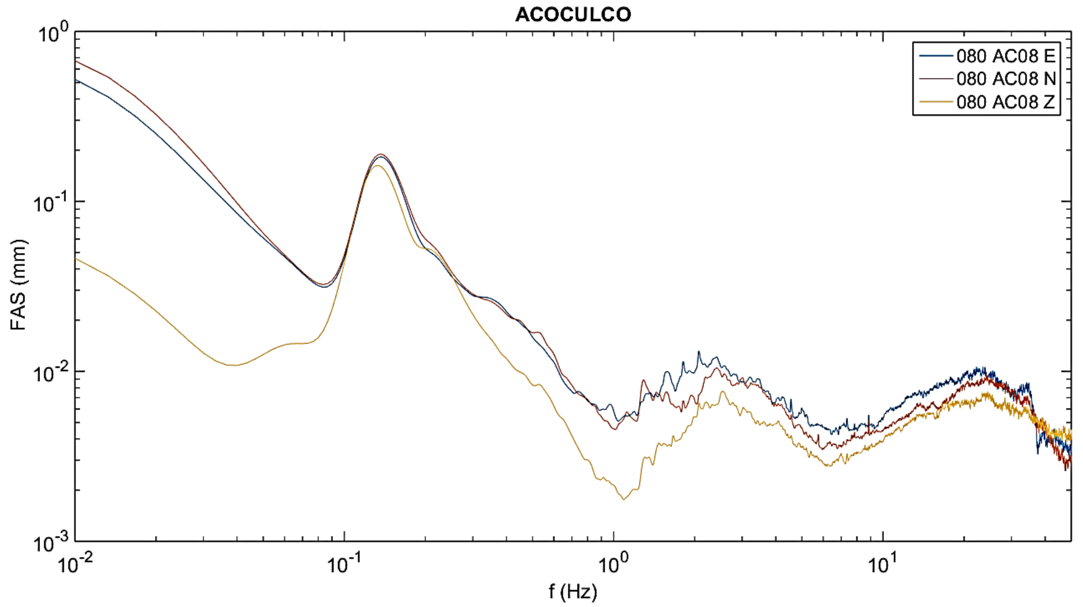
ACOCULCO
080 AC08 E
080 AC08 N
080 AC08 Z
FAS (mm)
f (Hz)

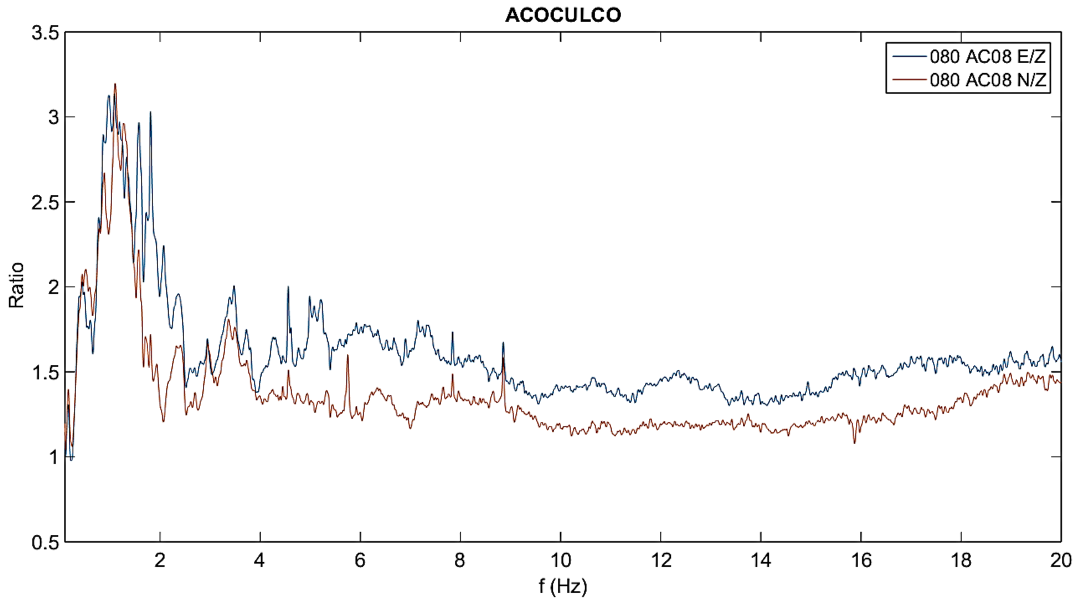
ACOCULCO
080 AC08 E/Z
080 AC08 N/Z
Ratio
f (Hz)

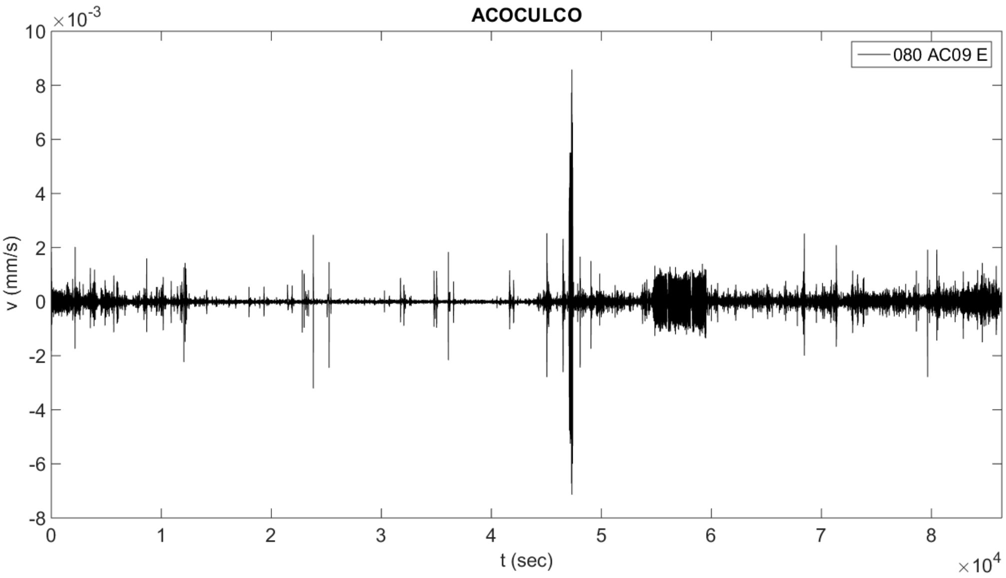
ACOCULCO
080 AC09 E
v (mm/s)
t (sec)
$\times 10^{-3}$
$\times 10^{4}$

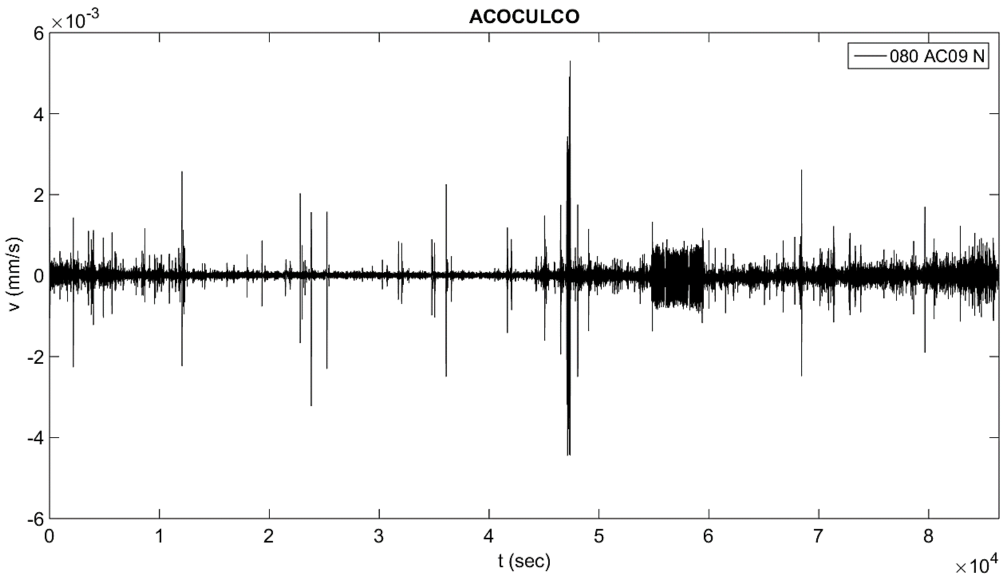
ACOCULCO
080 AC09 N
v (mm/s)
t (sec)
$\times 10^{-3}$
$\times 10^{4}$

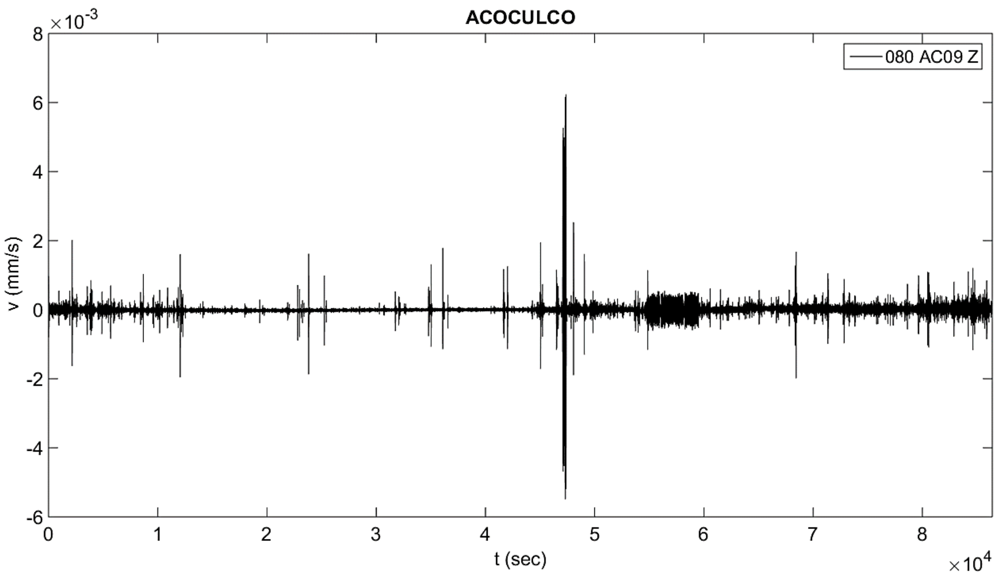
ACOCULCO
080 AC09 Z
v (mm/s)
t (sec)
$\times 10^{-3}$
$\times 10^{4}$

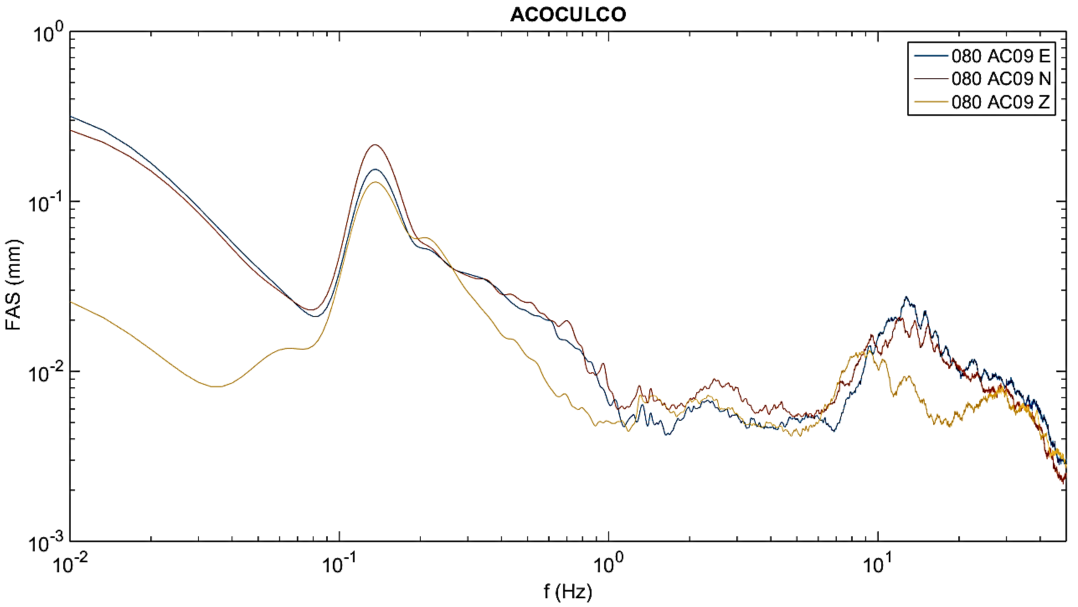
ACOCULCO
080 AC09 E
080 AC09 N
080 AC09 Z
FAS (mm)
f (Hz)

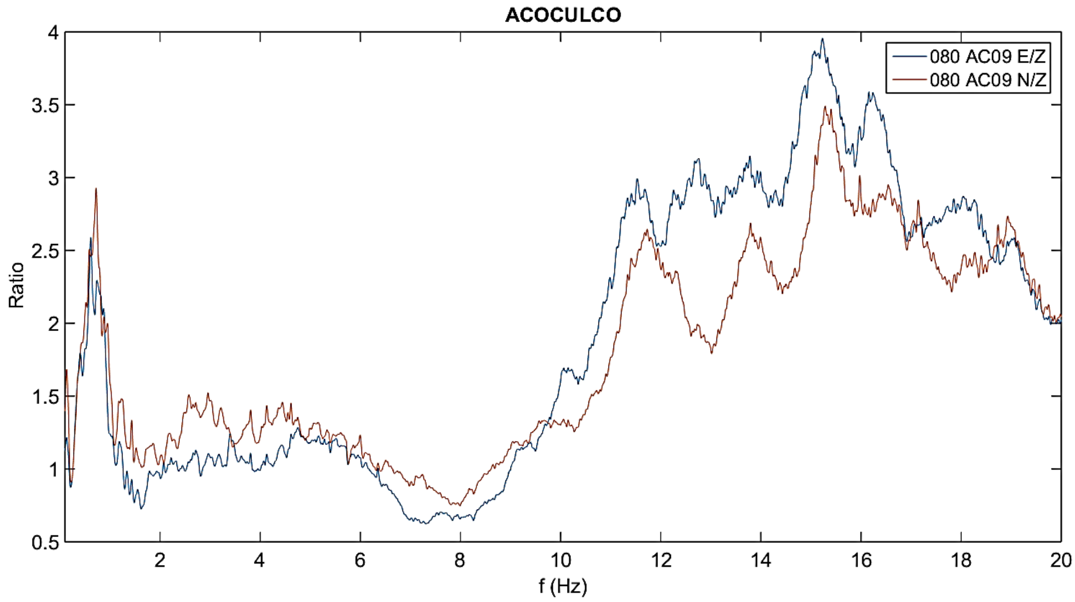
ACOCULCO
080 AC09 E/Z
080 AC09 N/Z
Ratio
f (Hz)

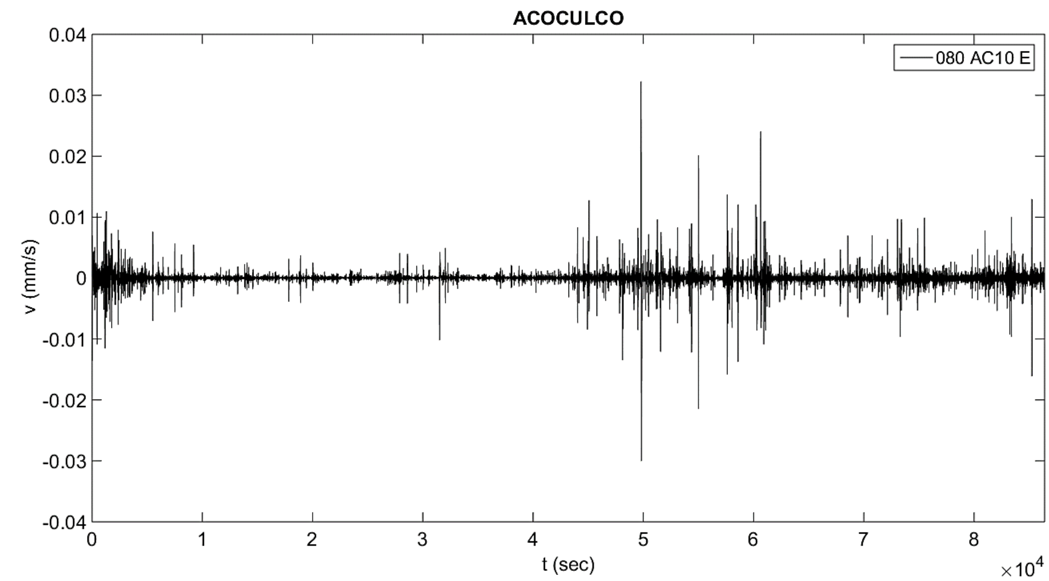
ACOCULCO
080 AC10 E
v (mm/s)
t (sec)
×10^4
0.04
0.03
0.02
0.01
0
-0.01
-0.02
-0.03
-0.04
0
1
2
3
4
5
6
7
8

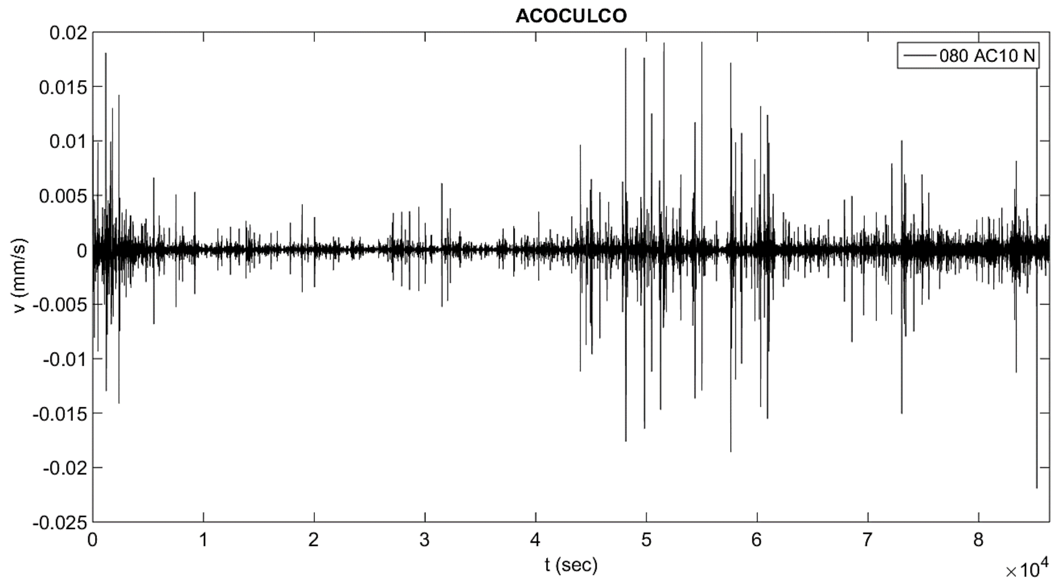
ACOCULCO
080 AC10 N
v (mm/s)
t (sec)
×10^4
0.02
0.015
0.01
0.005
0
-0.005
-0.01
-0.015
-0.02
-0.025
0
1
2
3
4
5
6
7
8

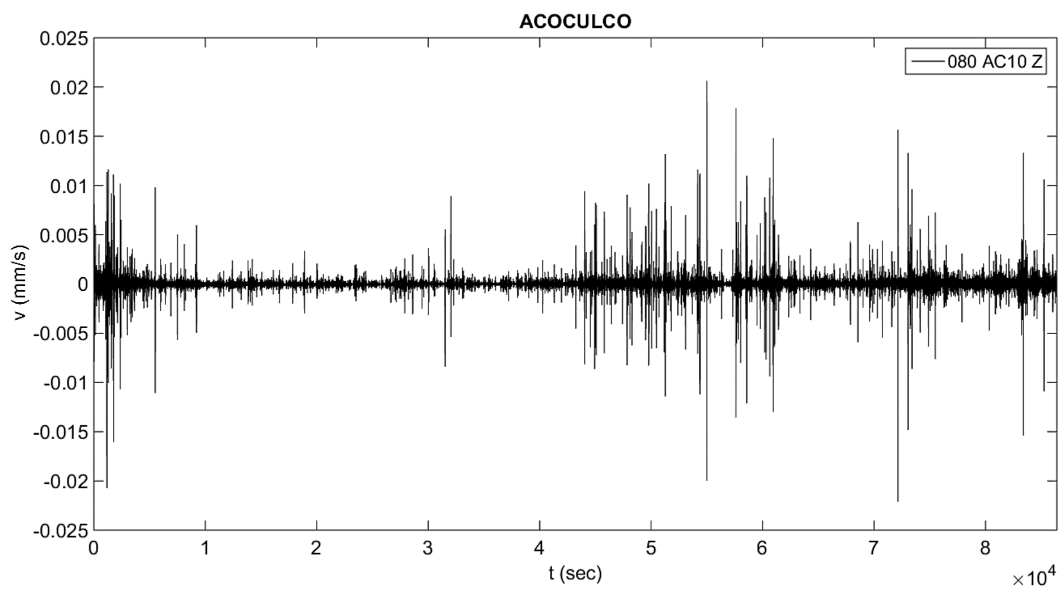
ACOCULCO
080 AC10 Z
v (mm/s)
t (sec)
×10^4
0.025
0.02
0.015
0.01
0.005
0
-0.005
-0.01
-0.015
-0.02
-0.025
0
1
2
3
4
5
6
7
8

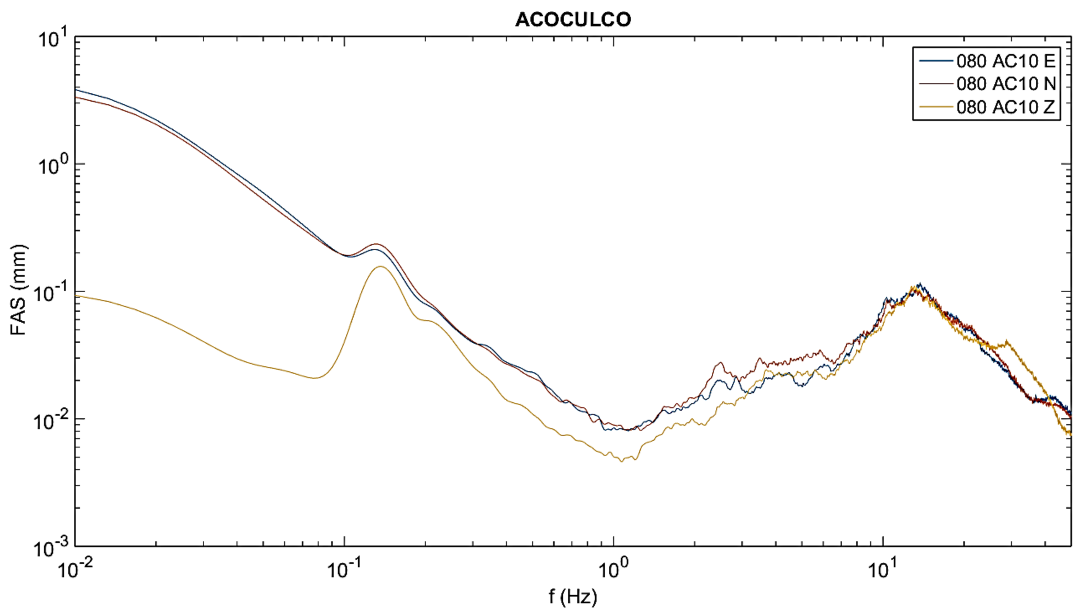
ACOCULCO
080 AC10 E
080 AC10 N
080 AC10 Z
FAS (mm)
f (Hz)

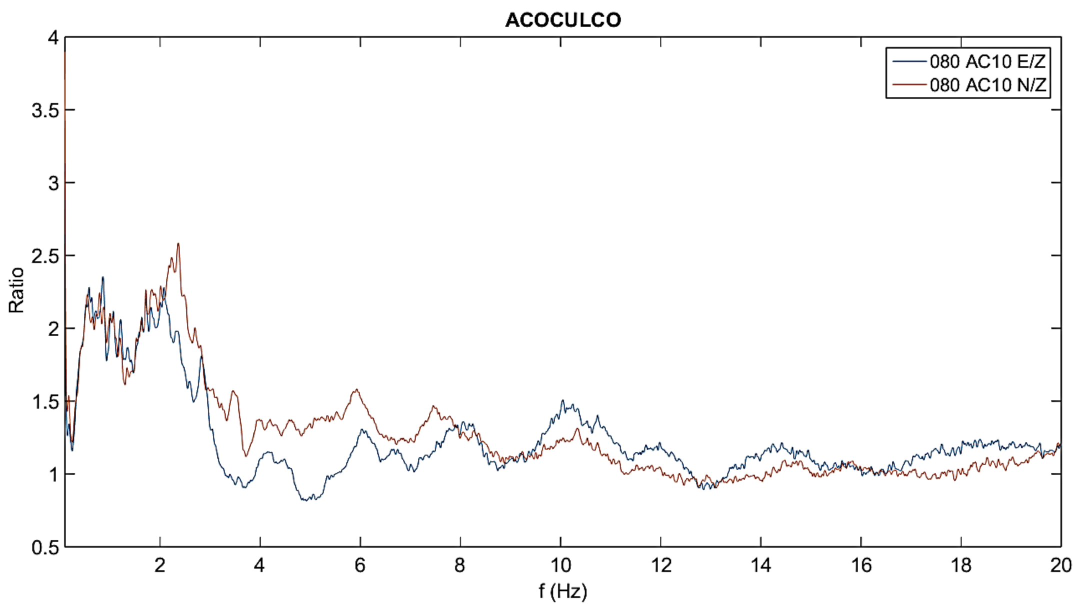
ACOCULCO
080 AC10 E/Z
080 AC10 N/Z
Ratio
f (Hz)

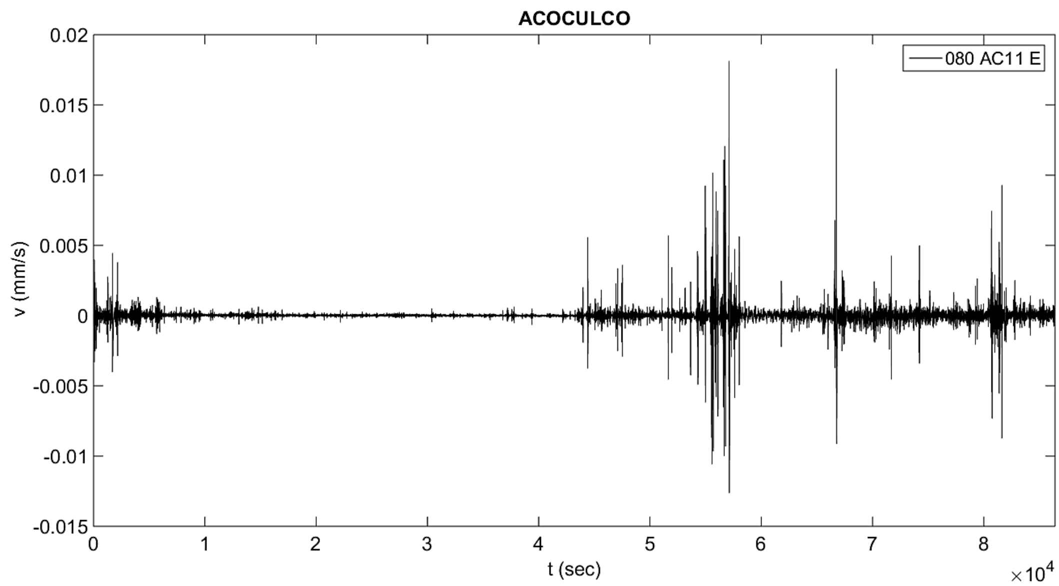
ACOCULCO
080 AC11 E
v (mm/s)
t (sec)
$\times 10^4$

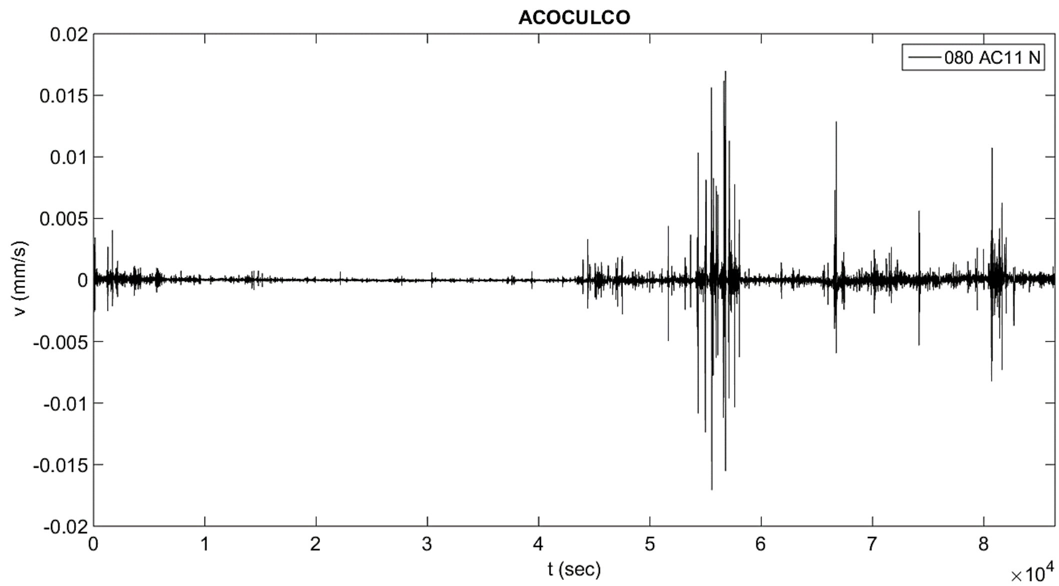
ACOCULCO
080 AC11 N
v (mm/s)
t (sec)
$\times 10^4$

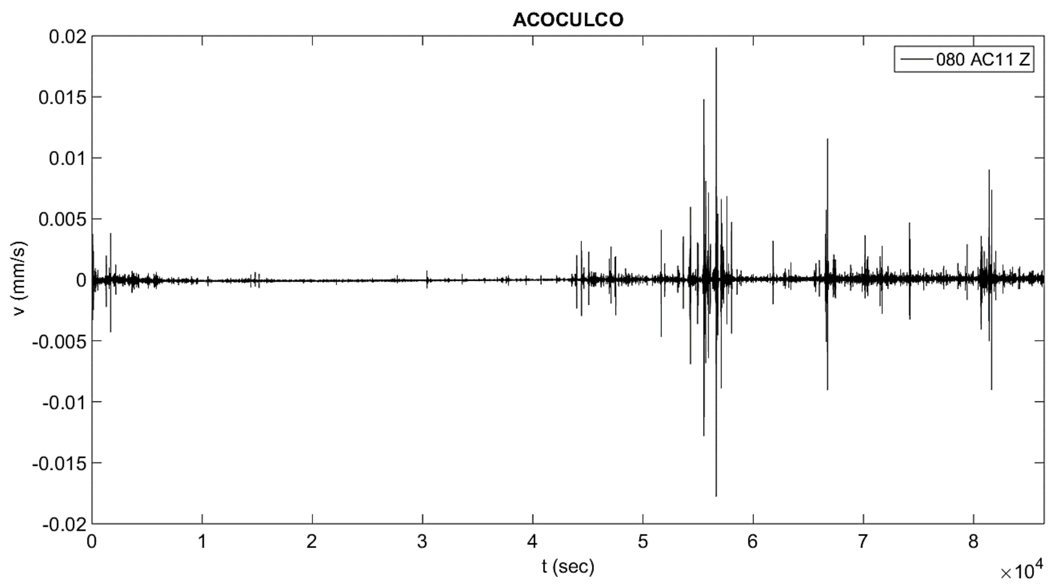
ACOCULCO
080 AC11 Z
v (mm/s)
t (sec)
$\times 10^4$

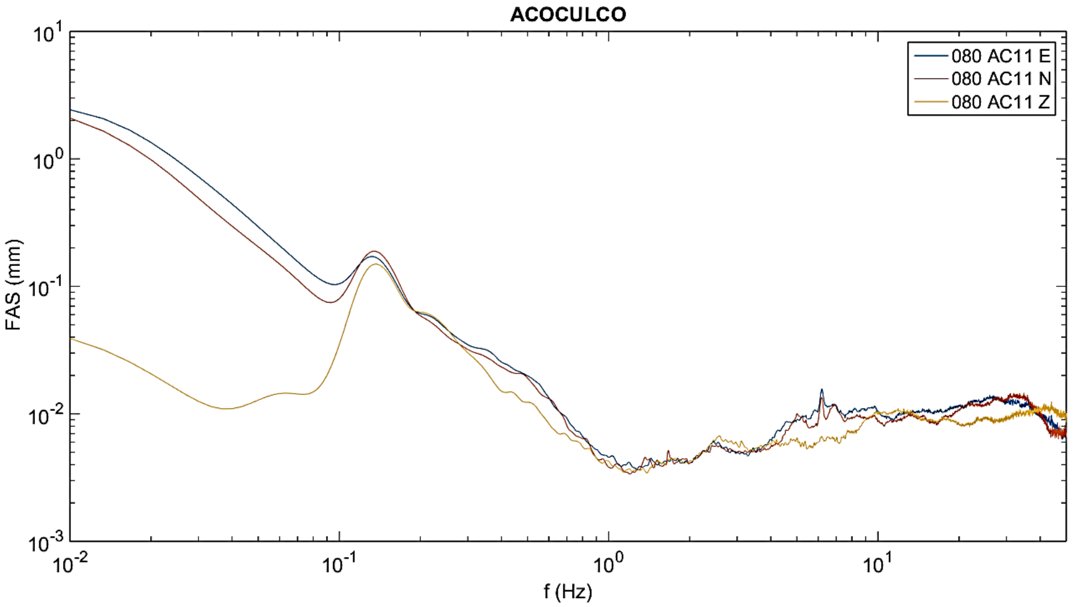
ACOCULCO
080 AC11 E
080 AC11 N
080 AC11 Z
FAS (mm)
f (Hz)

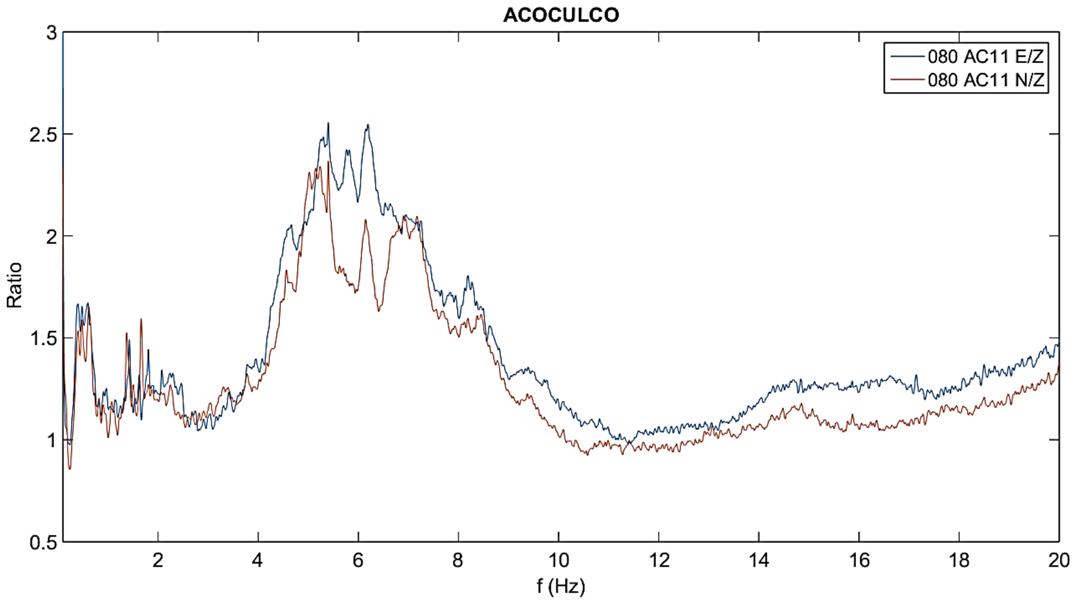
ACOCULCO
080 AC11 E/Z
080 AC11 N/Z
Ratio
f (Hz)

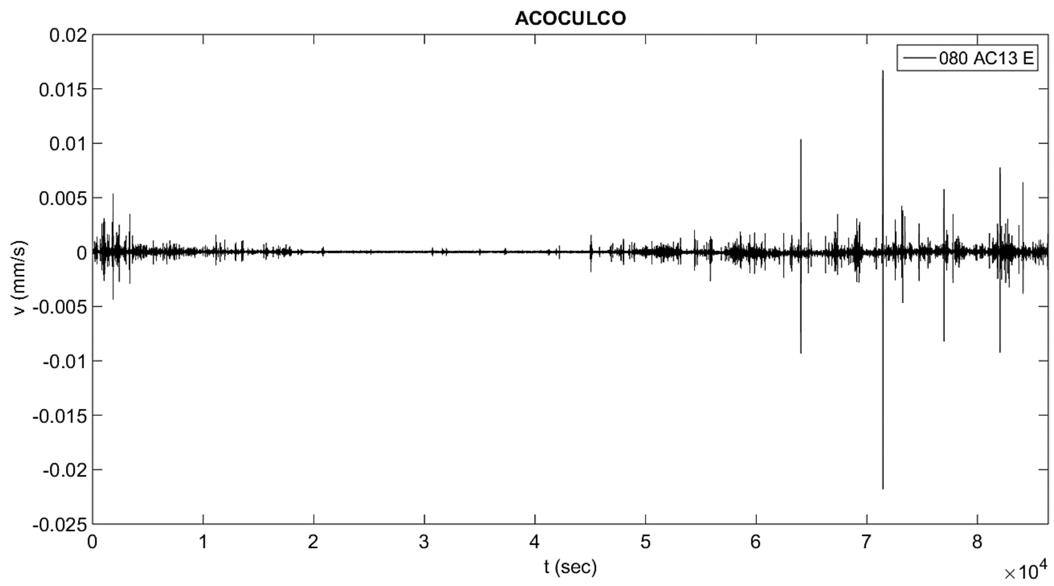
ACOCULCO
080 AC13 E
0.02
0.015
0.01
0.005
0
-0.005
-0.01
-0.015
-0.02
-0.025
v (mm/s)
0
1
2
3
4
5
6
7
8
t (sec)
×10^4

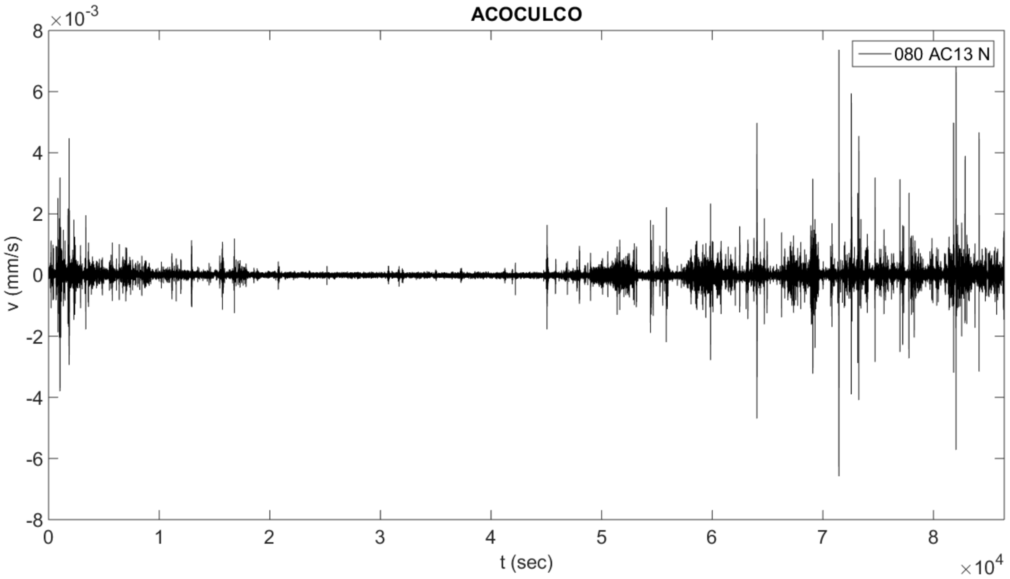
ACOCULCO
×10^-3
080 AC13 N
8
6
4
2
0
-2
-4
-6
-8
v (mm/s)
0
1
2
3
4
5
6
7
8
t (sec)
×10^4

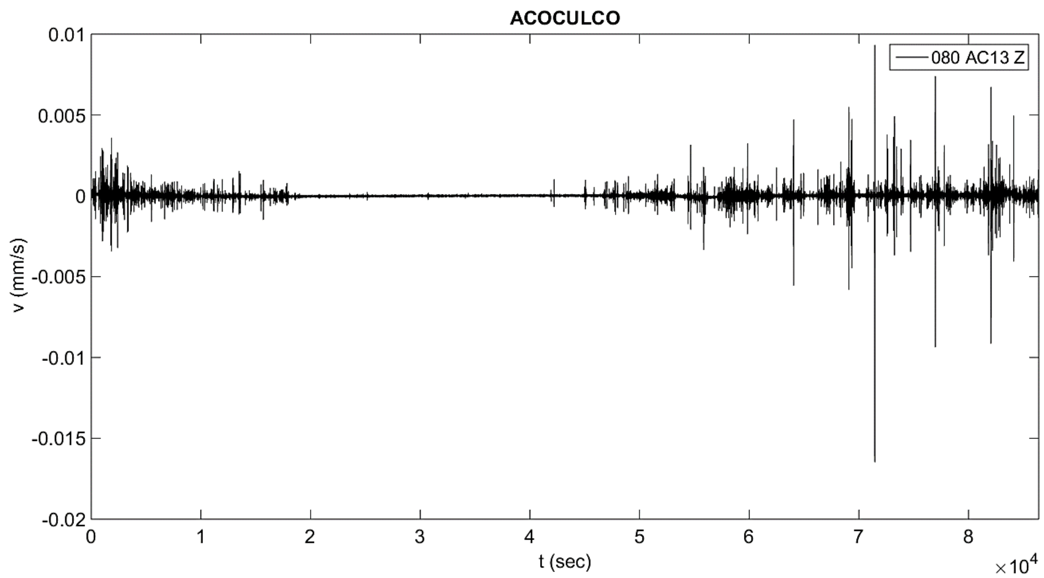
ACOCULCO
080 AC13 Z
0.01
0.005
0
-0.005
-0.01
-0.015
-0.02
v (mm/s)
0
1
2
3
4
5
6
7
8
t (sec)
×10^4

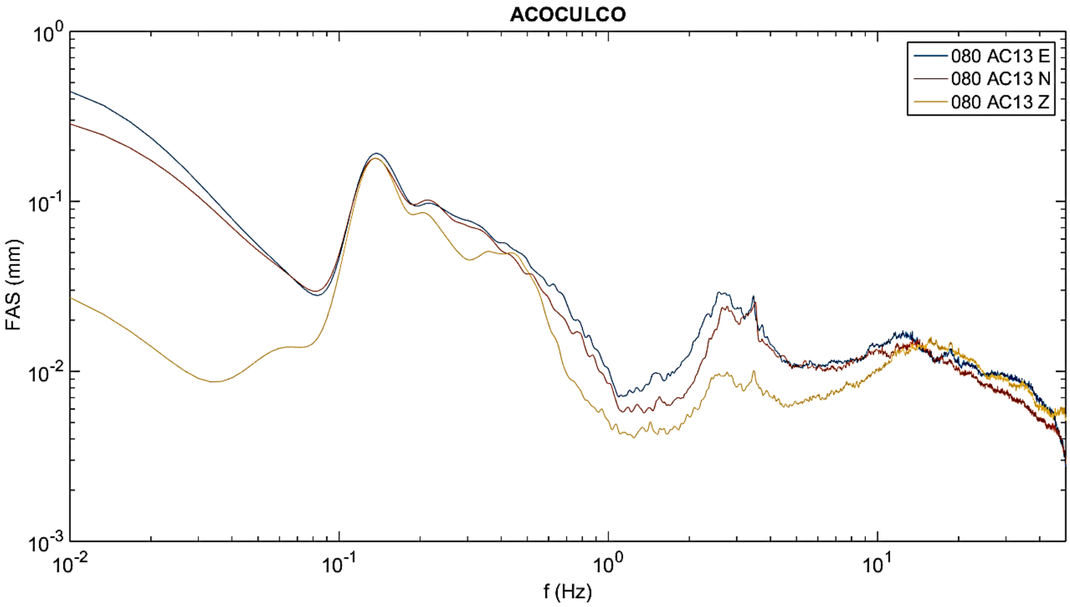
ACOCULCO
080 AC13 E
080 AC13 N
080 AC13 Z
FAS (mm)
f (Hz)

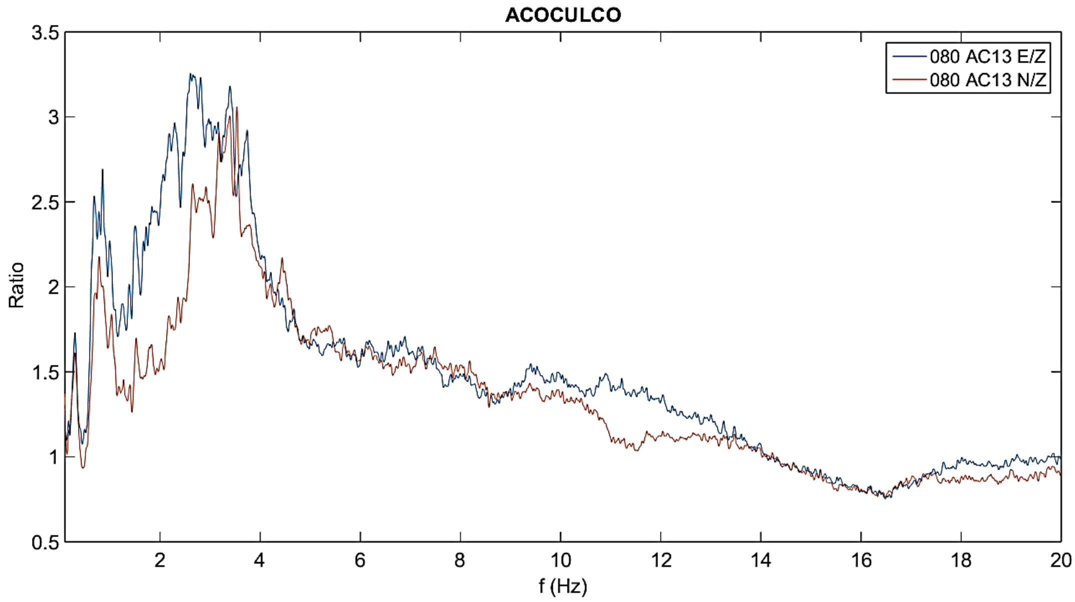
ACOCULCO
080 AC13 E/Z
080 AC13 N/Z
Ratio
f (Hz)

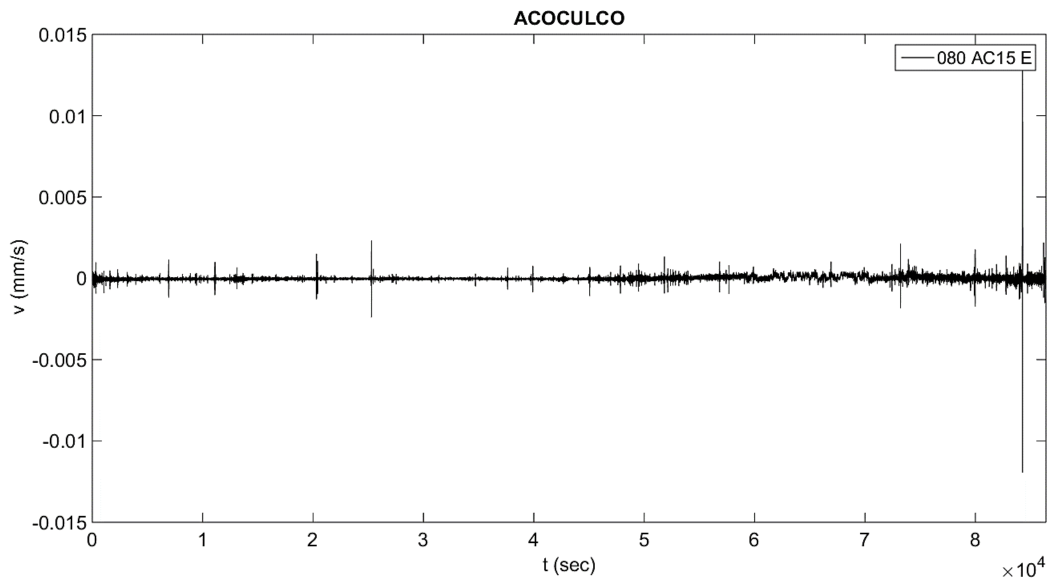
ACOCULCO
080 AC15 E
0.015
0.01
0.005
0
-0.005
-0.01
-0.015
v (mm/s)
0
1
2
3
4
5
6
7
8
t (sec)
×10^4

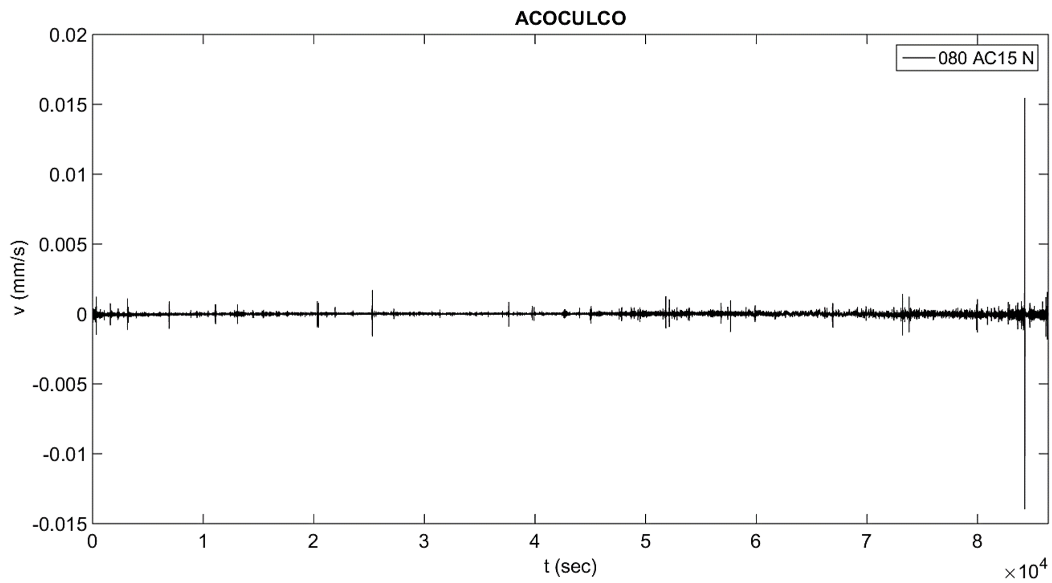
ACOCULCO
080 AC15 N
0.02
0.015
0.01
0.005
0
-0.005
-0.01
-0.015
v (mm/s)
0
1
2
3
4
5
6
7
8
t (sec)
×10^4

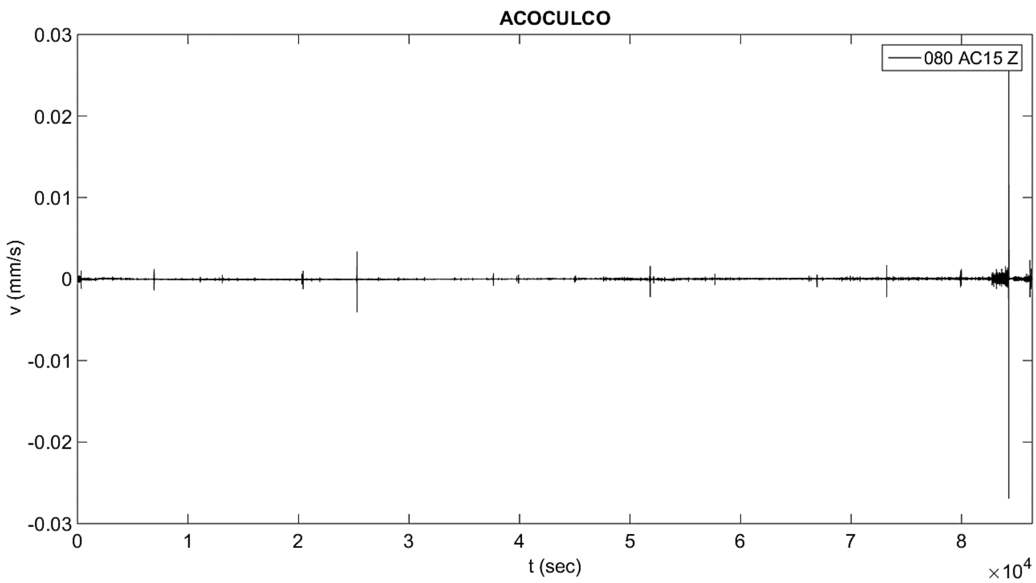
ACOCULCO
080 AC15 Z
0.03
0.02
0.01
0
-0.01
-0.02
-0.03
v (mm/s)
0
1
2
3
4
5
6
7
8
t (sec)
×10^4

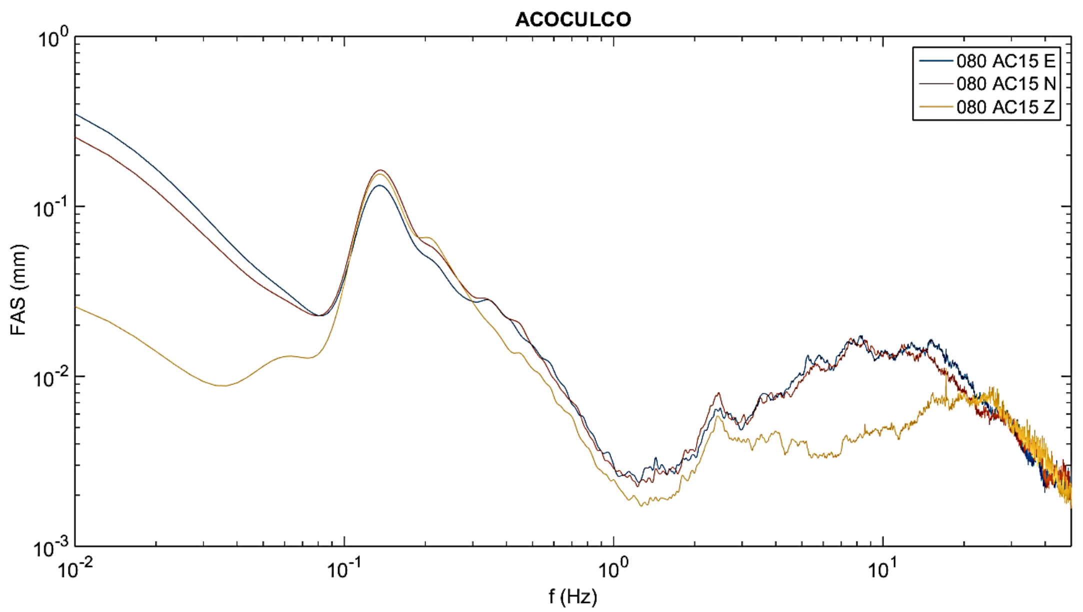
ACOCULCO
080 AC15 E
080 AC15 N
080 AC15 Z
FAS (mm)
f (Hz)

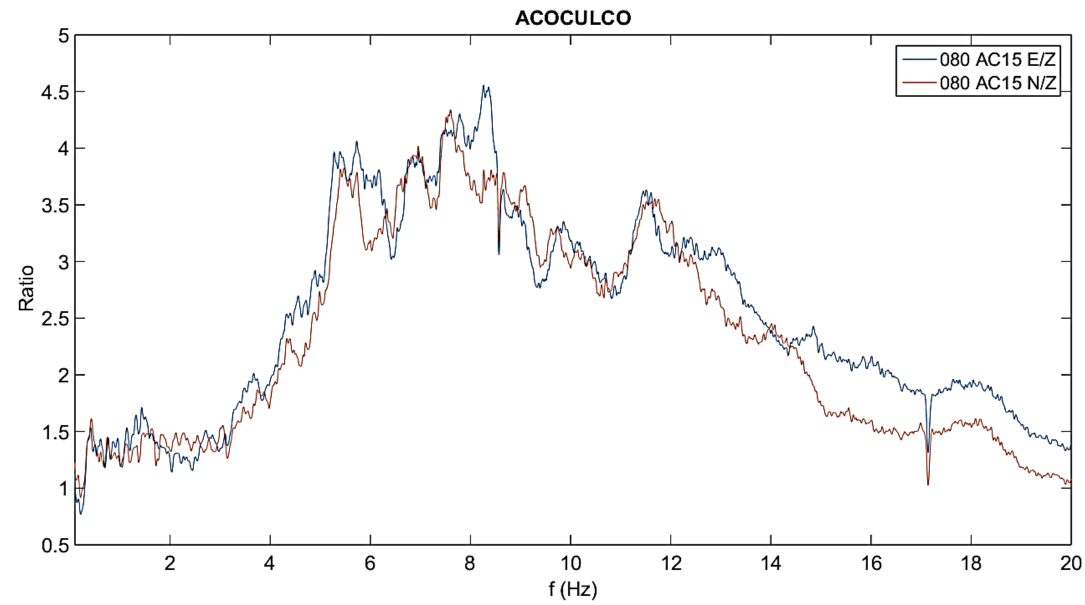
ACOCULCO
080 AC15 E/Z
080 AC15 N/Z
Ratio
f (Hz)

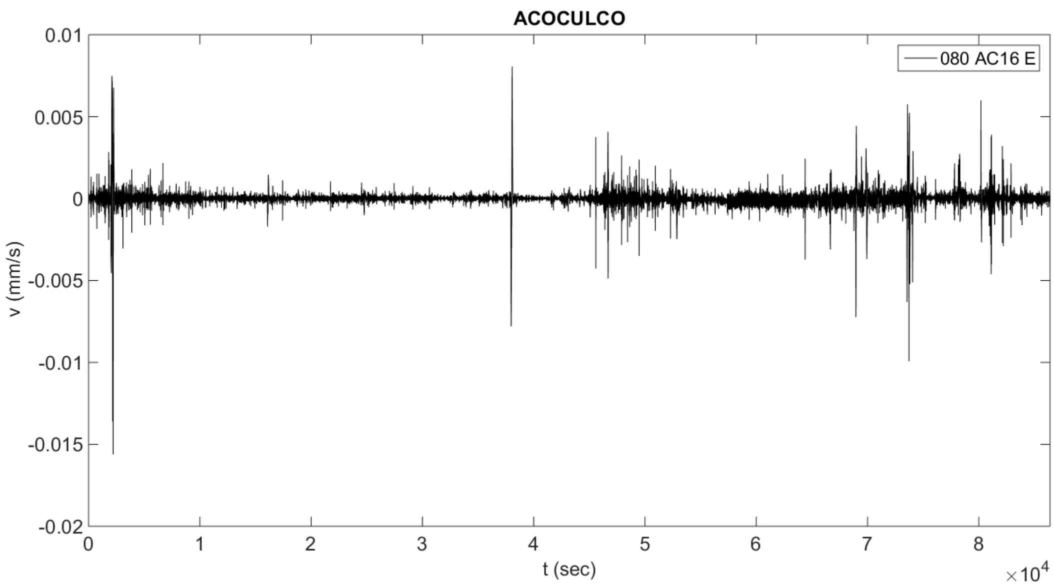
ACOCULCO
080 AC16 E
v (mm/s)
t (sec)
×10^4

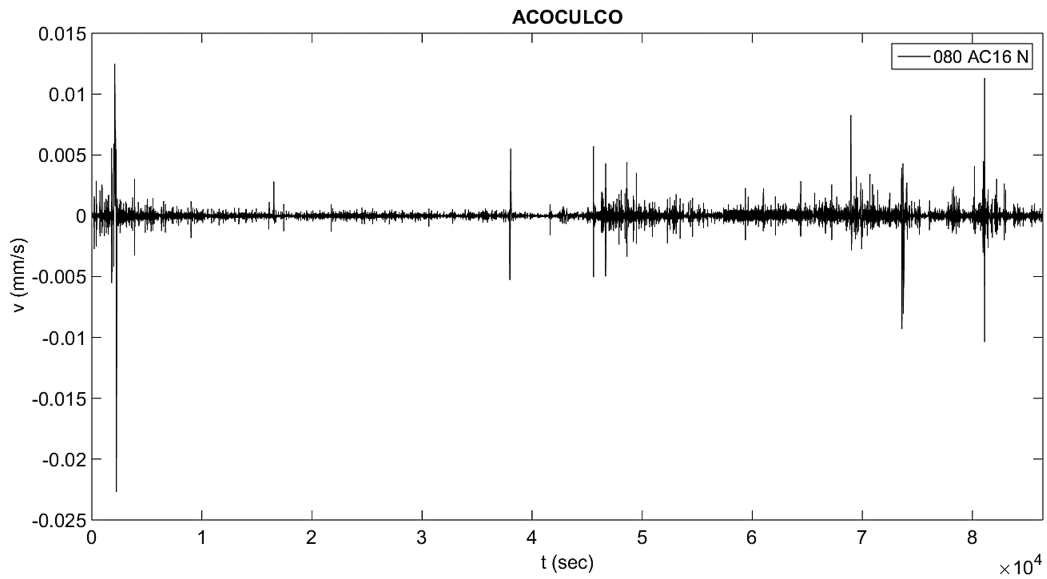
ACOCULCO
080 AC16 N
v (mm/s)
t (sec)
×10^4

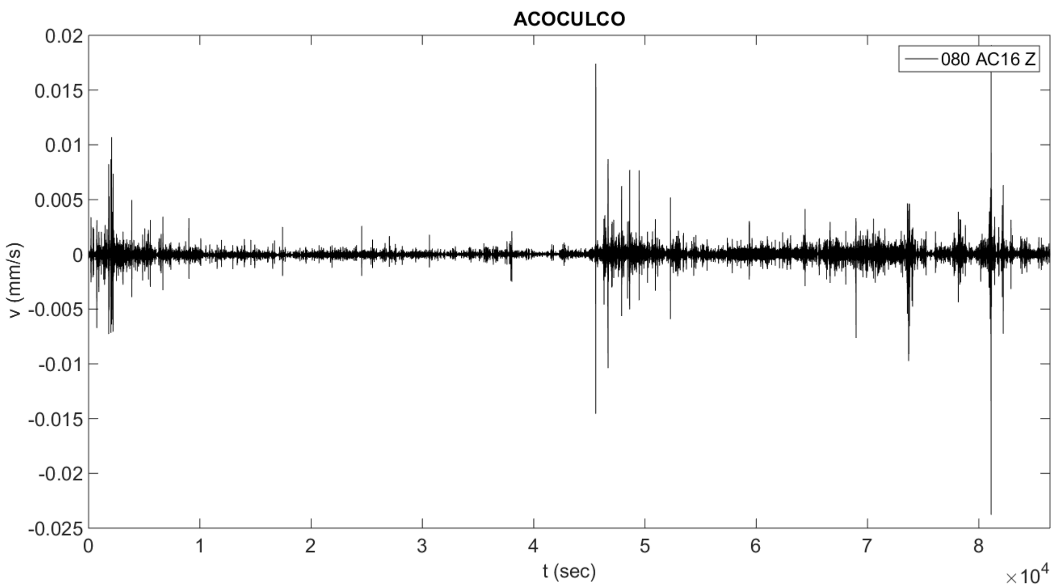
ACOCULCO
080 AC16 Z
v (mm/s)
t (sec)
×10^4

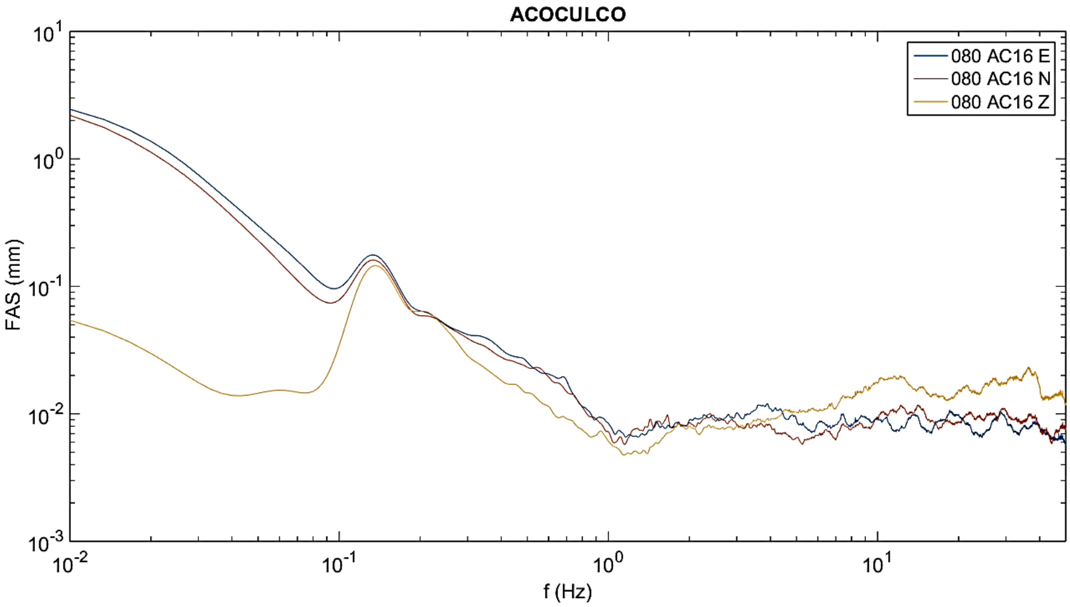
ACOCULCO
080 AC16 E
080 AC16 N
080 AC16 Z
FAS (mm)
f (Hz)

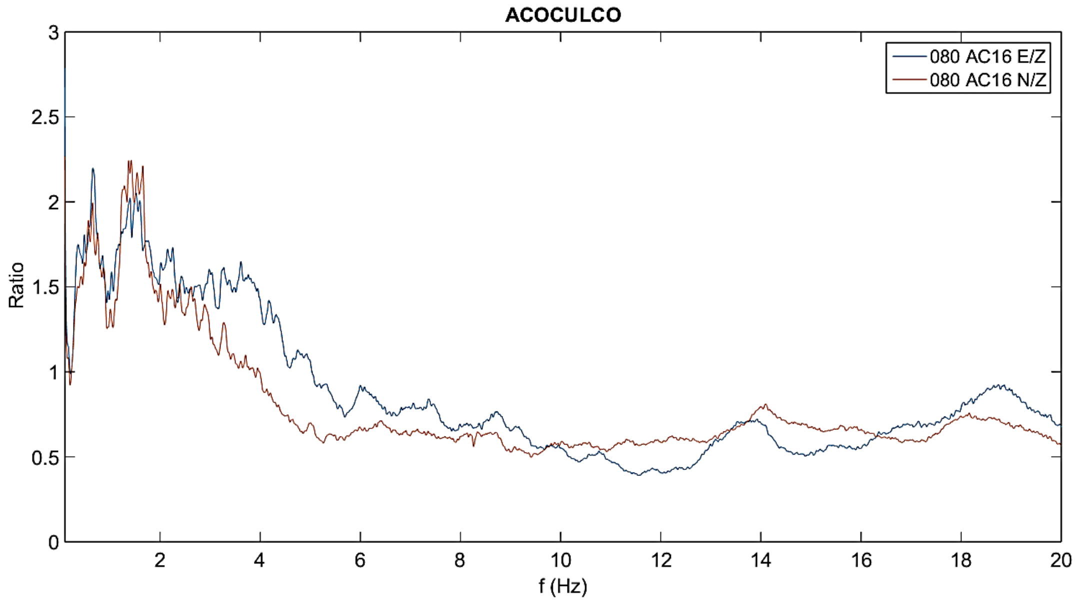
ACOCULCO
080 AC16 E/Z
080 AC16 N/Z
Ratio
f (Hz)

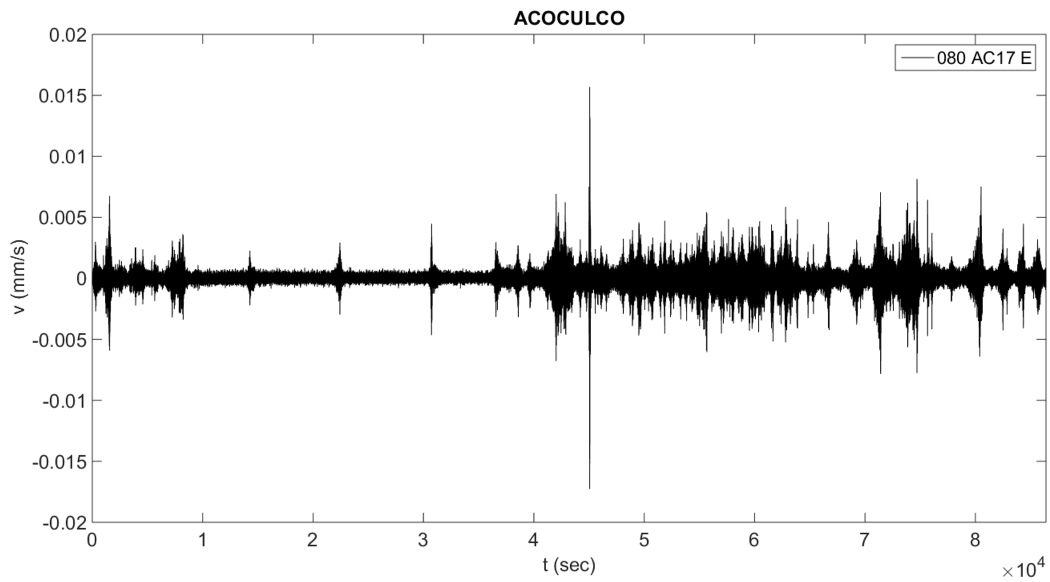
ACOCULCO
080 AC17 E
v (mm/s)
t (sec)
×10^4

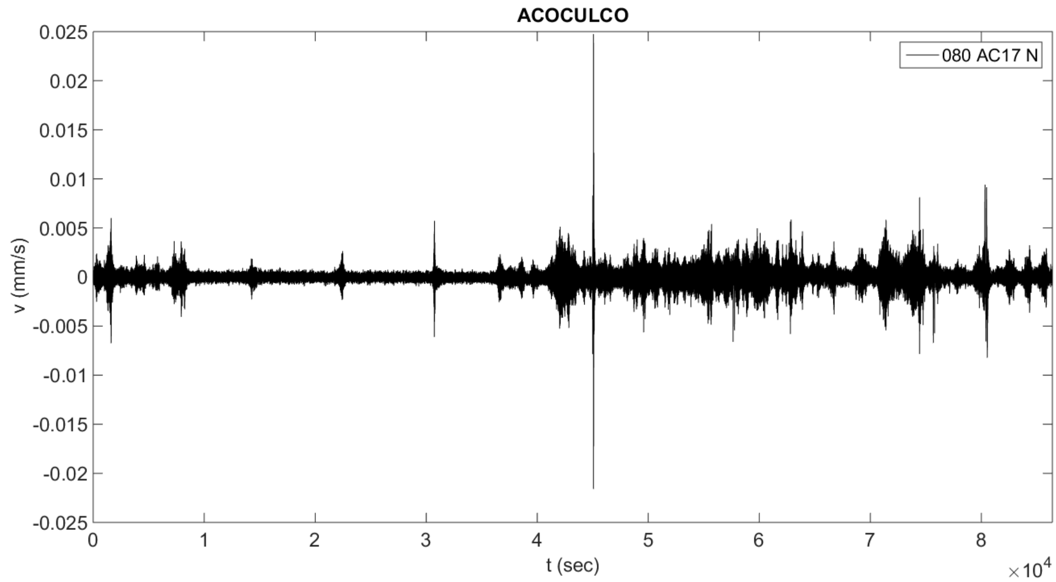
ACOCULCO
080 AC17 N
v (mm/s)
t (sec)
×10^4

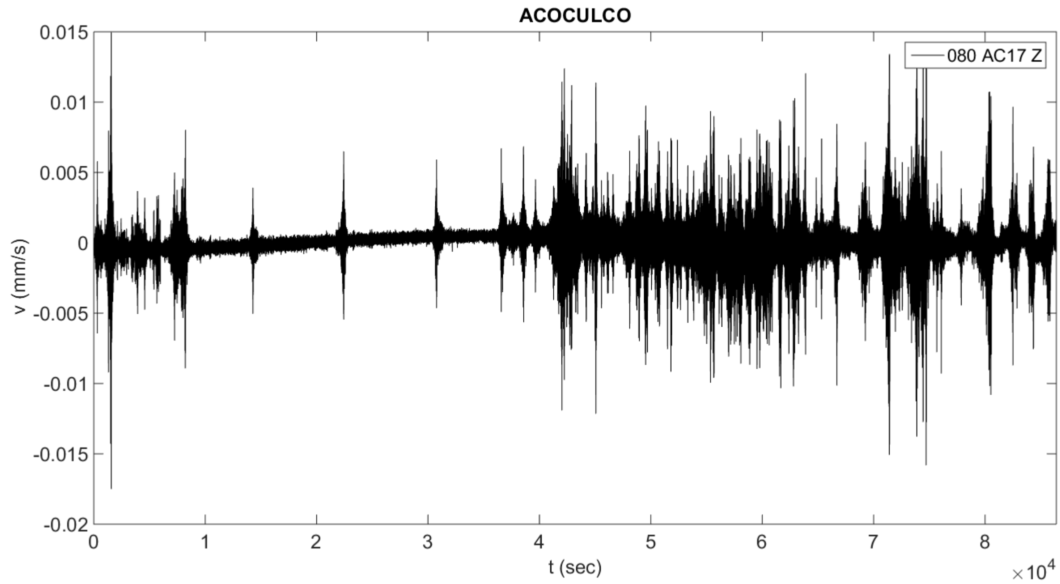
ACOCULCO
080 AC17 Z
v (mm/s)
t (sec)
×10^4

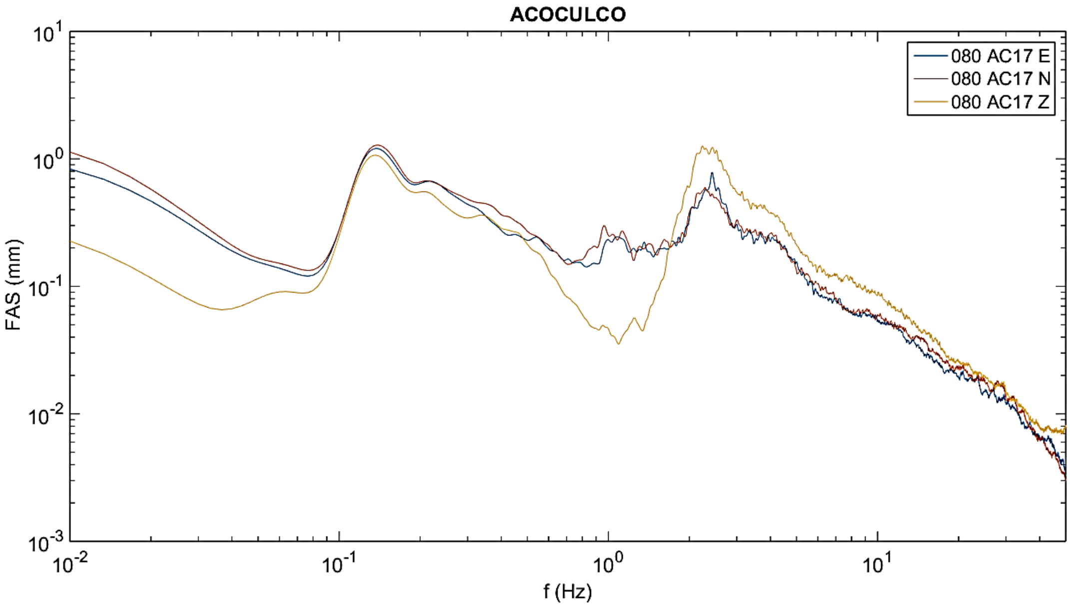
ACOCULCO
080 AC17 E
080 AC17 N
080 AC17 Z
FAS (mm)
f (Hz)

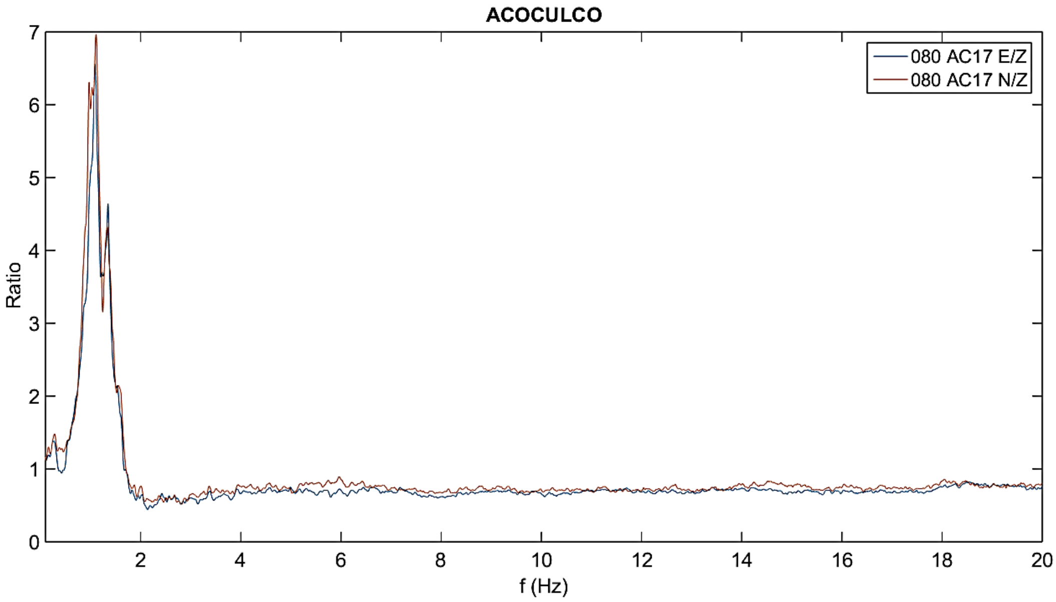
ACOCULCO
080 AC17 E/Z
080 AC17 N/Z
Ratio
f (Hz)

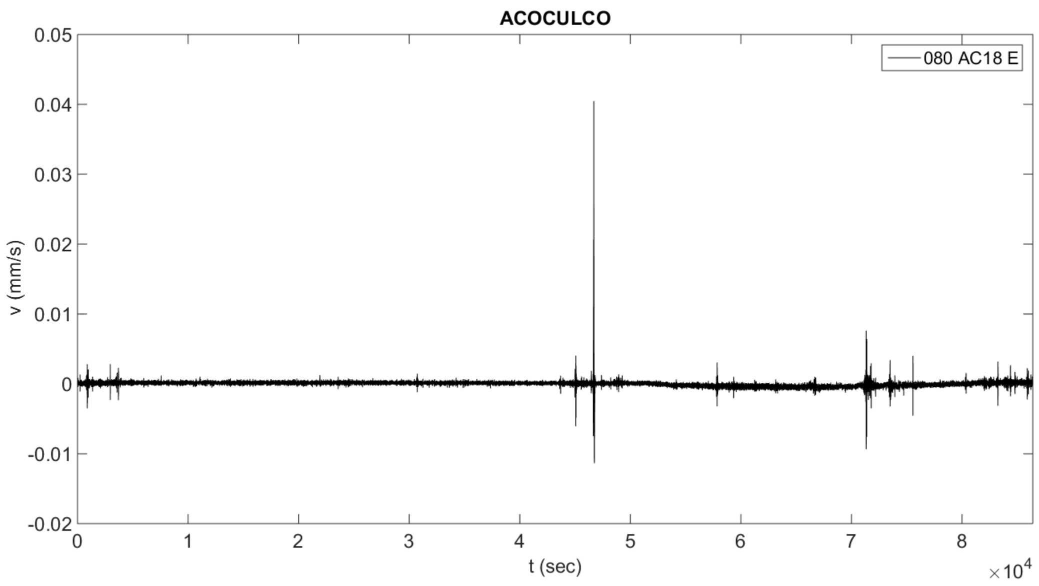
ACOCULCO
080 AC18 E
v (mm/s)
t (sec)
×10^4
0.05
0.04
0.03
0.02
0.01
0
-0.01
-0.02
0
1
2
3
4
5
6
7
8

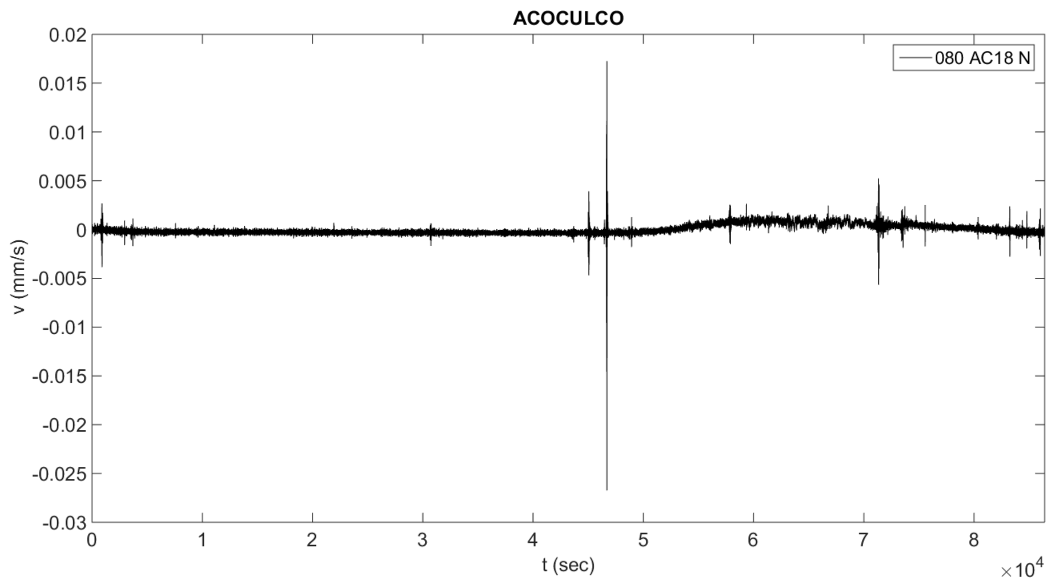
ACOCULCO
080 AC18 N
v (mm/s)
t (sec)
×10^4
0.02
0.015
0.01
0.005
0
-0.005
-0.01
-0.015
-0.02
-0.025
-0.03
0
1
2
3
4
5
6
7
8

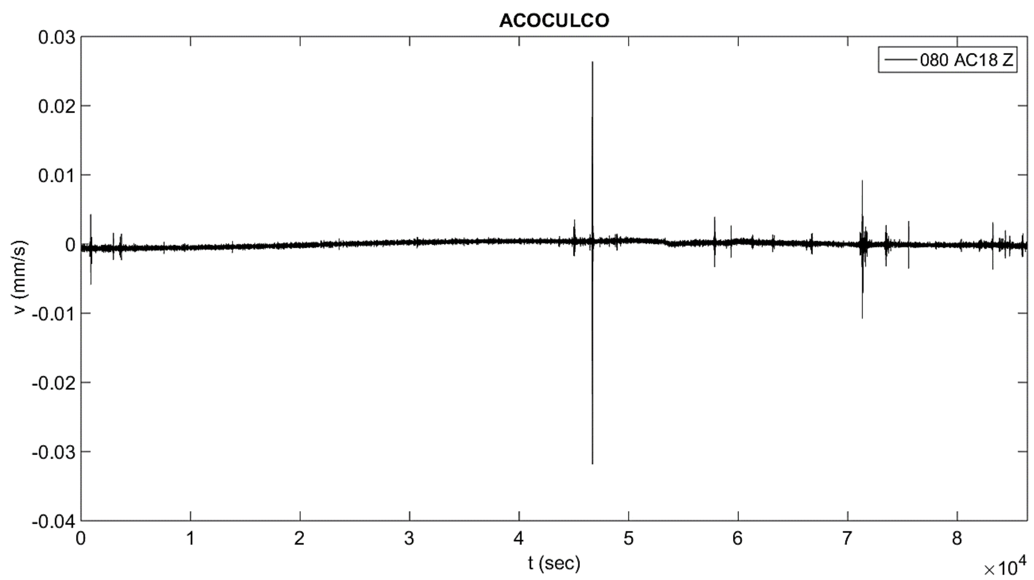
ACOCULCO
080 AC18 Z
v (mm/s)
t (sec)
×10^4
0.03
0.02
0.01
0
-0.01
-0.02
-0.03
-0.04
0
1
2
3
4
5
6
7
8

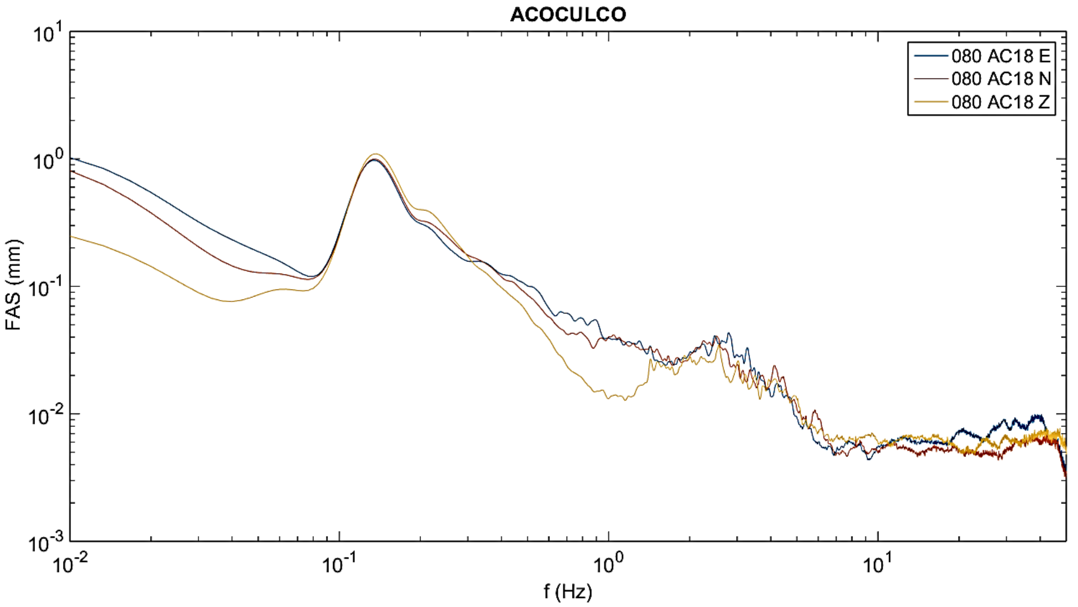
ACOCULCO
080 AC18 E
080 AC18 N
080 AC18 Z
FAS (mm)
f (Hz)

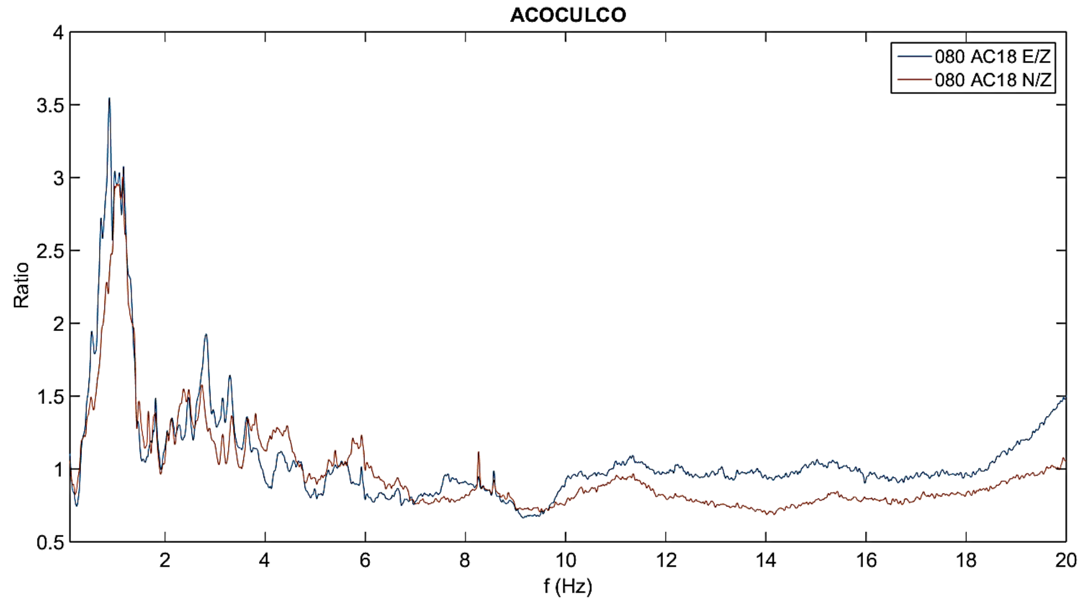
ACOCULCO
080 AC18 E/Z
080 AC18 N/Z
Ratio
f (Hz)

Appendix 4-B Day 087 Spectra and Spectral Ratios

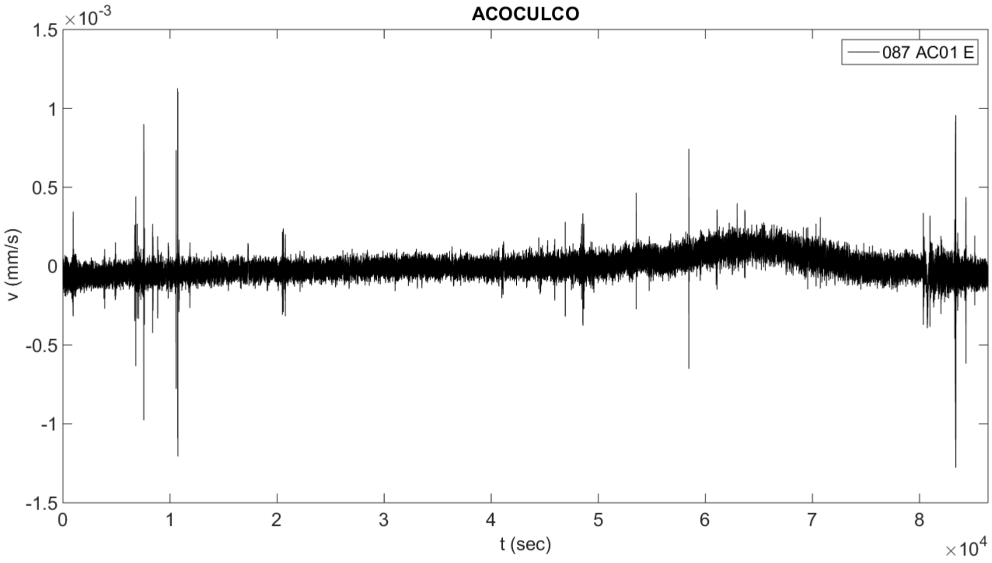

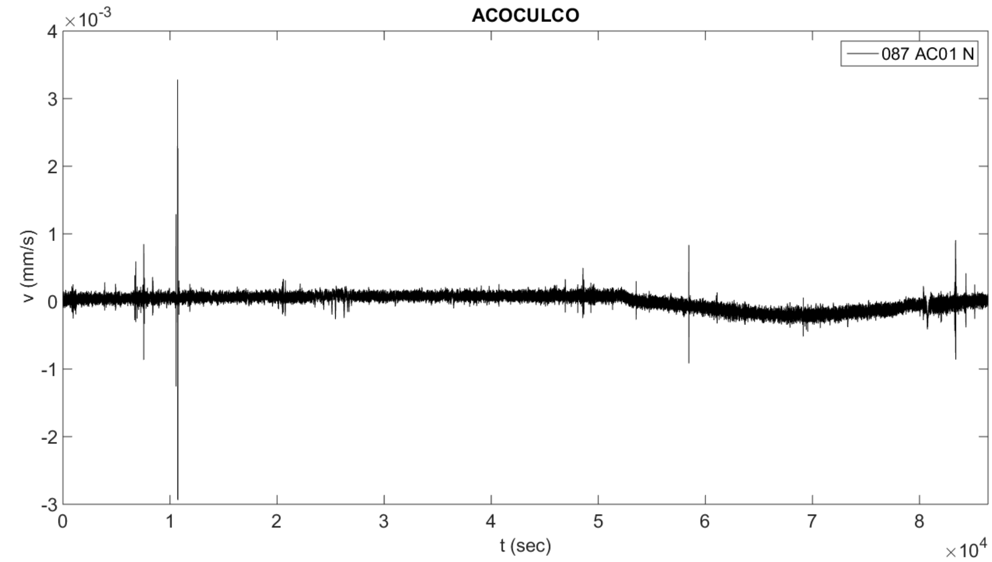

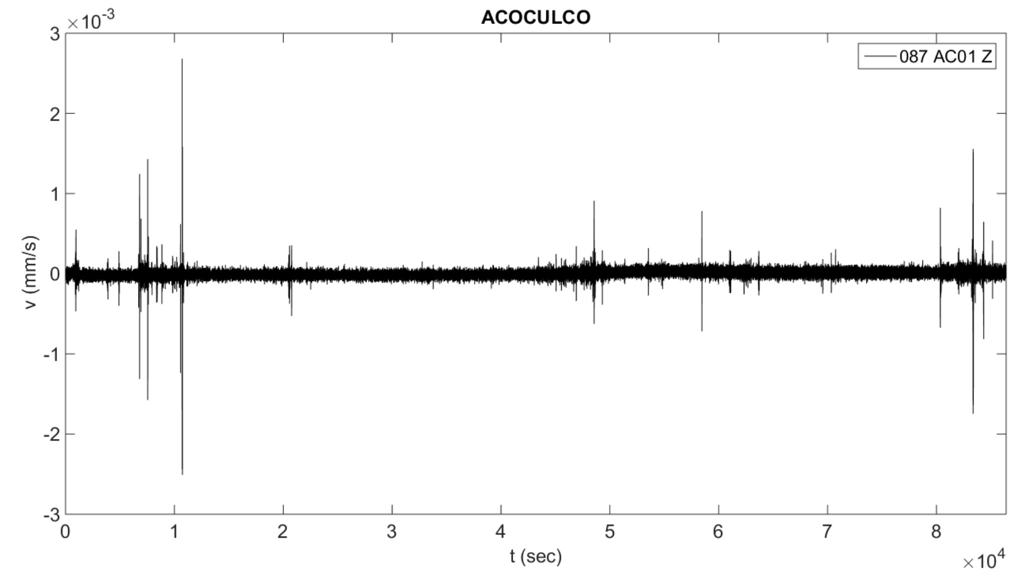

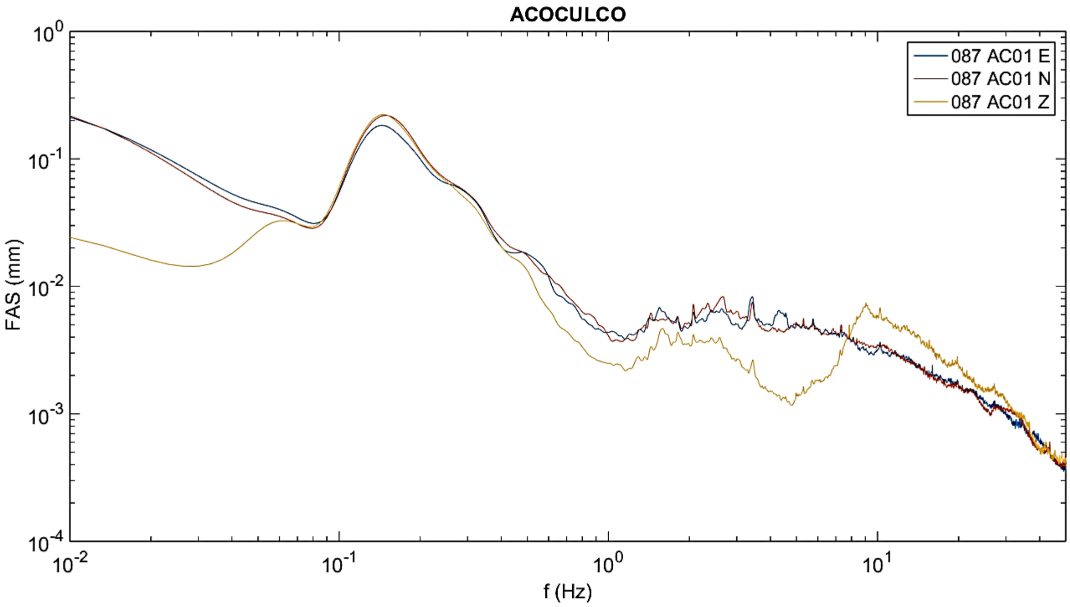
ACOCULCO
087 AC01 E
087 AC01 N
087 AC01 Z
FAS (mm)
f (Hz)

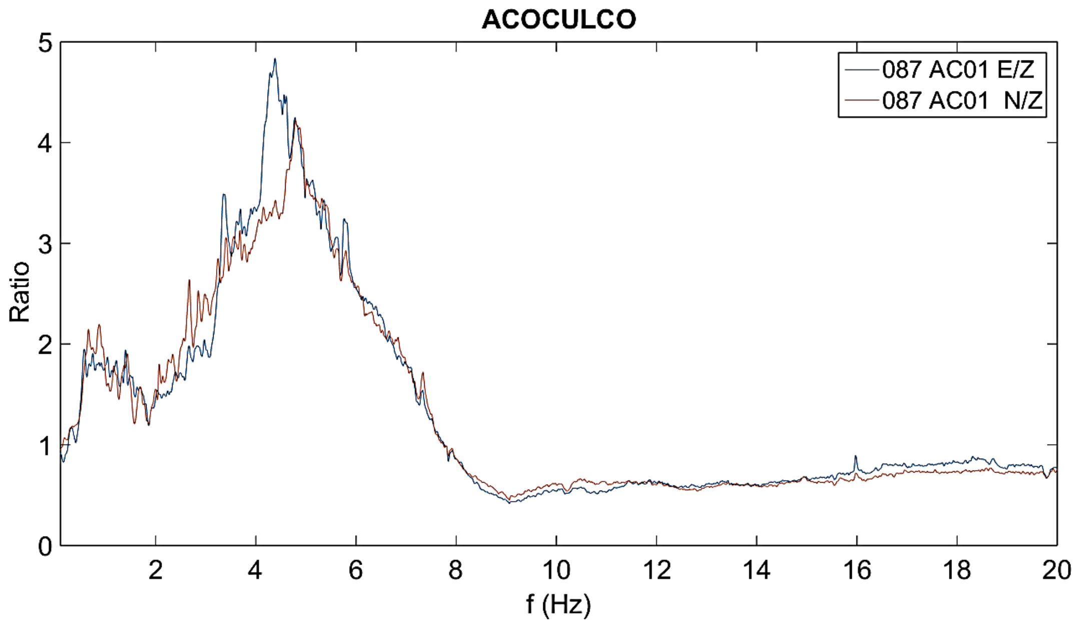
ACOCULCO
087 AC01 E/Z
087 AC01 N/Z
Ratio
f (Hz)

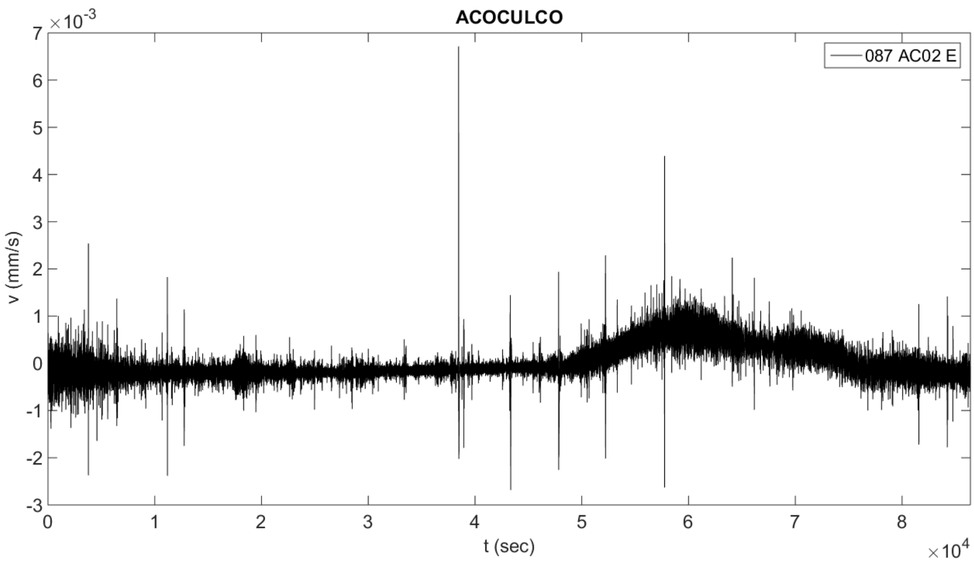
ACOCULCO
087 AC02 E
v (mm/s)
t (sec)
×10^-3
×10^4

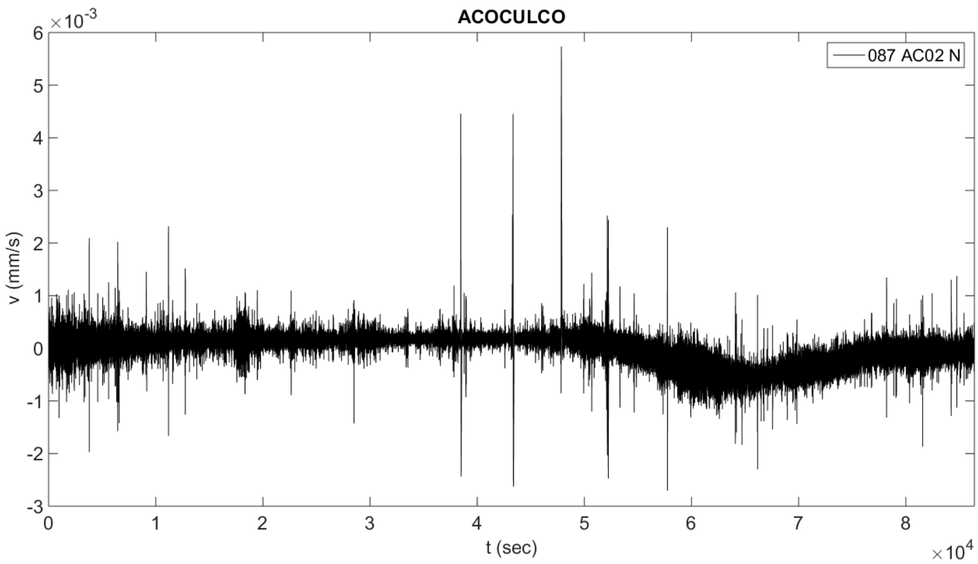
ACOCULCO
087 AC02 N
v (mm/s)
t (sec)
×10^-3
×10^4

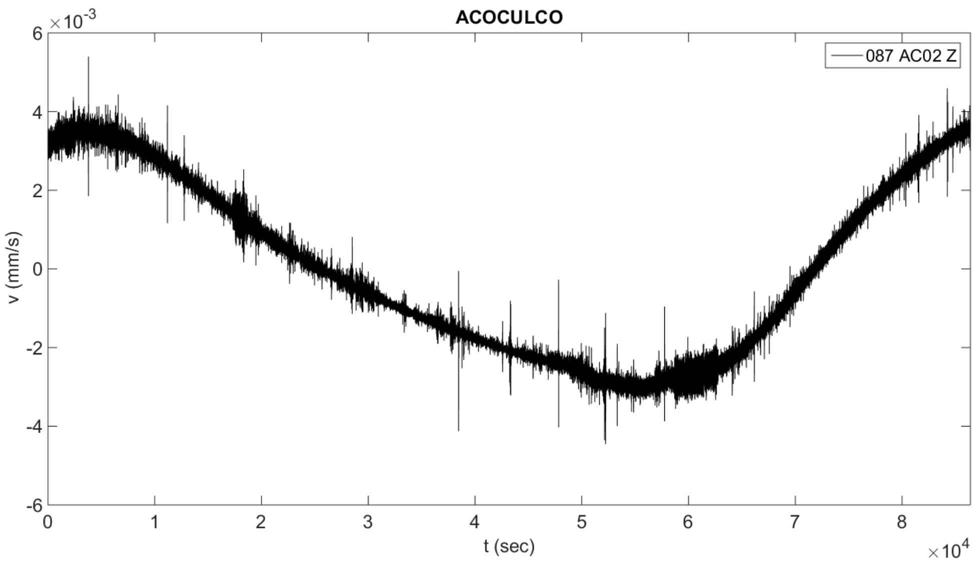
ACOCULCO
087 AC02 Z
v (mm/s)
t (sec)
×10^-3
×10^4

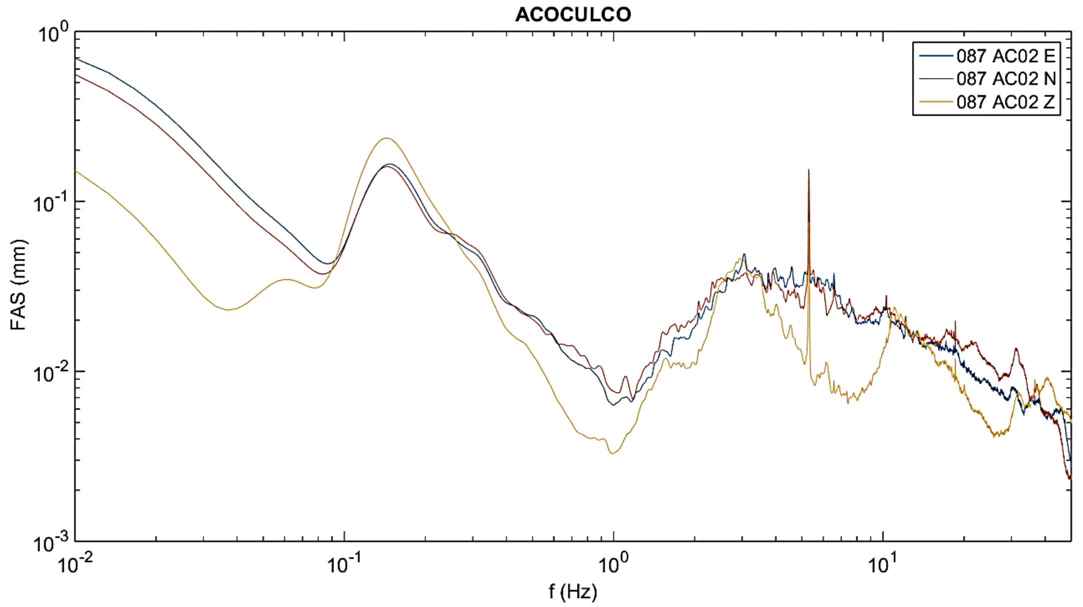

ACOCULCO
087 AC02 E
087 AC02 N
087 AC02 Z
FAS (mm)
f (Hz)

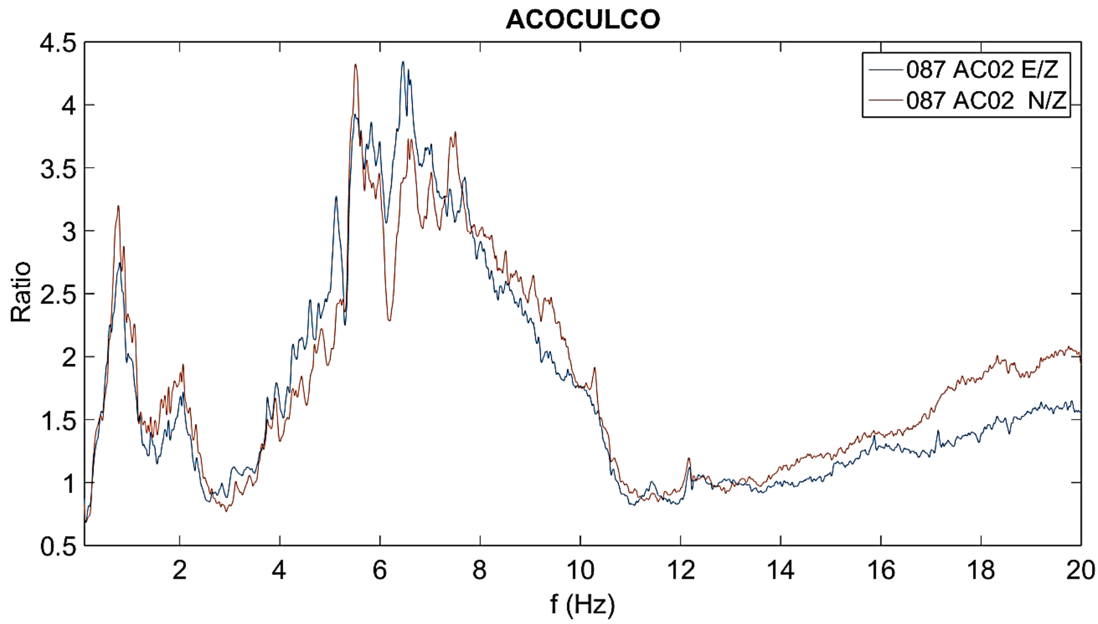

ACOCULCO
087 AC02 E/Z
087 AC02 N/Z
Ratio
f (Hz)

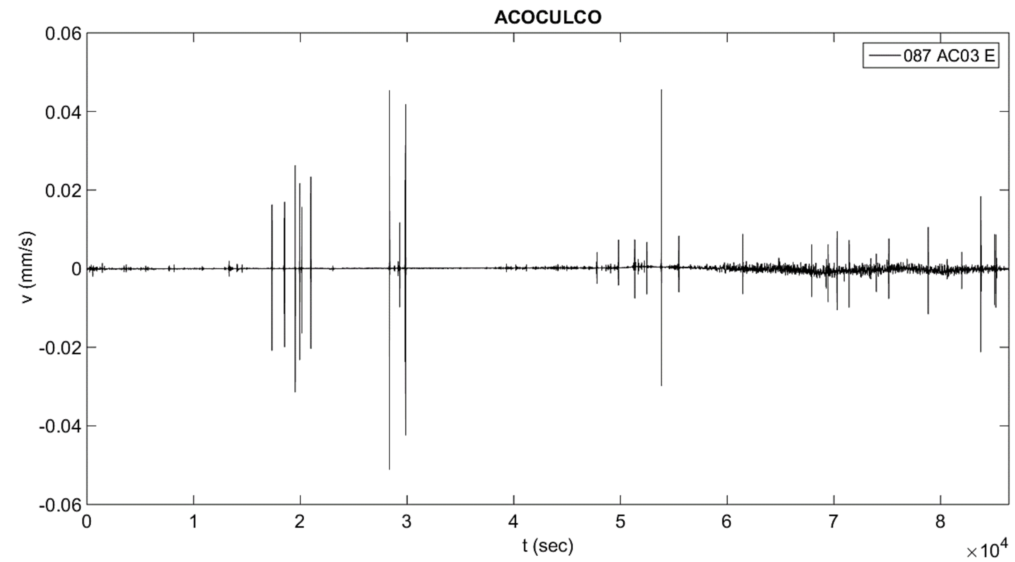
ACOCULCO
087 AC03 E
v (mm/s)
t (sec)
×10^4

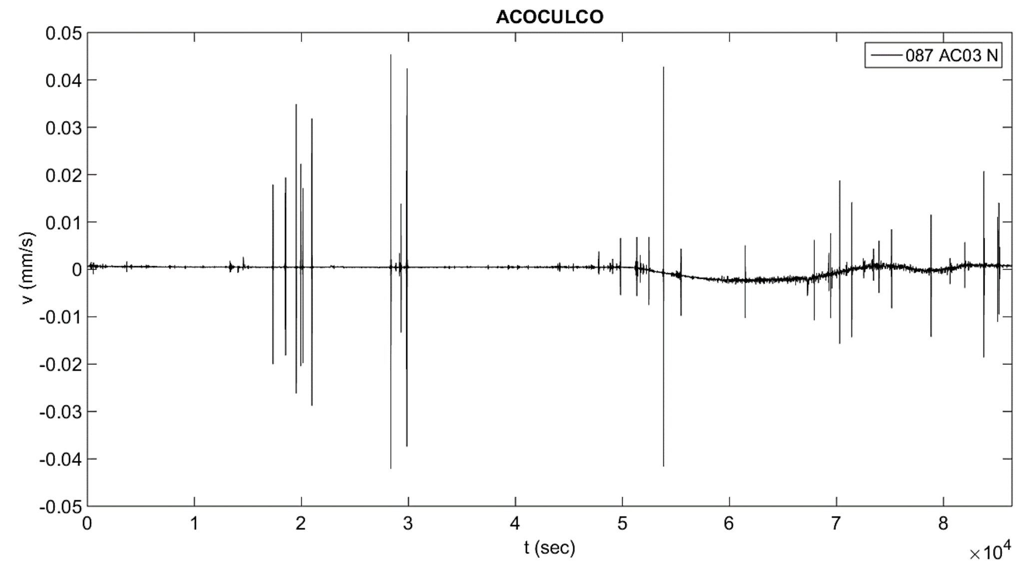
ACOCULCO
087 AC03 N
v (mm/s)
t (sec)
×10^4

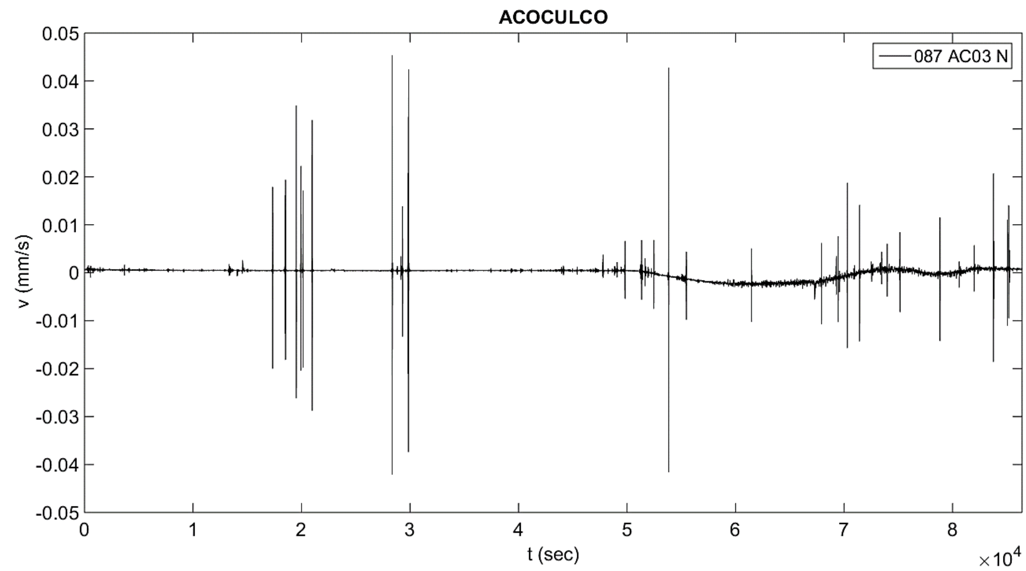
ACOCULCO
087 AC03 N
v (mm/s)
t (sec)
×10^4

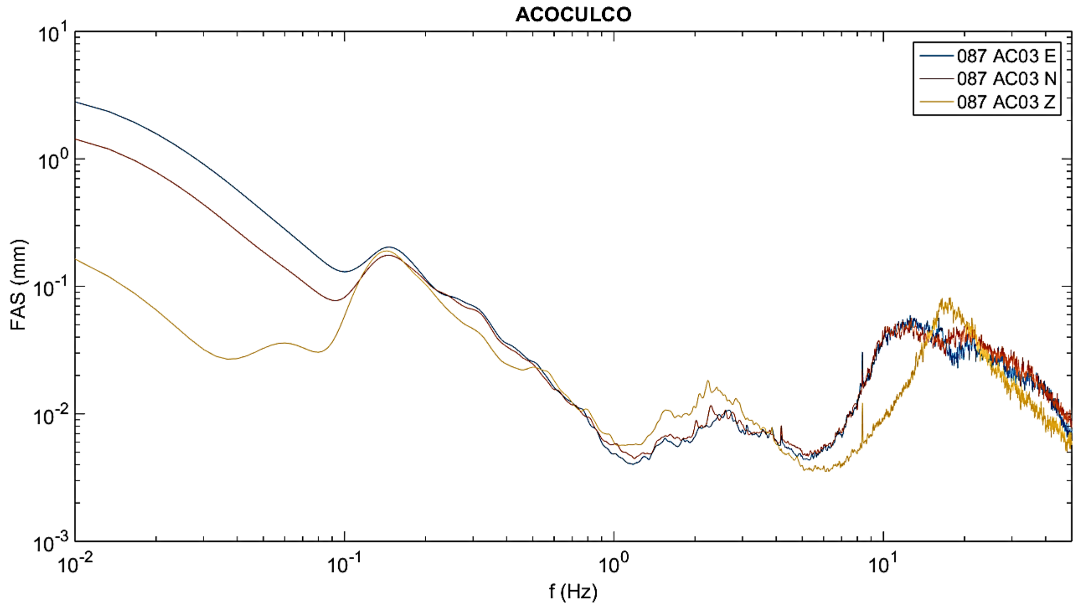
ACOCULCO
087 AC03 E
087 AC03 N
087 AC03 Z
FAS (mm)
f (Hz)

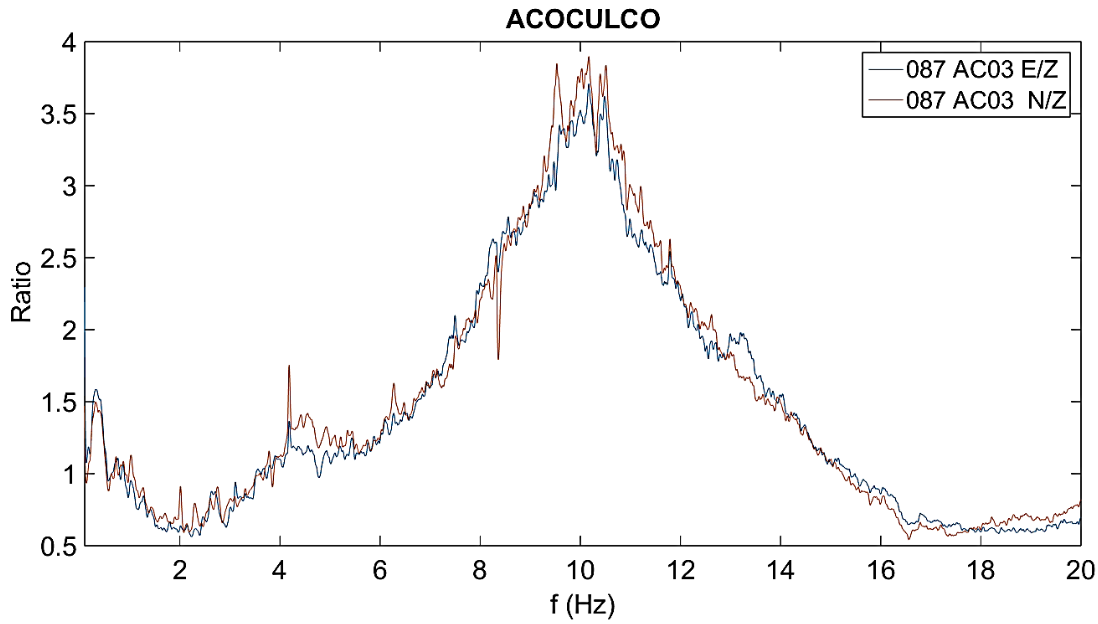
ACOCULCO
087 AC03 E/Z
087 AC03 N/Z
Ratio
f (Hz)

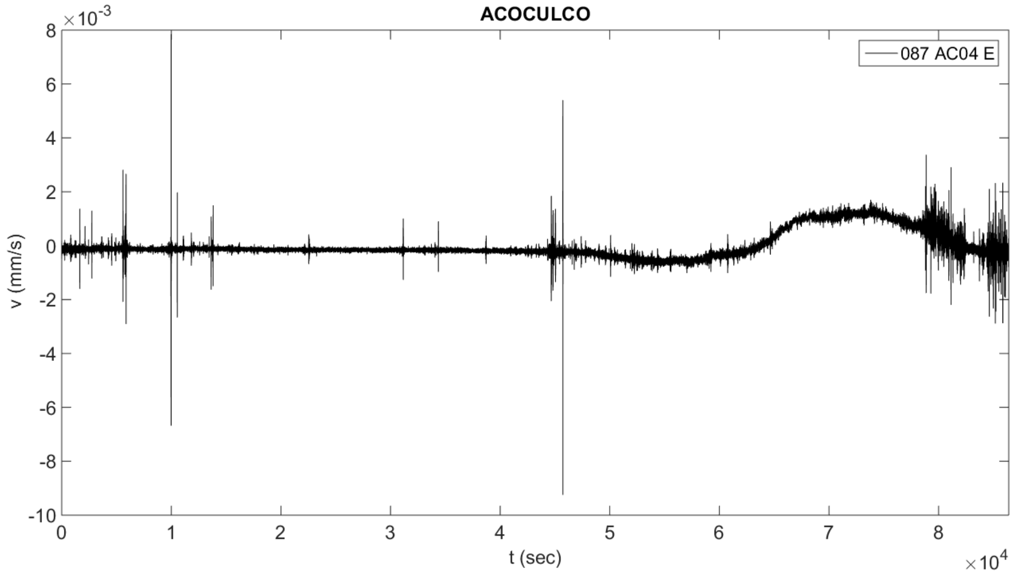
ACOCULCO
×10^-3
087 AC04 E
v (mm/s)
t (sec)
×10^4

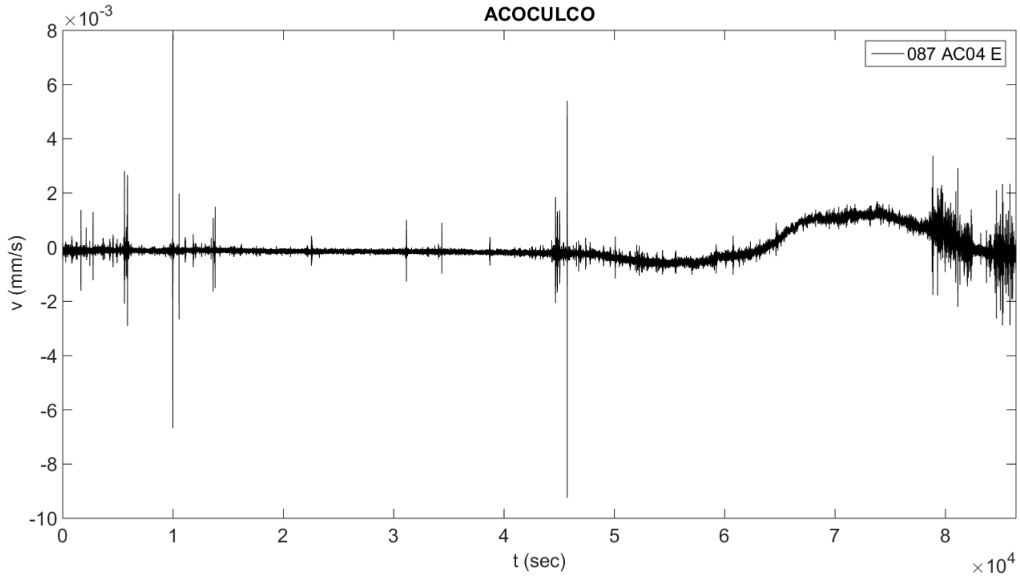
ACOCULCO
×10^-3
087 AC04 E
v (mm/s)
t (sec)
×10^4

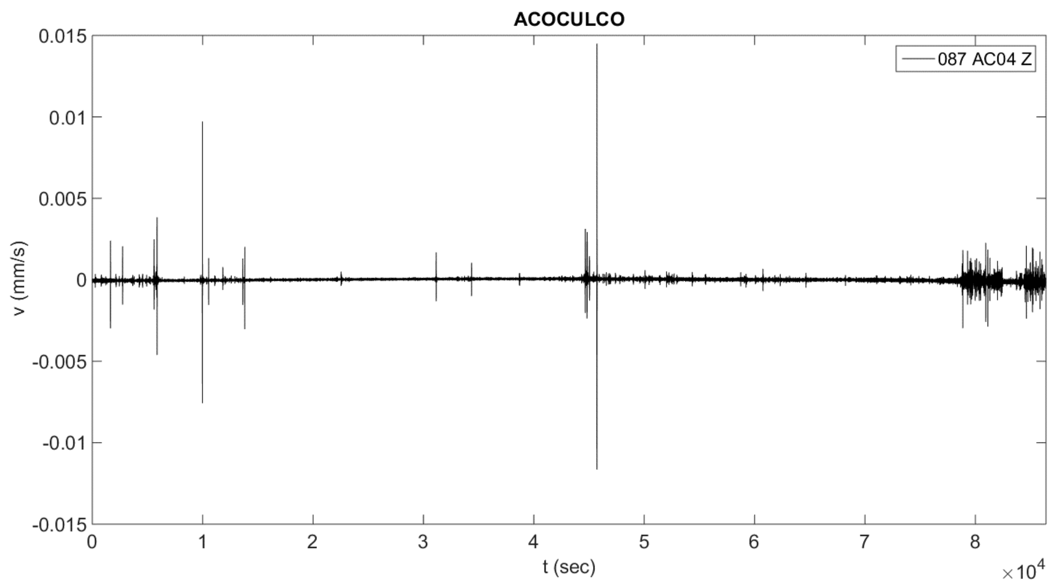
ACOCULCO
087 AC04 Z
v (mm/s)
t (sec)
×10^4

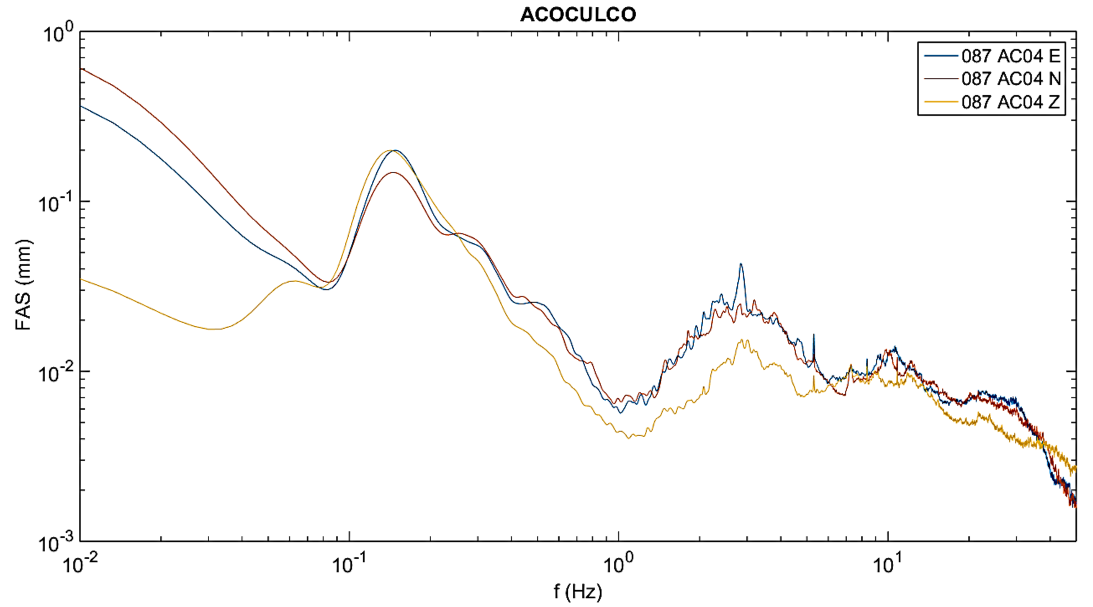
ACOCULCO
087 AC04 E
087 AC04 N
087 AC04 Z
FAS (mm)
f (Hz)

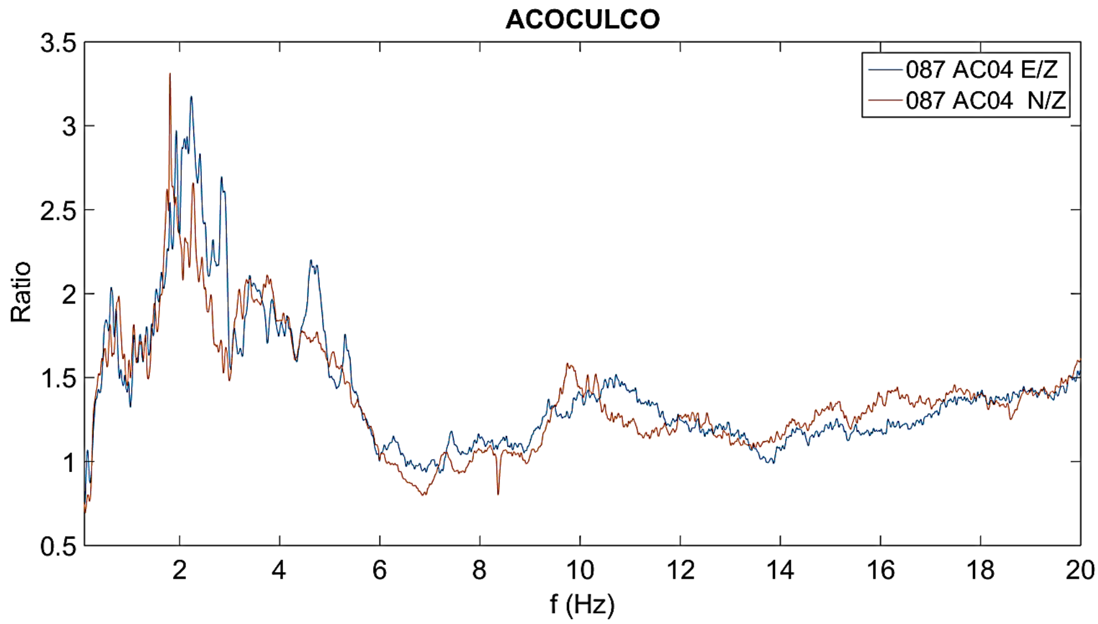
ACOCULCO
087 AC04 E/Z
087 AC04 N/Z
Ratio
f (Hz)

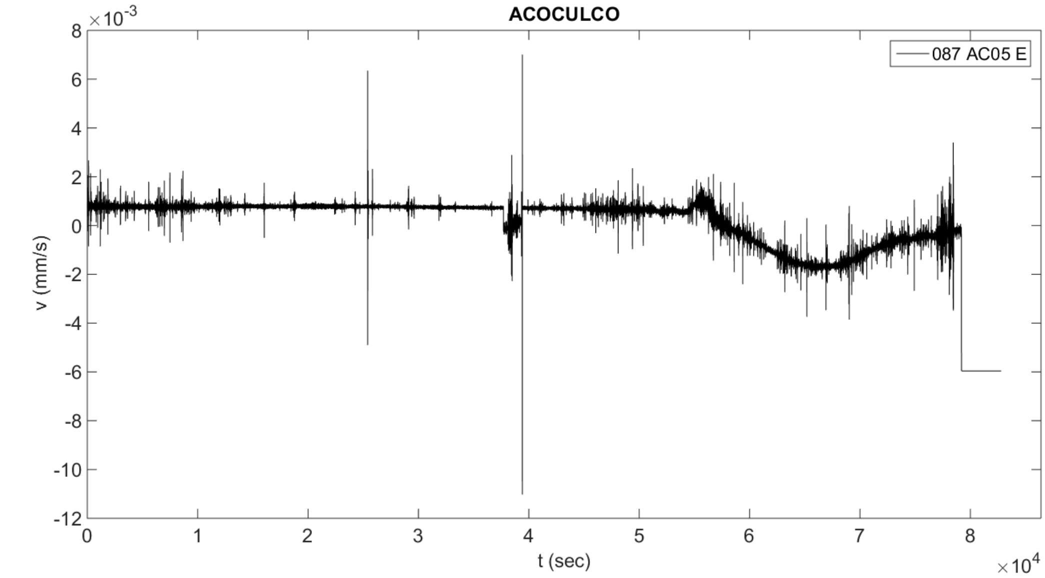
ACOCULCO
$\times 10^{-3}$
087 AC05 E
v (mm/s)
t (sec)
$\times 10^{4}$
8
6
4
2
0
-2
-4
-6
-8
-10
-12
0
1
2
3
4
5
6
7
8

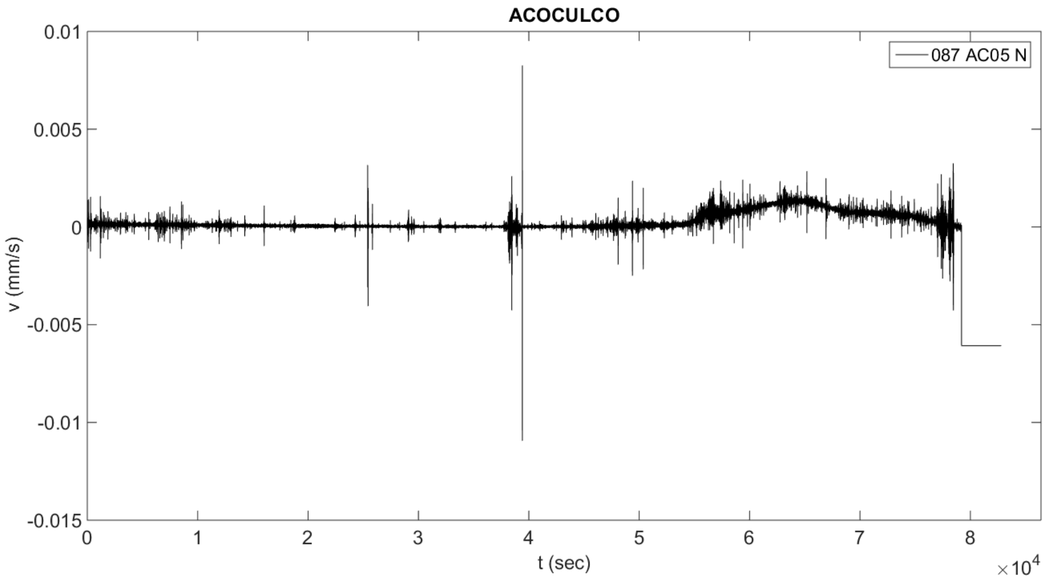
ACOCULCO
087 AC05 N
v (mm/s)
t (sec)
$\times 10^{4}$
0.01
0.005
0
-0.005
-0.01
-0.015
0
1
2
3
4
5
6
7
8

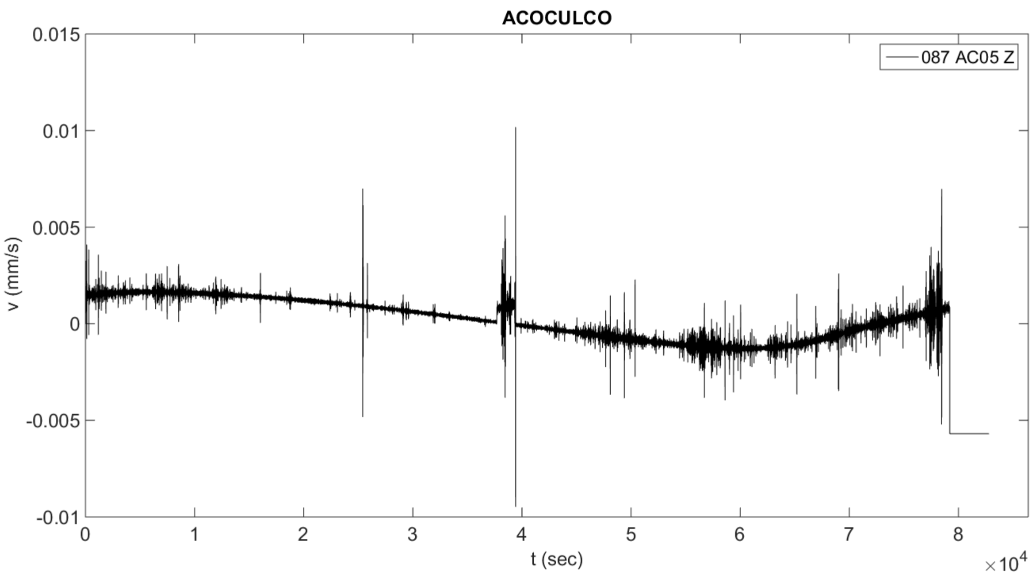
ACOCULCO
087 AC05 Z
v (mm/s)
t (sec)
$\times 10^{4}$
0.015
0.01
0.005
0
-0.005
-0.01
0
1
2
3
4
5
6
7
8

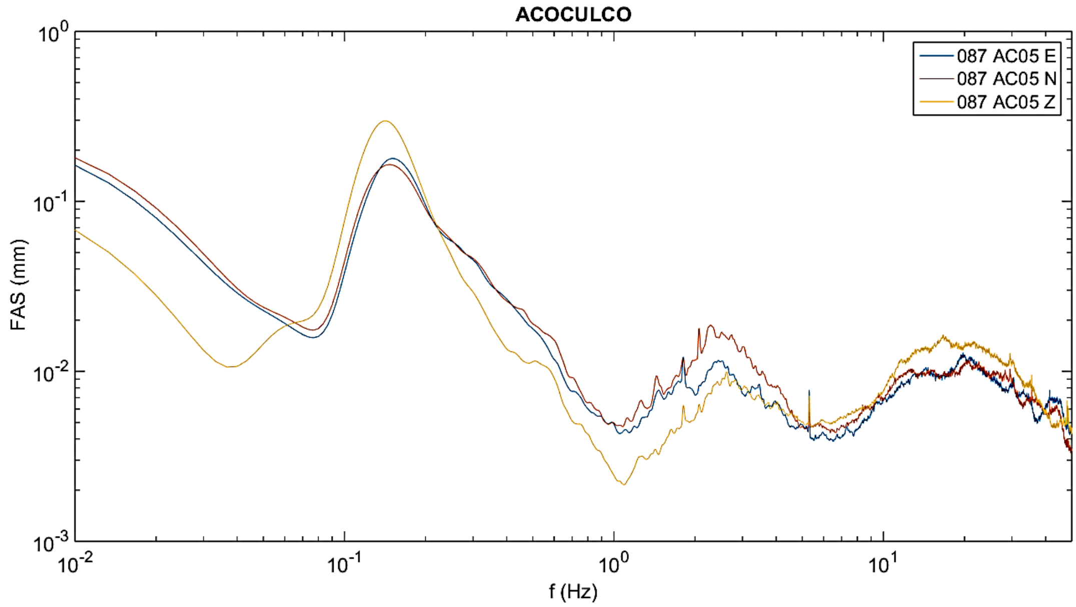
ACOCULCO
087 AC05 E
087 AC05 N
087 AC05 Z
FAS (mm)
f (Hz)

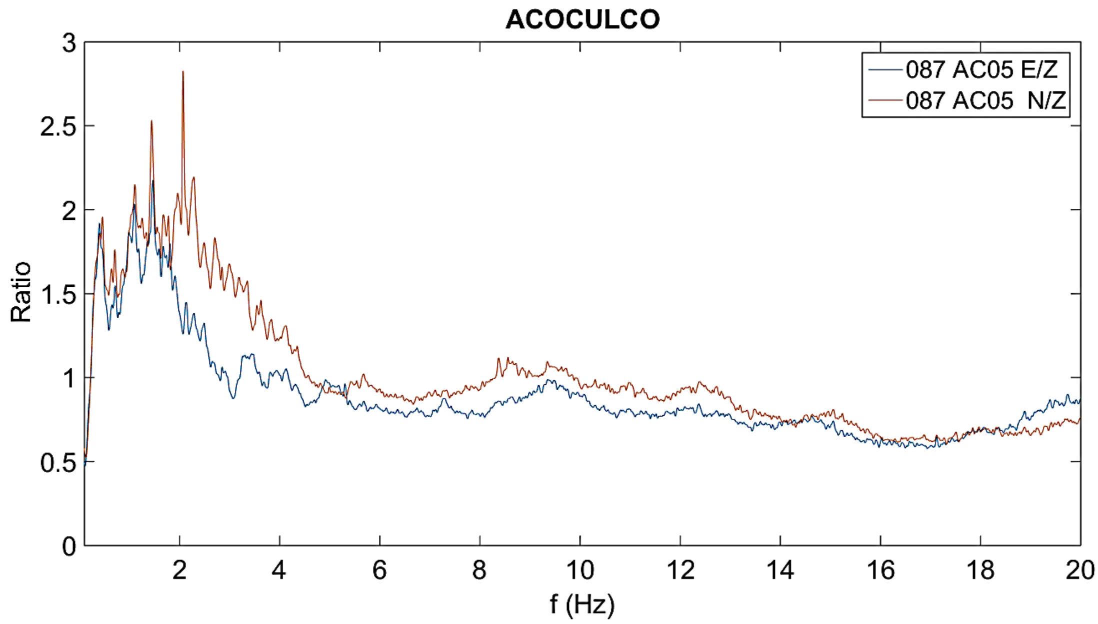
ACOCULCO
087 AC05 E/Z
087 AC05 N/Z
Ratio
f (Hz)

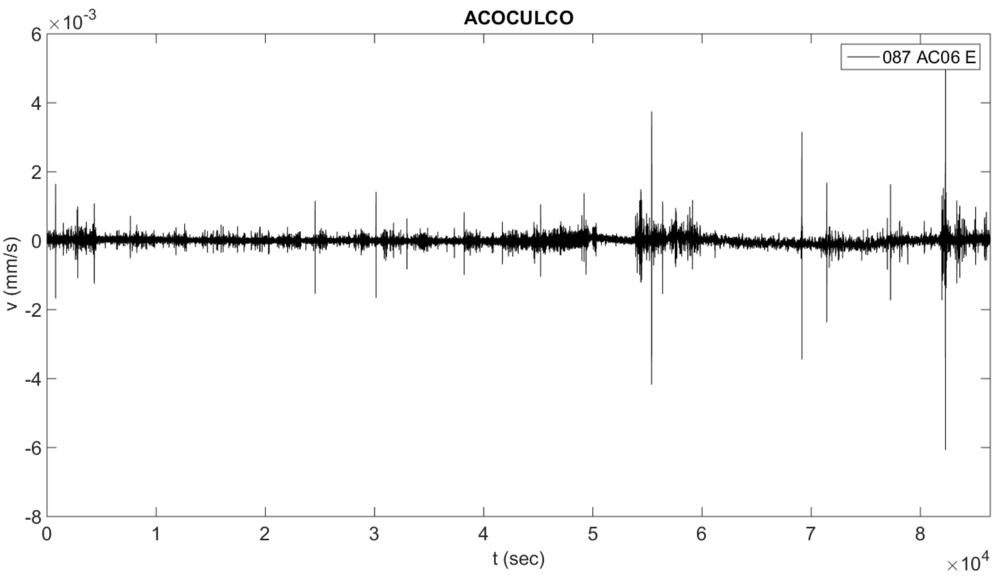
ACOCULCO
087 AC06 E
v (mm/s)
t (sec)

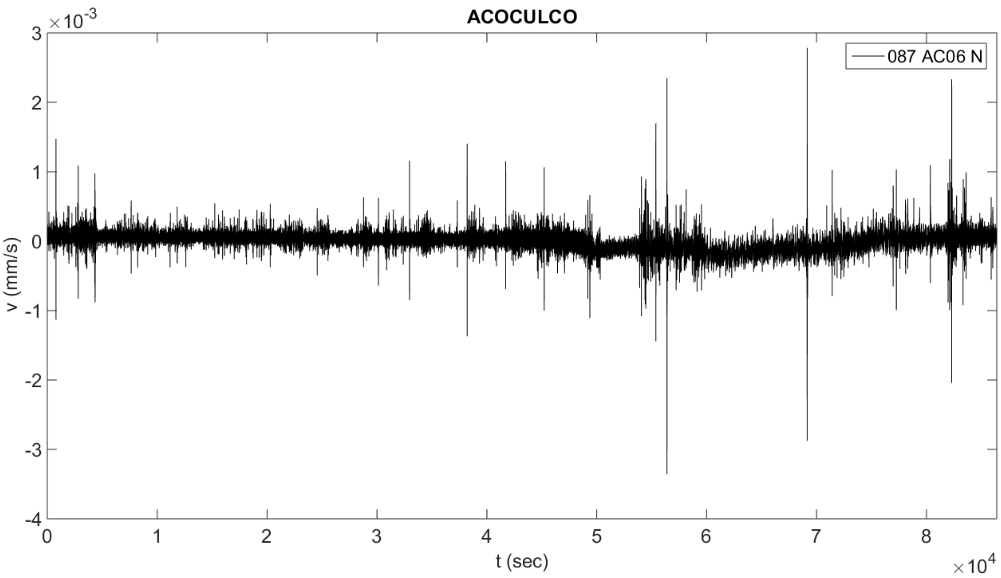
ACOCULCO
087 AC06 N
v (mm/s)
t (sec)

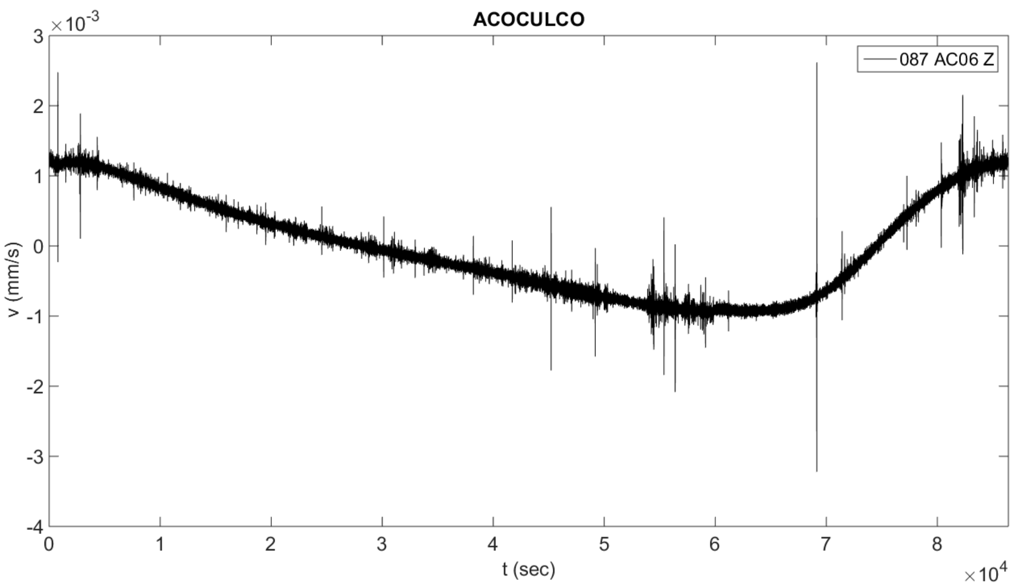
ACOCULCO
087 AC06 Z
v (mm/s)
t (sec)

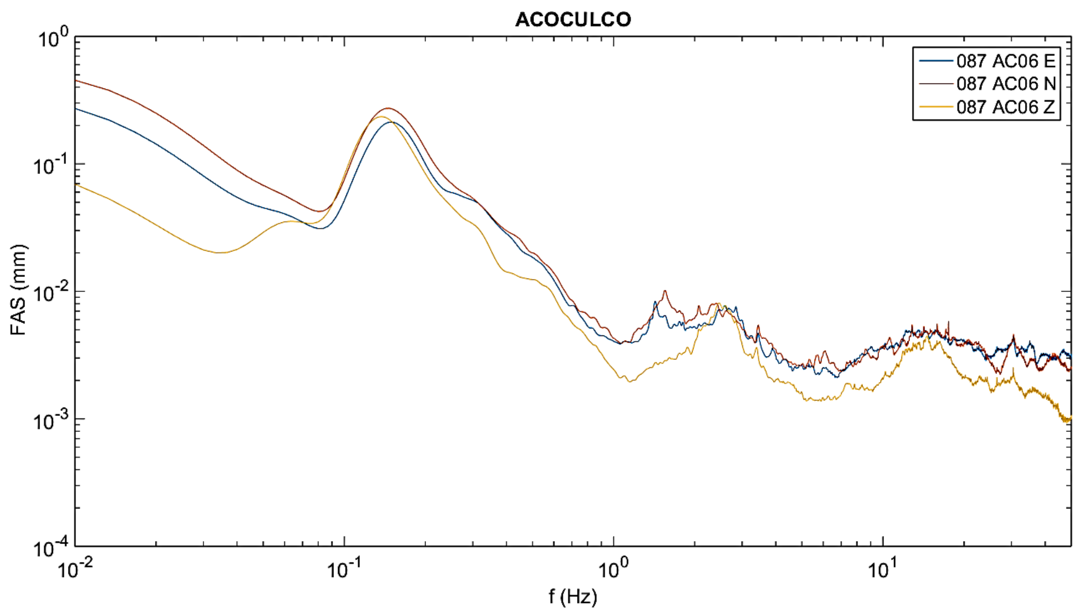
ACOCULCO
087 AC06 E
087 AC06 N
087 AC06 Z
FAS (mm)
f (Hz)

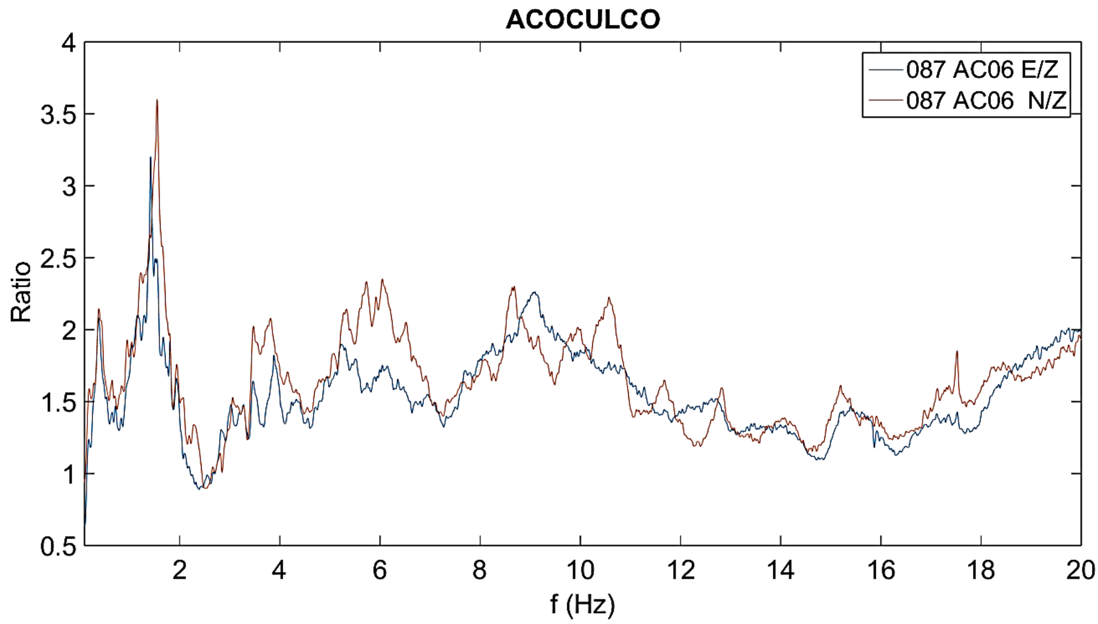
ACOCULCO
087 AC06 E/Z
087 AC06 N/Z
Ratio
f (Hz)

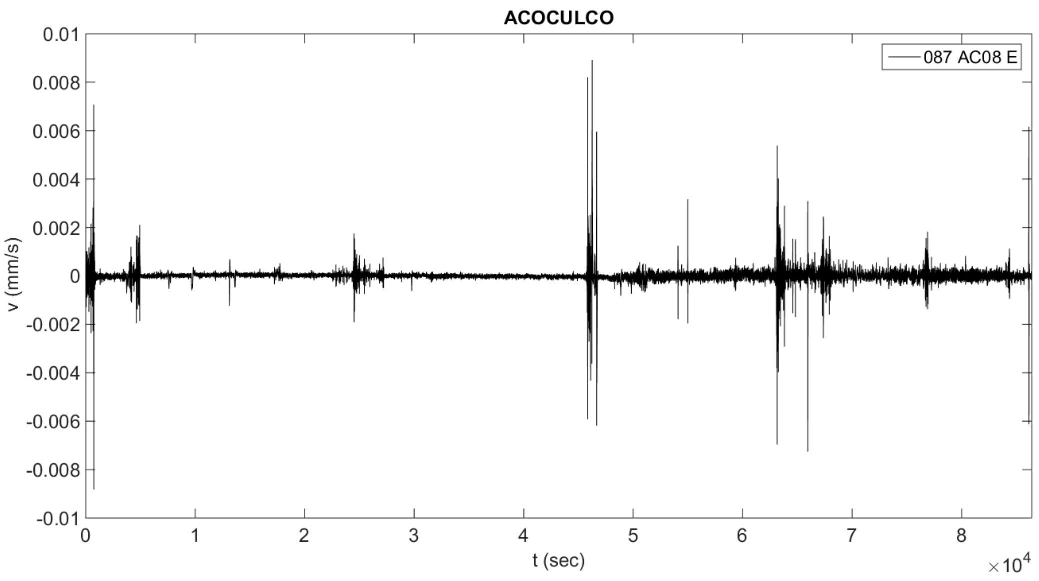
ACOCULCO
087 AC08 E
v (mm/s)
t (sec)
×10^4

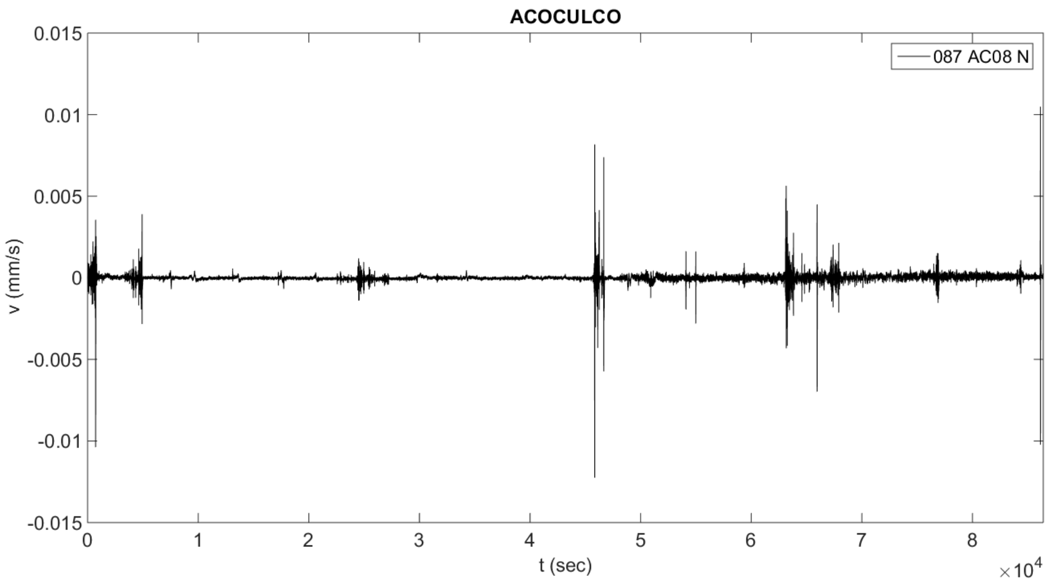
ACOCULCO
087 AC08 N
v (mm/s)
t (sec)
×10^4

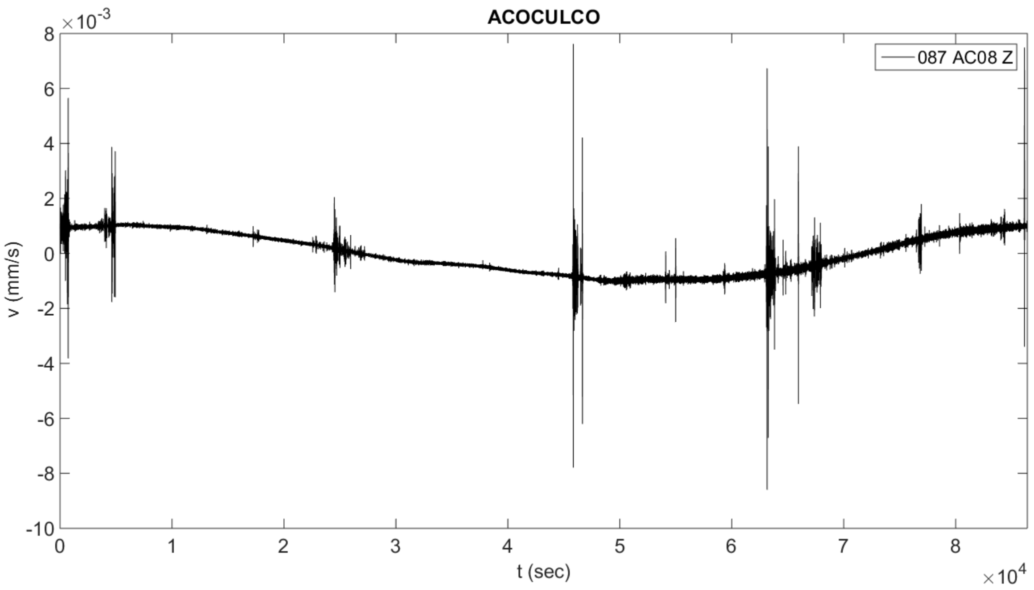
ACOCULCO
×10^-3
087 AC08 Z
v (mm/s)
t (sec)
×10^4

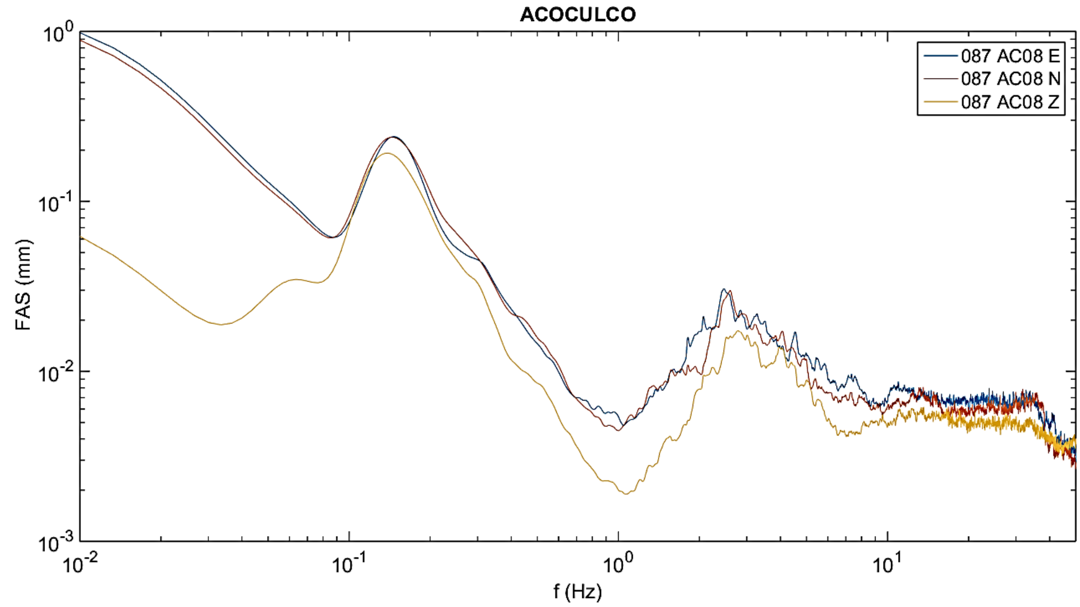
ACOCULCO
087 AC08 E
087 AC08 N
087 AC08 Z
FAS (mm)
f (Hz)

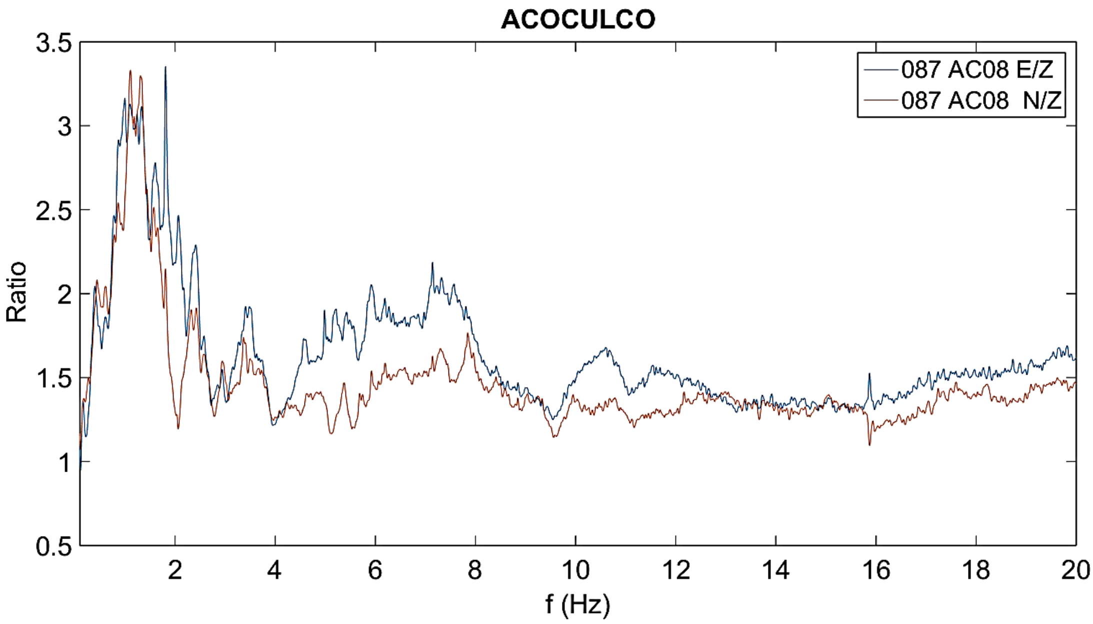
ACOCULCO
087 AC08 E/Z
087 AC08 N/Z
Ratio
f (Hz)

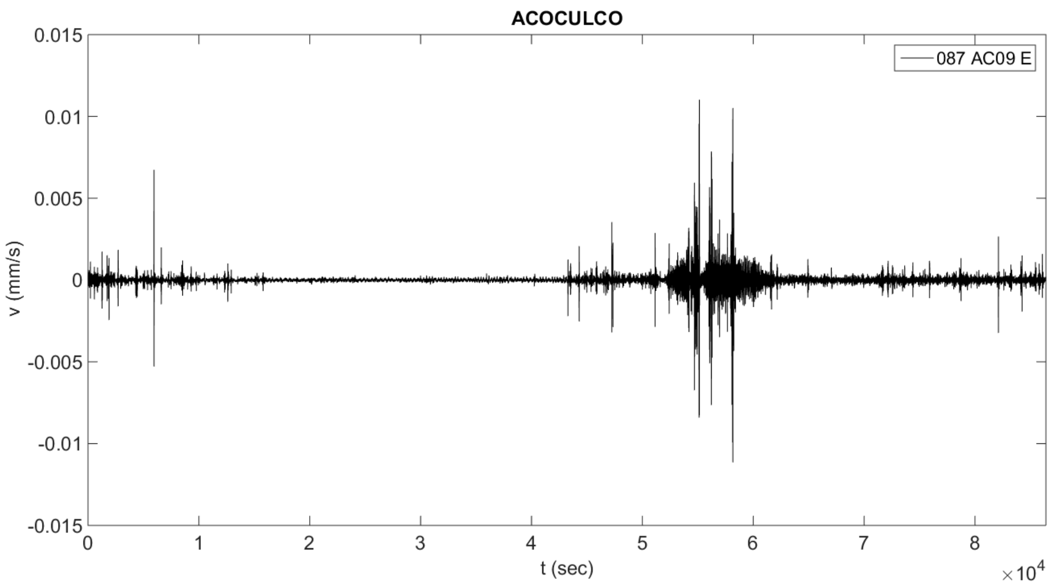
ACOCULCO
087 AC09 E
0.015
0.01
0.005
0
-0.005
-0.01
-0.015
v (mm/s)
0
1
2
3
4
5
6
7
8
t (sec)
×10^4

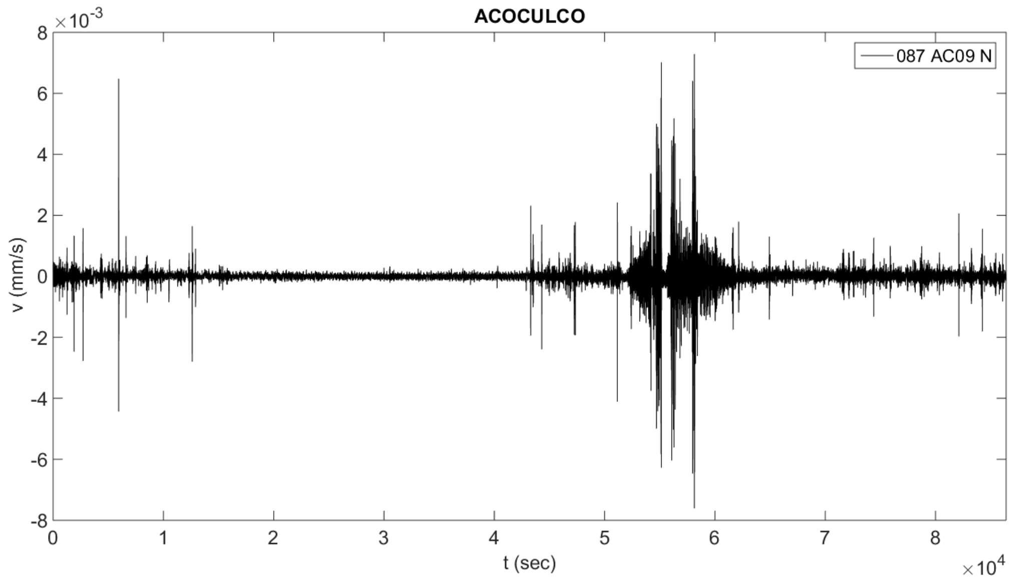
ACOCULCO
087 AC09 N
×10^-3
8
6
4
2
0
-2
-4
-6
-8
v (mm/s)
0
1
2
3
4
5
6
7
8
t (sec)
×10^4

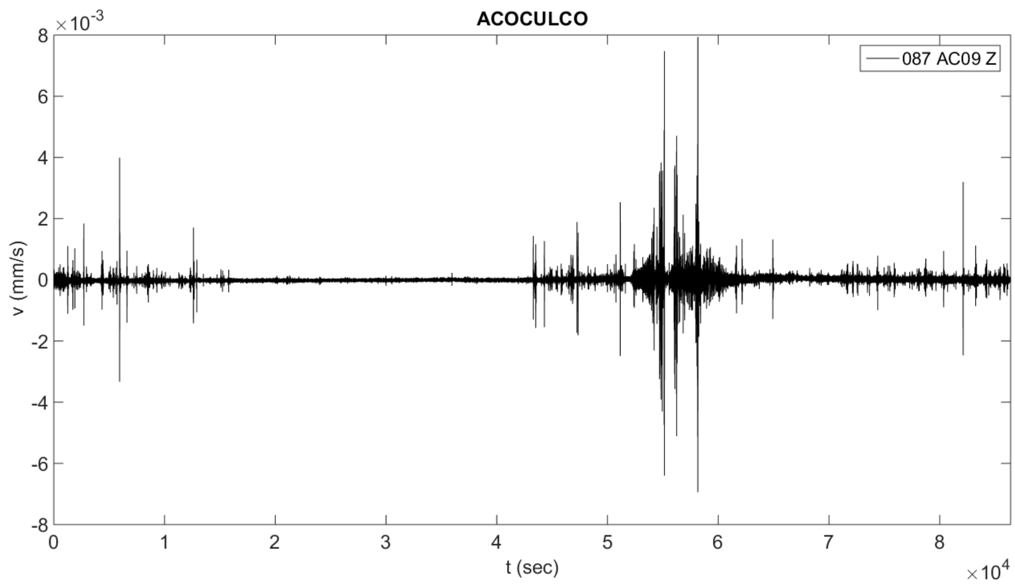
ACOCULCO
087 AC09 Z
×10^-3
8
6
4
2
0
-2
-4
-6
-8
v (mm/s)
0
1
2
3
4
5
6
7
8
t (sec)
×10^4

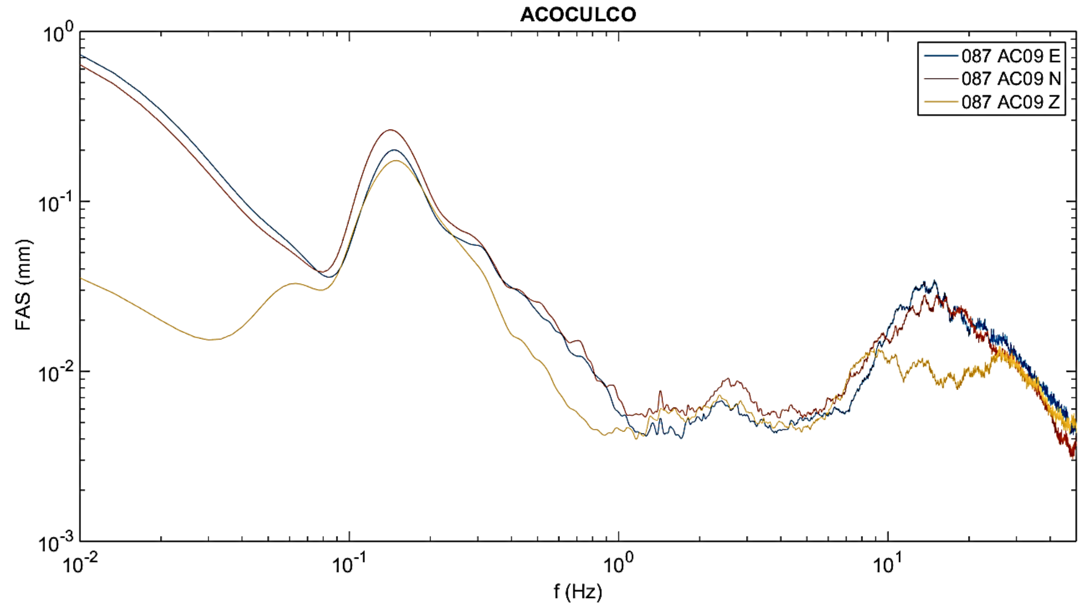
ACOCULCO
087 AC09 E
087 AC09 N
087 AC09 Z
FAS (mm)
f (Hz)

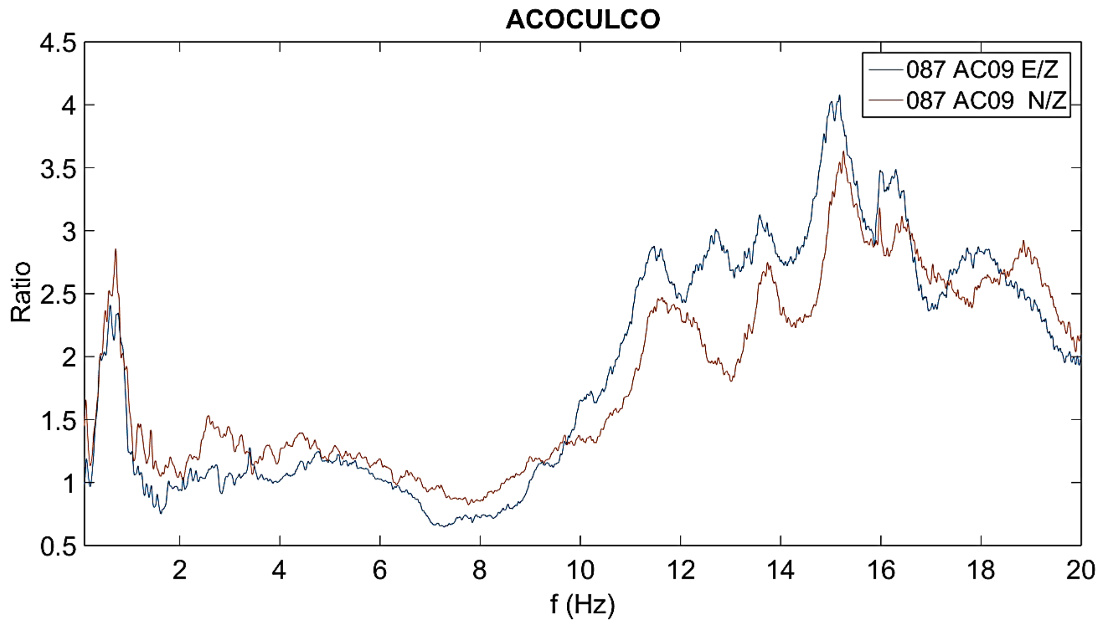
ACOCULCO
087 AC09 E/Z
087 AC09 N/Z
Ratio
f (Hz)

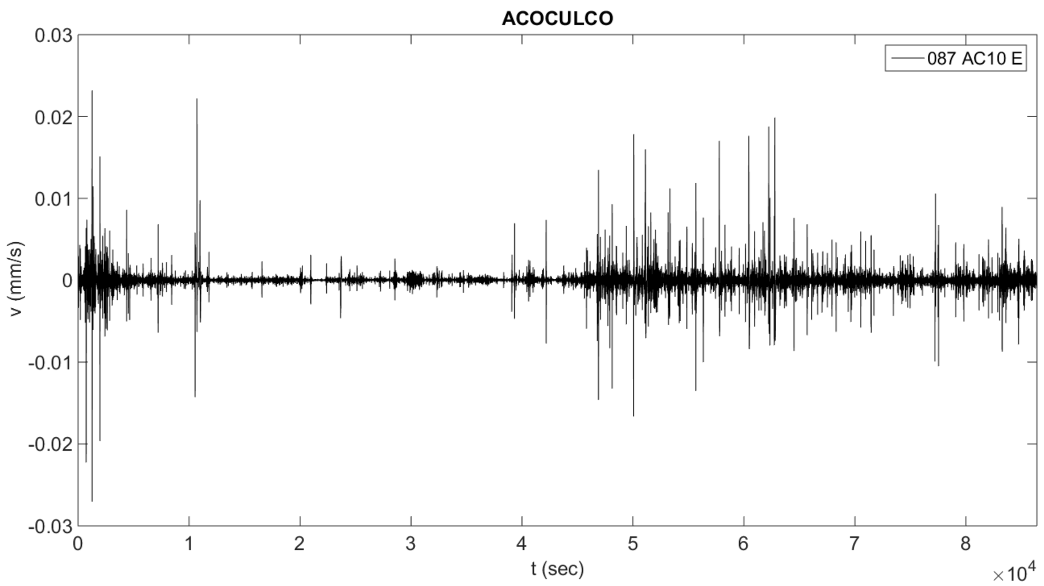
ACOCULCO
087 AC10 E
v (mm/s)
t (sec)
×10^4
0.03
0.02
0.01
0
-0.01
-0.02
-0.03
0
1
2
3
4
5
6
7
8

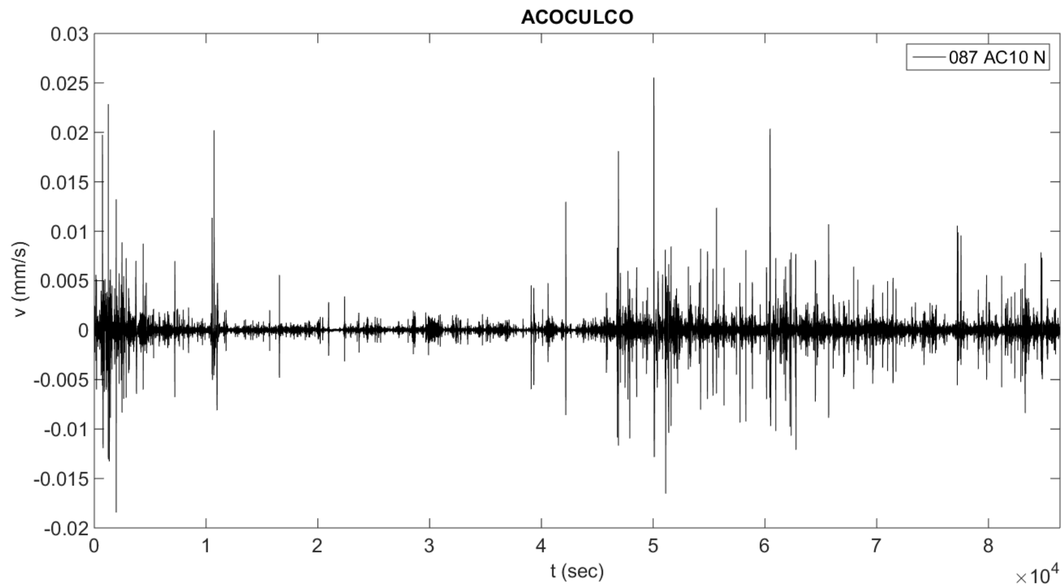
ACOCULCO
087 AC10 N
v (mm/s)
t (sec)
×10^4
0.03
0.025
0.02
0.015
0.01
0.005
0
-0.005
-0.01
-0.015
-0.02
0
1
2
3
4
5
6
7
8

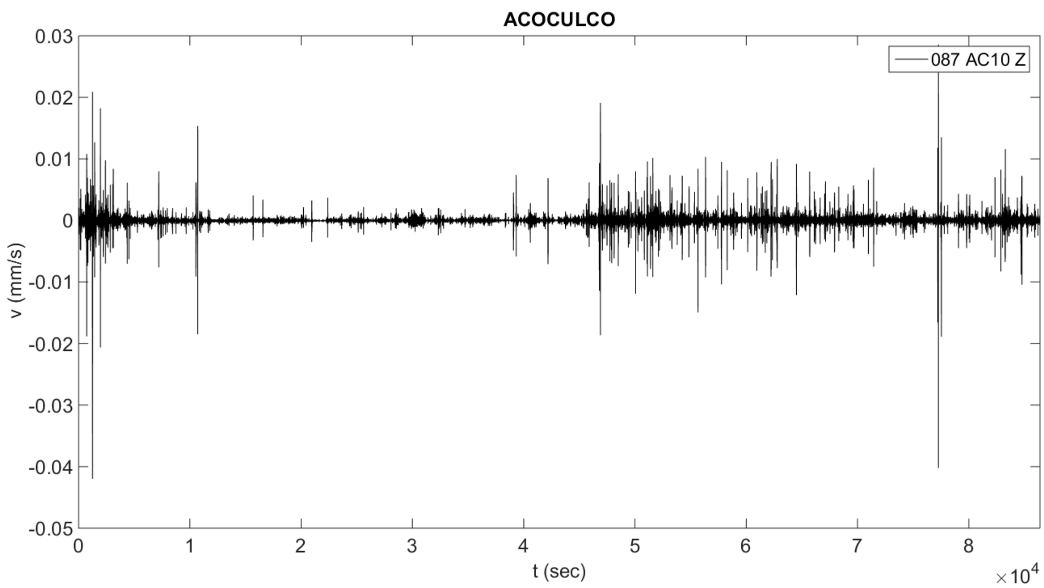
ACOCULCO
087 AC10 Z
v (mm/s)
t (sec)
×10^4
0.03
0.02
0.01
0
-0.01
-0.02
-0.03
-0.04
-0.05
0
1
2
3
4
5
6
7
8

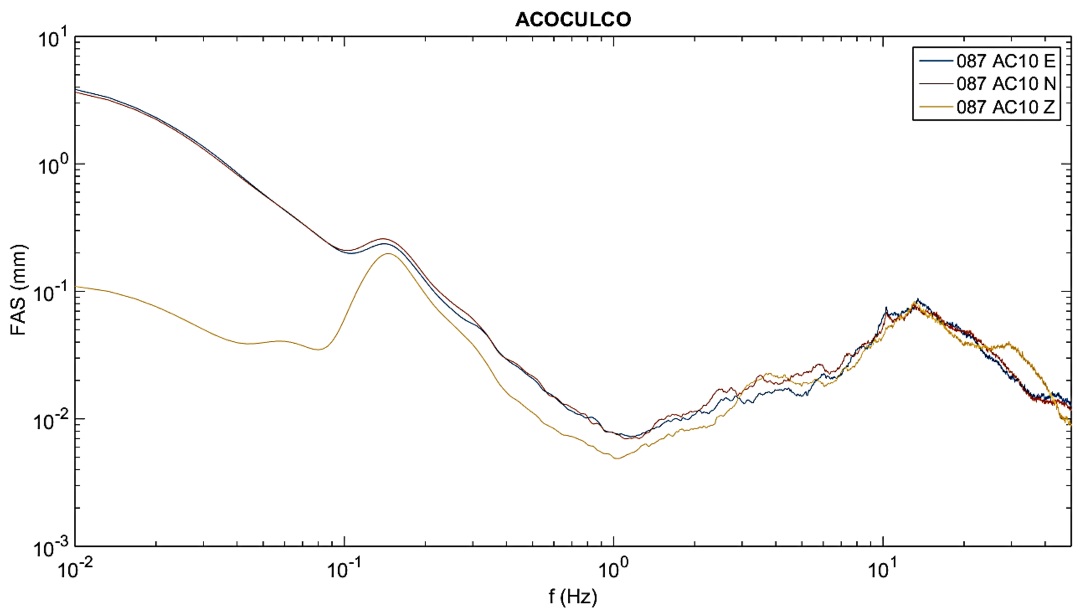
ACOCULCO
087 AC10 E
087 AC10 N
087 AC10 Z
FAS (mm)
f (Hz)

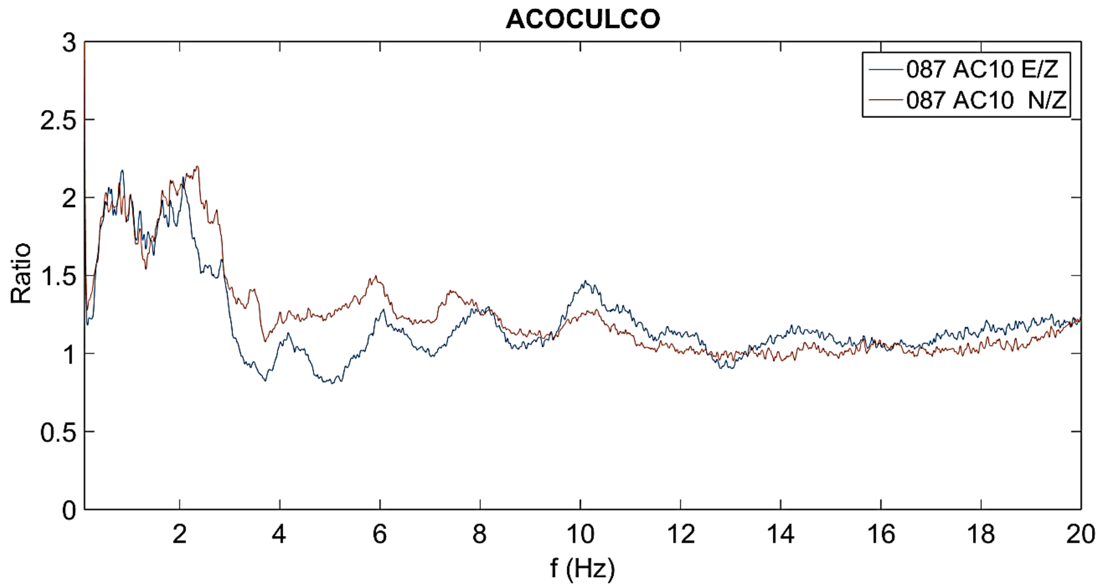
ACOCULCO
087 AC10 E/Z
087 AC10 N/Z
Ratio
f (Hz)

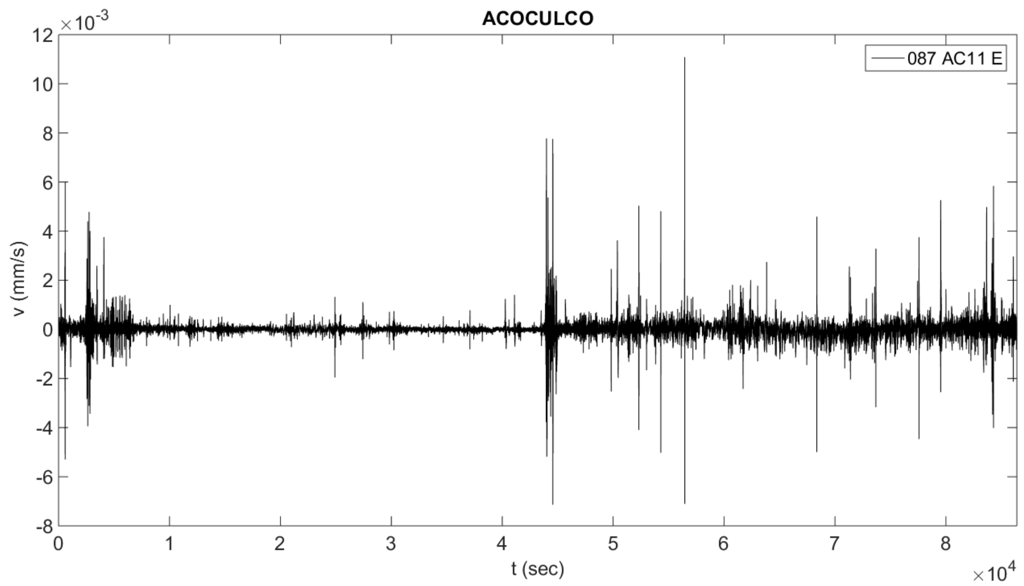
ACOCULCO
087 AC11 E
v (mm/s)
t (sec)
×10^-3
×10^4

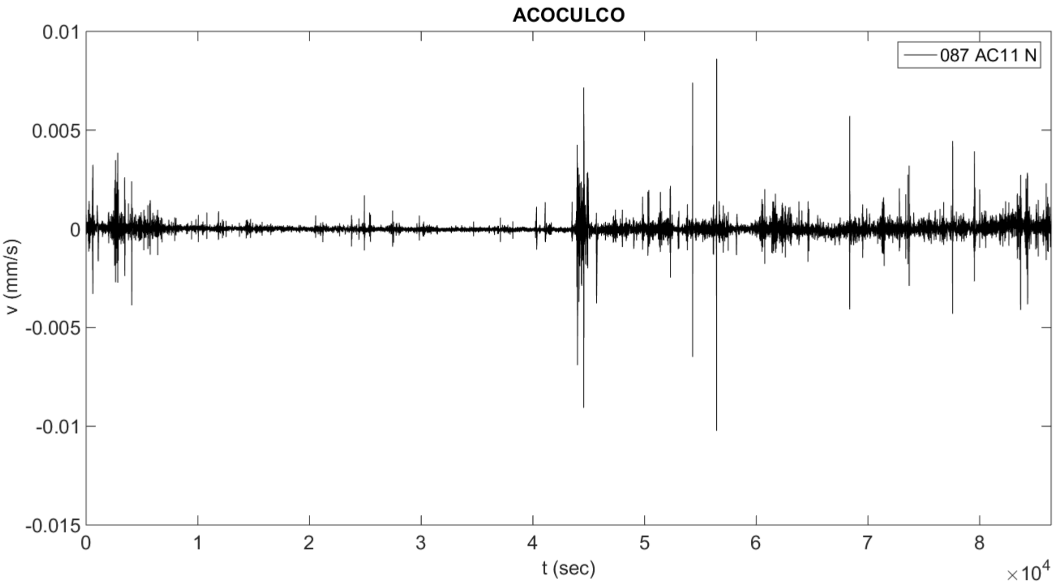
ACOCULCO
087 AC11 N
v (mm/s)
t (sec)
×10^4

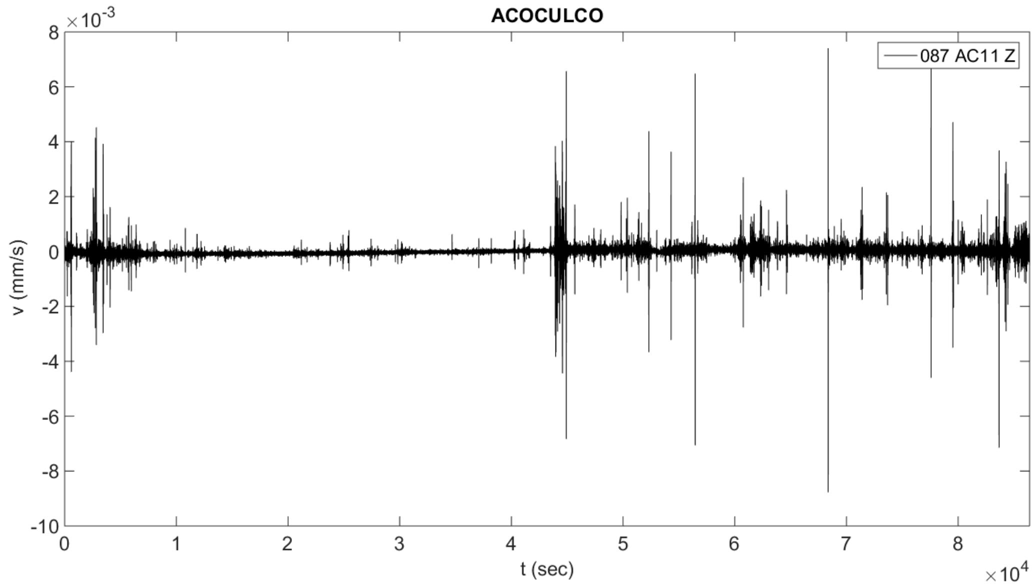
ACOCULCO
087 AC11 Z
v (mm/s)
t (sec)
×10^-3
×10^4

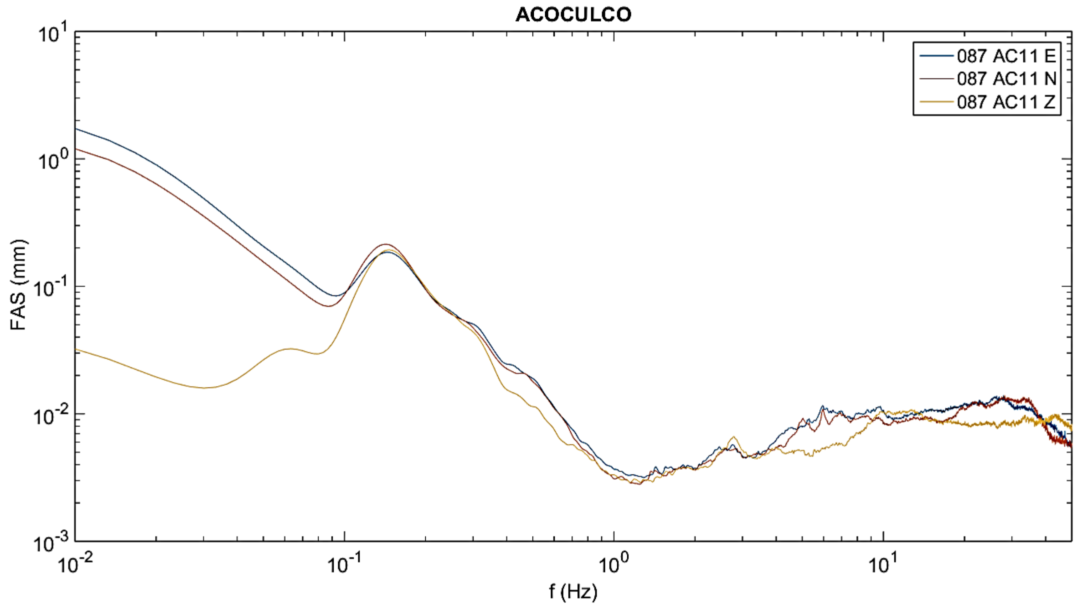
ACOCULCO
087 AC11 E
087 AC11 N
087 AC11 Z
FAS (mm)
f (Hz)

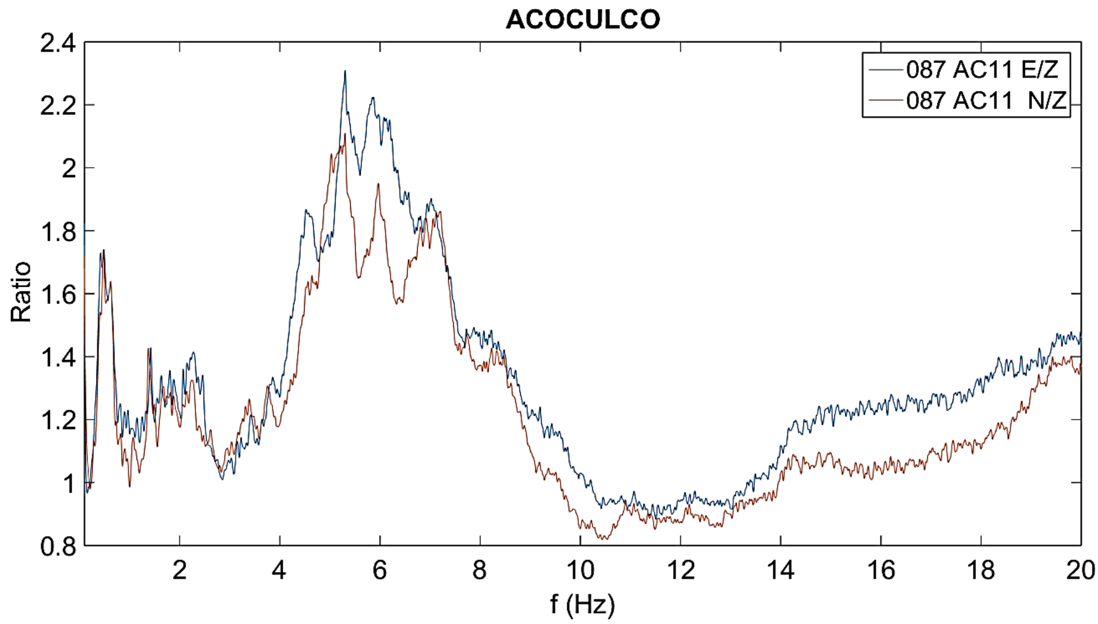
ACOCULCO
087 AC11 E/Z
087 AC11 N/Z
Ratio
f (Hz)

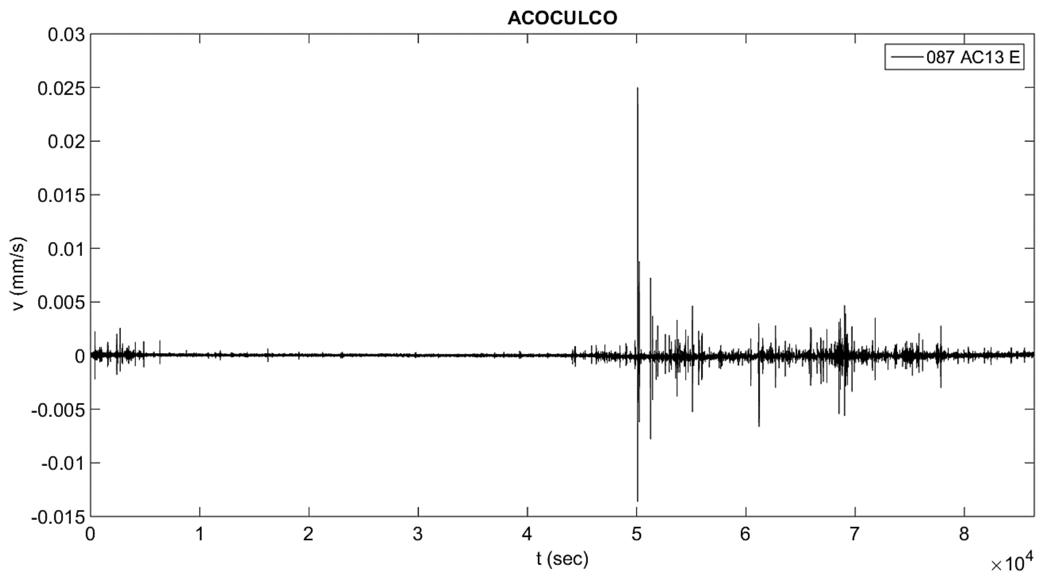
ACOCULCO
087 AC13 E
v (mm/s)
t (sec)
×10^4

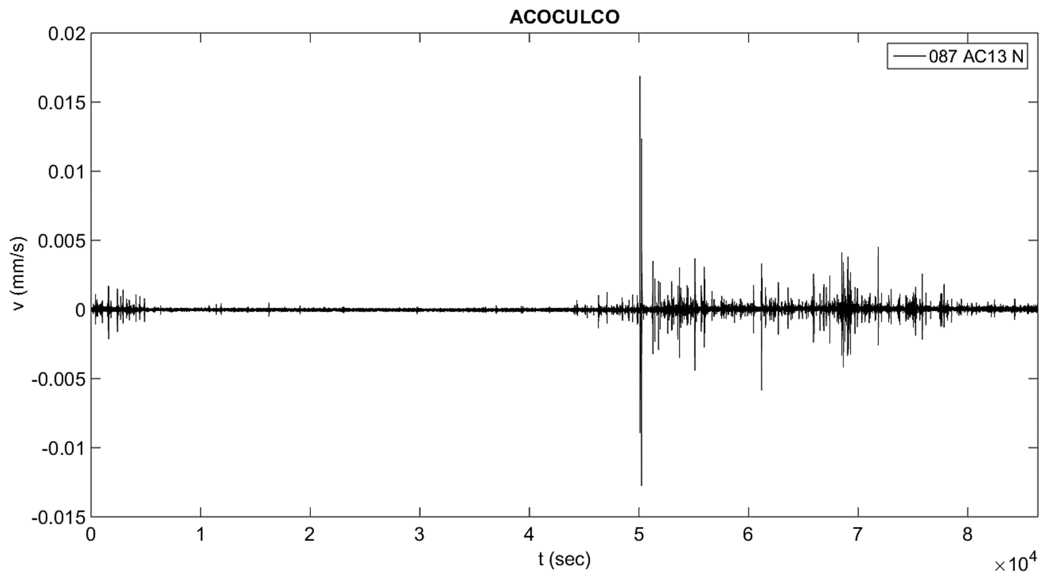
ACOCULCO
087 AC13 N
v (mm/s)
t (sec)
×10^4

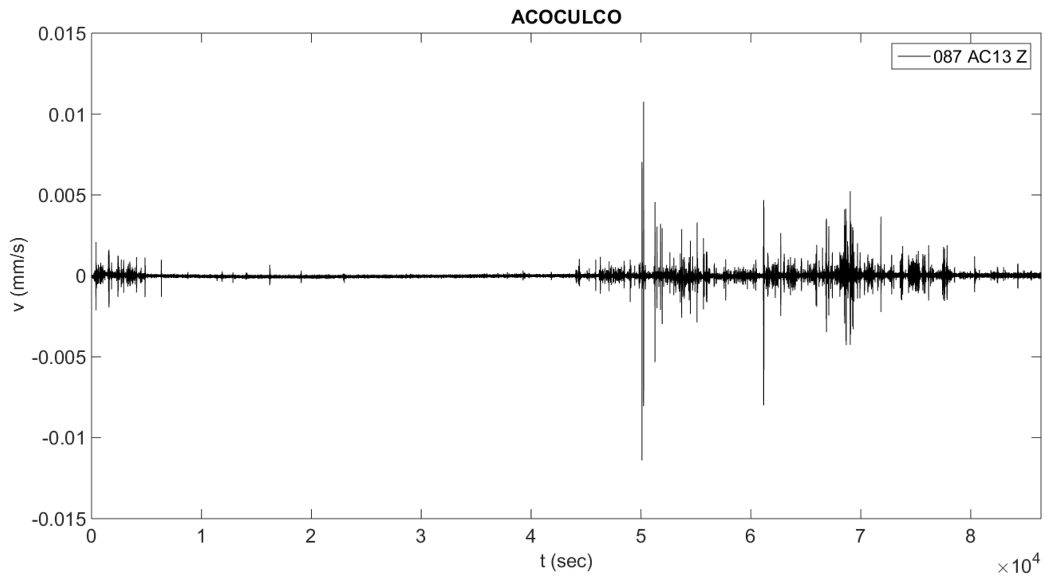
ACOCULCO
087 AC13 Z
v (mm/s)
t (sec)
×10^4

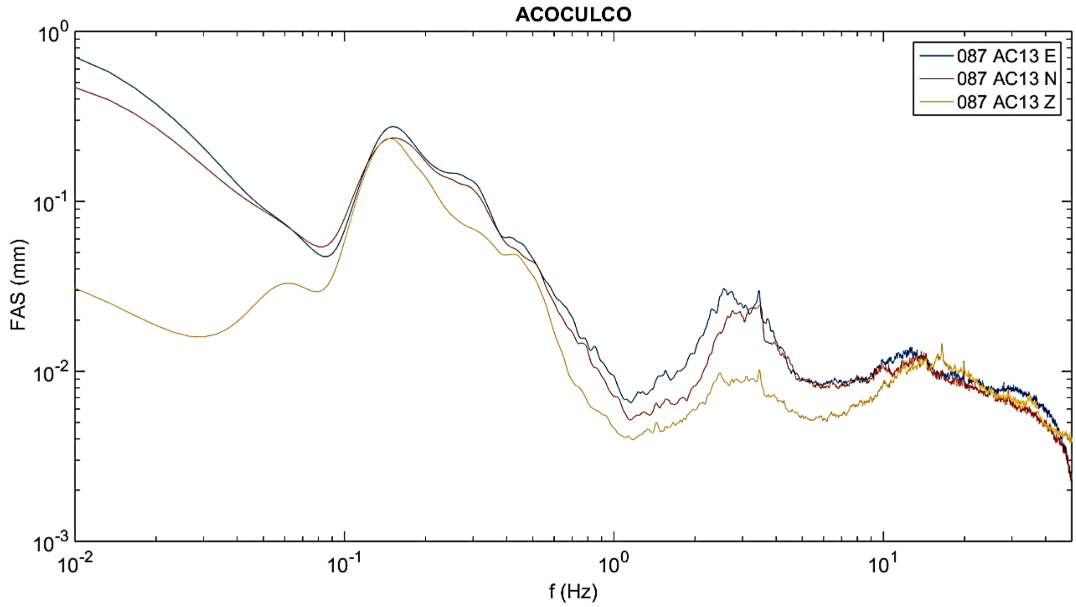
ACOCULCO
087 AC13 E
087 AC13 N
087 AC13 Z
FAS (mm)
f (Hz)

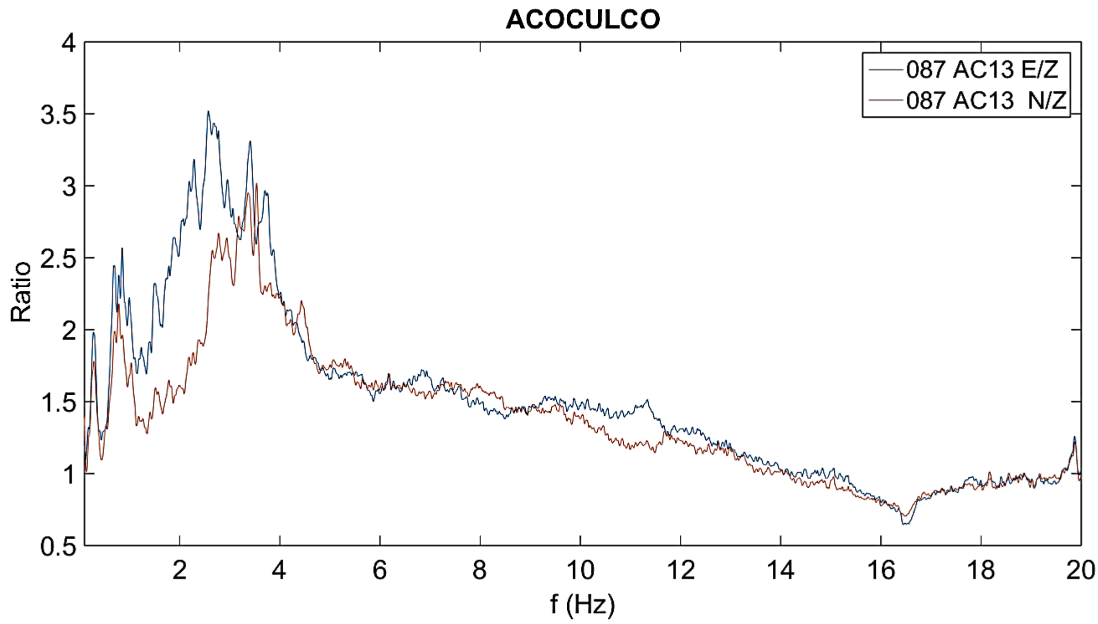
ACOCULCO
087 AC13 E/Z
087 AC13 N/Z
Ratio
f (Hz)

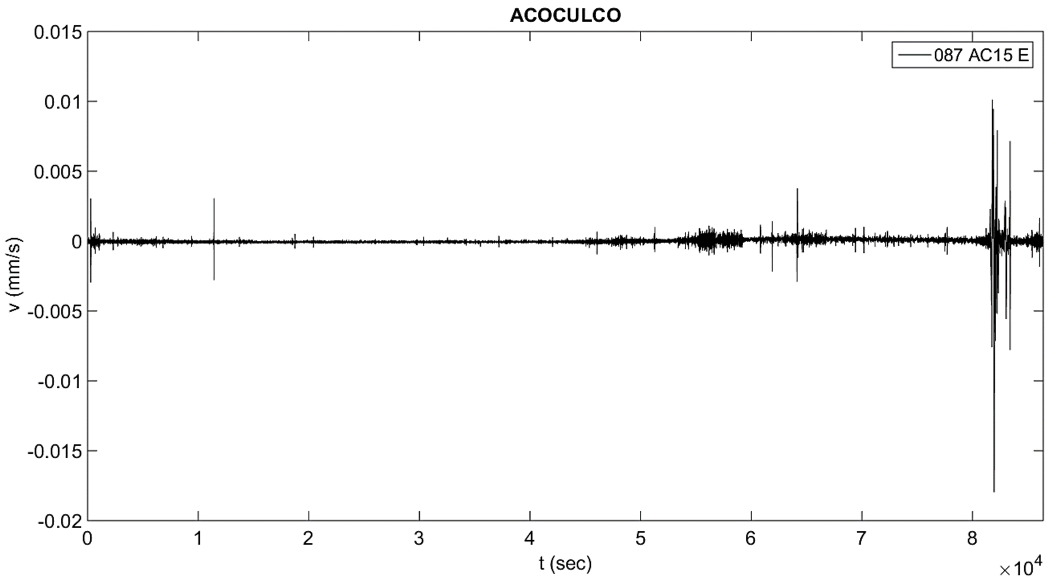
ACOCULCO
087 AC15 E
v (mm/s)
t (sec)
×10^4

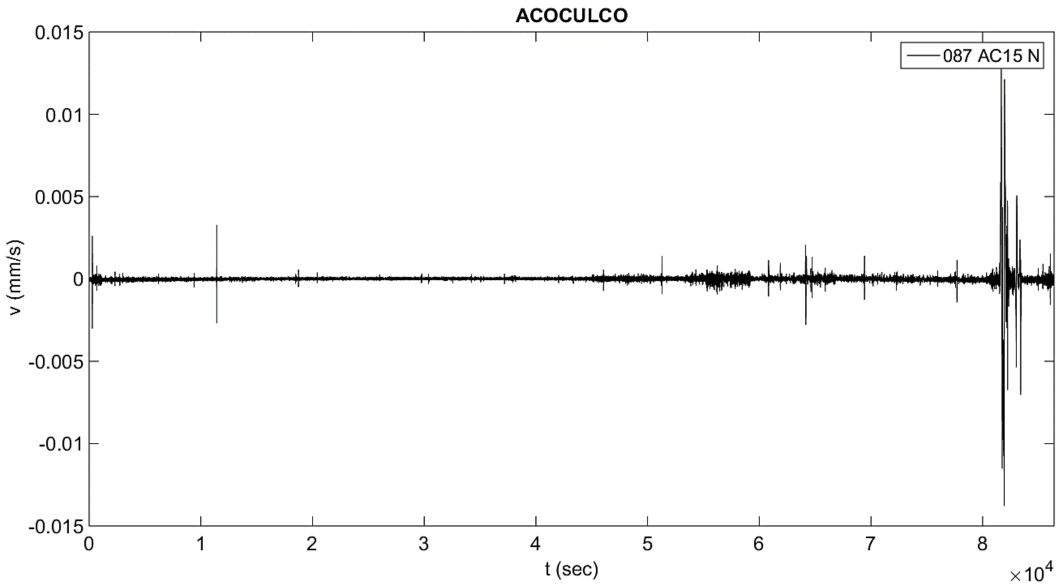
ACOCULCO
087 AC15 N
v (mm/s)
t (sec)
×10^4

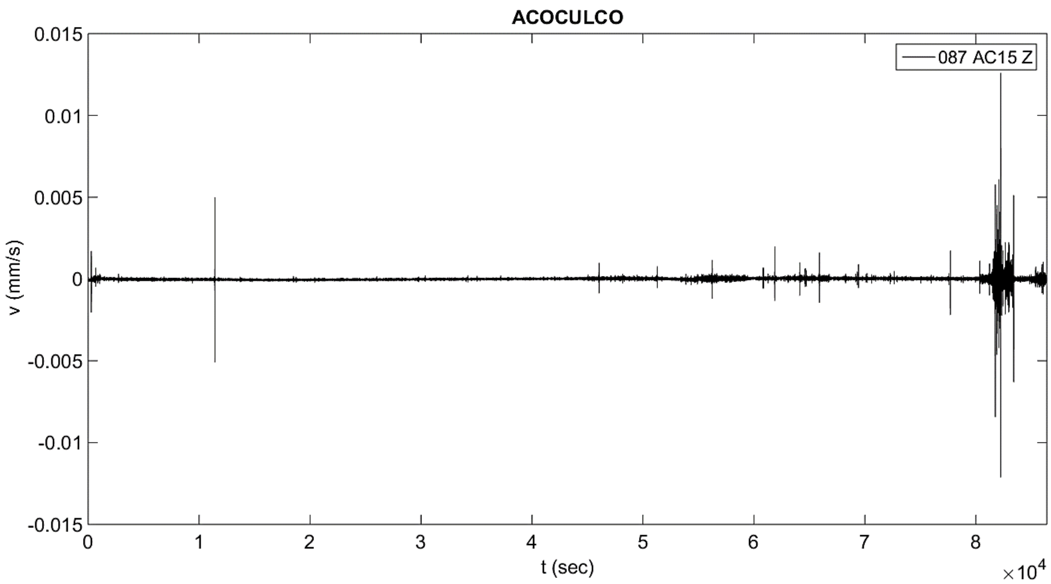
ACOCULCO
087 AC15 Z
v (mm/s)
t (sec)
×10^4

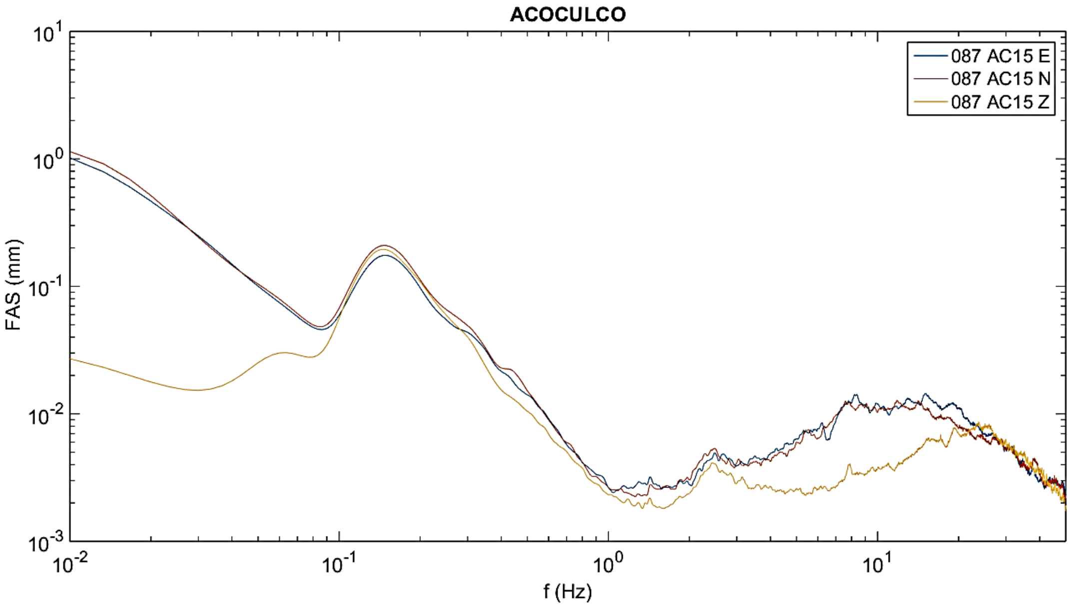
ACOCULCO
087 AC15 E
087 AC15 N
087 AC15 Z
FAS (mm)
f (Hz)

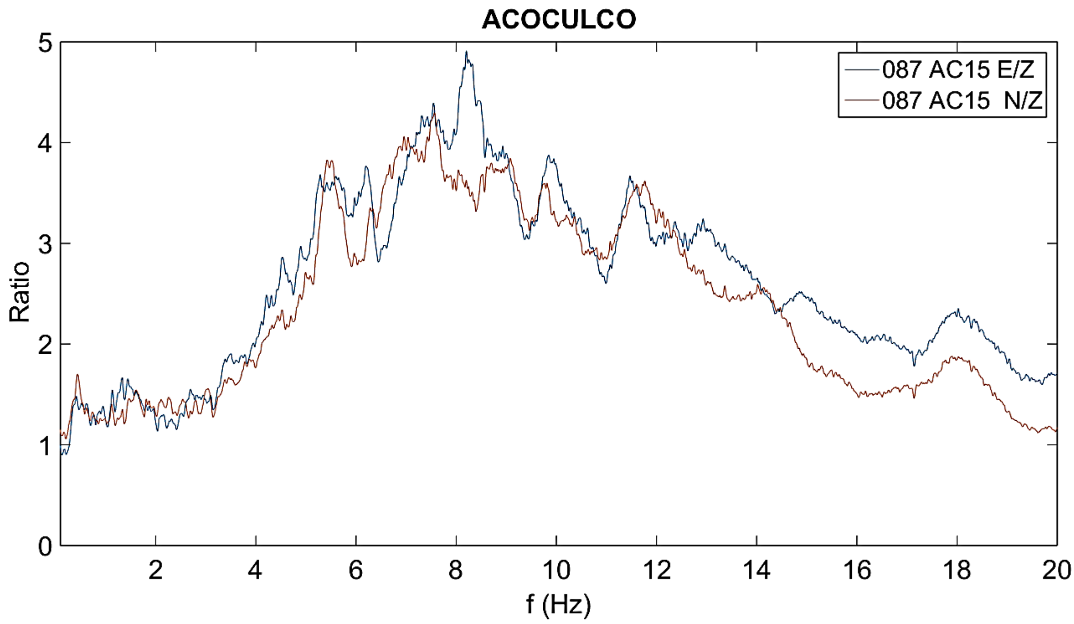
ACOCULCO
087 AC15 E/Z
087 AC15 N/Z
Ratio
f (Hz)

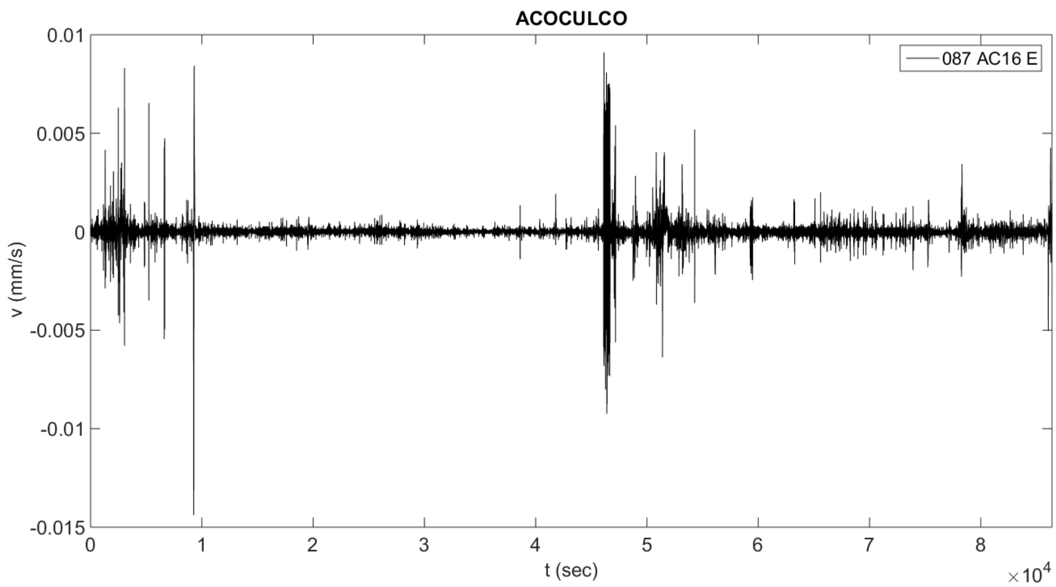
ACOCULCO
087 AC16 E
0.01
0.005
0
-0.005
-0.01
-0.015
v (mm/s)
0
1
2
3
4
5
6
7
8
t (sec)
$\times 10^4$

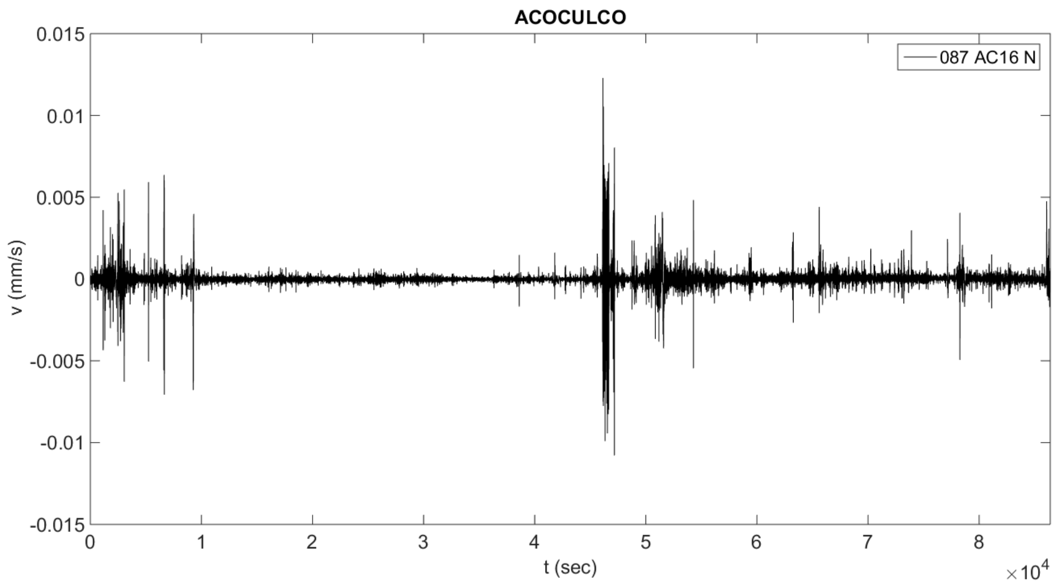
ACOCULCO
087 AC16 N
0.015
0.01
0.005
0
-0.005
-0.01
-0.015
v (mm/s)
0
1
2
3
4
5
6
7
8
t (sec)
$\times 10^4$

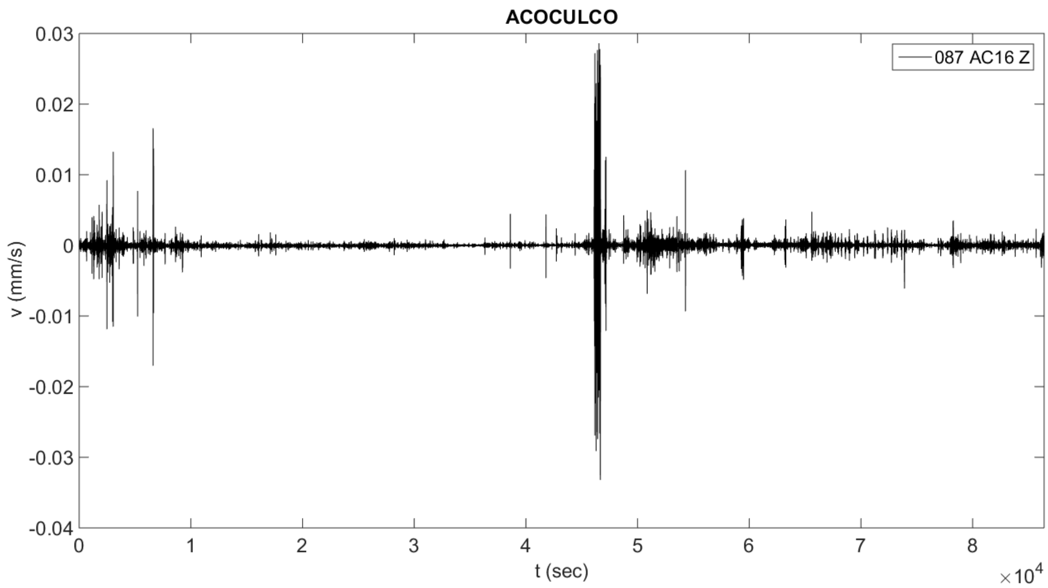
ACOCULCO
087 AC16 Z
0.03
0.02
0.01
0
-0.01
-0.02
-0.03
-0.04
v (mm/s)
0
1
2
3
4
5
6
7
8
t (sec)
$\times 10^4$

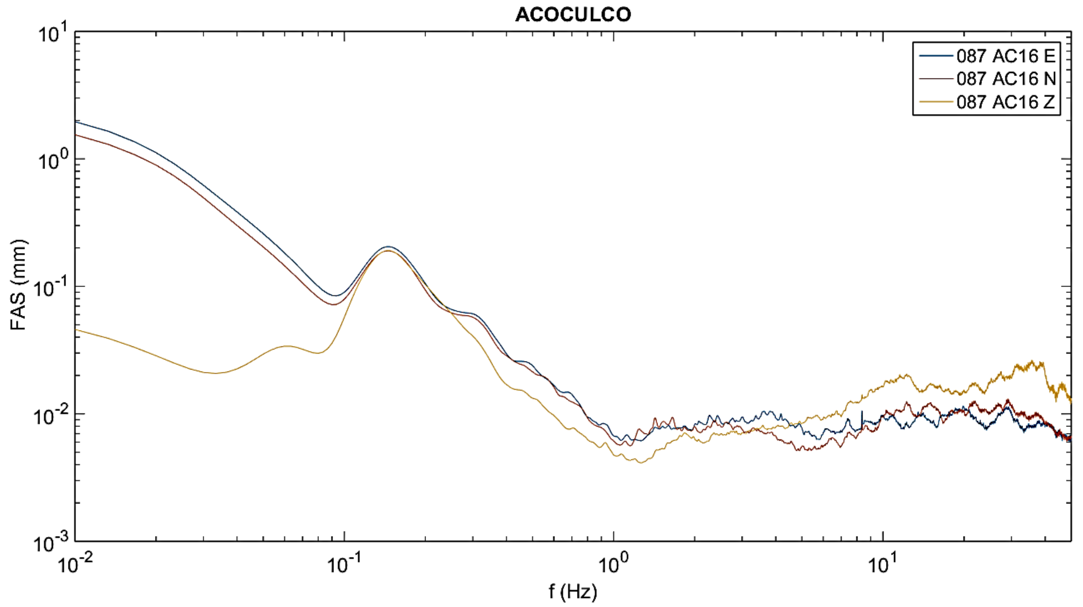
ACOCULCO
087 AC16 E
087 AC16 N
087 AC16 Z
FAS (mm)
f (Hz)

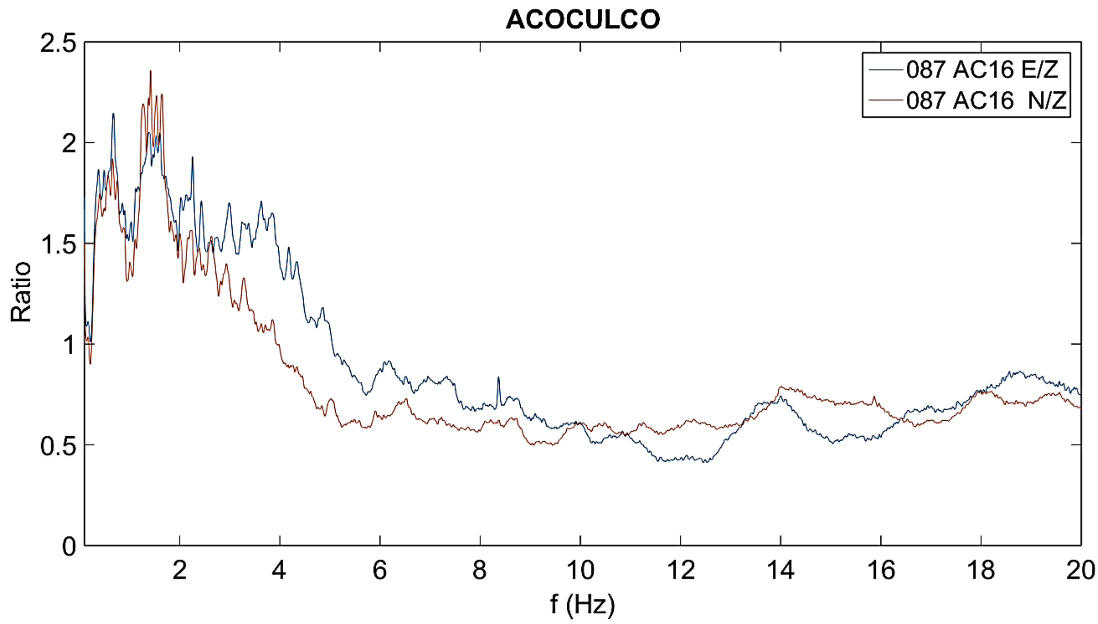
ACOCULCO
087 AC16 E/Z
087 AC16 N/Z
Ratio
f (Hz)

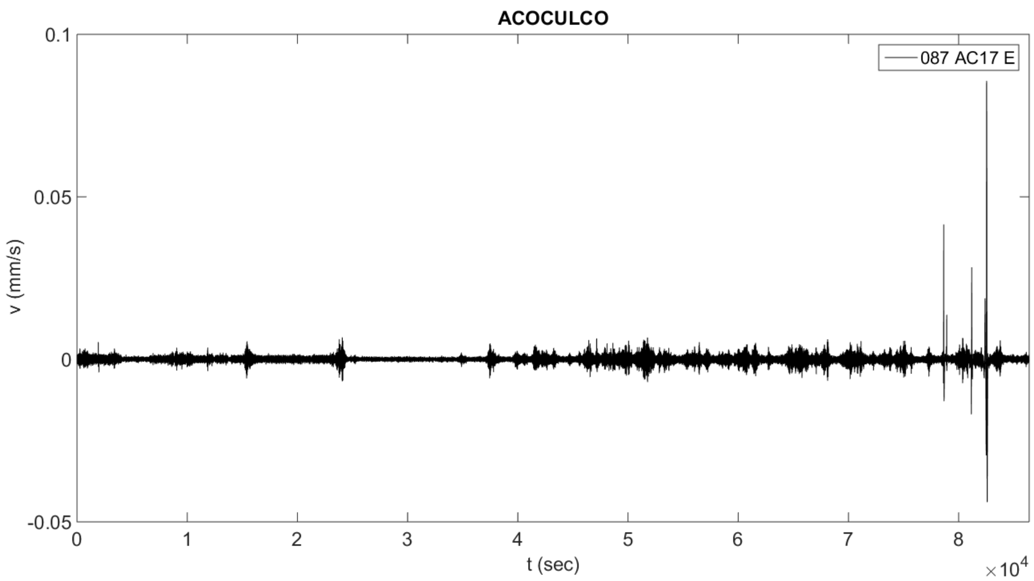
ACOCULCO
087 AC17 E
v (mm/s)
t (sec)
×10^4
0.1
0.05
0
-0.05
0
1
2
3
4
5
6
7
8

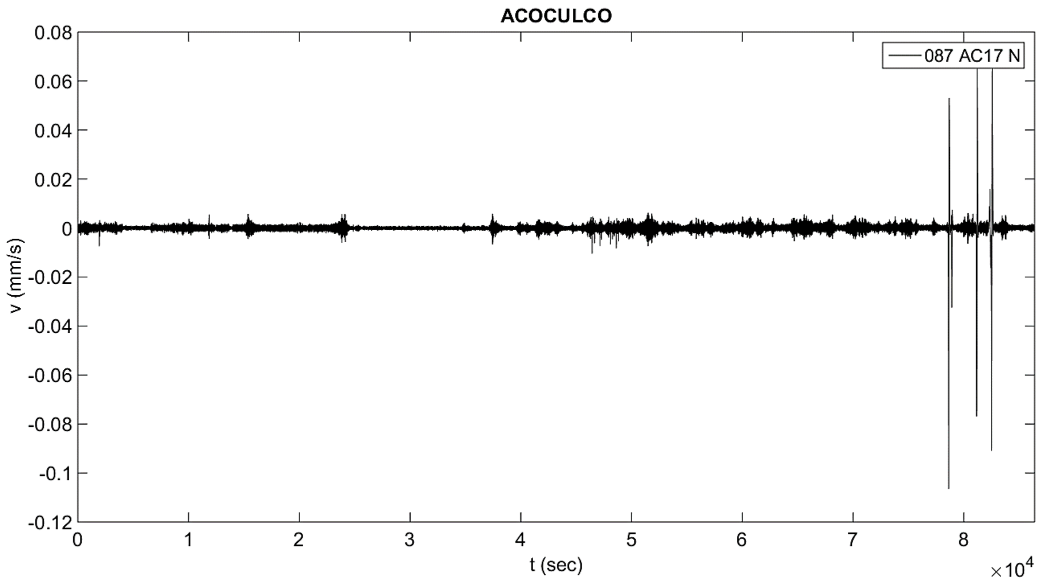
ACOCULCO
087 AC17 N
v (mm/s)
t (sec)
×10^4
0.08
0.06
0.04
0.02
0
-0.02
-0.04
-0.06
-0.08
-0.1
-0.12
0
1
2
3
4
5
6
7
8

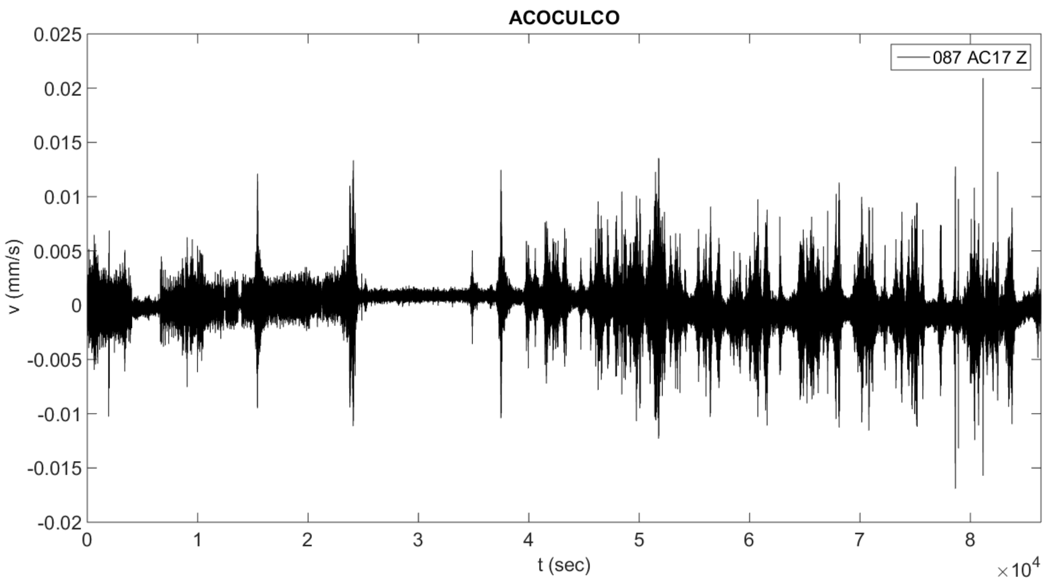
ACOCULCO
087 AC17 Z
v (mm/s)
t (sec)
×10^4
0.025
0.02
0.015
0.01
0.005
0
-0.005
-0.01
-0.015
-0.02
0
1
2
3
4
5
6
7
8

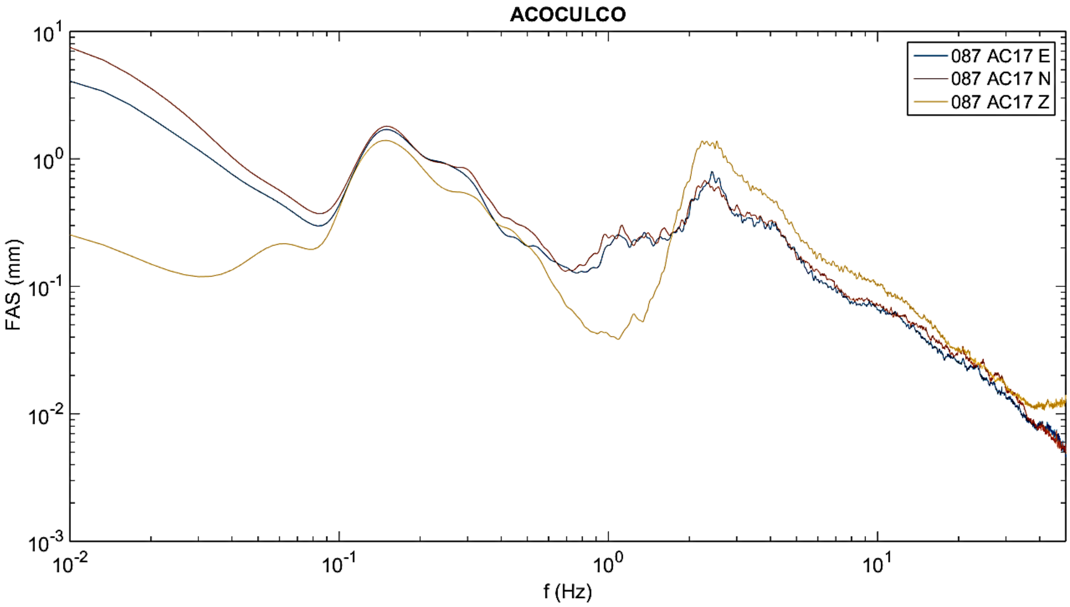
ACOCULCO
087 AC17 E
087 AC17 N
087 AC17 Z
FAS (mm)
f (Hz)

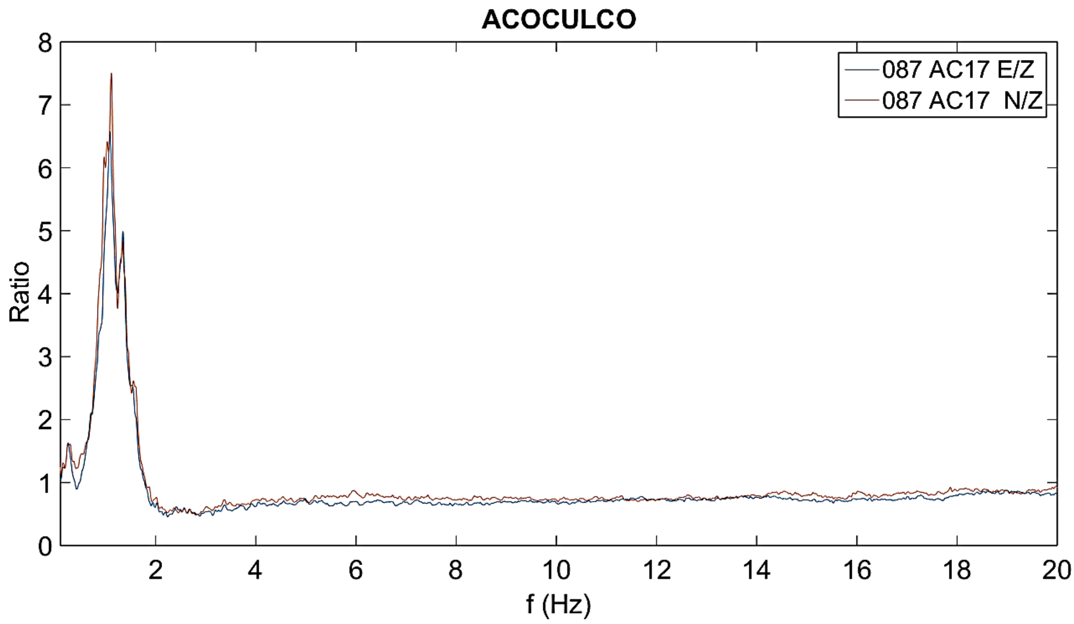
ACOCULCO
087 AC17 E/Z
087 AC17 N/Z
Ratio
f (Hz)

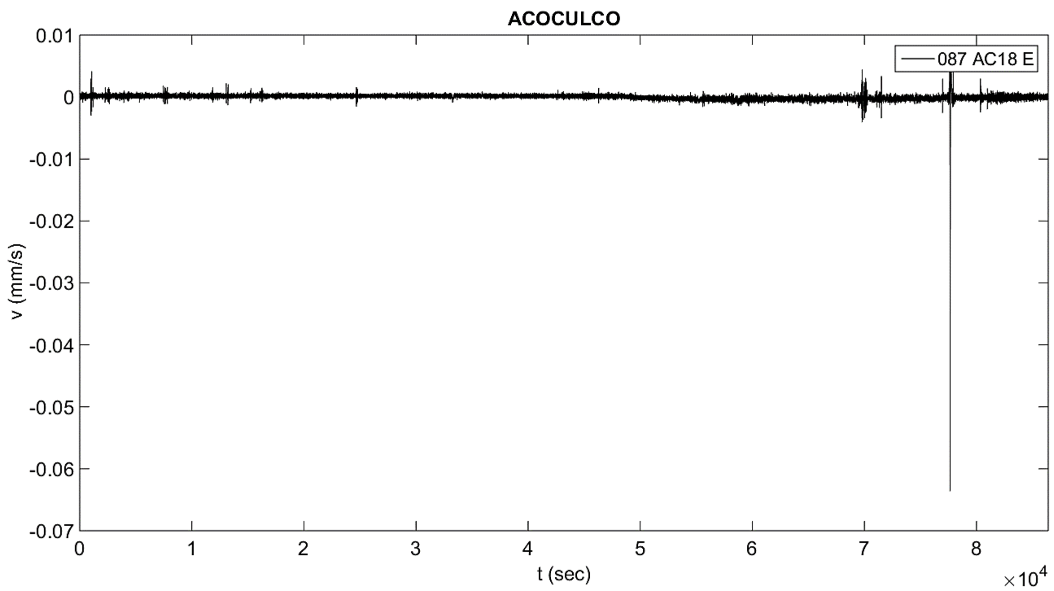
ACOCULCO
087 AC18 E
v (mm/s)
t (sec)
×10^4
0.01
0
-0.01
-0.02
-0.03
-0.04
-0.05
-0.06
-0.07
0
1
2
3
4
5
6
7
8

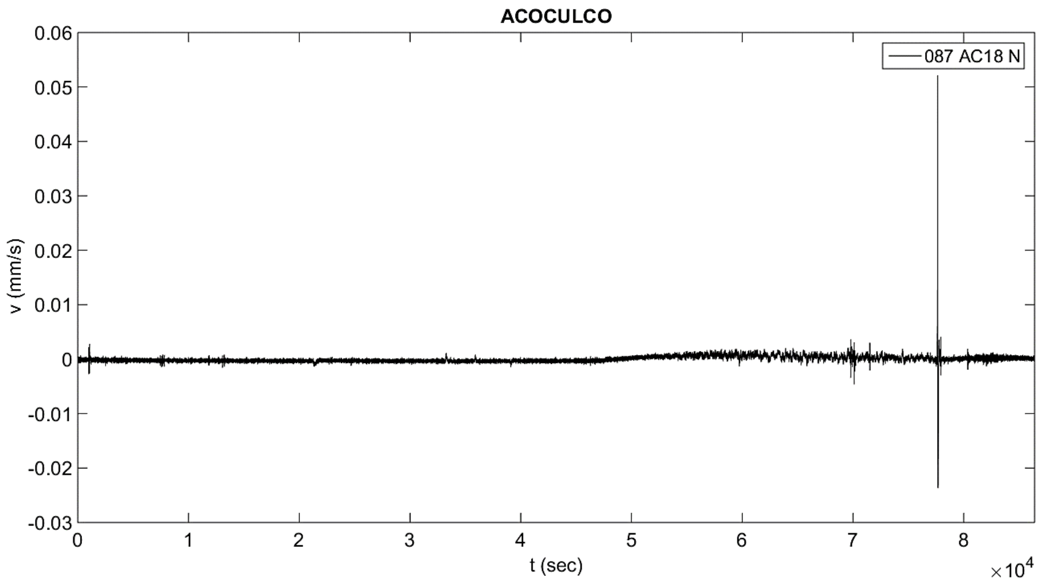
ACOCULCO
087 AC18 N
v (mm/s)
t (sec)
×10^4
0.06
0.05
0.04
0.03
0.02
0.01
0
-0.01
-0.02
-0.03
0
1
2
3
4
5
6
7
8

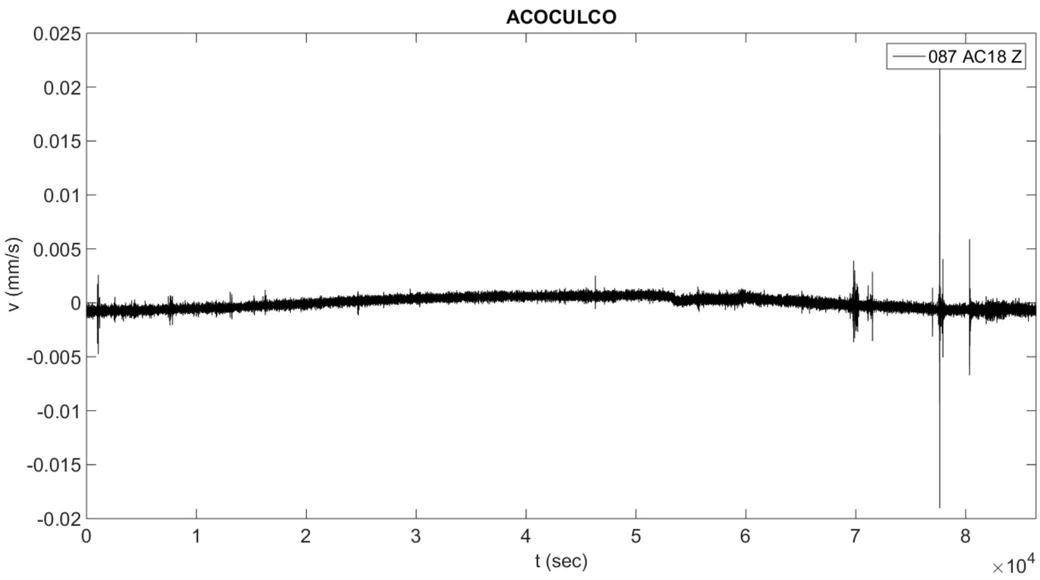
ACOCULCO
087 AC18 Z
v (mm/s)
t (sec)
×10^4
0.025
0.02
0.015
0.01
0.005
0
-0.005
-0.01
-0.015
-0.02
0
1
2
3
4
5
6
7
8

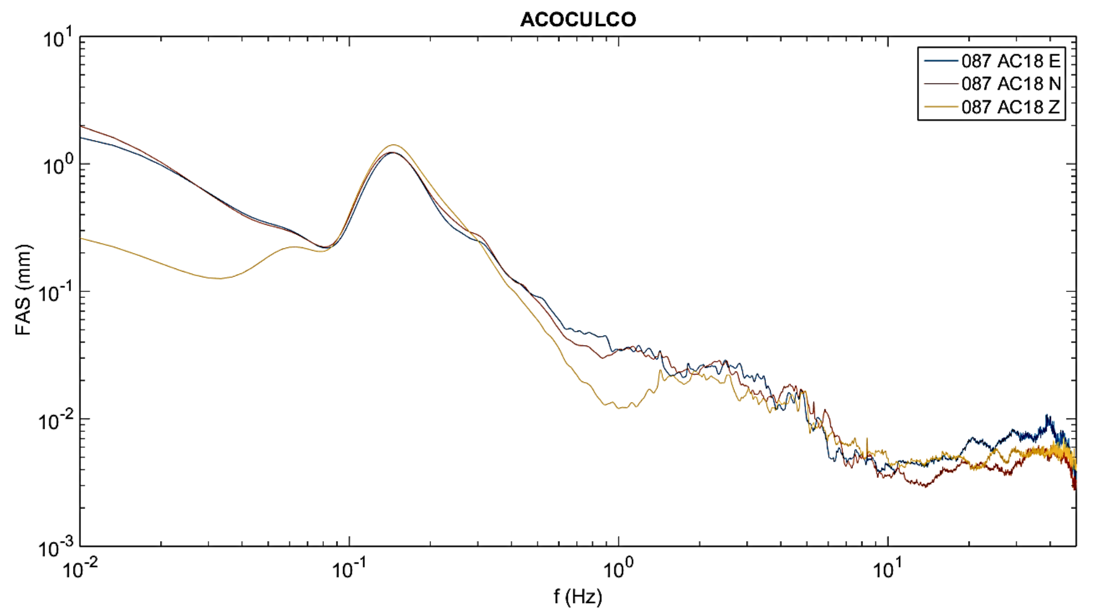
ACOCULCO
087 AC18 E
087 AC18 N
087 AC18 Z
FAS (mm)
f (Hz)

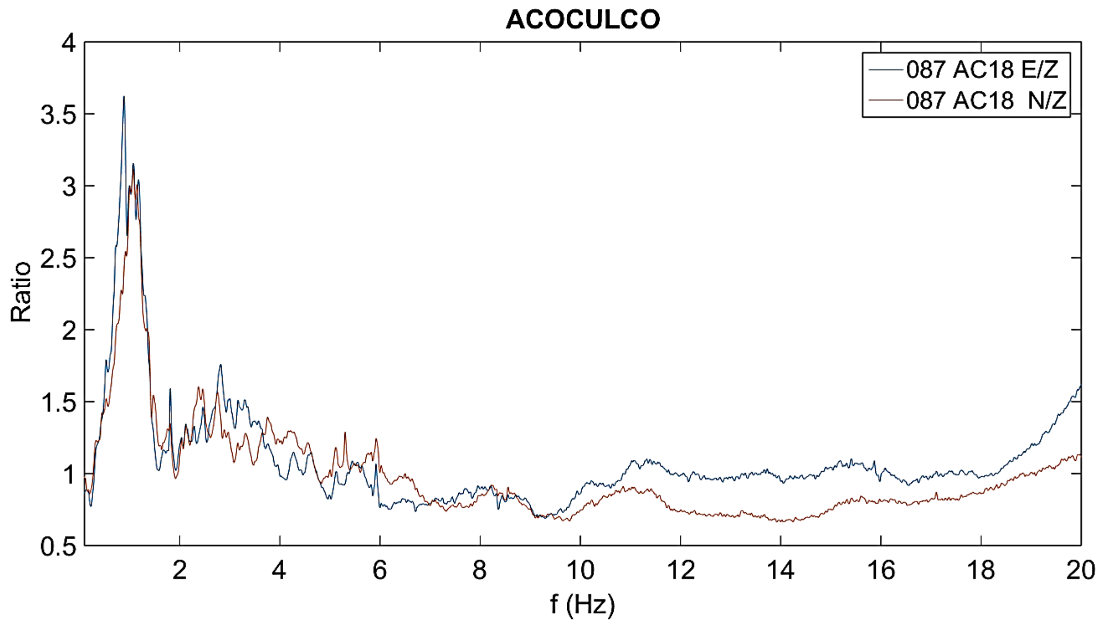
ACOCULCO
087 AC18 E/Z
087 AC18 N/Z
Ratio
f (Hz)

Appendix 4-C Day 081, Earthquake. Time histories, spectra and spectral ratios

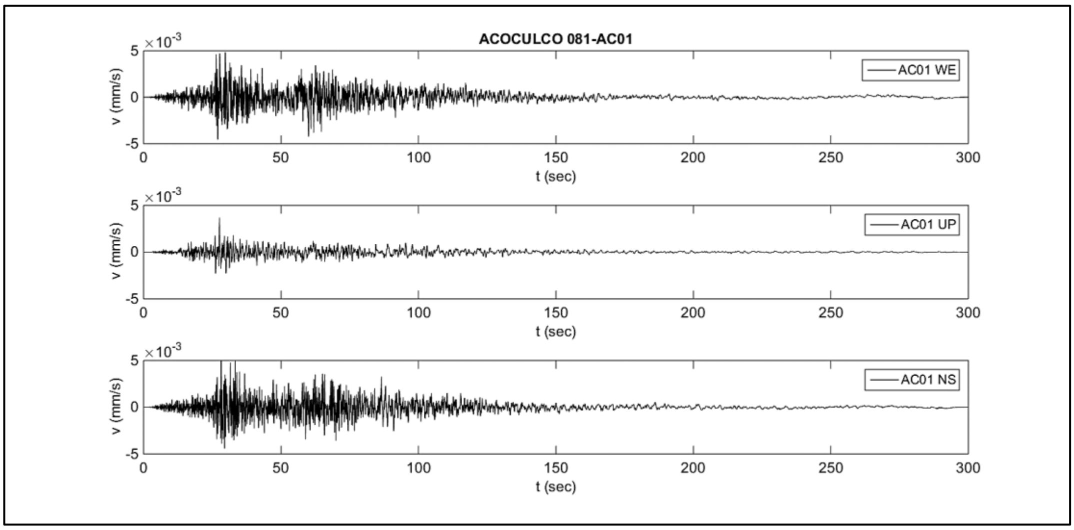

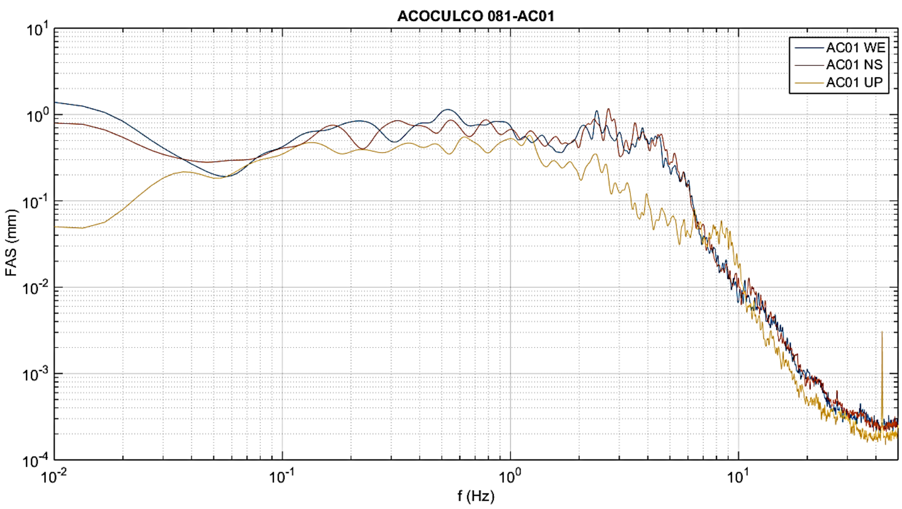

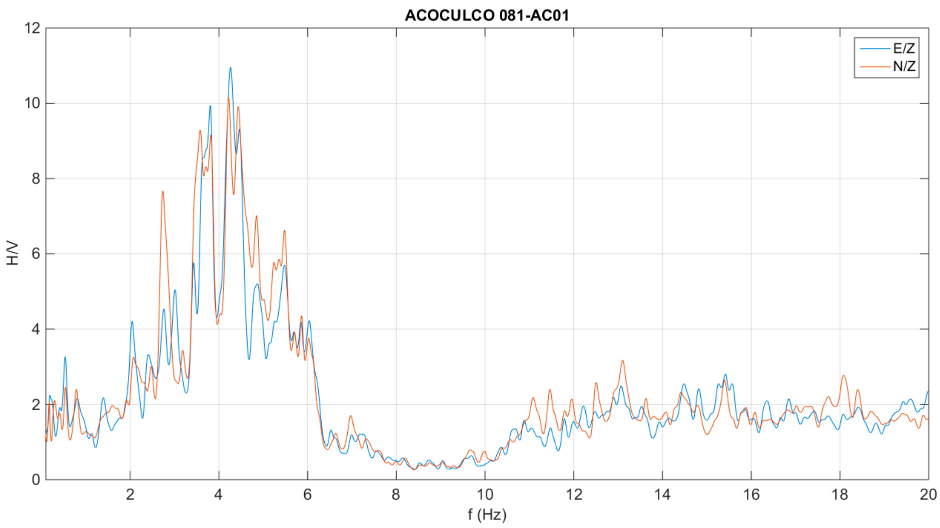

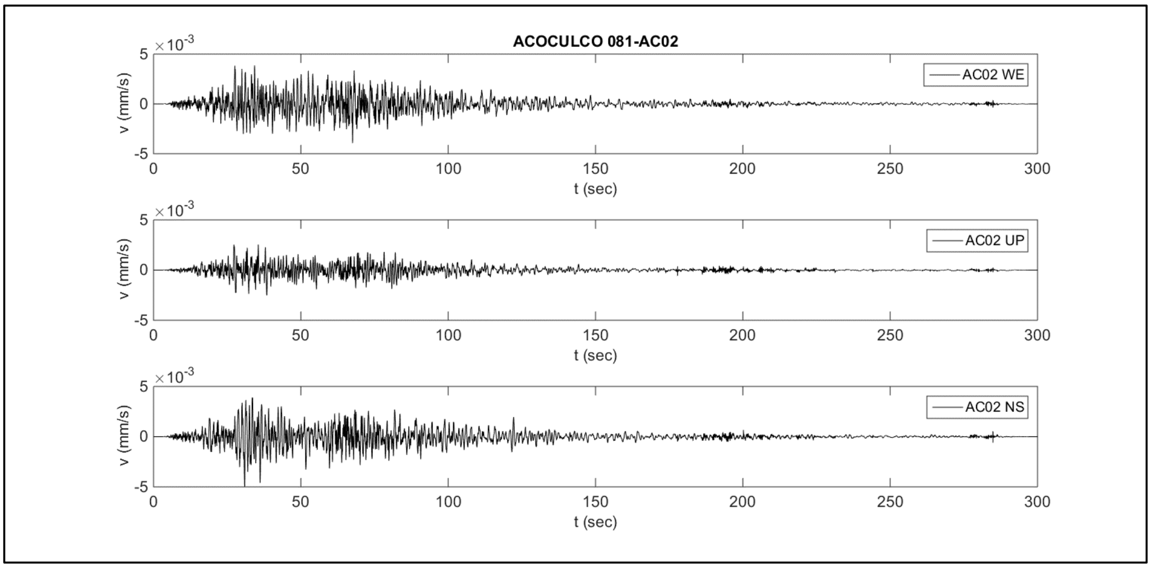

ACOCULCO 081-AC02
AC02 WE
AC02 UP
AC02 NS
v (mm/s)
t (sec)

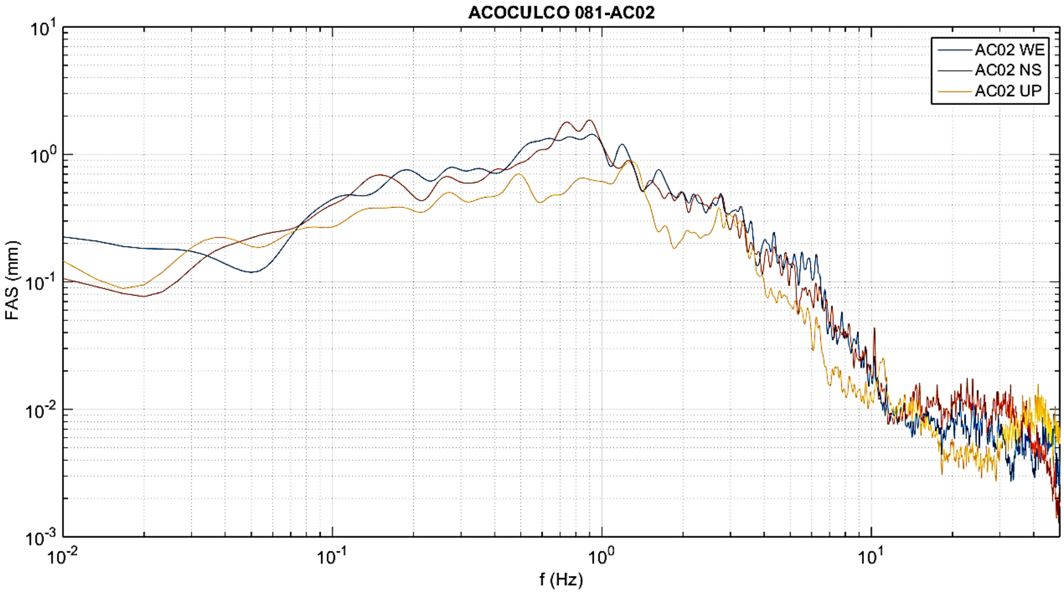

ACOCULCO 081-AC02
AC02 WE
AC02 NS
AC02 UP
FAS (mm)
f (Hz)

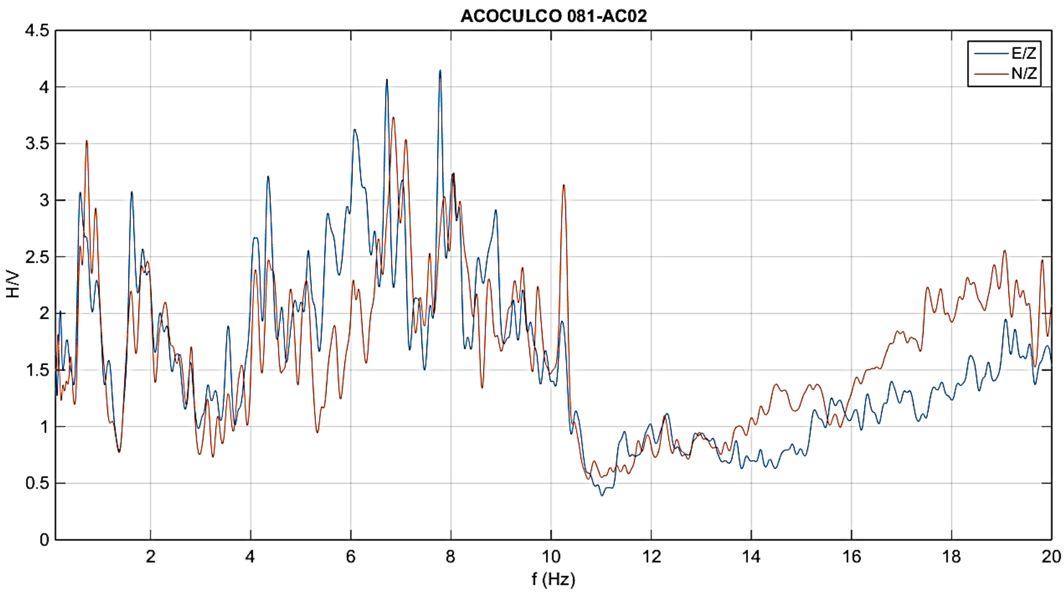

ACOCULCO 081-AC02
E/Z
N/Z
H/V
f (Hz)

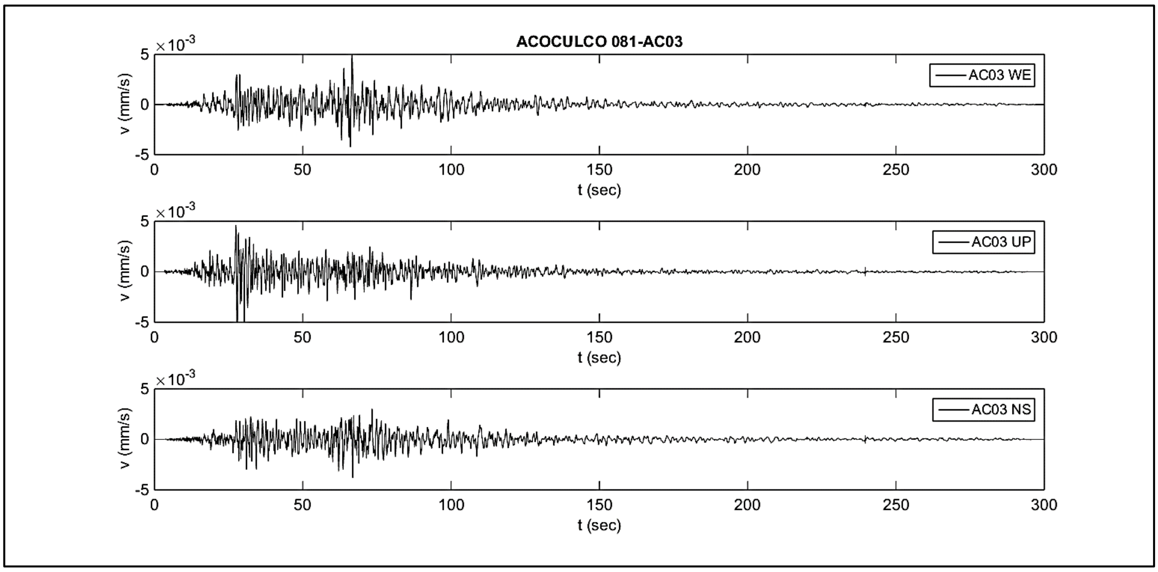
ACOCULCO 081-AC03
AC03 WE
AC03 UP
AC03 NS
v (mm/s)
t (sec)
×10^-3

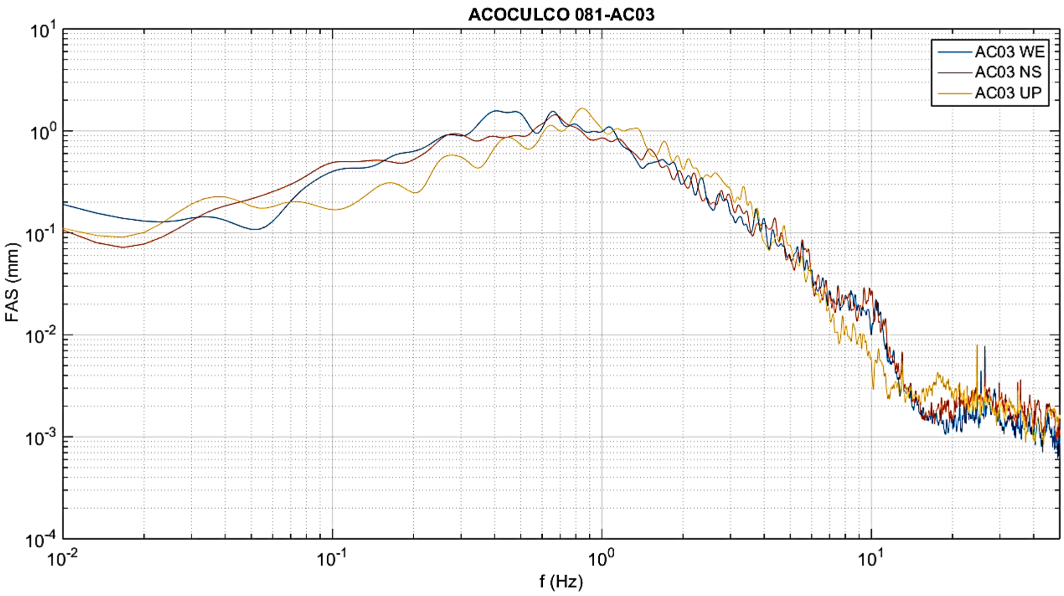
ACOCULCO 081-AC03
AC03 WE
AC03 NS
AC03 UP
FAS (mm)
f (Hz)

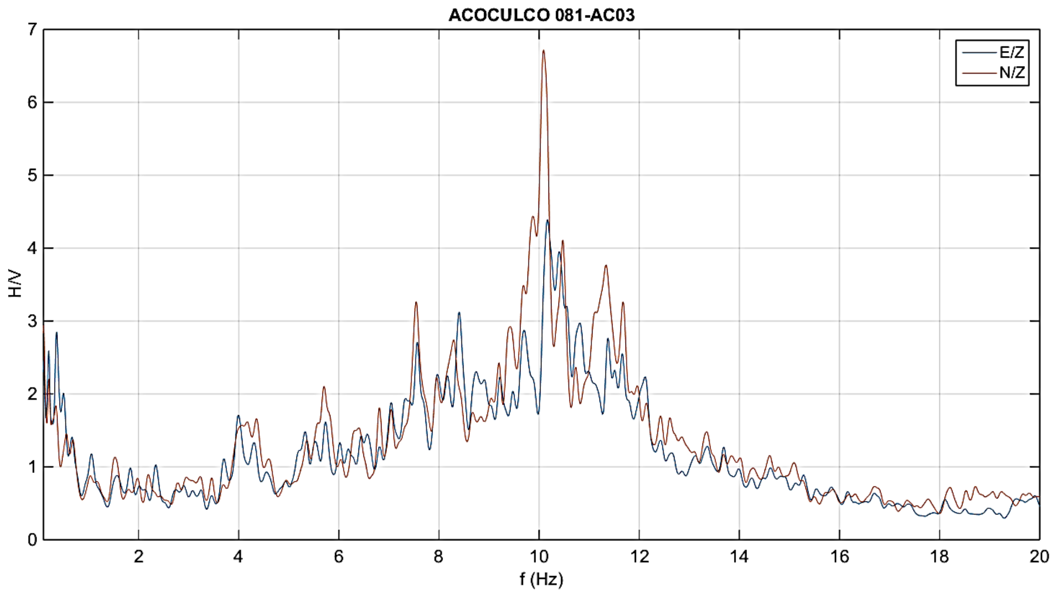
ACOCULCO 081-AC03
E/Z
N/Z
H/V
f (Hz)

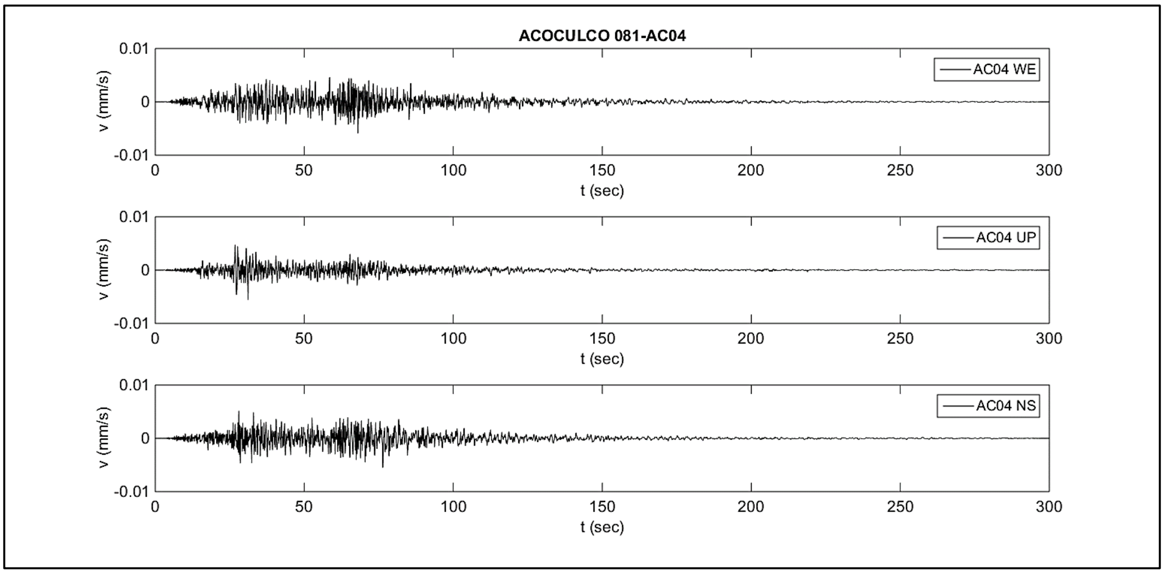
ACOCULCO 081-AC04
AC04 WE
AC04 UP
AC04 NS
v (mm/s)
0.01
0
-0.01
0
50
100
150
200
250
300
t (sec)

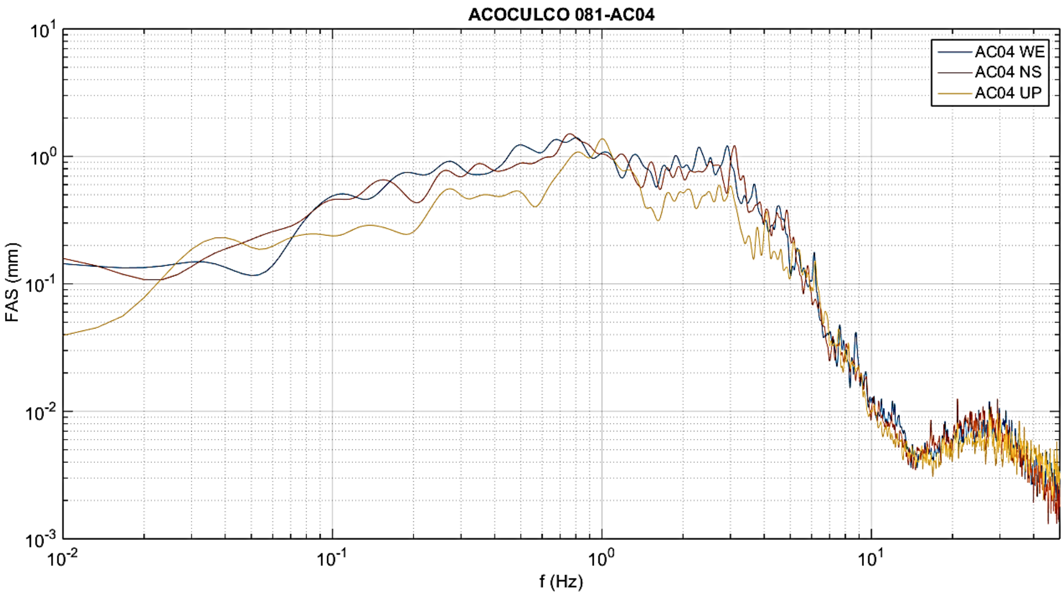
ACOCULCO 081-AC04
AC04 WE
AC04 NS
AC04 UP
FAS (mm)
f (Hz)

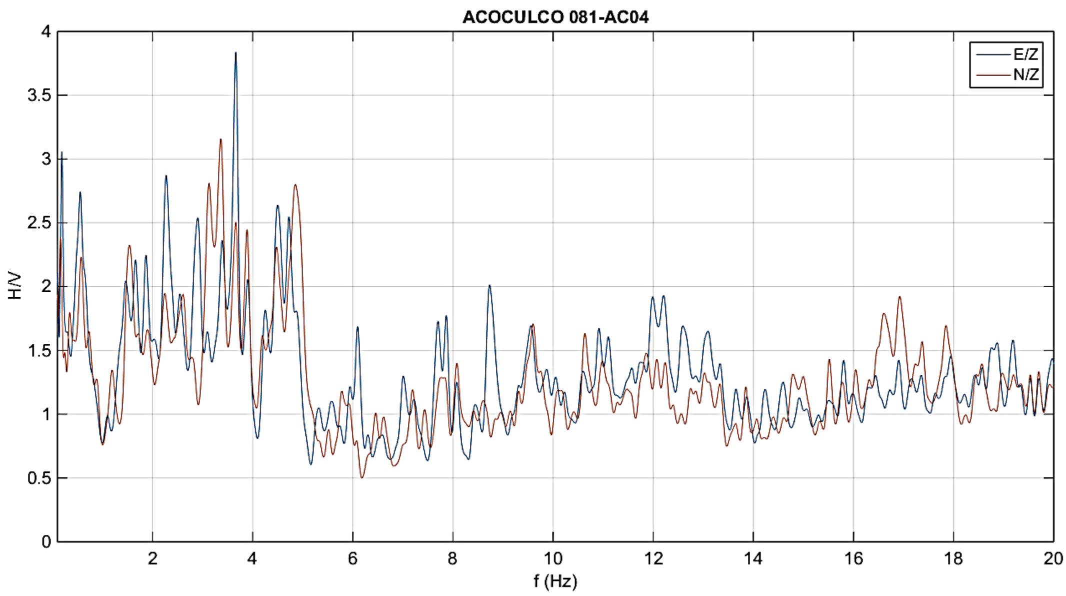
ACOCULCO 081-AC04
E/Z
N/Z
H/V
f (Hz)

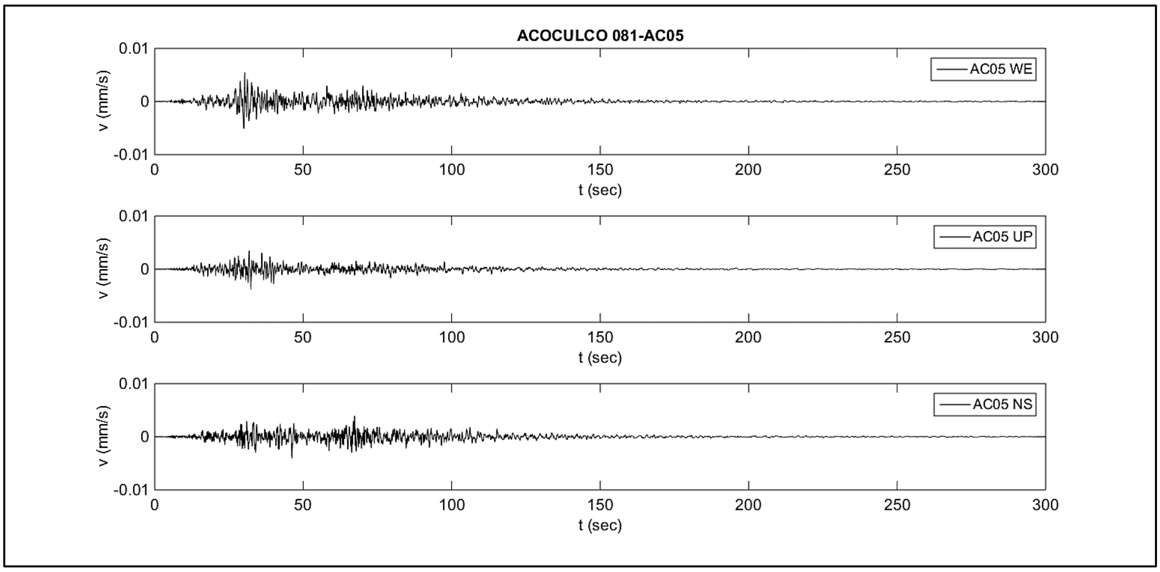
ACOCULCO 081-AC05
AC05 WE
AC05 UP
AC05 NS
v (mm/s)
t (sec)

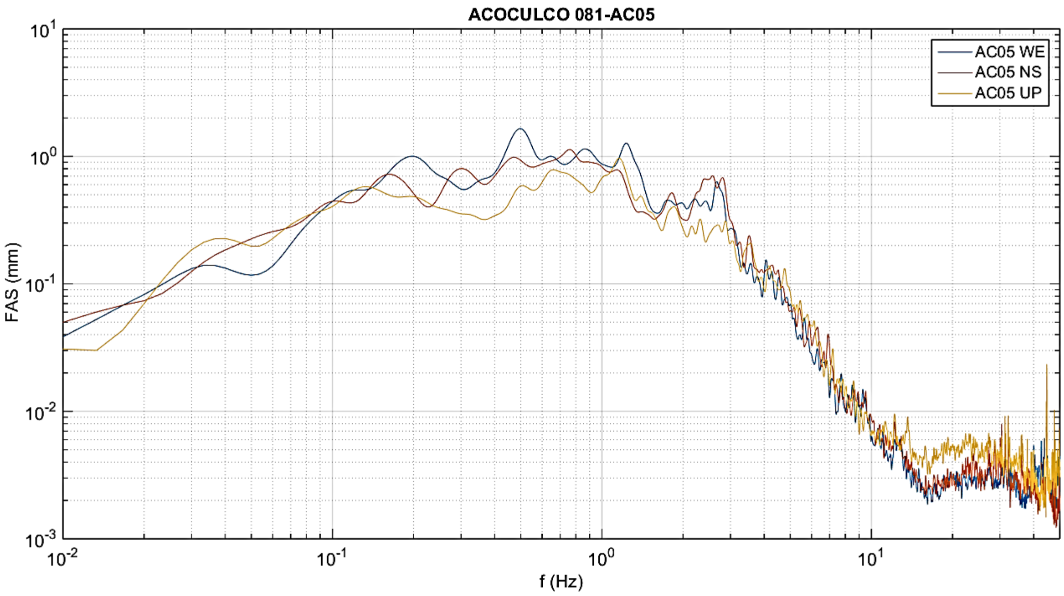
ACOCULCO 081-AC05
AC05 WE
AC05 NS
AC05 UP
FAS (mm)
f (Hz)

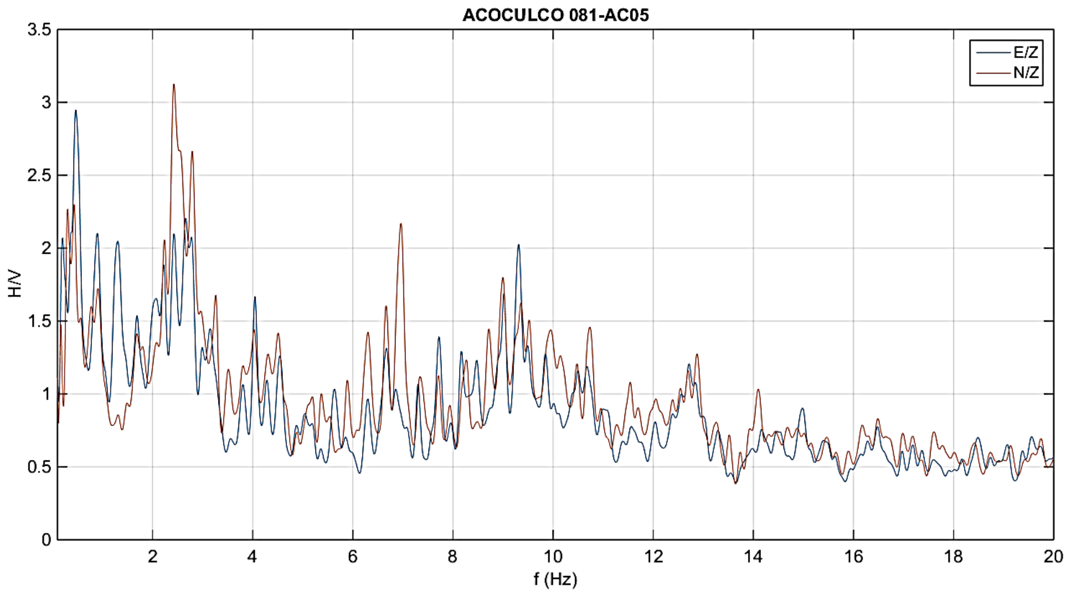
ACOCULCO 081-AC05
E/Z
N/Z
H/V
f (Hz)

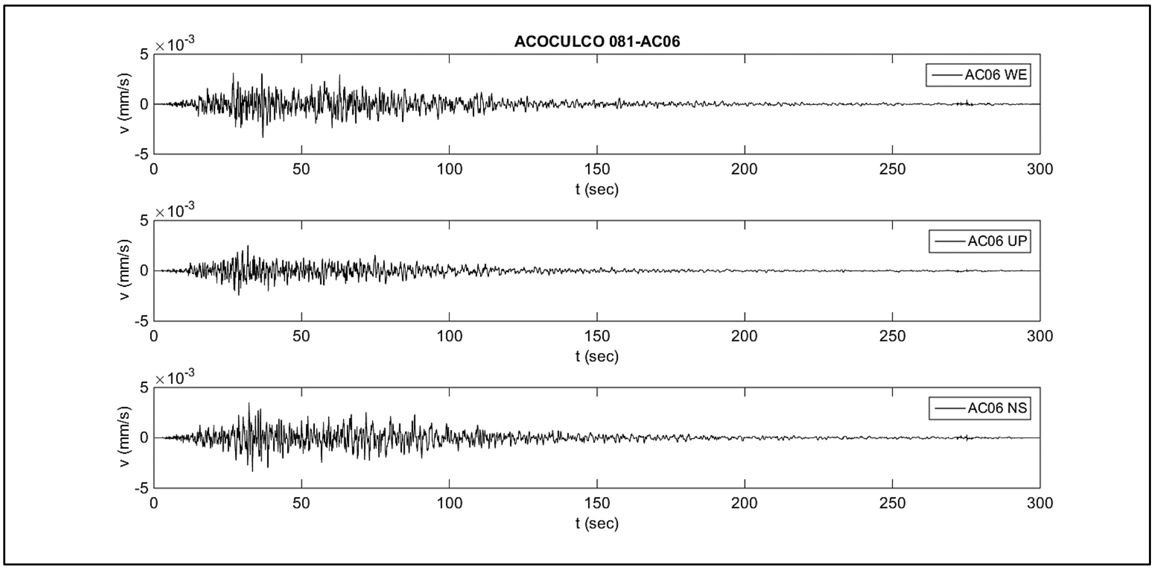
ACOCULCO 081-AC06
AC06 WE
AC06 UP
AC06 NS
v (mm/s)
t (sec)

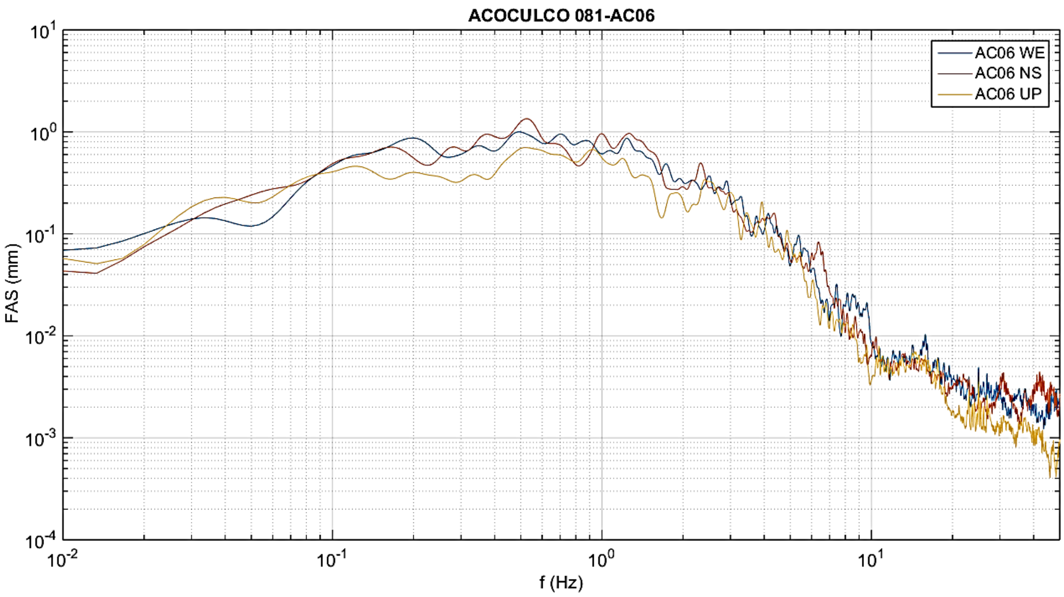
ACOCULCO 081-AC06
AC06 WE
AC06 NS
AC06 UP
FAS (mm)
f (Hz)

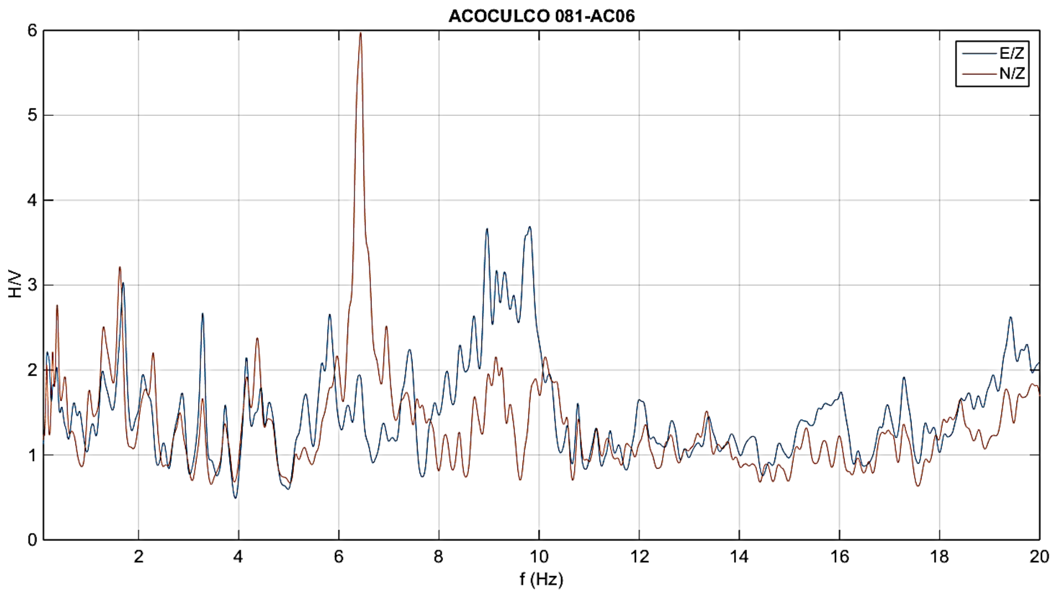
ACOCULCO 081-AC06
E/Z
N/Z
H/V
f (Hz)

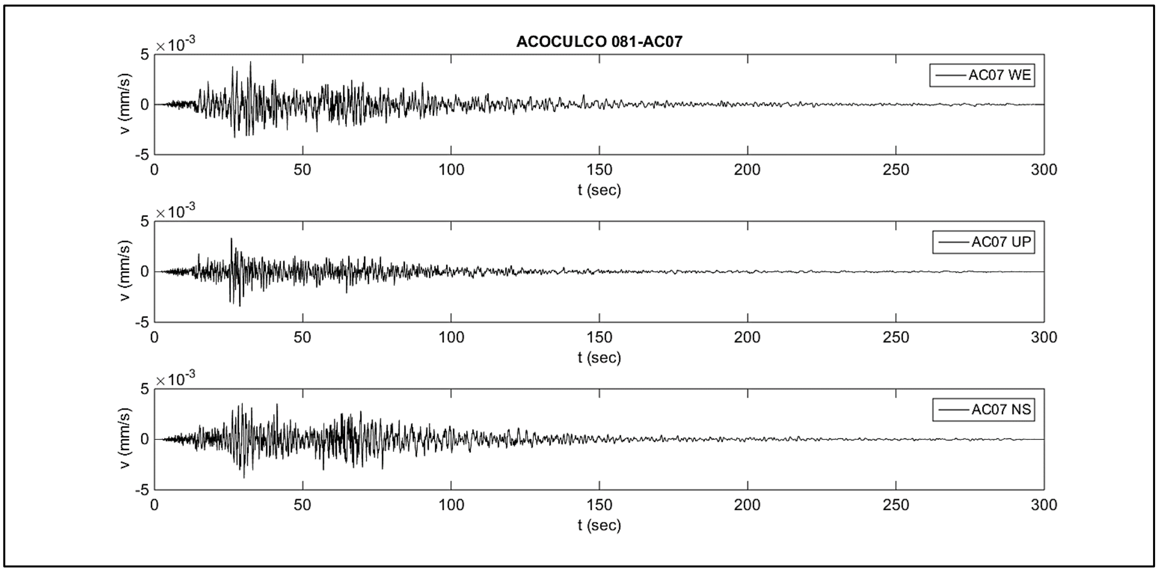
ACOCULCO 081-AC07
AC07 WE
AC07 UP
AC07 NS
v (mm/s)
t (sec)

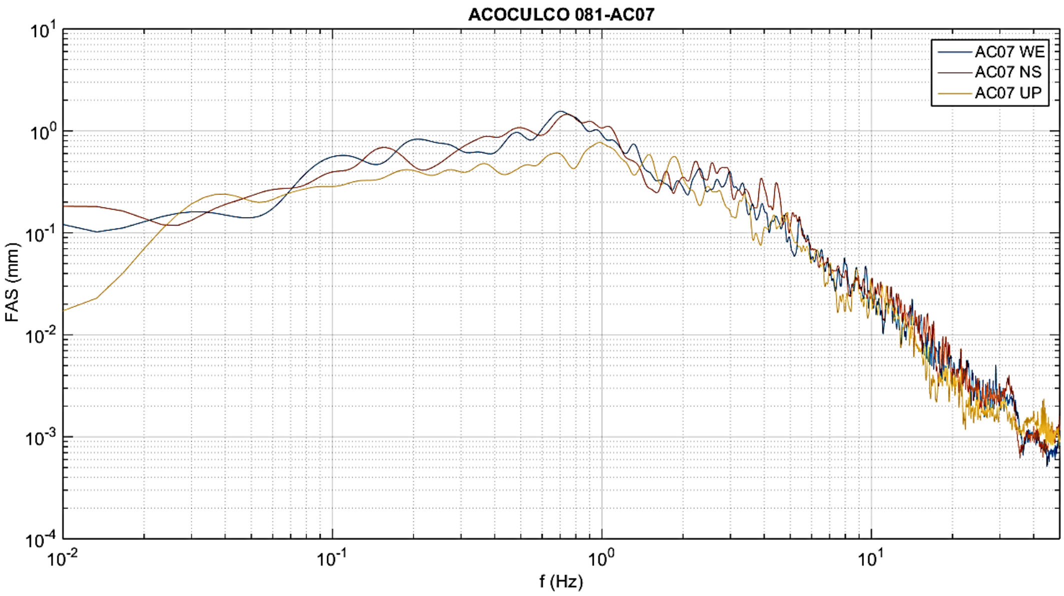
ACOCULCO 081-AC07
AC07 WE
AC07 NS
AC07 UP
FAS (mm)
f (Hz)

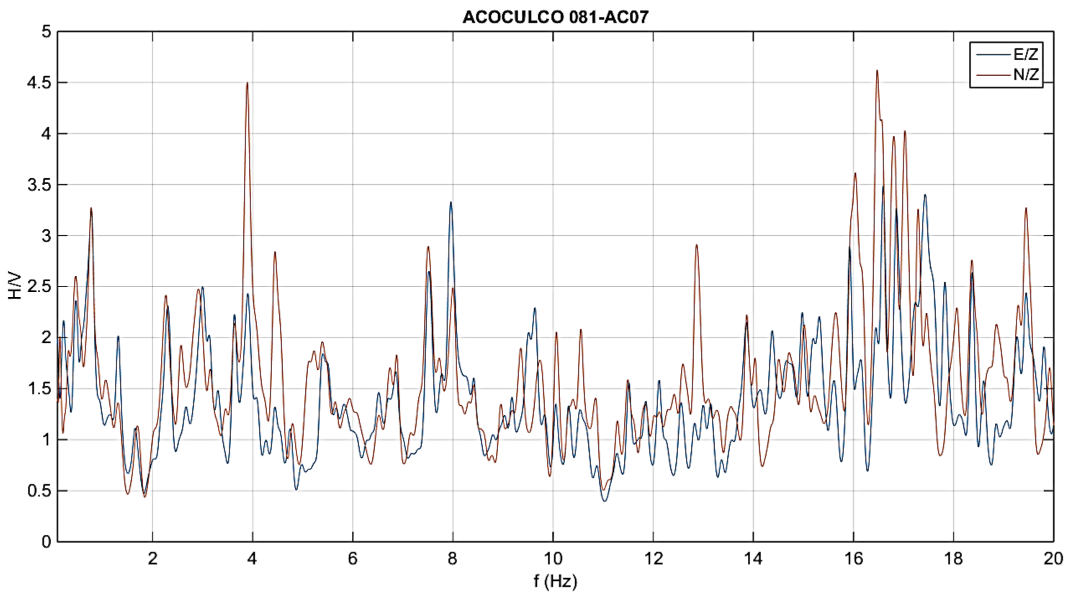
ACOCULCO 081-AC07
E/Z
N/Z
H/V
f (Hz)

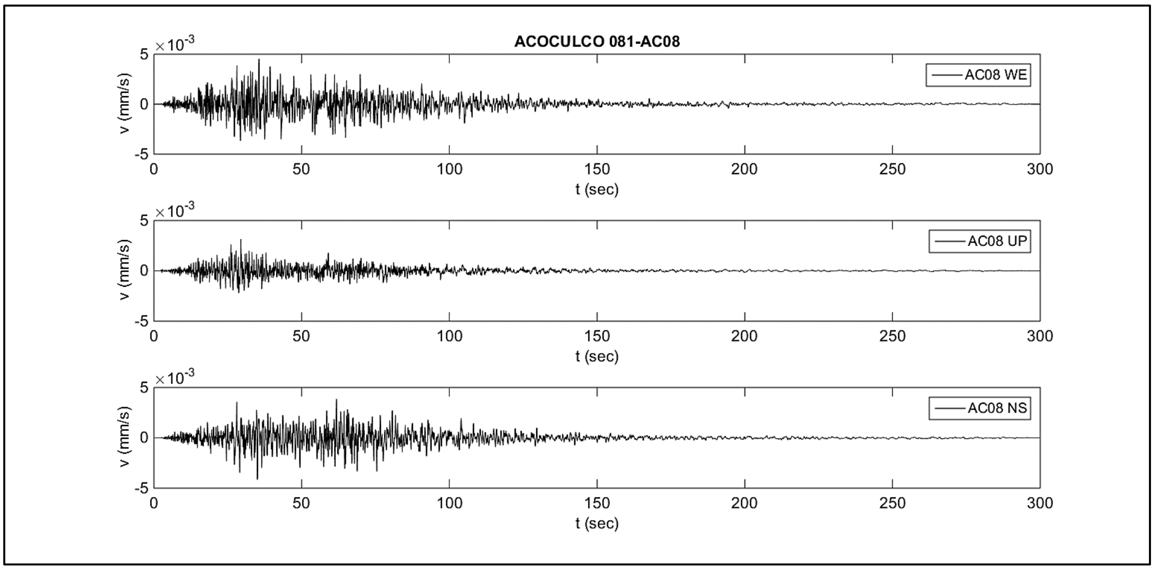
ACOCULCO 081-AC08
AC08 WE
AC08 UP
AC08 NS
v (mm/s)
t (sec)

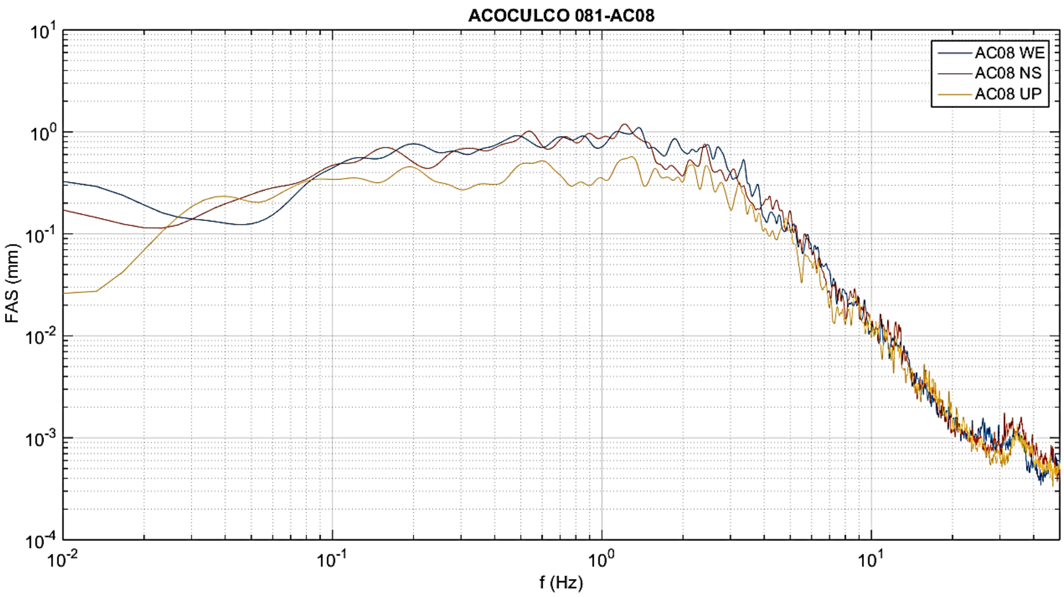
ACOCULCO 081-AC08
AC08 WE
AC08 NS
AC08 UP
FAS (mm)
f (Hz)

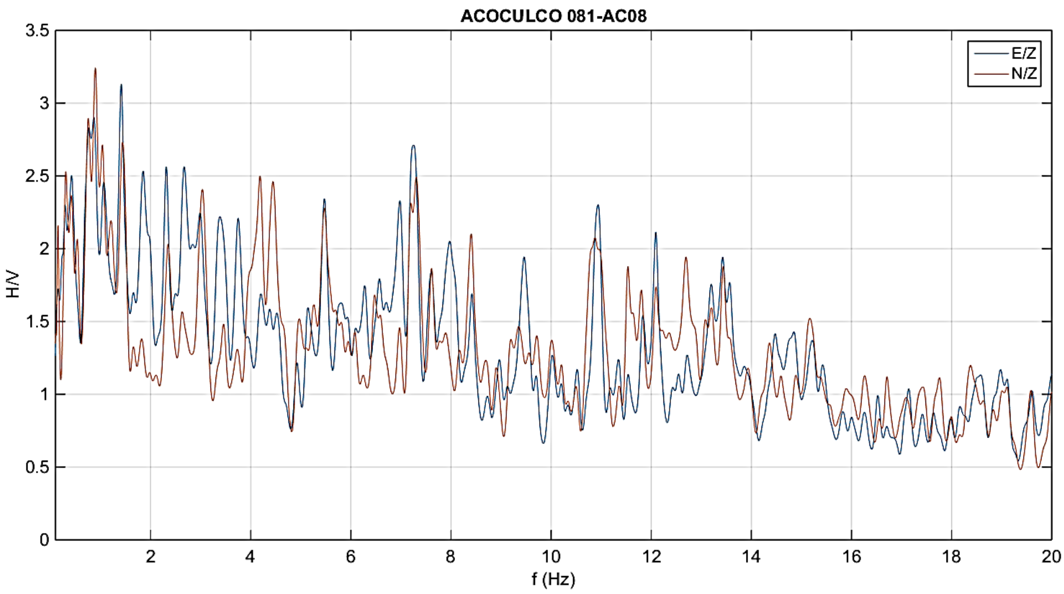
ACOCULCO 081-AC08
E/Z
N/Z
H/V
f (Hz)

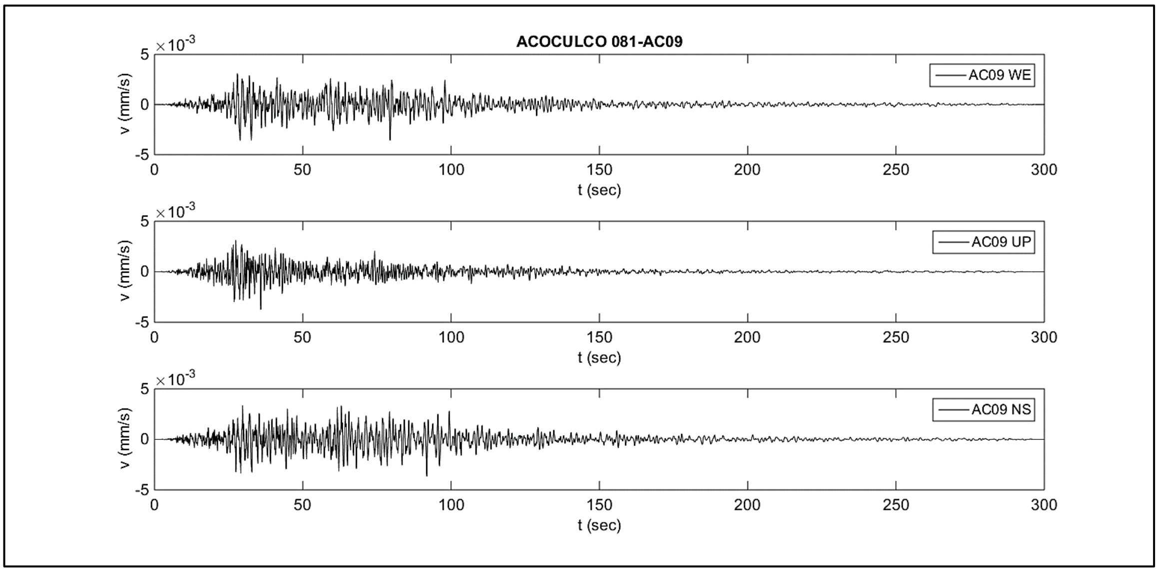
ACOCULCO 081-AC09
AC09 WE
AC09 UP
AC09 NS
v (mm/s)
t (sec)
×10^-3

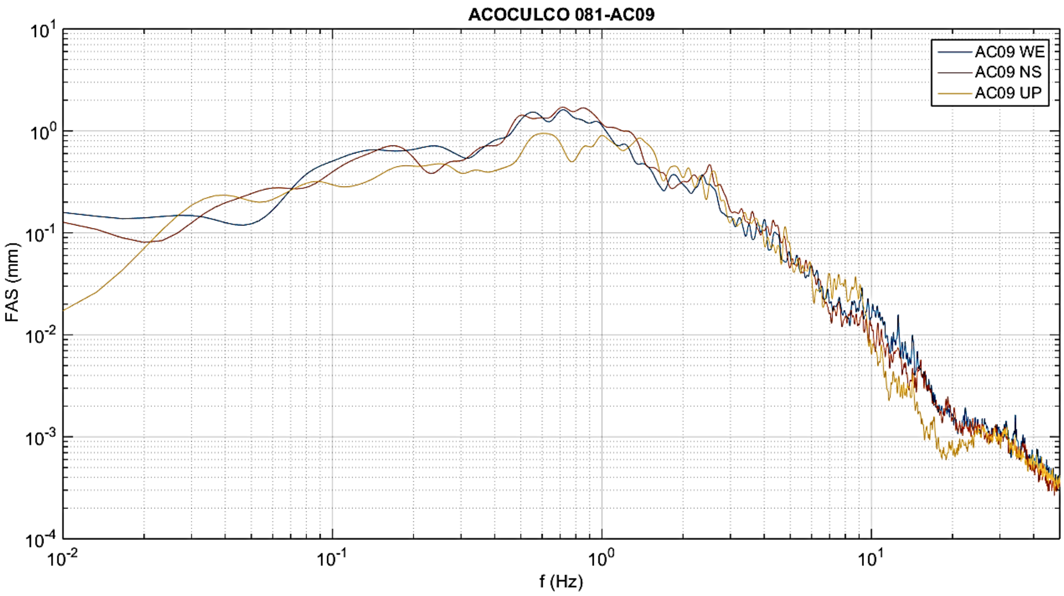
ACOCULCO 081-AC09
AC09 WE
AC09 NS
AC09 UP
FAS (mm)
f (Hz)

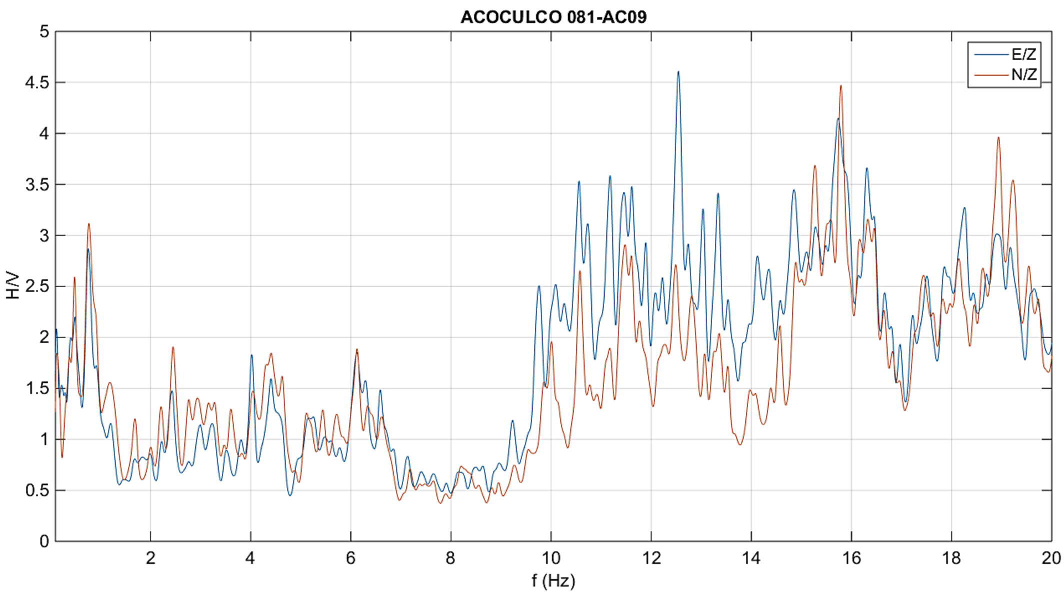
ACOCULCO 081-AC09
E/Z
N/Z
H/V
f (Hz)

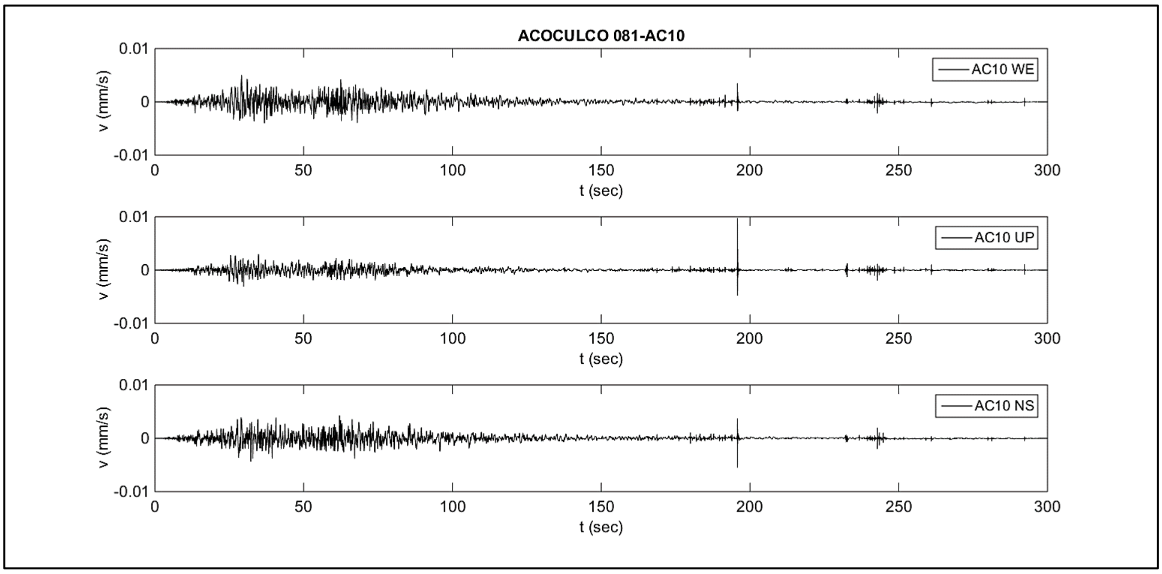
ACOCULCO 081-AC10
AC10 WE
AC10 UP
AC10 NS
v (mm/s)
t (sec)

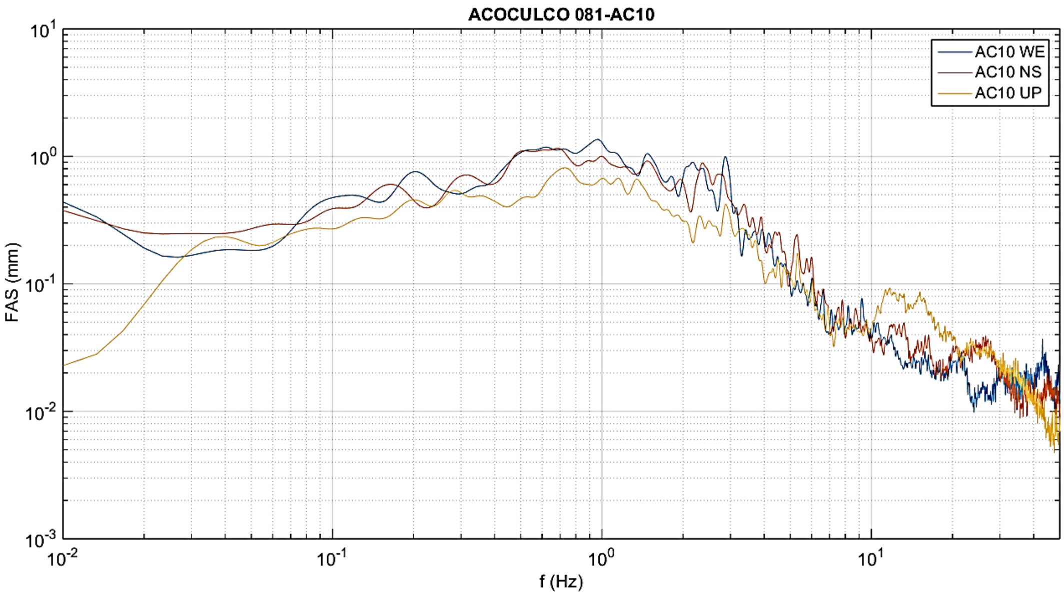
ACOCULCO 081-AC10
AC10 WE
AC10 NS
AC10 UP
FAS (mm)
f (Hz)

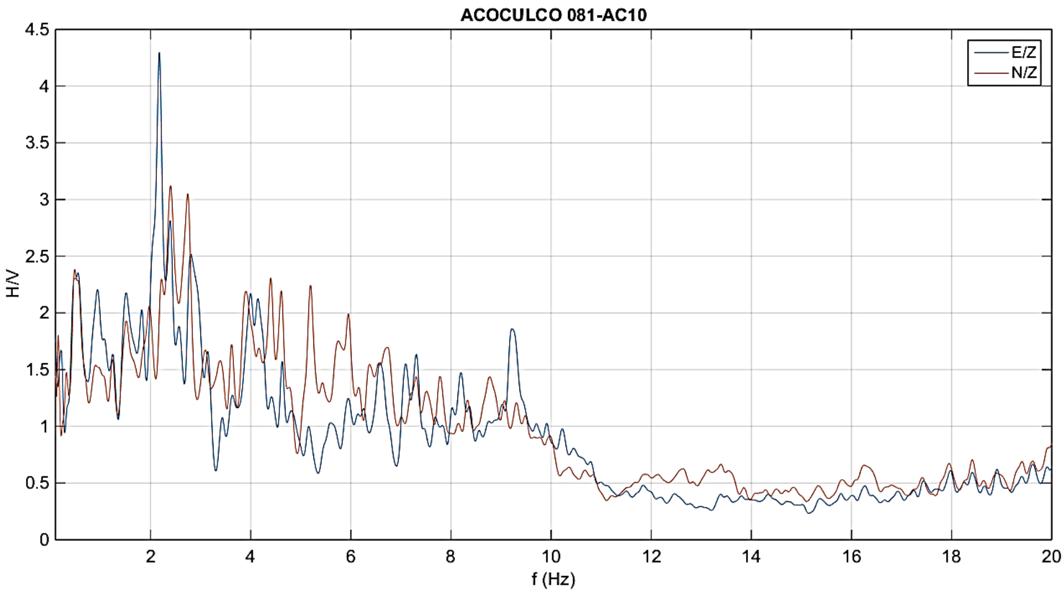
ACOCULCO 081-AC10
E/Z
N/Z
H/V
f (Hz)

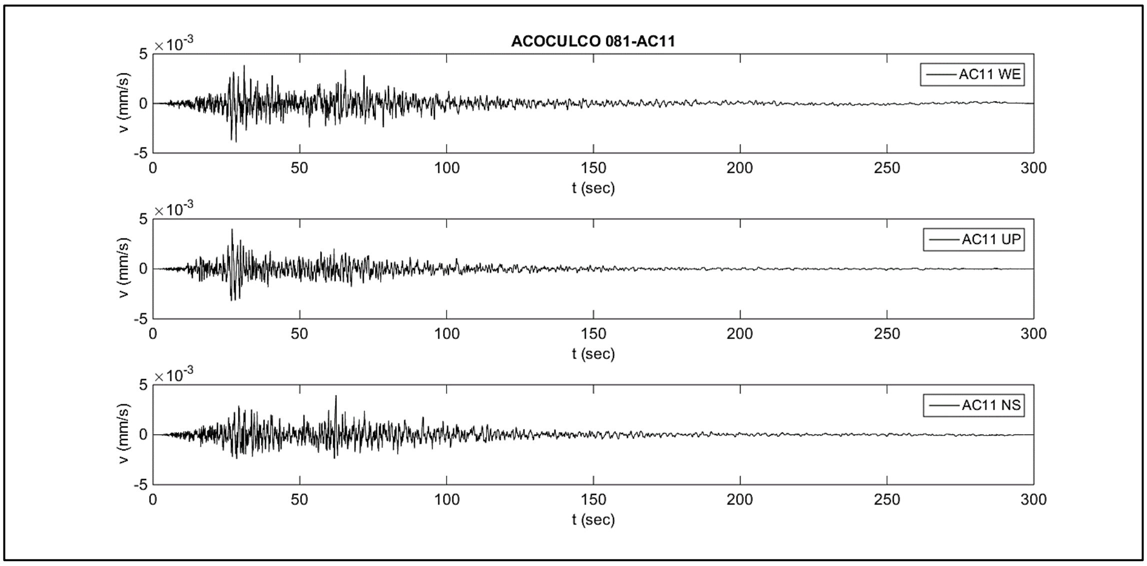
ACOCULCO 081-AC11
AC11 WE
AC11 UP
AC11 NS
v (mm/s)
t (sec)

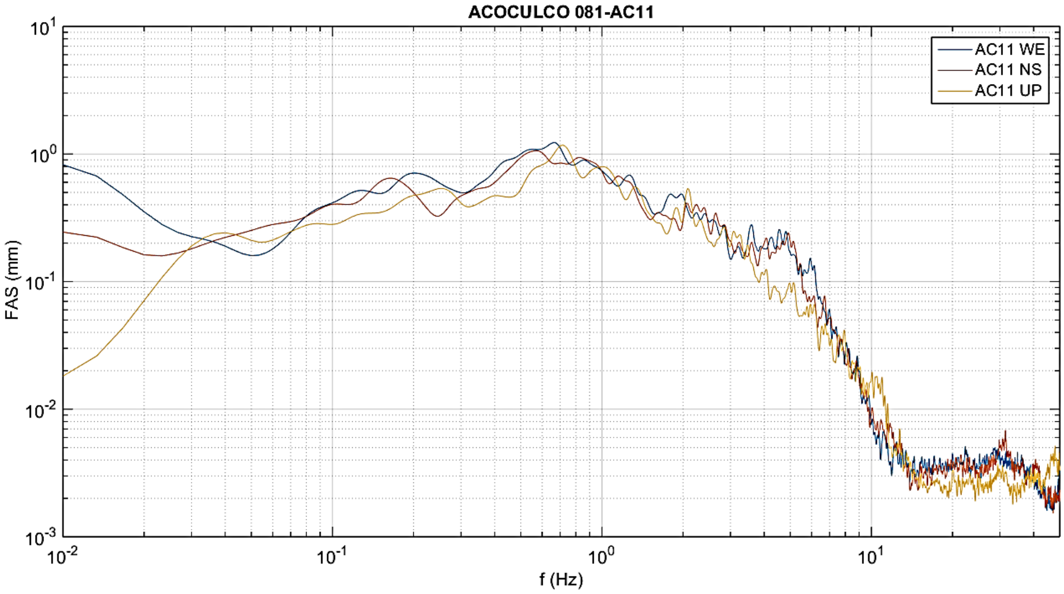
ACOCULCO 081-AC11
AC11 WE
AC11 NS
AC11 UP
FAS (mm)
f (Hz)

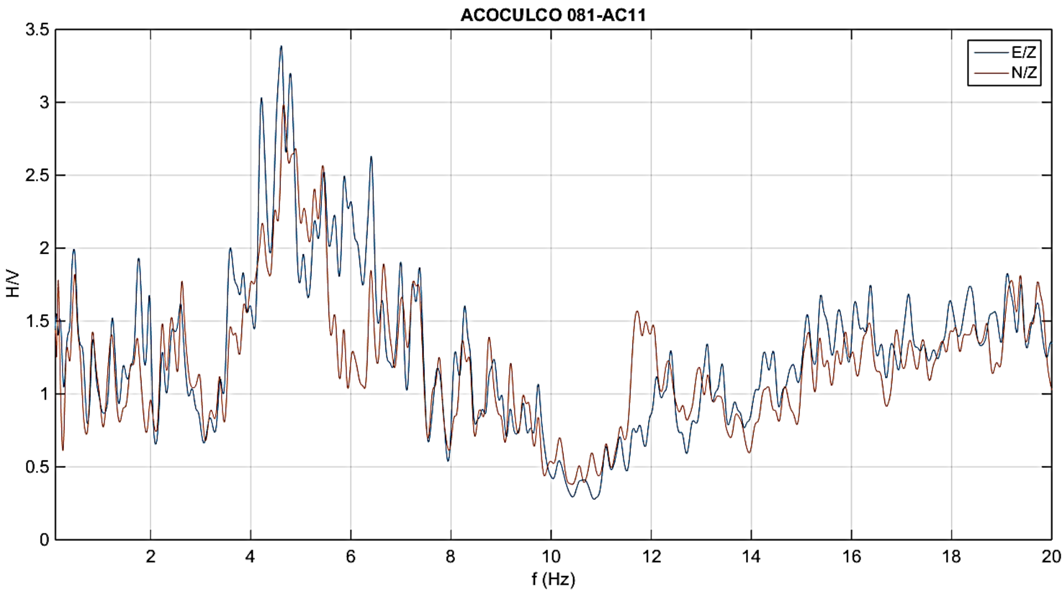
ACOCULCO 081-AC11
E/Z
N/Z
H/V
f (Hz)

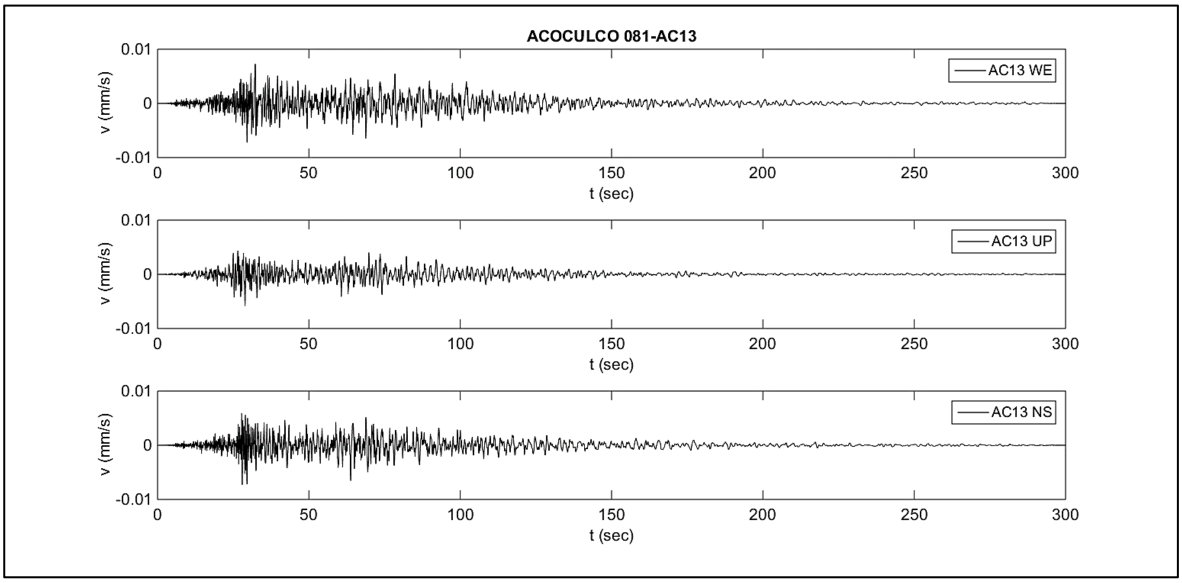
ACOCULCO 081-AC13
AC13 WE
AC13 UP
AC13 NS
v (mm/s)
t (sec)
0.01
0
-0.01
0
50
100
150
200
250
300

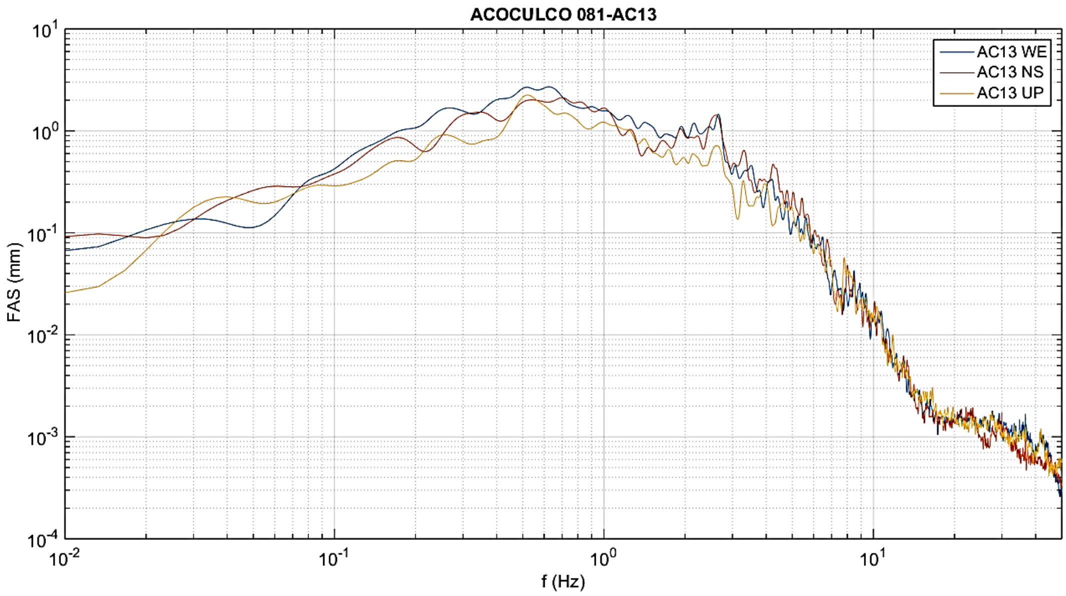
ACOCULCO 081-AC13
AC13 WE
AC13 NS
AC13 UP
FAS (mm)
f (Hz)

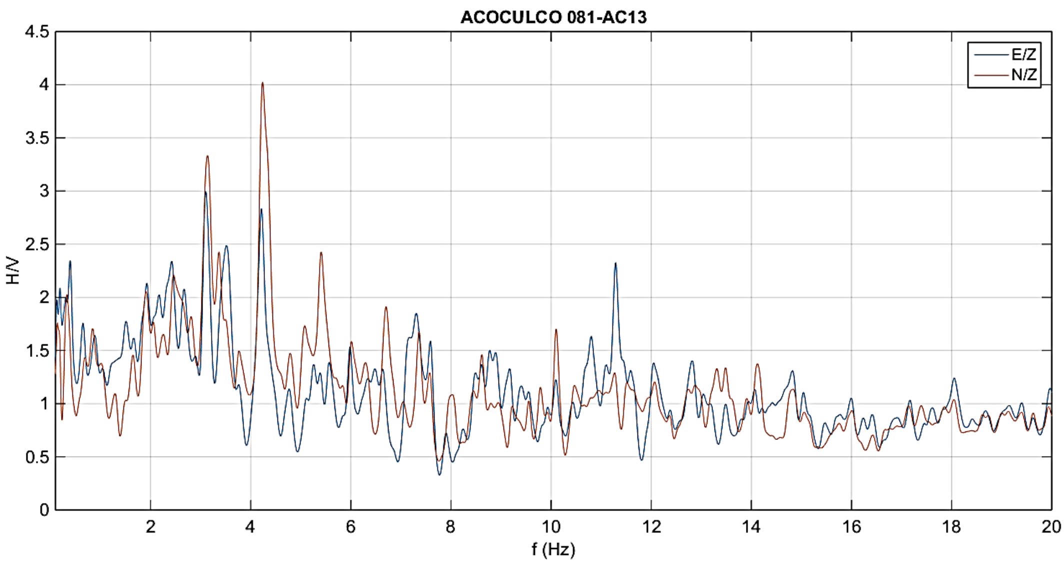
ACOCULCO 081-AC13
E/Z
N/Z
H/V
f (Hz)

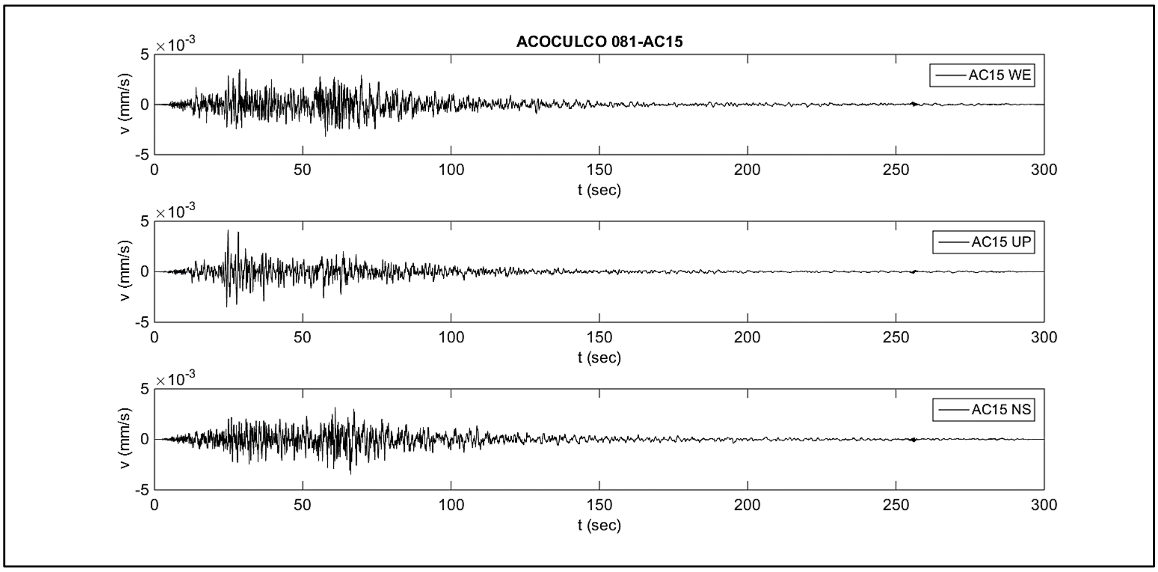
ACOCULCO 081-AC15
AC15 WE
AC15 UP
AC15 NS
v (mm/s)
t (sec)
×10^-3

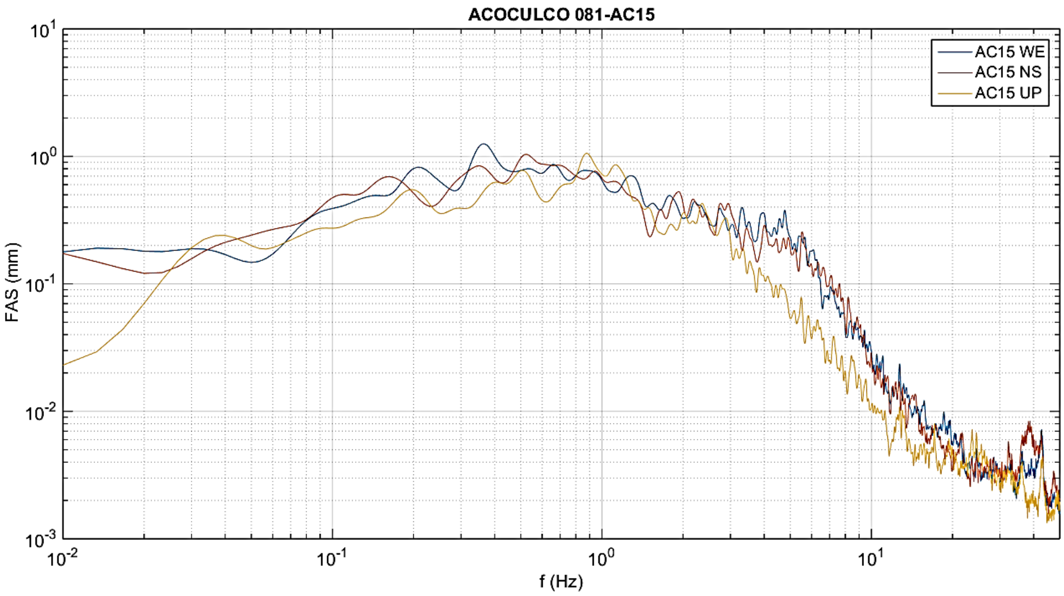
ACOCULCO 081-AC15
AC15 WE
AC15 NS
AC15 UP
FAS (mm)
f (Hz)

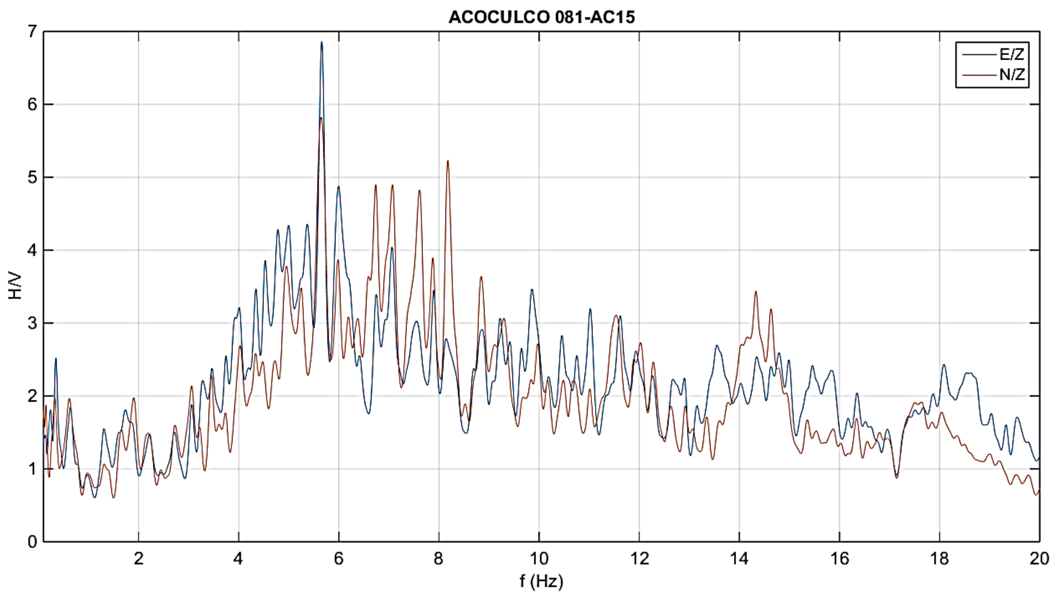
ACOCULCO 081-AC15
E/Z
N/Z
H/V
f (Hz)

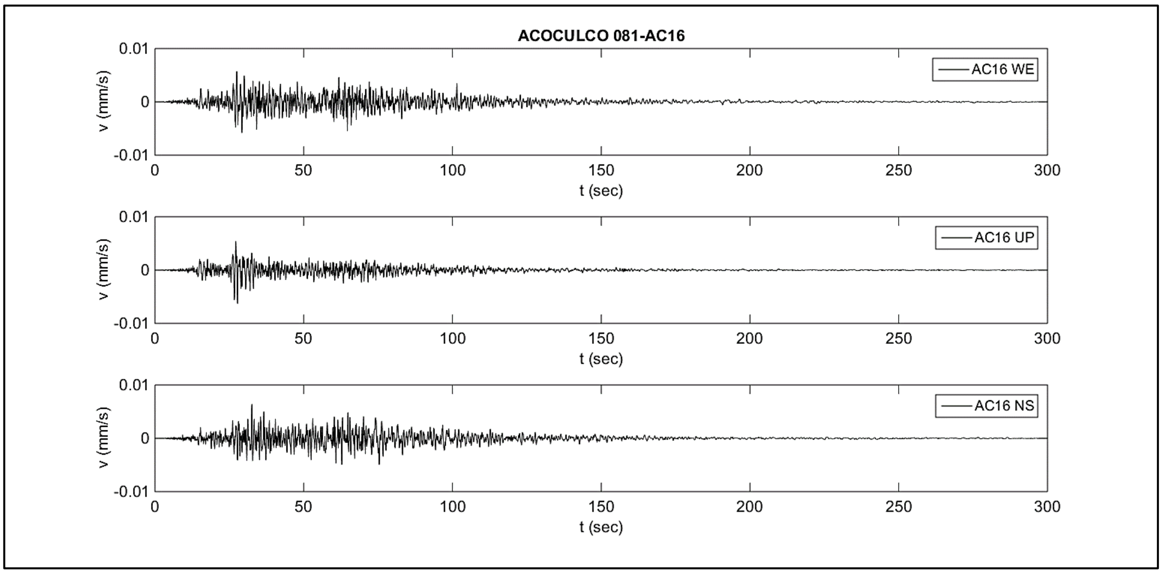
ACOCULCO 081-AC16
AC16 WE
AC16 UP
AC16 NS
v (mm/s)
t (sec)
0.01
0
-0.01
0
50
100
150
200
250
300

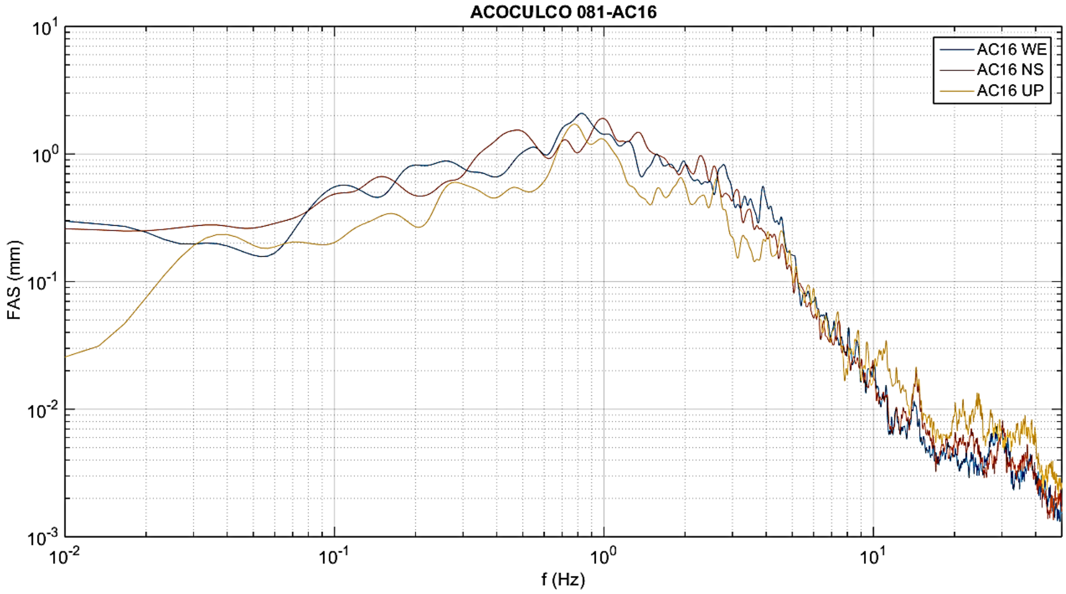
ACOCULCO 081-AC16
AC16 WE
AC16 NS
AC16 UP
FAS (mm)
f (Hz)
10^1
10^0
10^{-1}
10^{-2}
10^{-3}

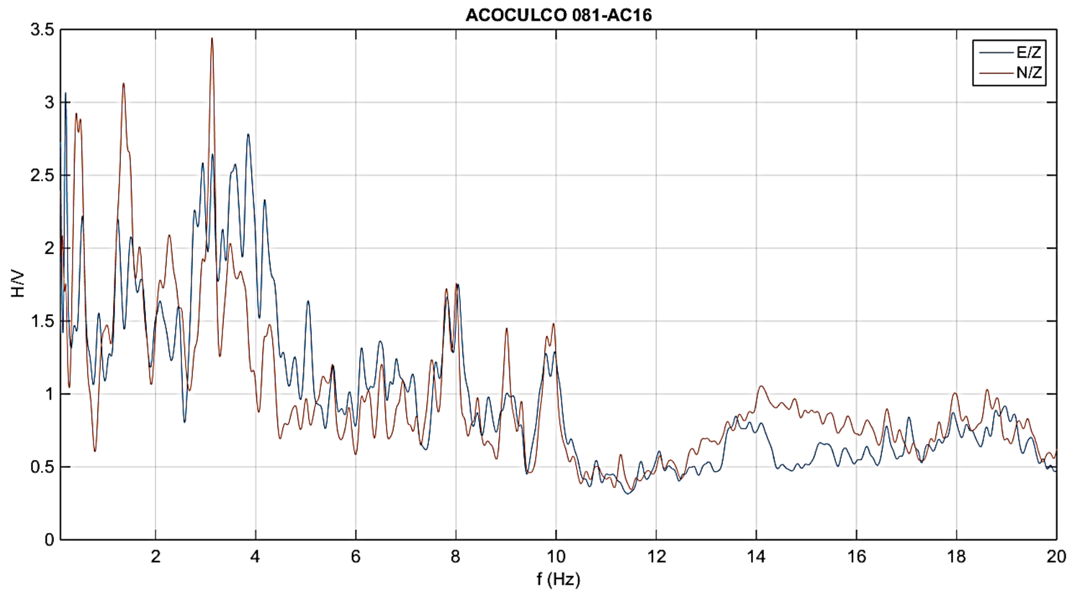
ACOCULCO 081-AC16
E/Z
N/Z
H/V
f (Hz)
3.5
3
2.5
2
1.5
1
0.5
0
2
4
6
8
10
12
14
16
18
20

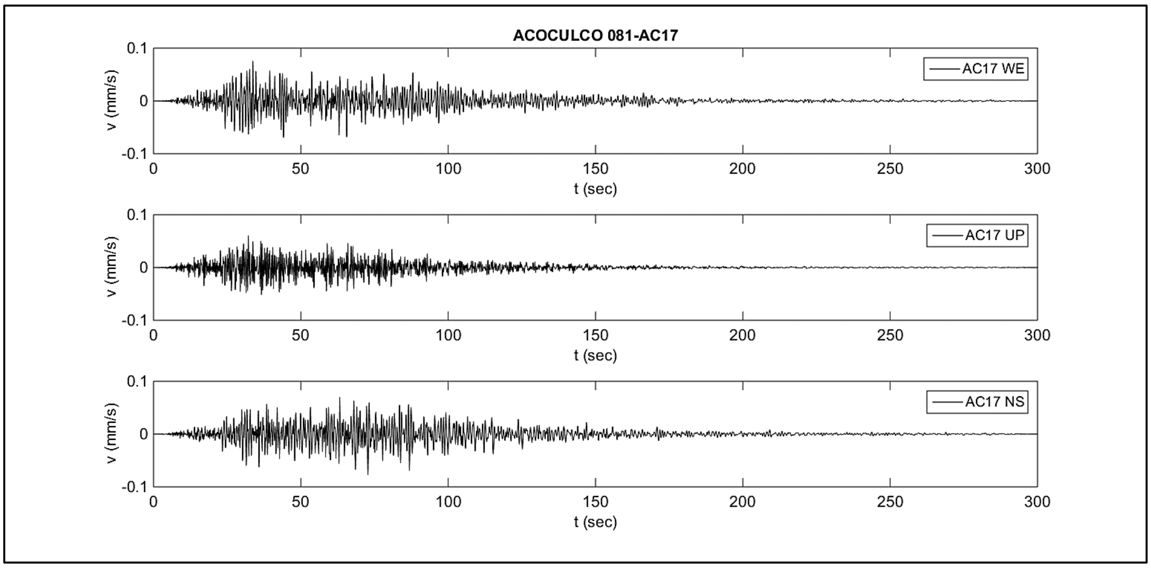
ACOCULCO 081-AC17
AC17 WE
AC17 UP
AC17 NS
v (mm/s)
t (sec)

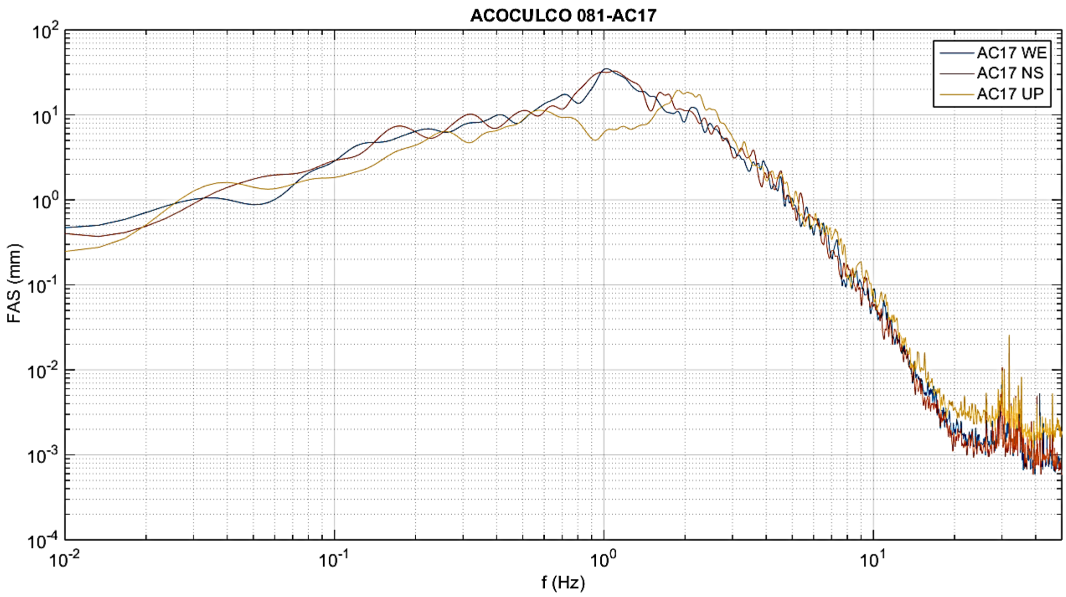
ACOCULCO 081-AC17
AC17 WE
AC17 NS
AC17 UP
FAS (mm)
f (Hz)

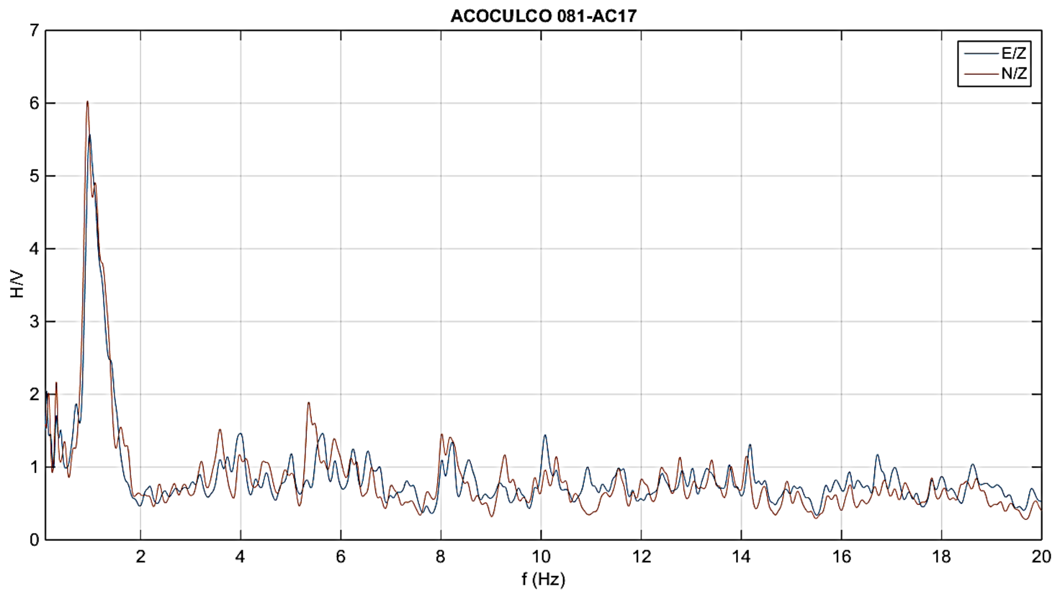
ACOCULCO 081-AC17
E/Z
N/Z
H/V
f (Hz)

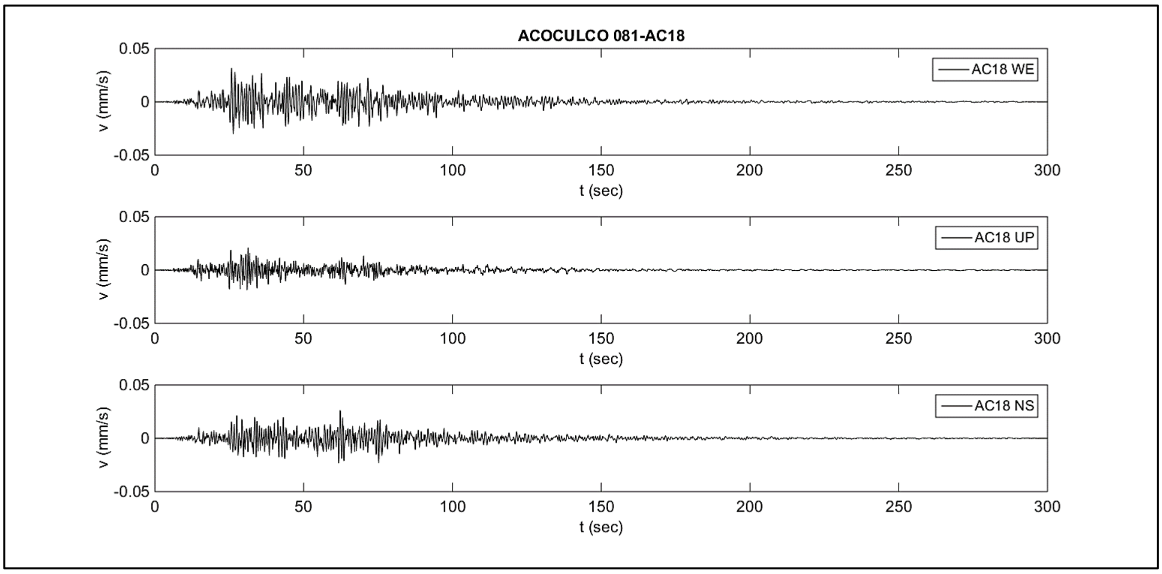
ACOCULCO 081-AC18
AC18 WE
AC18 UP
AC18 NS
v (mm/s)
t (sec)

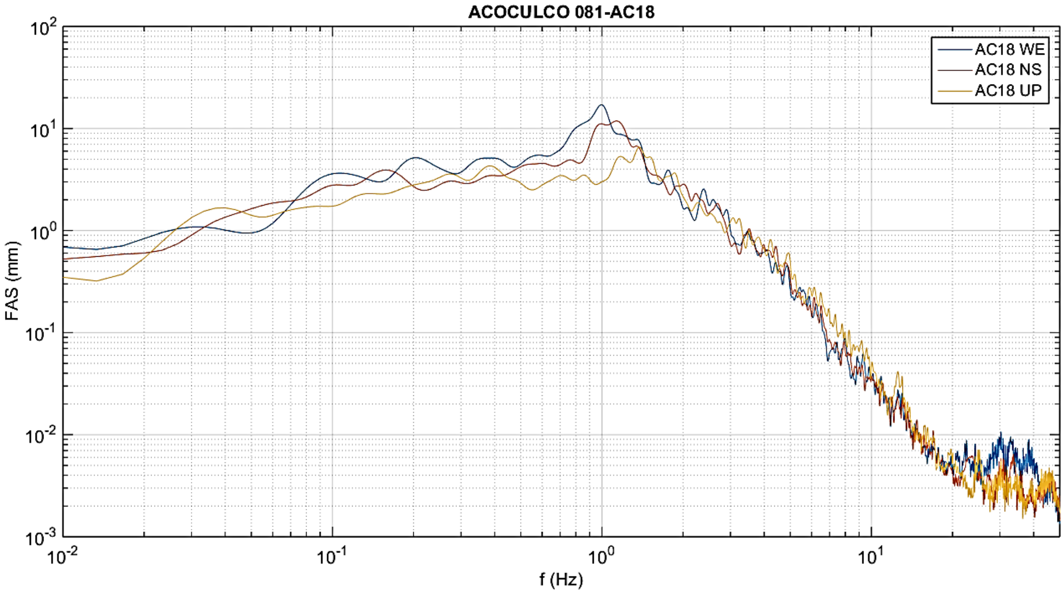
ACOCULCO 081-AC18
AC18 WE
AC18 NS
AC18 UP
FAS (mm)
f (Hz)

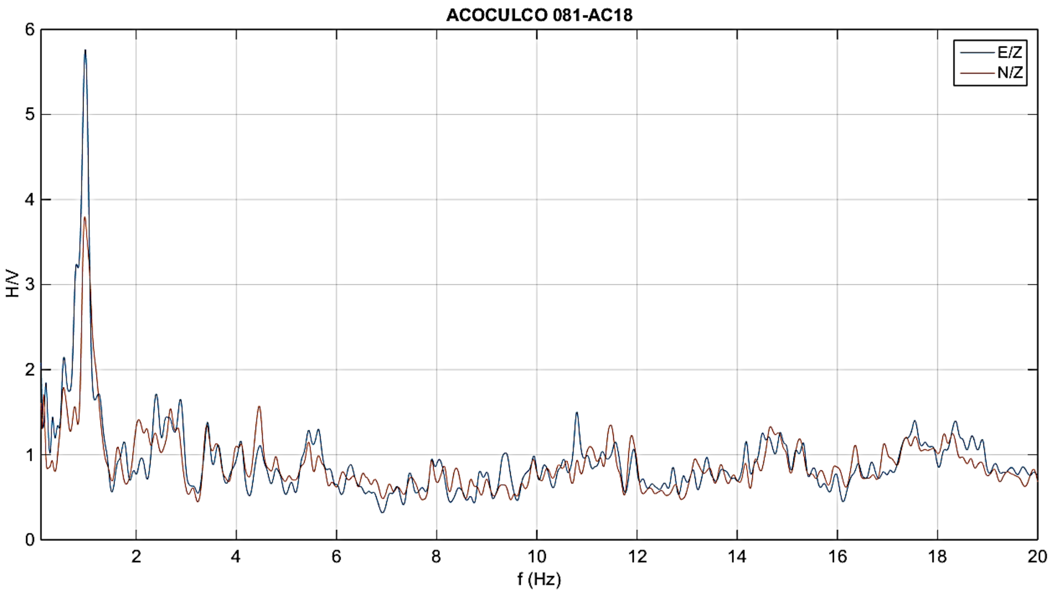
ACOCULCO 081-AC18
E/Z
N/Z
H/V
f (Hz)

Appendix 4-D Day 082, Earthquake. Time histories, spectra and spectral ratios

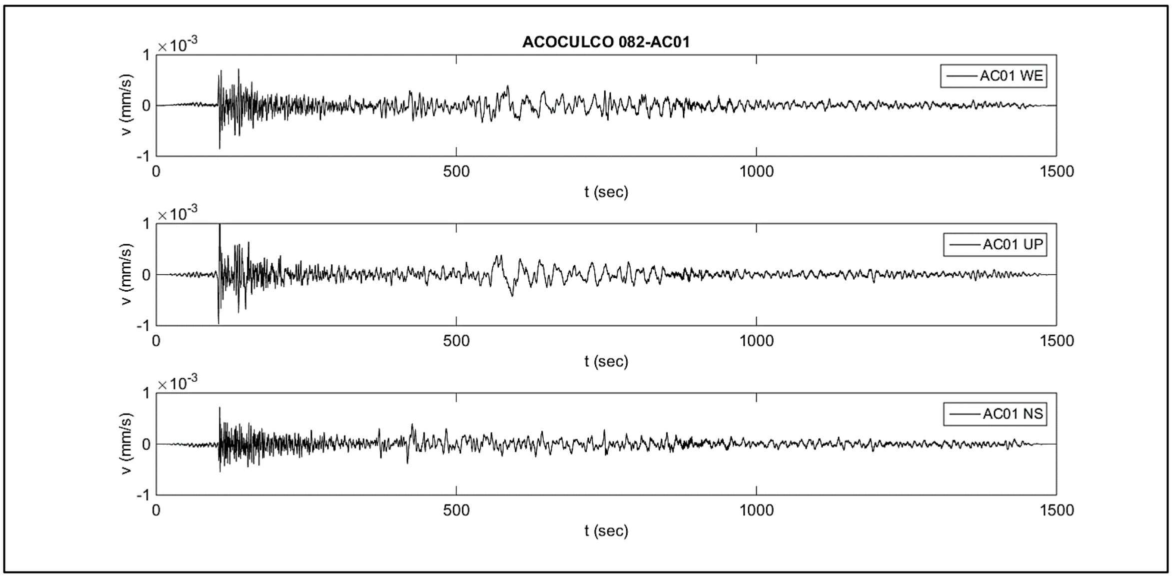

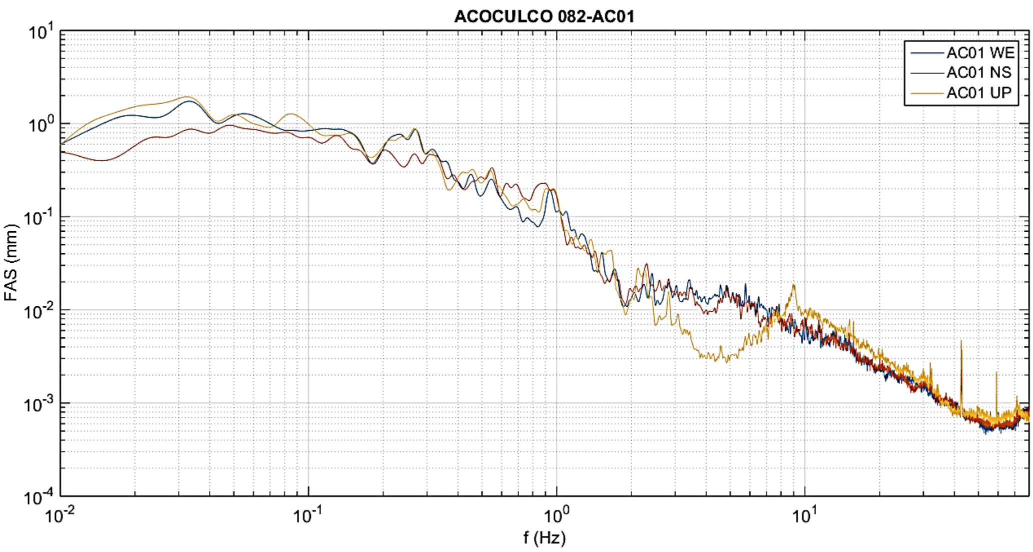

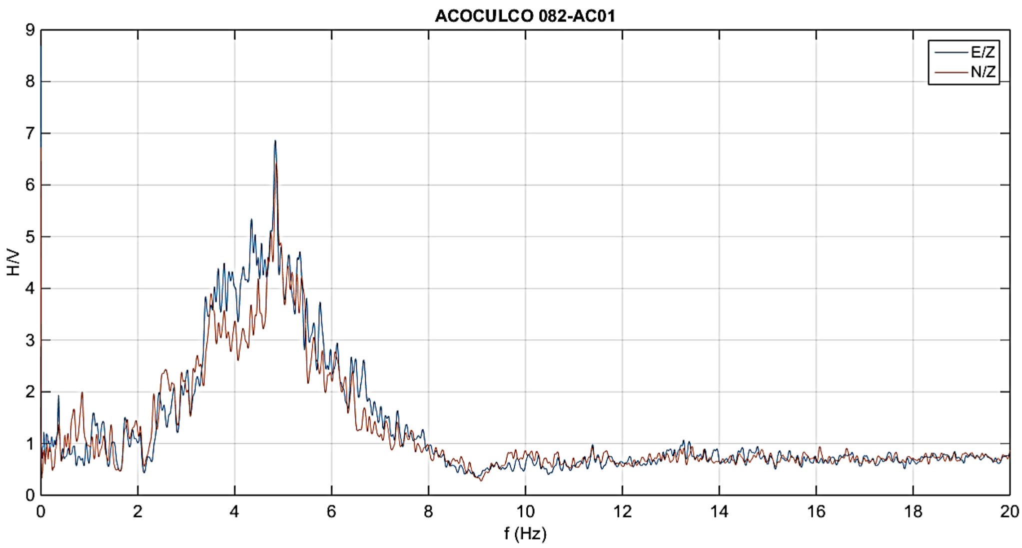

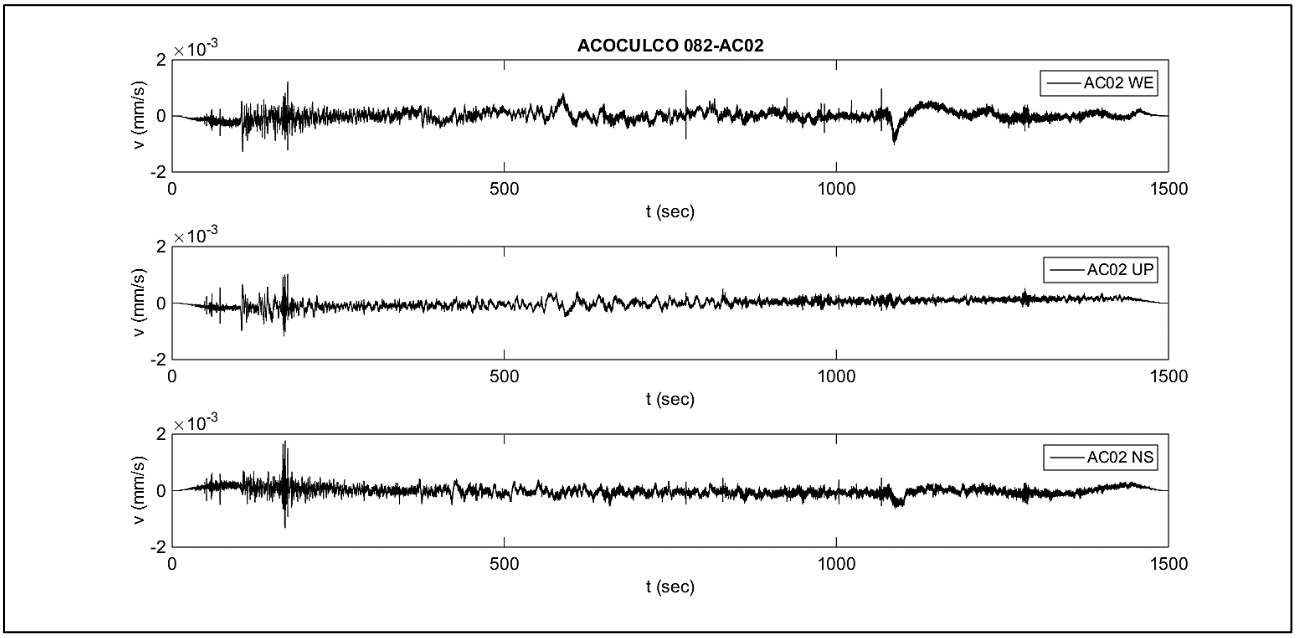
ACOCULCO 082-AC02
AC02 WE
AC02 UP
AC02 NS
v (mm/s)
t (sec)
×10-3
0
500
1000
1500

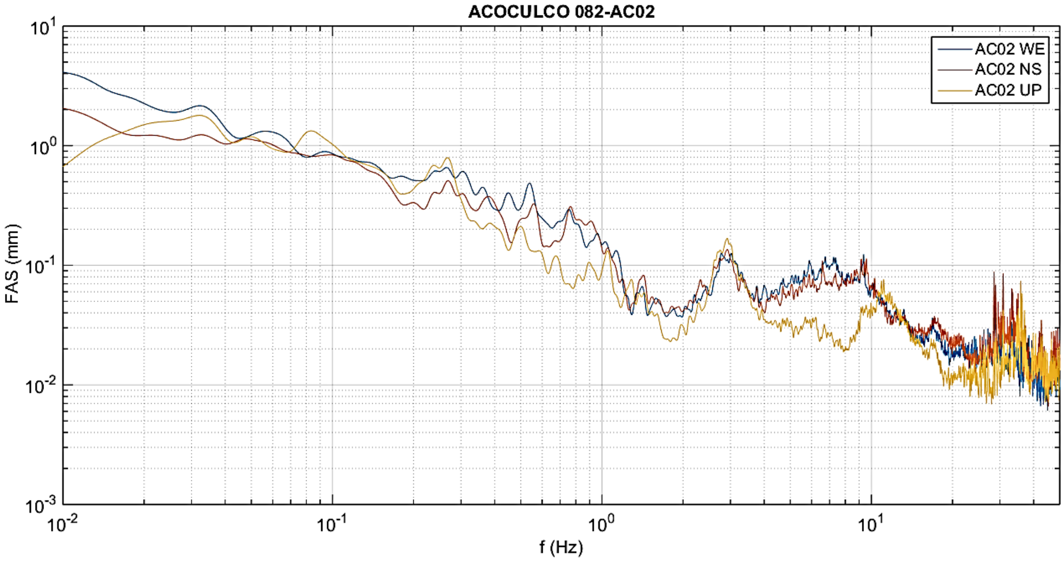
ACOCULCO 082-AC02
AC02 WE
AC02 NS
AC02 UP
FAS (mm)
f (Hz)

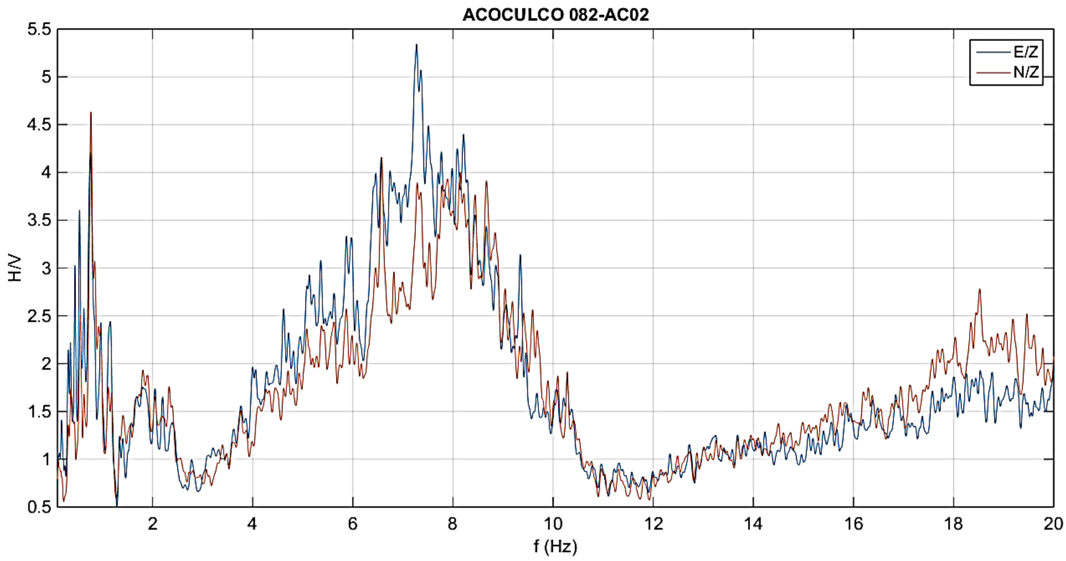
ACOCULCO 082-AC02
E/Z
N/Z
H/V
f (Hz)

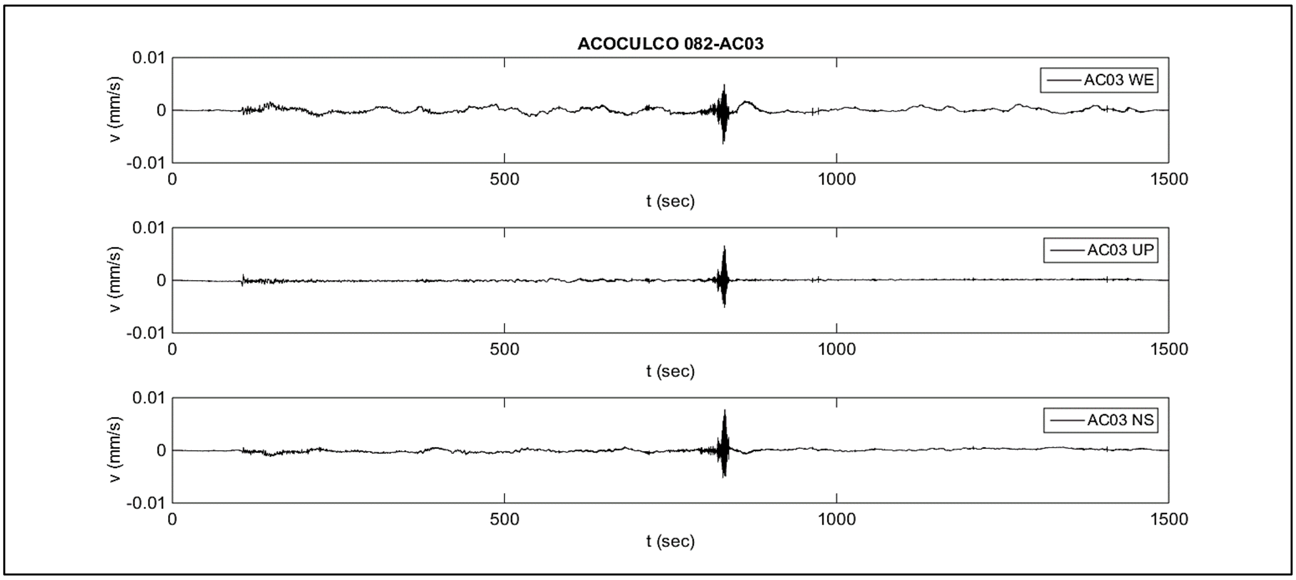
ACOCULCO 082-AC03
AC03 WE
AC03 UP
AC03 NS
v (mm/s)
t (sec)
0.01
0
-0.01
0
500
1000
1500

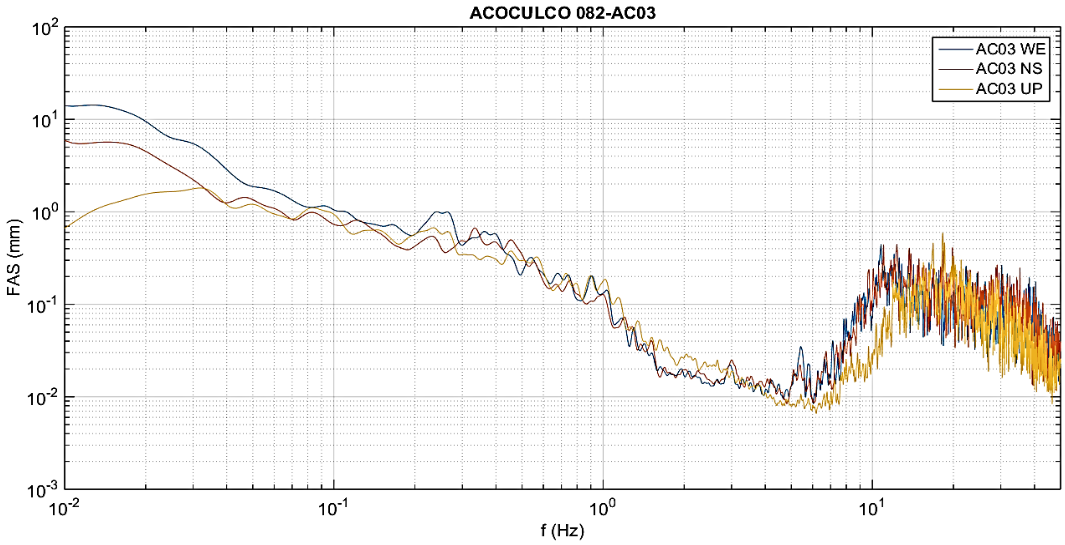
ACOCULCO 082-AC03
AC03 WE
AC03 NS
AC03 UP
FAS (mm)
f (Hz)

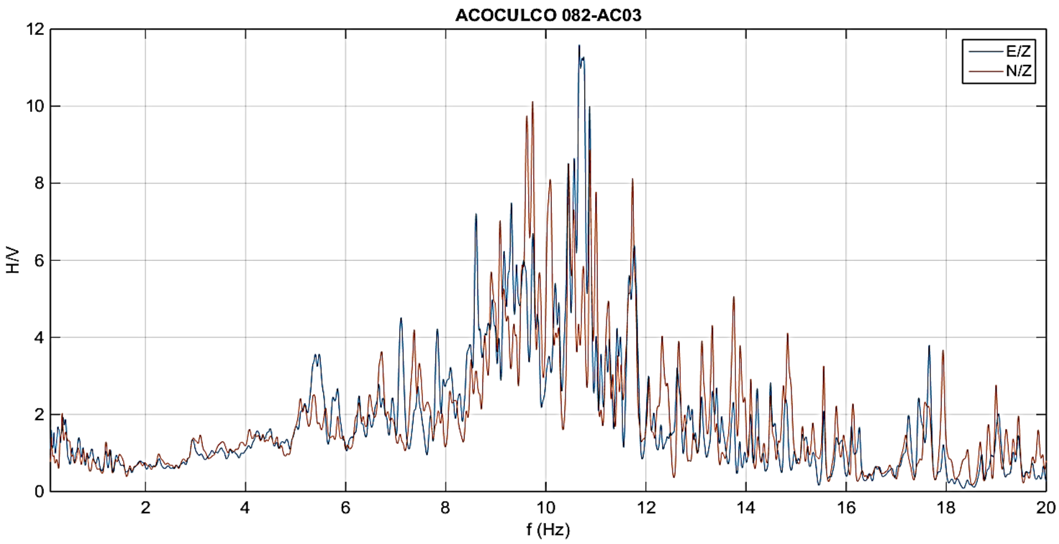
ACOCULCO 082-AC03
E/Z
N/Z
H/V
f (Hz)

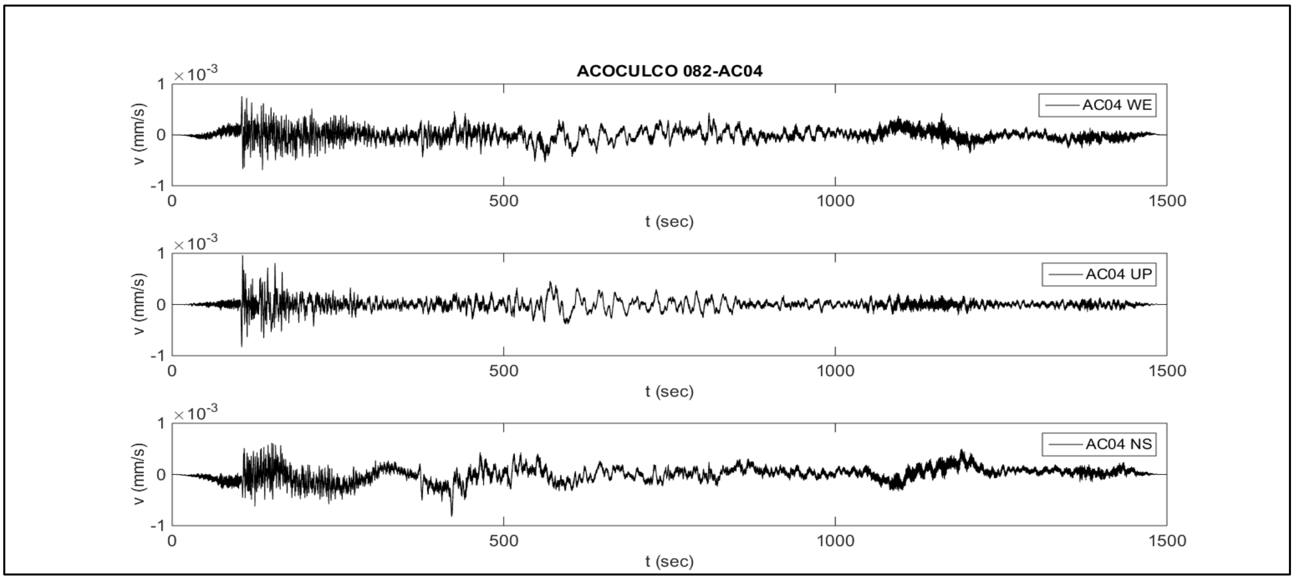
ACOCULCO 082-AC04
AC04 WE
AC04 UP
AC04 NS
v (mm/s)
t (sec)
×10-3

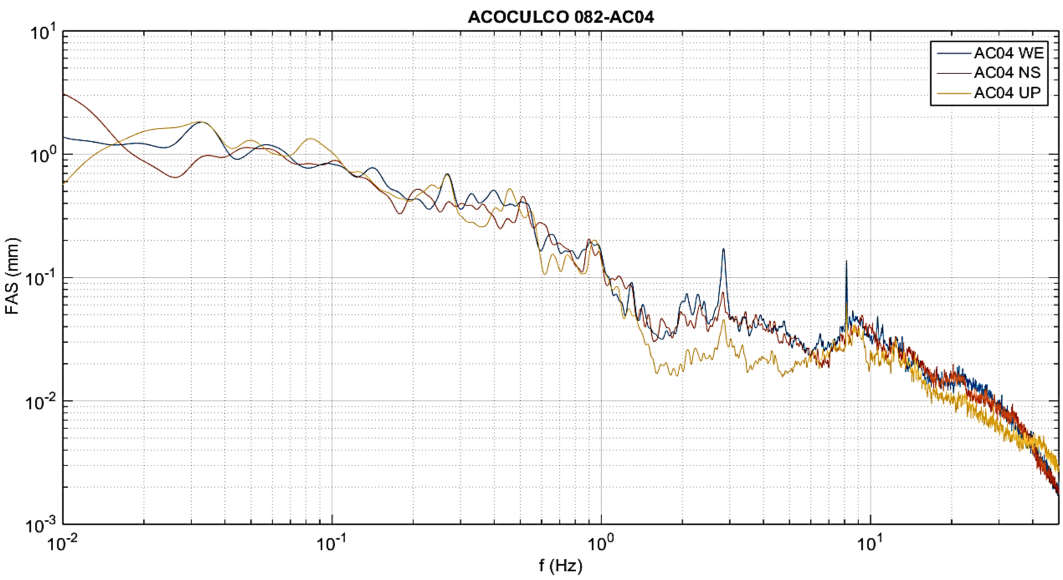
ACOCULCO 082-AC04
AC04 WE
AC04 NS
AC04 UP
FAS (mm)
f (Hz)

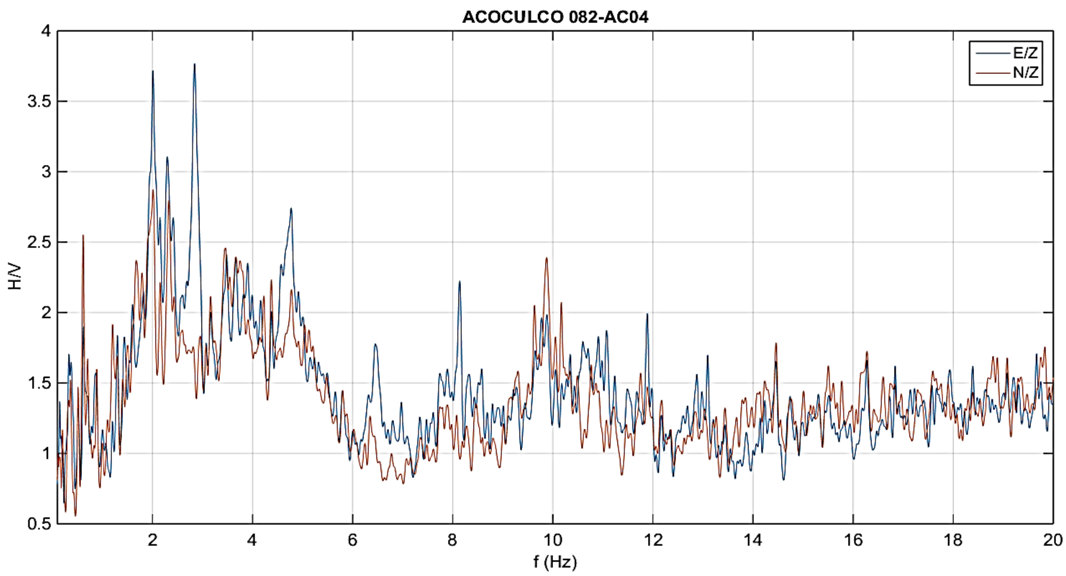
ACOCULCO 082-AC04
E/Z
N/Z
H/V
f (Hz)

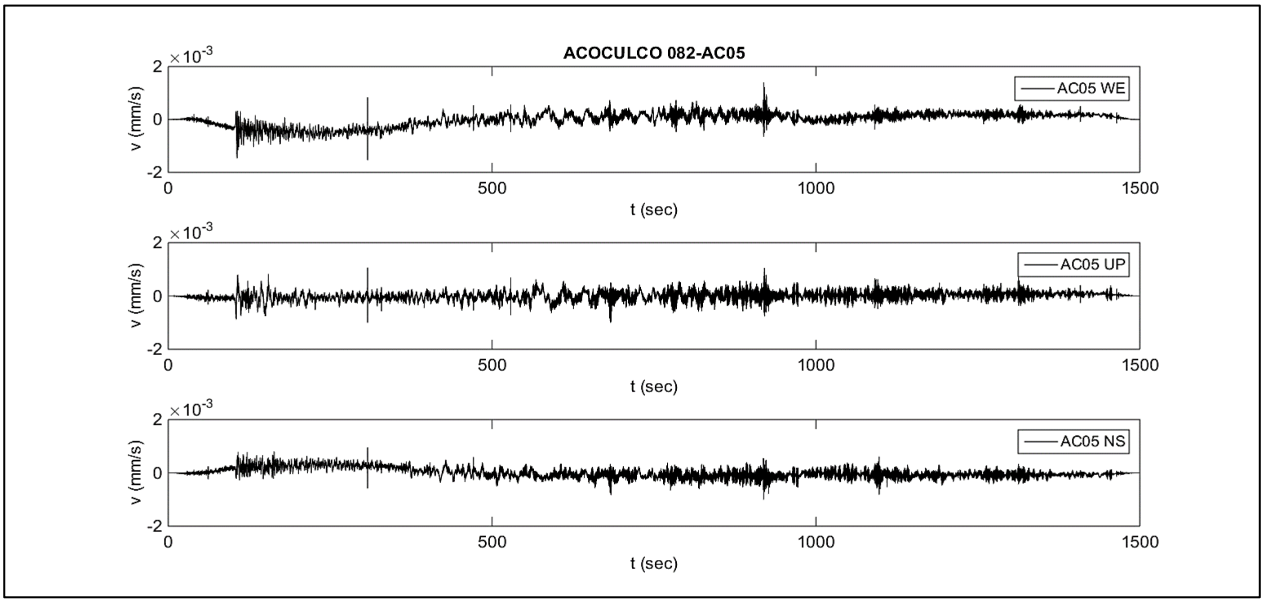
ACOCULCO 082-AC05
AC05 WE
AC05 UP
AC05 NS
v (mm/s)
t (sec)

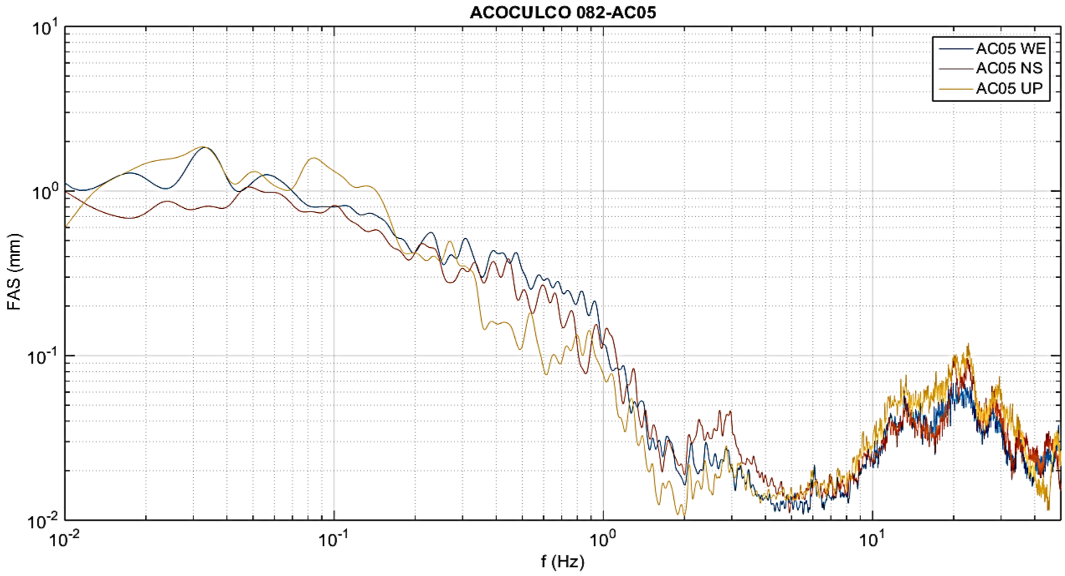
ACOCULCO 082-AC05
AC05 WE
AC05 NS
AC05 UP
FAS (mm)
f (Hz)

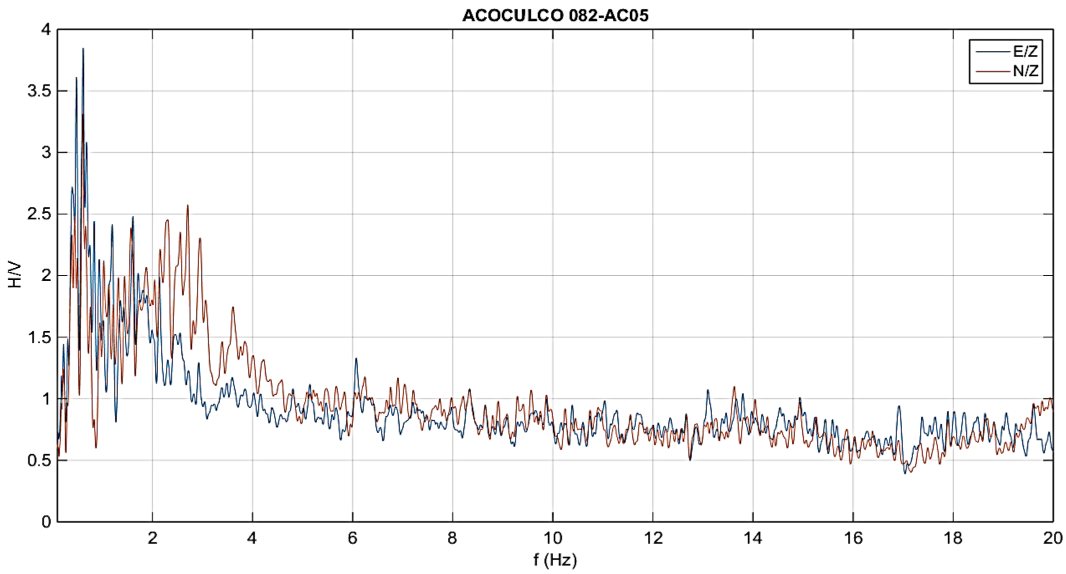
ACOCULCO 082-AC05
E/Z
N/Z
H/V
f (Hz)

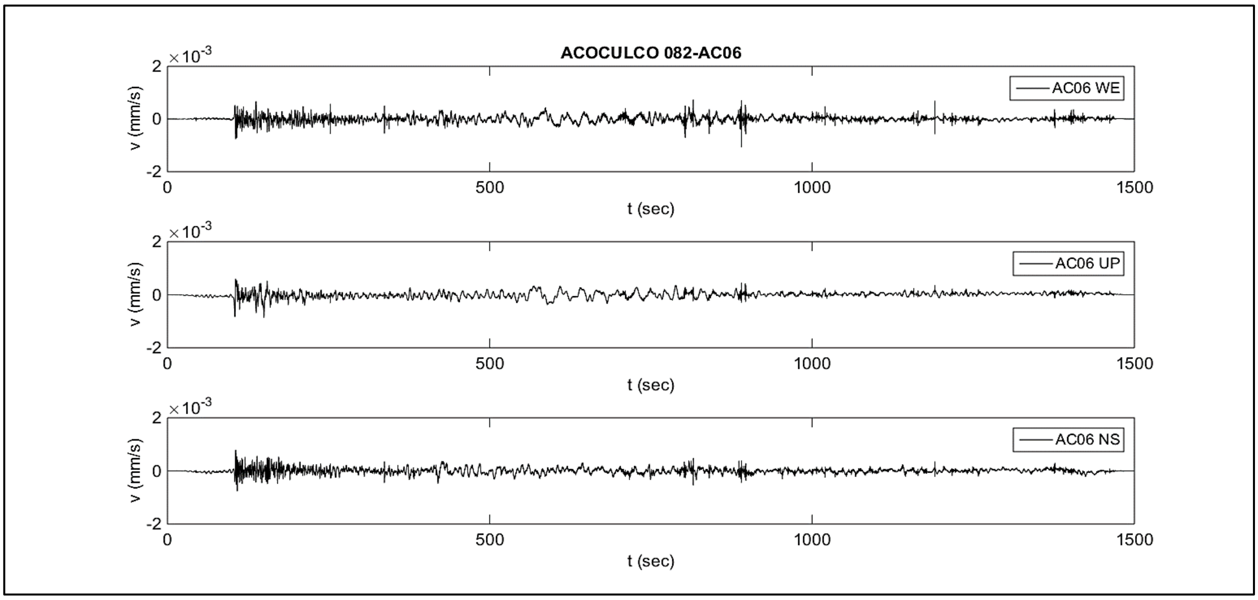
ACOCULCO 082-AC06
AC06 WE
AC06 UP
AC06 NS
v (mm/s)
t (sec)

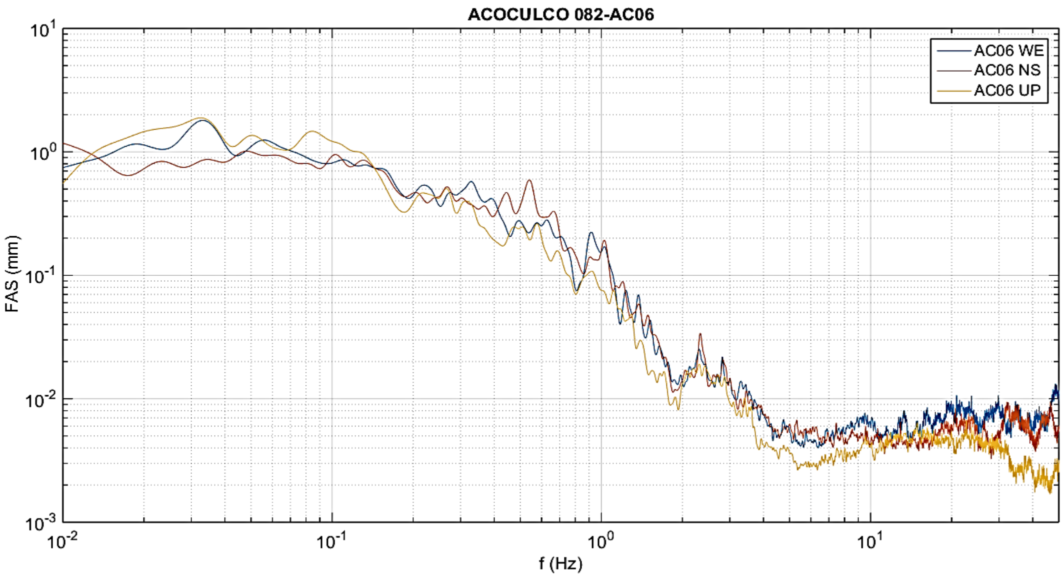
ACOCULCO 082-AC06
AC06 WE
AC06 NS
AC06 UP
FAS (mm)
f (Hz)

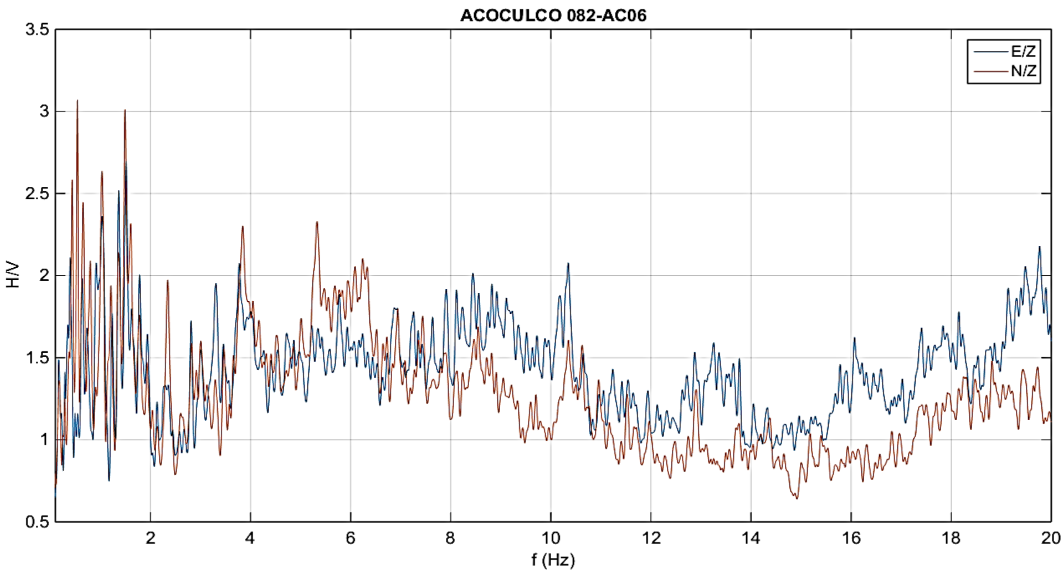
ACOCULCO 082-AC06
E/Z
N/Z
H/V
f (Hz)

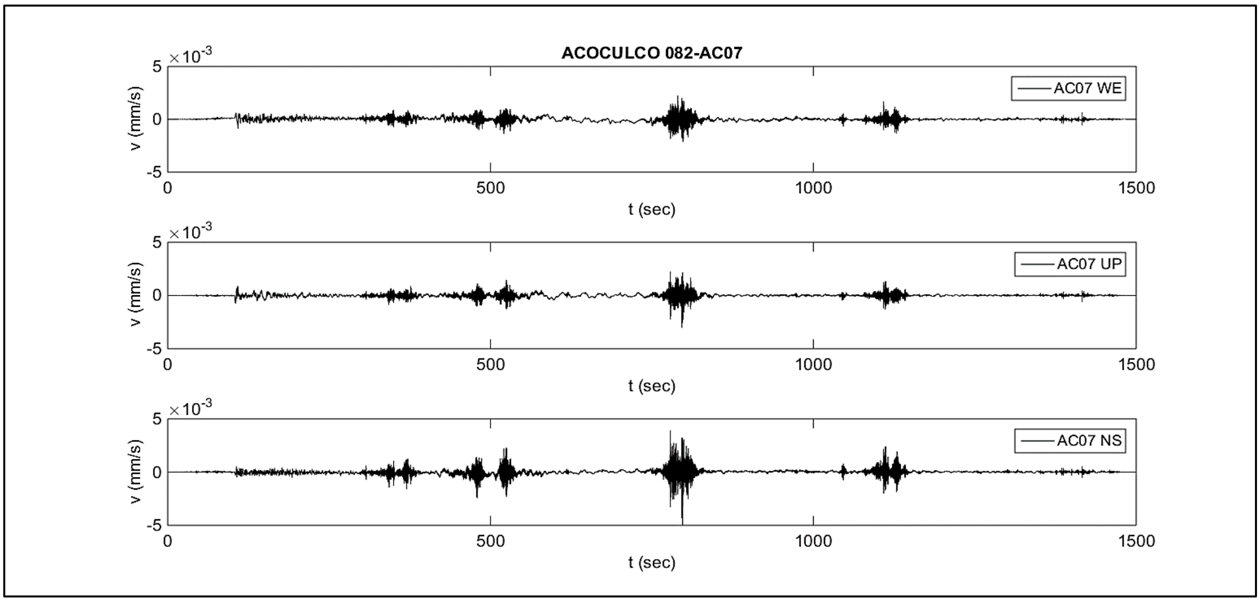
ACOCULCO 082-AC07
AC07 WE
AC07 UP
AC07 NS
v (mm/s)
t (sec)
$\times 10^{-3}$

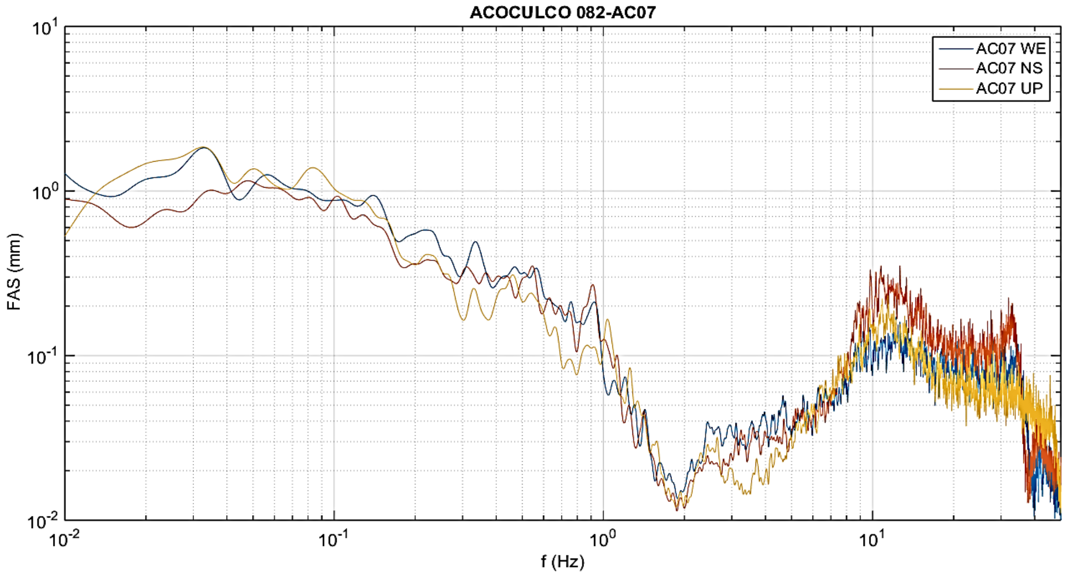
ACOCULCO 082-AC07
AC07 WE
AC07 NS
AC07 UP
FAS (mm)
f (Hz)

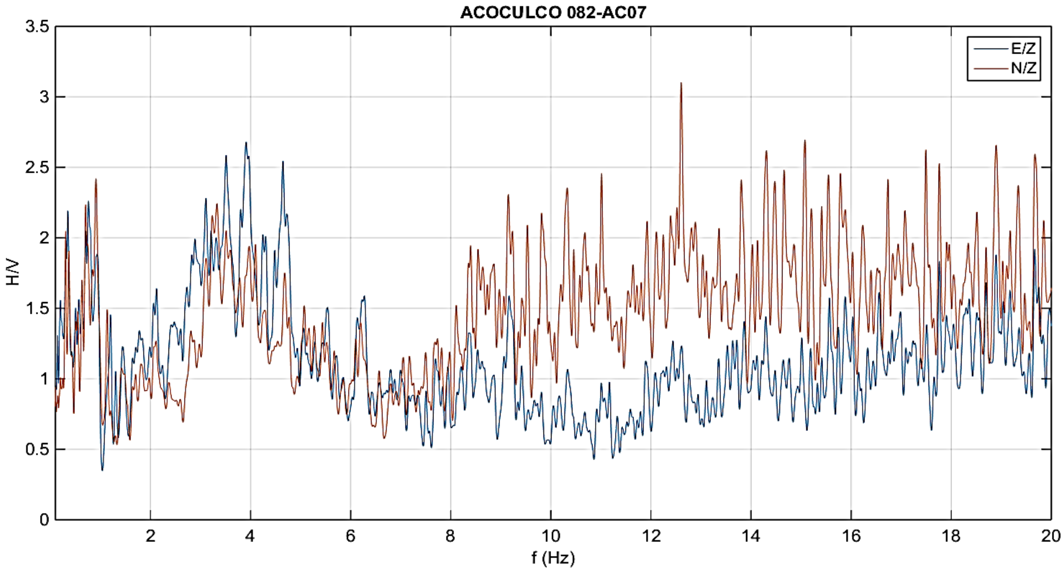
ACOCULCO 082-AC07
E/Z
N/Z
H/V
f (Hz)

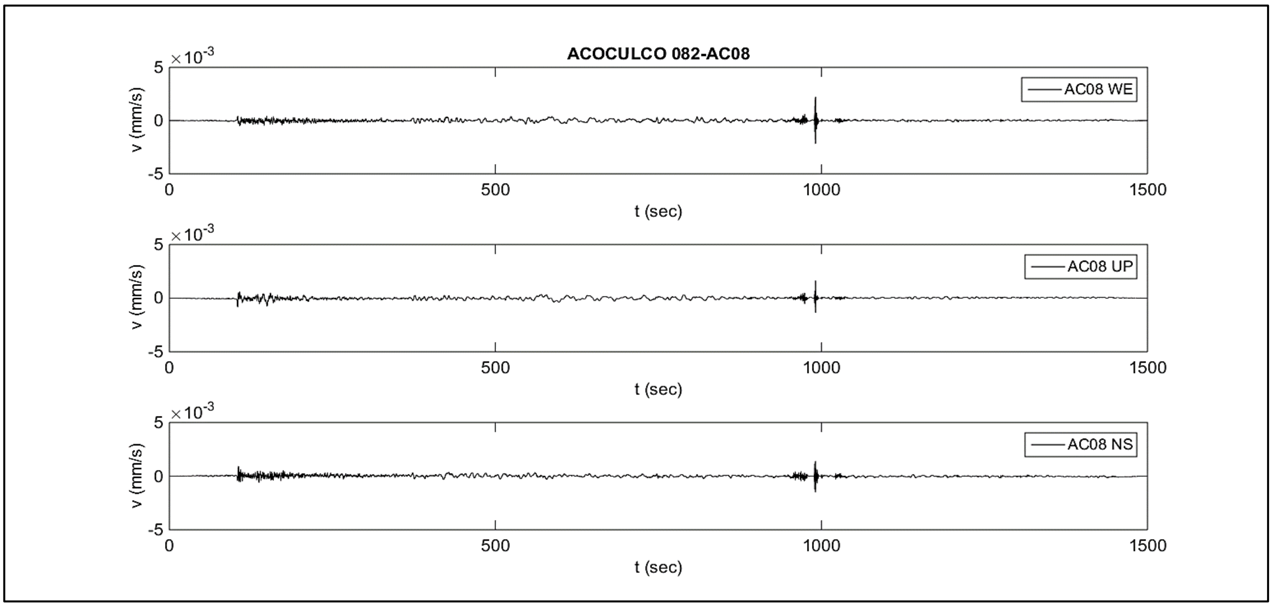
ACOCULCO 082-AC08
AC08 WE
AC08 UP
AC08 NS
v (mm/s)
t (sec)

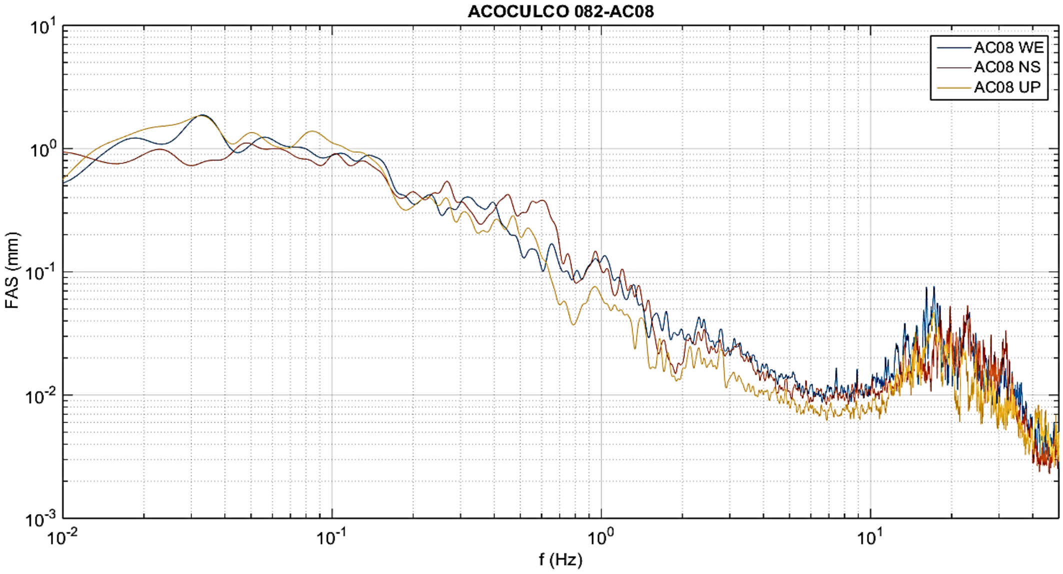
ACOCULCO 082-AC08
AC08 WE
AC08 NS
AC08 UP
FAS (mm)
f (Hz)

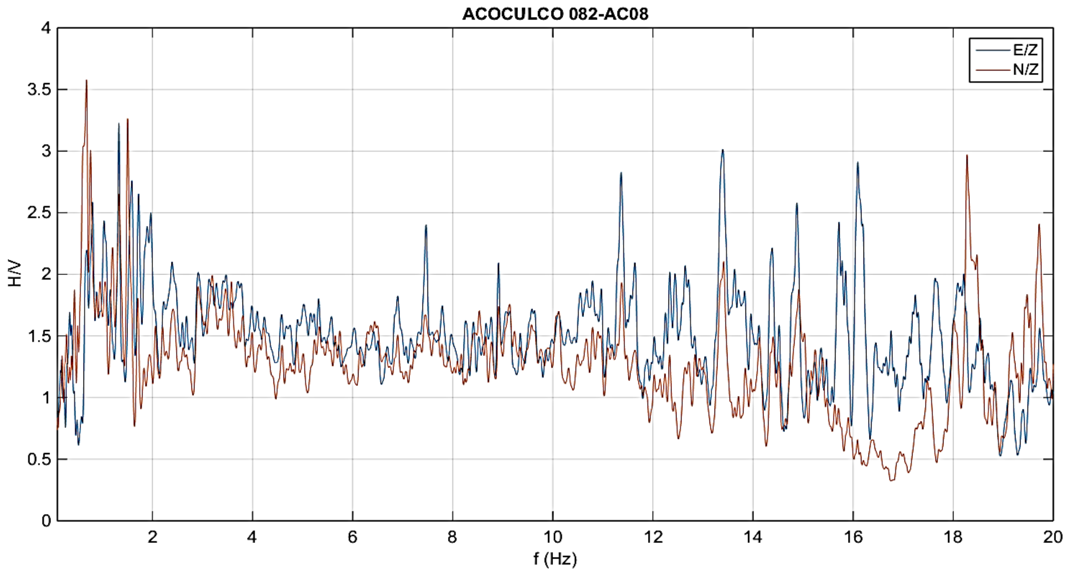
ACOCULCO 082-AC08
E/Z
N/Z
H/V
f (Hz)

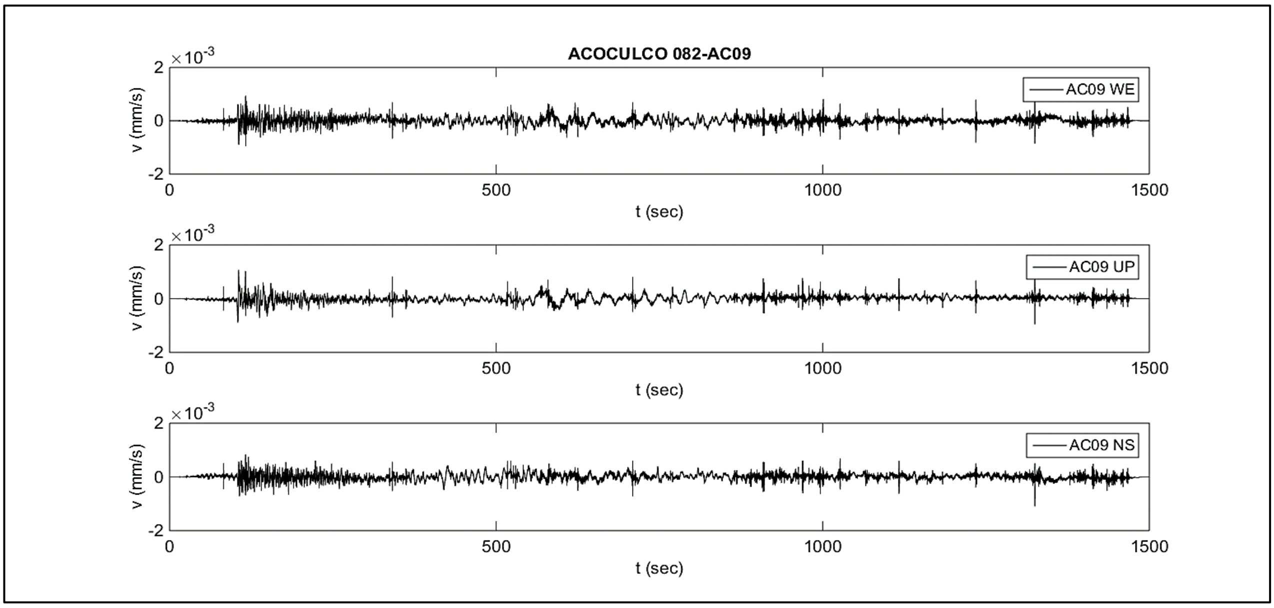
ACOCULCO 082-AC09
AC09 WE
AC09 UP
AC09 NS
v (mm/s)
t (sec)
$\times 10^{-3}$

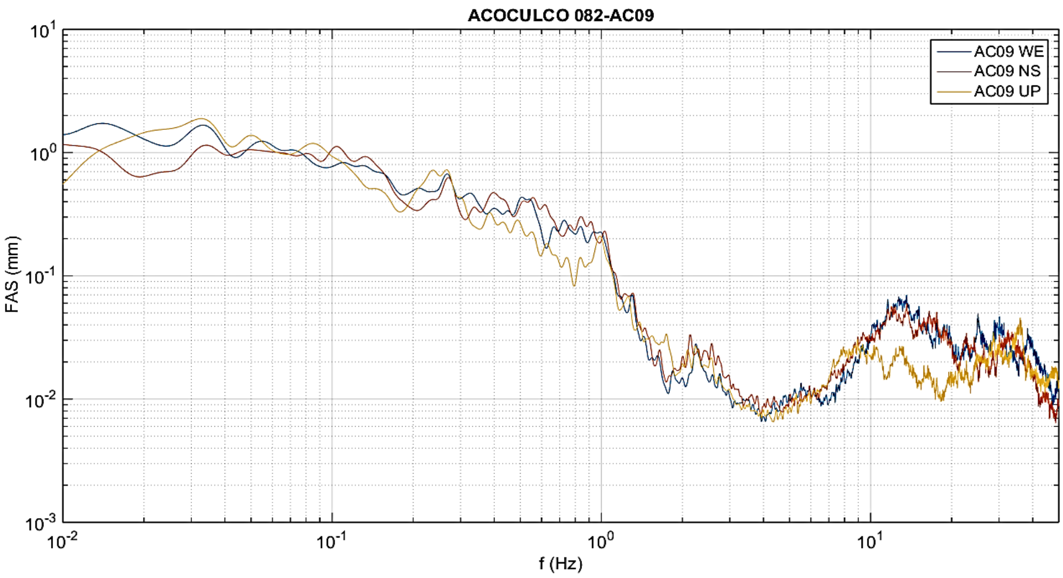
ACOCULCO 082-AC09
AC09 WE
AC09 NS
AC09 UP
FAS (mm)
f (Hz)

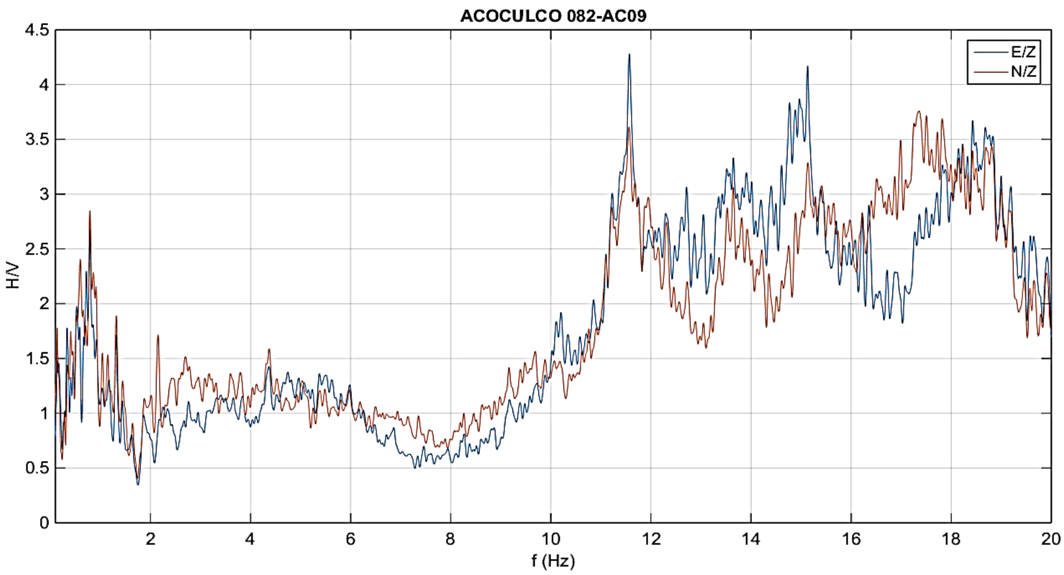
ACOCULCO 082-AC09
E/Z
N/Z
H/V
f (Hz)

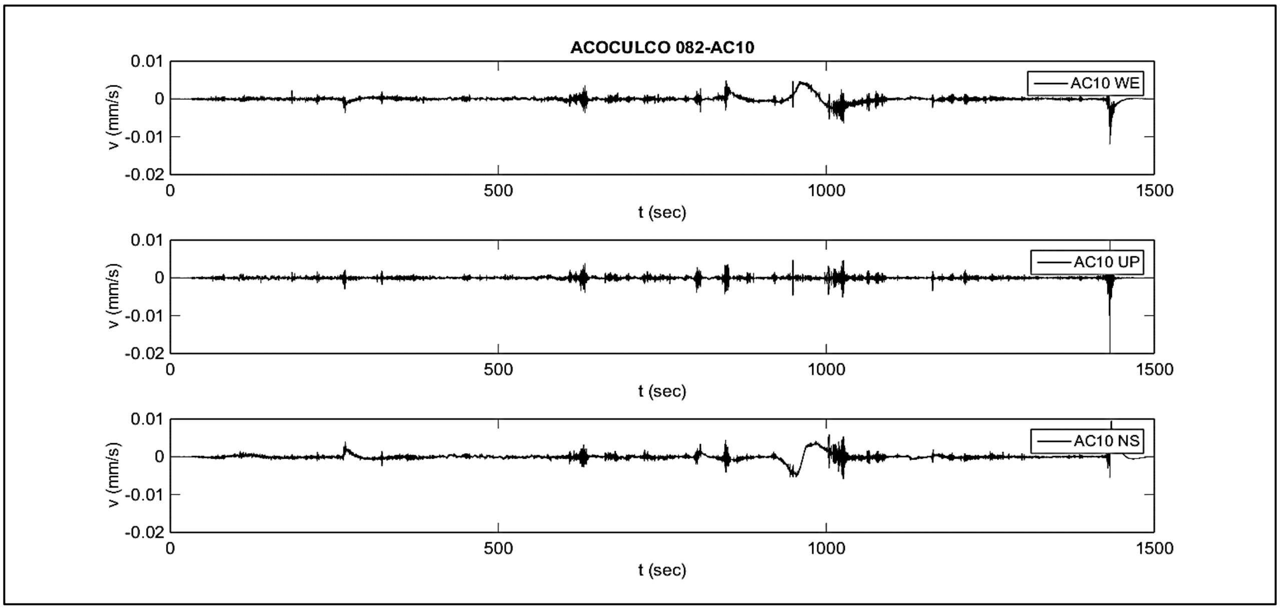
ACOCULCO 082-AC10
AC10 WE
AC10 UP
AC10 NS
v (mm/s)
t (sec)

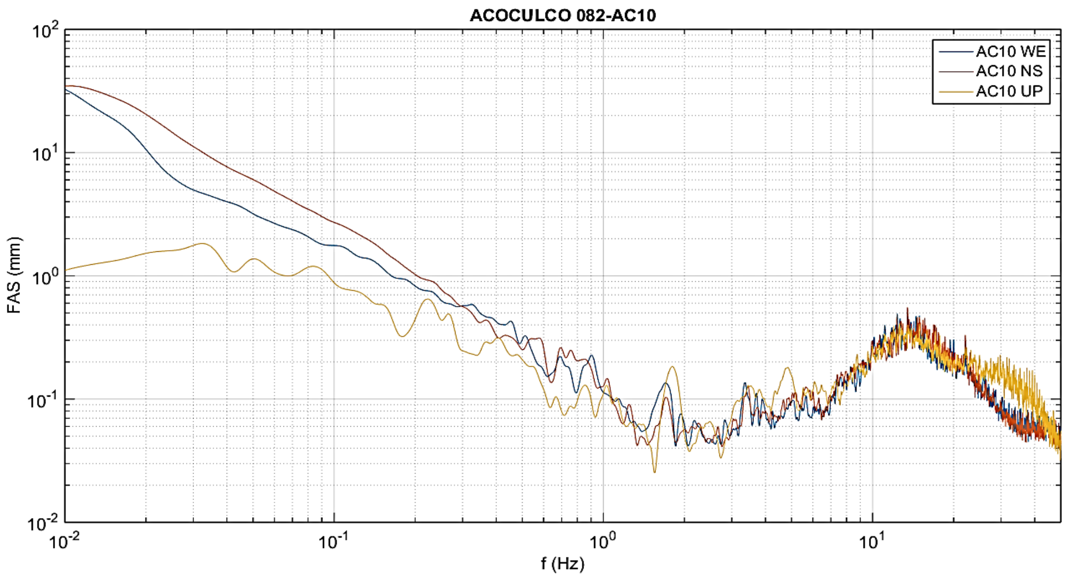
ACOCULCO 082-AC10
AC10 WE
AC10 NS
AC10 UP
FAS (mm)
f (Hz)

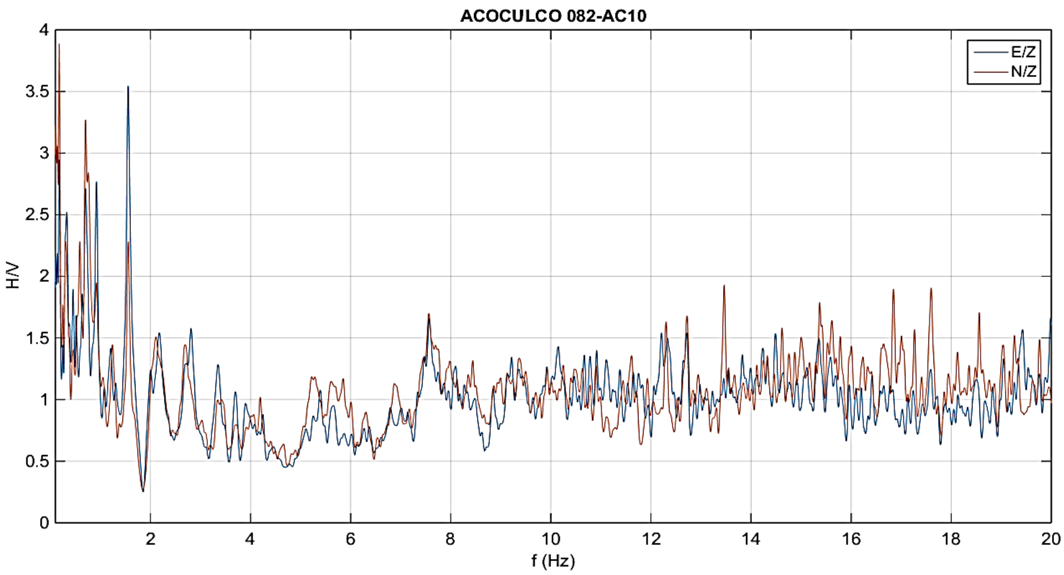
ACOCULCO 082-AC10
E/Z
N/Z
H/V
f (Hz)

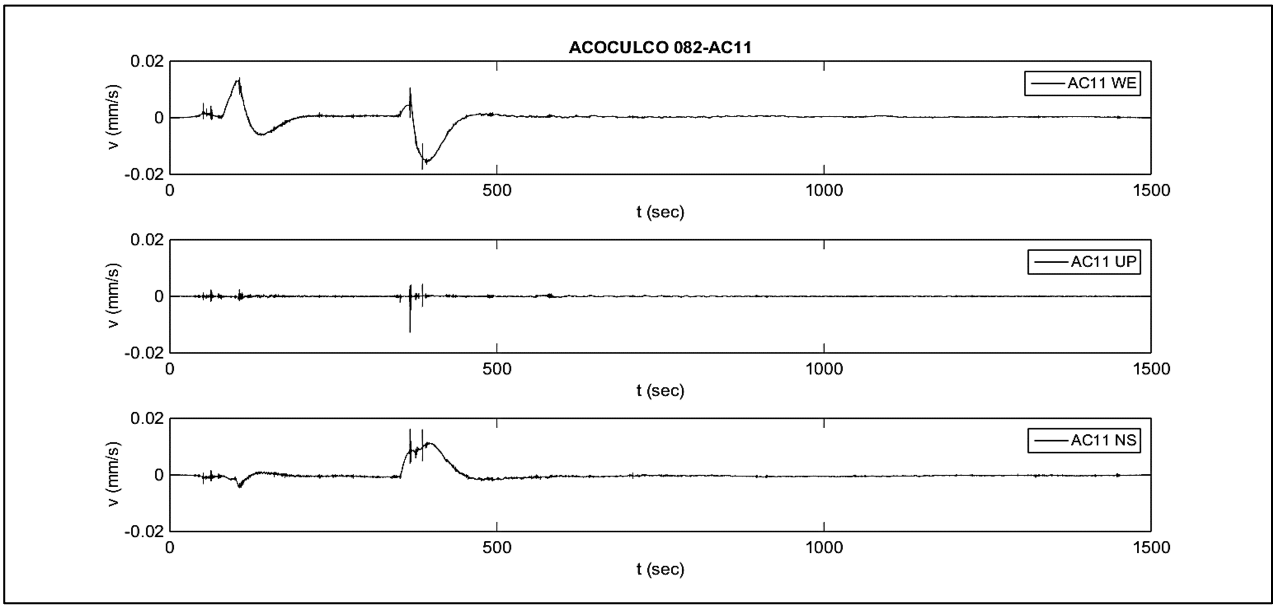
ACOCULCO 082-AC11
AC11 WE
AC11 UP
AC11 NS
v (mm/s)
0.02
0
-0.02
0
500
1000
1500
t (sec)

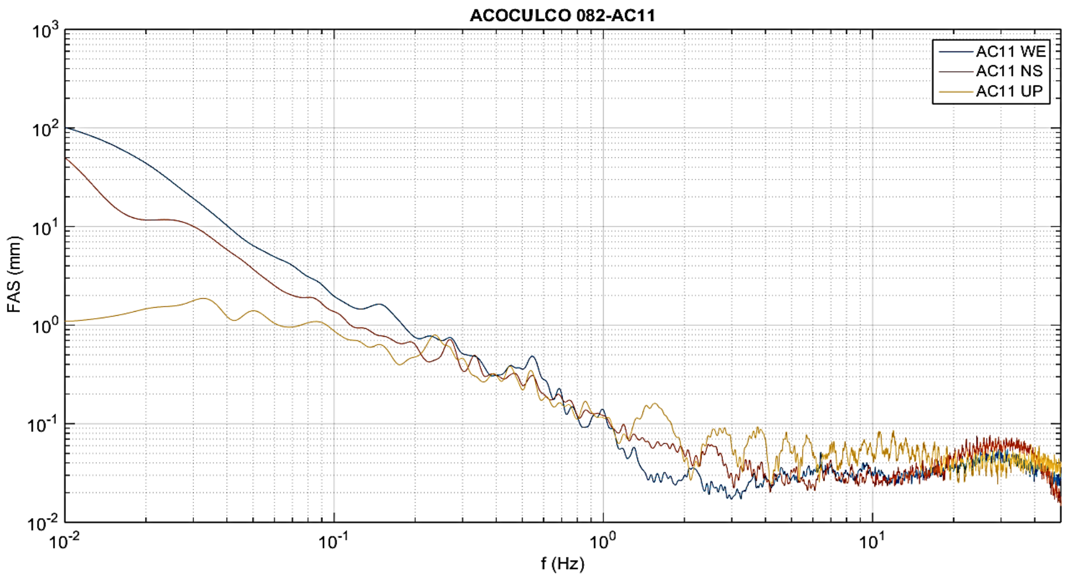
ACOCULCO 082-AC11
AC11 WE
AC11 NS
AC11 UP
FAS (mm)
f (Hz)

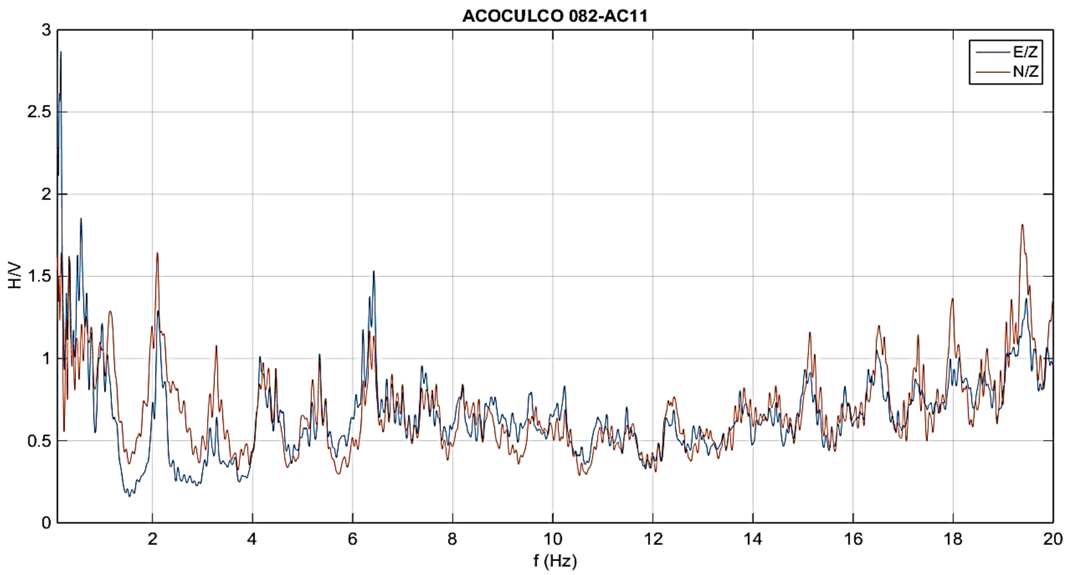
ACOCULCO 082-AC11
E/Z
N/Z
H/V
f (Hz)

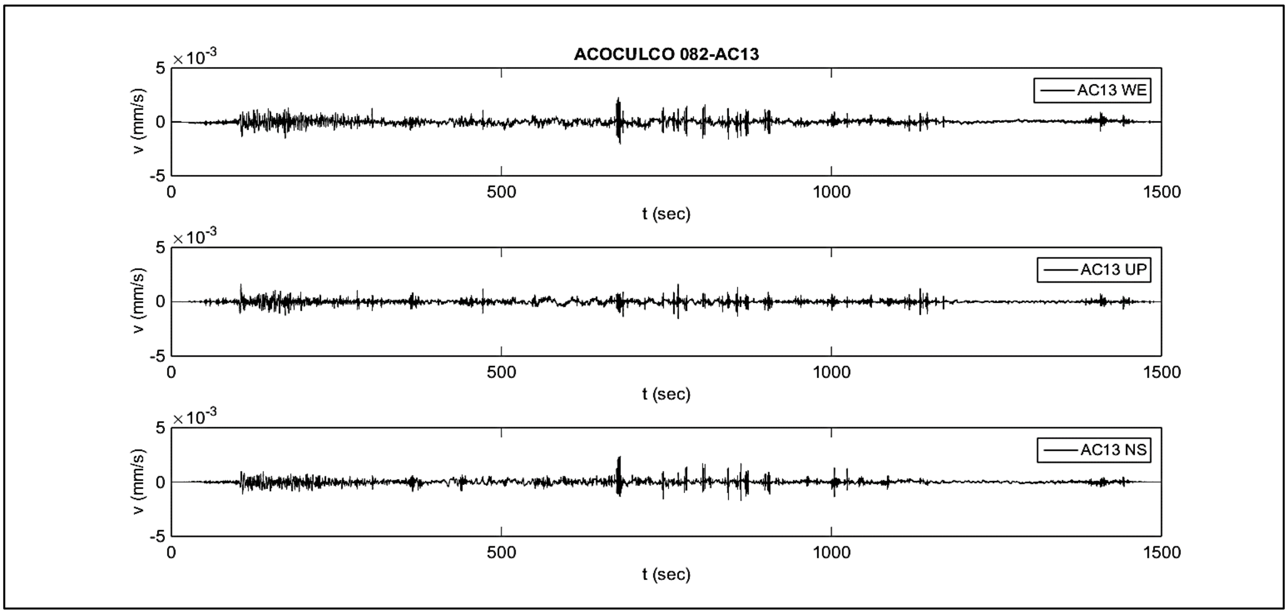
ACOCULCO 082-AC13
AC13 WE
AC13 UP
AC13 NS
v (mm/s)
t (sec)

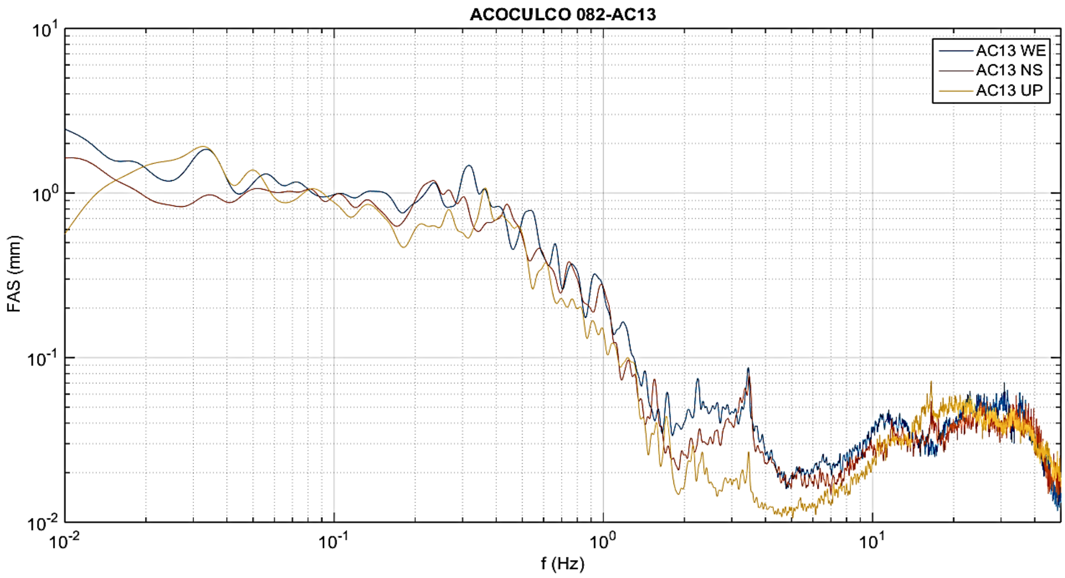
ACOCULCO 082-AC13
AC13 WE
AC13 NS
AC13 UP
FAS (mm)
f (Hz)

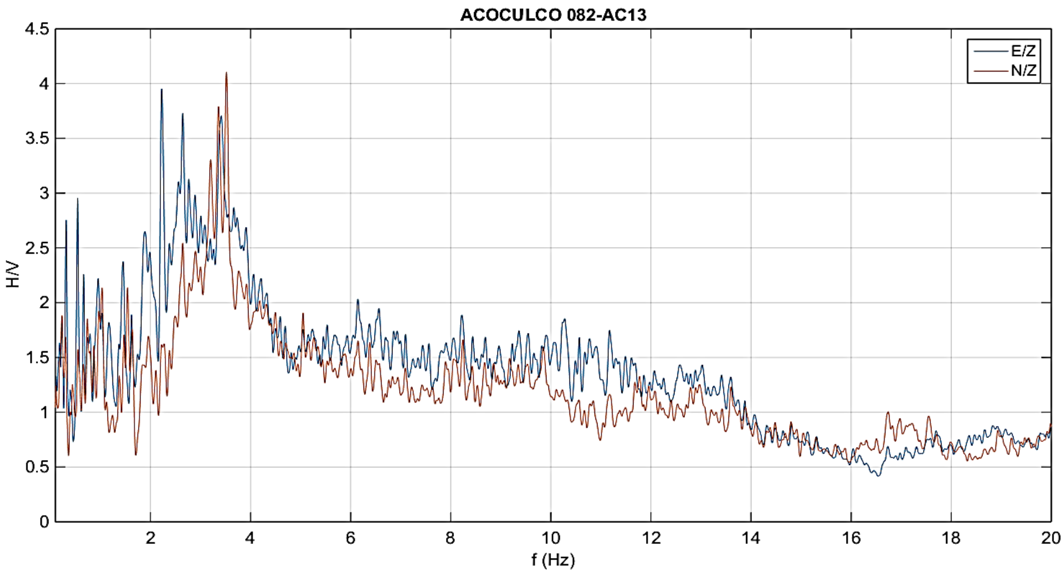
ACOCULCO 082-AC13
E/Z
N/Z
H/V
f (Hz)

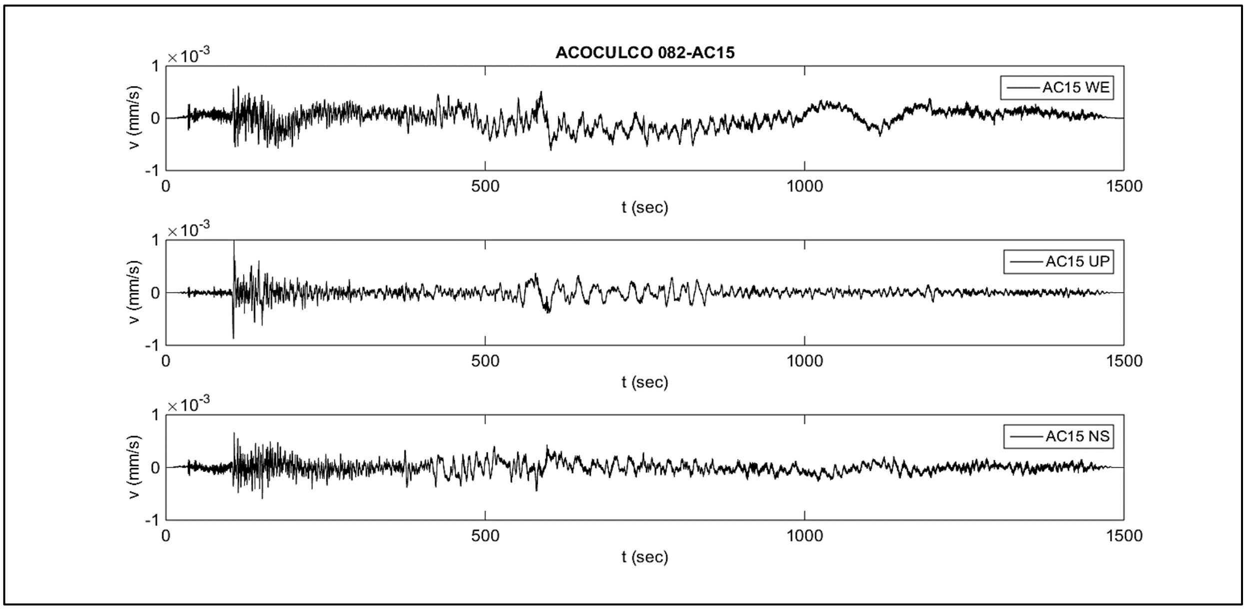
ACOCULCO 082-AC15
AC15 WE
AC15 UP
AC15 NS
v (mm/s)
t (sec)

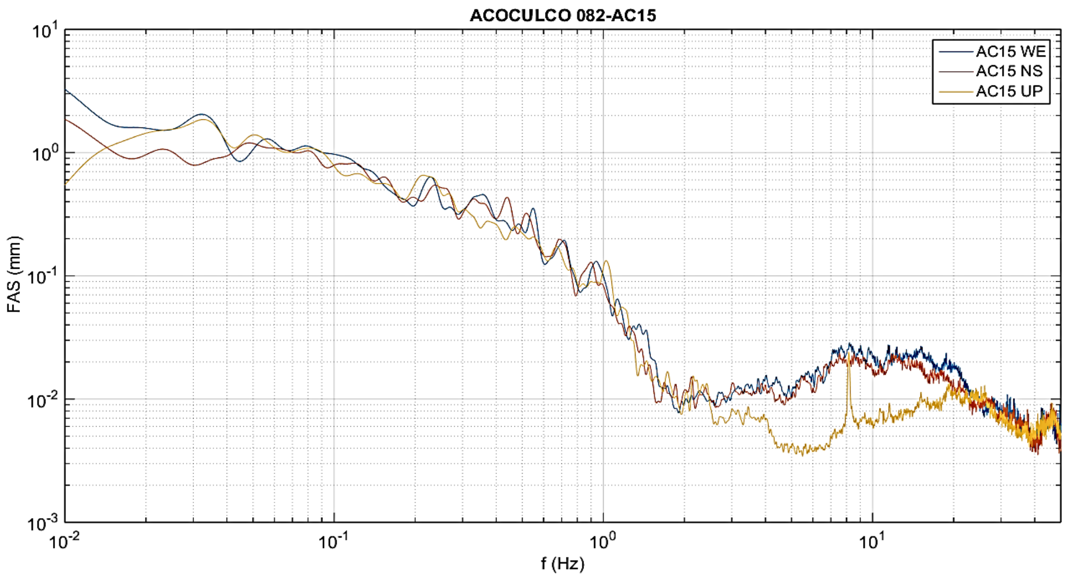
ACOCULCO 082-AC15
AC15 WE
AC15 NS
AC15 UP
FAS (mm)
f (Hz)

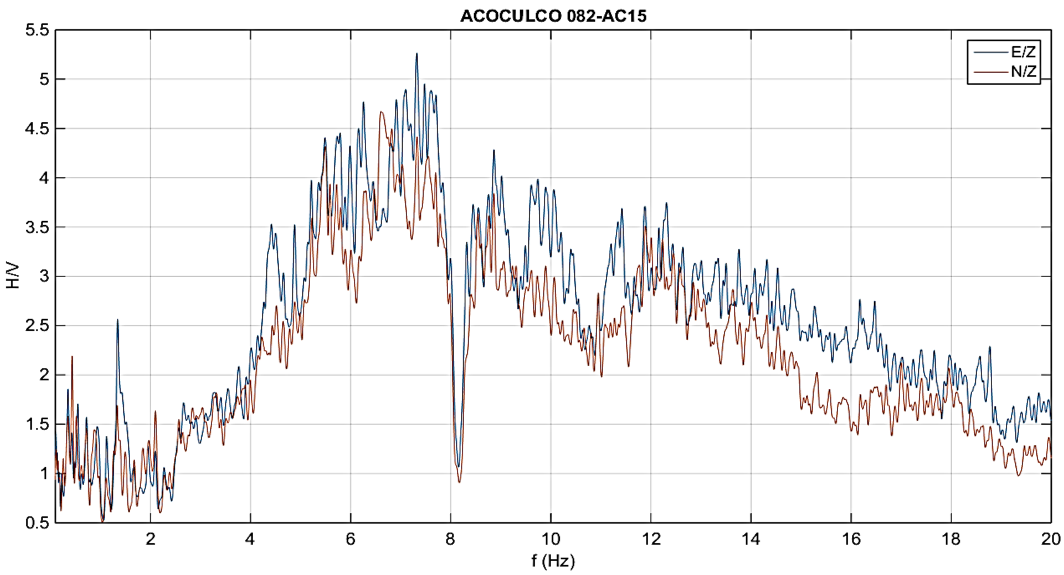
ACOCULCO 082-AC15
E/Z
N/Z
H/V
f (Hz)

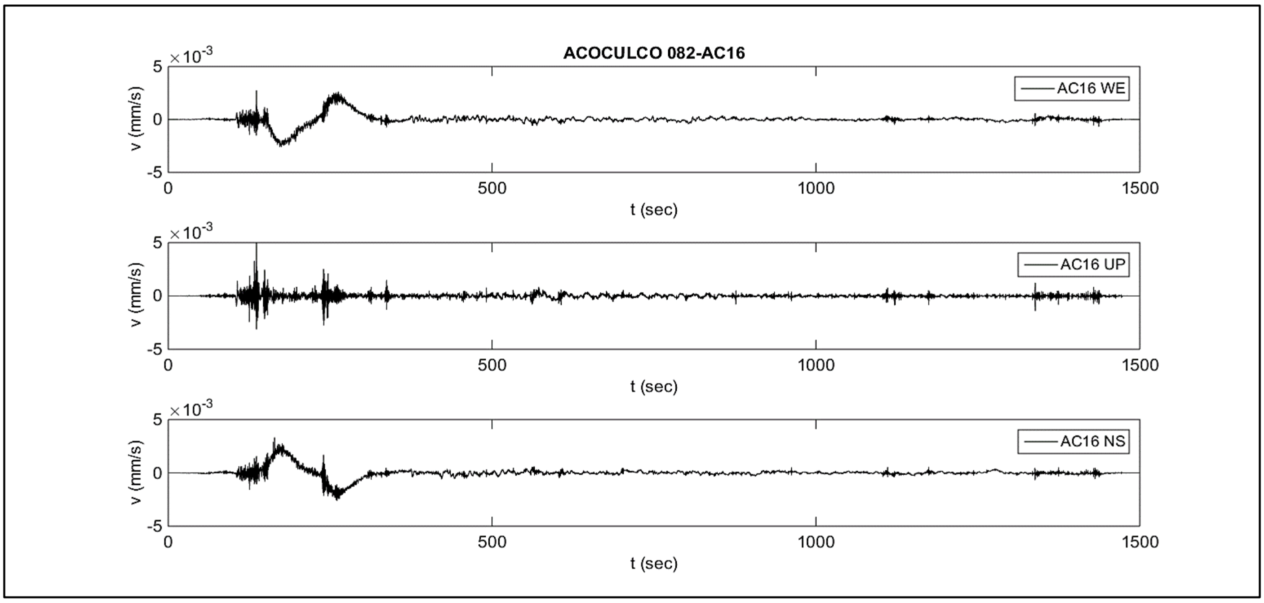
ACOCULCO 082-AC16
AC16 WE
AC16 UP
AC16 NS
v (mm/s)
t (sec)

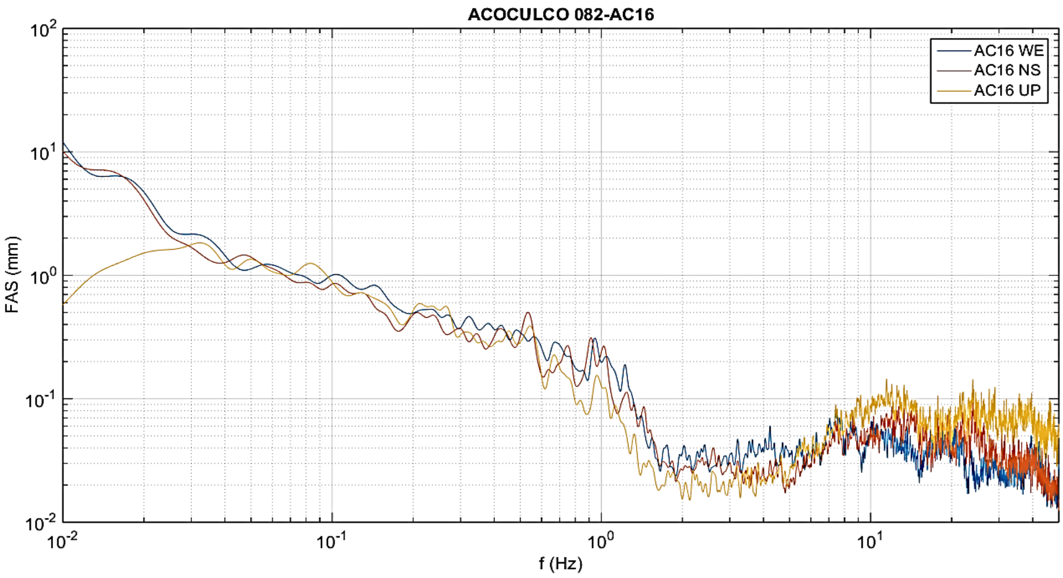
ACOCULCO 082-AC16
AC16 WE
AC16 NS
AC16 UP
FAS (mm)
f (Hz)

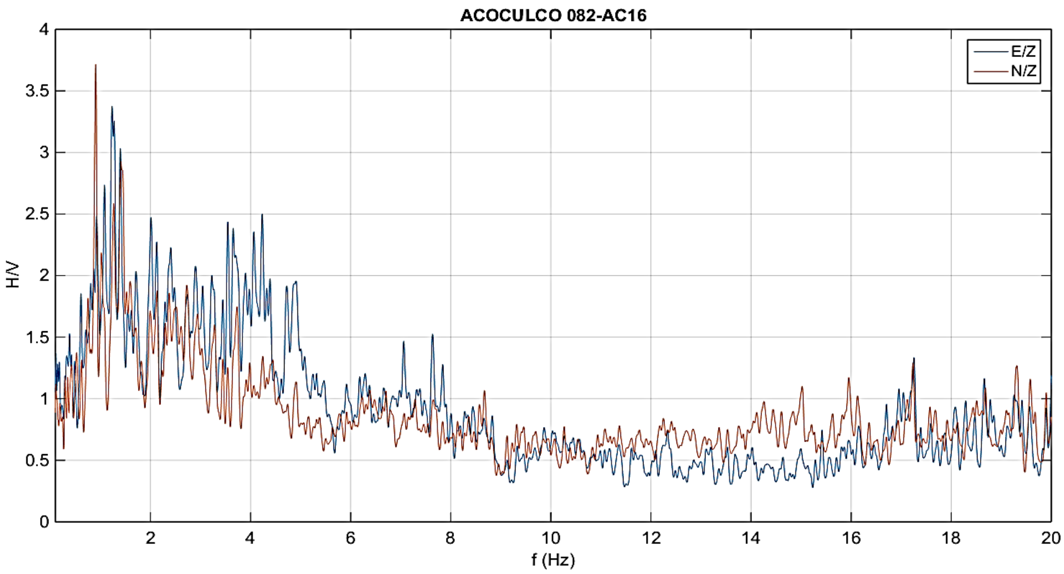
ACOCULCO 082-AC16
E/Z
N/Z
H/V
f (Hz)

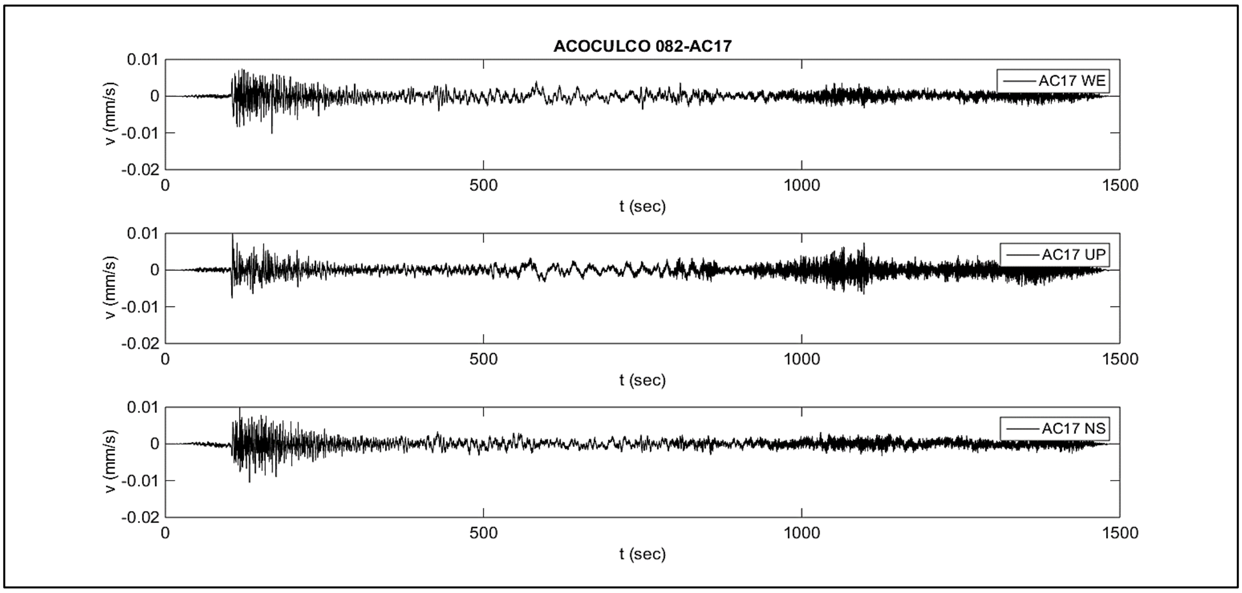
ACOCULCO 082-AC17
AC17 WE
AC17 UP
AC17 NS
v (mm/s)
t (sec)

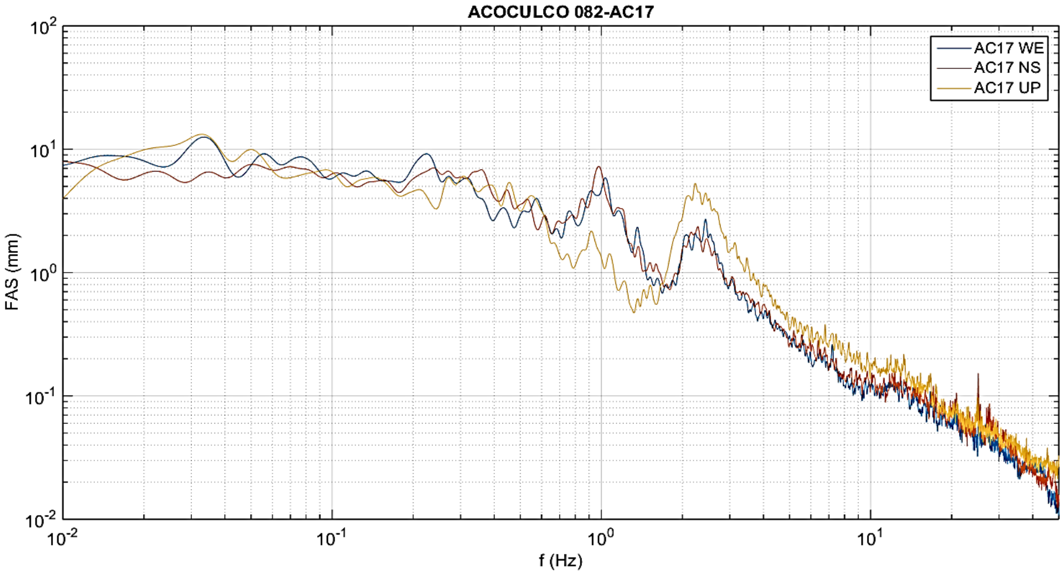
ACOCULCO 082-AC17
AC17 WE
AC17 NS
AC17 UP
FAS (mm)
f (Hz)

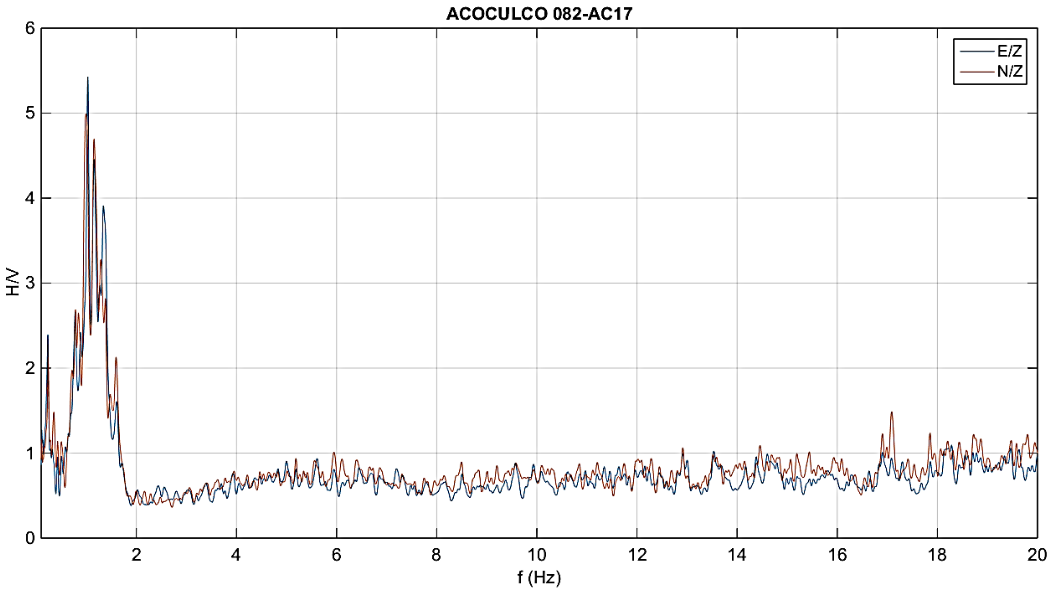
ACOCULCO 082-AC17
E/Z
N/Z
H/V
f (Hz)

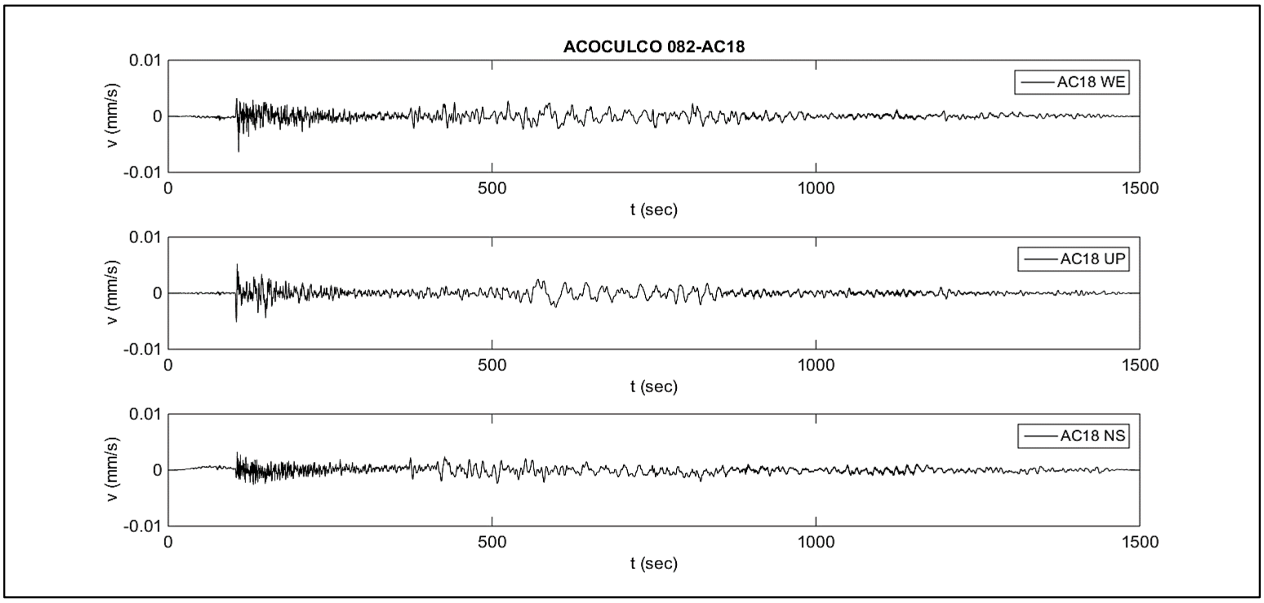
ACOCULCO 082-AC18
AC18 WE
AC18 UP
AC18 NS
v (mm/s)
t (sec)
0.01
0
-0.01
0
500
1000
1500

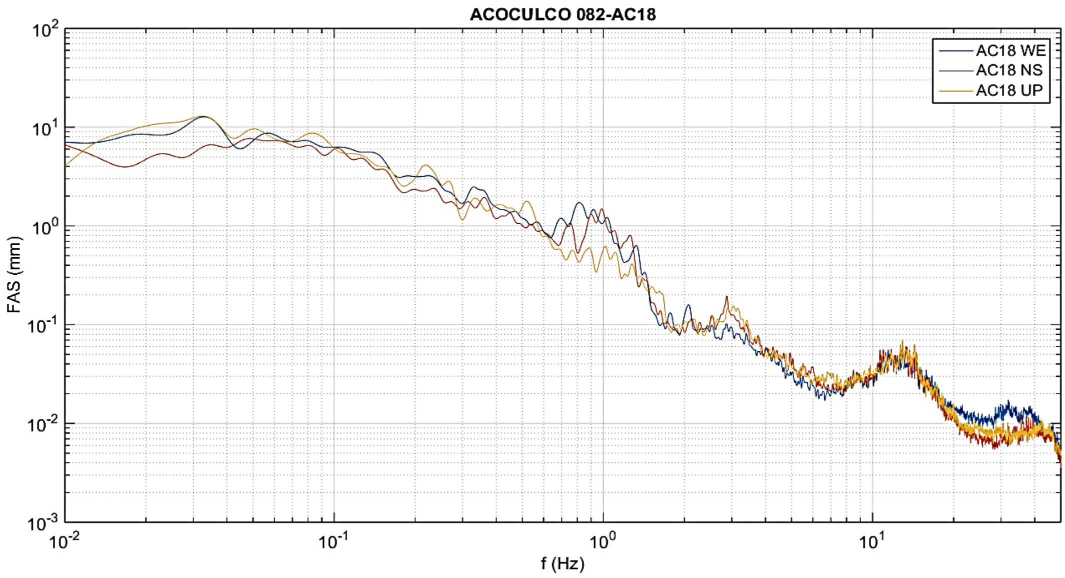
ACOCULCO 082-AC18
AC18 WE
AC18 NS
AC18 UP
FAS (mm)
f (Hz)

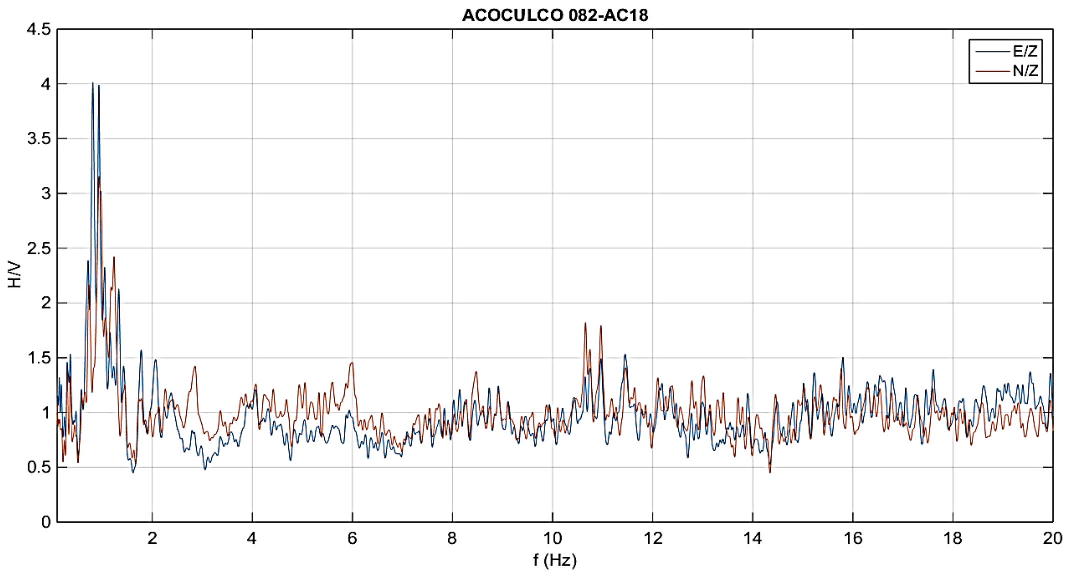
ACOCULCO 082-AC18
E/Z
N/Z
H/V
f (Hz)

Appendix 4-E Day 083, Earthquake. Time histories, spectra and spectral ratios

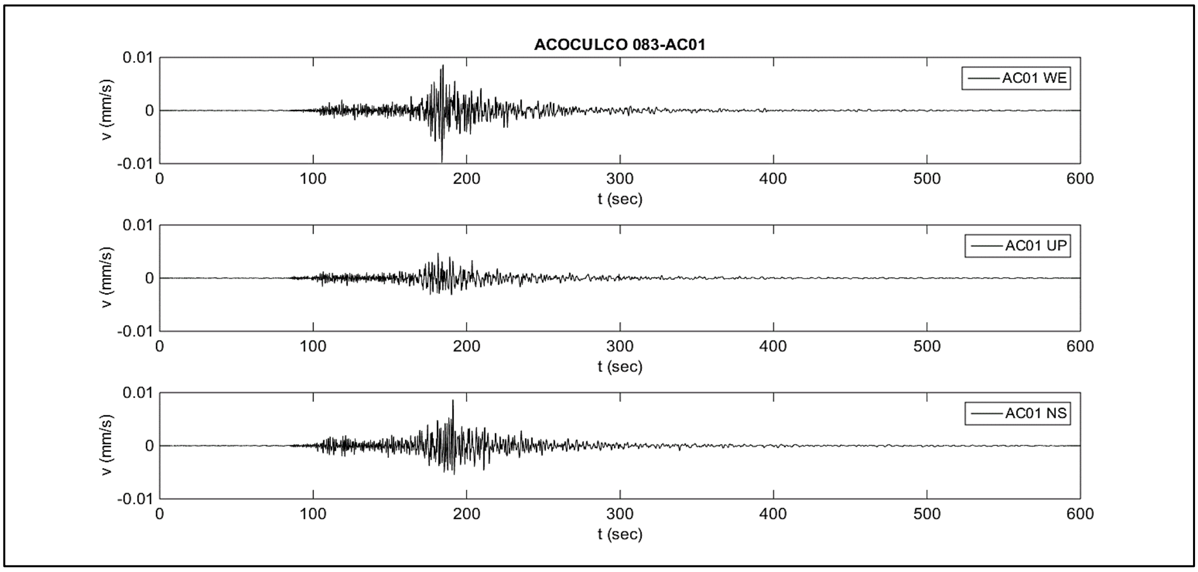

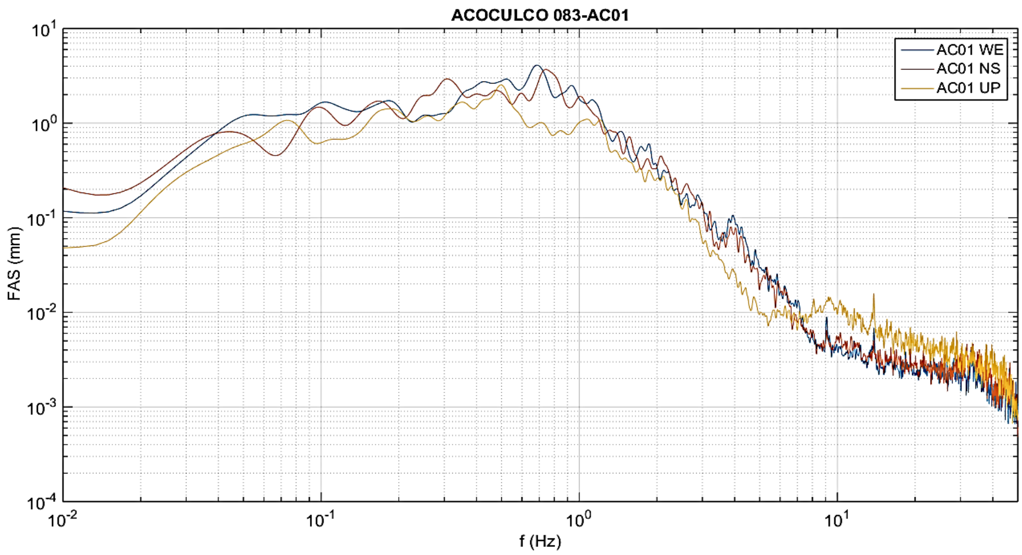

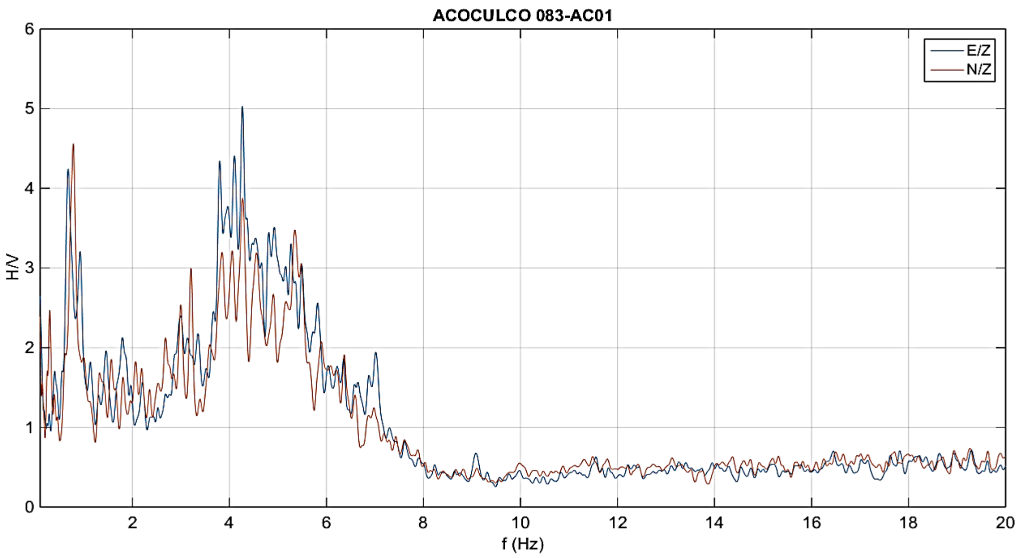

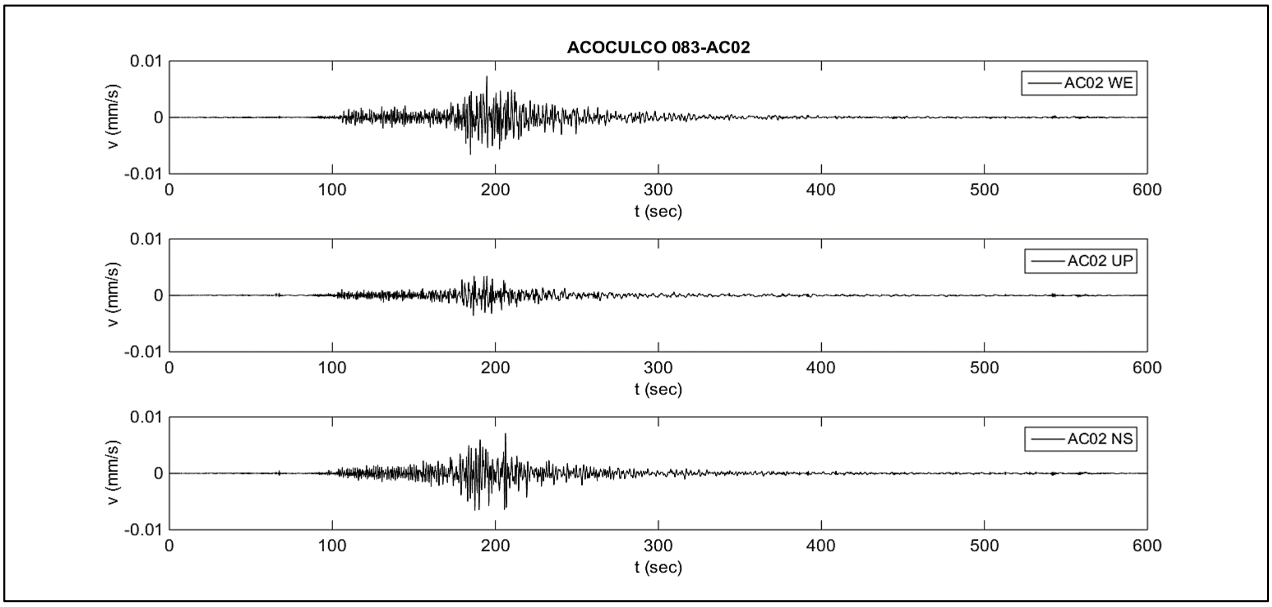
ACOCULCO 083-AC02
AC02 WE
AC02 UP
AC02 NS
v (mm/s)
t (sec)

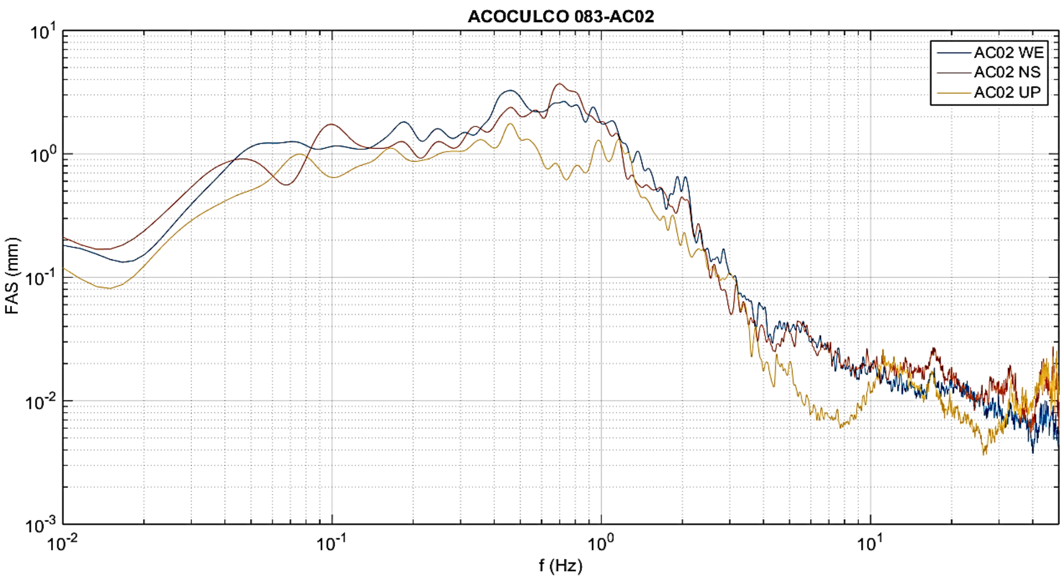
ACOCULCO 083-AC02
AC02 WE
AC02 NS
AC02 UP
FAS (mm)
f (Hz)

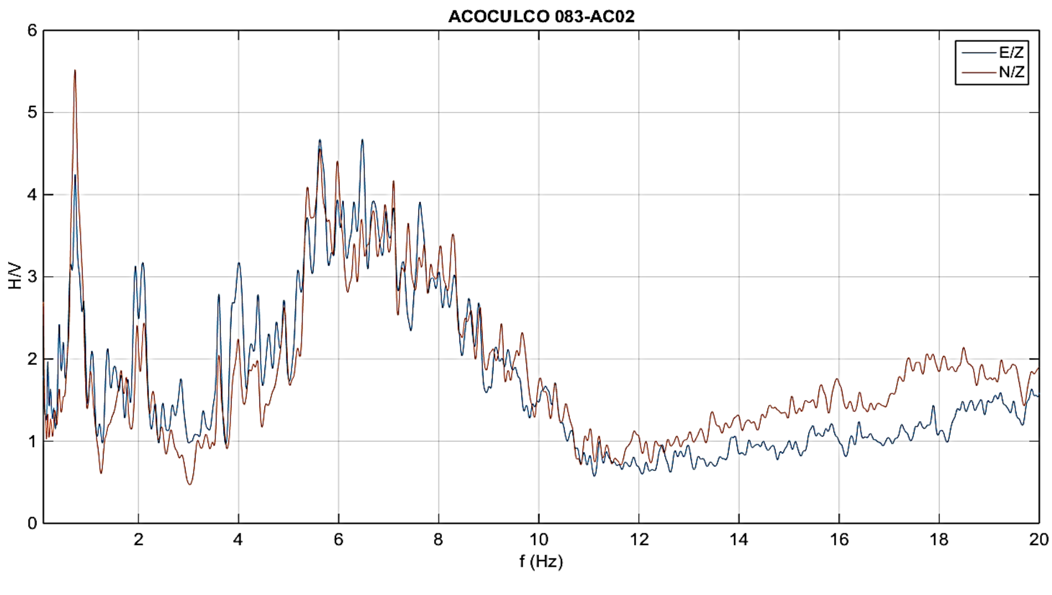
ACOCULCO 083-AC02
E/Z
N/Z
H/V
f (Hz)

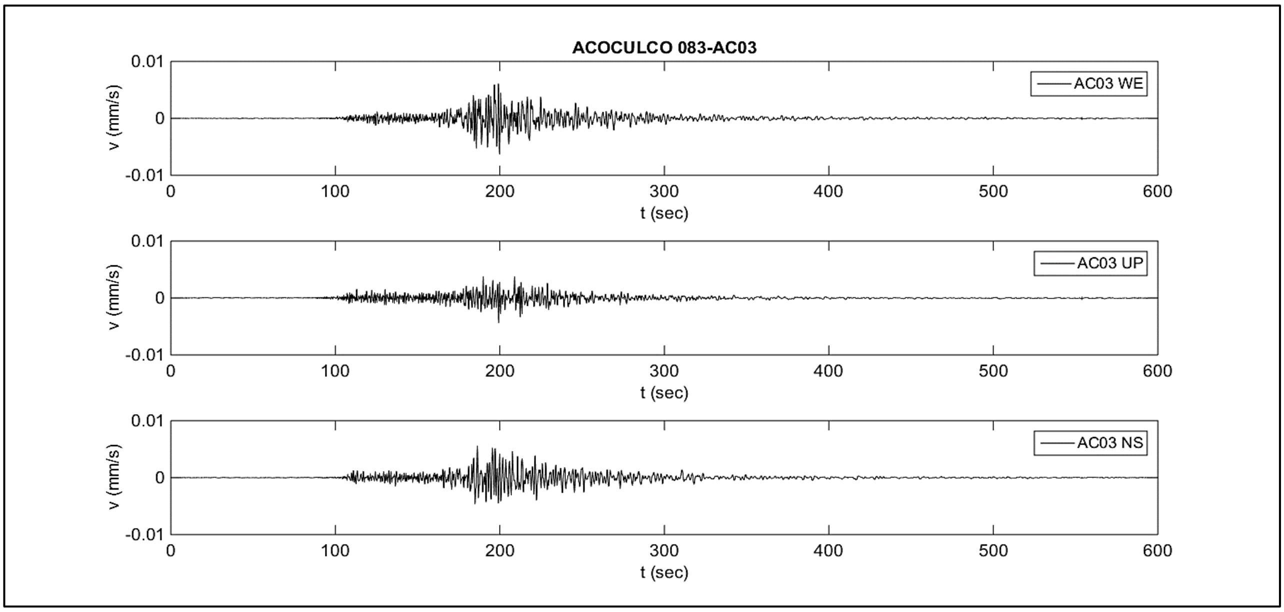
ACOCULCO 083-AC03
AC03 WE
AC03 UP
AC03 NS
v (mm/s)
t (sec)

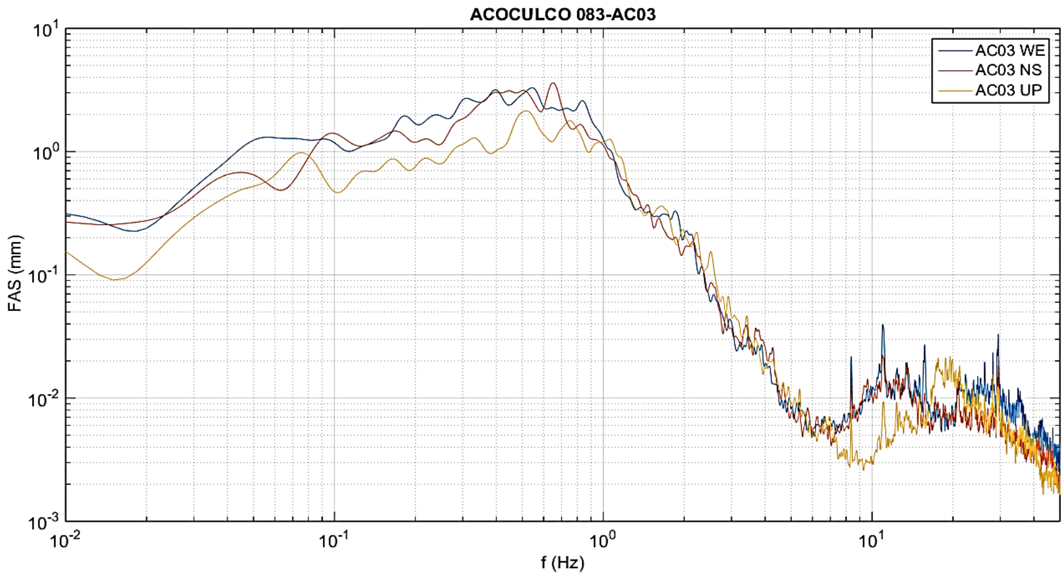
ACOCULCO 083-AC03
AC03 WE
AC03 NS
AC03 UP
FAS (mm)
f (Hz)

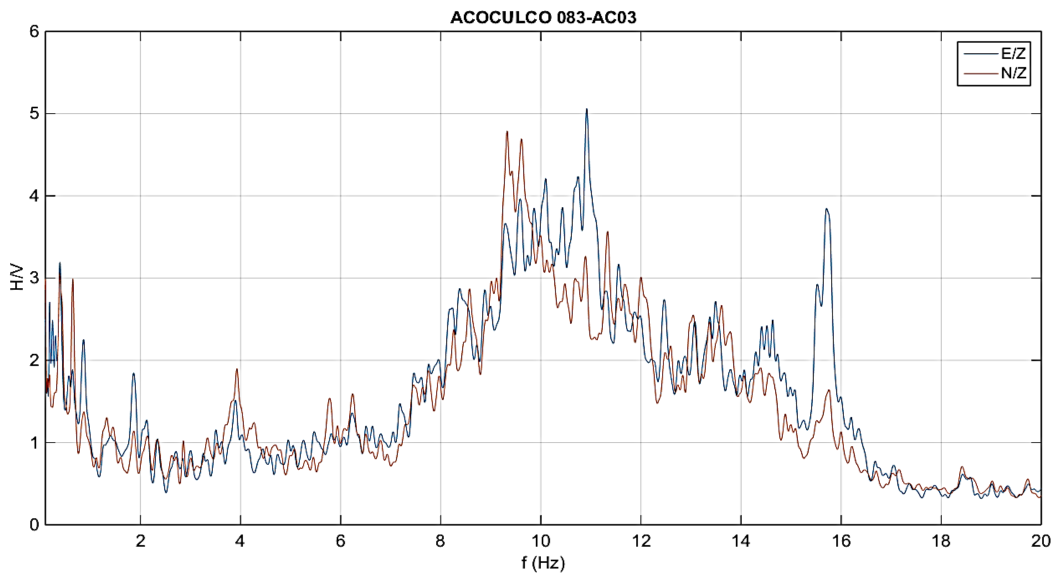
ACOCULCO 083-AC03
E/Z
N/Z
H/V
f (Hz)

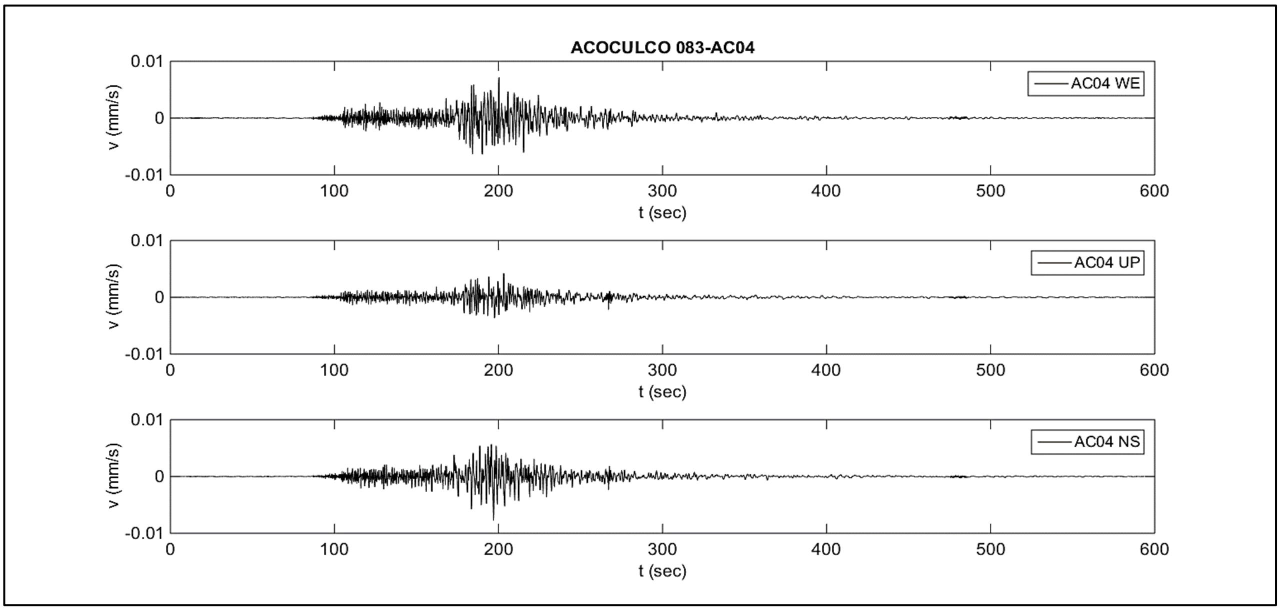
ACOCULCO 083-AC04
AC04 WE
AC04 UP
AC04 NS
v (mm/s)
0.01
0
-0.01
0
100
200
300
400
500
600
t (sec)

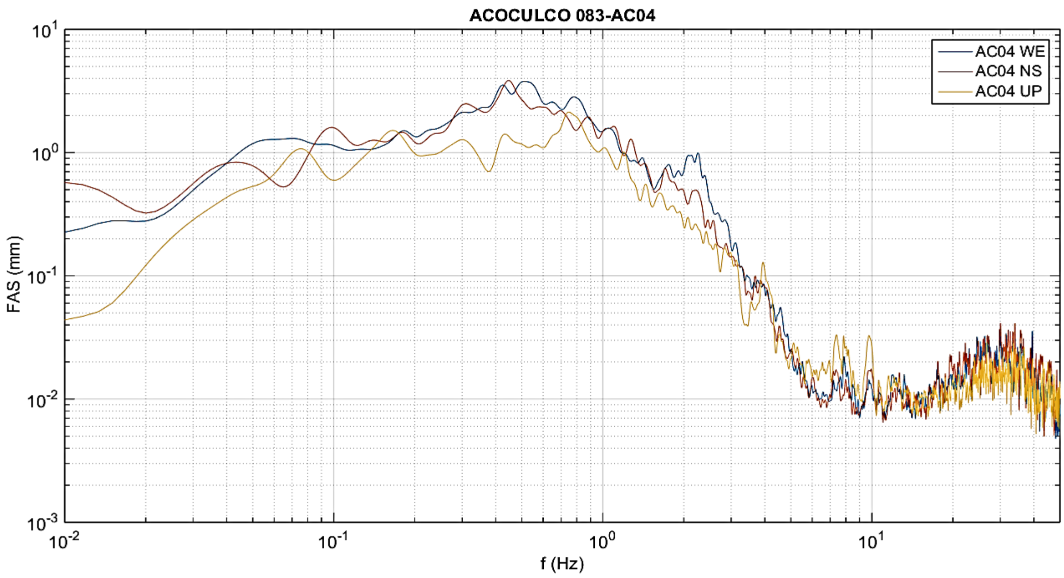
ACOCULCO 083-AC04
AC04 WE
AC04 NS
AC04 UP
FAS (mm)
10^1
10^0
10^{-1}
10^{-2}
10^{-3}
f (Hz)

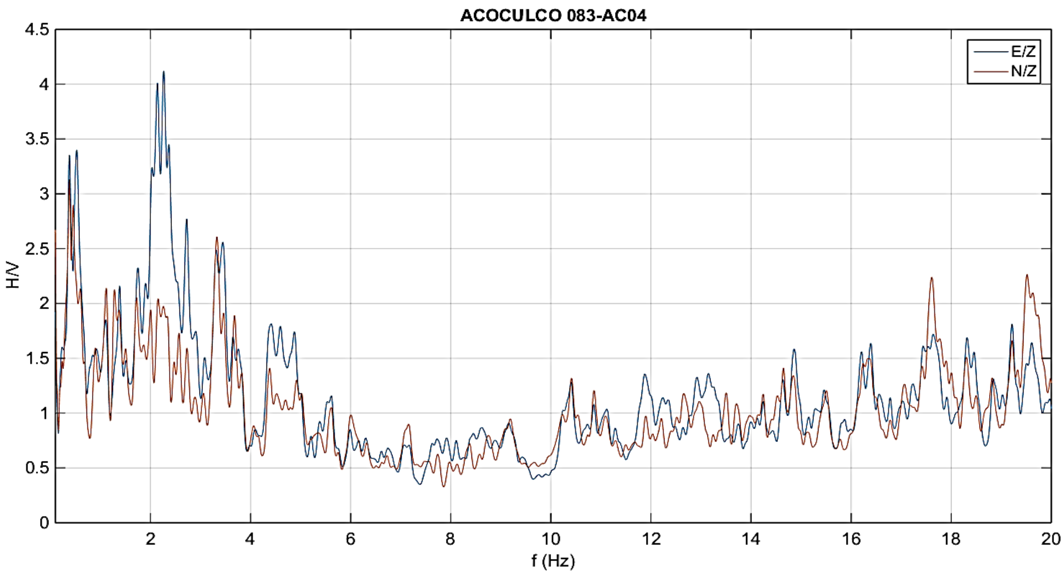
ACOCULCO 083-AC04
E/Z
N/Z
H/V
4.5
4
3.5
3
2.5
2
1.5
1
0.5
0
2
4
6
8
10
12
14
16
18
20
f (Hz)

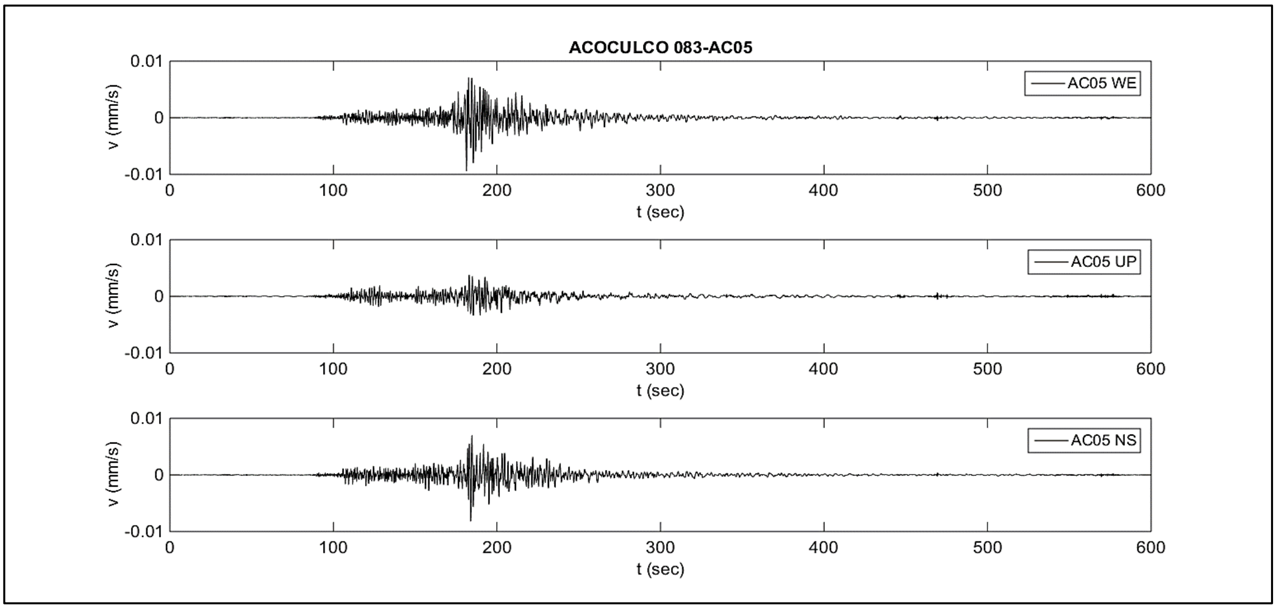
ACOCULCO 083-AC05
AC05 WE
AC05 UP
AC05 NS
v (mm/s)
t (sec)

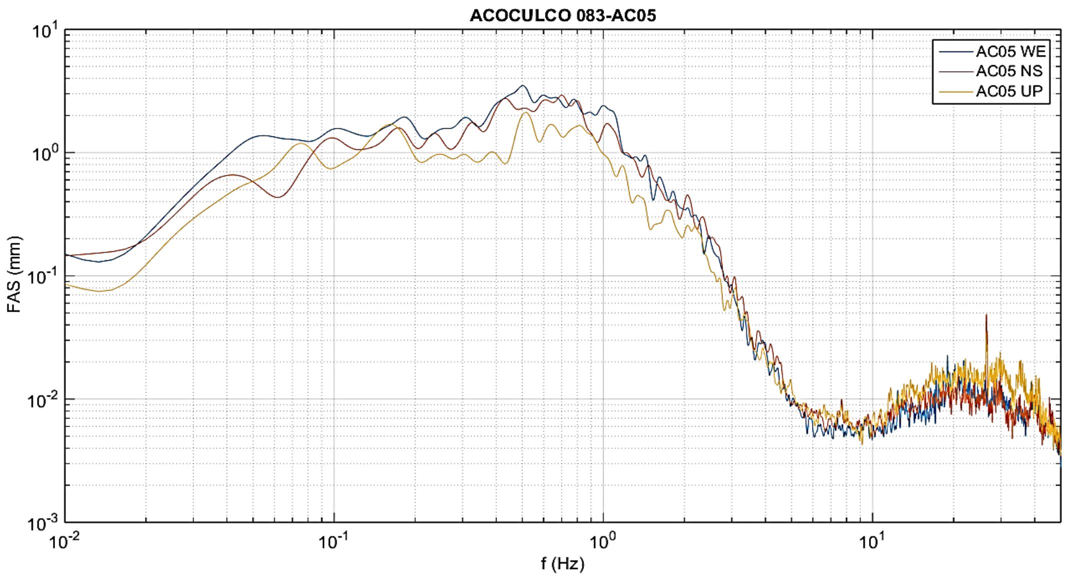
ACOCULCO 083-AC05
AC05 WE
AC05 NS
AC05 UP
FAS (mm)
f (Hz)

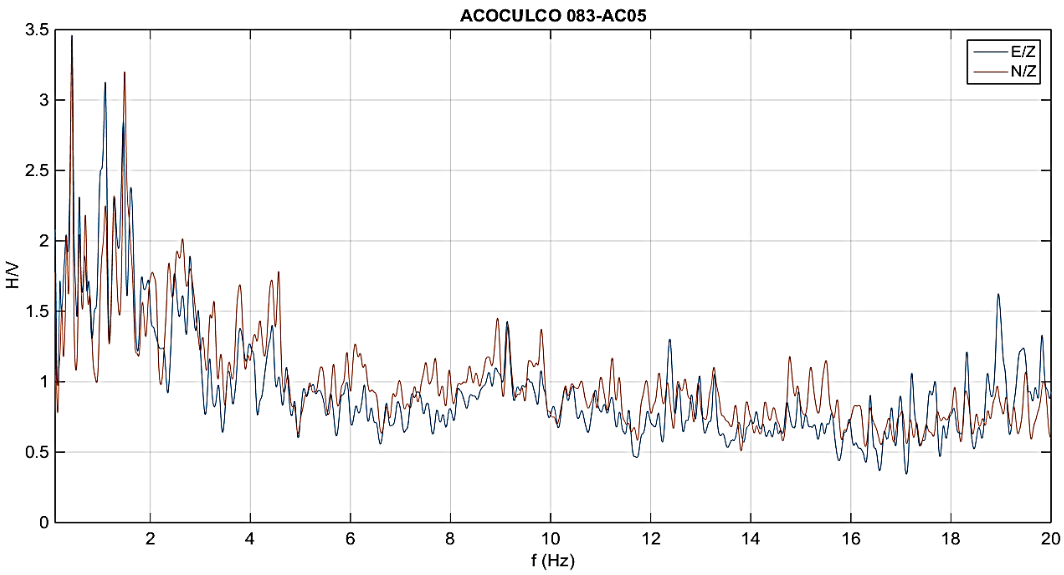
ACOCULCO 083-AC05
E/Z
N/Z
H/V
f (Hz)

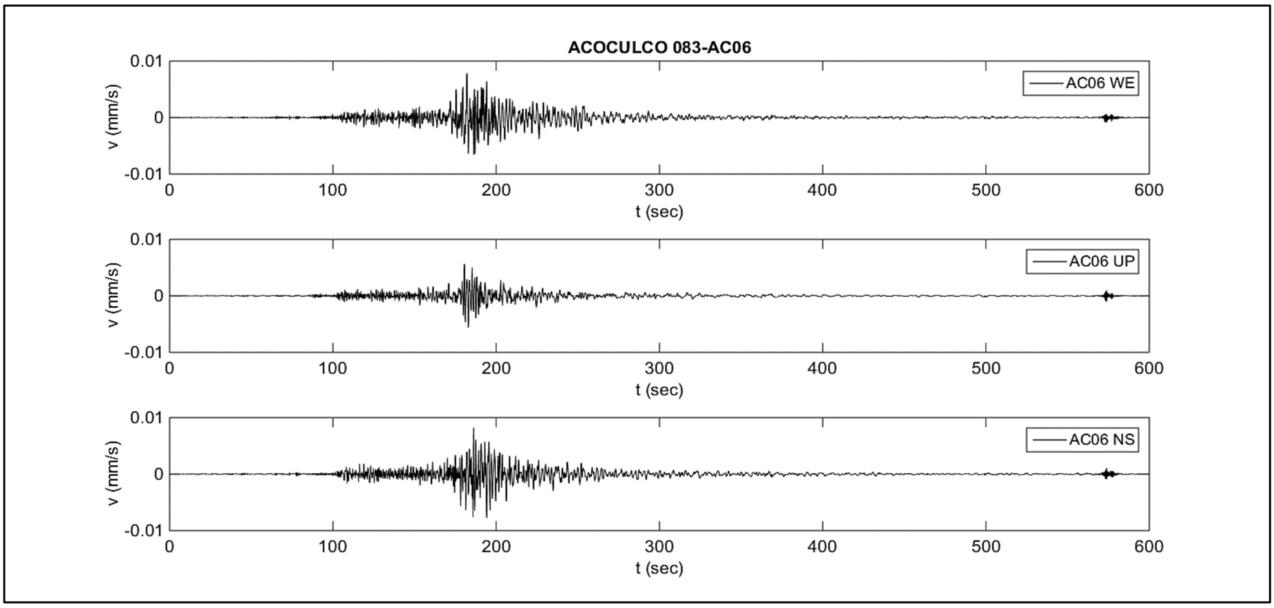

ACOCULCO 083-AC06
AC06 WE
AC06 UP
AC06 NS
v (mm/s)
t (sec)
0.01
0
-0.01
0
100
200
300
400
500
600

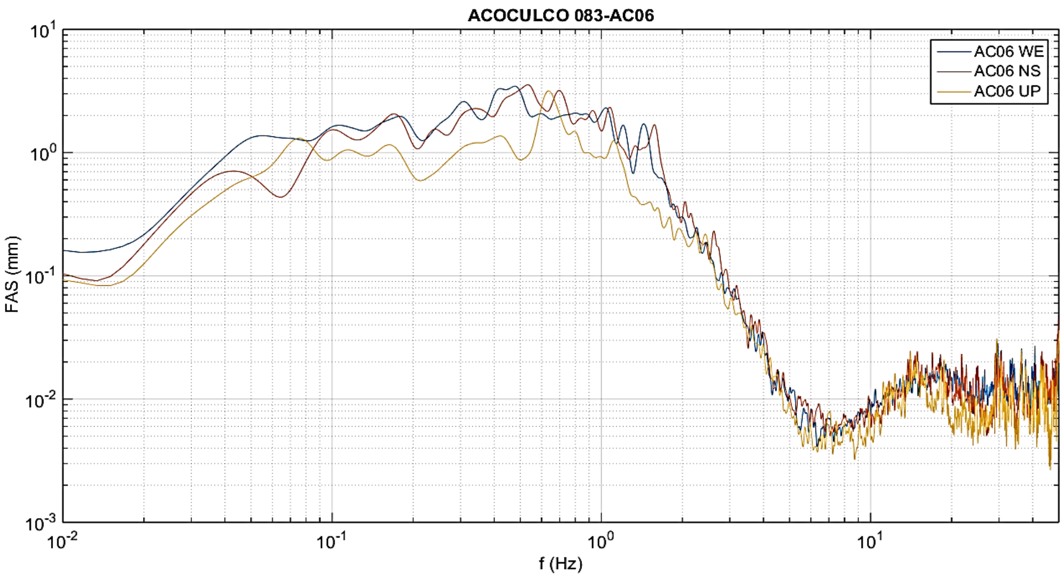

ACOCULCO 083-AC06
AC06 WE
AC06 NS
AC06 UP
FAS (mm)
f (Hz)

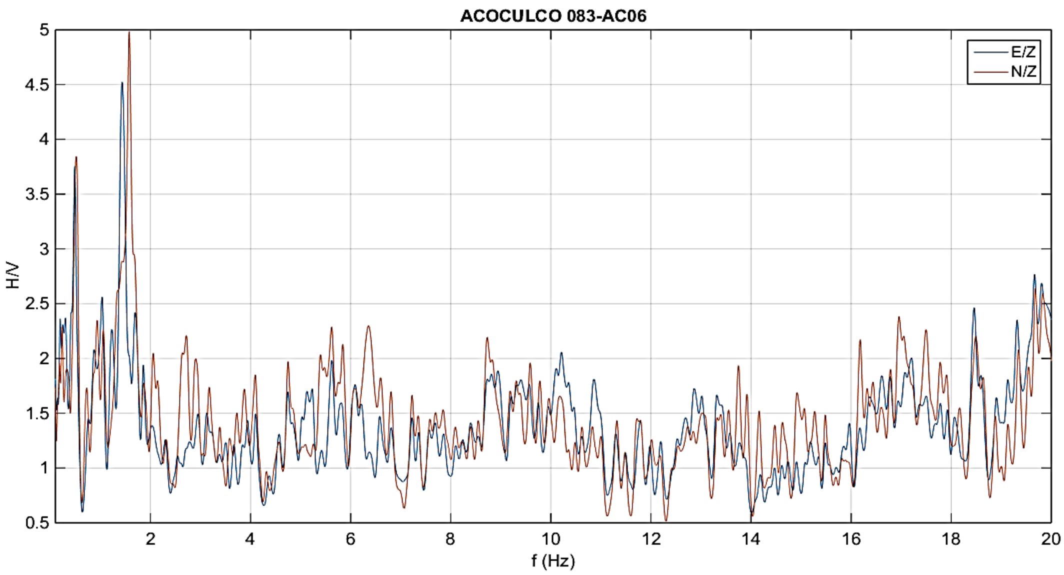

ACOCULCO 083-AC06
E/Z
N/Z
H/V
f (Hz)

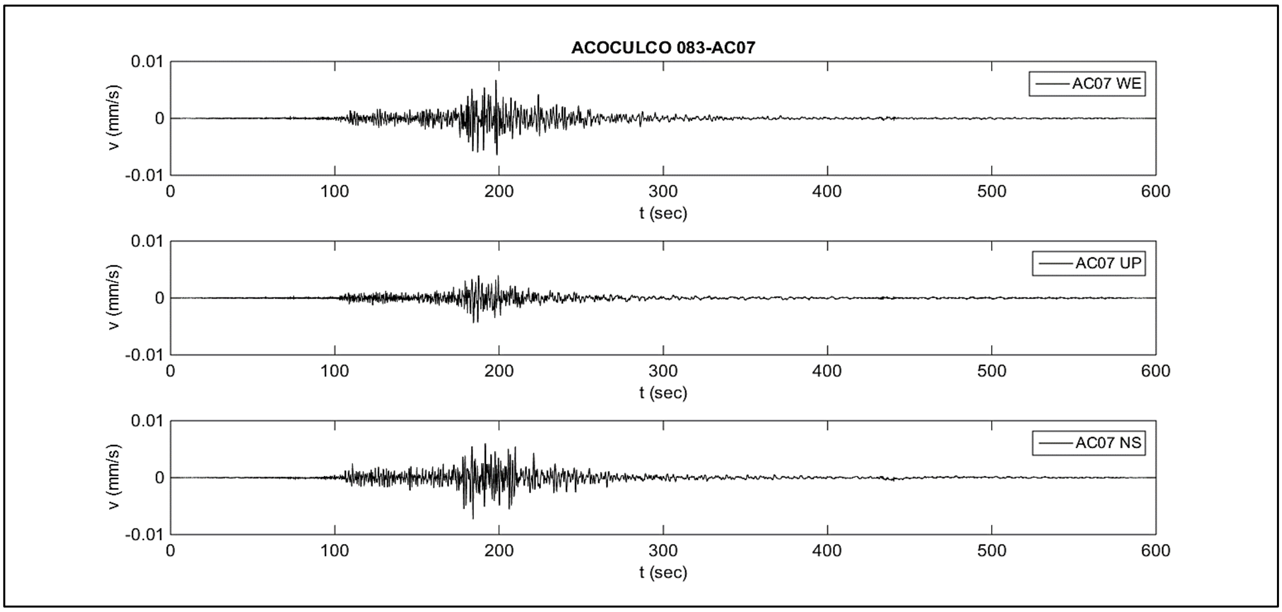
ACOCULCO 083-AC07
v (mm/s)
t (sec)
AC07 WE
AC07 UP
AC07 NS

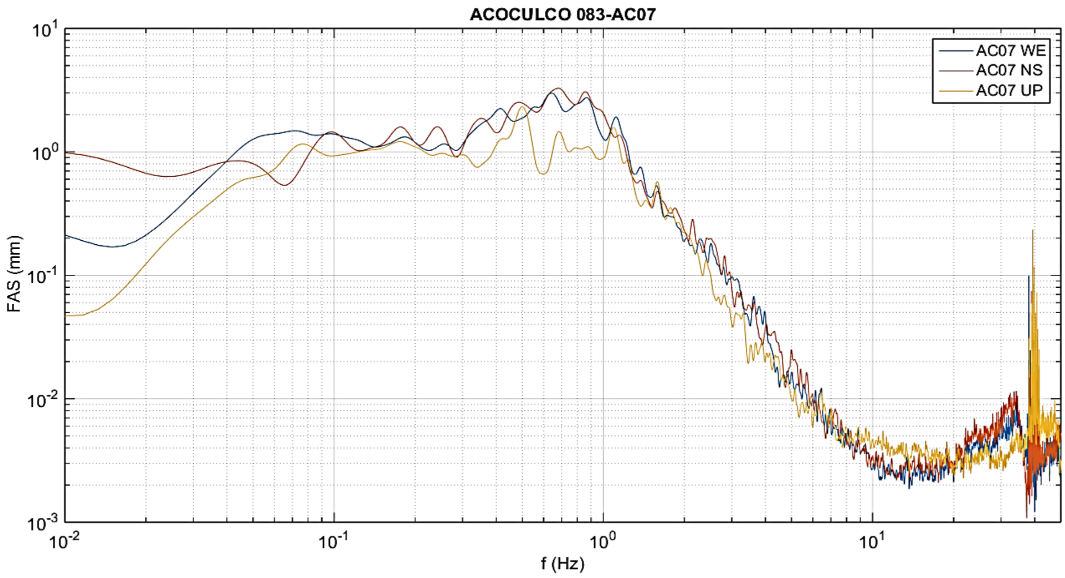
ACOCULCO 083-AC07
FAS (mm)
f (Hz)
AC07 WE
AC07 NS
AC07 UP

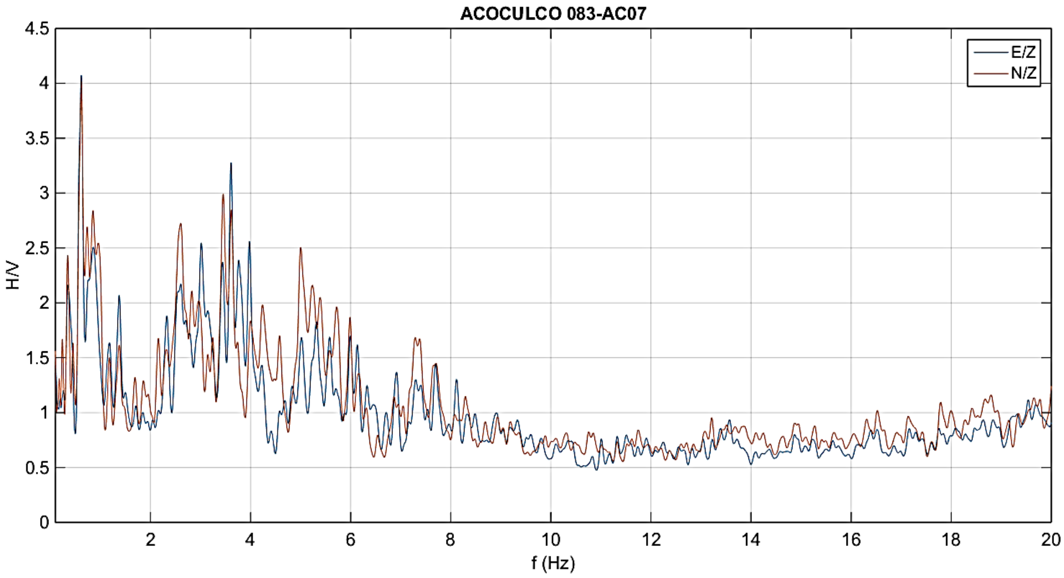
ACOCULCO 083-AC07
H/V
f (Hz)
E/Z
N/Z

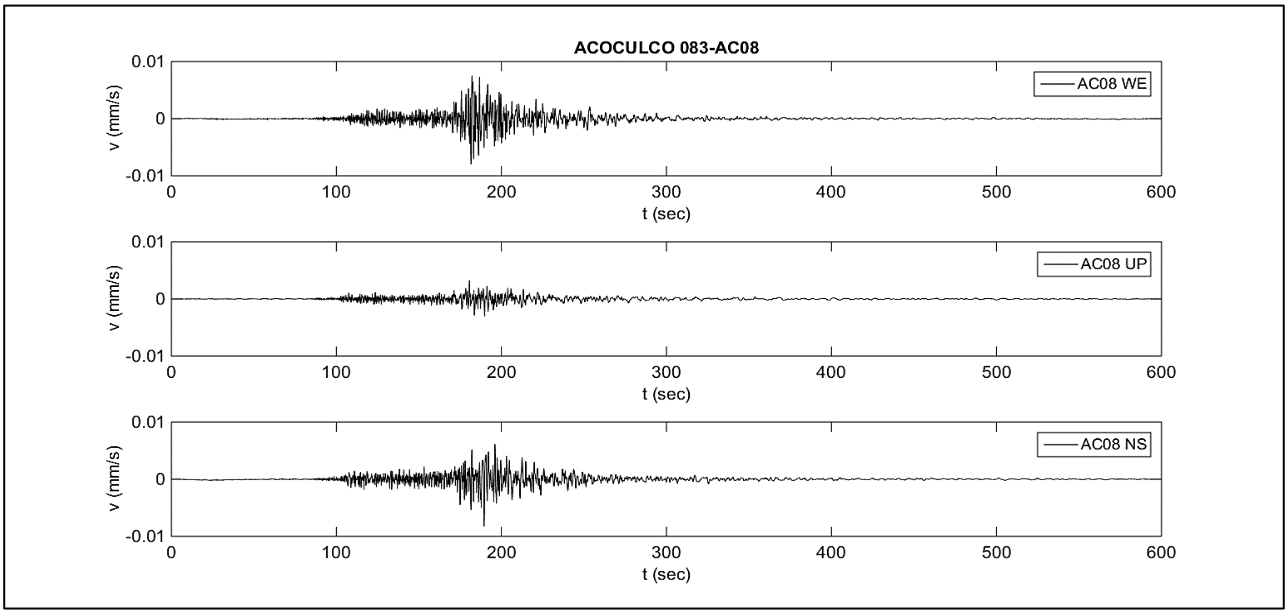
ACOCULCO 083-AC08
AC08 WE
AC08 UP
AC08 NS
v (mm/s)
t (sec)
0.01
0
-0.01
0
100
200
300
400
500
600

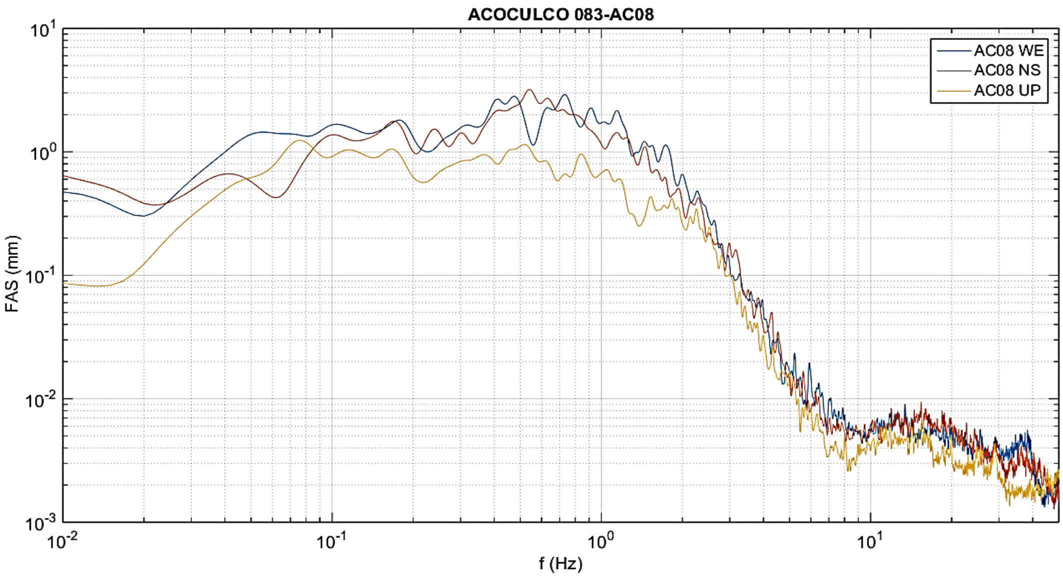
ACOCULCO 083-AC08
AC08 WE
AC08 NS
AC08 UP
FAS (mm)
f (Hz)

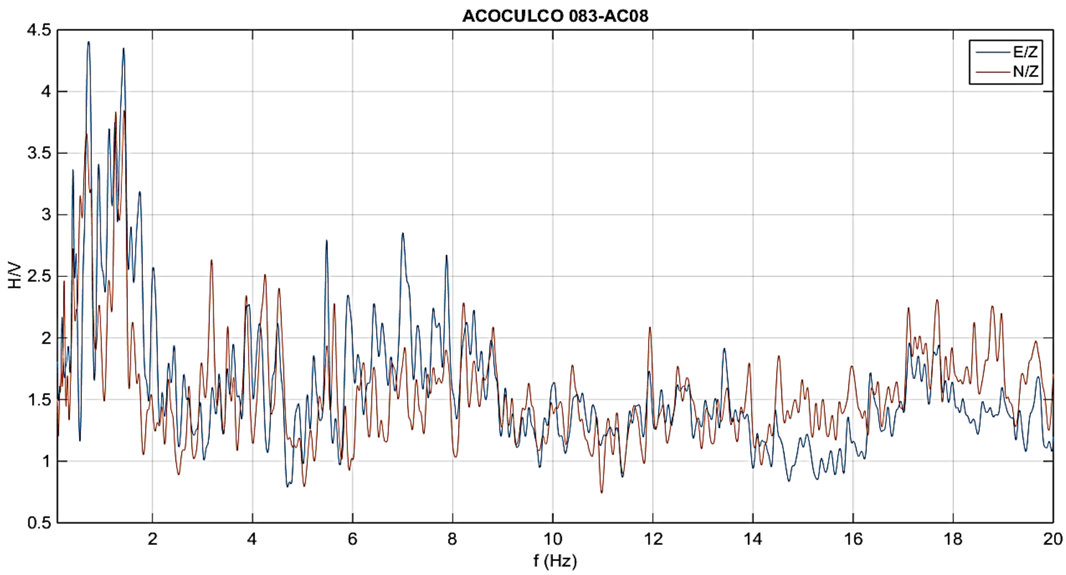
ACOCULCO 083-AC08
E/Z
N/Z
H/V
f (Hz)

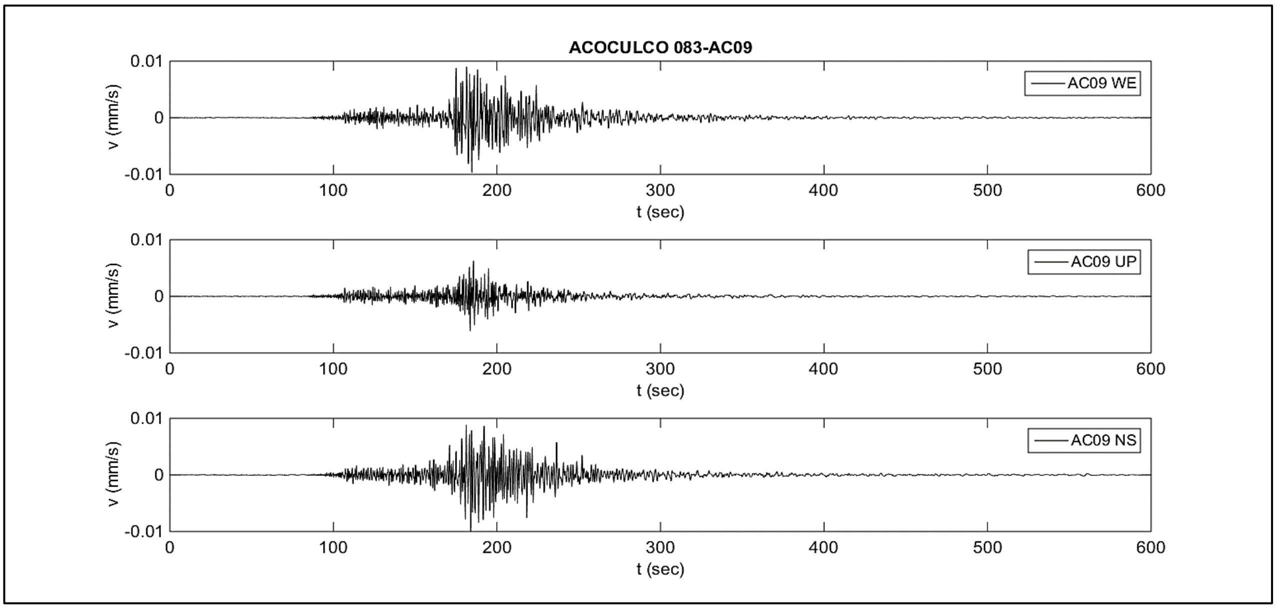
ACOCULCO 083-AC09
AC09 WE
AC09 UP
AC09 NS
v (mm/s)
t (sec)

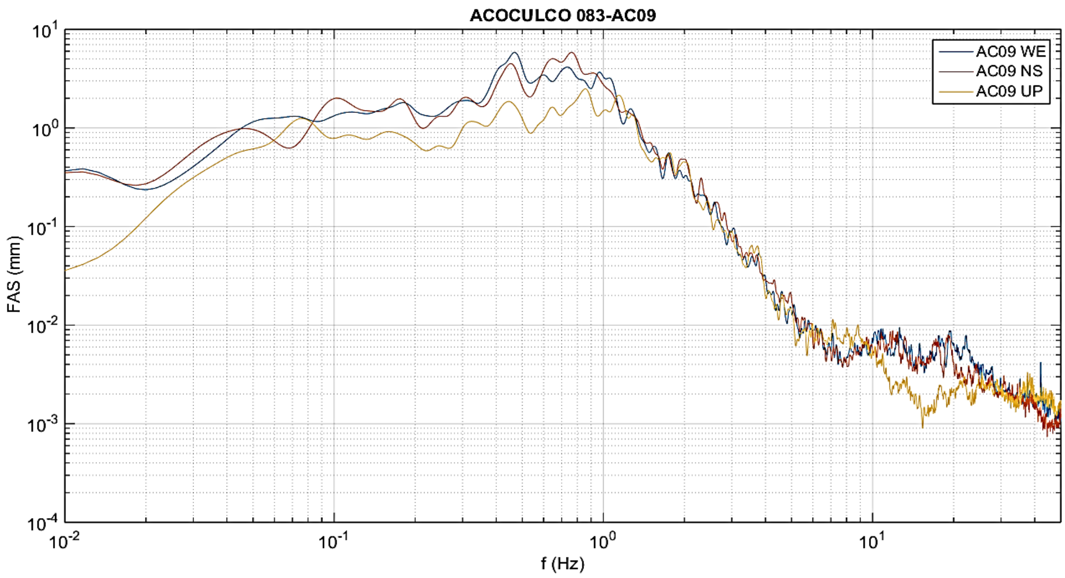
ACOCULCO 083-AC09
AC09 WE
AC09 NS
AC09 UP
FAS (mm)
f (Hz)

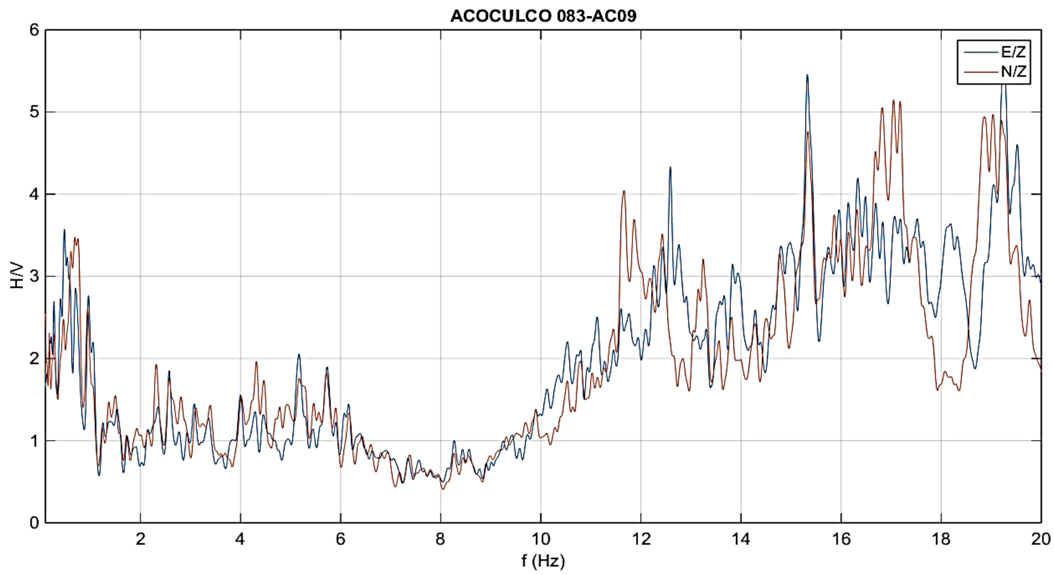
ACOCULCO 083-AC09
E/Z
N/Z
H/V
f (Hz)

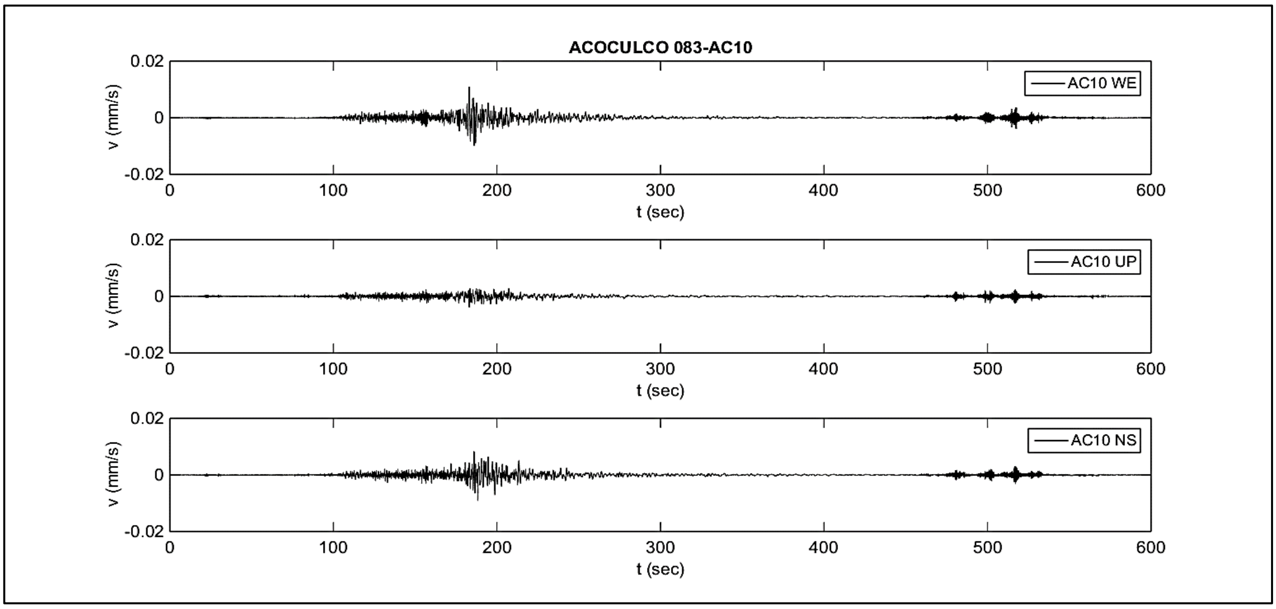
ACOCULCO 083-AC10
AC10 WE
AC10 UP
AC10 NS
v (mm/s)
t (sec)
0.02
0
-0.02
0
100
200
300
400
500
600

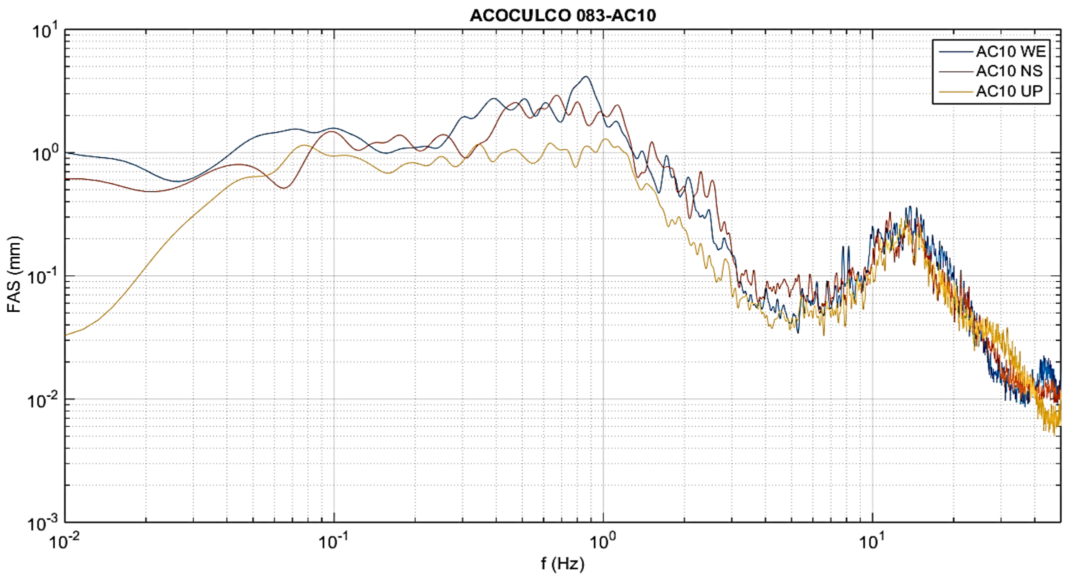
ACOCULCO 083-AC10
AC10 WE
AC10 NS
AC10 UP
FAS (mm)
f (Hz)

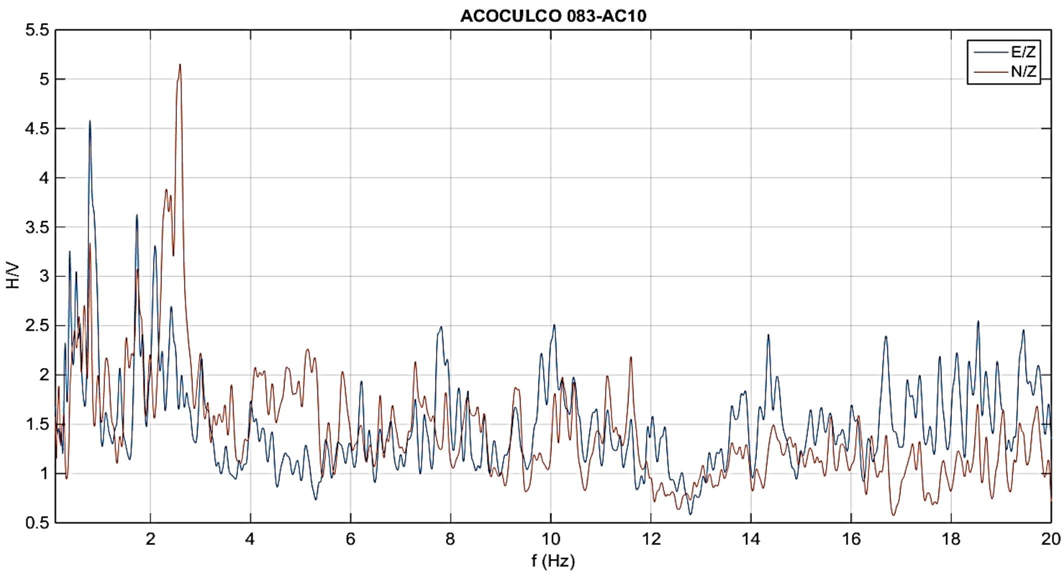
ACOCULCO 083-AC10
E/Z
N/Z
H/V
f (Hz)

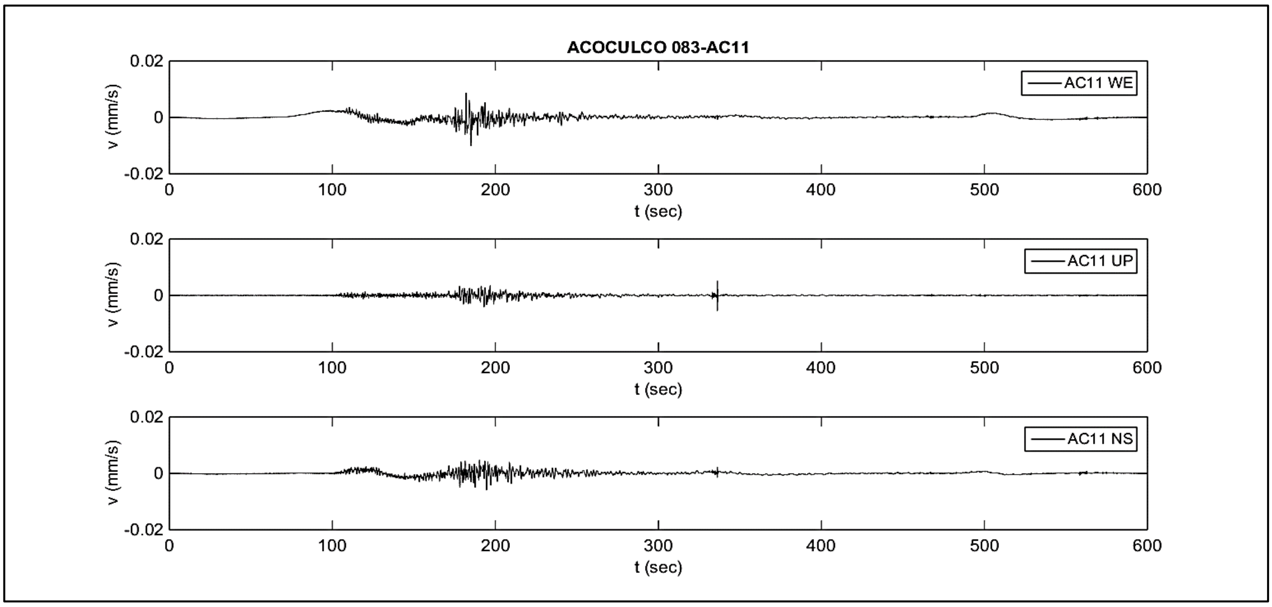
ACOCULCO 083-AC11
AC11 WE
AC11 UP
AC11 NS
v (mm/s)
t (sec)

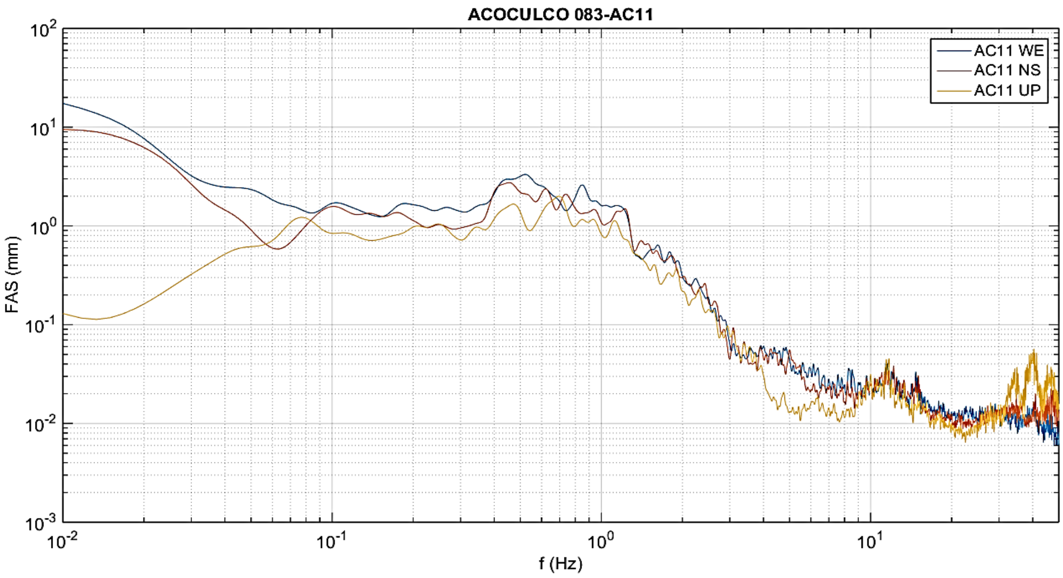
ACOCULCO 083-AC11
AC11 WE
AC11 NS
AC11 UP
FAS (mm)
f (Hz)

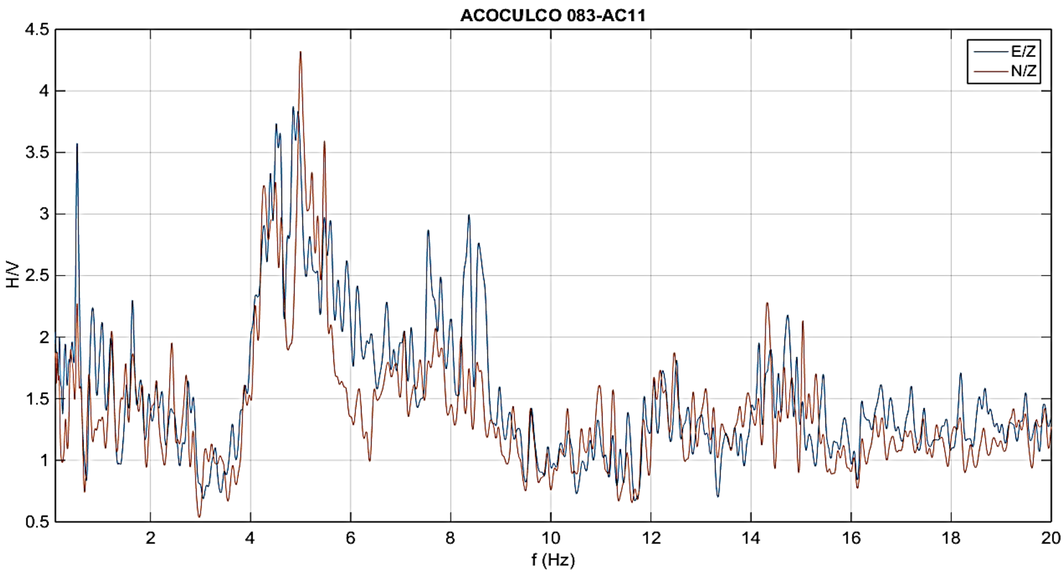
ACOCULCO 083-AC11
E/Z
N/Z
H/V
f (Hz)

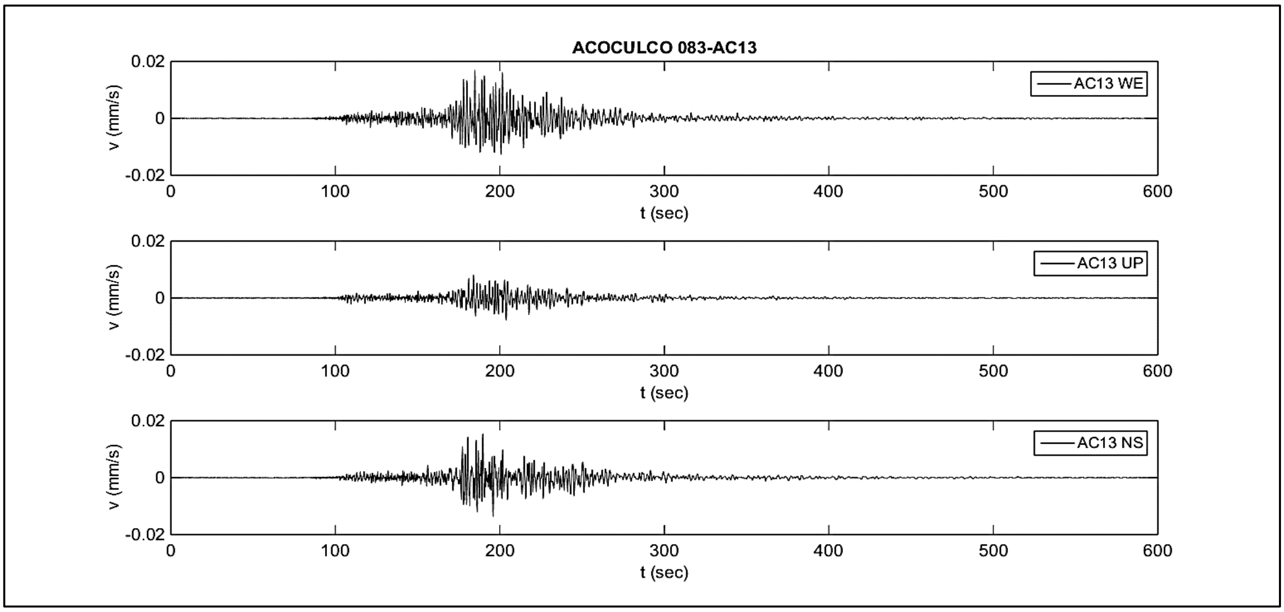

ACOCULCO 083-AC13
AC13 WE
AC13 UP
AC13 NS
v (mm/s)
t (sec)

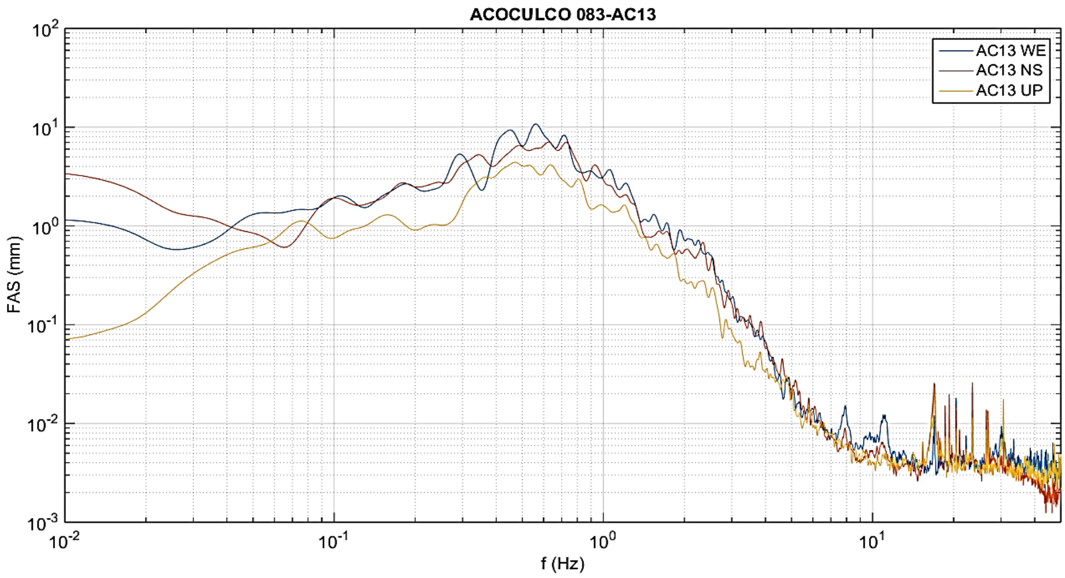

ACOCULCO 083-AC13
AC13 WE
AC13 NS
AC13 UP
FAS (mm)
f (Hz)

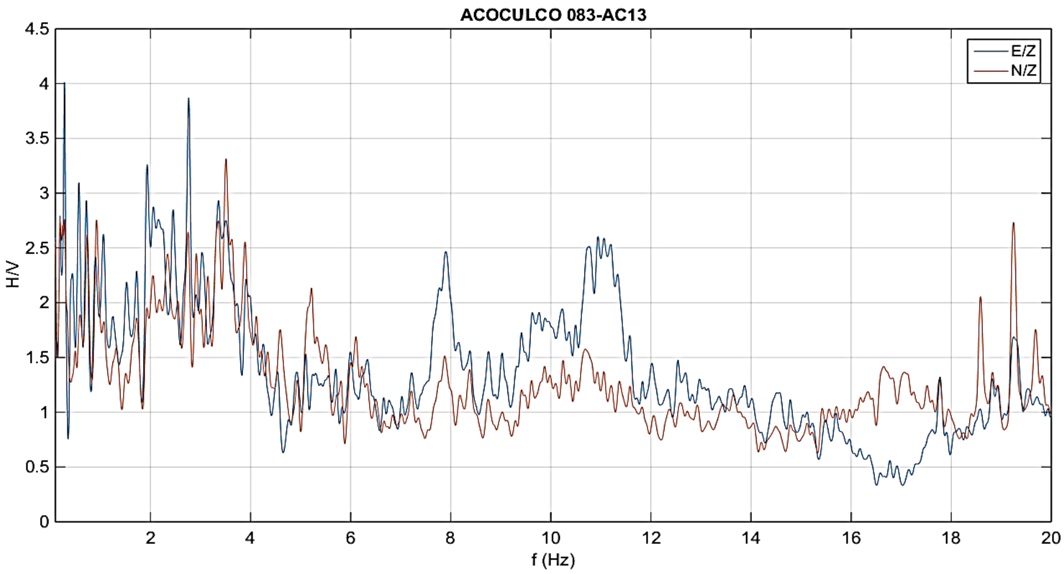

ACOCULCO 083-AC13
E/Z
N/Z
H/V
f (Hz)

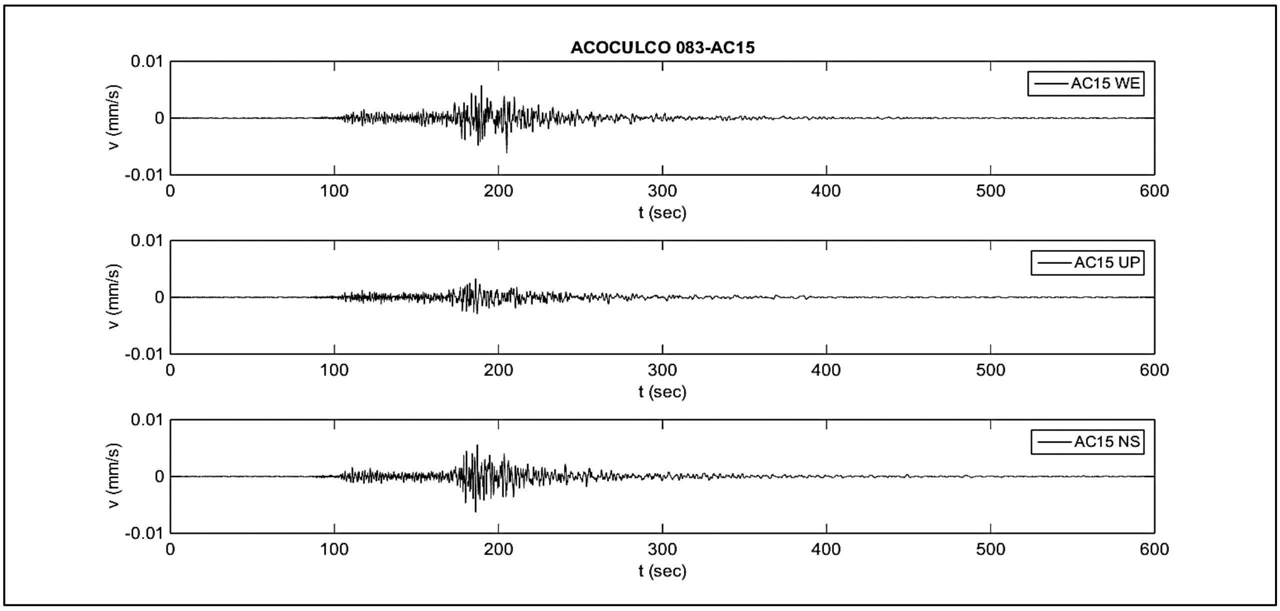
ACOCULCO 083-AC15
AC15 WE
AC15 UP
AC15 NS
v (mm/s)
0.01
0
-0.01
0
100
200
300
400
500
600
t (sec)

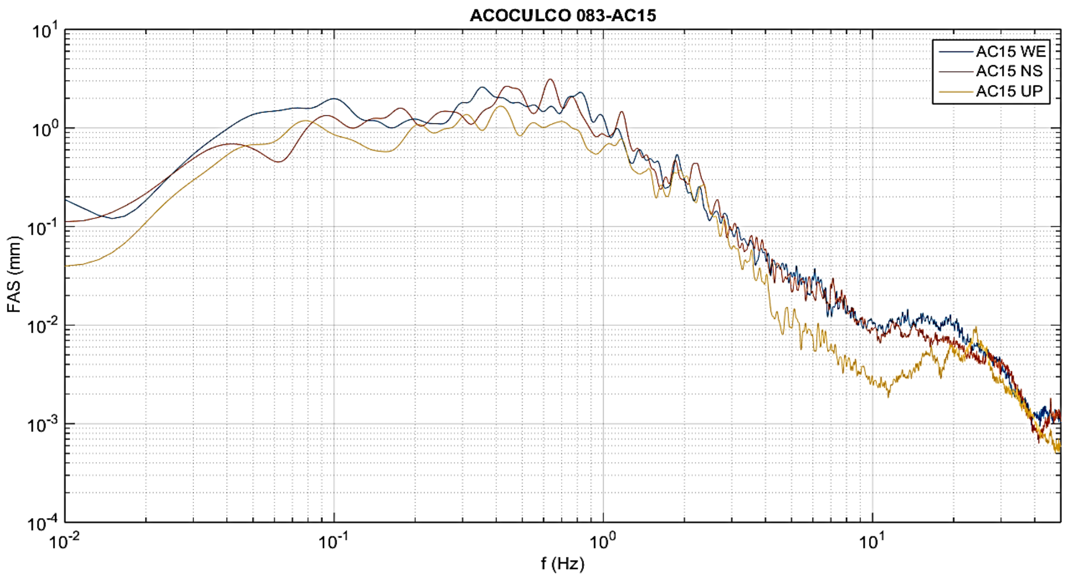
ACOCULCO 083-AC15
AC15 WE
AC15 NS
AC15 UP
FAS (mm)
f (Hz)

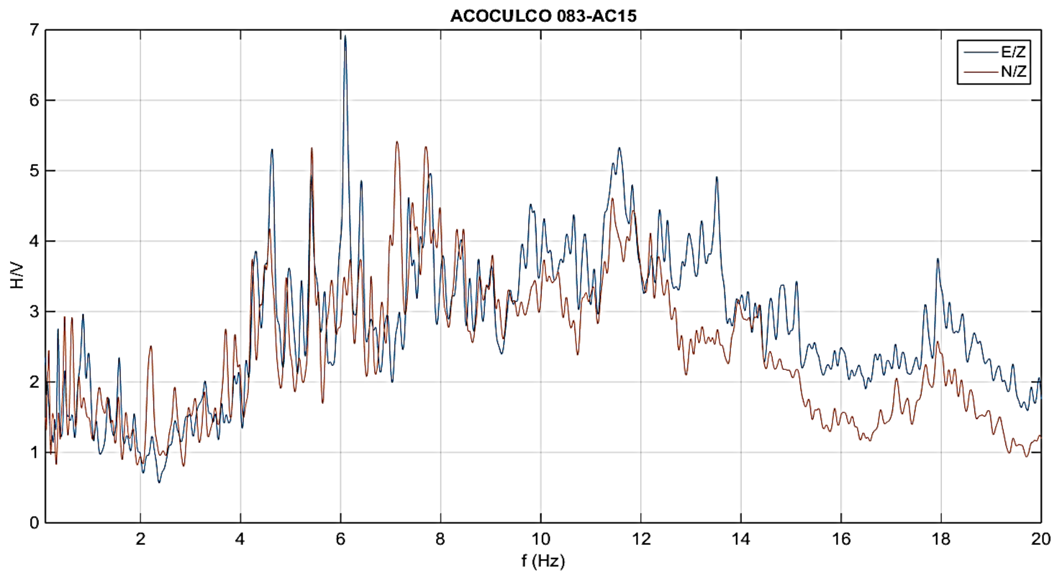
ACOCULCO 083-AC15
E/Z
N/Z
H/V
f (Hz)

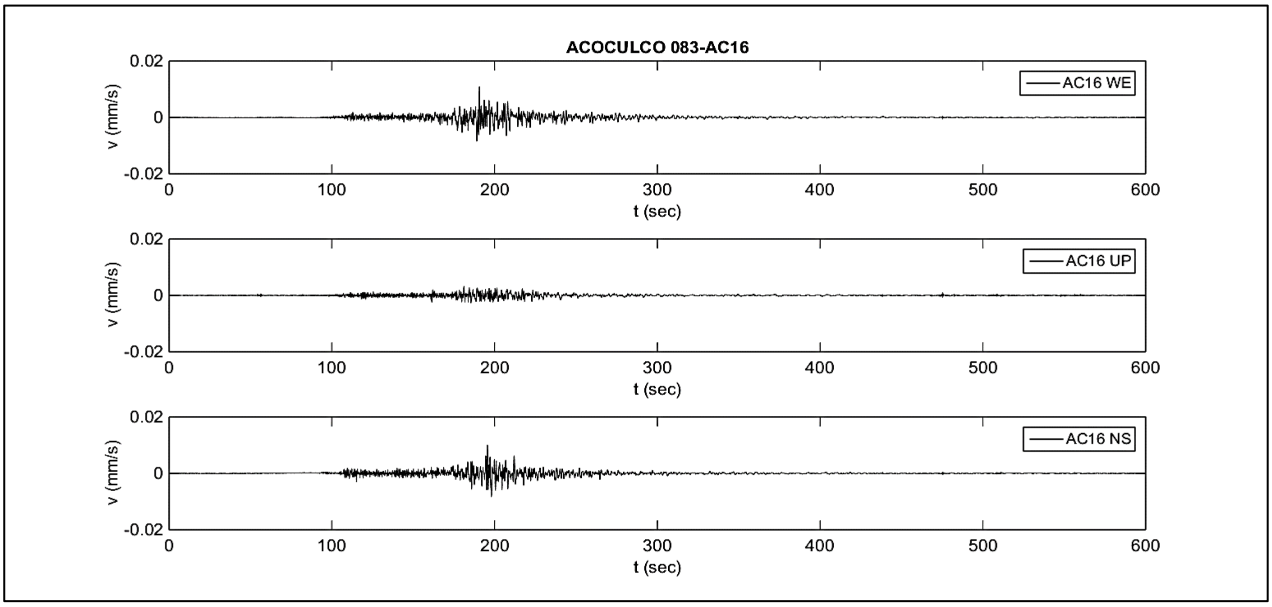
ACOCULCO 083-AC16
AC16 WE
AC16 UP
AC16 NS
v (mm/s)
t (sec)
0.02
0
-0.02
0
100
200
300
400
500
600

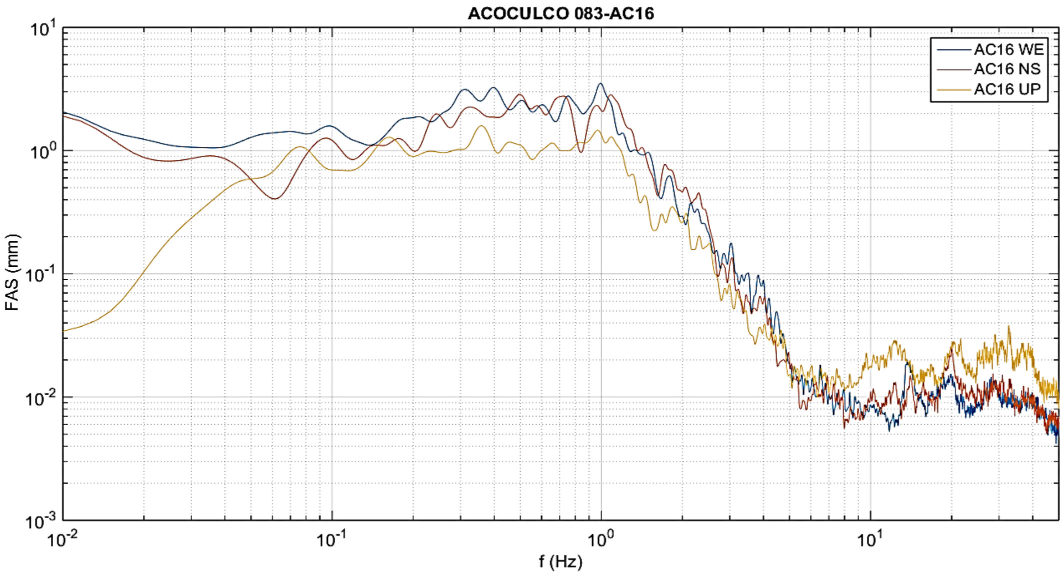
ACOCULCO 083-AC16
AC16 WE
AC16 NS
AC16 UP
FAS (mm)
f (Hz)

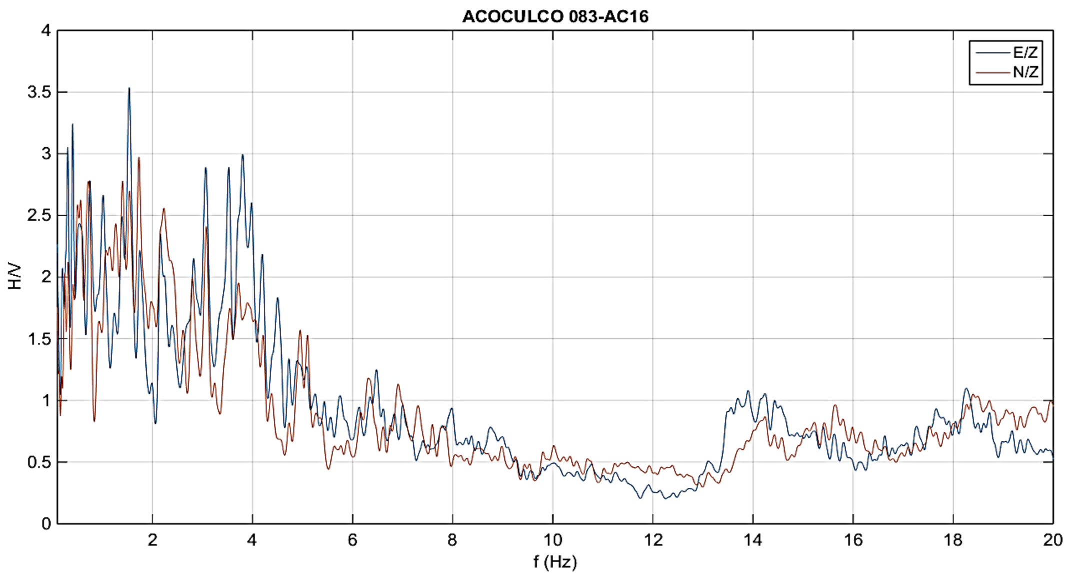
ACOCULCO 083-AC16
E/Z
N/Z
H/V
f (Hz)

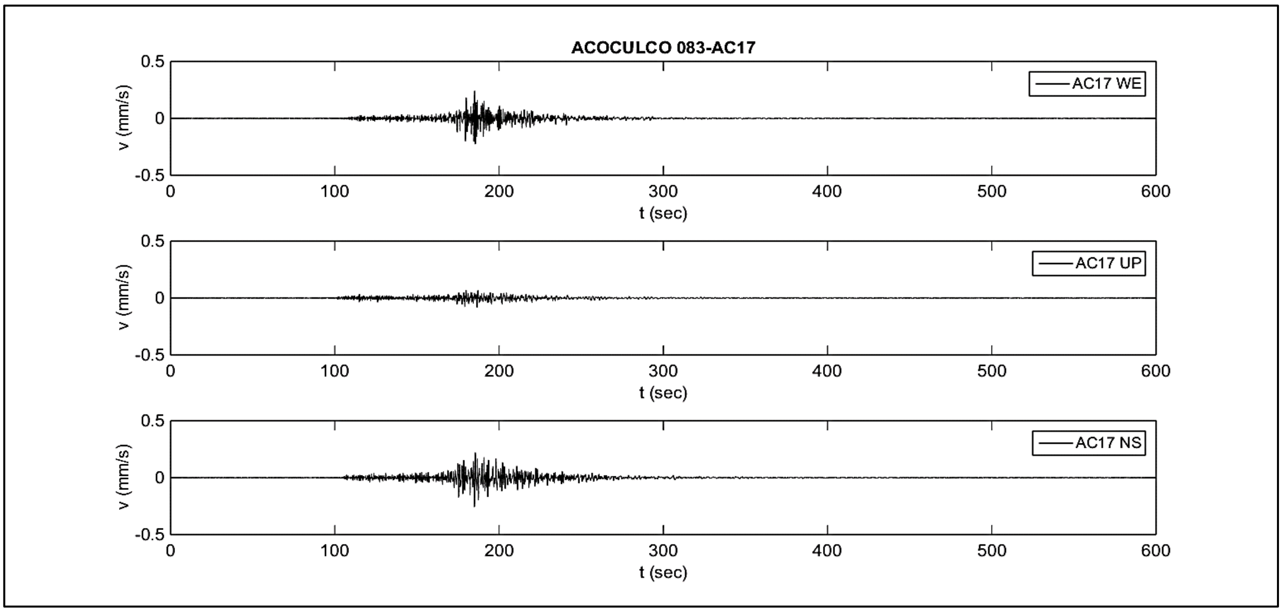
ACOCULCO 083-AC17
AC17 WE
AC17 UP
AC17 NS
v (mm/s)
t (sec)

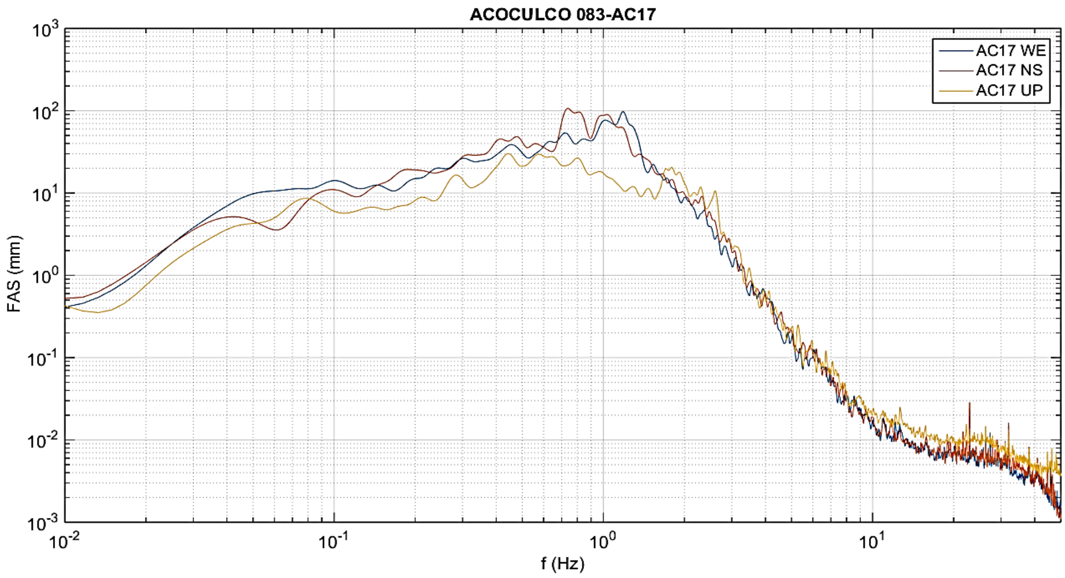
ACOCULCO 083-AC17
AC17 WE
AC17 NS
AC17 UP
FAS (mm)
f (Hz)

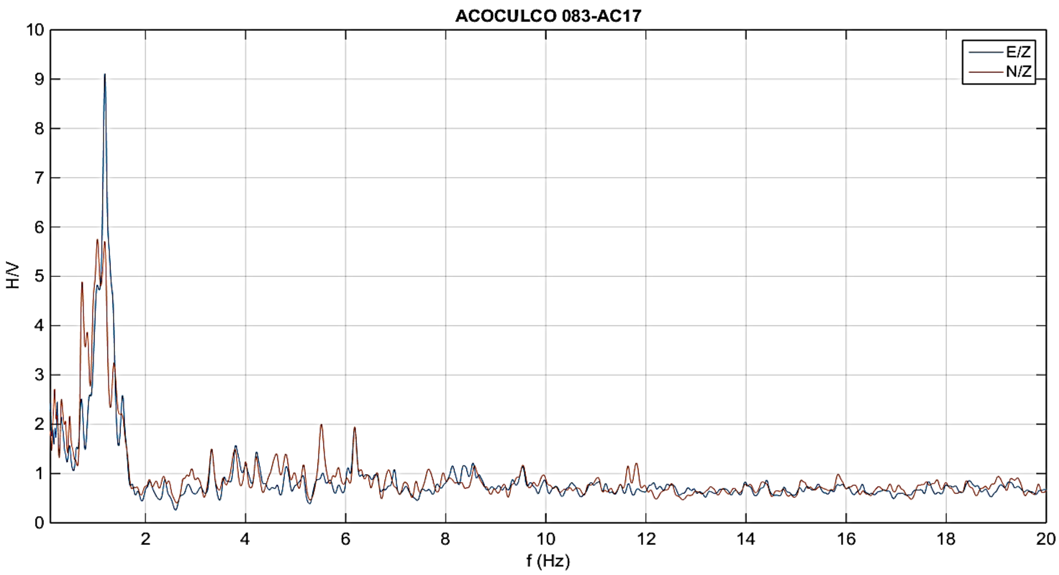
ACOCULCO 083-AC17
E/Z
N/Z
H/V
f (Hz)

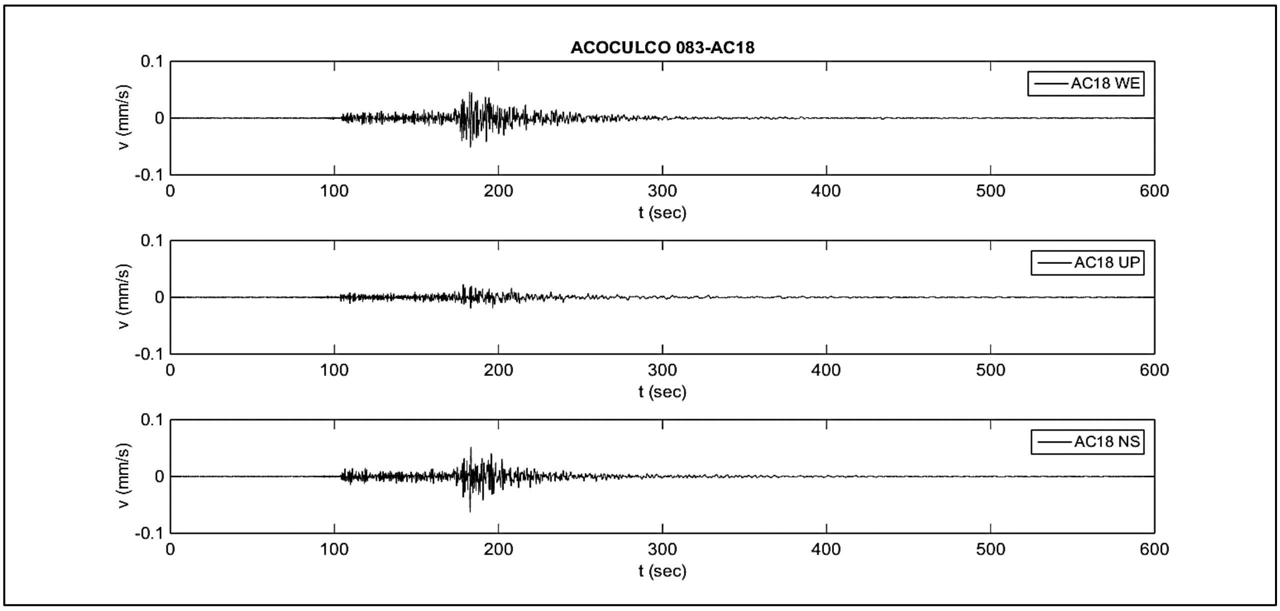
ACOCULCO 083-AC18
AC18 WE
AC18 UP
AC18 NS
v (mm/s)
t (sec)
0.1
0
-0.1
0
100
200
300
400
500
600

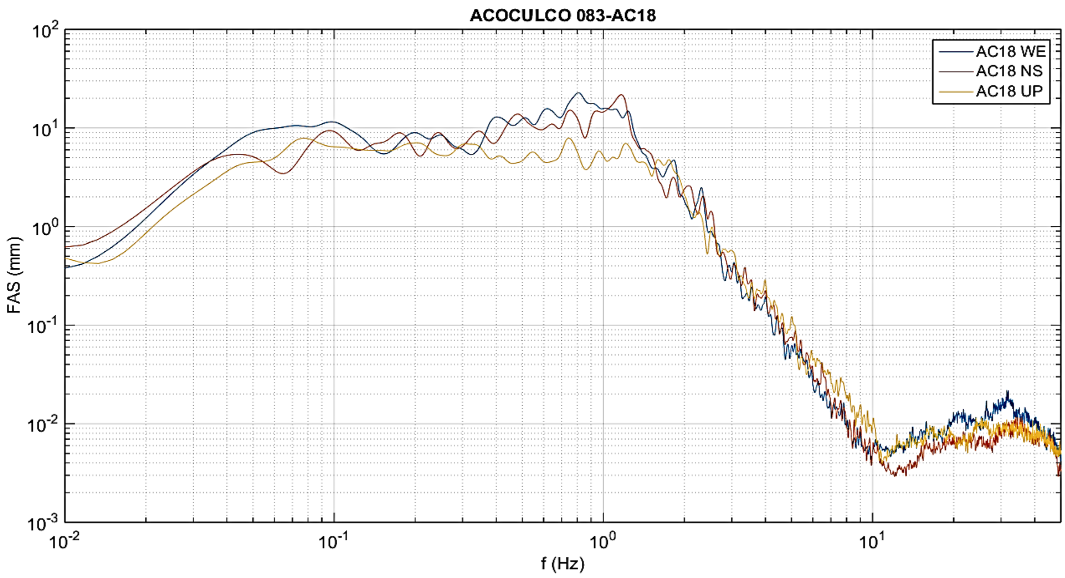
ACOCULCO 083-AC18
AC18 WE
AC18 NS
AC18 UP
FAS (mm)
f (Hz)
10^2
10^1
10^0
10^{-1}
10^{-2}
10^{-3}
10^{-2}
10^{-1}
10^0
10^1

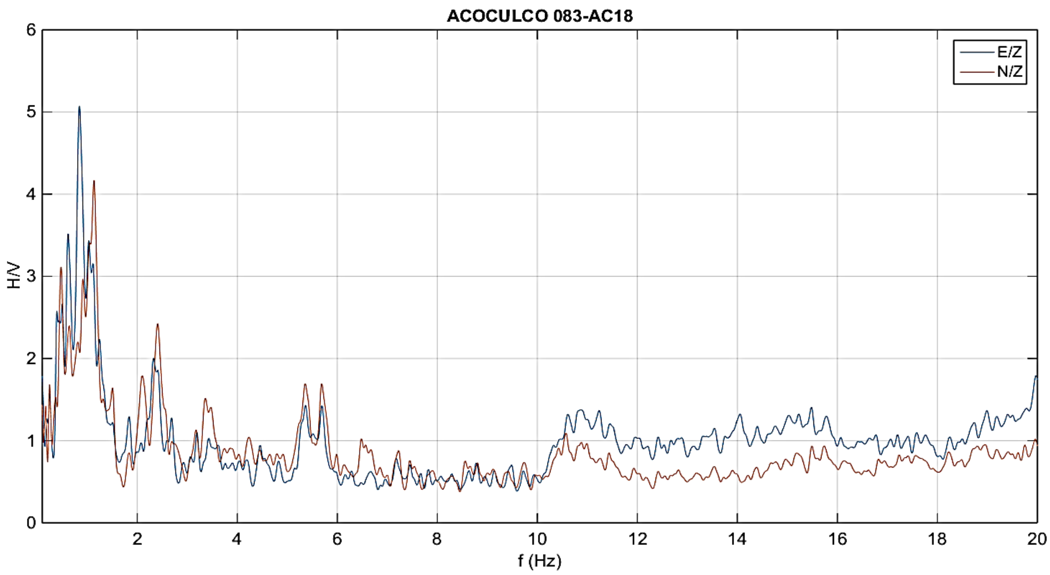
ACOCULCO 083-AC18
E/Z
N/Z
H/V
f (Hz)
0
1
2
3
4
5
6
2
4
6
8
10
12
14
16
18
20

Appendix 4-F Day 085, Earthquake. Time histories, spectra and spectral ratios

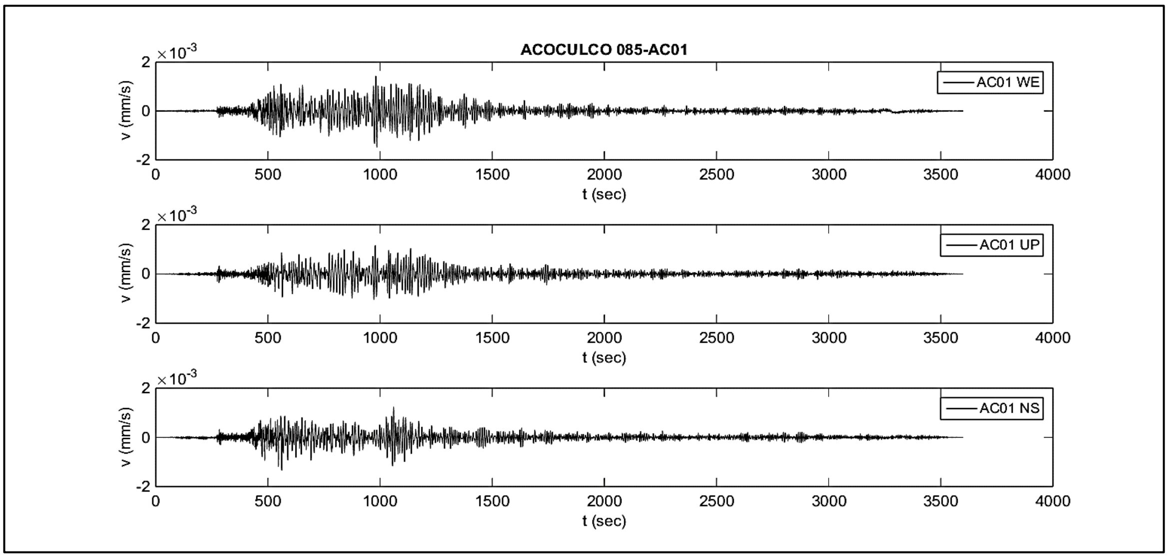

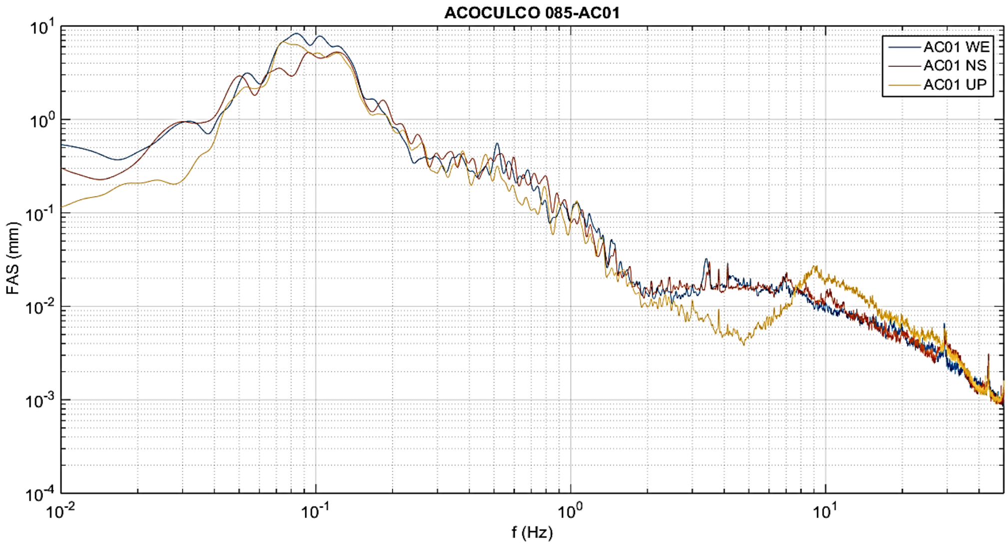

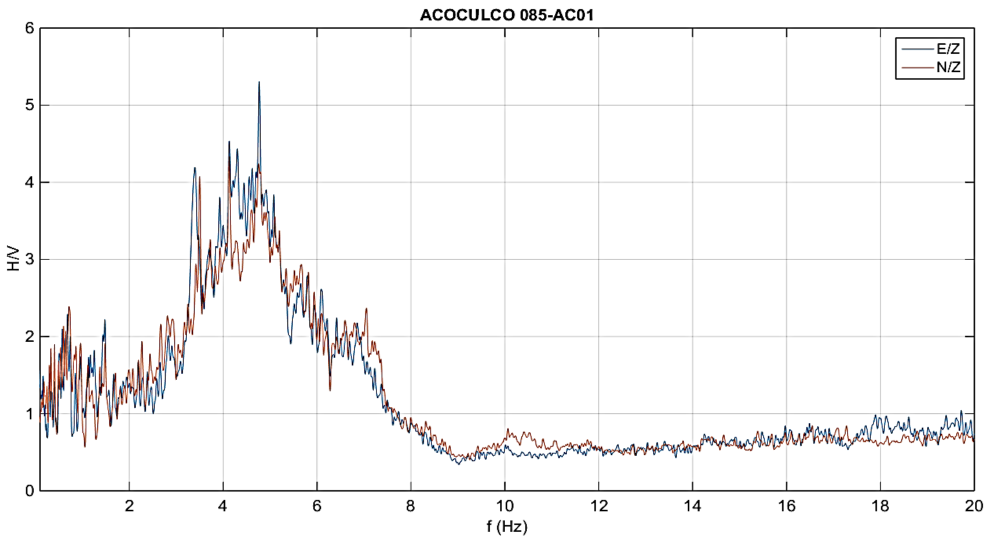

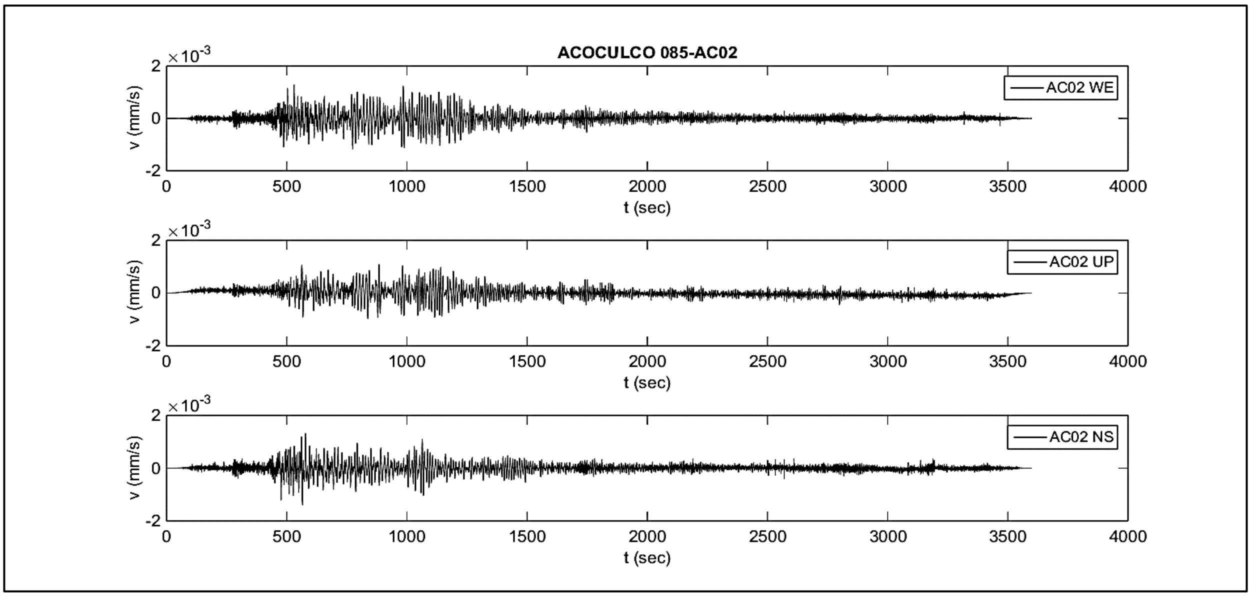
ACOCULCO 085-AC02
AC02 WE
AC02 UP
AC02 NS
v (mm/s)
t (sec)

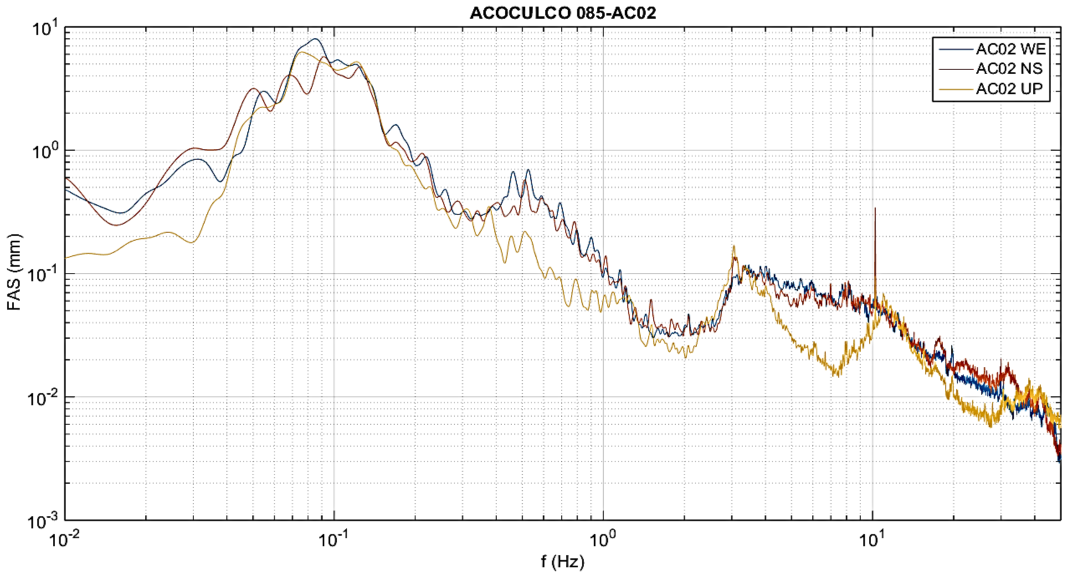
ACOCULCO 085-AC02
AC02 WE
AC02 NS
AC02 UP
FAS (mm)
f (Hz)

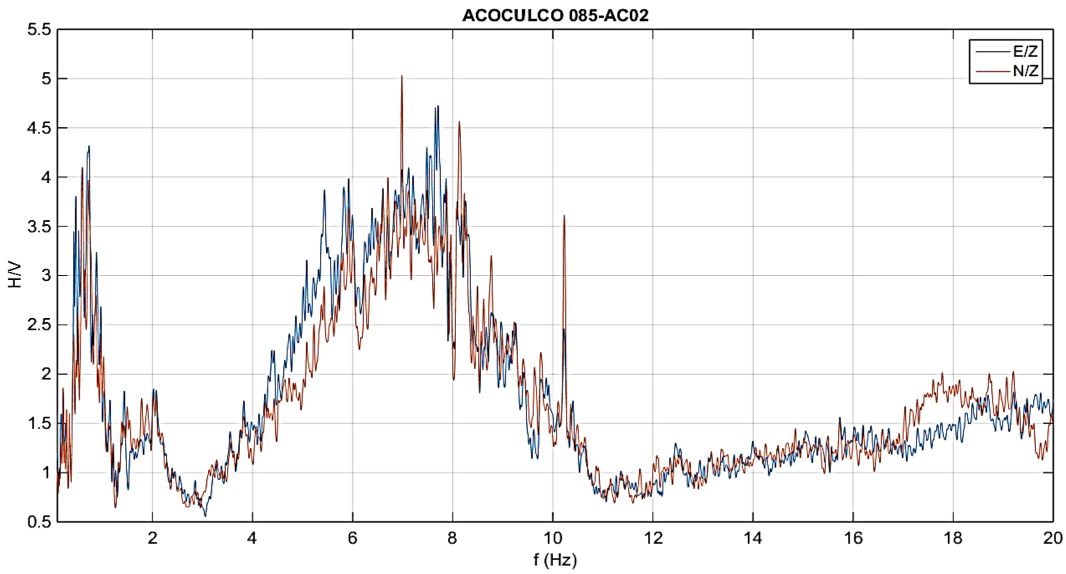
ACOCULCO 085-AC02
E/Z
N/Z
H/V
f (Hz)

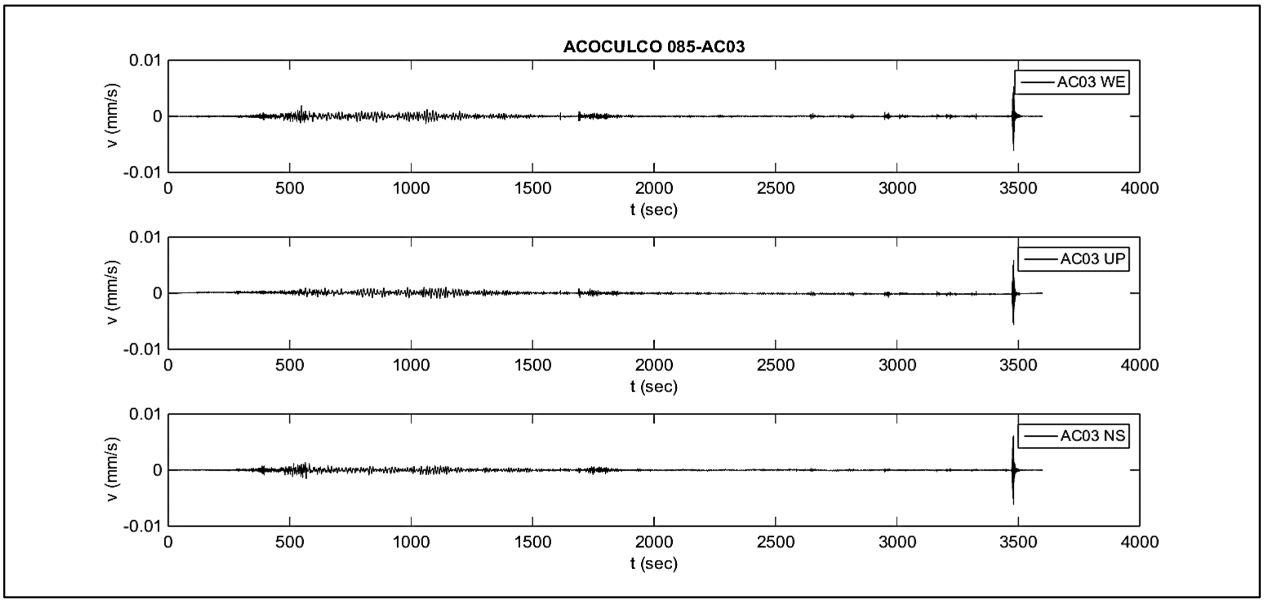
ACOCULCO 085-AC03
AC03 WE
AC03 UP
AC03 NS
v (mm/s)
t (sec)

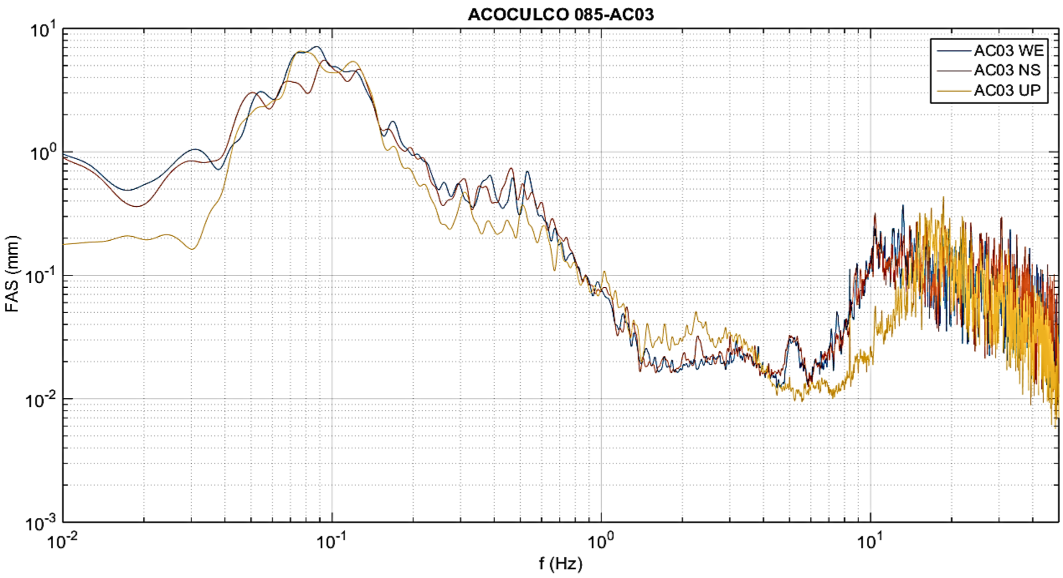
ACOCULCO 085-AC03
AC03 WE
AC03 NS
AC03 UP
FAS (mm)
f (Hz)

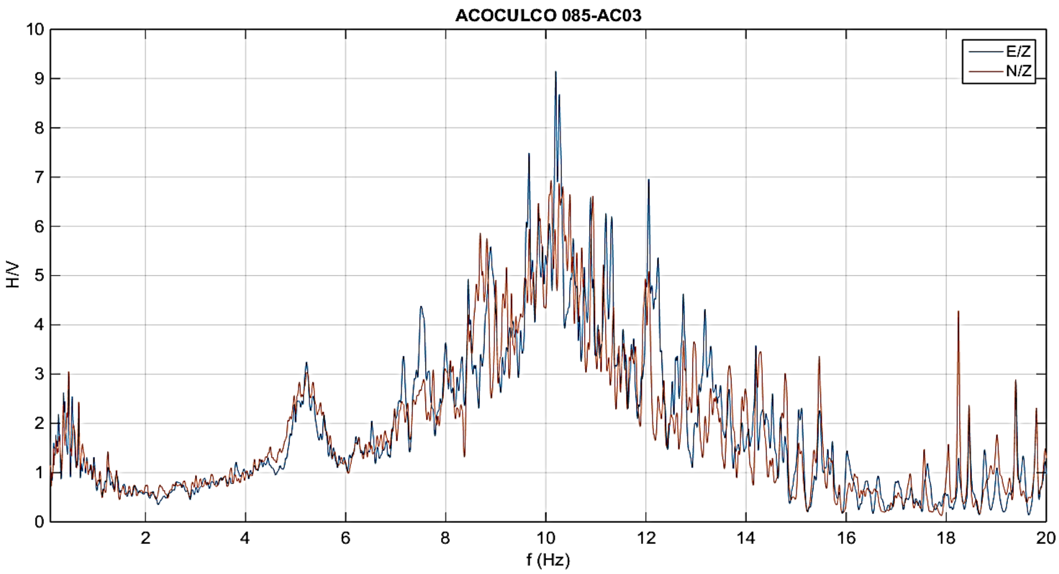
ACOCULCO 085-AC03
E/Z
N/Z
H/V
f (Hz)

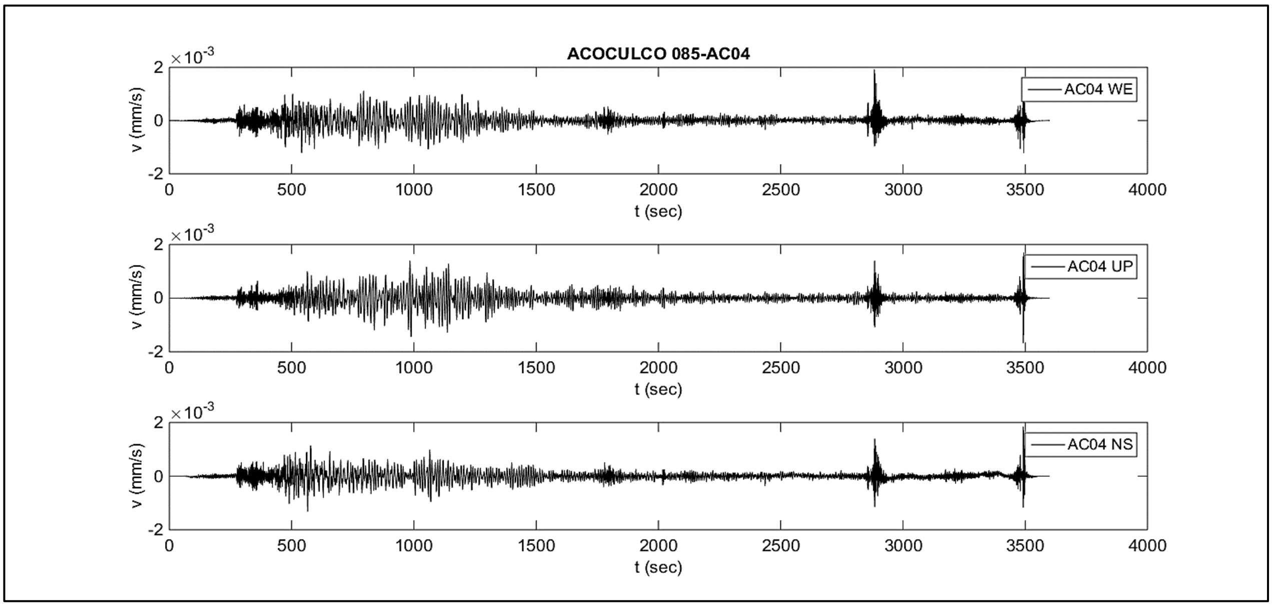
ACOCULCO 085-AC04
AC04 WE
AC04 UP
AC04 NS
v (mm/s)
t (sec)
×10-3

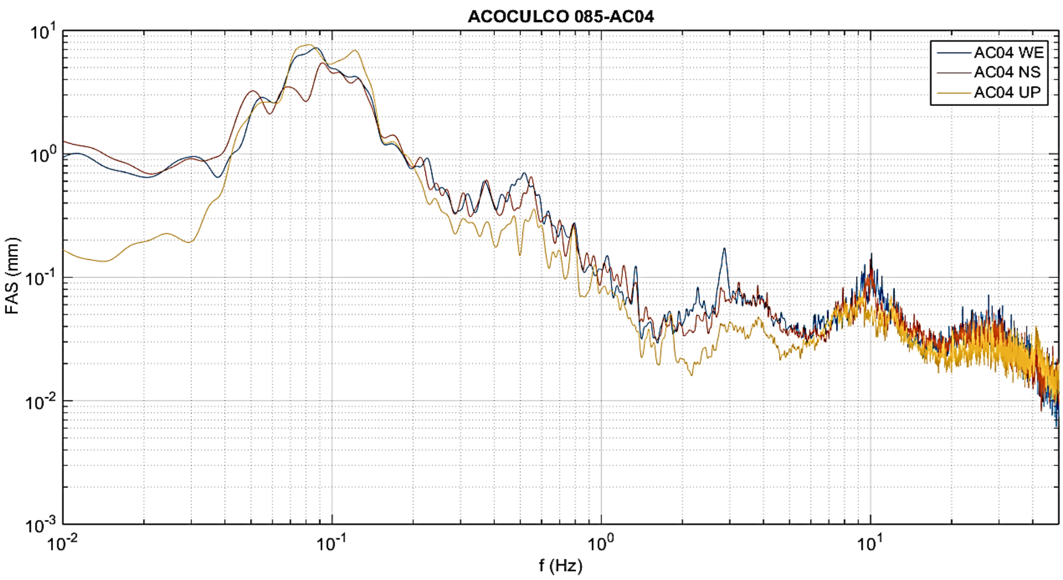
ACOCULCO 085-AC04
AC04 WE
AC04 NS
AC04 UP
FAS (mm)
f (Hz)

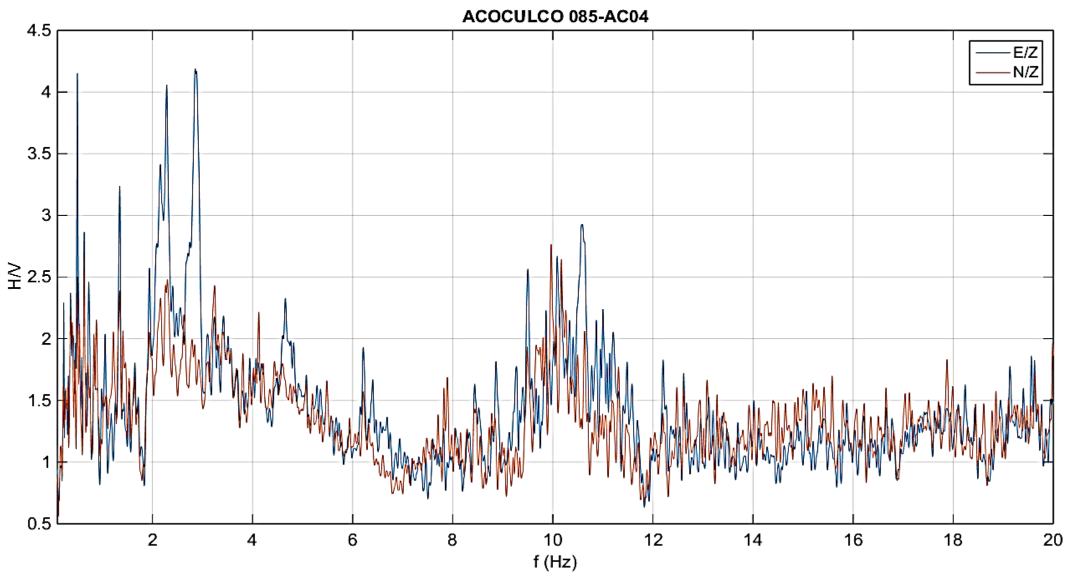
ACOCULCO 085-AC04
E/Z
N/Z
H/V
f (Hz)

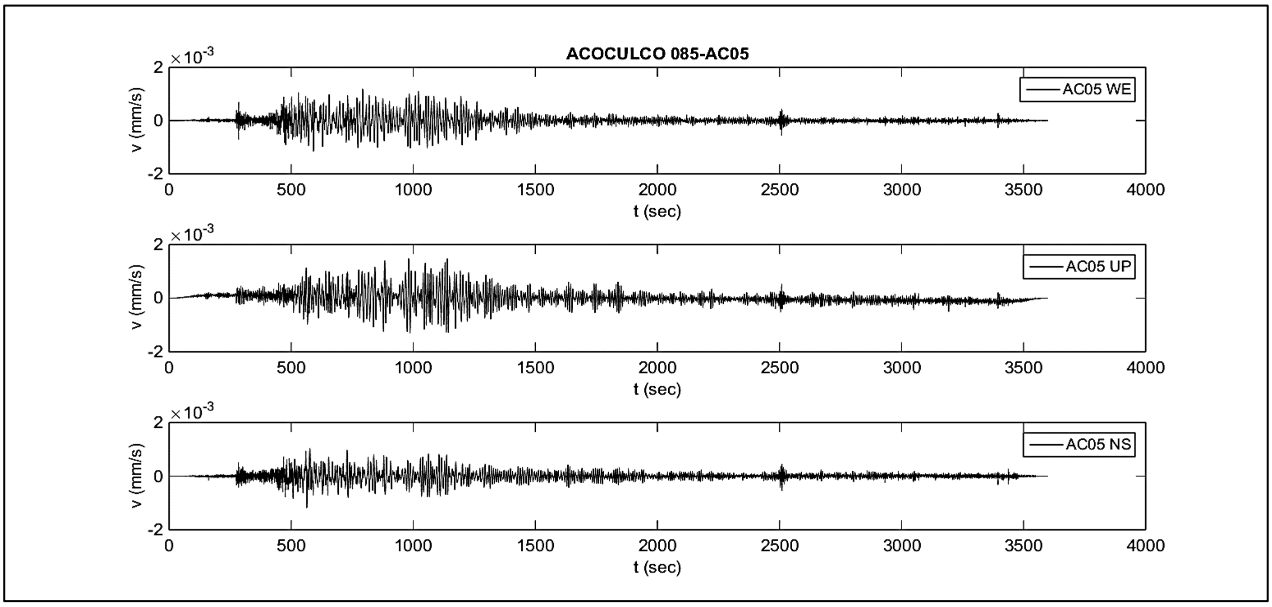
ACOCULCO 085-AC05
AC05 WE
AC05 UP
AC05 NS
v (mm/s)
t (sec)
×10^-3

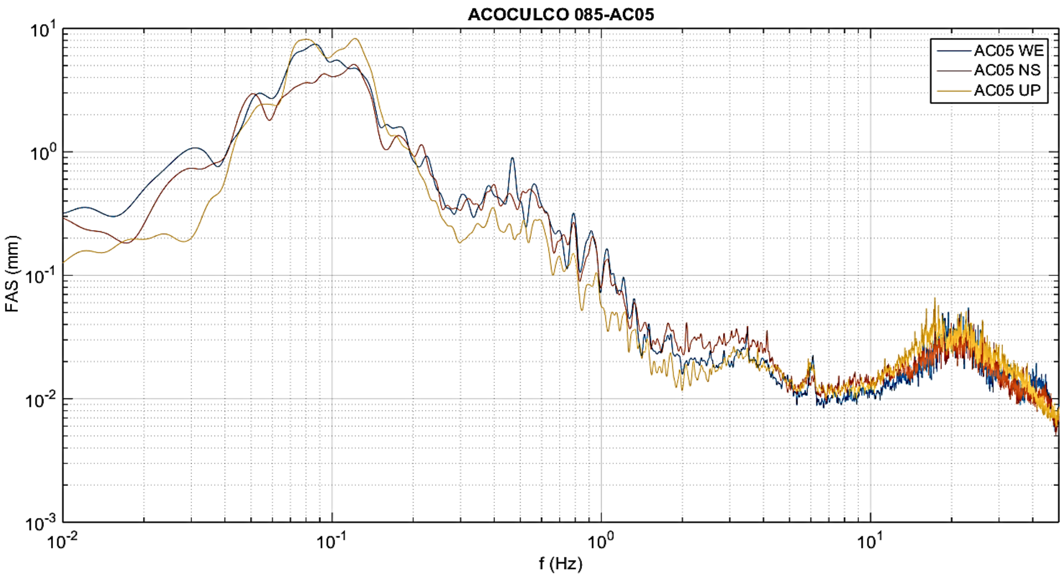
ACOCULCO 085-AC05
AC05 WE
AC05 NS
AC05 UP
FAS (mm)
f (Hz)

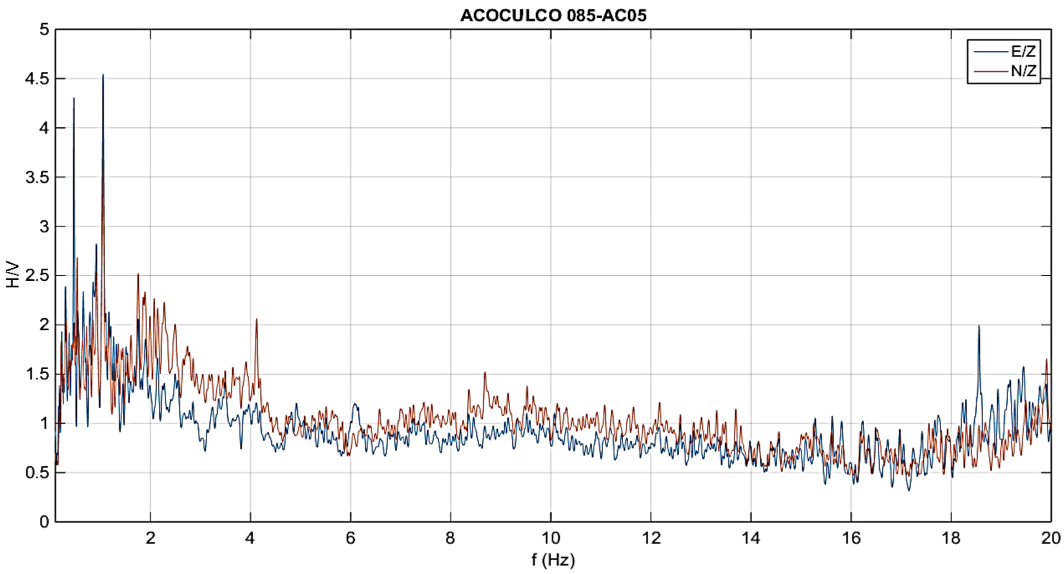
ACOCULCO 085-AC05
E/Z
N/Z
H/V
f (Hz)

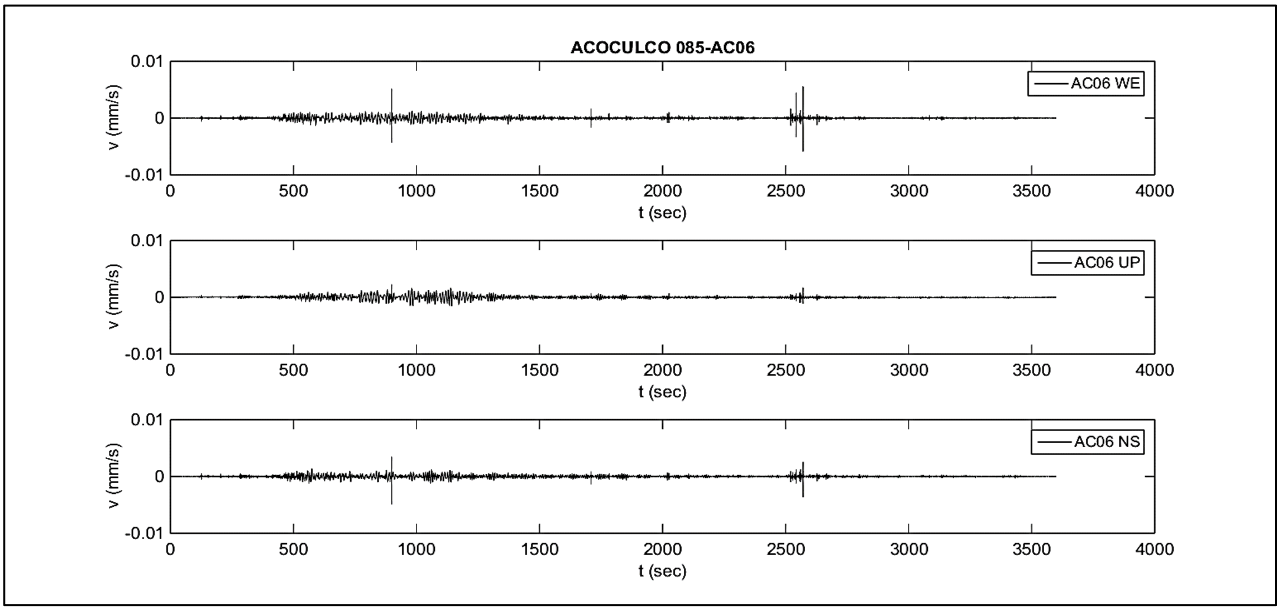
ACOCULCO 085-AC06
AC06 WE
AC06 UP
AC06 NS
v (mm/s)
t (sec)

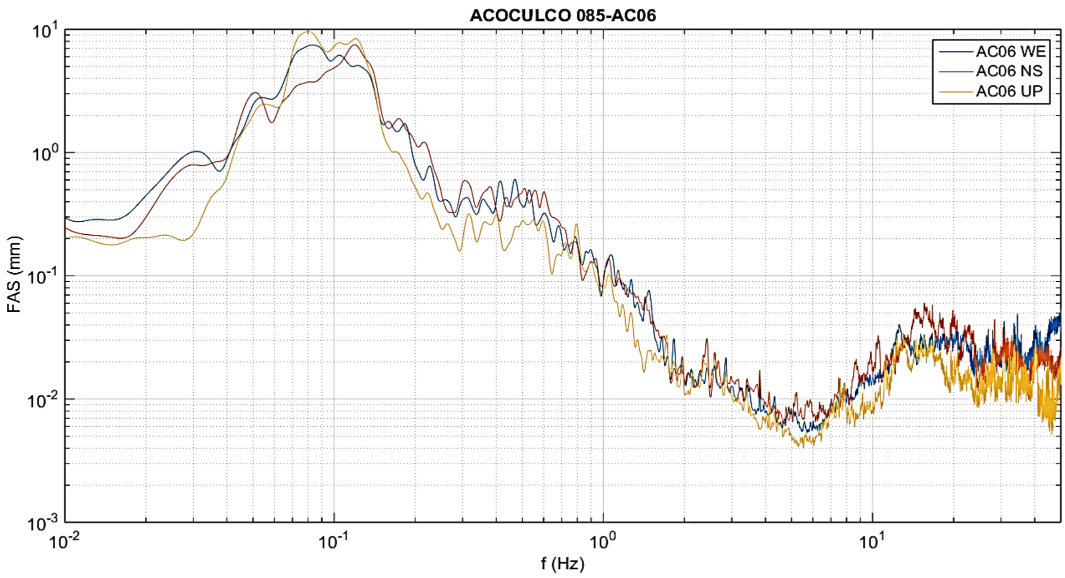
ACOCULCO 085-AC06
AC06 WE
AC06 NS
AC06 UP
FAS (mm)
f (Hz)

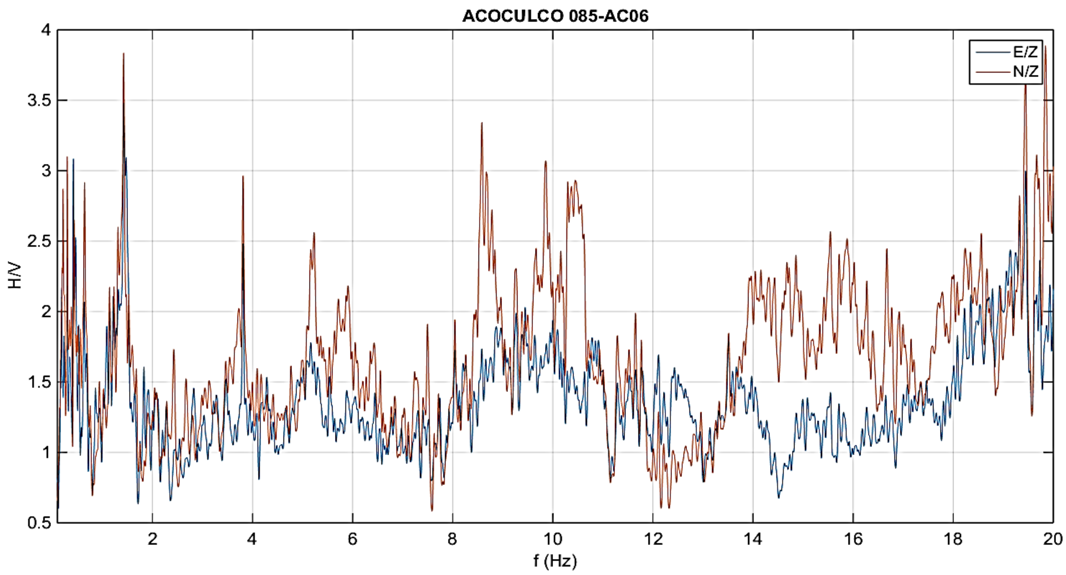
ACOCULCO 085-AC06
E/Z
N/Z
H/V
f (Hz)

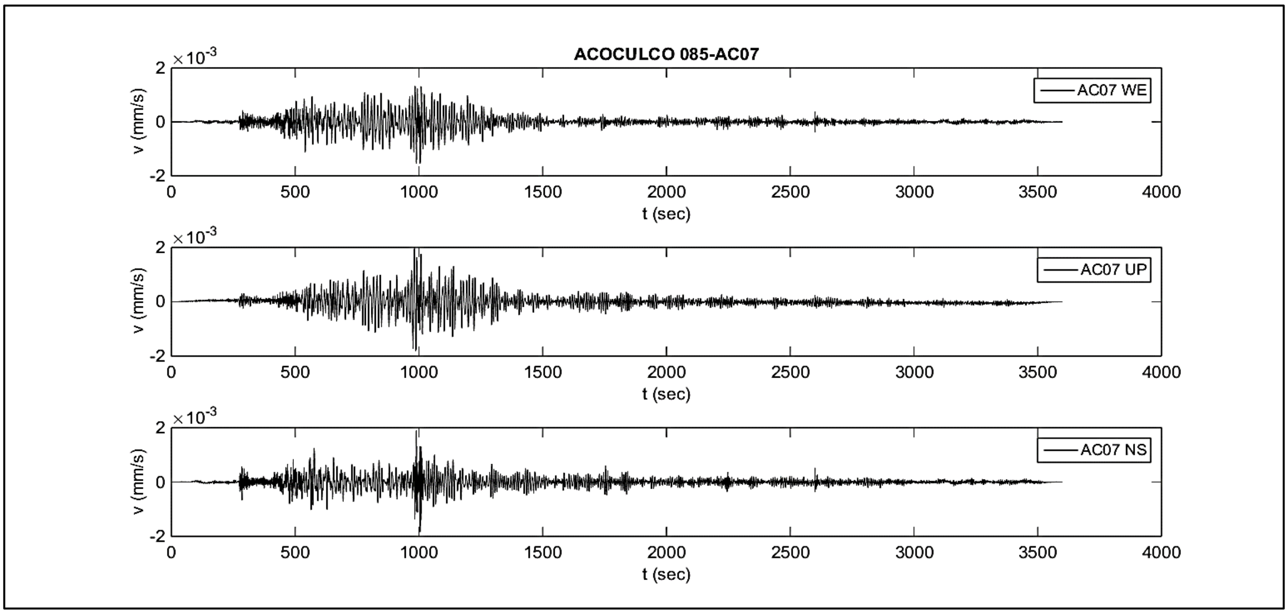
ACOCULCO 085-AC07
AC07 WE
AC07 UP
AC07 NS
v (mm/s)
t (sec)

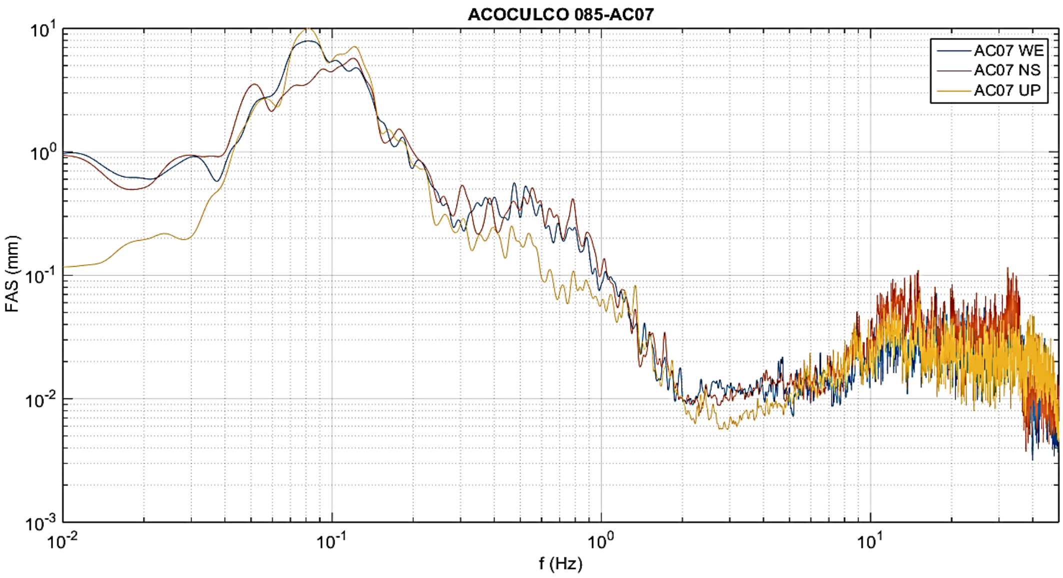
ACOCULCO 085-AC07
AC07 WE
AC07 NS
AC07 UP
FAS (mm)
f (Hz)

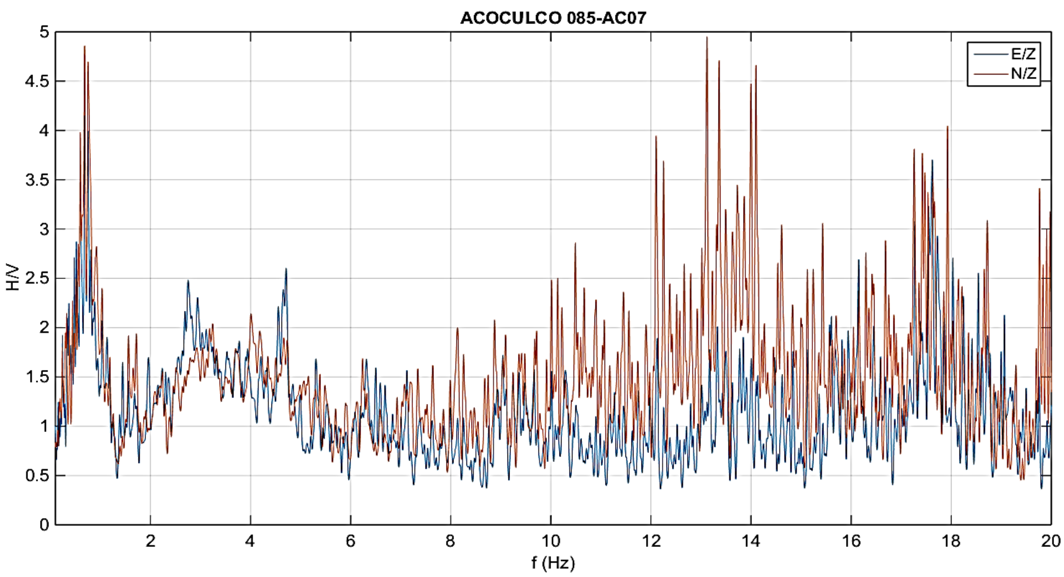
ACOCULCO 085-AC07
E/Z
N/Z
H/V
f (Hz)

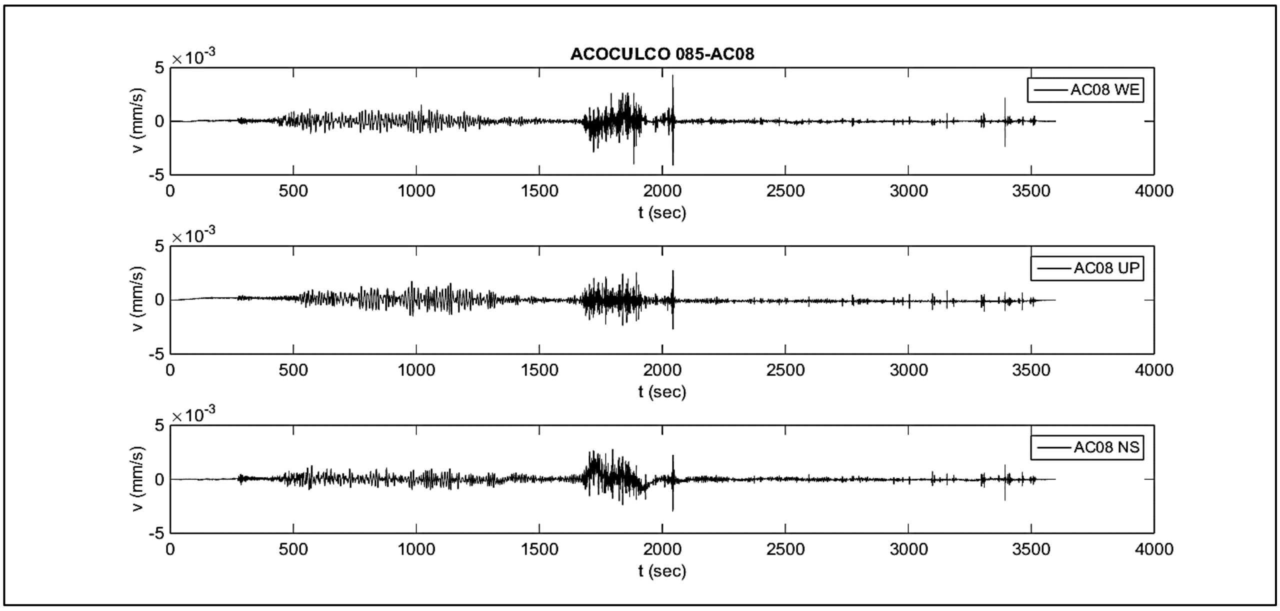
ACOCULCO 085-AC08
AC08 WE
AC08 UP
AC08 NS
v (mm/s)
t (sec)

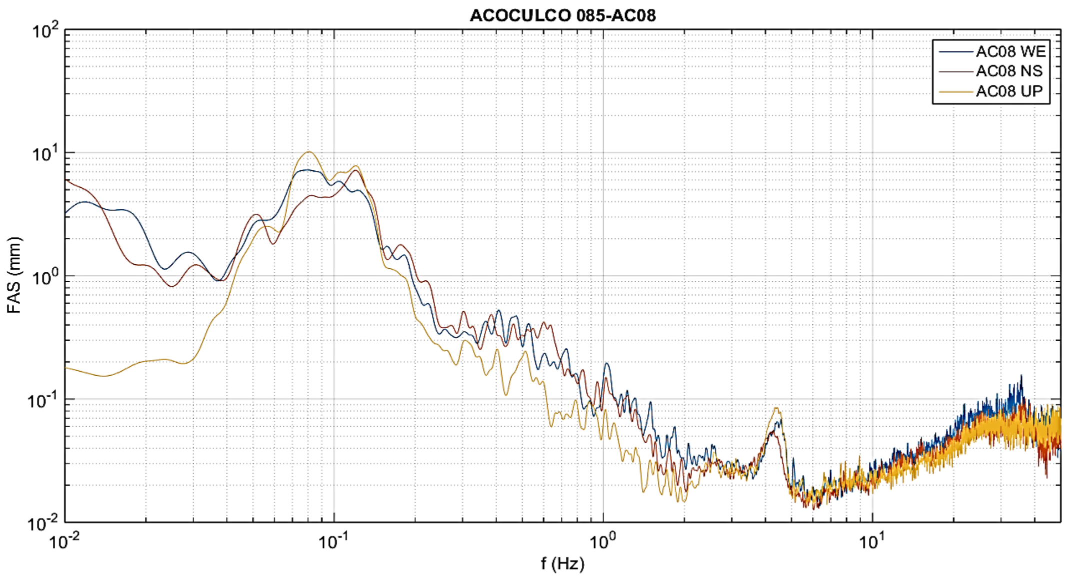
ACOCULCO 085-AC08
AC08 WE
AC08 NS
AC08 UP
FAS (mm)
f (Hz)

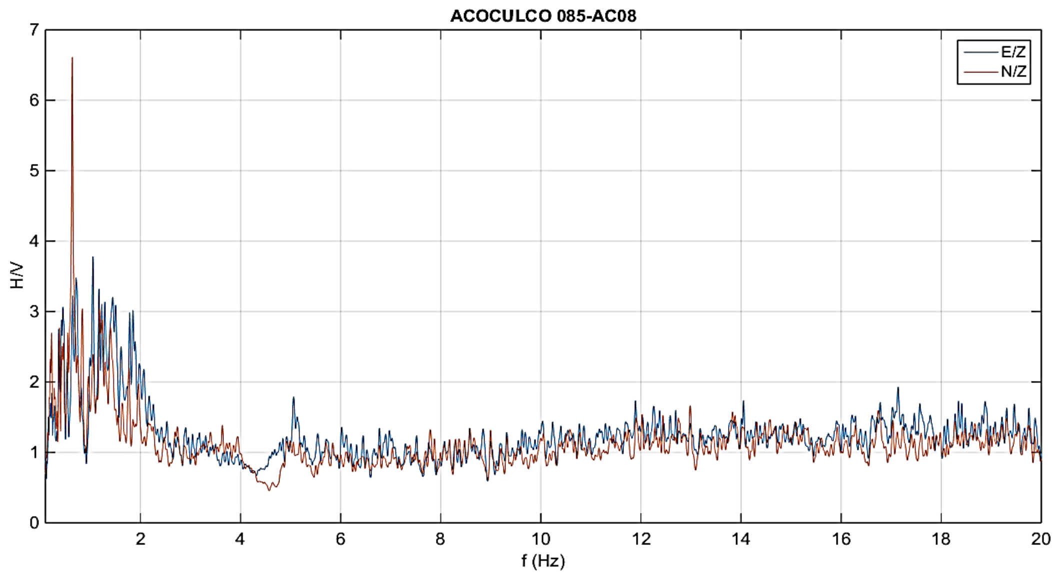
ACOCULCO 085-AC08
E/Z
N/Z
H/V
f (Hz)

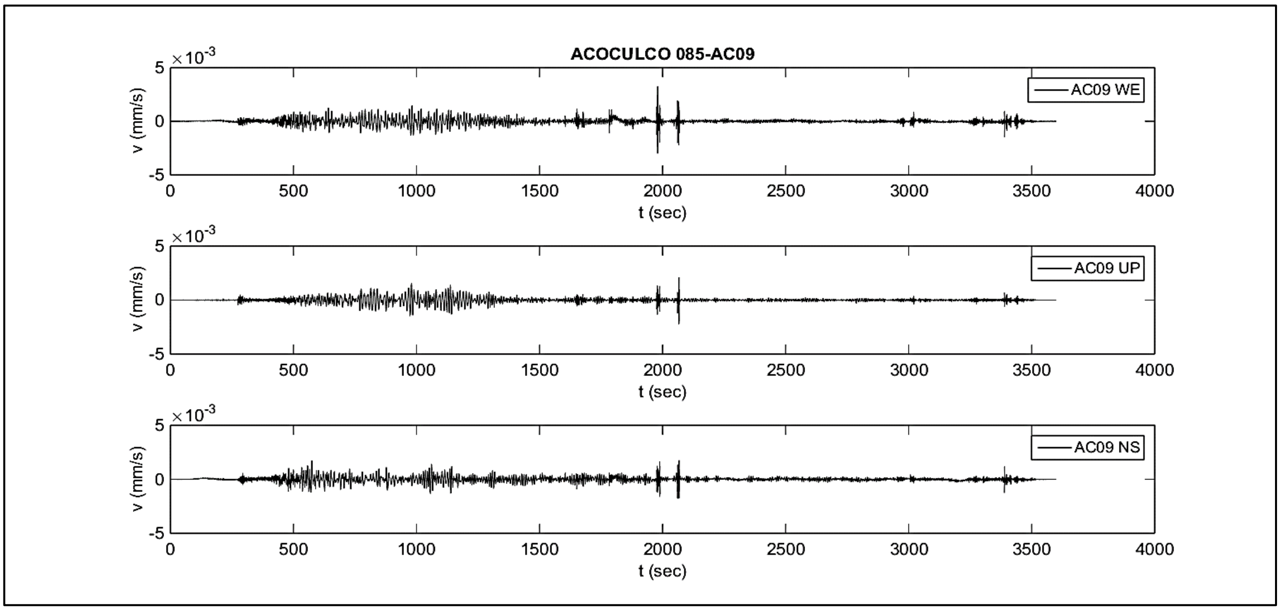
ACOCULCO 085-AC09
AC09 WE
AC09 UP
AC09 NS
v (mm/s)
t (sec)

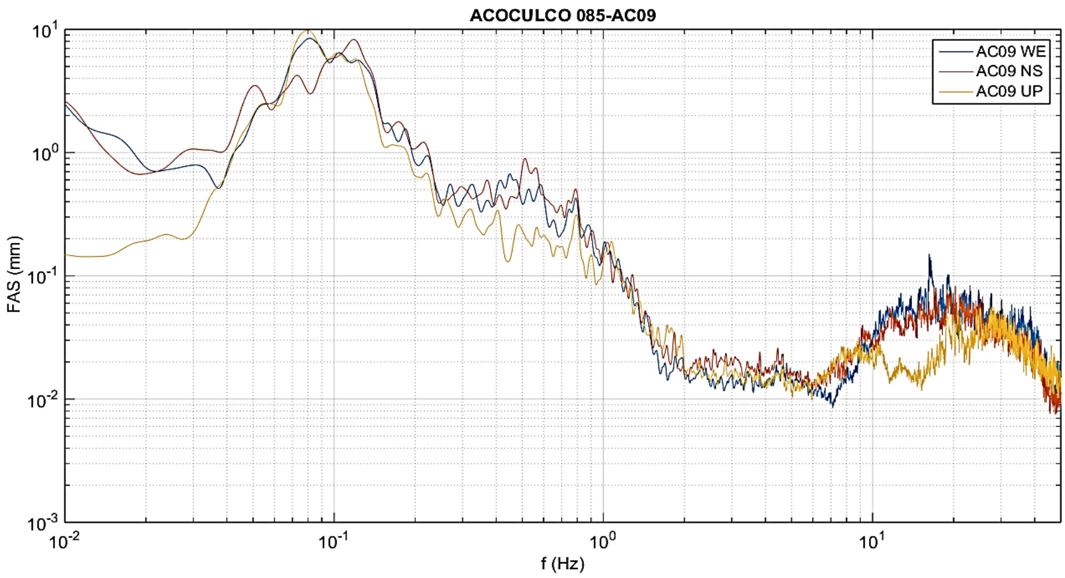
ACOCULCO 085-AC09
AC09 WE
AC09 NS
AC09 UP
FAS (mm)
f (Hz)

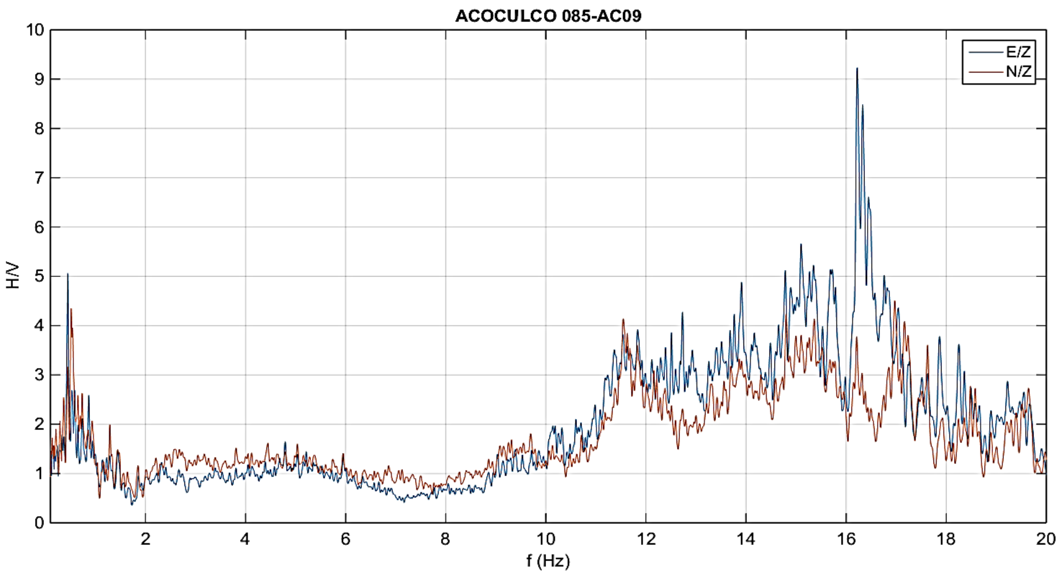
ACOCULCO 085-AC09
E/Z
N/Z
H/V
f (Hz)

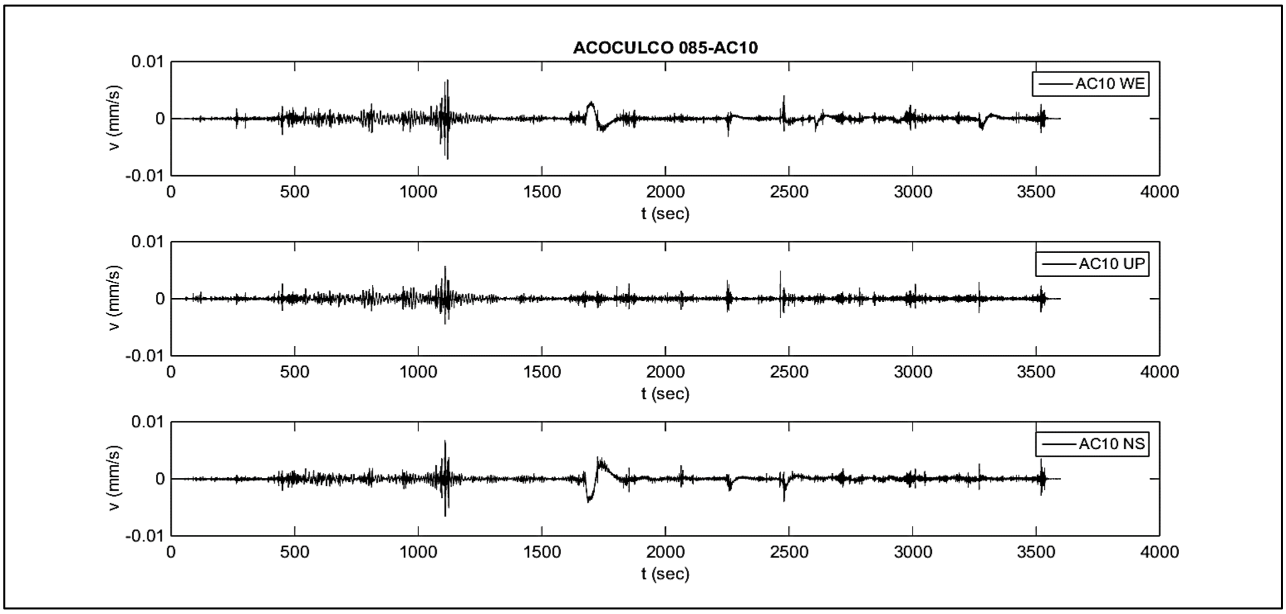
ACOCULCO 085-AC10
AC10 WE
AC10 UP
AC10 NS
v (mm/s)
t (sec)

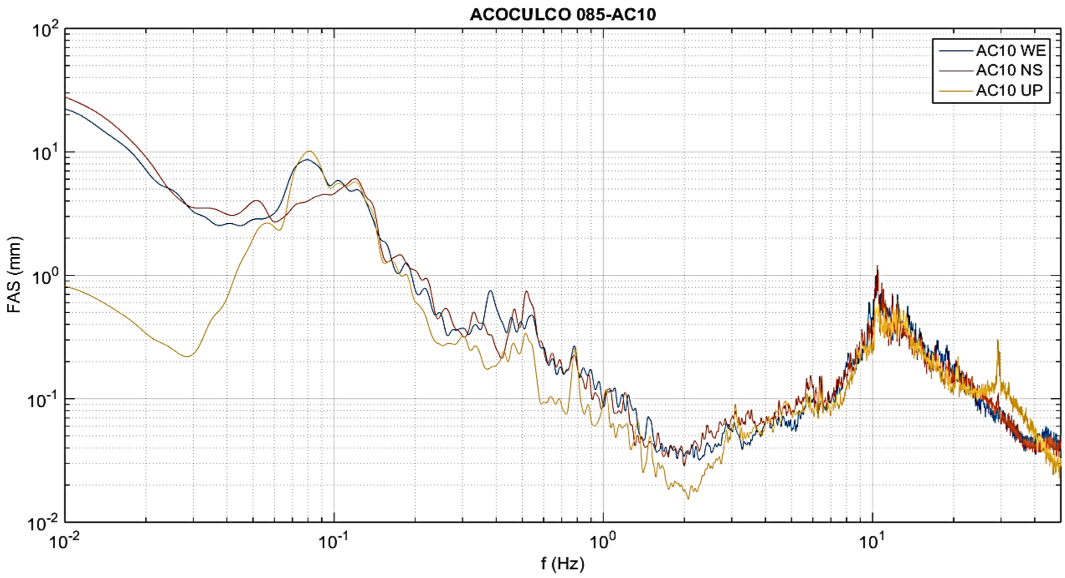
ACOCULCO 085-AC10
AC10 WE
AC10 NS
AC10 UP
FAS (mm)
f (Hz)

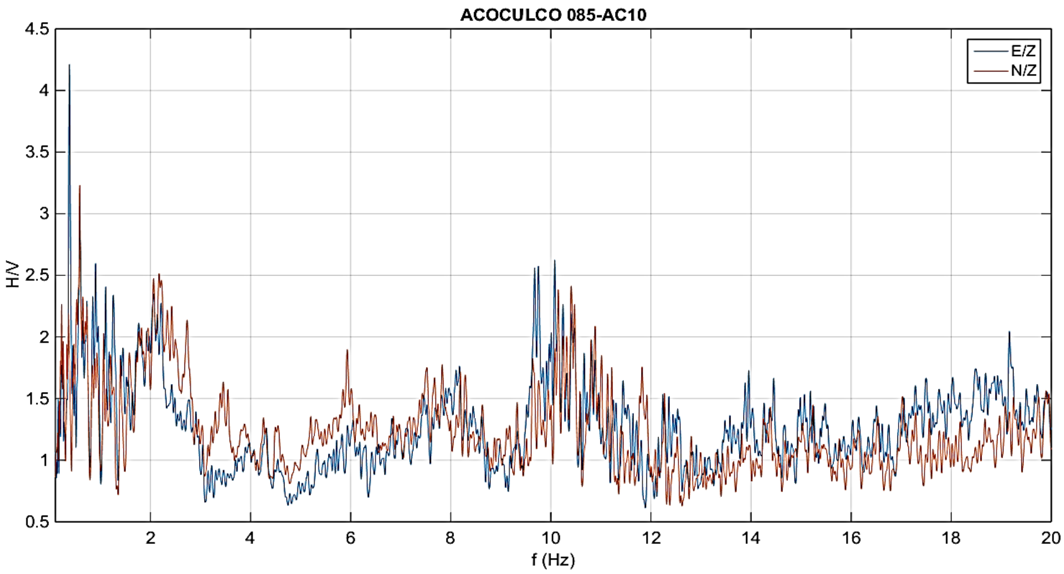
ACOCULCO 085-AC10
E/Z
N/Z
H/V
f (Hz)

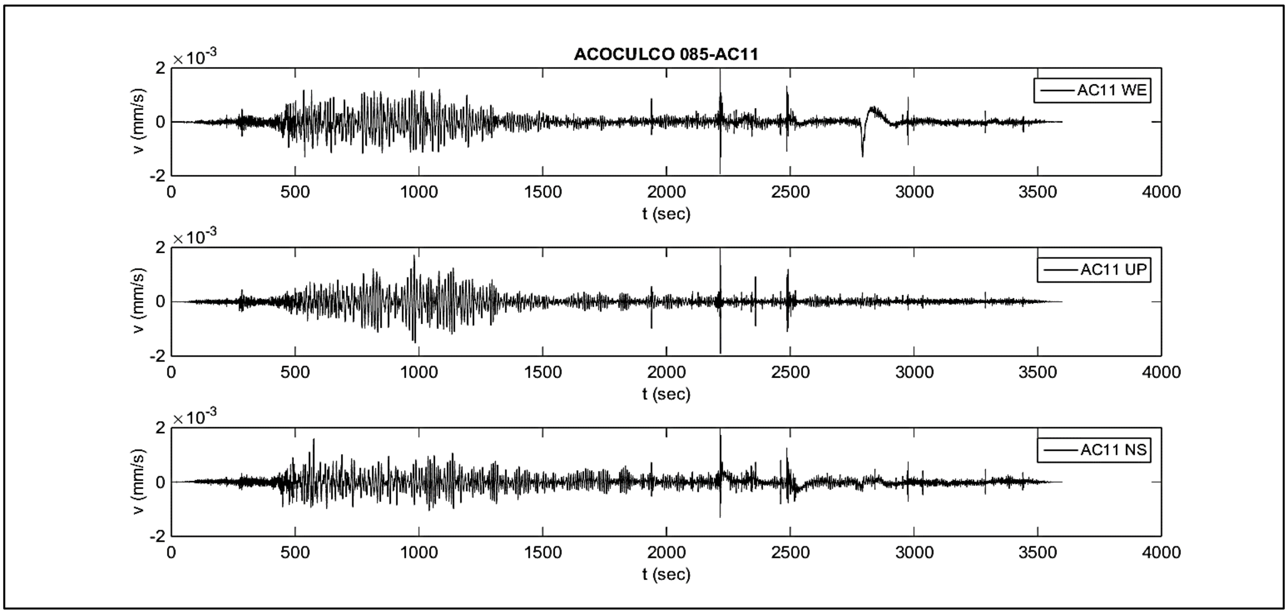
ACOCULCO 085-AC11
AC11 WE
AC11 UP
AC11 NS
v (mm/s)
t (sec)

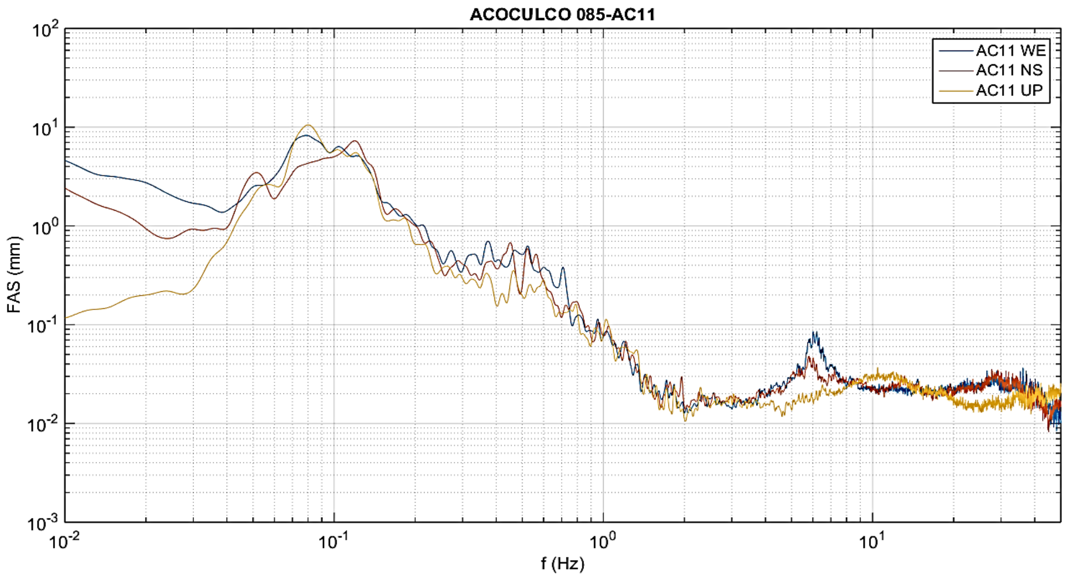
ACOCULCO 085-AC11
AC11 WE
AC11 NS
AC11 UP
FAS (mm)
f (Hz)

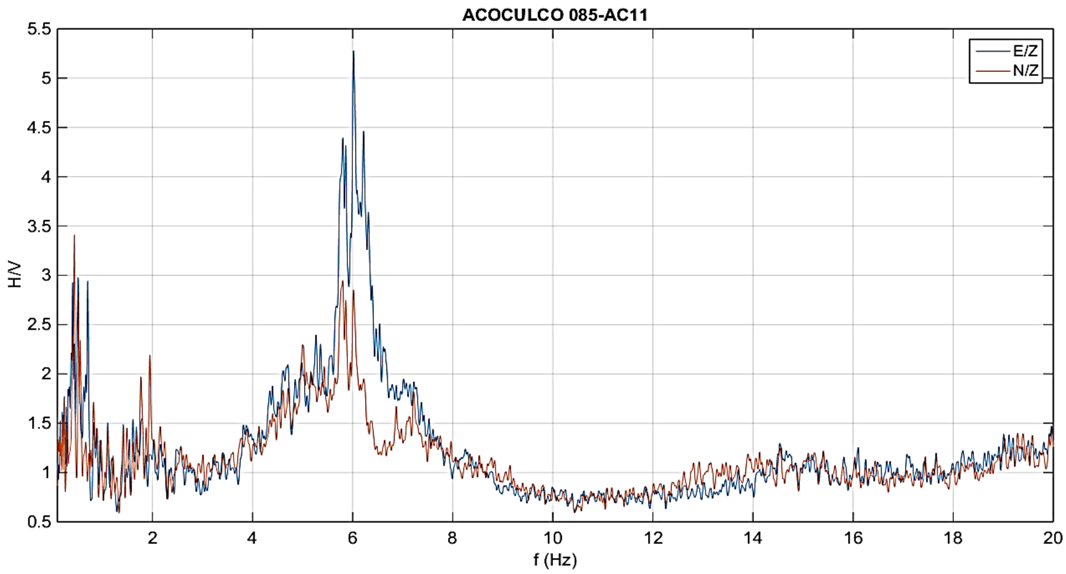
ACOCULCO 085-AC11
E/Z
N/Z
H/V
f (Hz)

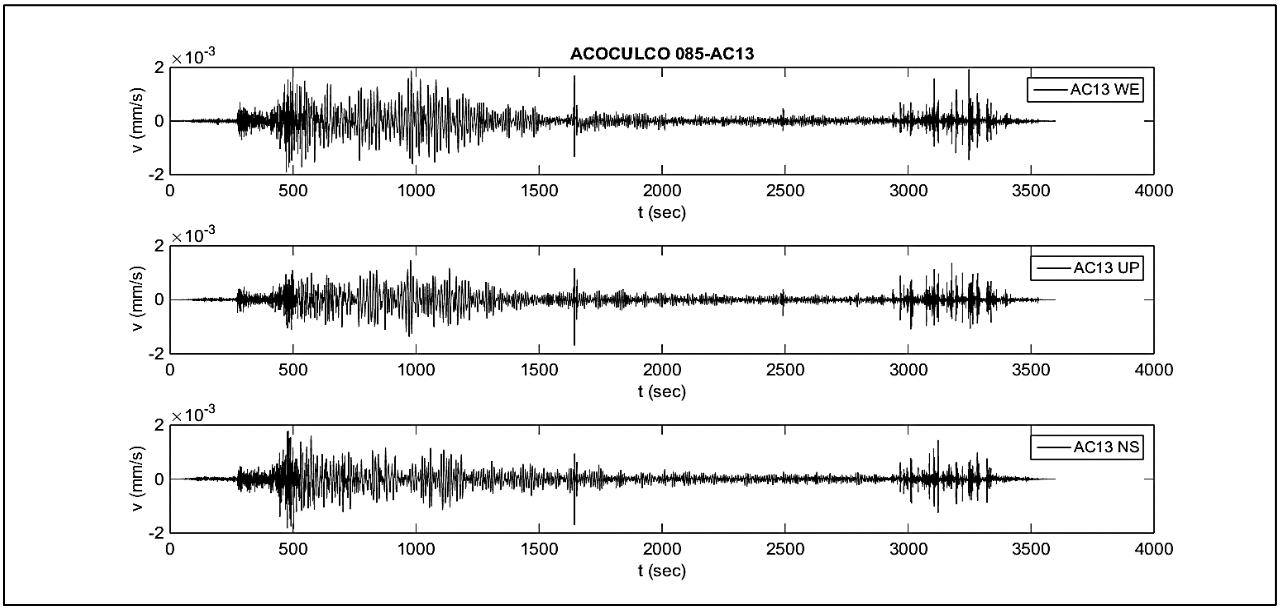
ACOCULCO 085-AC13
AC13 WE
AC13 UP
AC13 NS
v (mm/s)
t (sec)
×10^-3

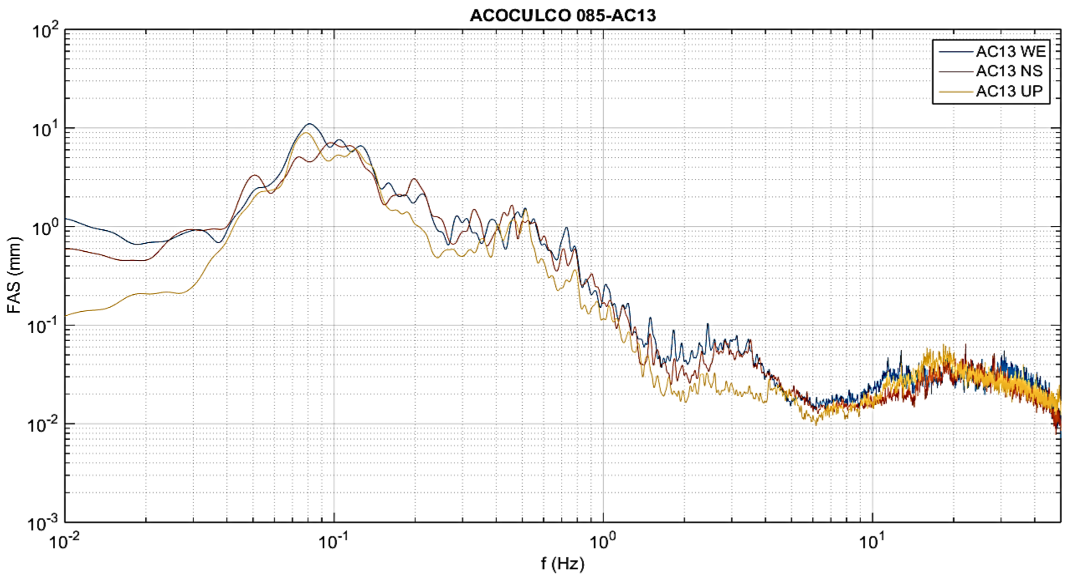
ACOCULCO 085-AC13
AC13 WE
AC13 NS
AC13 UP
FAS (mm)
f (Hz)

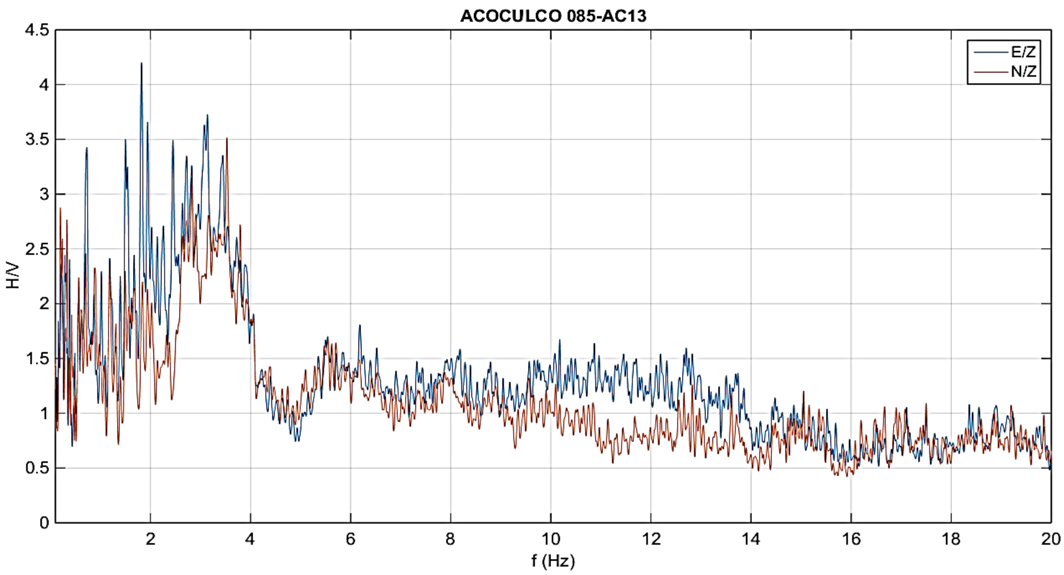
ACOCULCO 085-AC13
E/Z
N/Z
H/V
f (Hz)

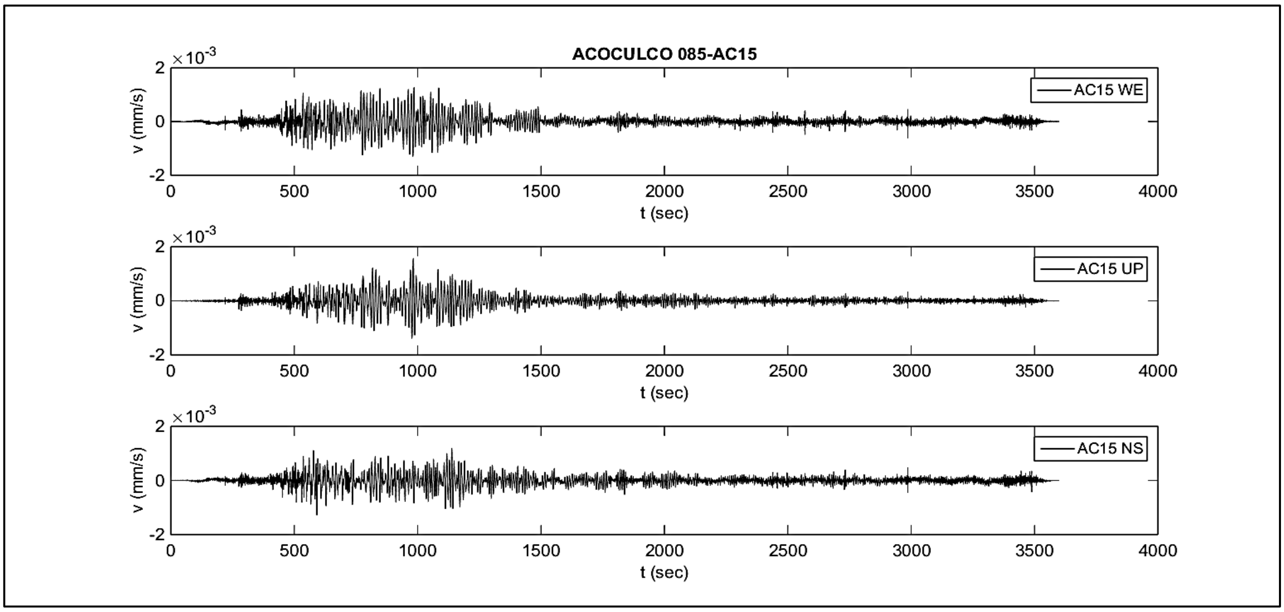

ACOCULCO 085-AC15
AC15 WE
AC15 UP
AC15 NS
v (mm/s)
t (sec)

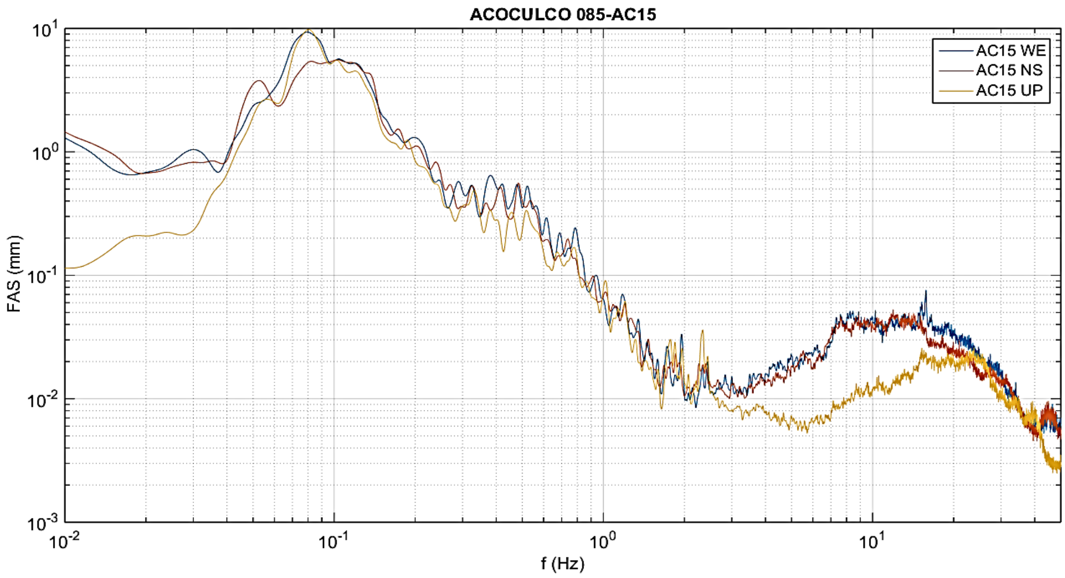

ACOCULCO 085-AC15
AC15 WE
AC15 NS
AC15 UP
FAS (mm)
f (Hz)

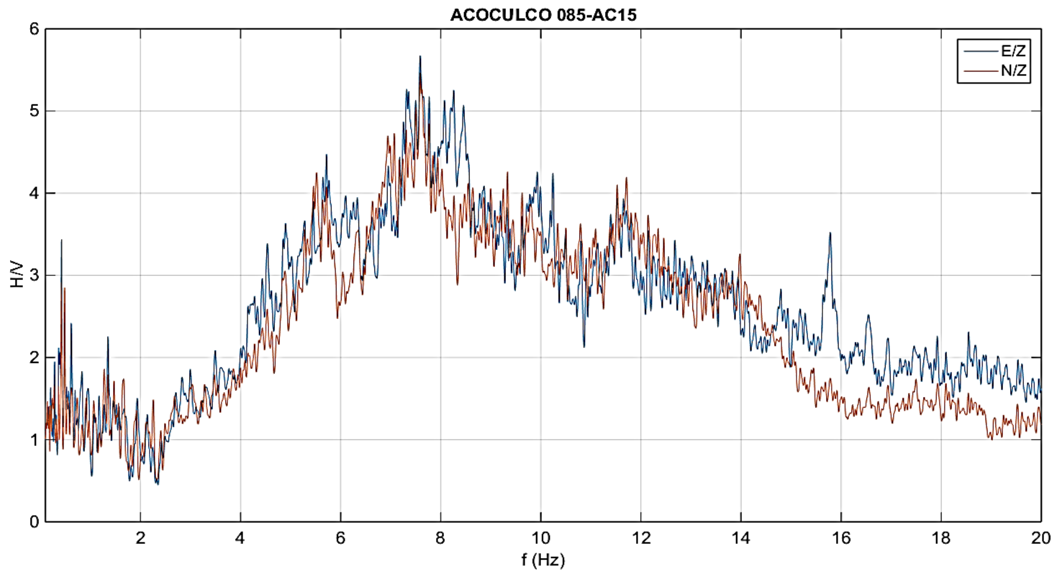

ACOCULCO 085-AC15
E/Z
N/Z
H/V
f (Hz)

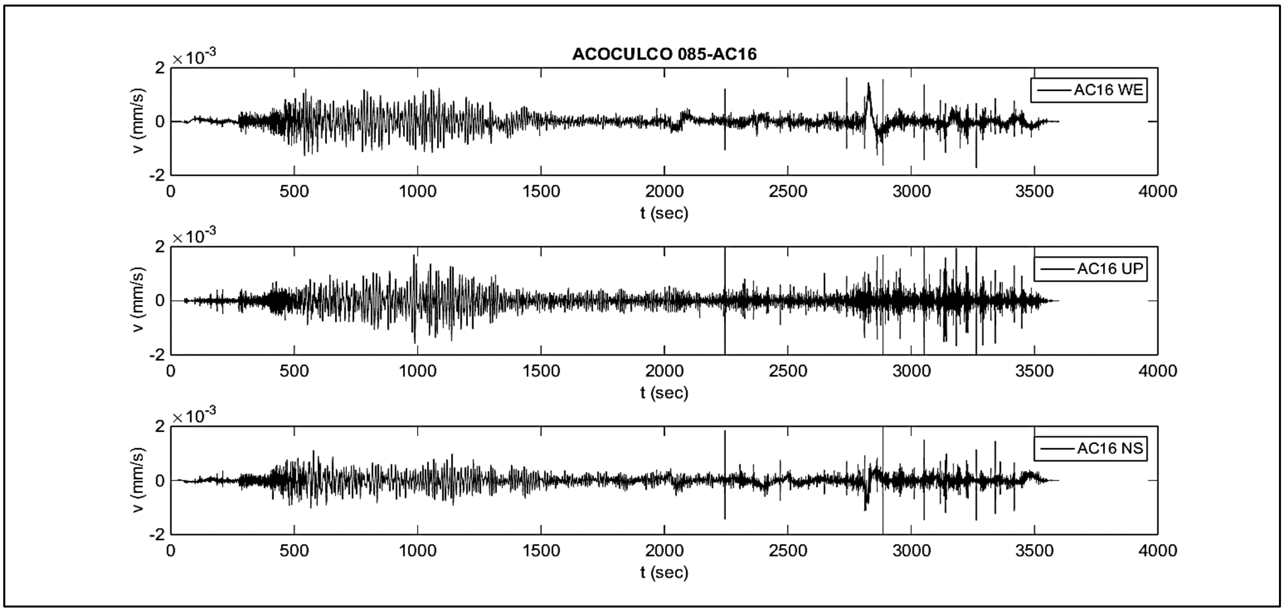
ACOCULCO 085-AC16
AC16 WE
AC16 UP
AC16 NS
v (mm/s)
t (sec)

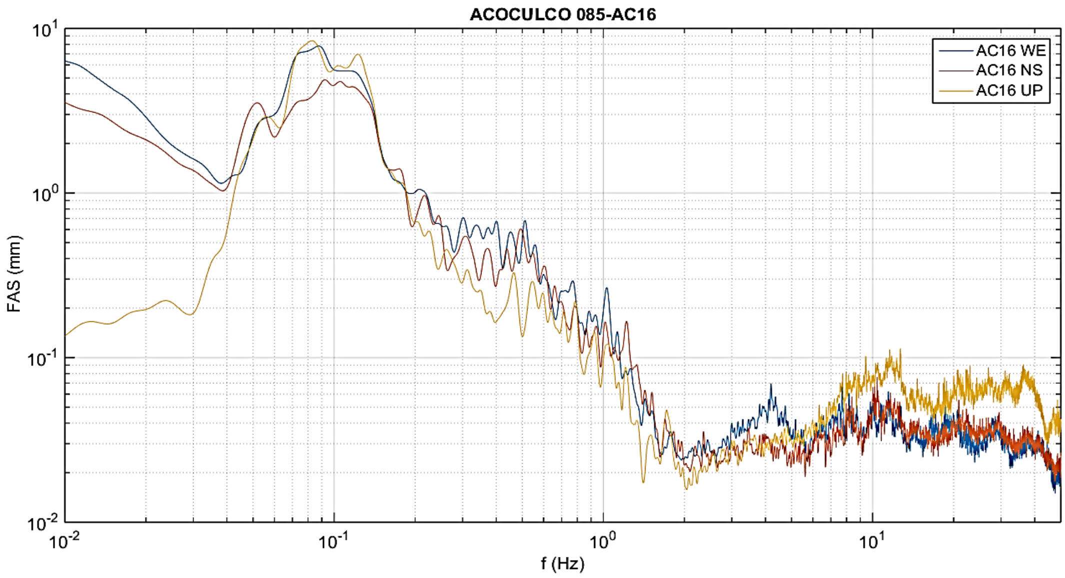
ACOCULCO 085-AC16
AC16 WE
AC16 NS
AC16 UP
FAS (mm)
f (Hz)

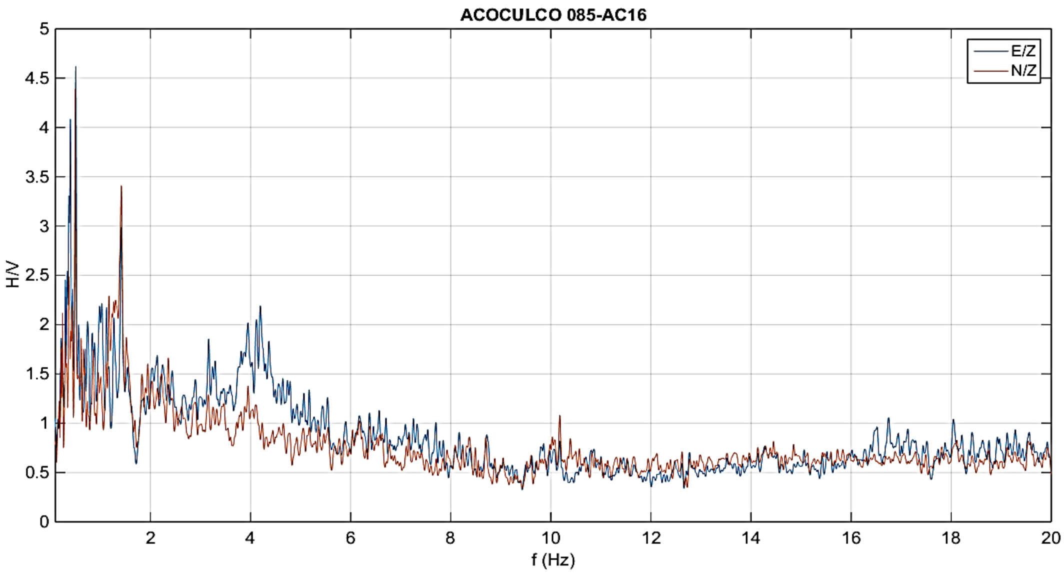
ACOCULCO 085-AC16
E/Z
N/Z
H/V
f (Hz)

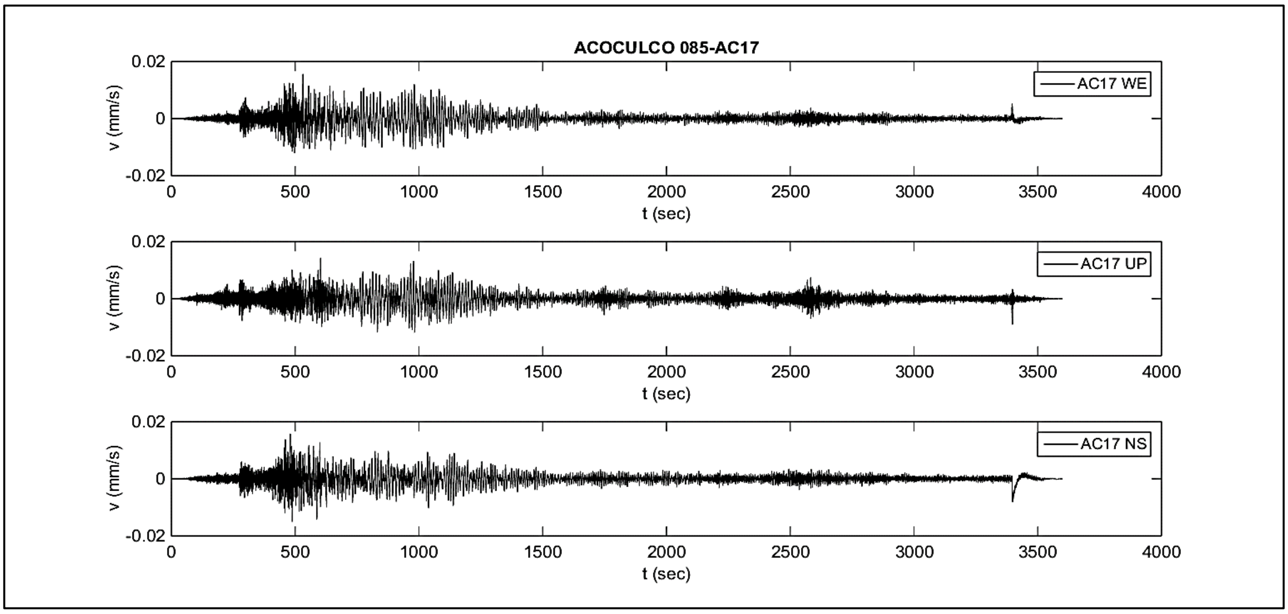
ACOCULCO 085-AC17
AC17 WE
AC17 UP
AC17 NS
v (mm/s)
t (sec)

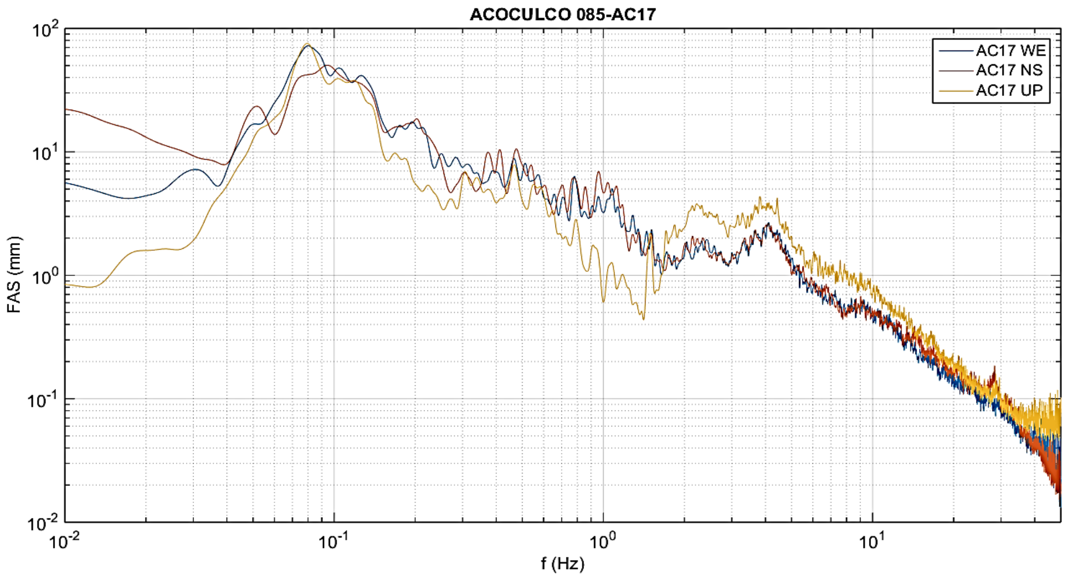
ACOCULCO 085-AC17
AC17 WE
AC17 NS
AC17 UP
FAS (mm)
f (Hz)

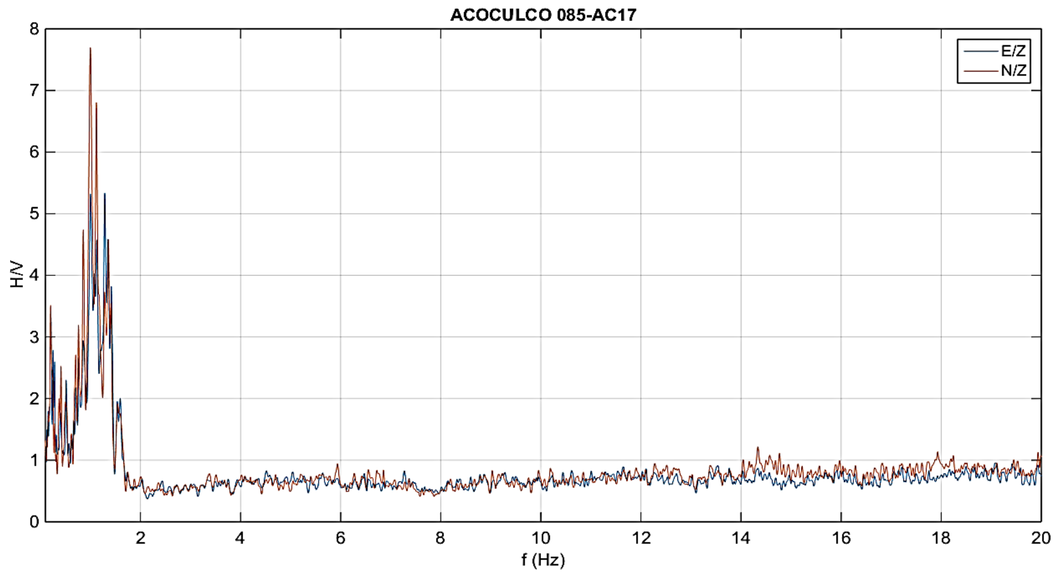
ACOCULCO 085-AC17
E/Z
N/Z
H/V
f (Hz)

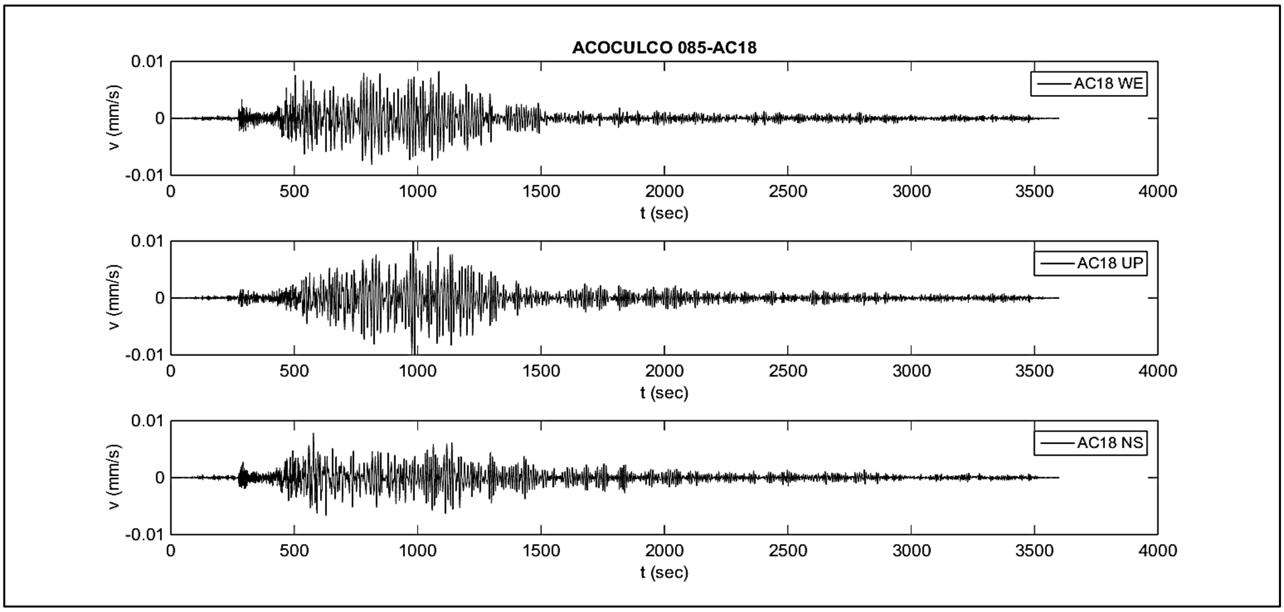
ACOCULCO 085-AC18
AC18 WE
AC18 UP
AC18 NS
v (mm/s)
t (sec)

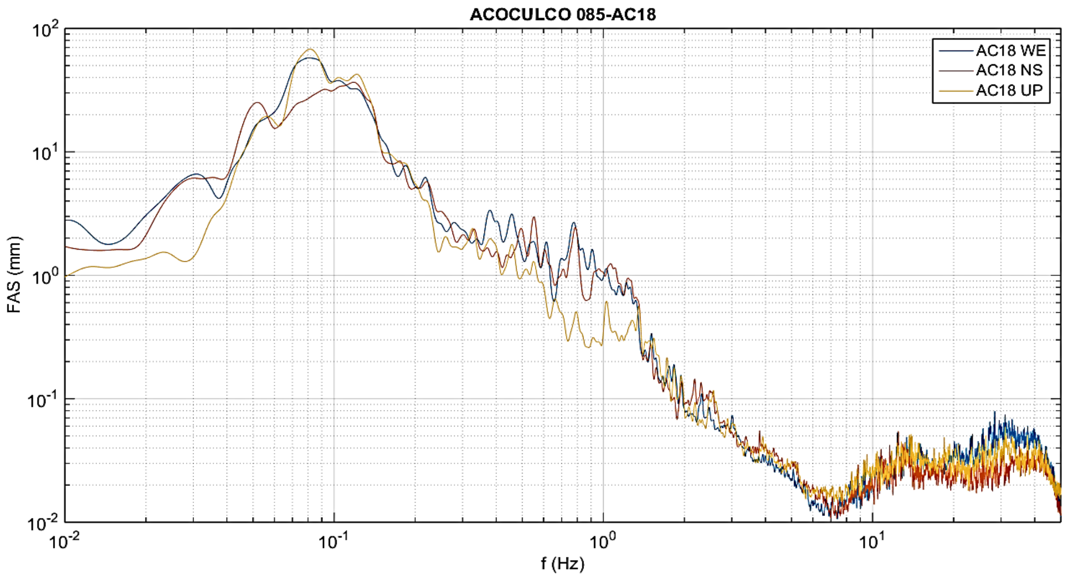
ACOCULCO 085-AC18
AC18 WE
AC18 NS
AC18 UP
FAS (mm)
f (Hz)

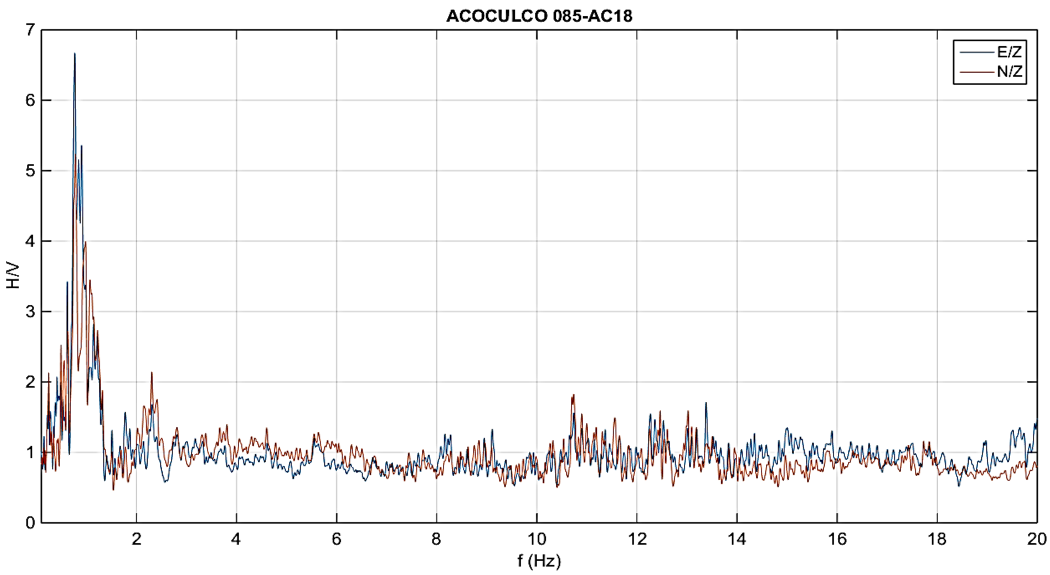
ACOCULCO 085-AC18
E/Z
N/Z
H/V
f (Hz)

Appendix 4-G Day 086, Earthquake. Time histories, spectra and spectral ratios

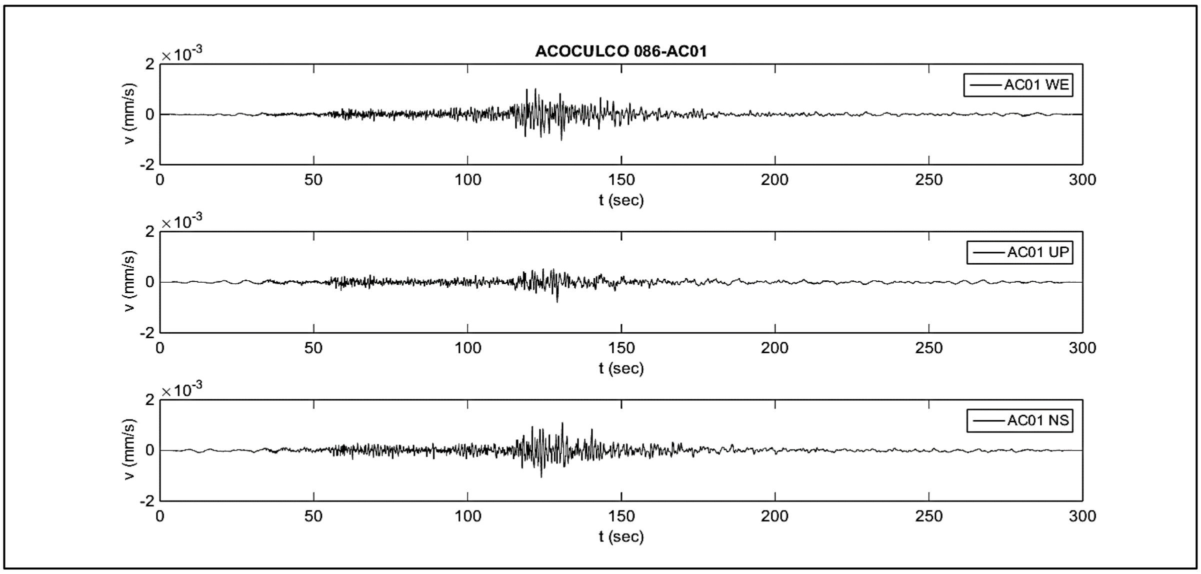

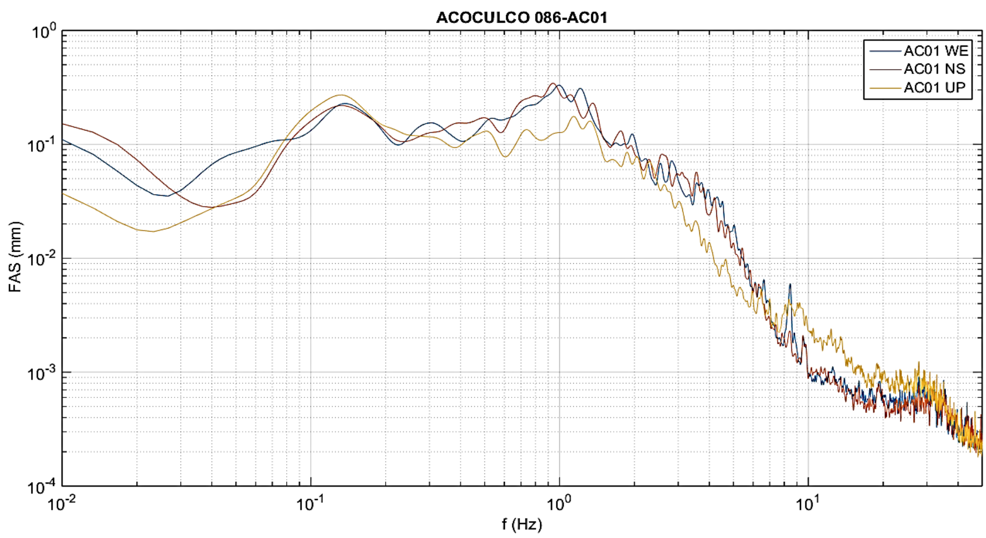

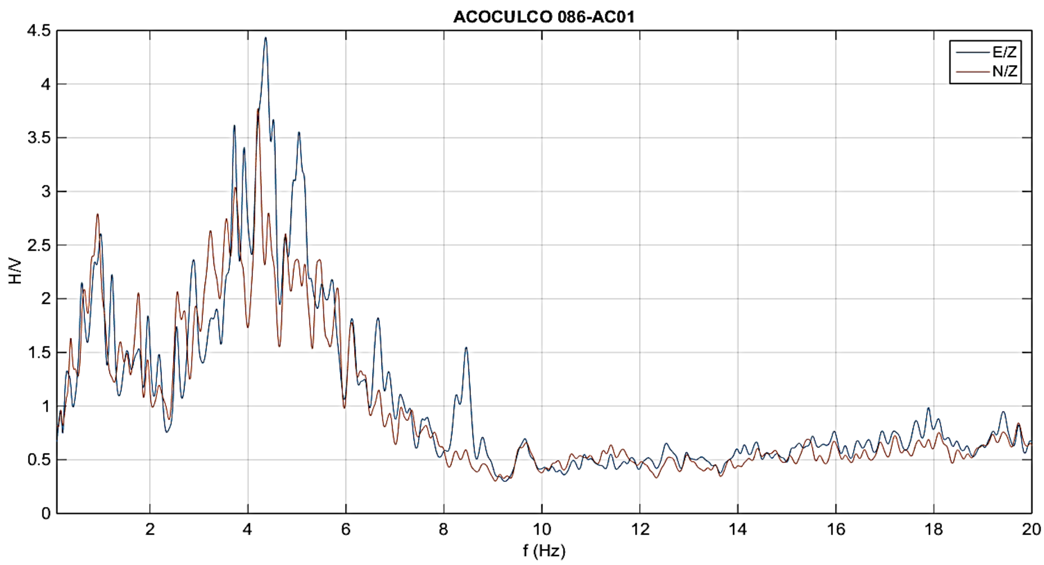

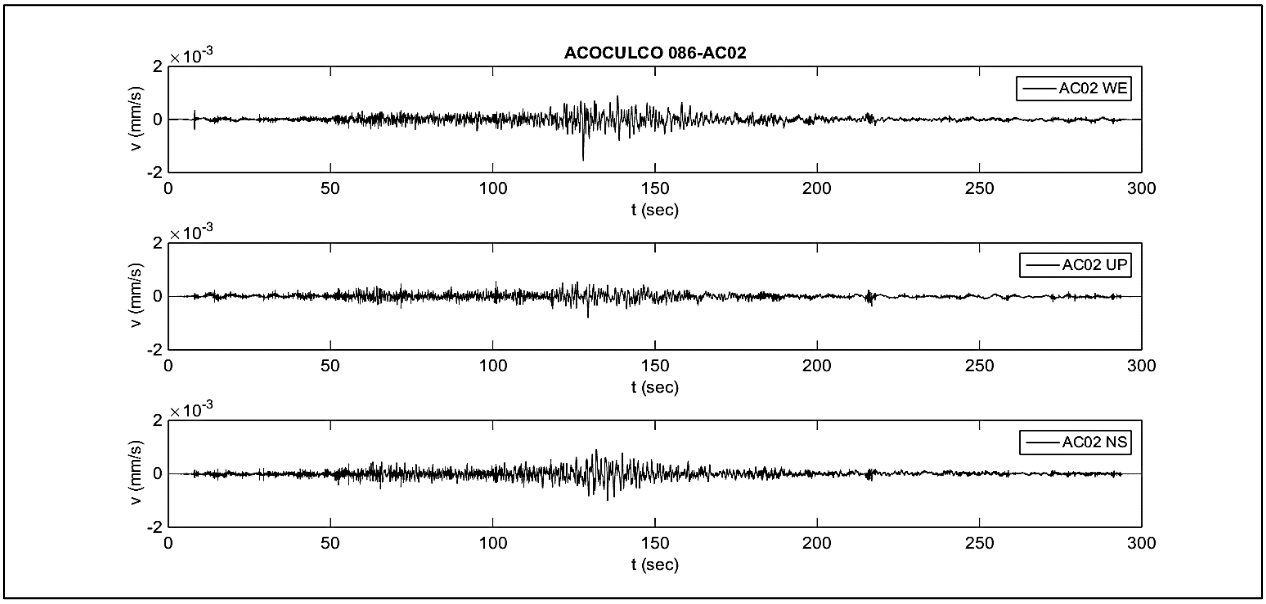
ACOCULCO 086-AC02
AC02 WE
AC02 UP
AC02 NS
v (mm/s)
t (sec)

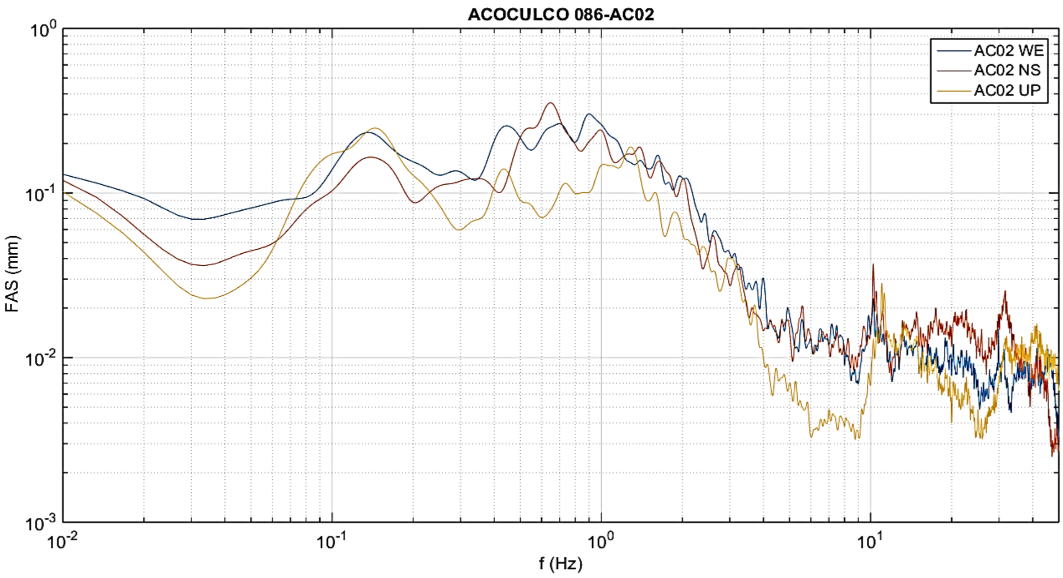
ACOCULCO 086-AC02
AC02 WE
AC02 NS
AC02 UP
FAS (mm)
f (Hz)

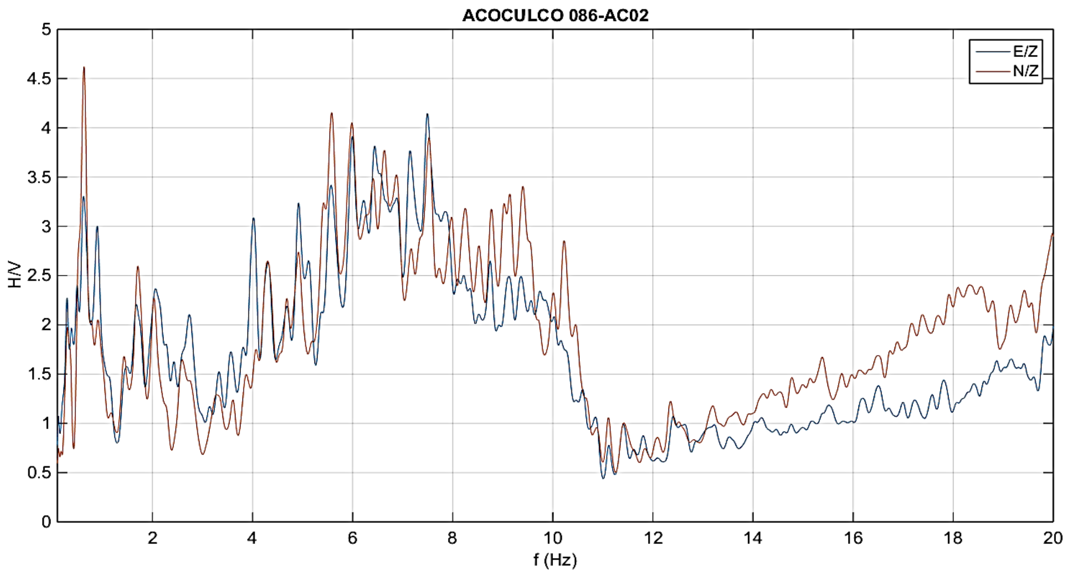
ACOCULCO 086-AC02
E/Z
N/Z
H/V
f (Hz)

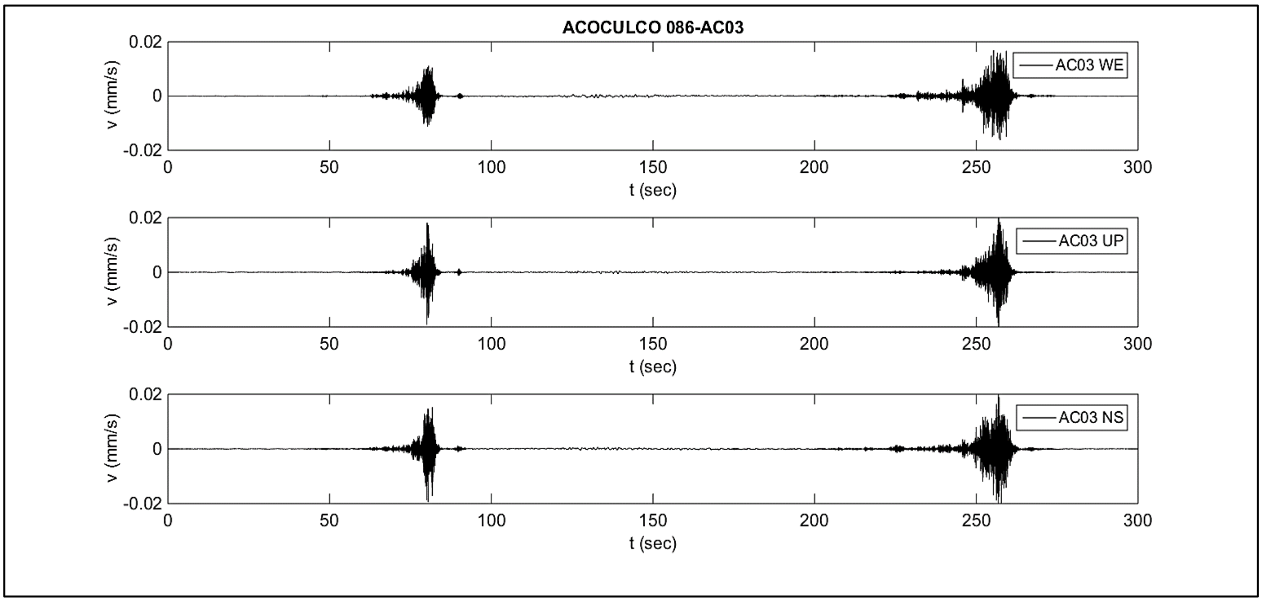

ACOCULCO 086-AC03
AC03 WE
AC03 UP
AC03 NS
v (mm/s)
t (sec)

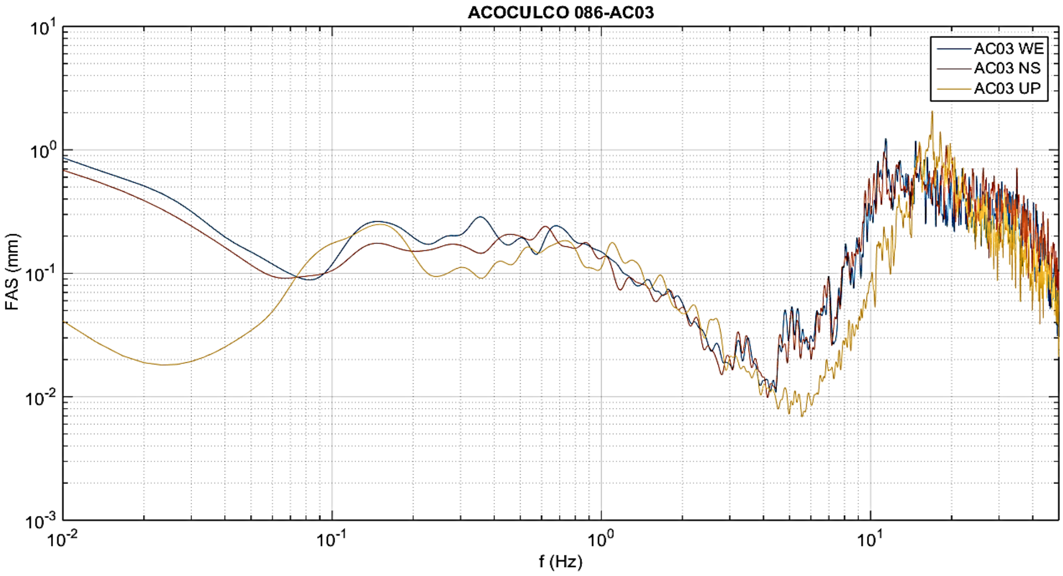

ACOCULCO 086-AC03
AC03 WE
AC03 NS
AC03 UP
FAS (mm)
f (Hz)

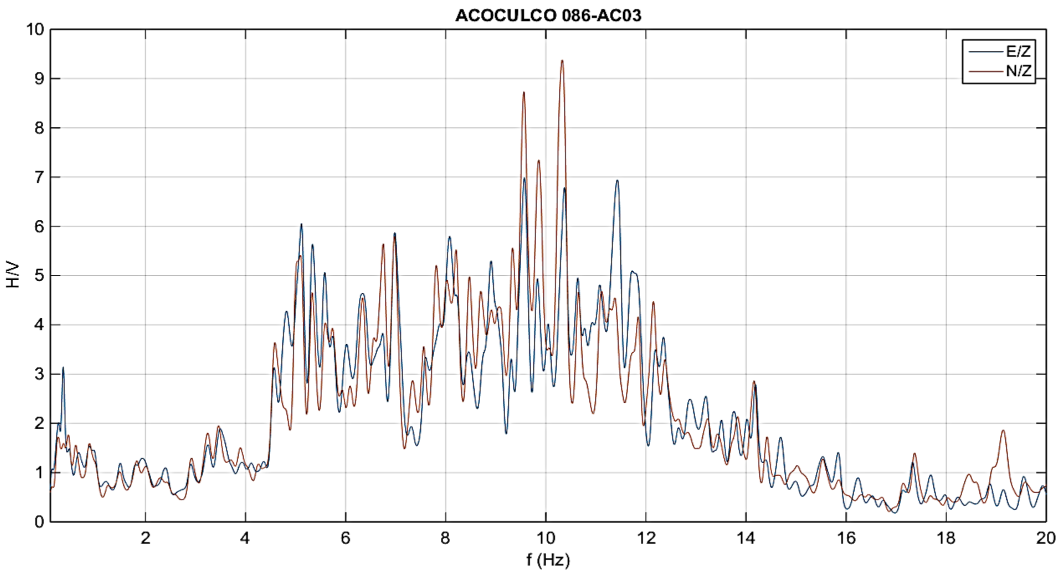

ACOCULCO 086-AC03
E/Z
N/Z
H/V
f (Hz)

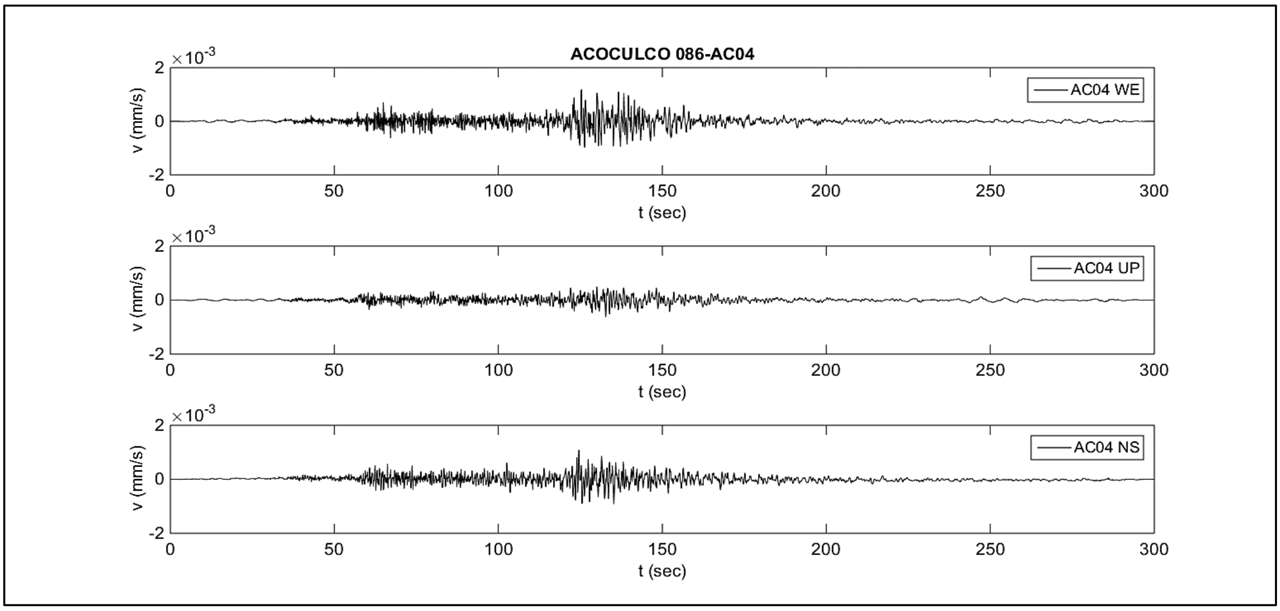
ACOCULCO 086-AC04
AC04 WE
AC04 UP
AC04 NS
v (mm/s)
t (sec)

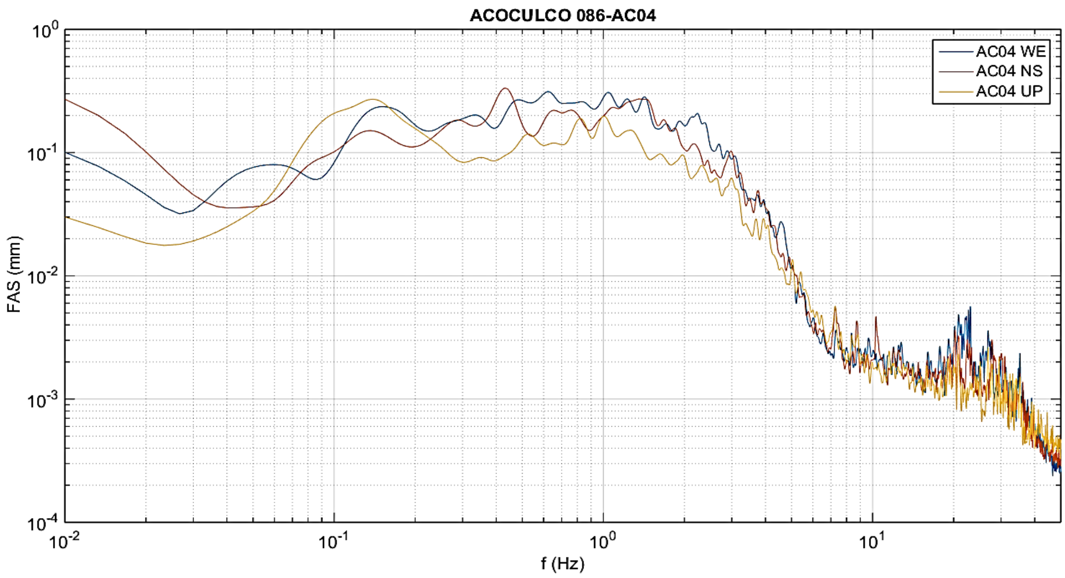
ACOCULCO 086-AC04
AC04 WE
AC04 NS
AC04 UP
FAS (mm)
f (Hz)

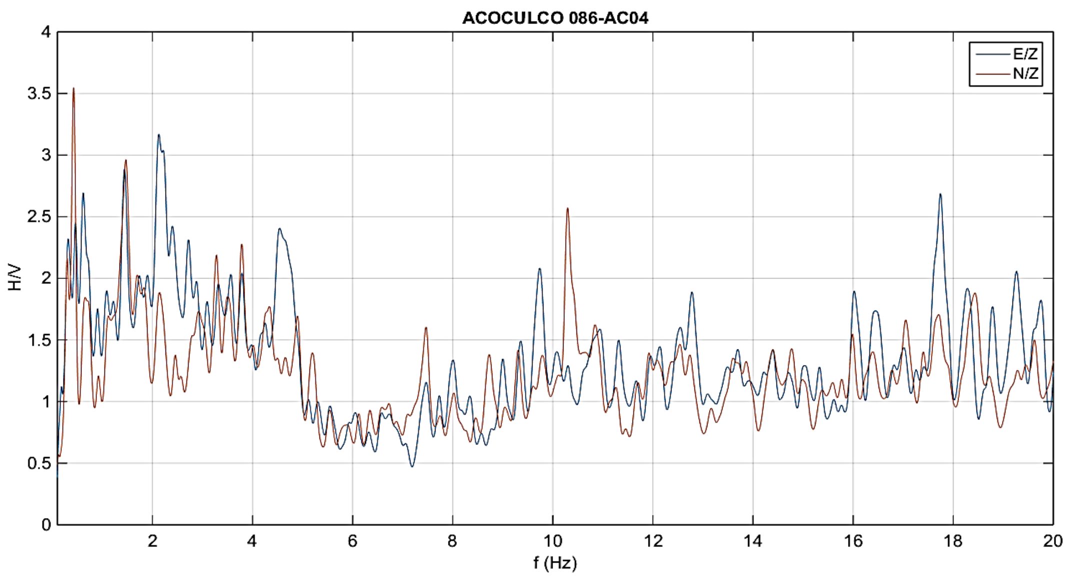
ACOCULCO 086-AC04
E/Z
N/Z
H/V
f (Hz)

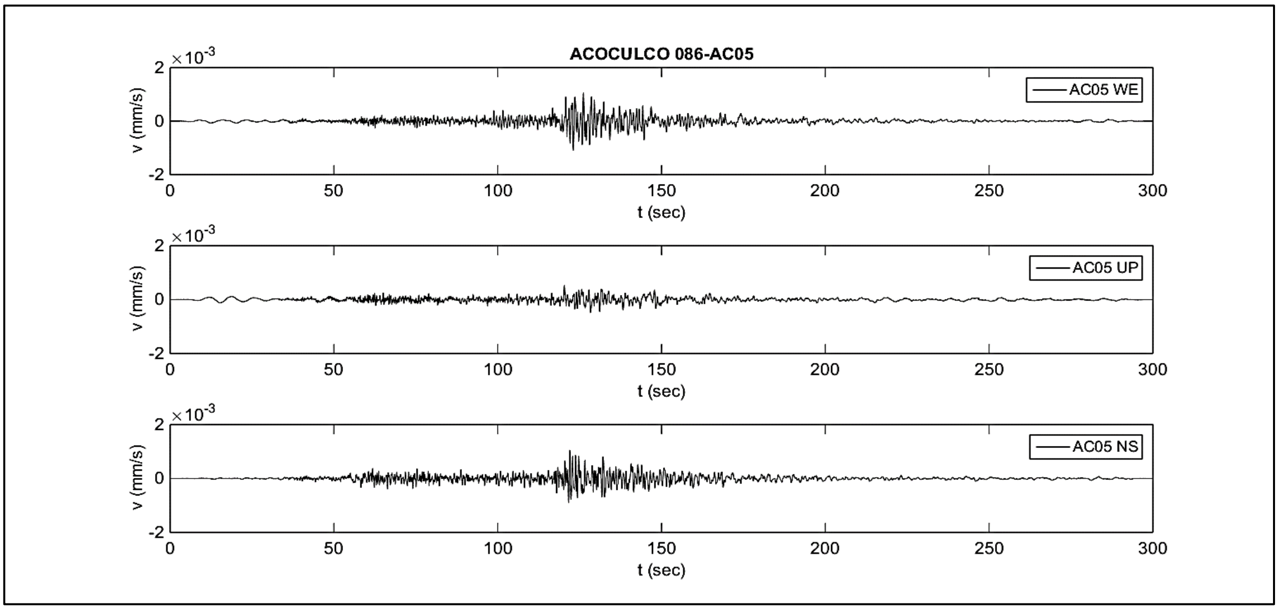
ACOCULCO 086-AC05
AC05 WE
AC05 UP
AC05 NS
v (mm/s)
t (sec)
$\times10^{-3}$

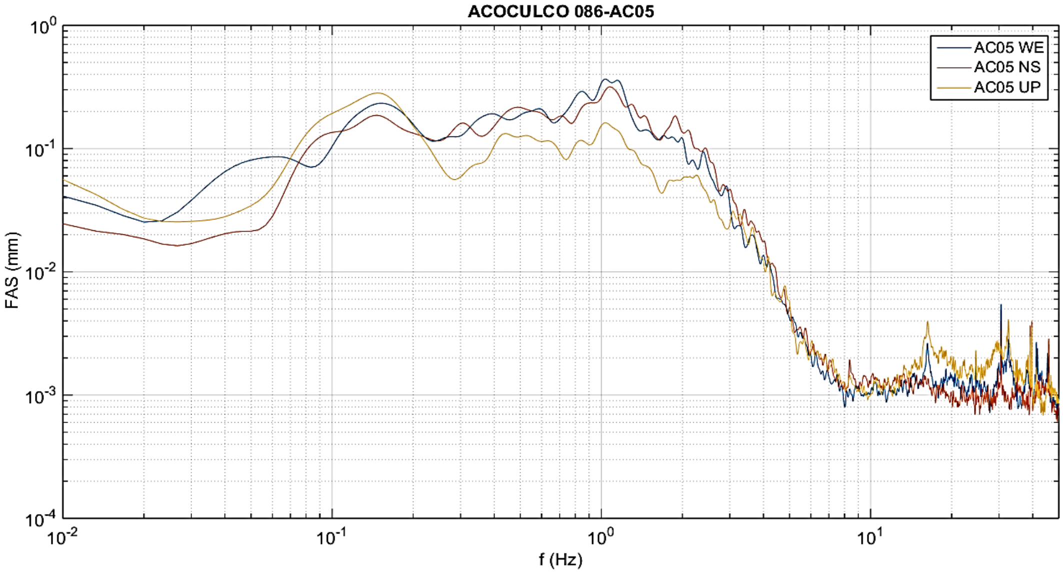
ACOCULCO 086-AC05
AC05 WE
AC05 NS
AC05 UP
FAS (mm)
f (Hz)

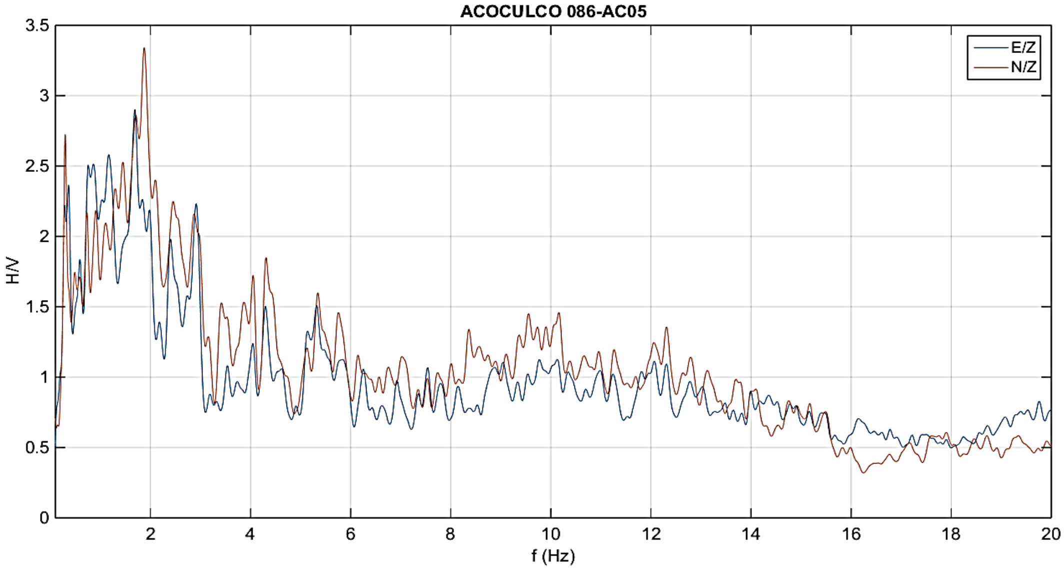
ACOCULCO 086-AC05
E/Z
N/Z
H/V
f (Hz)

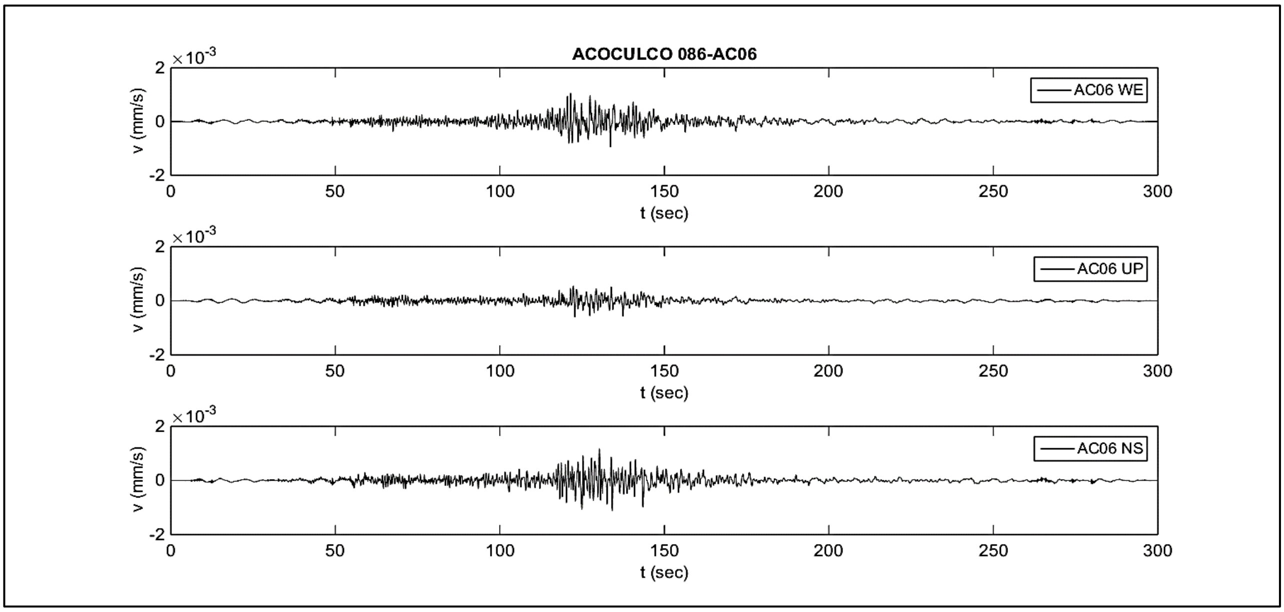
ACOCULCO 086-AC06
AC06 WE
AC06 UP
AC06 NS
v (mm/s)
t (sec)

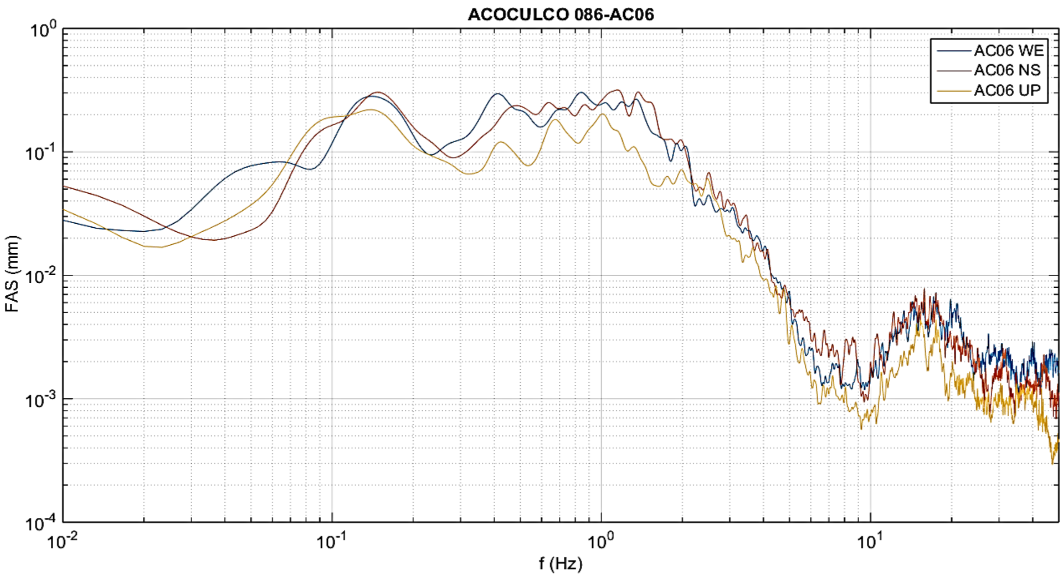
ACOCULCO 086-AC06
AC06 WE
AC06 NS
AC06 UP
FAS (mm)
f (Hz)

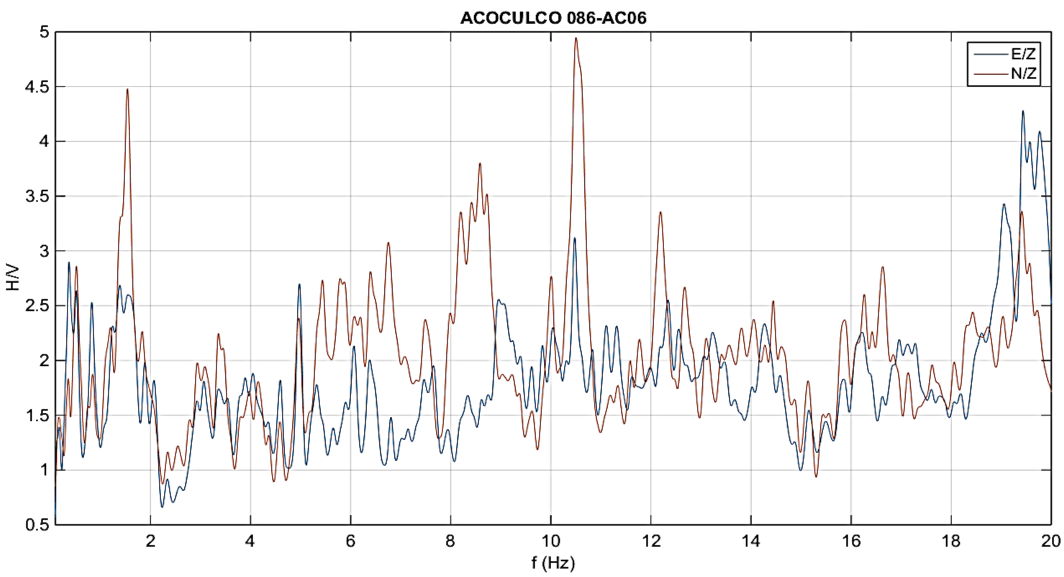
ACOCULCO 086-AC06
E/Z
N/Z
H/V
f (Hz)

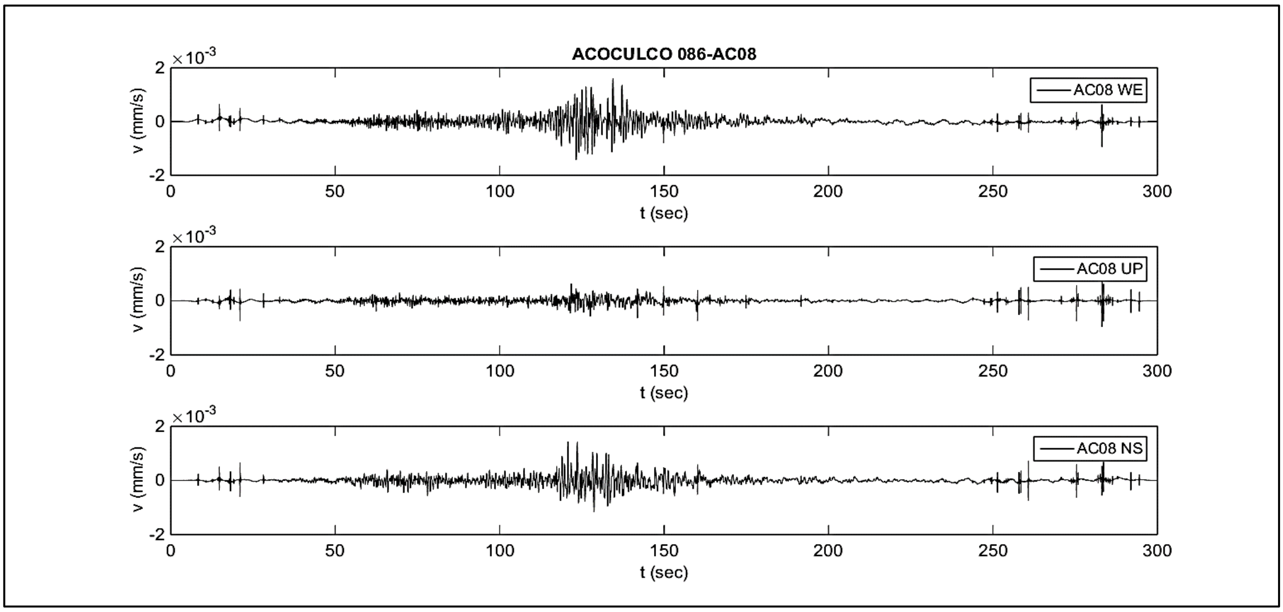
ACOCULCO 086-AC08
AC08 WE
AC08 UP
AC08 NS
v (mm/s)
t (sec)
×10-3

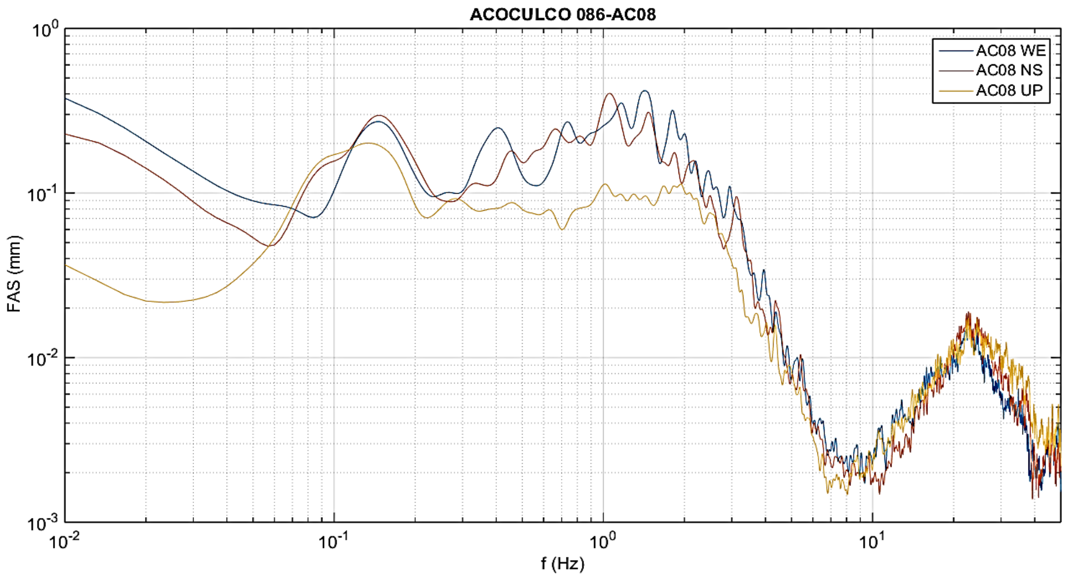
ACOCULCO 086-AC08
AC08 WE
AC08 NS
AC08 UP
FAS (mm)
f (Hz)

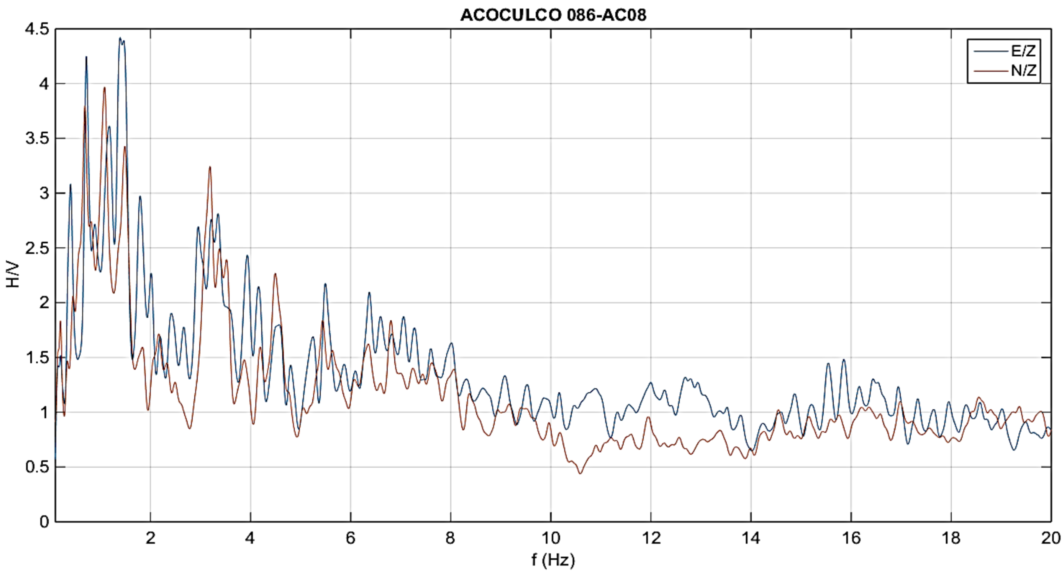
ACOCULCO 086-AC08
E/Z
N/Z
H/V
f (Hz)

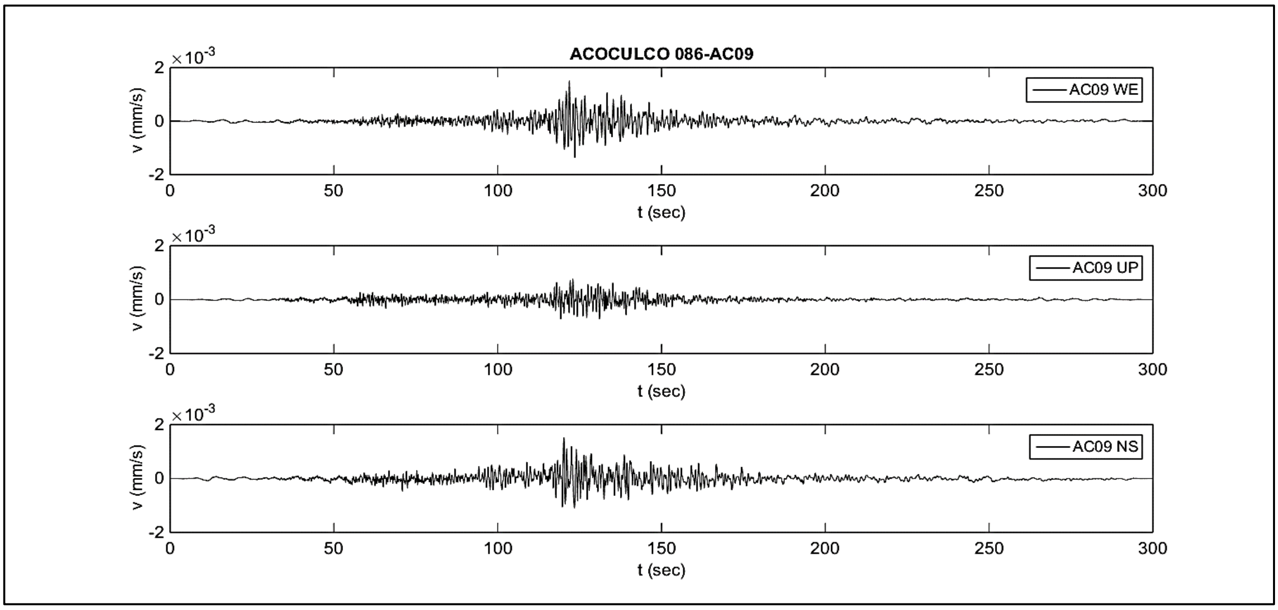
ACOCULCO 086-AC09
AC09 WE
AC09 UP
AC09 NS
v (mm/s)
t (sec)

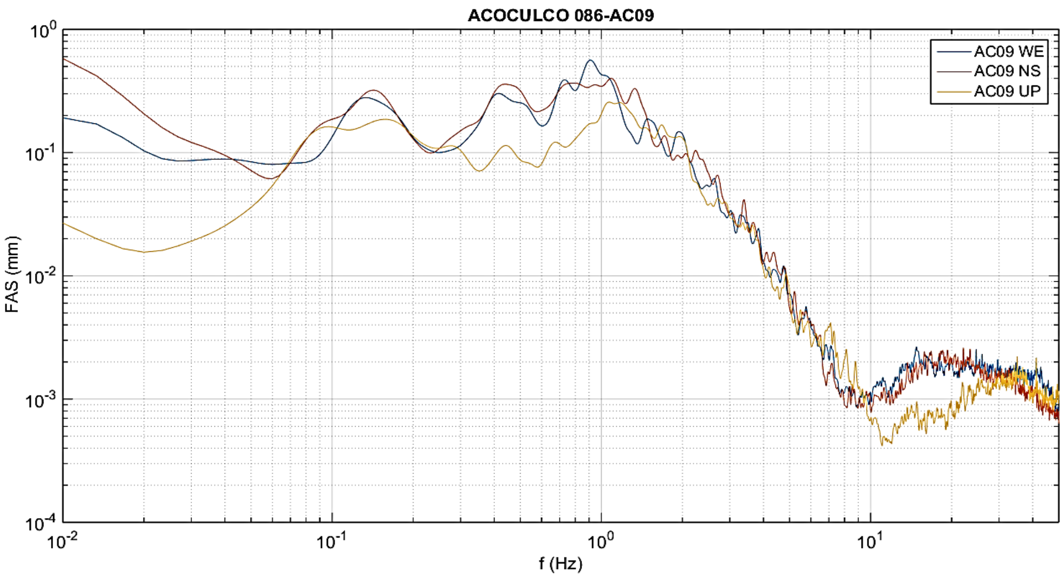
ACOCULCO 086-AC09
AC09 WE
AC09 NS
AC09 UP
FAS (mm)
f (Hz)

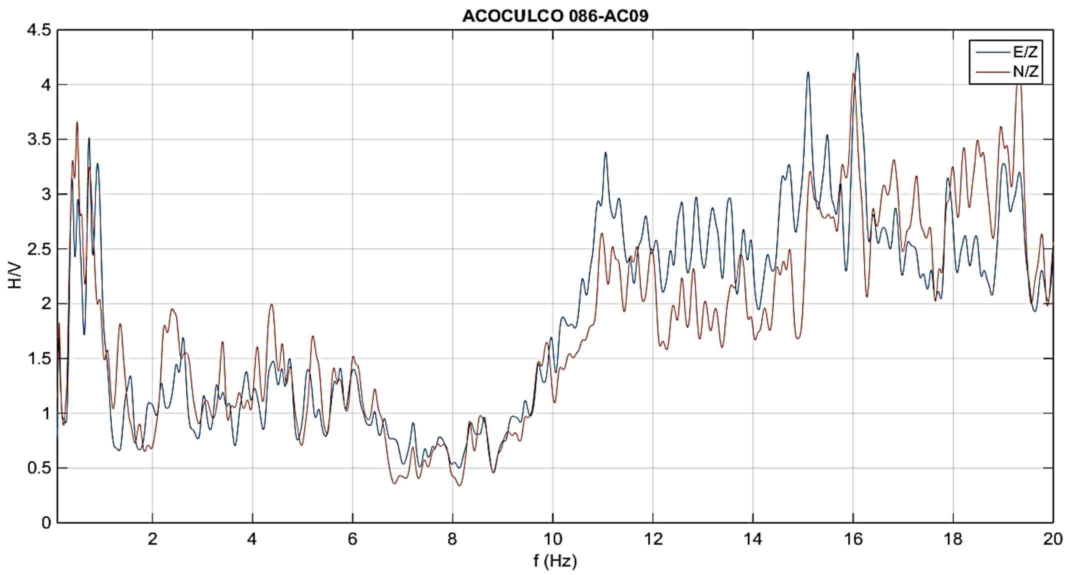
ACOCULCO 086-AC09
E/Z
N/Z
H/V
f (Hz)

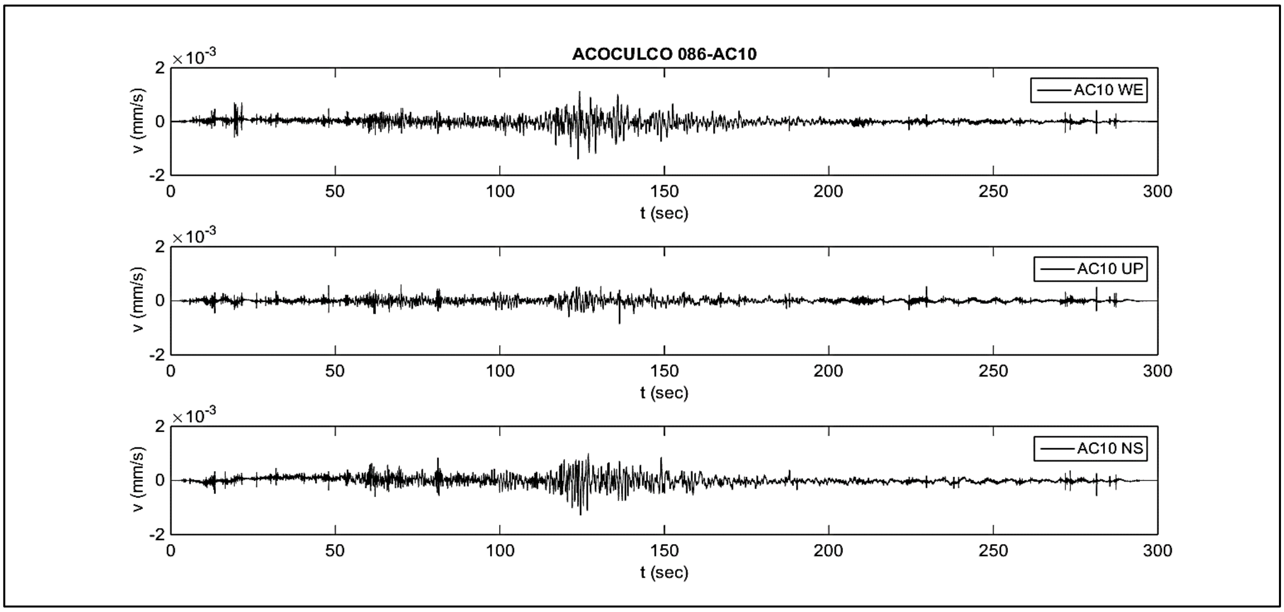
ACOCULCO 086-AC10
AC10 WE
AC10 UP
AC10 NS
v (mm/s)
t (sec)

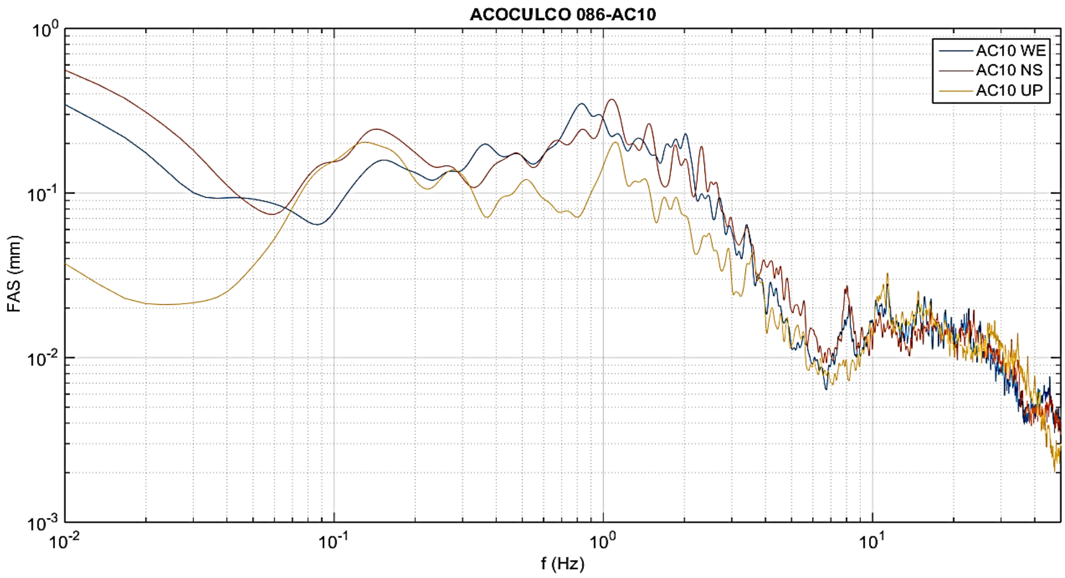
ACOCULCO 086-AC10
AC10 WE
AC10 NS
AC10 UP
FAS (mm)
f (Hz)

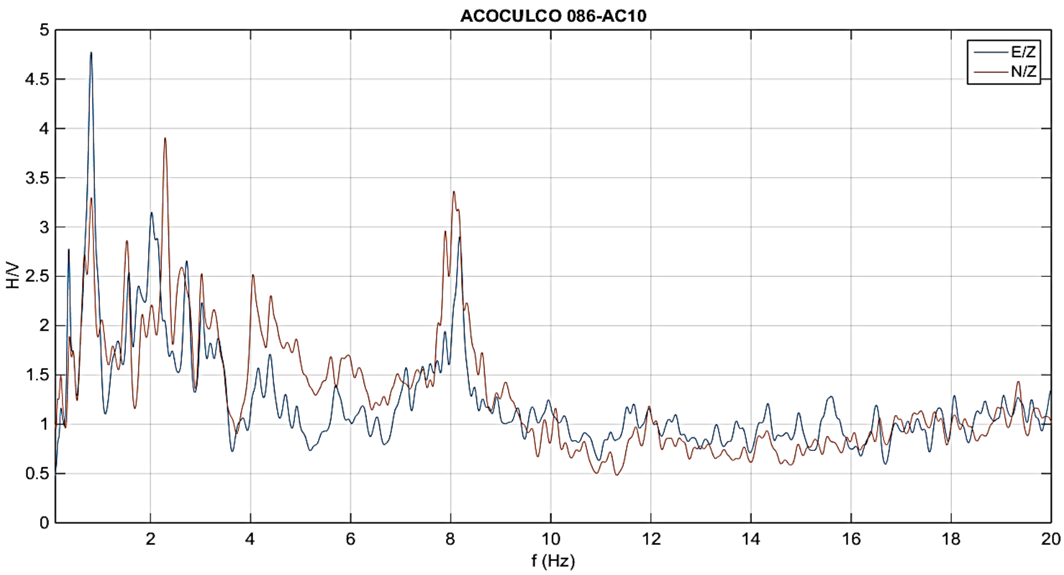
ACOCULCO 086-AC10
E/Z
N/Z
H/V
f (Hz)

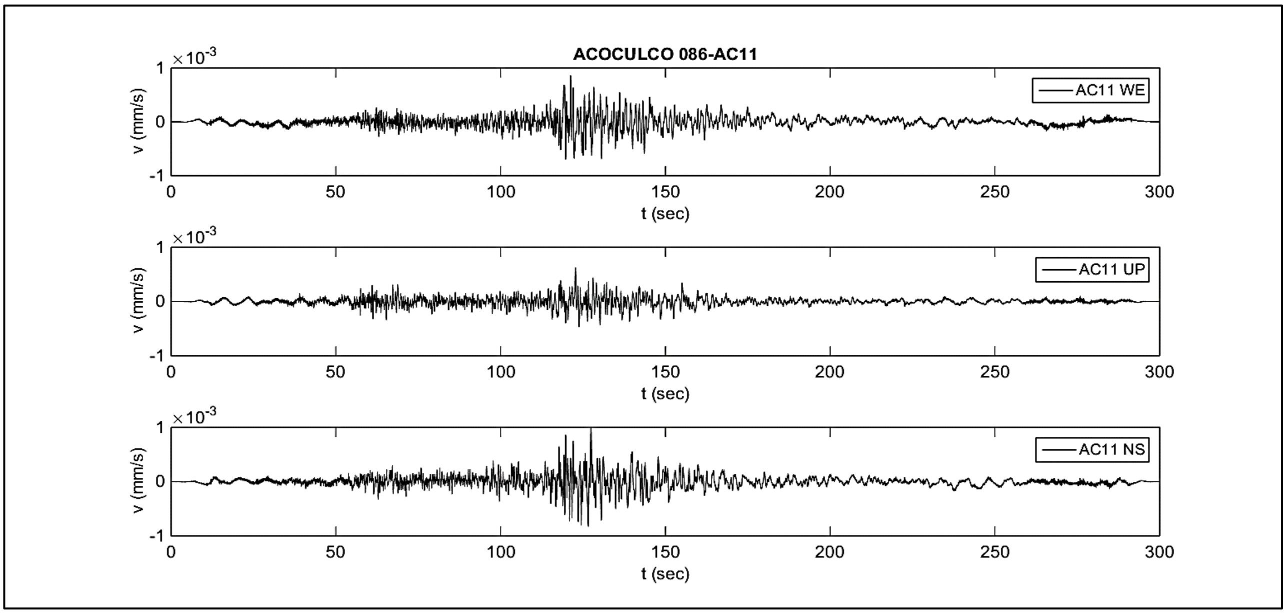
ACOCULCO 086-AC11
AC11 WE
AC11 UP
AC11 NS
v (mm/s)
t (sec)

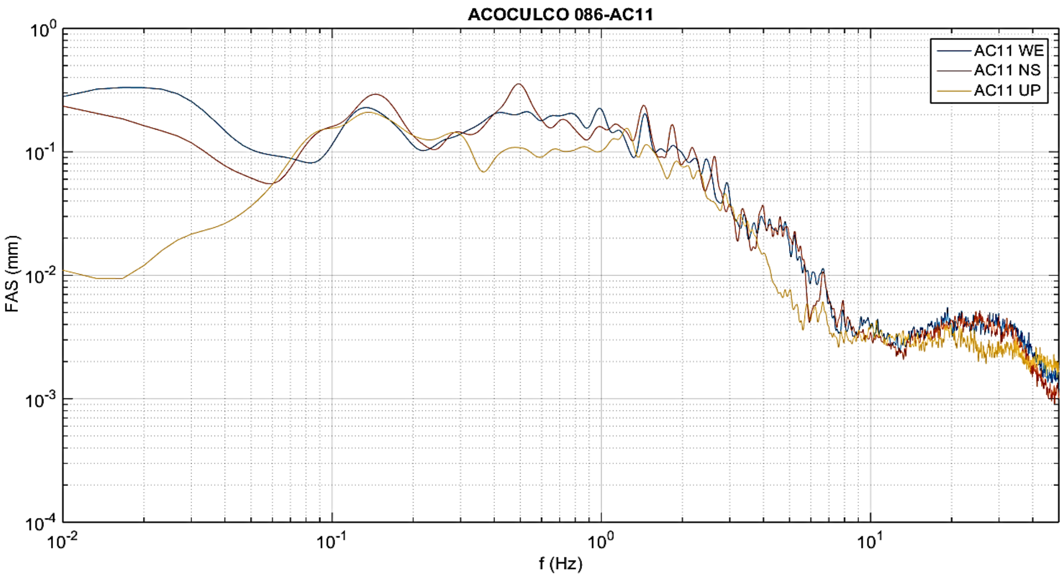
ACOCULCO 086-AC11
AC11 WE
AC11 NS
AC11 UP
FAS (mm)
f (Hz)

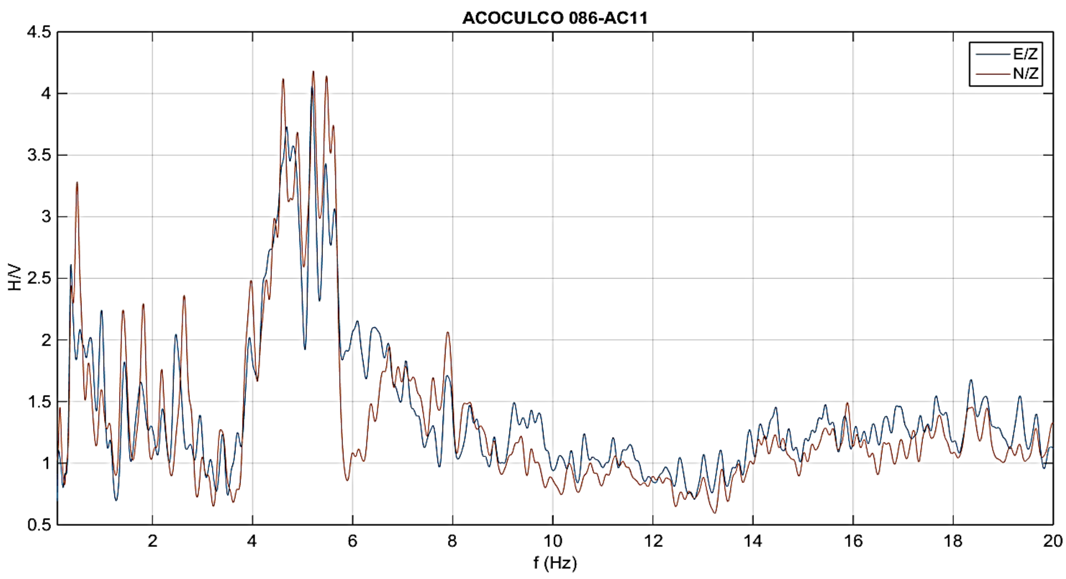
ACOCULCO 086-AC11
E/Z
N/Z
H/V
f (Hz)

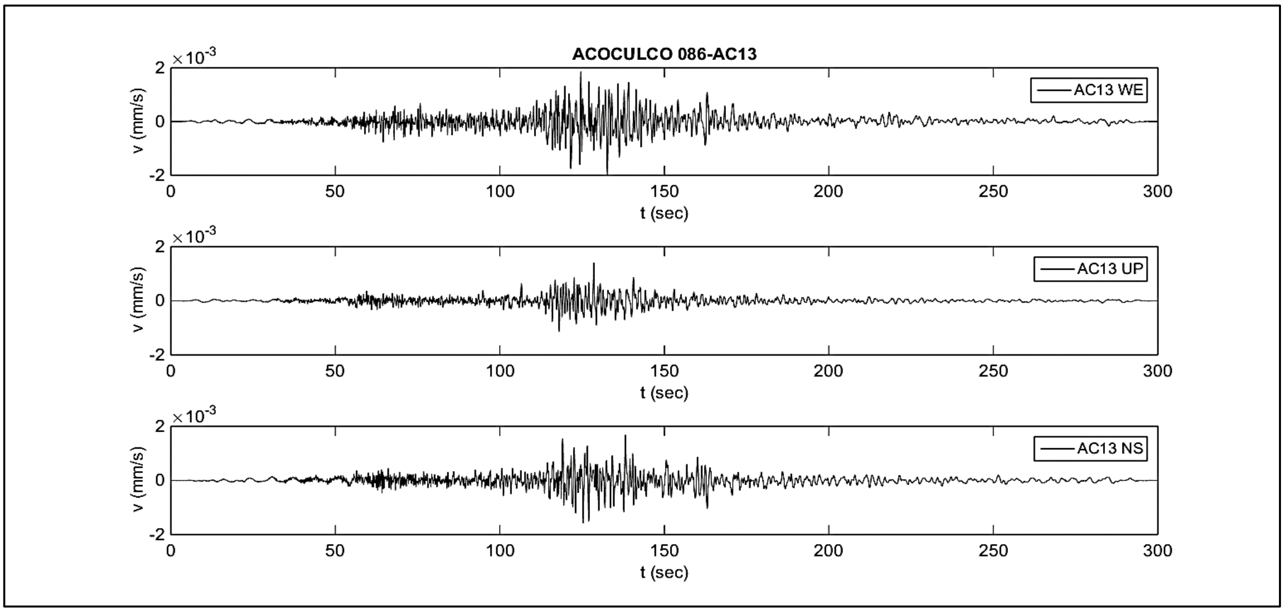
ACOCULCO 086-AC13
AC13 WE
AC13 UP
AC13 NS
v (mm/s)
t (sec)
×10^-3

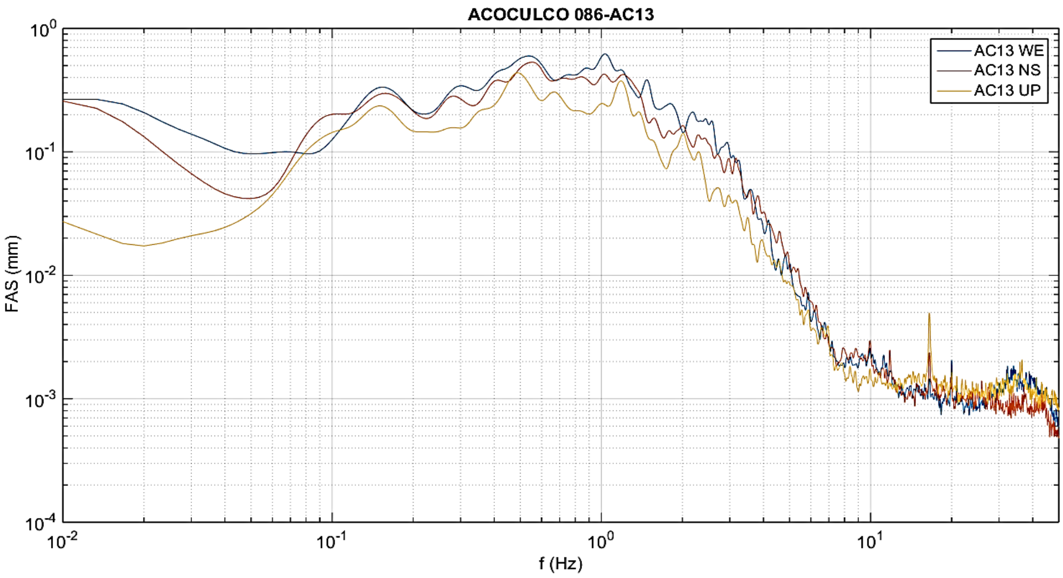
ACOCULCO 086-AC13
AC13 WE
AC13 NS
AC13 UP
FAS (mm)
f (Hz)

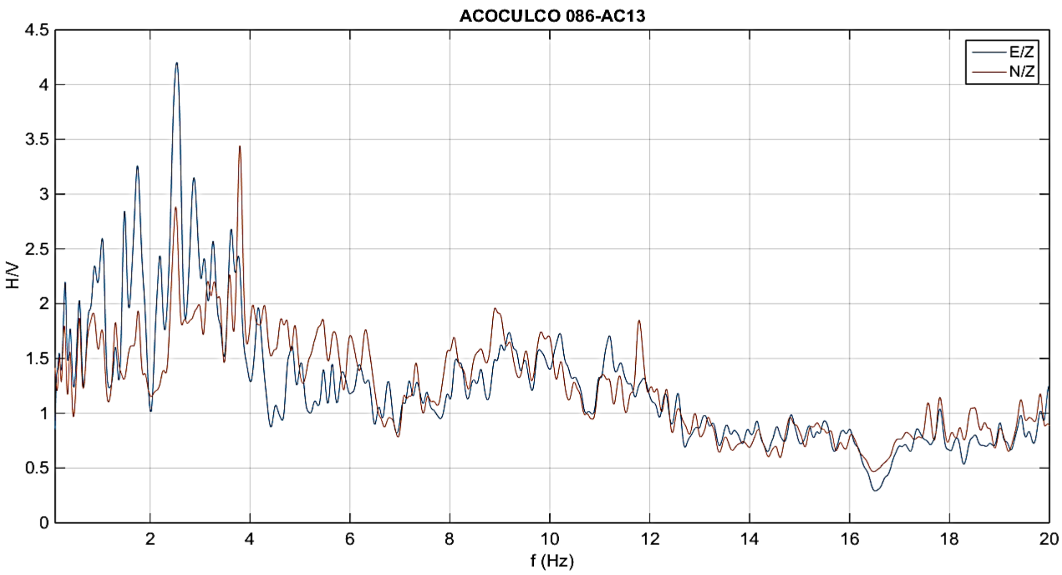
ACOCULCO 086-AC13
E/Z
N/Z
H/V
f (Hz)

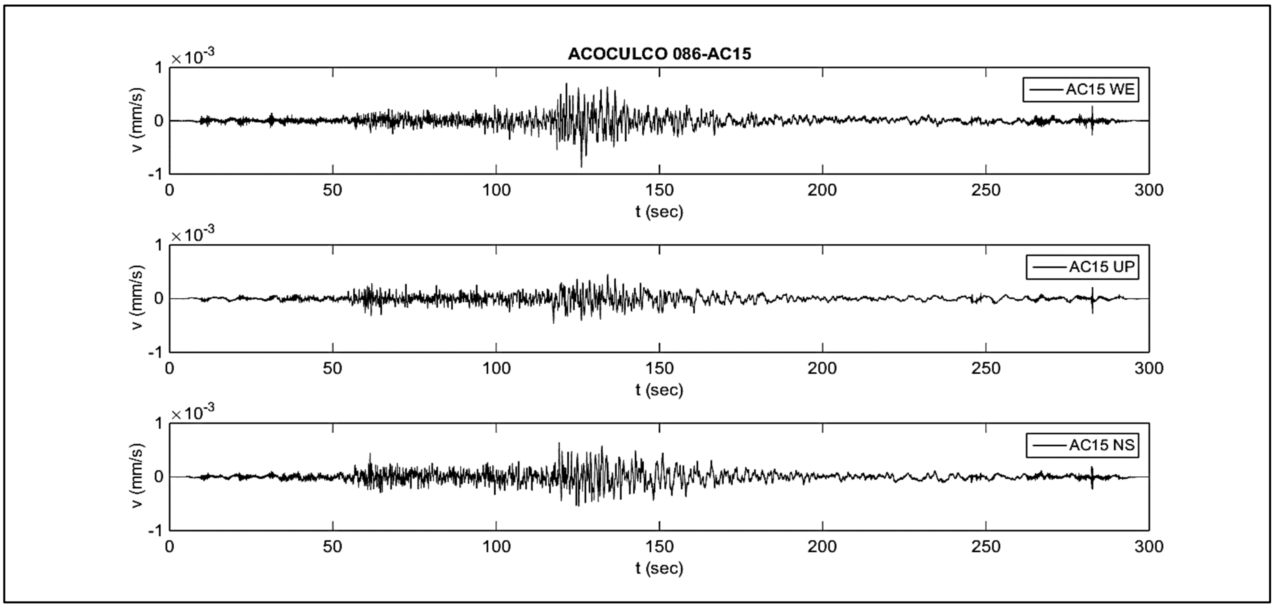

ACOCULCO 086-AC15
AC15 WE
AC15 UP
AC15 NS
v (mm/s)
t (sec)

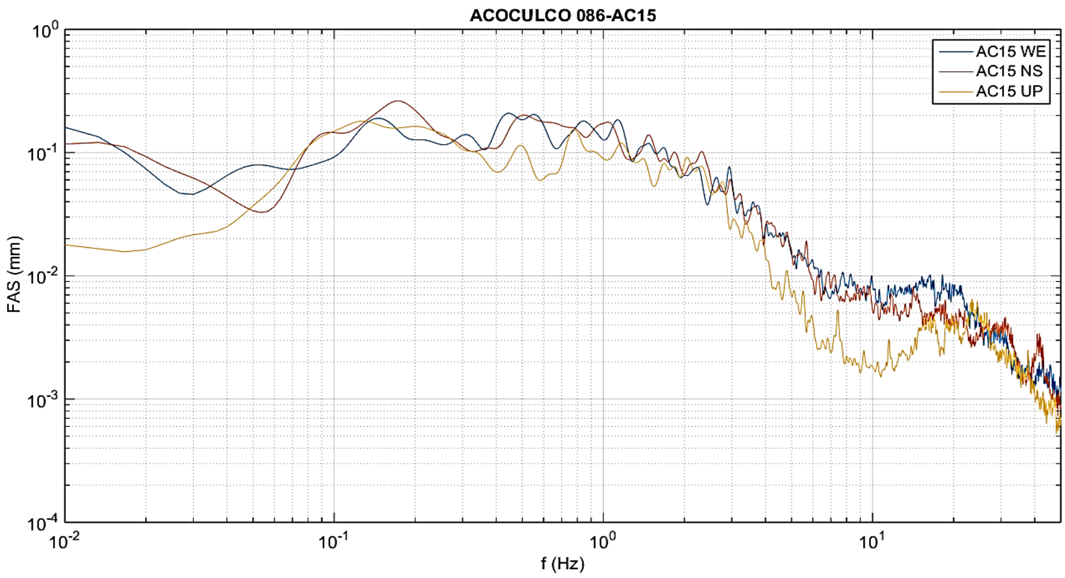

ACOCULCO 086-AC15
AC15 WE
AC15 NS
AC15 UP
FAS (mm)
f (Hz)

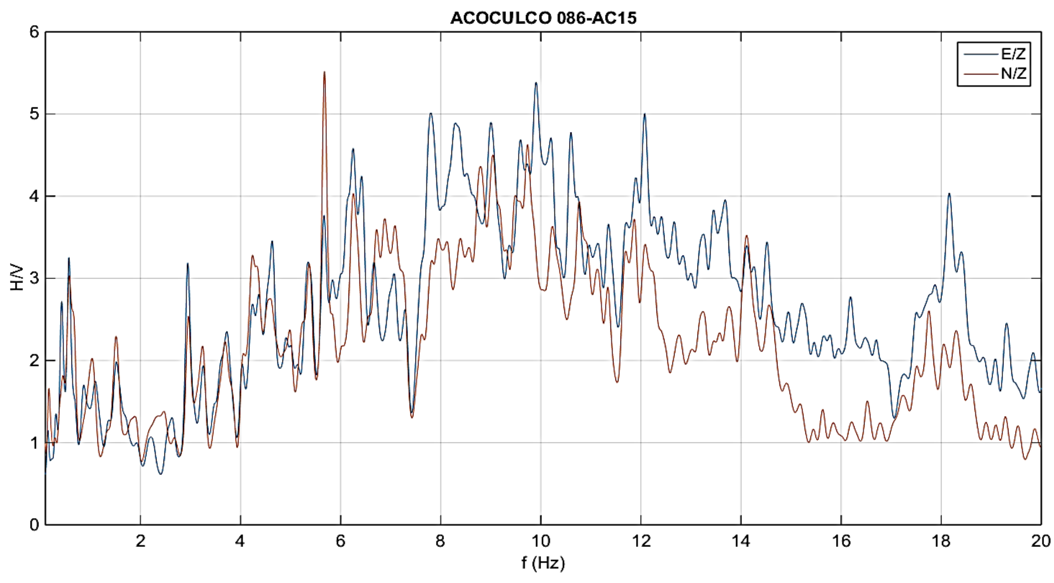

ACOCULCO 086-AC15
E/Z
N/Z
H/V
f (Hz)

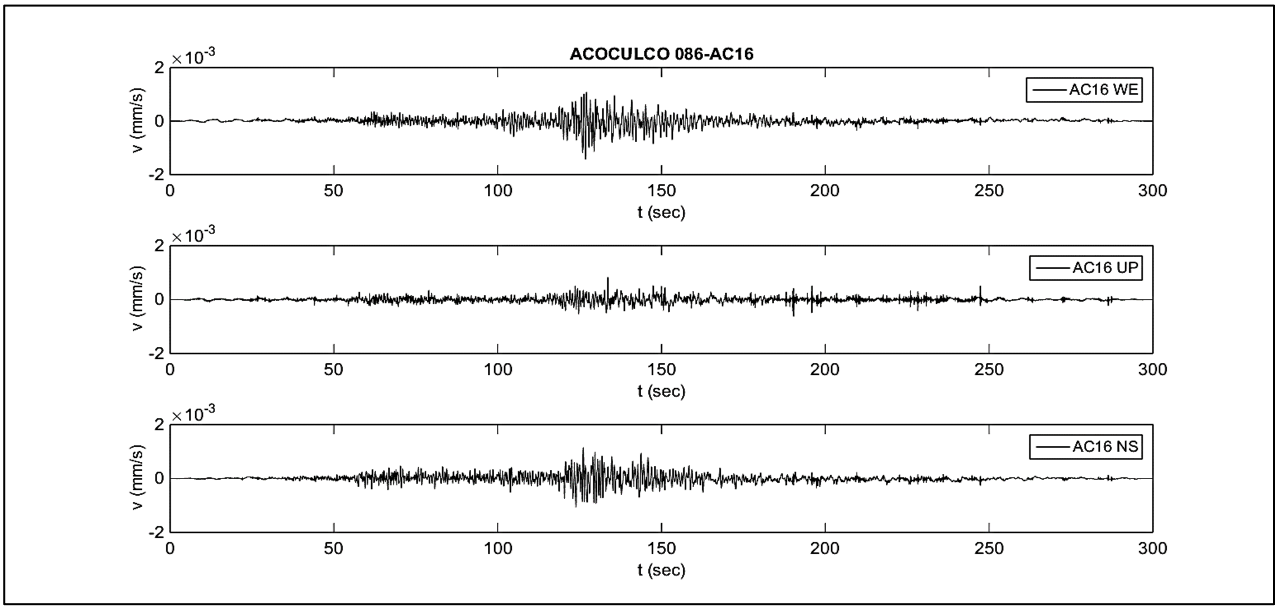
ACOCULCO 086-AC16
AC16 WE
AC16 UP
AC16 NS
v (mm/s)
t (sec)

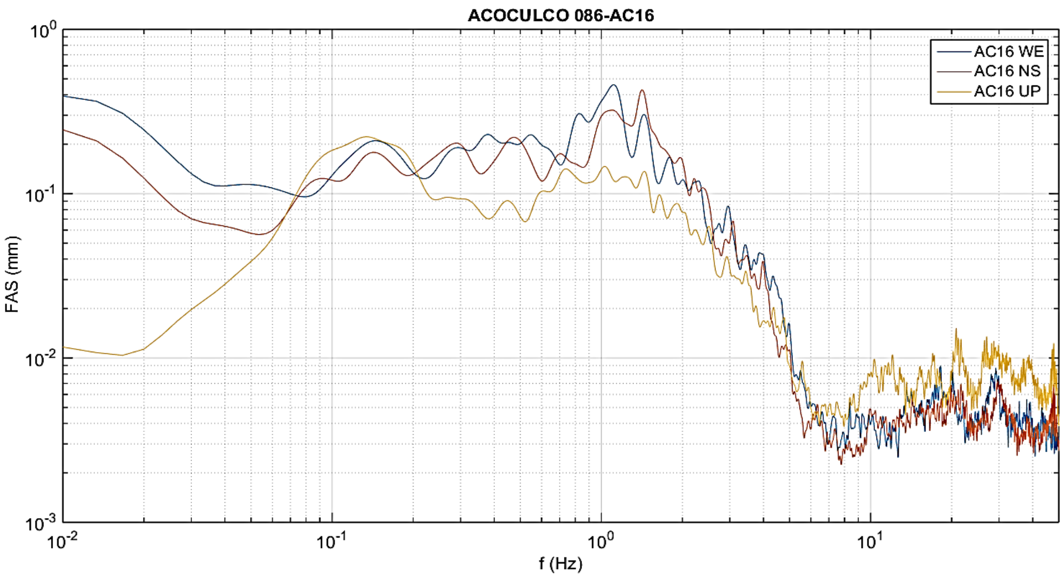
ACOCULCO 086-AC16
AC16 WE
AC16 NS
AC16 UP
FAS (mm)
f (Hz)

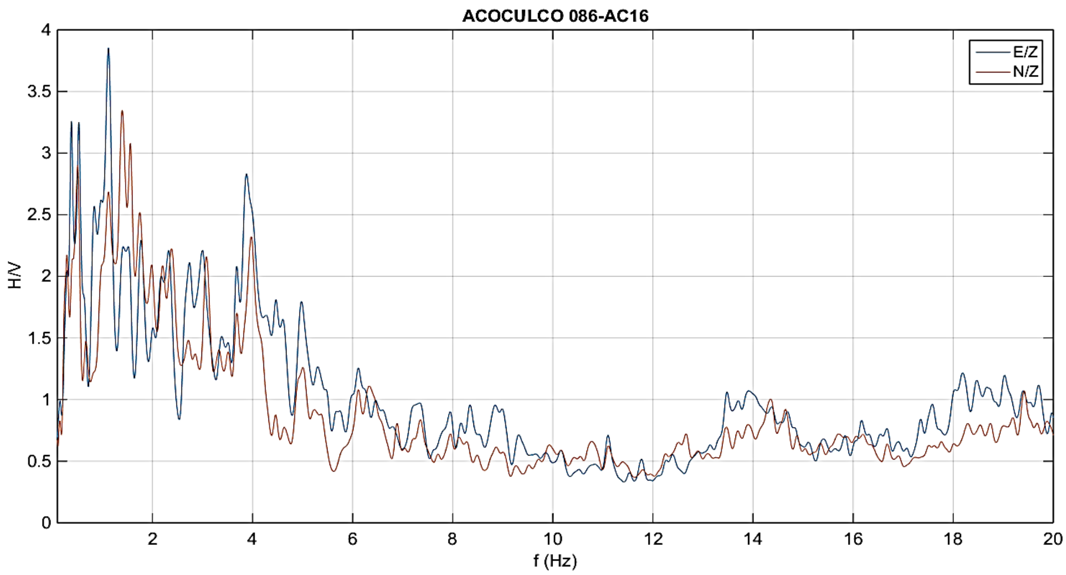
ACOCULCO 086-AC16
E/Z
N/Z
H/V
f (Hz)

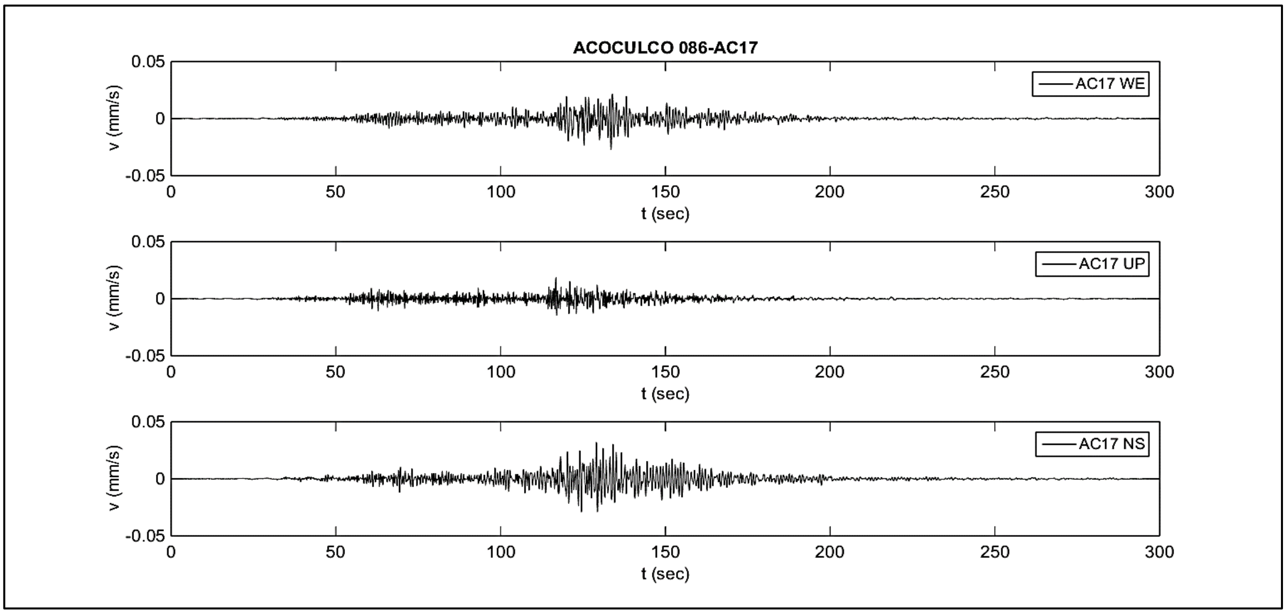
ACOCULCO 086-AC17
AC17 WE
AC17 UP
AC17 NS
v (mm/s)
t (sec)

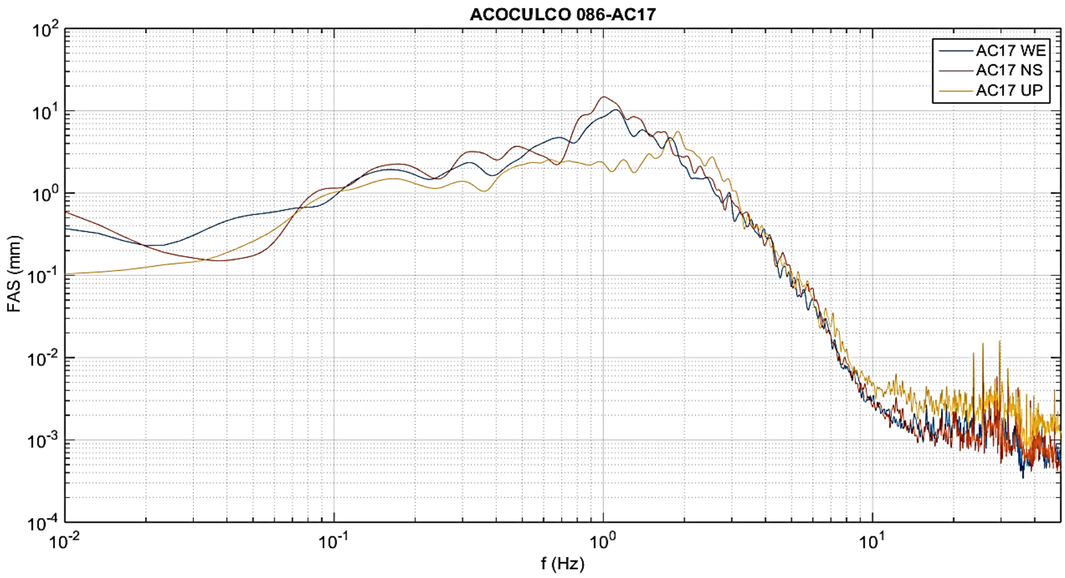
ACOCULCO 086-AC17
AC17 WE
AC17 NS
AC17 UP
FAS (mm)
f (Hz)

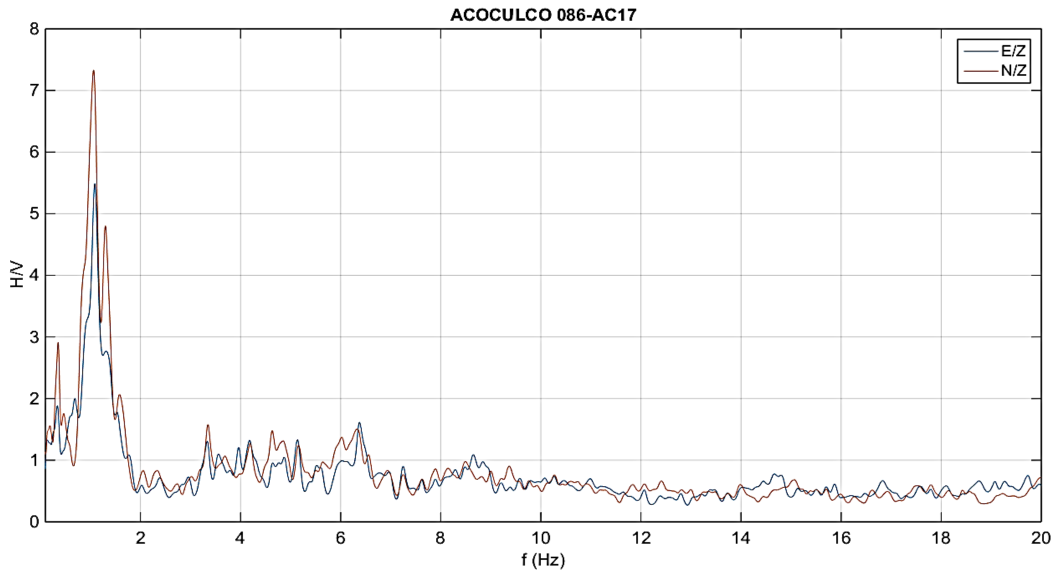
ACOCULCO 086-AC17
E/Z
N/Z
H/V
f (Hz)

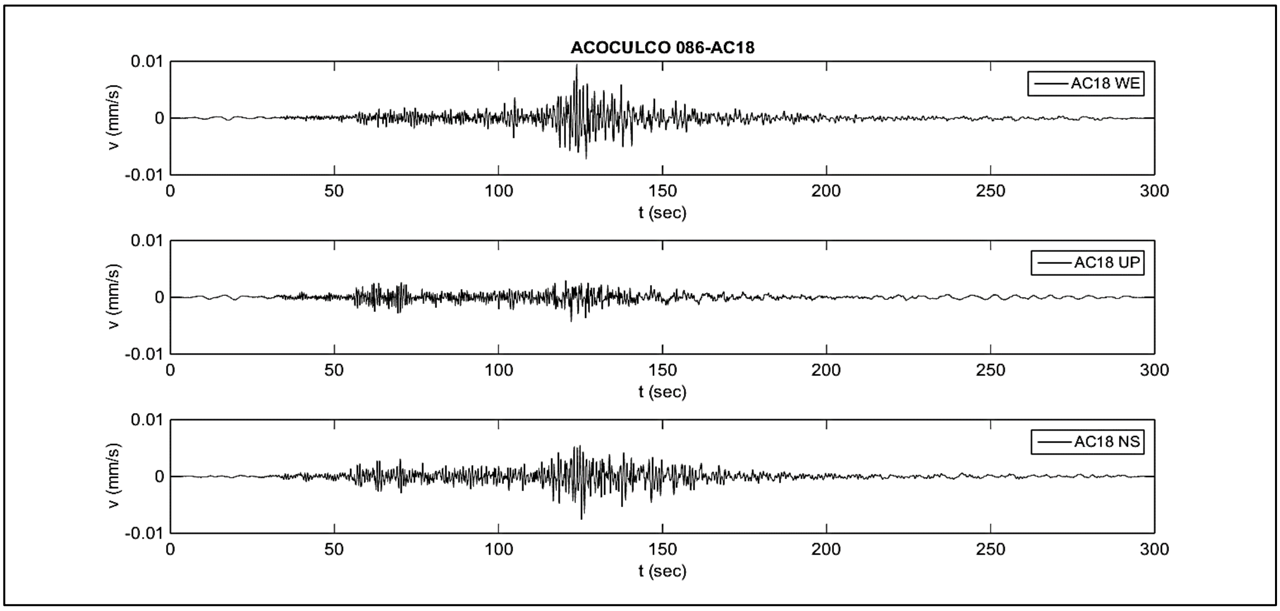
ACOCULCO 086-AC18
AC18 WE
AC18 UP
AC18 NS
v (mm/s)
t (sec)
0.01
0
-0.01
0 50 100 150 200 250 300

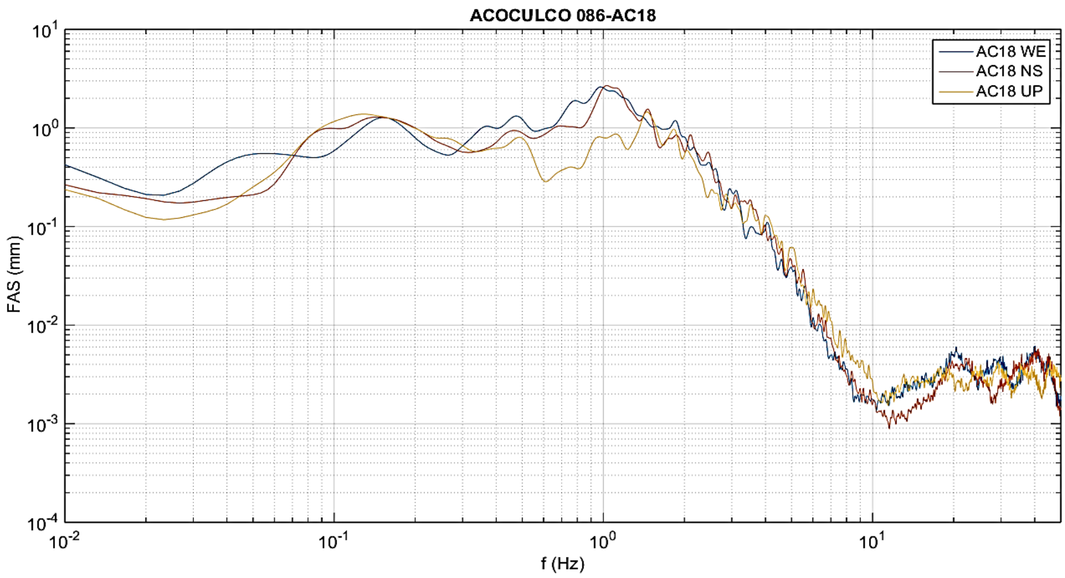
ACOCULCO 086-AC18
AC18 WE
AC18 NS
AC18 UP
FAS (mm)
f (Hz)

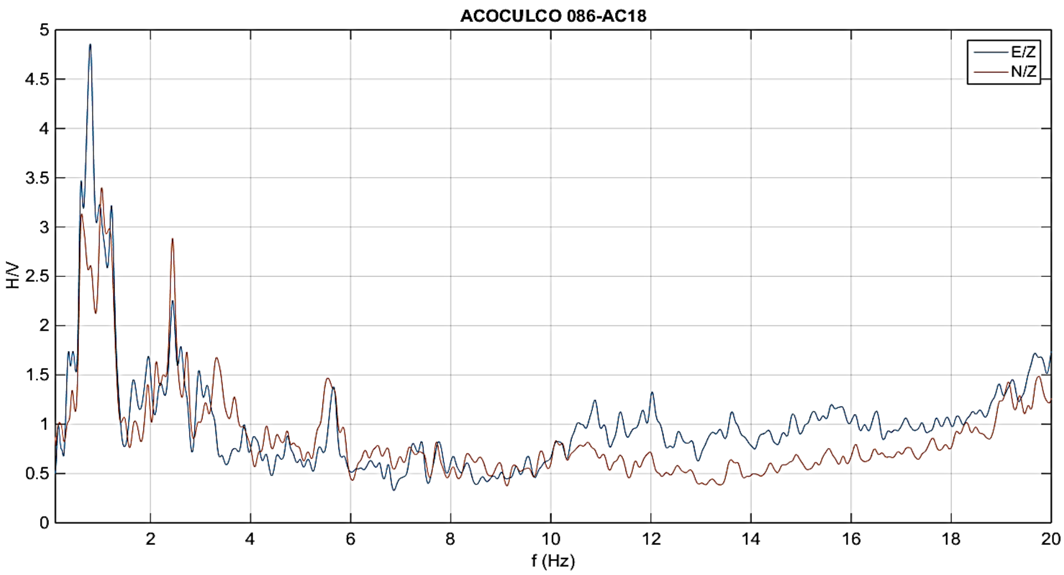
ACOCULCO 086-AC18
E/Z
N/Z
H/V
f (Hz)

Appendix 4-H Day 086 Comparison of the spectra

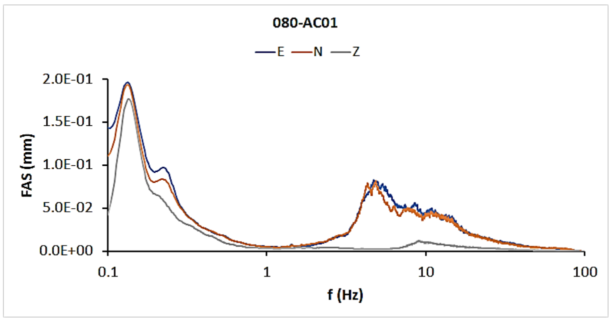

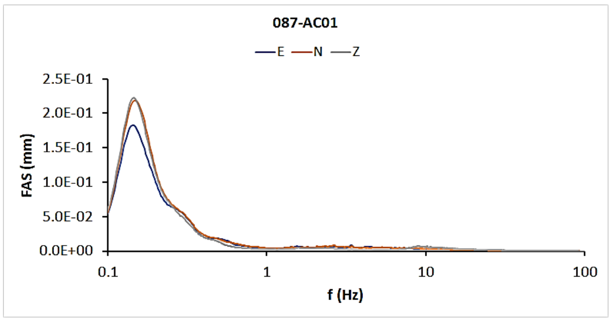

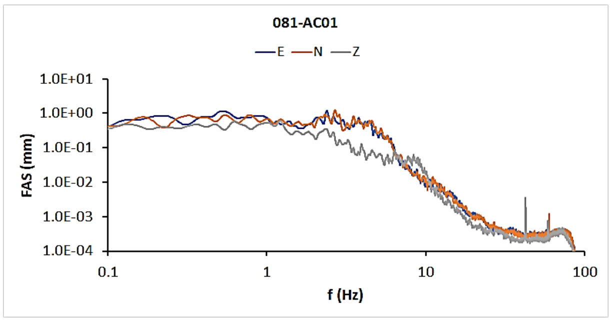

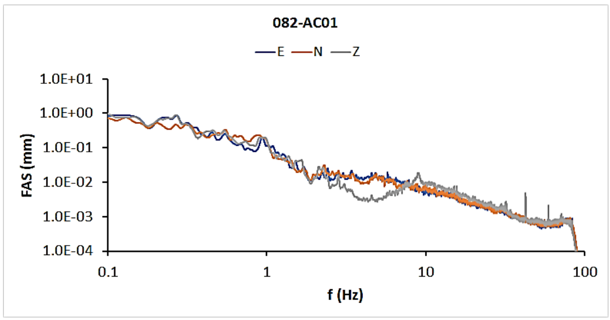

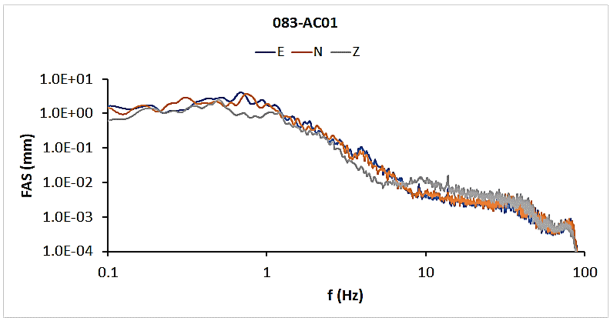

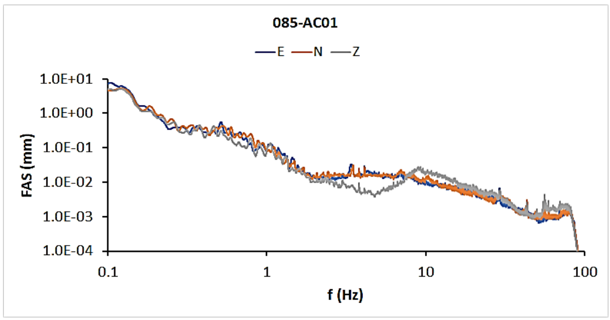

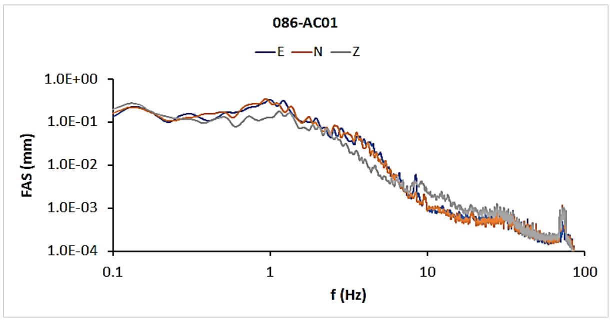

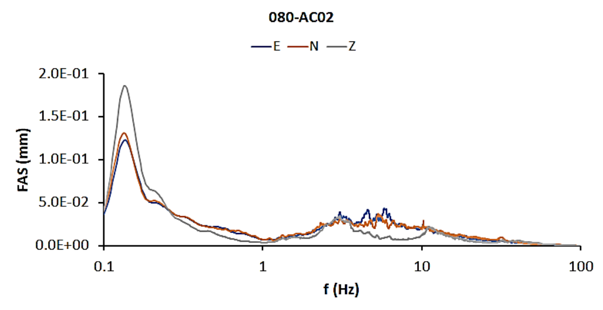
080-AC02
E N Z
2.0E-01
1.5E-01
1.0E-01
5.0E-02
0.0E+00
FAS (mm)
0.1
1
10
100
f (Hz)

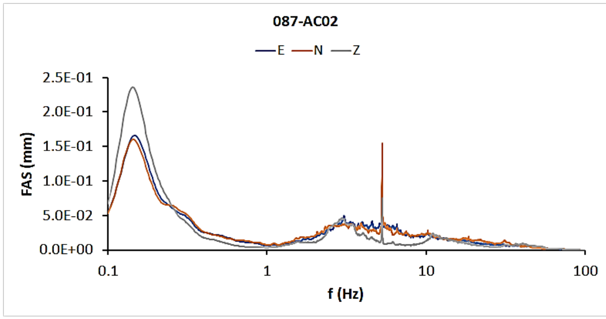
087-AC02
E N Z
2.5E-01
2.0E-01
1.5E-01
1.0E-01
5.0E-02
0.0E+00
FAS (mm)
0.1
1
10
100
f (Hz)

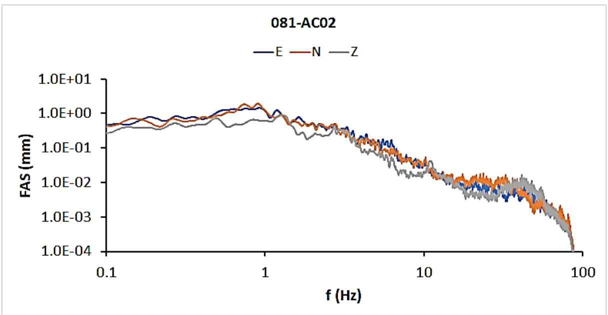
081-AC02
E N Z
1.0E+01
1.0E+00
1.0E-01
1.0E-02
1.0E-03
1.0E-04
FAS (mm)
0.1
1
10
100
f (Hz)

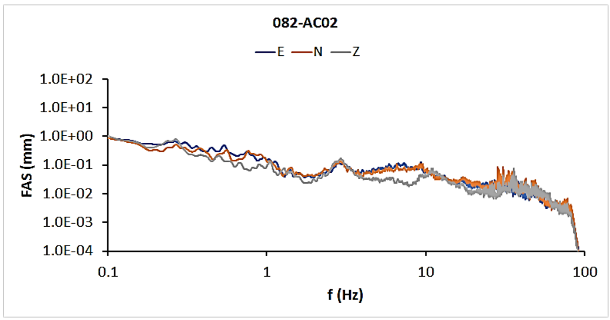
082-AC02
E N Z
1.0E+02
1.0E+01
1.0E+00
1.0E-01
1.0E-02
1.0E-03
1.0E-04
FAS (mm)
0.1
1
10
100
f (Hz)

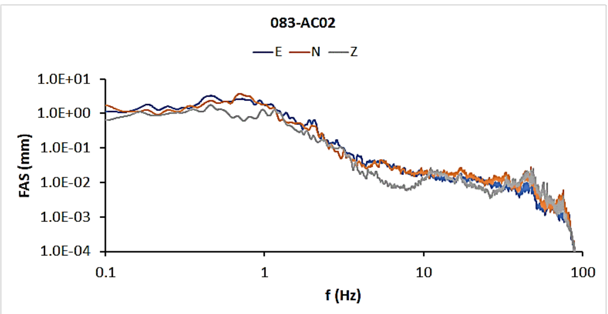
083-AC02
E N Z
1.0E+01
1.0E+00
1.0E-01
1.0E-02
1.0E-03
1.0E-04
FAS (mm)
0.1
1
10
100
f (Hz)

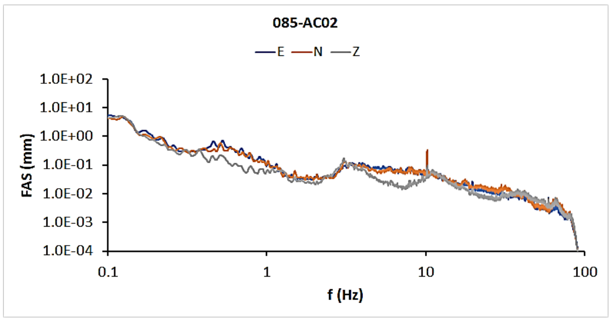
085-AC02
E N Z
1.0E+02
1.0E+01
1.0E+00
1.0E-01
1.0E-02
1.0E-03
1.0E-04
FAS (mm)
0.1
1
10
100
f (Hz)

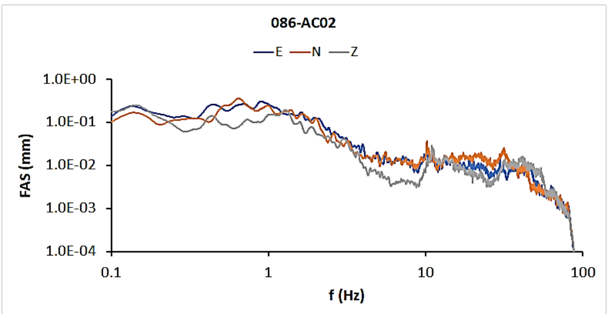
086-AC02
E N Z
1.0E+00
1.0E-01
1.0E-02
1.0E-03
1.0E-04
FAS (mm)
0.1
1
10
100
f (Hz)

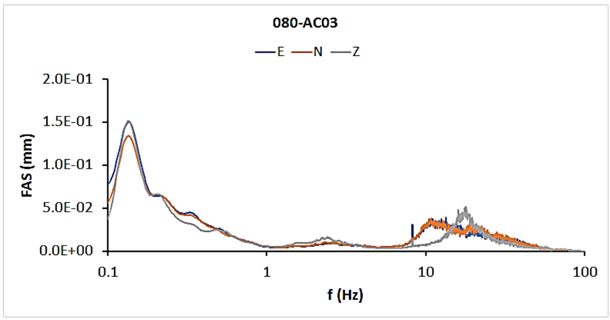
080-AC03
E
N
Z
FAS (mm)
f (Hz)

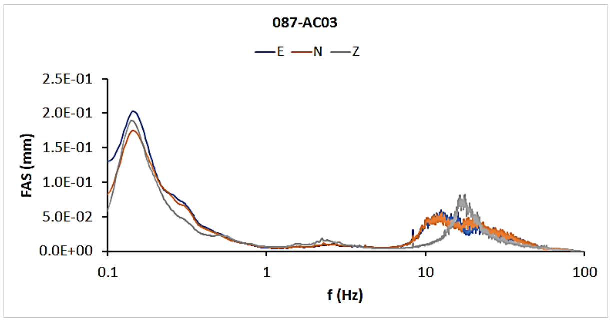
087-AC03
E
N
Z
FAS (mm)
f (Hz)

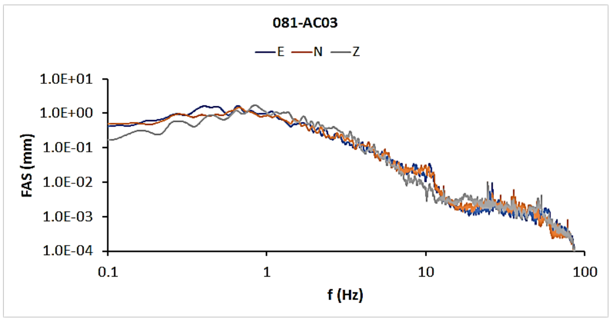
081-AC03
E
N
Z
FAS (mm)
f (Hz)

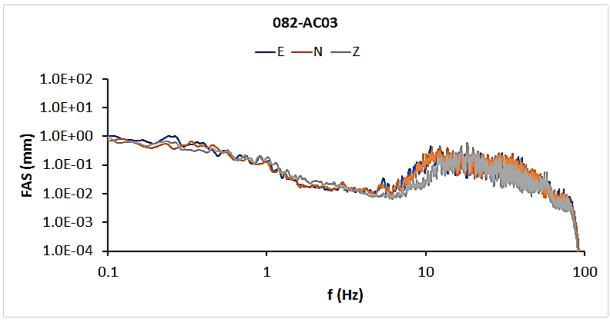
082-AC03
E
N
Z
FAS (mm)
f (Hz)

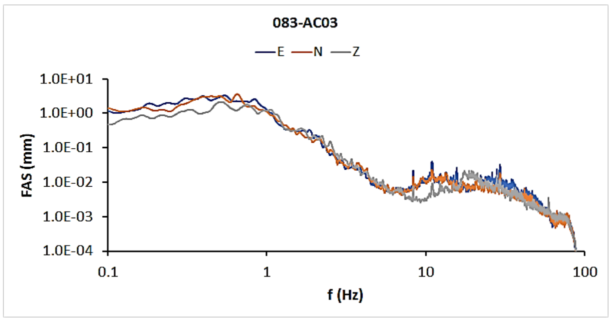
083-AC03
E
N
Z
FAS (mm)
f (Hz)

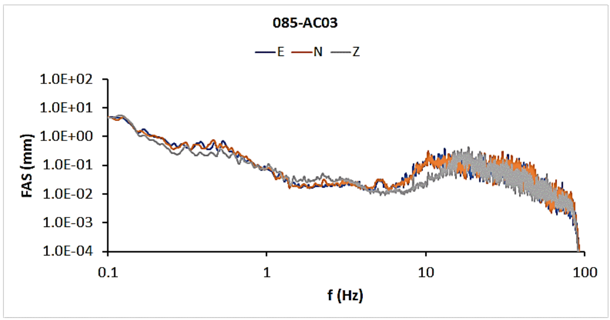
085-AC03
E
N
Z
FAS (mm)
f (Hz)

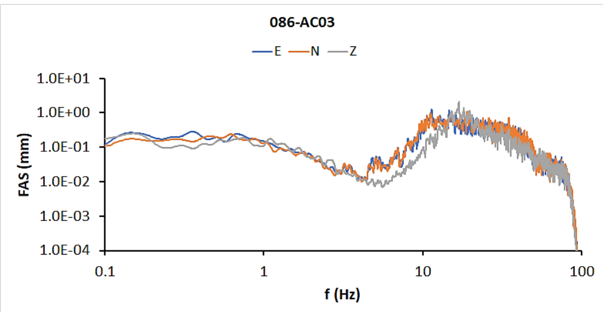
086-AC03
E
N
Z
FAS (mm)
f (Hz)

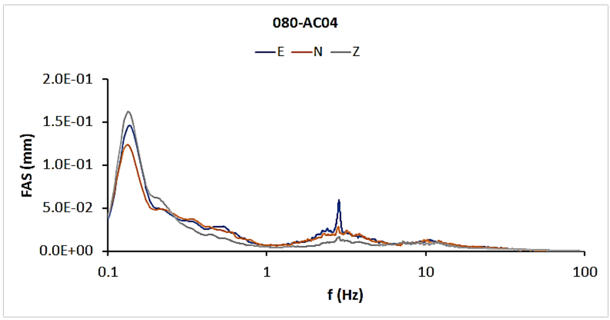
080-AC04
E N Z
FAS (mm)
2.0E-01
1.5E-01
1.0E-01
5.0E-02
0.0E+00
0.1
1
10
100
f (Hz)

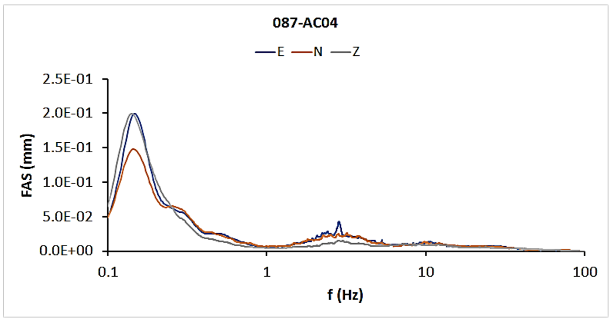
087-AC04
E N Z
FAS (mm)
2.5E-01
2.0E-01
1.5E-01
1.0E-01
5.0E-02
0.0E+00
0.1
1
10
100
f (Hz)

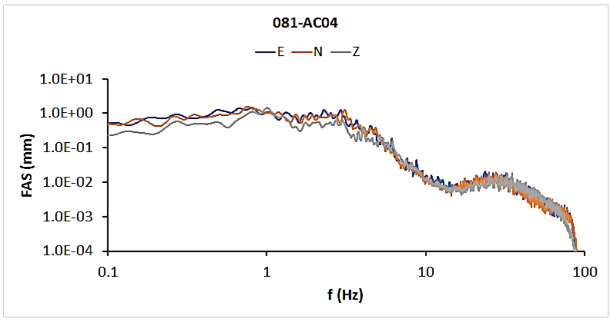
081-AC04
E N Z
FAS (mm)
1.0E+01
1.0E+00
1.0E-01
1.0E-02
1.0E-03
1.0E-04
0.1
1
10
100
f (Hz)

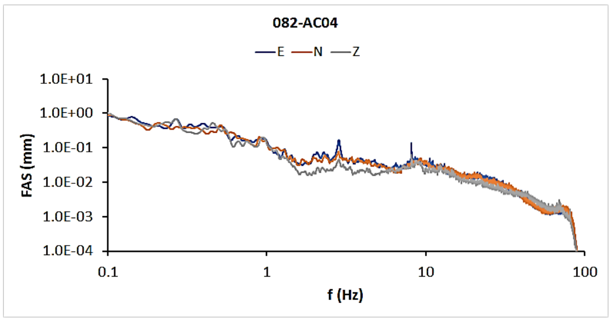
082-AC04
E N Z
FAS (mm)
1.0E+01
1.0E+00
1.0E-01
1.0E-02
1.0E-03
1.0E-04
0.1
1
10
100
f (Hz)

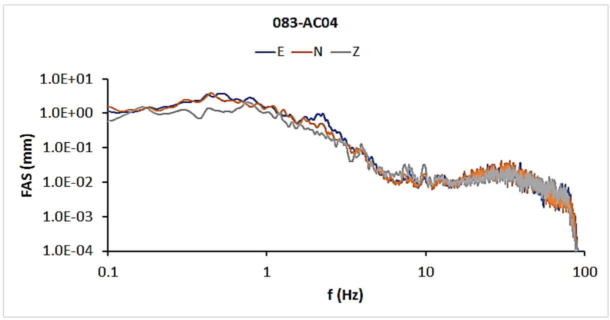
083-AC04
E N Z
FAS (mm)
1.0E+01
1.0E+00
1.0E-01
1.0E-02
1.0E-03
1.0E-04
0.1
1
10
100
f (Hz)

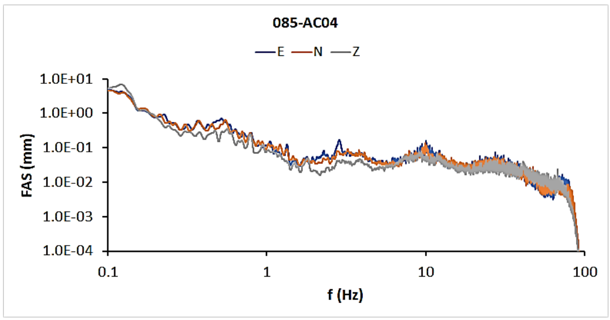
085-AC04
E N Z
FAS (mm)
1.0E+01
1.0E+00
1.0E-01
1.0E-02
1.0E-03
1.0E-04
0.1
1
10
100
f (Hz)

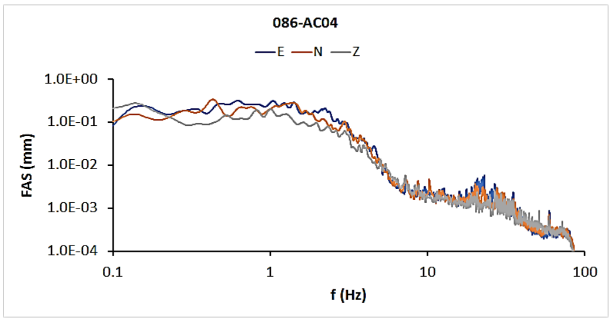
086-AC04
E N Z
FAS (mm)
1.0E+00
1.0E-01
1.0E-02
1.0E-03
1.0E-04
0.1
1
10
100
f (Hz)

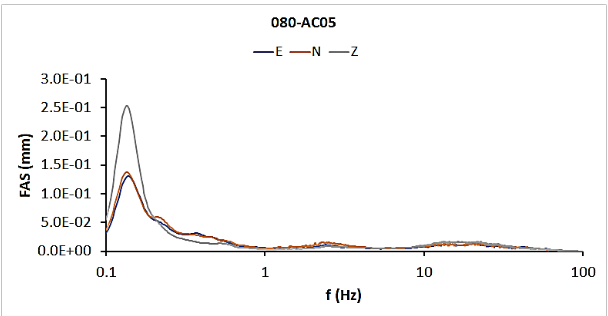
080-AC05
E N Z
3.0E-01
2.5E-01
2.0E-01
1.5E-01
1.0E-01
5.0E-02
0.0E+00
FAS (mm)
0.1
1
10
100
f (Hz)

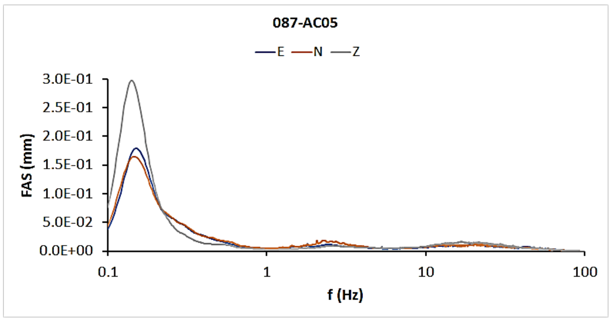
087-AC05
E N Z
3.0E-01
2.5E-01
2.0E-01
1.5E-01
1.0E-01
5.0E-02
0.0E+00
FAS (mm)
0.1
1
10
100
f (Hz)

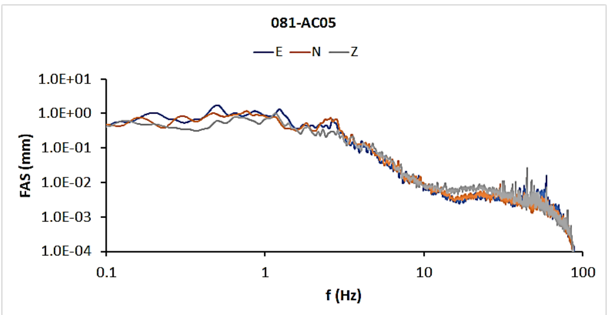
081-AC05
E N Z
1.0E+01
1.0E+00
1.0E-01
1.0E-02
1.0E-03
1.0E-04
FAS (mm)
0.1
1
10
100
f (Hz)

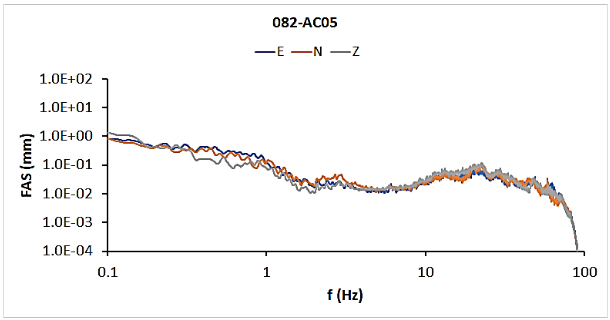
082-AC05
E N Z
1.0E+02
1.0E+01
1.0E+00
1.0E-01
1.0E-02
1.0E-03
1.0E-04
FAS (mm)
0.1
1
10
100
f (Hz)

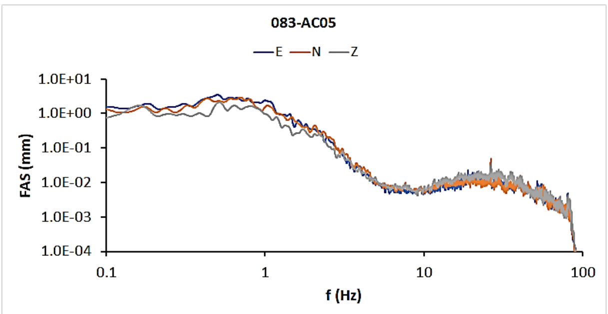
083-AC05
E N Z
1.0E+01
1.0E+00
1.0E-01
1.0E-02
1.0E-03
1.0E-04
FAS (mm)
0.1
1
10
100
f (Hz)

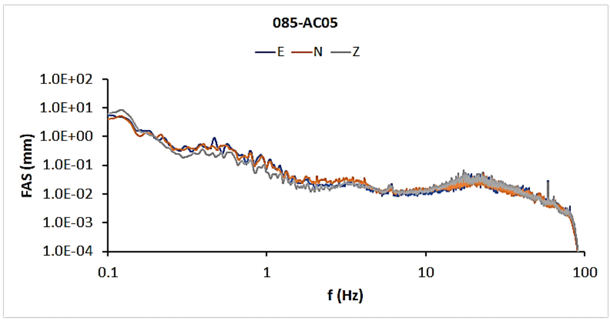
085-AC05
E N Z
1.0E+02
1.0E+01
1.0E+00
1.0E-01
1.0E-02
1.0E-03
1.0E-04
FAS (mm)
0.1
1
10
100
f (Hz)

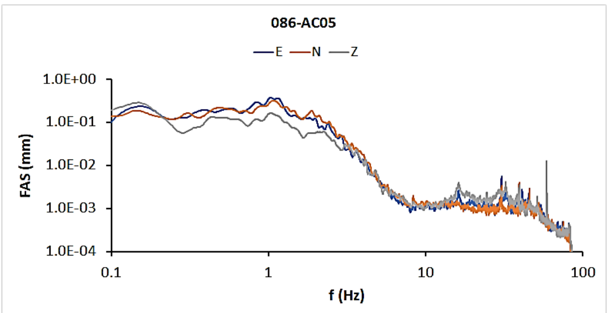
086-AC05
E N Z
1.0E+00
1.0E-01
1.0E-02
1.0E-03
1.0E-04
FAS (mm)
0.1
1
10
100
f (Hz)

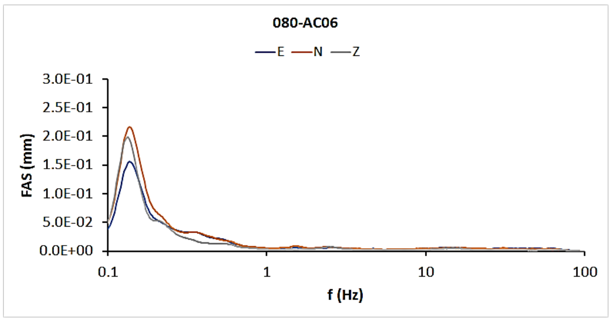
080-AC06
E
N
Z
3.0E-01
2.5E-01
2.0E-01
1.5E-01
1.0E-01
5.0E-02
0.0E+00
FAS (mm)
0.1
1
10
100
f (Hz)

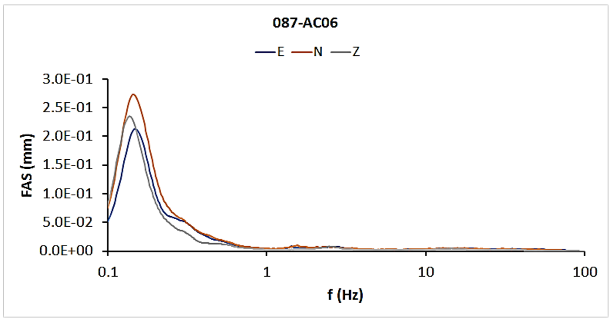
087-AC06
E
N
Z
3.0E-01
2.5E-01
2.0E-01
1.5E-01
1.0E-01
5.0E-02
0.0E+00
FAS (mm)
0.1
1
10
100
f (Hz)

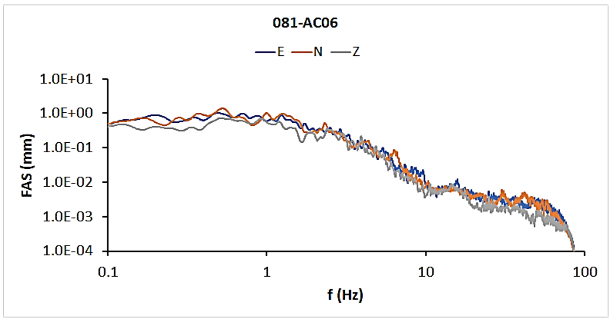
081-AC06
E
N
Z
1.0E+01
1.0E+00
1.0E-01
1.0E-02
1.0E-03
1.0E-04
FAS (mm)
0.1
1
10
100
f (Hz)

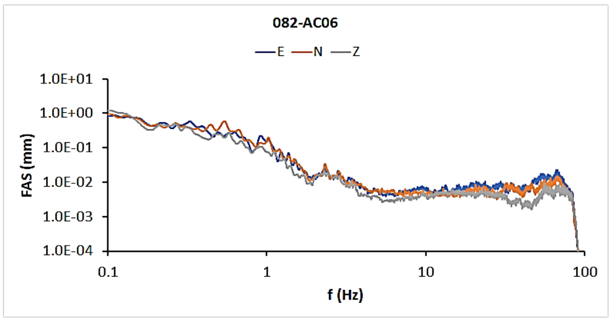
082-AC06
E
N
Z
1.0E+01
1.0E+00
1.0E-01
1.0E-02
1.0E-03
1.0E-04
FAS (mm)
0.1
1
10
100
f (Hz)

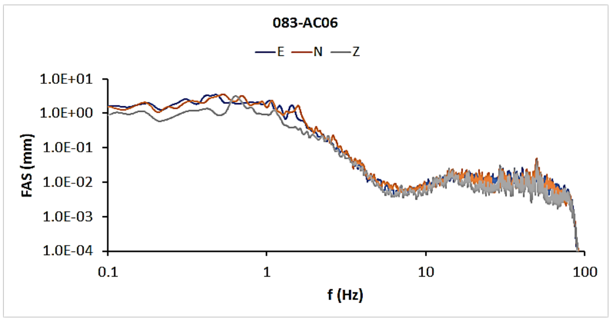
083-AC06
E
N
Z
1.0E+01
1.0E+00
1.0E-01
1.0E-02
1.0E-03
1.0E-04
FAS (mm)
0.1
1
10
100
f (Hz)

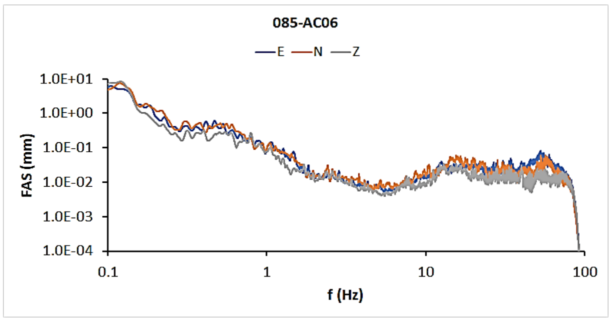
085-AC06
E
N
Z
1.0E+01
1.0E+00
1.0E-01
1.0E-02
1.0E-03
1.0E-04
FAS (mm)
0.1
1
10
100
f (Hz)

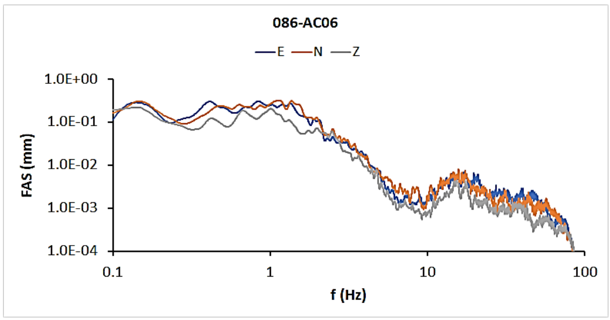
086-AC06
E
N
Z
1.0E+00
1.0E-01
1.0E-02
1.0E-03
1.0E-04
FAS (mm)
0.1
1
10
100
f (Hz)

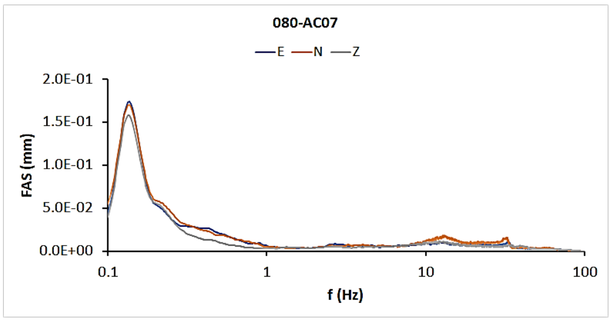
080-AC07
E
N
Z
2.0E-01
1.5E-01
1.0E-01
5.0E-02
0.0E+00
FAS (mm)
0.1
1
10
100
f (Hz)

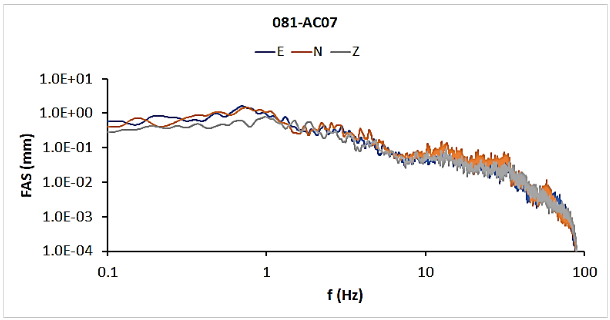
081-AC07
E
N
Z
1.0E+01
1.0E+00
1.0E-01
1.0E-02
1.0E-03
1.0E-04
FAS (mm)
0.1
1
10
100
f (Hz)

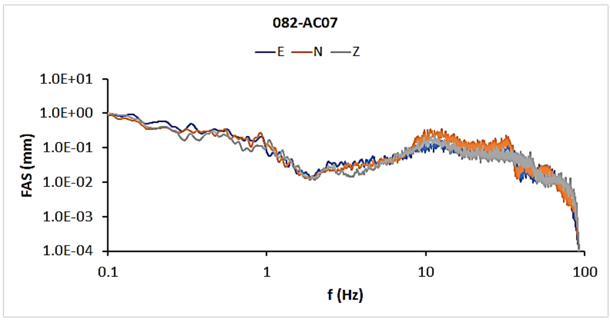
082-AC07
E
N
Z
1.0E+01
1.0E+00
1.0E-01
1.0E-02
1.0E-03
1.0E-04
FAS (mm)
0.1
1
10
100
f (Hz)

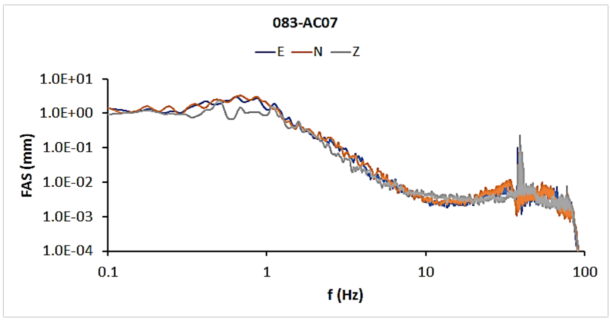
083-AC07
E
N
Z
1.0E+01
1.0E+00
1.0E-01
1.0E-02
1.0E-03
1.0E-04
FAS (mm)
0.1
1
10
100
f (Hz)

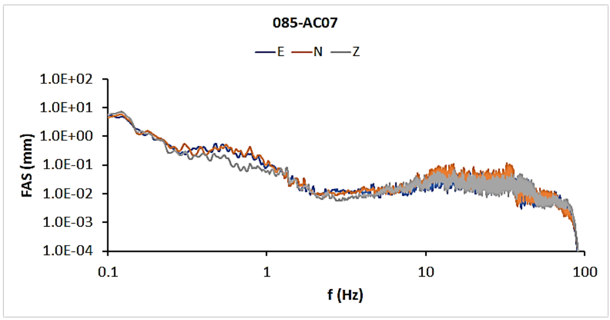
085-AC07
E
N
Z
1.0E+02
1.0E+01
1.0E+00
1.0E-01
1.0E-02
1.0E-03
1.0E-04
FAS (mm)
0.1
1
10
100
f (Hz)

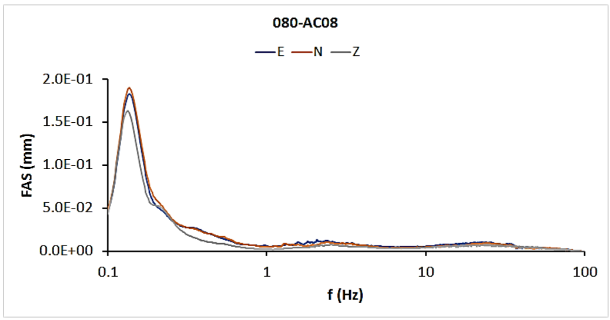
080-AC08
E
N
Z
FAS (mm)
2.0E-01
1.5E-01
1.0E-01
5.0E-02
0.0E+00
0.1
1
10
100
f (Hz)

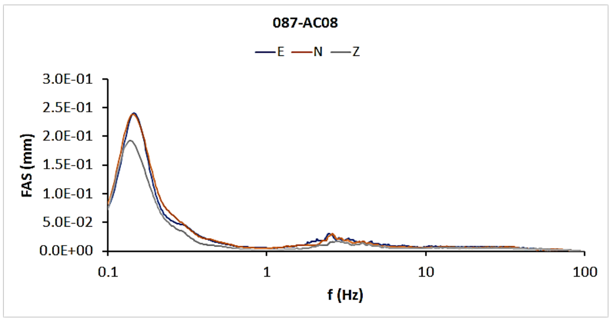
087-AC08
E
N
Z
FAS (mm)
3.0E-01
2.5E-01
2.0E-01
1.5E-01
1.0E-01
5.0E-02
0.0E+00
0.1
1
10
100
f (Hz)

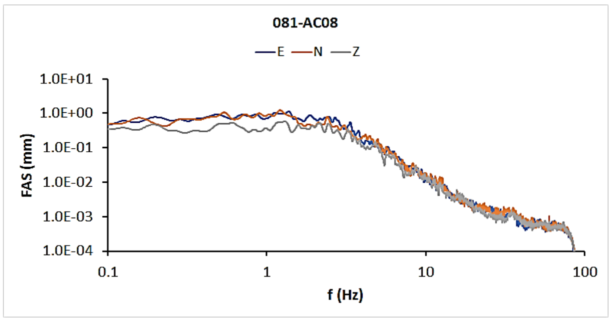
081-AC08
E
N
Z
FAS (mm)
1.0E+01
1.0E+00
1.0E-01
1.0E-02
1.0E-03
1.0E-04
0.1
1
10
100
f (Hz)

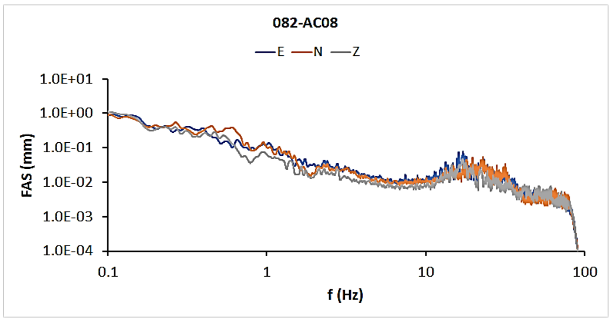
082-AC08
E
N
Z
FAS (mm)
1.0E+01
1.0E+00
1.0E-01
1.0E-02
1.0E-03
1.0E-04
0.1
1
10
100
f (Hz)

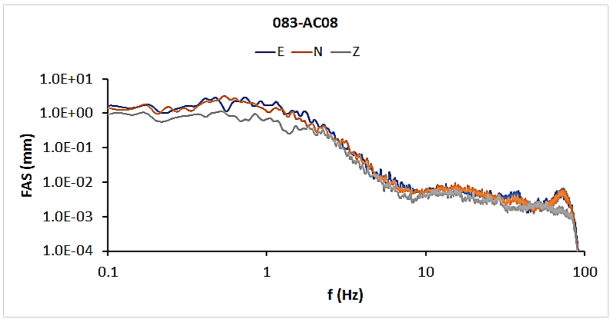
083-AC08
E
N
Z
FAS (mm)
1.0E+01
1.0E+00
1.0E-01
1.0E-02
1.0E-03
1.0E-04
0.1
1
10
100
f (Hz)

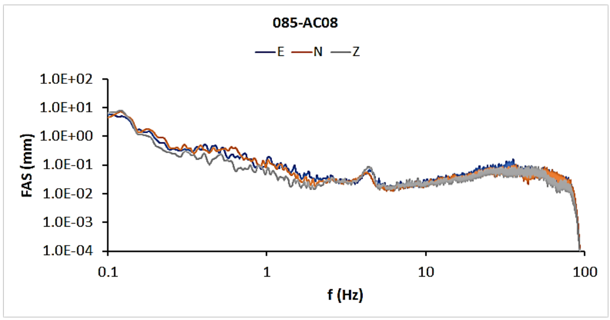
085-AC08
E
N
Z
FAS (mm)
1.0E+02
1.0E+01
1.0E+00
1.0E-01
1.0E-02
1.0E-03
1.0E-04
0.1
1
10
100
f (Hz)

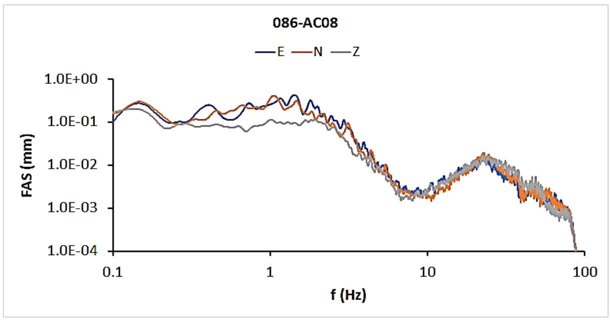
086-AC08
E
N
Z
FAS (mm)
1.0E+00
1.0E-01
1.0E-02
1.0E-03
1.0E-04
0.1
1
10
100
f (Hz)

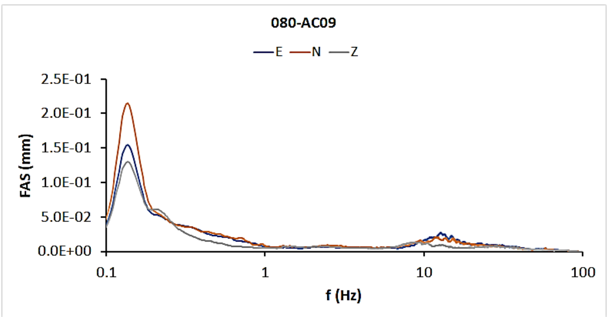

080-AC09
E N Z
FAS (mm)
f (Hz)

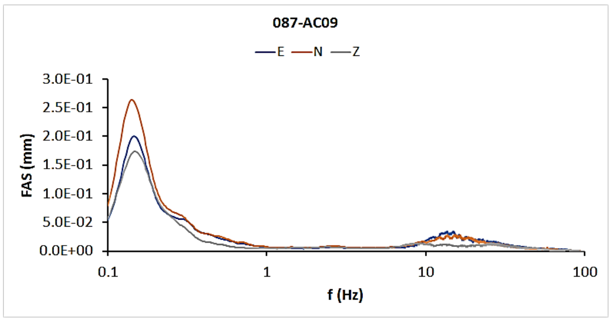

087-AC09
E N Z
FAS (mm)
f (Hz)

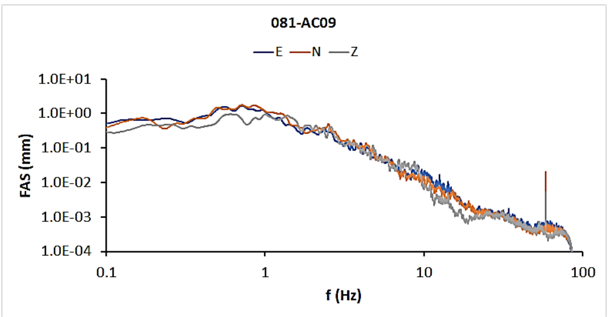

081-AC09
E N Z
FAS (mm)
f (Hz)

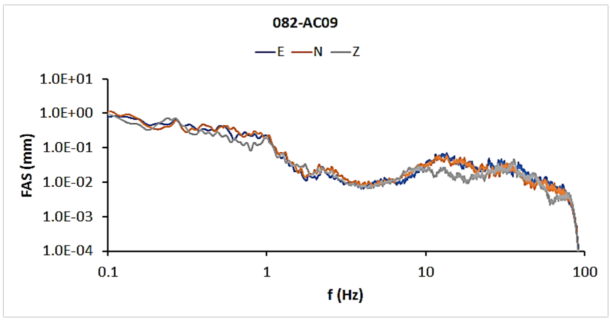

082-AC09
E N Z
FAS (mm)
f (Hz)

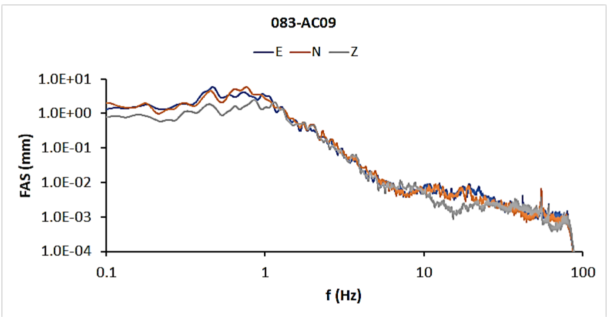

083-AC09
E N Z
FAS (mm)
f (Hz)

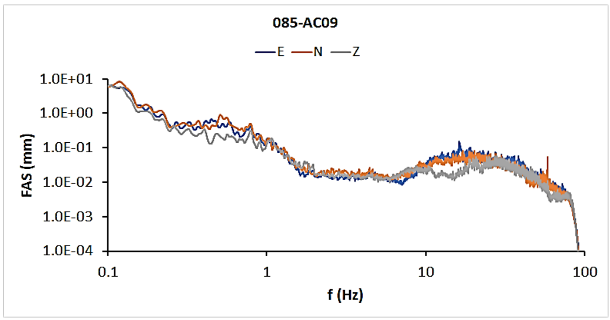

085-AC09
E N Z
FAS (mm)
f (Hz)

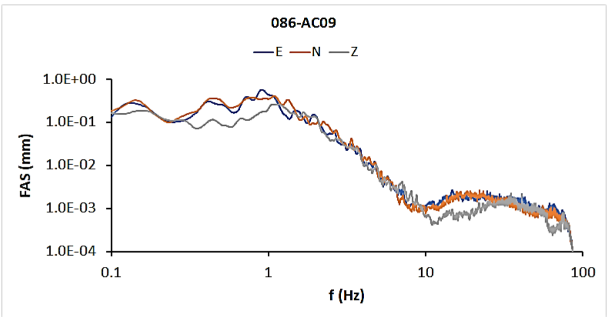

086-AC09
E N Z
FAS (mm)
f (Hz)

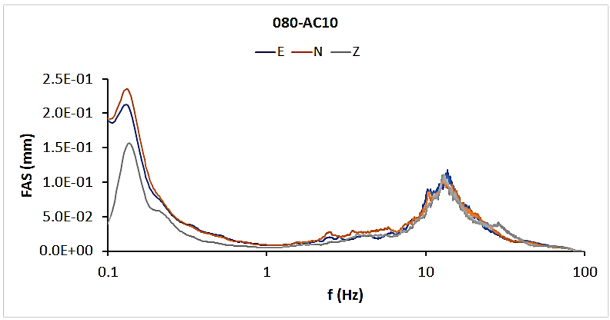
080-AC10
E N Z
FAS (mm)
2.5E-01
2.0E-01
1.5E-01
1.0E-01
5.0E-02
0.0E+00
0.1
1
10
100
f (Hz)

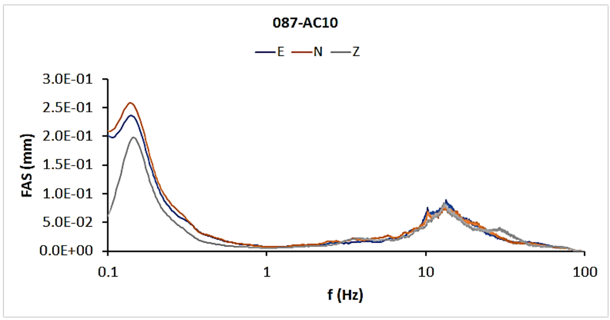
087-AC10
E N Z
FAS (mm)
3.0E-01
2.5E-01
2.0E-01
1.5E-01
1.0E-01
5.0E-02
0.0E+00
0.1
1
10
100
f (Hz)

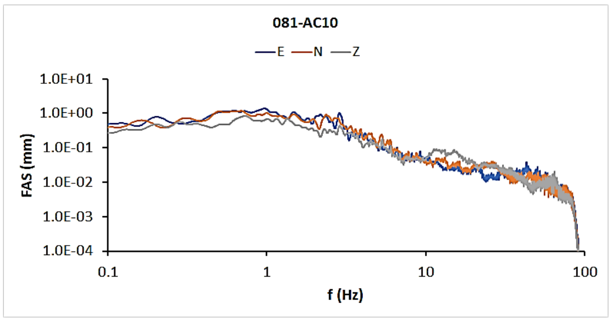
081-AC10
E N Z
FAS (mm)
1.0E+01
1.0E+00
1.0E-01
1.0E-02
1.0E-03
1.0E-04
0.1
1
10
100
f (Hz)

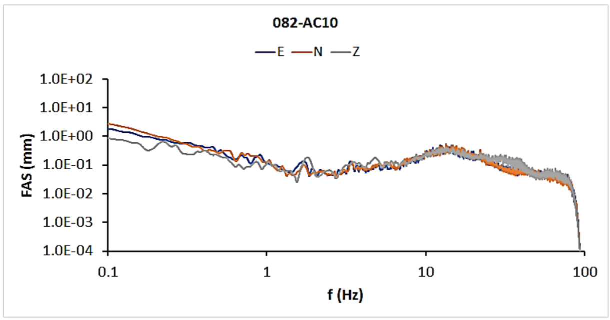
082-AC10
E N Z
FAS (mm)
1.0E+02
1.0E+01
1.0E+00
1.0E-01
1.0E-02
1.0E-03
1.0E-04
0.1
1
10
100
f (Hz)

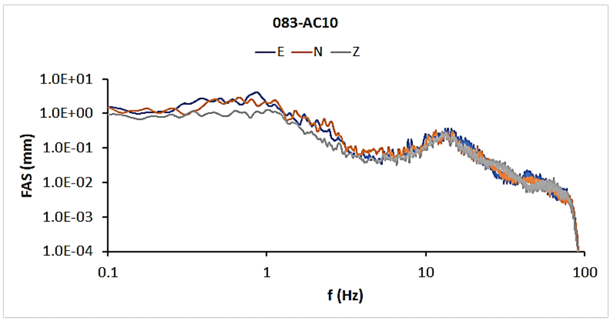
083-AC10
E N Z
FAS (mm)
1.0E+01
1.0E+00
1.0E-01
1.0E-02
1.0E-03
1.0E-04
0.1
1
10
100
f (Hz)

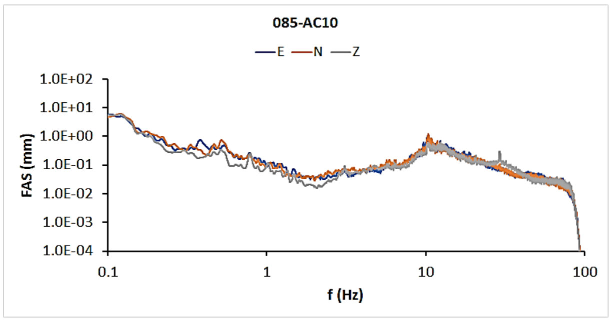
085-AC10
E N Z
FAS (mm)
1.0E+02
1.0E+01
1.0E+00
1.0E-01
1.0E-02
1.0E-03
1.0E-04
0.1
1
10
100
f (Hz)

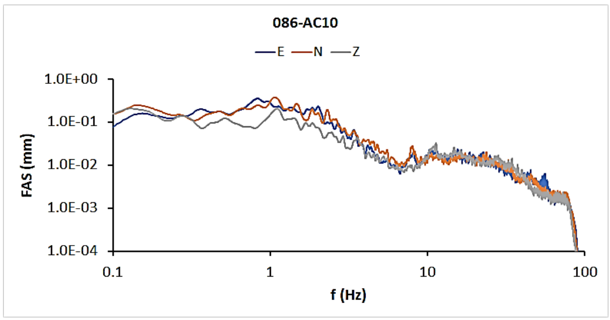
086-AC10
E N Z
FAS (mm)
1.0E+00
1.0E-01
1.0E-02
1.0E-03
1.0E-04
0.1
1
10
100
f (Hz)

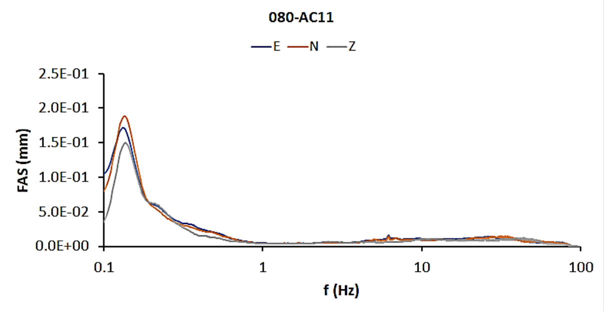
080-AC11
E
N
Z
2.5E-01
2.0E-01
1.5E-01
1.0E-01
5.0E-02
0.0E+00
FAS (mm)
0.1
1
10
100
f (Hz)

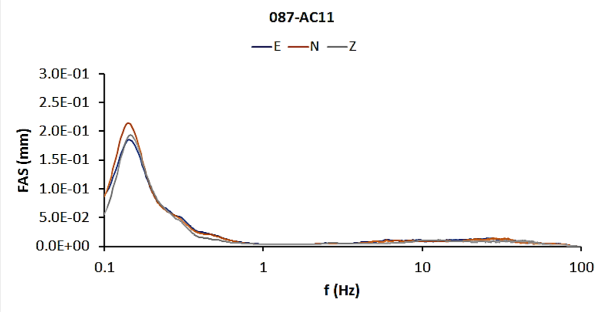
087-AC11
E
N
Z
3.0E-01
2.5E-01
2.0E-01
1.5E-01
1.0E-01
5.0E-02
0.0E+00
FAS (mm)
0.1
1
10
100
f (Hz)

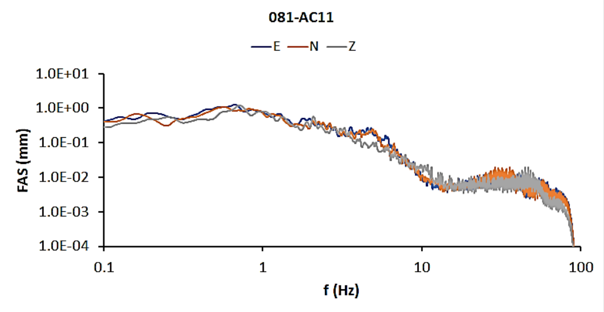
081-AC11
E
N
Z
1.0E+01
1.0E+00
1.0E-01
1.0E-02
1.0E-03
1.0E-04
FAS (mm)
0.1
1
10
100
f (Hz)

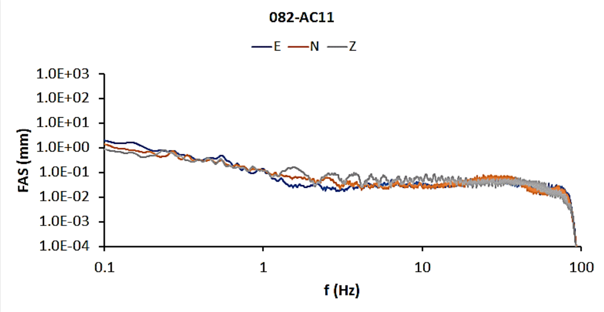
082-AC11
E
N
Z
1.0E+03
1.0E+02
1.0E+01
1.0E+00
1.0E-01
1.0E-02
1.0E-03
1.0E-04
FAS (mm)
0.1
1
10
100
f (Hz)

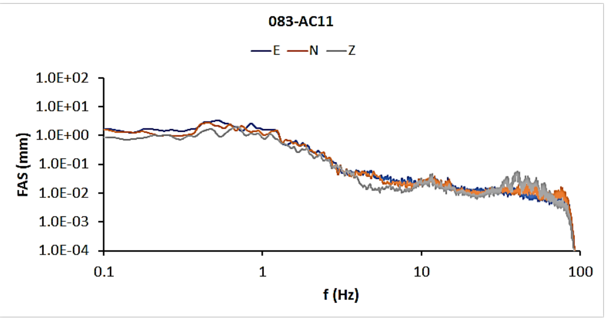
083-AC11
E
N
Z
1.0E+02
1.0E+01
1.0E+00
1.0E-01
1.0E-02
1.0E-03
1.0E-04
FAS (mm)
0.1
1
10
100
f (Hz)

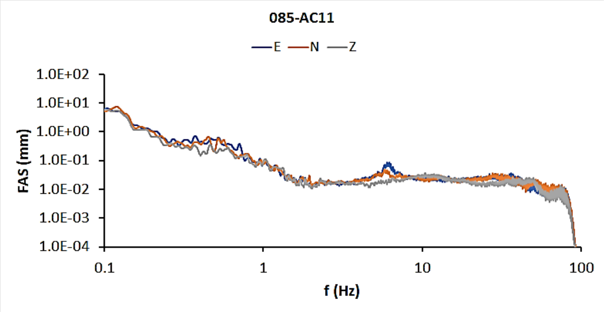
085-AC11
E
N
Z
1.0E+02
1.0E+01
1.0E+00
1.0E-01
1.0E-02
1.0E-03
1.0E-04
FAS (mm)
0.1
1
10
100
f (Hz)

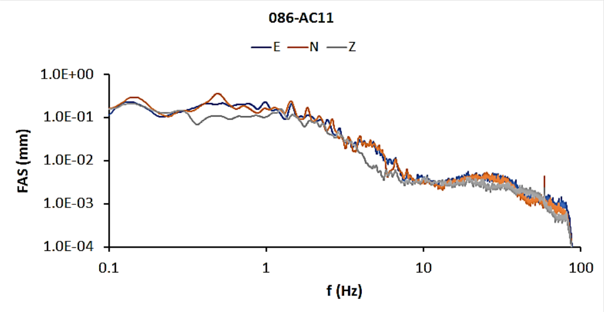
086-AC11
E
N
Z
1.0E+00
1.0E-01
1.0E-02
1.0E-03
1.0E-04
FAS (mm)
0.1
1
10
100
f (Hz)

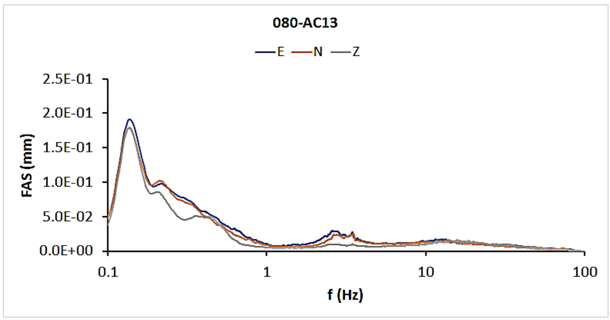
080-AC13
E
N
Z
FAS (mm)
2.5E-01
2.0E-01
1.5E-01
1.0E-01
5.0E-02
0.0E+00
0.1
1
10
100
f (Hz)

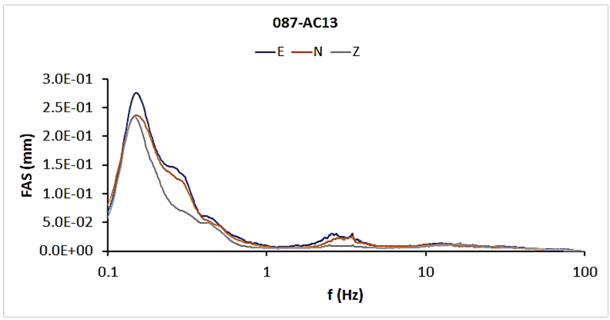
087-AC13
E
N
Z
FAS (mm)
3.0E-01
2.5E-01
2.0E-01
1.5E-01
1.0E-01
5.0E-02
0.0E+00
0.1
1
10
100
f (Hz)

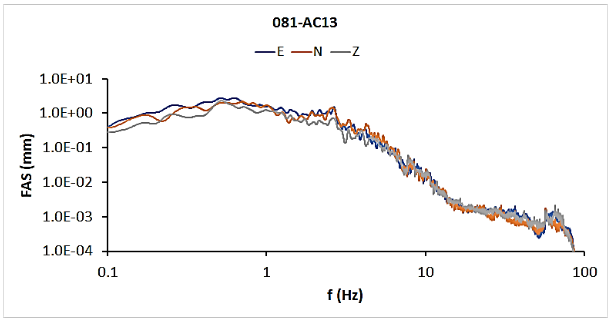
081-AC13
E
N
Z
FAS (mm)
1.0E+01
1.0E+00
1.0E-01
1.0E-02
1.0E-03
1.0E-04
0.1
1
10
100
f (Hz)

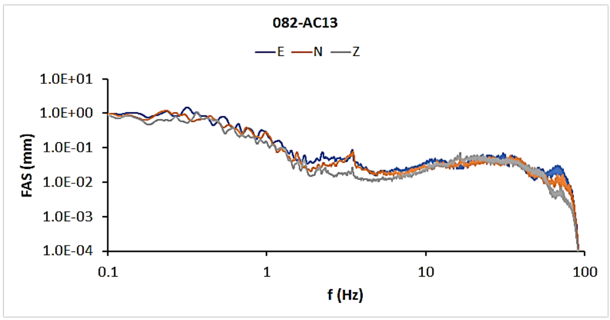
082-AC13
E
N
Z
FAS (mm)
1.0E+01
1.0E+00
1.0E-01
1.0E-02
1.0E-03
1.0E-04
0.1
1
10
100
f (Hz)

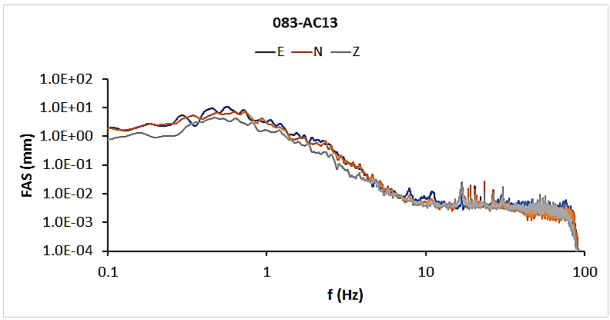
083-AC13
E
N
Z
FAS (mm)
1.0E+02
1.0E+01
1.0E+00
1.0E-01
1.0E-02
1.0E-03
1.0E-04
0.1
1
10
100
f (Hz)

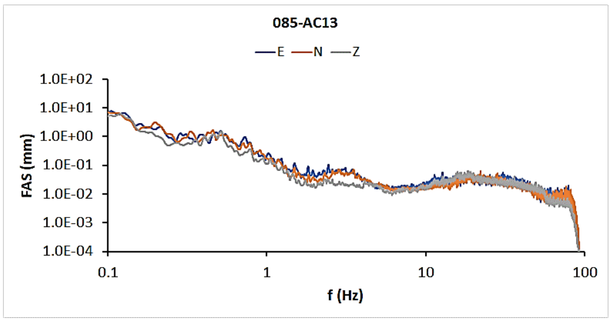
085-AC13
E
N
Z
FAS (mm)
1.0E+02
1.0E+01
1.0E+00
1.0E-01
1.0E-02
1.0E-03
1.0E-04
0.1
1
10
100
f (Hz)

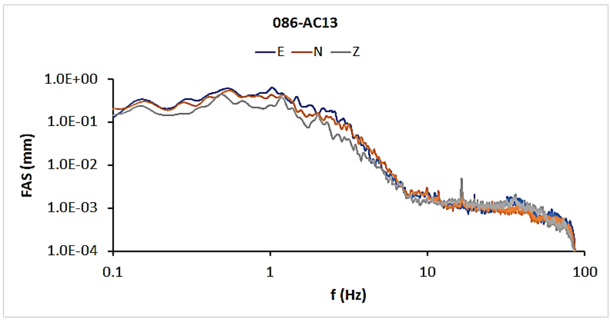
086-AC13
E
N
Z
FAS (mm)
1.0E+00
1.0E-01
1.0E-02
1.0E-03
1.0E-04
0.1
1
10
100
f (Hz)

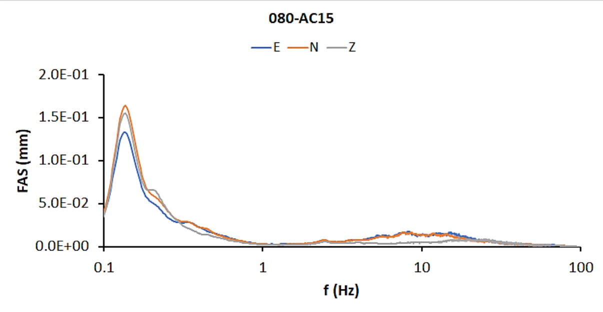
080-AC15
E N Z
2.0E-01
1.5E-01
1.0E-01
5.0E-02
0.0E+00
FAS (mm)
0.1
1
10
100
f (Hz)

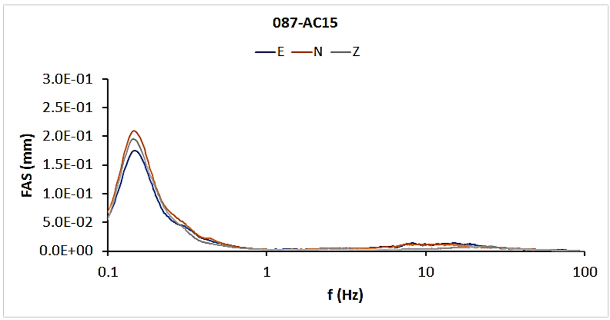
087-AC15
E N Z
3.0E-01
2.5E-01
2.0E-01
1.5E-01
1.0E-01
5.0E-02
0.0E+00
FAS (mm)
0.1
1
10
100
f (Hz)

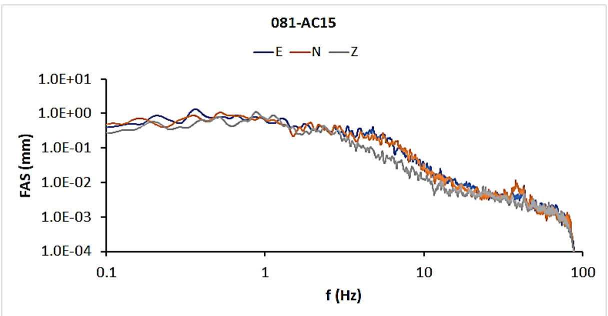
081-AC15
E N Z
1.0E+01
1.0E+00
1.0E-01
1.0E-02
1.0E-03
1.0E-04
FAS (mm)
0.1
1
10
100
f (Hz)

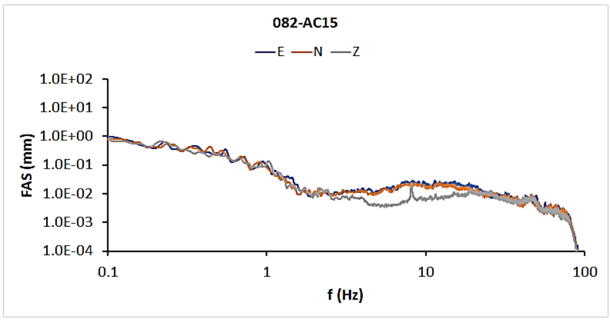
082-AC15
E N Z
1.0E+02
1.0E+01
1.0E+00
1.0E-01
1.0E-02
1.0E-03
1.0E-04
FAS (mm)
0.1
1
10
100
f (Hz)

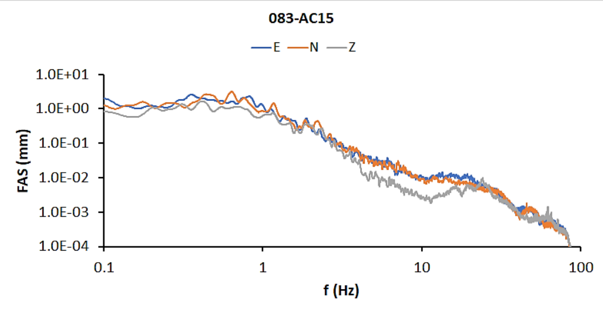
083-AC15
E N Z
1.0E+01
1.0E+00
1.0E-01
1.0E-02
1.0E-03
1.0E-04
FAS (mm)
0.1
1
10
100
f (Hz)

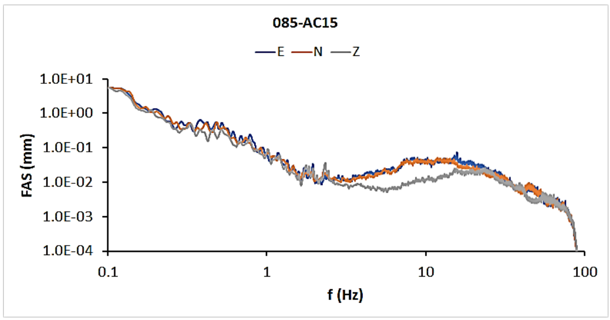
085-AC15
E N Z
1.0E+01
1.0E+00
1.0E-01
1.0E-02
1.0E-03
1.0E-04
FAS (mm)
0.1
1
10
100
f (Hz)

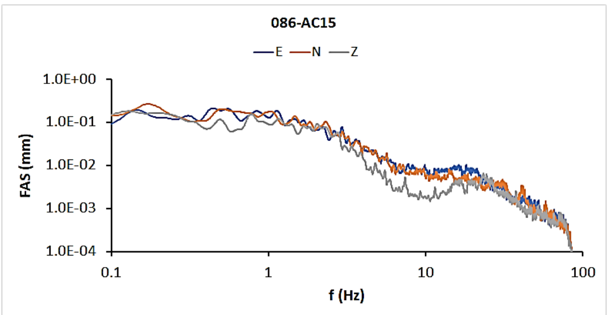
086-AC15
E N Z
1.0E+00
1.0E-01
1.0E-02
1.0E-03
1.0E-04
FAS (mm)
0.1
1
10
100
f (Hz)

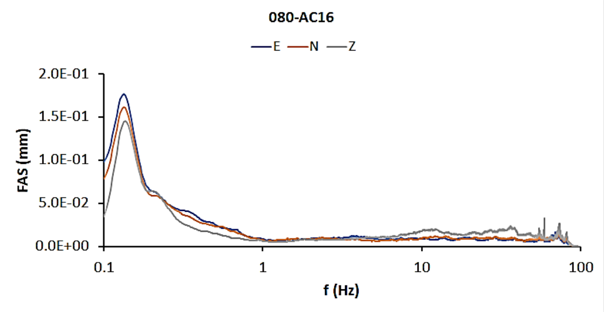
080-AC16
E N Z
2.0E-01
1.5E-01
1.0E-01
5.0E-02
0.0E+00
FAS (mm)
0.1
1
10
100
f (Hz)

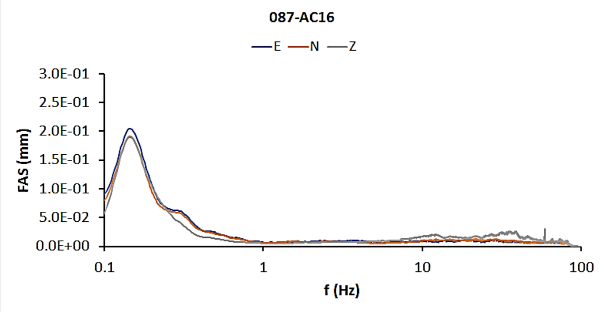
087-AC16
E N Z
3.0E-01
2.5E-01
2.0E-01
1.5E-01
1.0E-01
5.0E-02
0.0E+00
FAS (mm)
0.1
1
10
100
f (Hz)

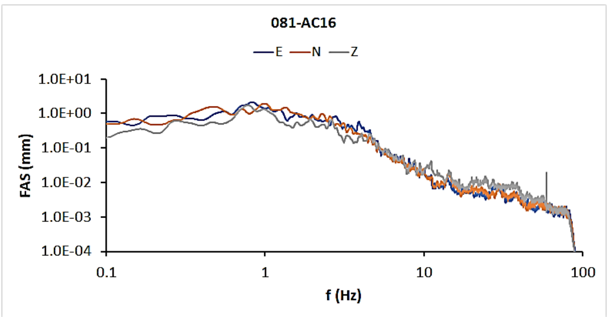
081-AC16
E N Z
1.0E+01
1.0E+00
1.0E-01
1.0E-02
1.0E-03
1.0E-04
FAS (mm)
0.1
1
10
100
f (Hz)

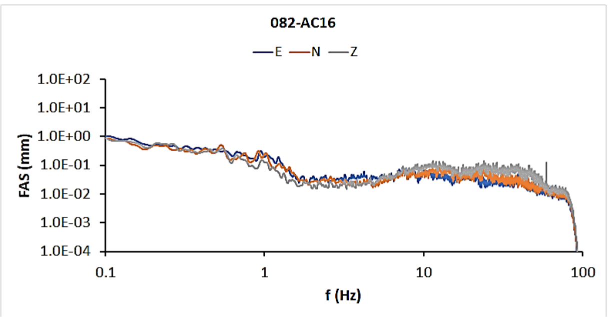
082-AC16
E N Z
1.0E+02
1.0E+01
1.0E+00
1.0E-01
1.0E-02
1.0E-03
1.0E-04
FAS (mm)
0.1
1
10
100
f (Hz)

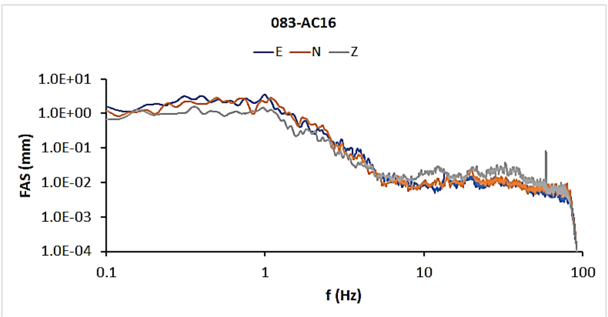
083-AC16
E N Z
1.0E+01
1.0E+00
1.0E-01
1.0E-02
1.0E-03
1.0E-04
FAS (mm)
0.1
1
10
100
f (Hz)

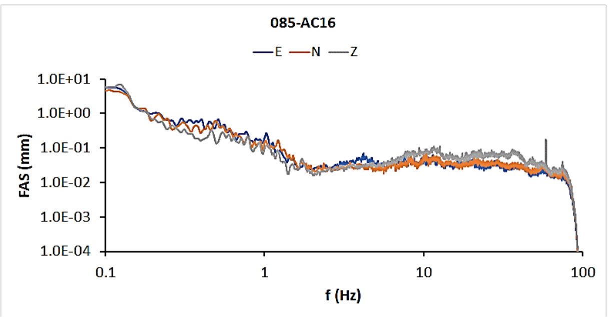
085-AC16
E N Z
1.0E+01
1.0E+00
1.0E-01
1.0E-02
1.0E-03
1.0E-04
FAS (mm)
0.1
1
10
100
f (Hz)

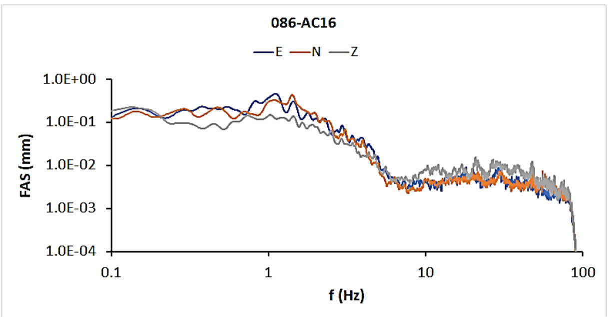
086-AC16
E N Z
1.0E+00
1.0E-01
1.0E-02
1.0E-03
1.0E-04
FAS (mm)
0.1
1
10
100
f (Hz)

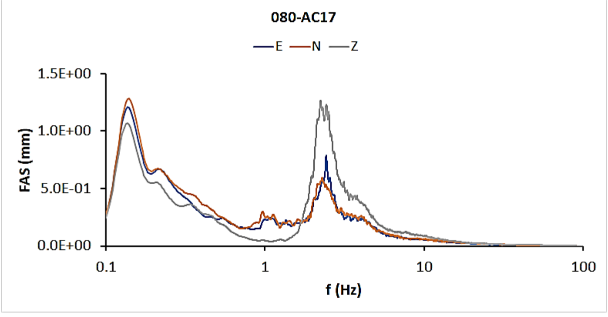
080-AC17
E N Z
FAS (mm)
f (Hz)

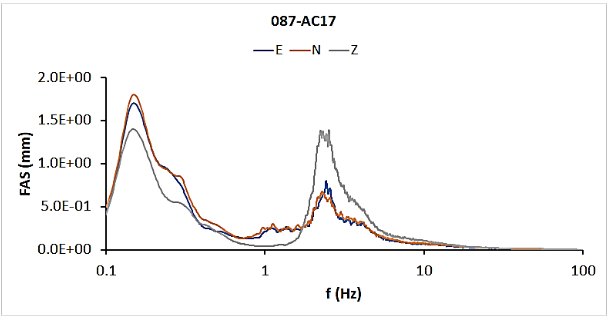
087-AC17
E N Z
FAS (mm)
f (Hz)

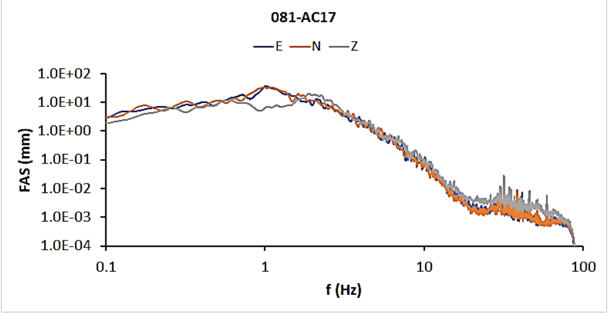
081-AC17
E N Z
FAS (mm)
f (Hz)

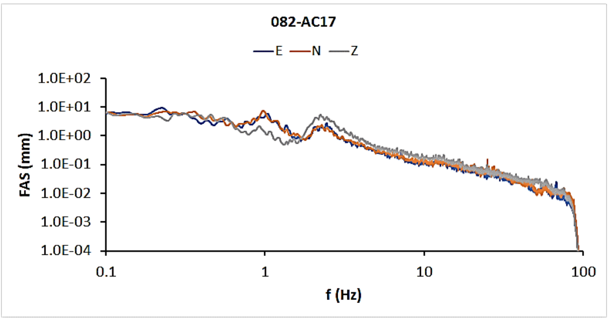
082-AC17
E N Z
FAS (mm)
f (Hz)

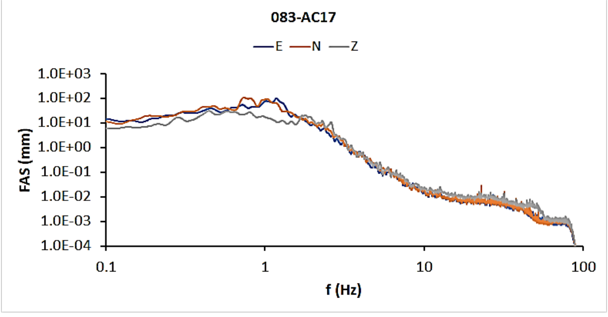
083-AC17
E N Z
FAS (mm)
f (Hz)

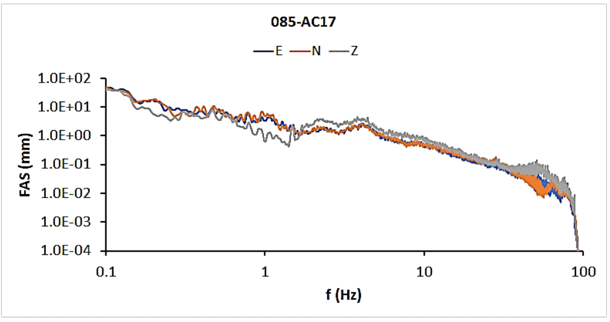
085-AC17
E N Z
FAS (mm)
f (Hz)

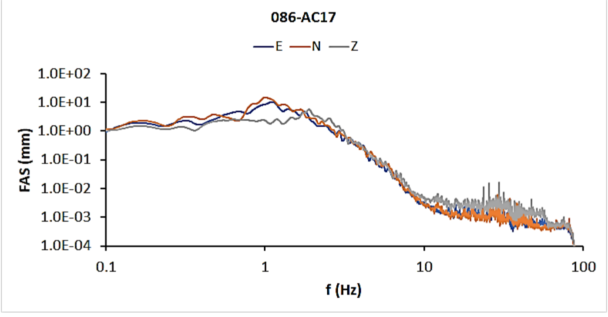
086-AC17
E N Z
FAS (mm)
f (Hz)

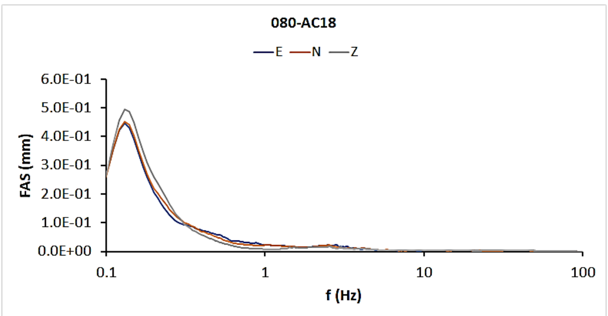
080-AC18
E
N
Z
6.0E-01
5.0E-01
4.0E-01
3.0E-01
2.0E-01
1.0E-01
0.0E+00
FAS (mm)
0.1
1
10
100
f (Hz)

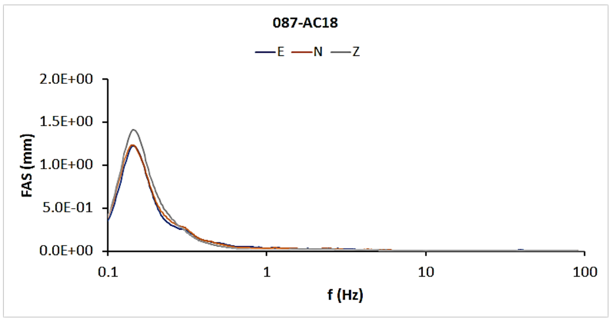
087-AC18
E
N
Z
2.0E+00
1.5E+00
1.0E+00
5.0E-01
0.0E+00
FAS (mm)
0.1
1
10
100
f (Hz)

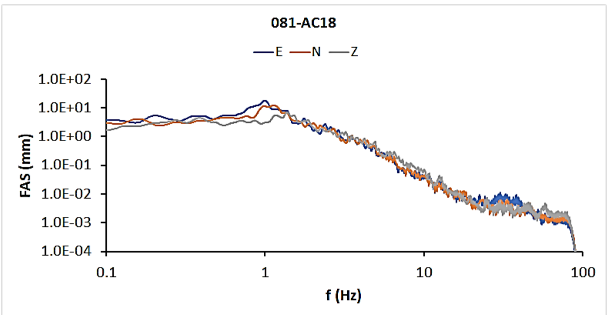
081-AC18
E
N
Z
1.0E+02
1.0E+01
1.0E+00
1.0E-01
1.0E-02
1.0E-03
1.0E-04
FAS (mm)
0.1
1
10
100
f (Hz)

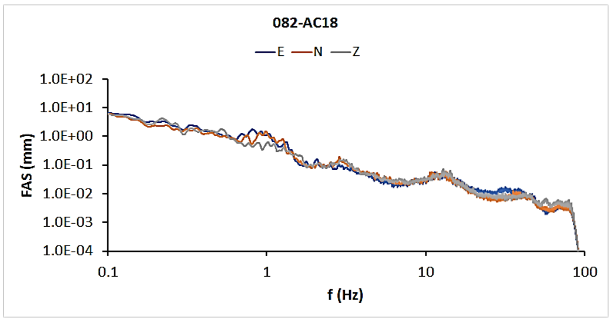
082-AC18
E
N
Z
1.0E+02
1.0E+01
1.0E+00
1.0E-01
1.0E-02
1.0E-03
1.0E-04
FAS (mm)
0.1
1
10
100
f (Hz)

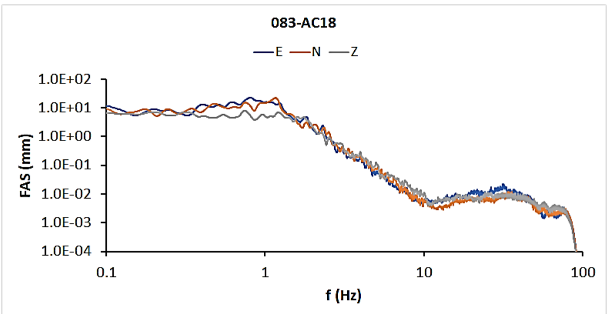
083-AC18
E
N
Z
1.0E+02
1.0E+01
1.0E+00
1.0E-01
1.0E-02
1.0E-03
1.0E-04
FAS (mm)
0.1
1
10
100
f (Hz)

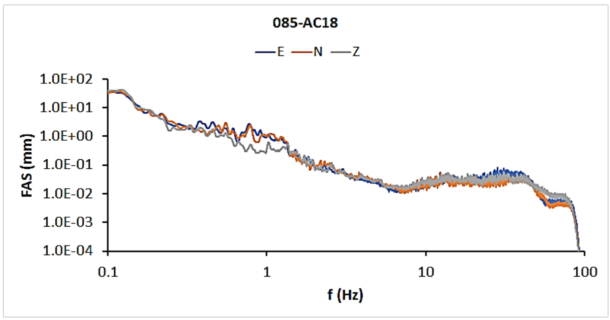
085-AC18
E
N
Z
1.0E+02
1.0E+01
1.0E+00
1.0E-01
1.0E-02
1.0E-03
1.0E-04
FAS (mm)
0.1
1
10
100
f (Hz)

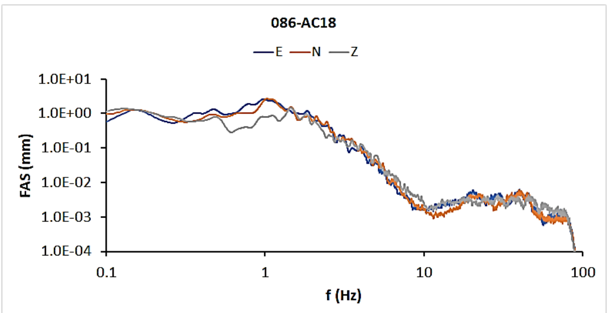
086-AC18
E
N
Z
1.0E+01
1.0E+00
1.0E-01
1.0E-02
1.0E-03
1.0E-04
FAS (mm)
0.1
1
10
100
f (Hz)

Appendix 4-I Day 086 Comparison of spectral ratios

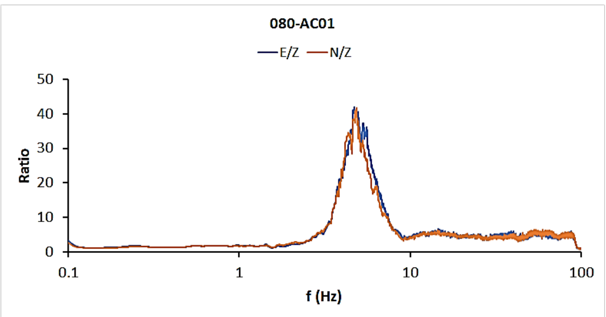

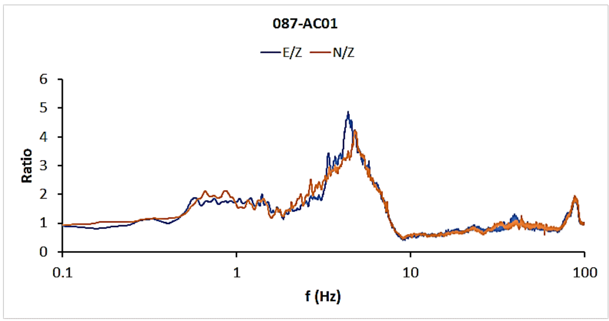

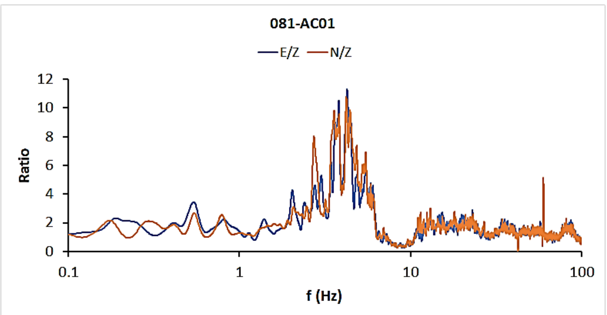

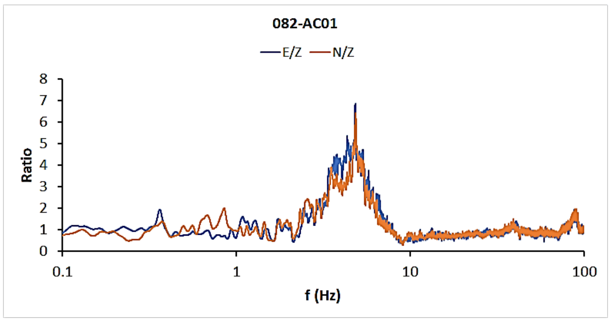

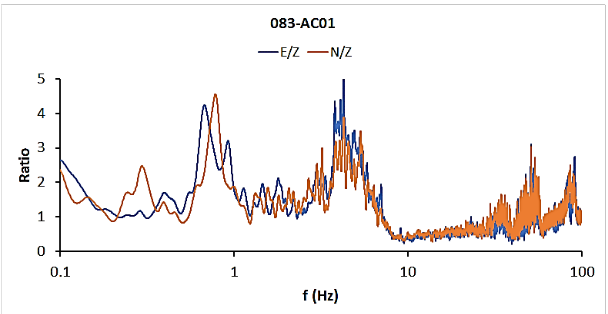

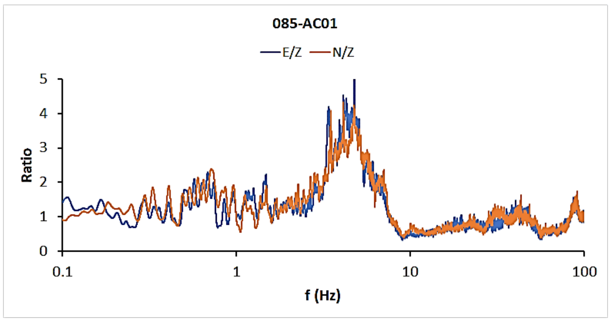

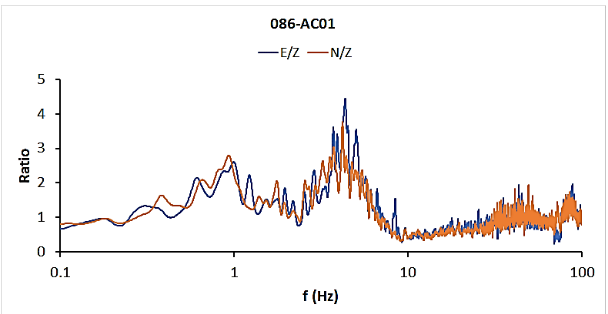

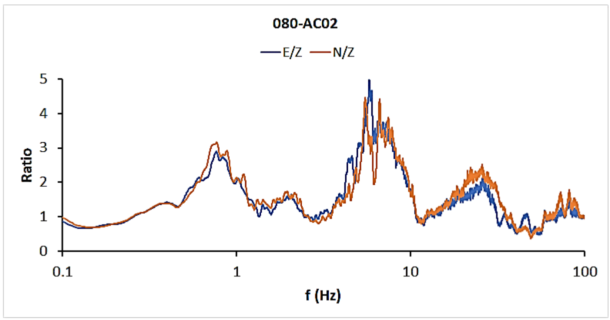
080-AC02
E/Z N/Z
Ratio
f (Hz)

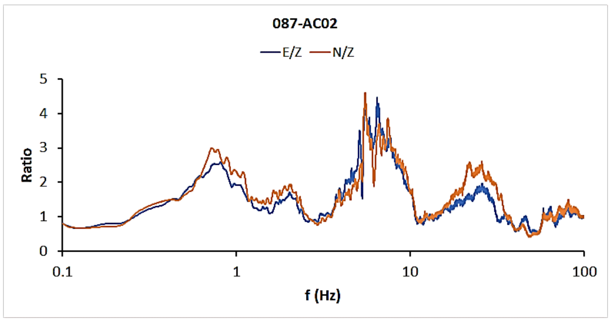
087-AC02
E/Z N/Z
Ratio
f (Hz)

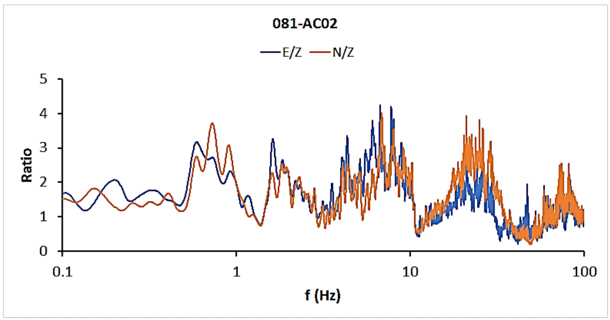
081-AC02
E/Z N/Z
Ratio
f (Hz)

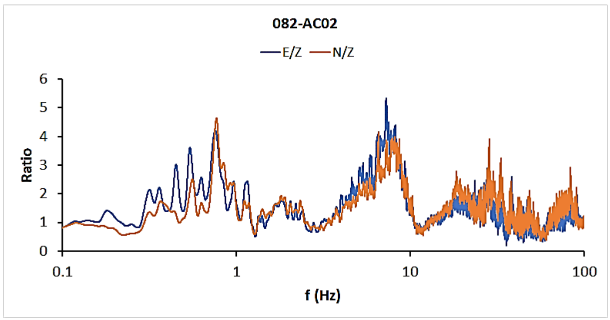
082-AC02
E/Z N/Z
Ratio
f (Hz)

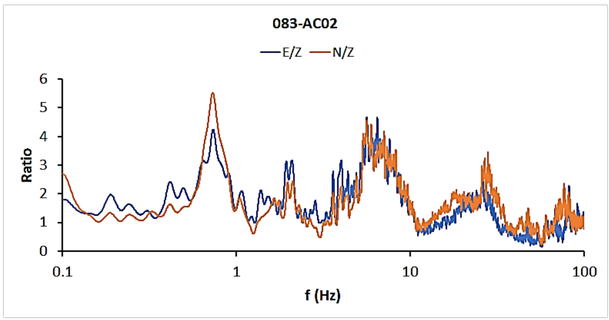
083-AC02
E/Z N/Z
Ratio
f (Hz)

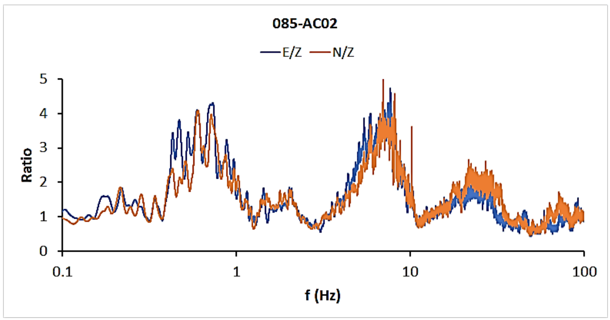
085-AC02
E/Z N/Z
Ratio
f (Hz)

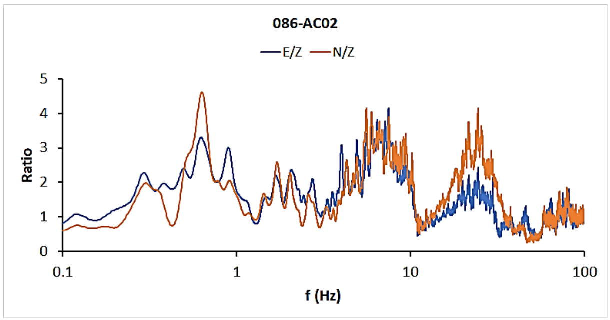
086-AC02
E/Z N/Z
Ratio
f (Hz)

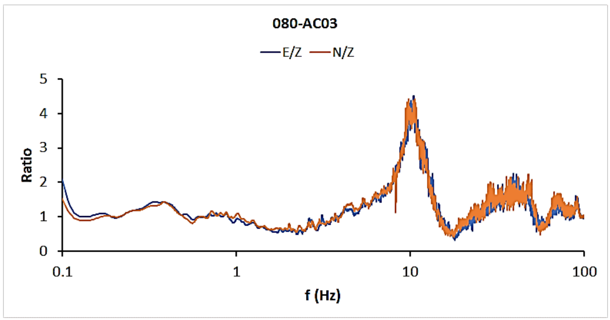
080-AC03
E/Z
N/Z
Ratio
f (Hz)

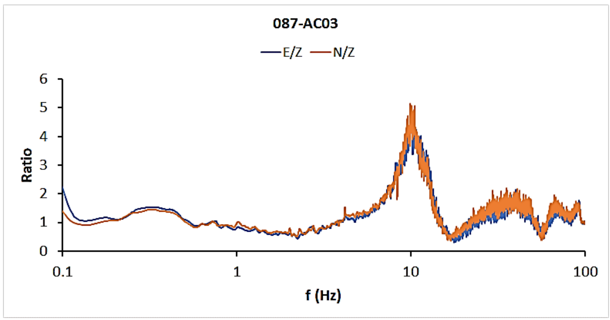
087-AC03
E/Z
N/Z
Ratio
f (Hz)

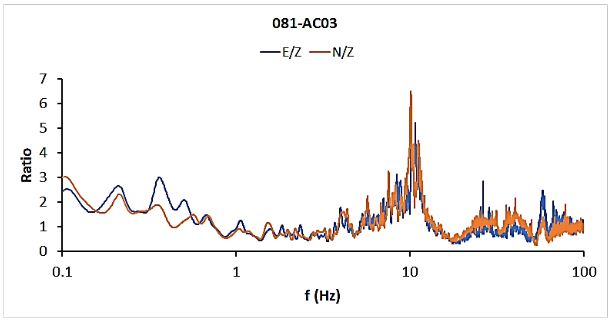
081-AC03
E/Z
N/Z
Ratio
f (Hz)

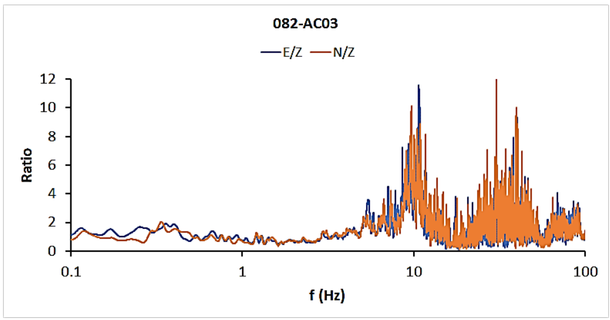
082-AC03
E/Z
N/Z
Ratio
f (Hz)

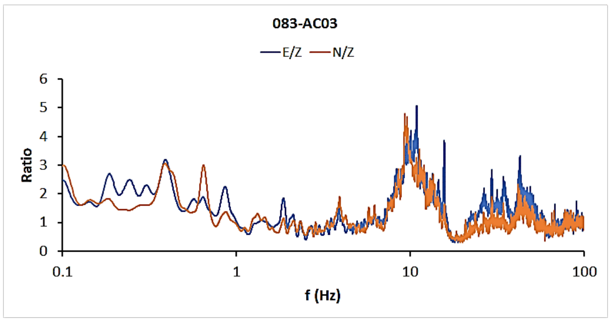
083-AC03
E/Z
N/Z
Ratio
f (Hz)

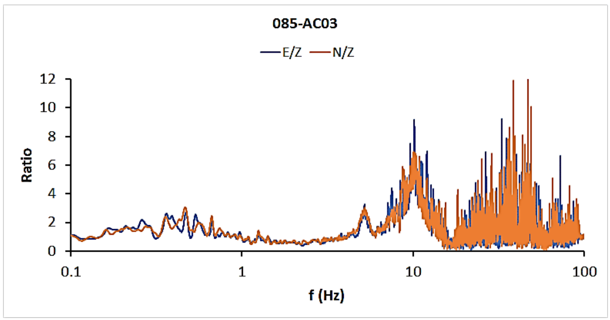
085-AC03
E/Z
N/Z
Ratio
f (Hz)

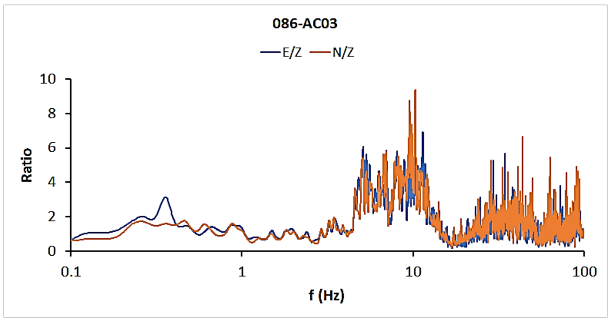
086-AC03
E/Z
N/Z
Ratio
f (Hz)

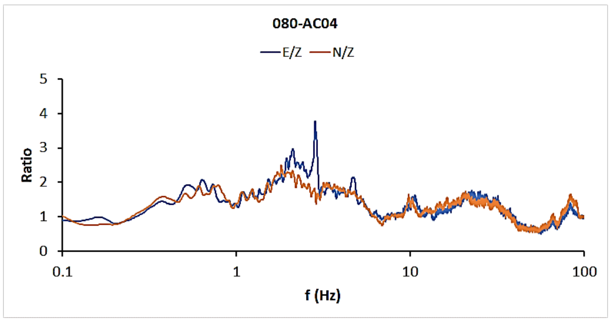
080-AC04
E/Z N/Z
Ratio
f (Hz)

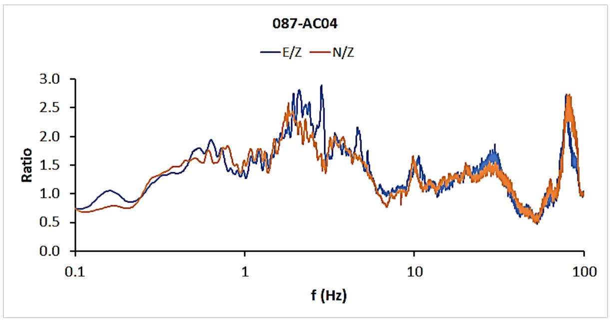
087-AC04
E/Z N/Z
Ratio
f (Hz)

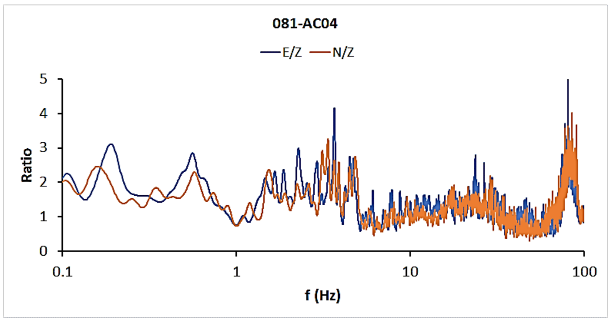
081-AC04
E/Z N/Z
Ratio
f (Hz)

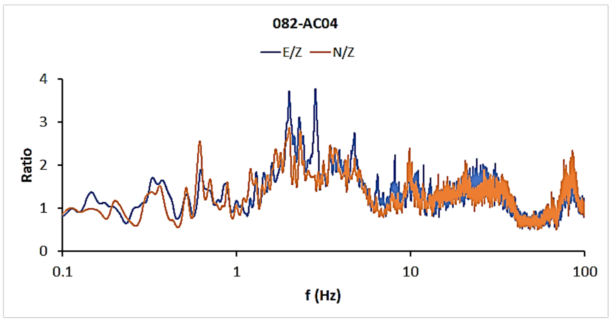
082-AC04
E/Z N/Z
Ratio
f (Hz)

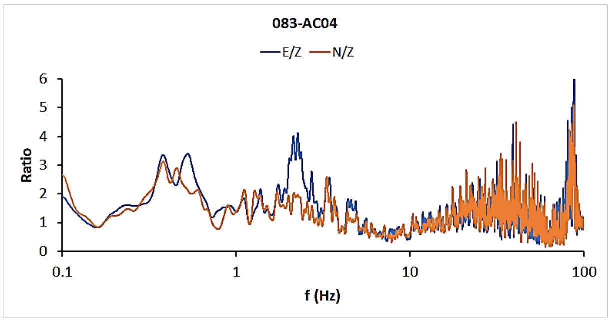
083-AC04
E/Z N/Z
Ratio
f (Hz)

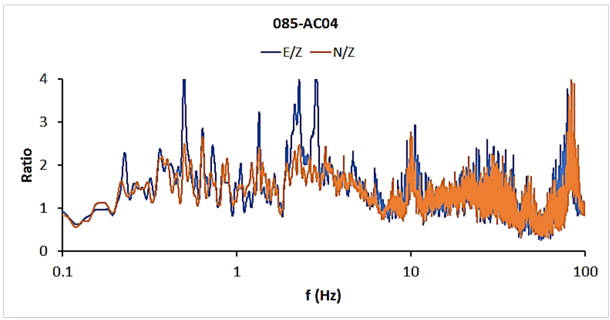
085-AC04
E/Z N/Z
Ratio
f (Hz)

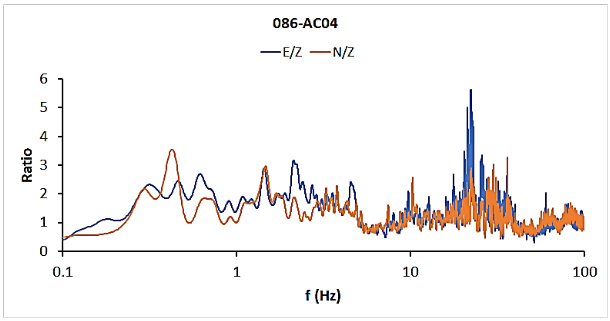
086-AC04
E/Z N/Z
Ratio
f (Hz)

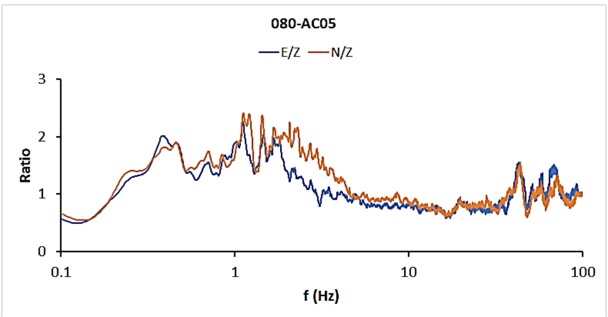
080-AC05
E/Z
N/Z
Ratio
f (Hz)

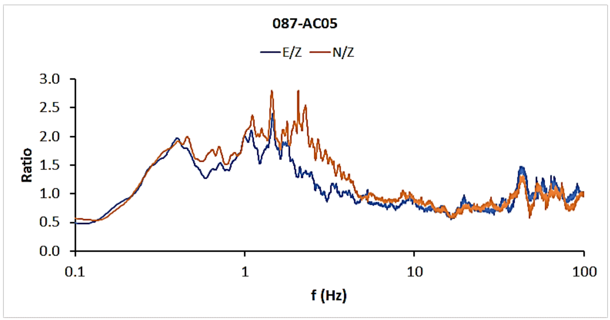
087-AC05
E/Z
N/Z
Ratio
f (Hz)

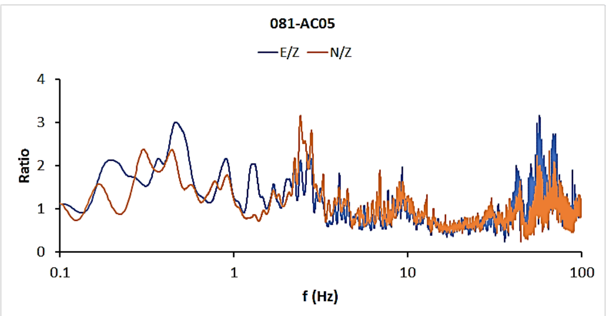
081-AC05
E/Z
N/Z
Ratio
f (Hz)

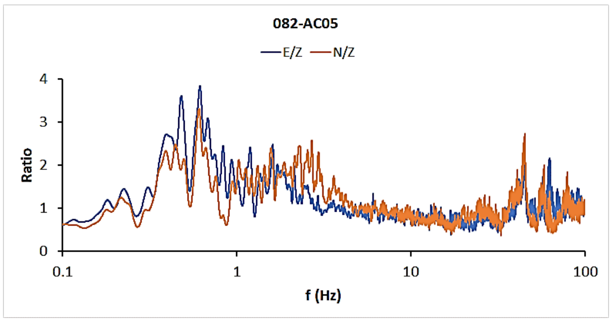
082-AC05
E/Z
N/Z
Ratio
f (Hz)

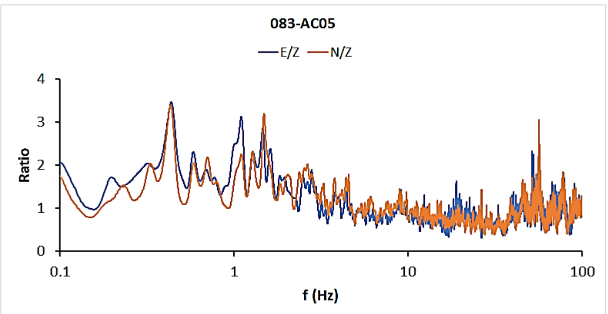
083-AC05
E/Z
N/Z
Ratio
f (Hz)

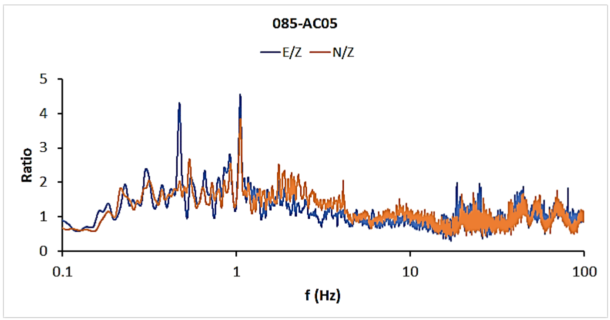
085-AC05
E/Z
N/Z
Ratio
f (Hz)

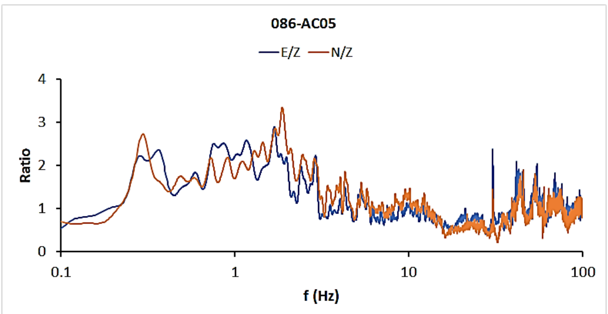
086-AC05
E/Z
N/Z
Ratio
f (Hz)

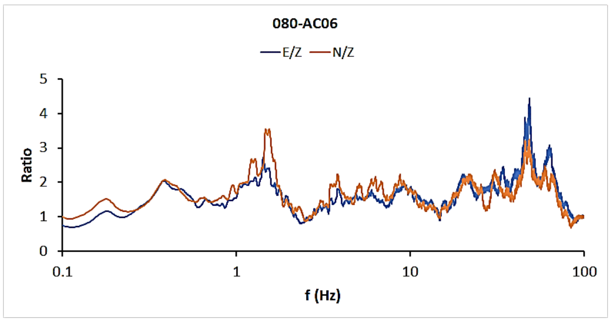
080-AC06
E/Z N/Z
Ratio
0 1 2 3 4 5
0.1 1 10 100
f (Hz)

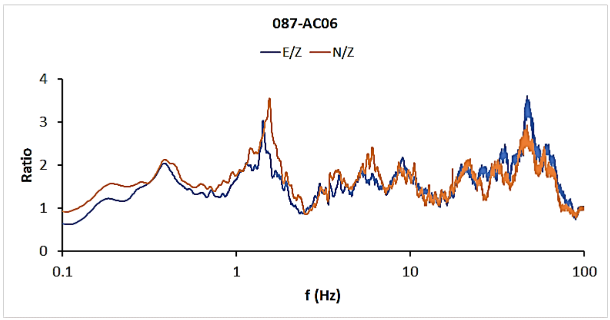
087-AC06
E/Z N/Z
Ratio
0 1 2 3 4
0.1 1 10 100
f (Hz)

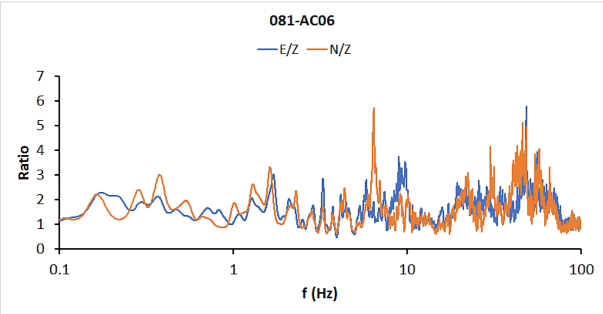
081-AC06
E/Z N/Z
Ratio
0 1 2 3 4 5 6 7
0.1 1 10 100
f (Hz)

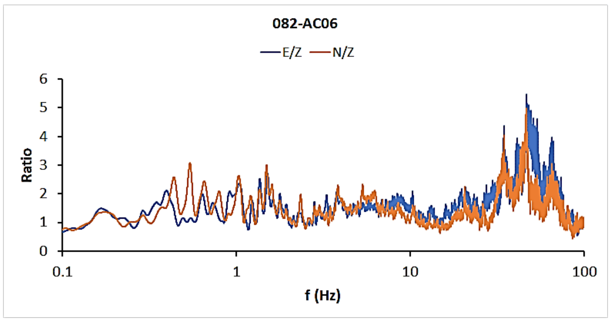
082-AC06
E/Z N/Z
Ratio
0 1 2 3 4 5 6
0.1 1 10 100
f (Hz)

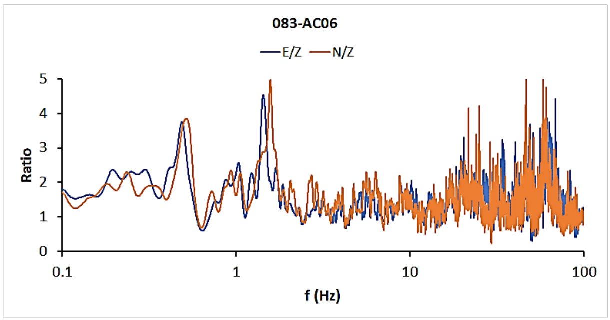
083-AC06
E/Z N/Z
Ratio
0 1 2 3 4 5
0.1 1 10 100
f (Hz)

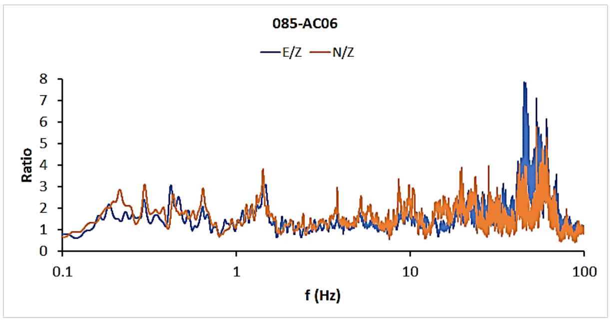
085-AC06
E/Z N/Z
Ratio
0 1 2 3 4 5 6 7 8
0.1 1 10 100
f (Hz)

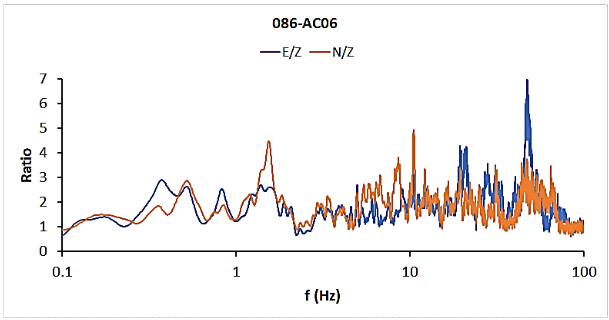
086-AC06
E/Z N/Z
Ratio
0 1 2 3 4 5 6 7
0.1 1 10 100
f (Hz)

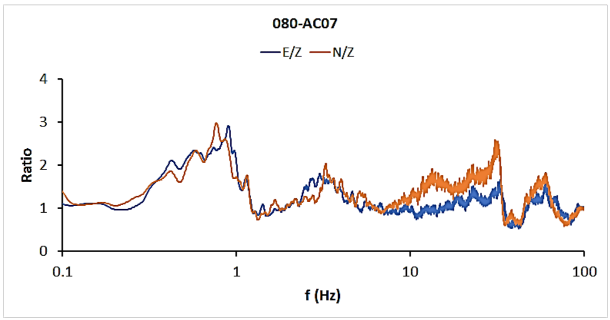
080-AC07
E/Z
N/Z
Ratio
f (Hz)
0
1
2
3
4
0.1
1
10
100

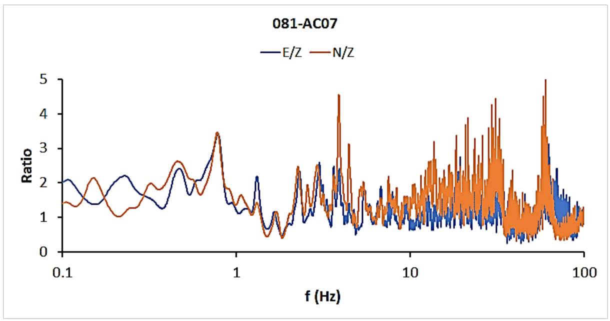
081-AC07
E/Z
N/Z
Ratio
f (Hz)
0
1
2
3
4
5
0.1
1
10
100

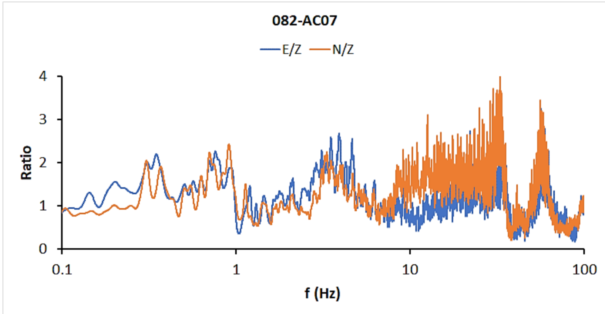
082-AC07
E/Z
N/Z
Ratio
f (Hz)
0
1
2
3
4
0.1
1
10
100

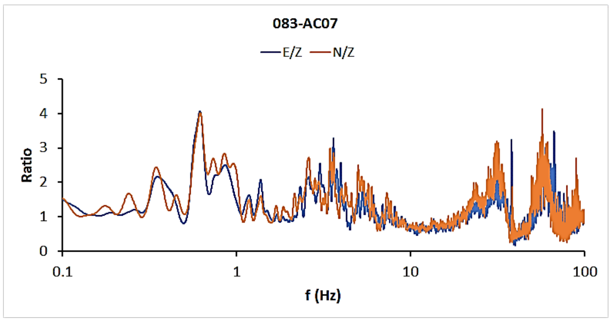
083-AC07
E/Z
N/Z
Ratio
f (Hz)
0
1
2
3
4
5
0.1
1
10
100

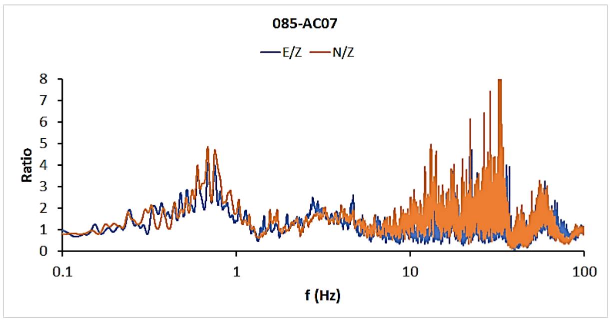
085-AC07
E/Z
N/Z
Ratio
f (Hz)
0
1
2
3
4
5
6
7
8
0.1
1
10
100

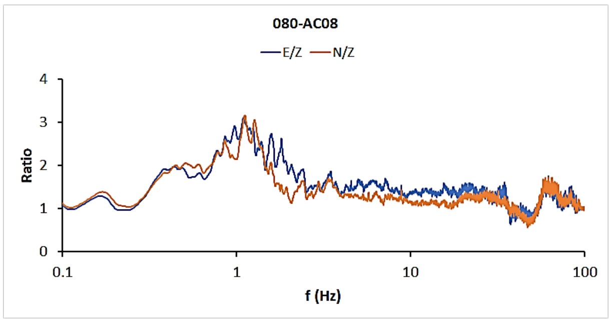
080-AC08
E/Z
N/Z
Ratio
f (Hz)

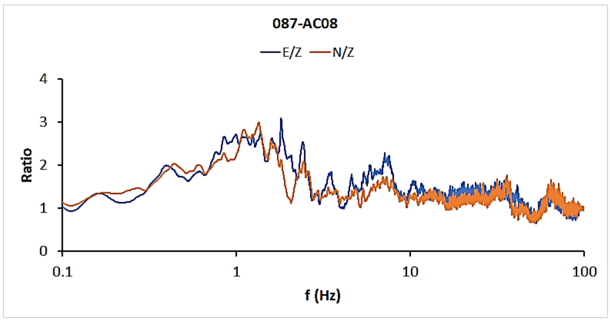
087-AC08
E/Z
N/Z
Ratio
f (Hz)

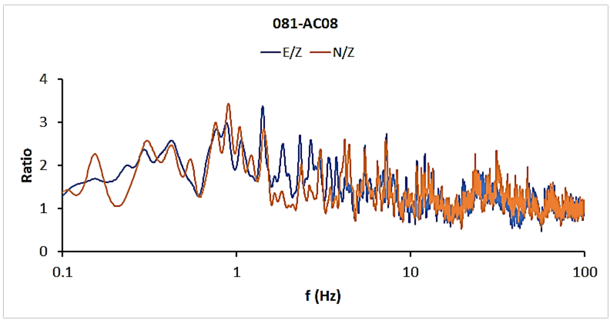
081-AC08
E/Z
N/Z
Ratio
f (Hz)

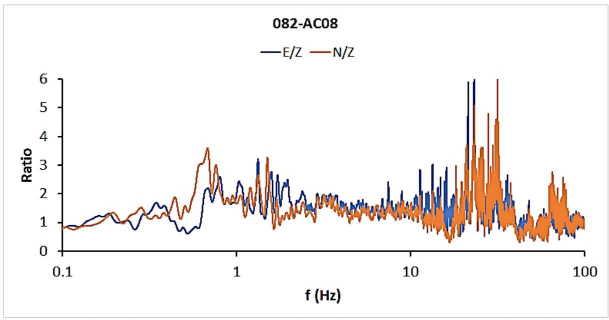
082-AC08
E/Z
N/Z
Ratio
f (Hz)

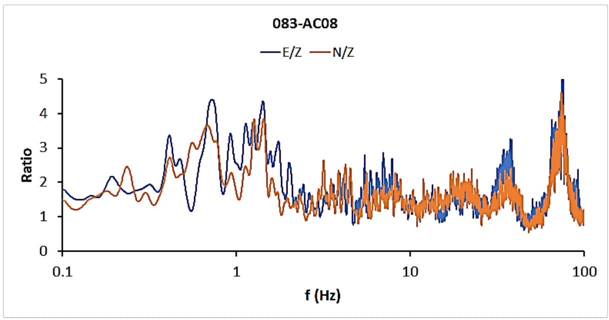
083-AC08
E/Z
N/Z
Ratio
f (Hz)

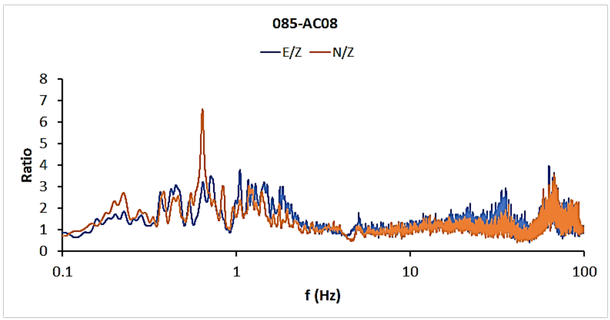
085-AC08
E/Z
N/Z
Ratio
f (Hz)

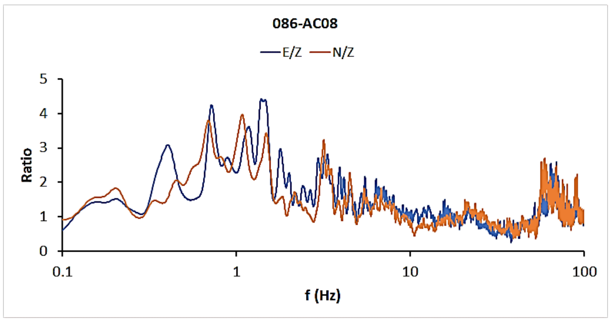
086-AC08
E/Z
N/Z
Ratio
f (Hz)

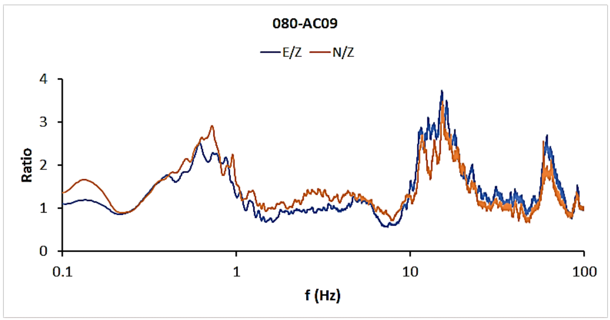
080-AC09
E/Z N/Z
Ratio
f (Hz)

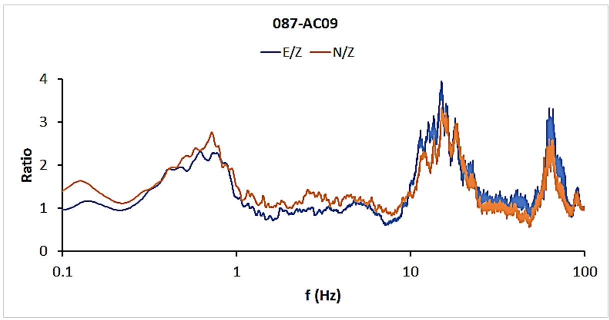
087-AC09
E/Z N/Z
Ratio
f (Hz)

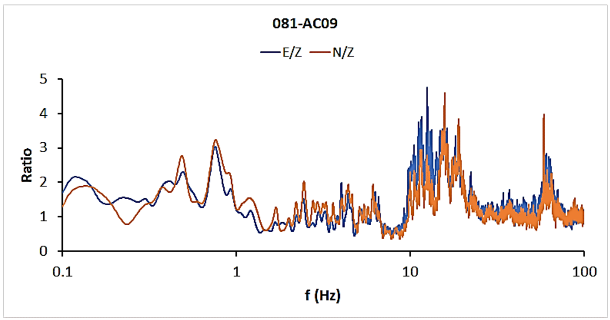
081-AC09
E/Z N/Z
Ratio
f (Hz)

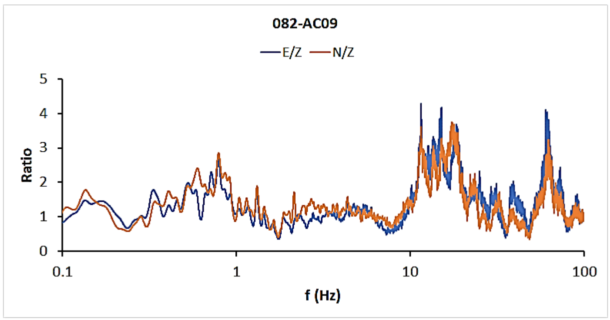
082-AC09
E/Z N/Z
Ratio
f (Hz)

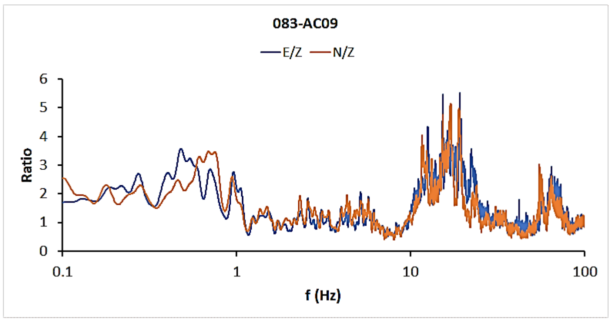
083-AC09
E/Z N/Z
Ratio
f (Hz)

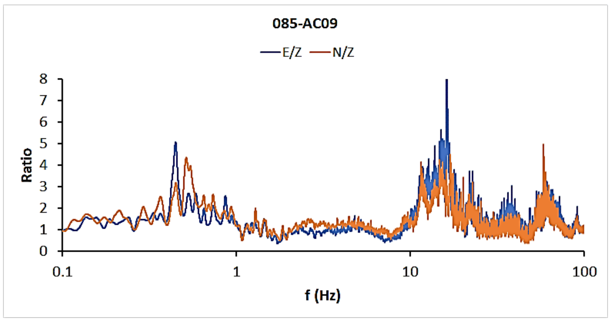
085-AC09
E/Z N/Z
Ratio
f (Hz)

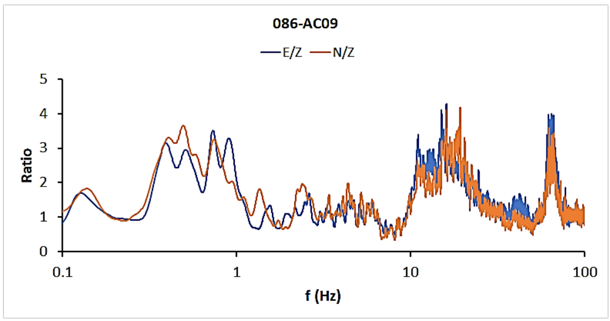
086-AC09
E/Z N/Z
Ratio
f (Hz)

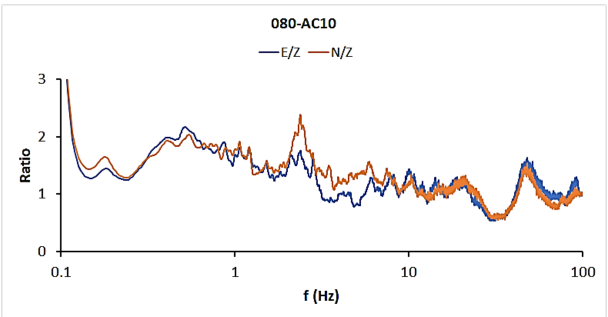
080-AC10
E/Z N/Z
Ratio
f (Hz)

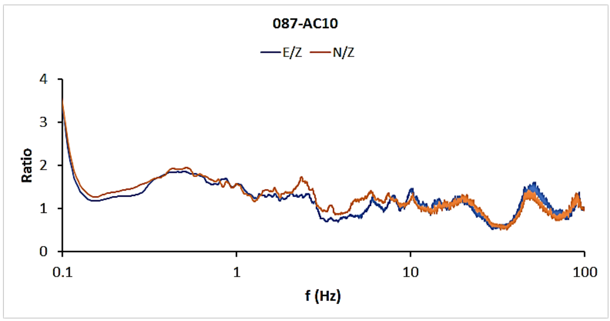
087-AC10
E/Z N/Z
Ratio
f (Hz)

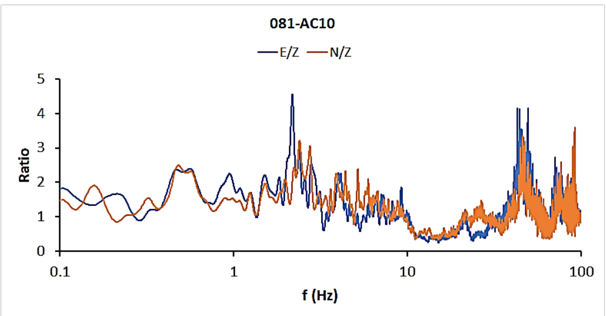
081-AC10
E/Z N/Z
Ratio
f (Hz)

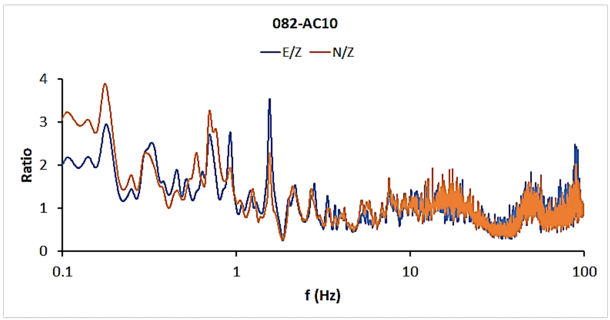
082-AC10
E/Z N/Z
Ratio
f (Hz)

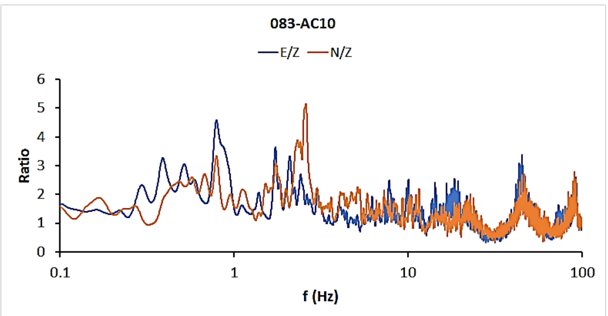
083-AC10
E/Z N/Z
Ratio
f (Hz)

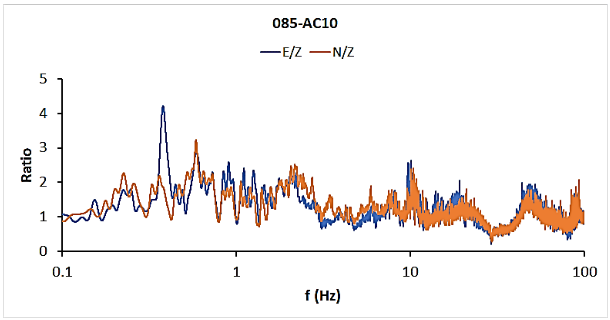
085-AC10
E/Z N/Z
Ratio
f (Hz)

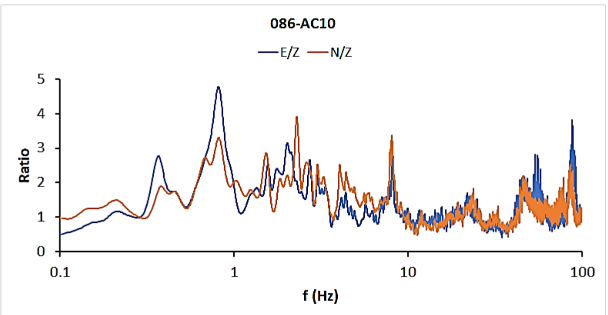
086-AC10
E/Z N/Z
Ratio
f (Hz)

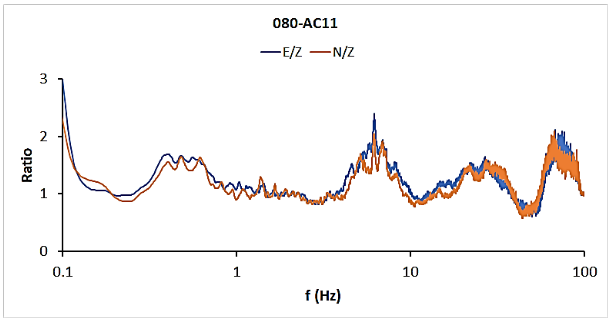
080-AC11
E/Z
N/Z
Ratio
f (Hz)
0
1
2
3
0.1
1
10
100

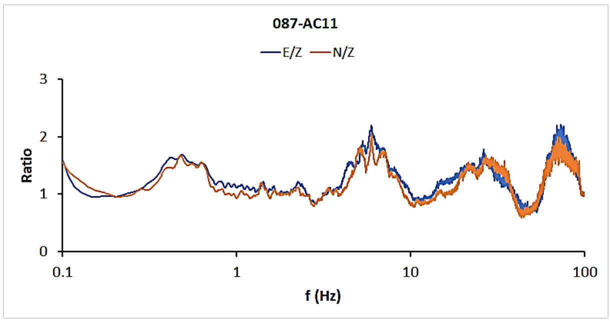
087-AC11
E/Z
N/Z
Ratio
f (Hz)
0
1
2
3
0.1
1
10
100

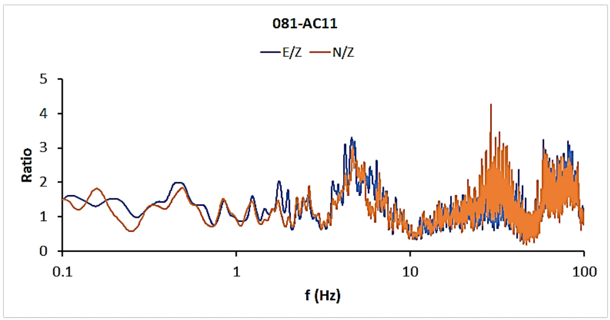
081-AC11
E/Z
N/Z
Ratio
f (Hz)
0
1
2
3
4
5
0.1
1
10
100

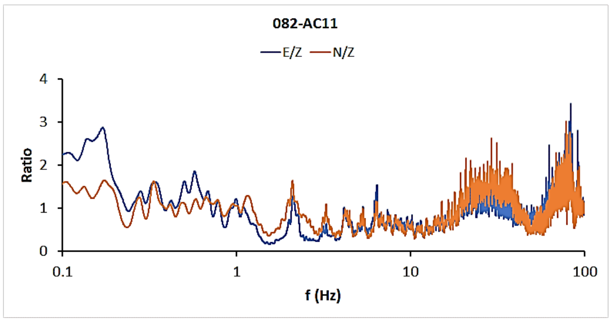
082-AC11
E/Z
N/Z
Ratio
f (Hz)
0
1
2
3
4
0.1
1
10
100

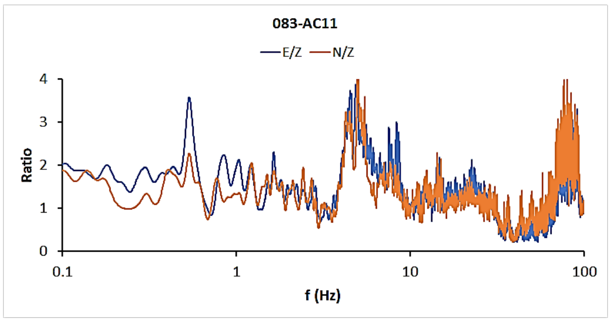
083-AC11
E/Z
N/Z
Ratio
f (Hz)
0
1
2
3
4
0.1
1
10
100

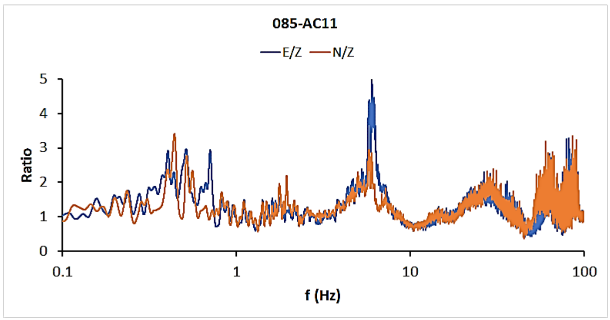
085-AC11
E/Z
N/Z
Ratio
f (Hz)
0
1
2
3
4
5
0.1
1
10
100

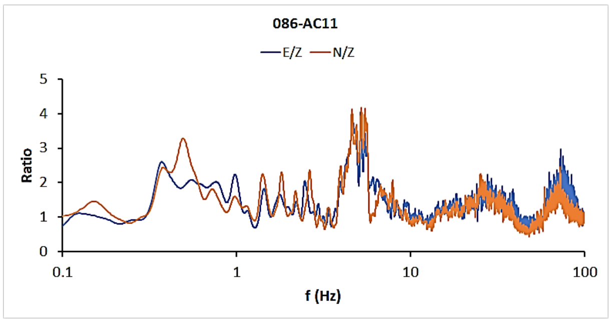
086-AC11
E/Z
N/Z
Ratio
f (Hz)
0
1
2
3
4
5
0.1
1
10
100

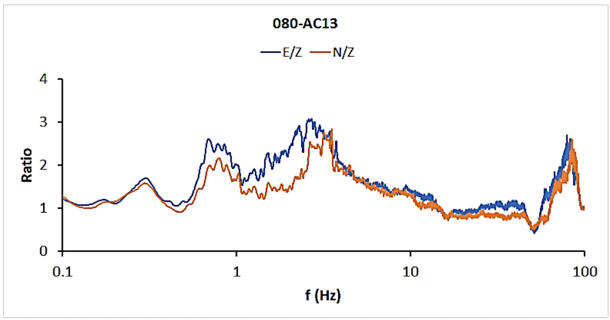
080-AC13
E/Z N/Z
Ratio
f (Hz)

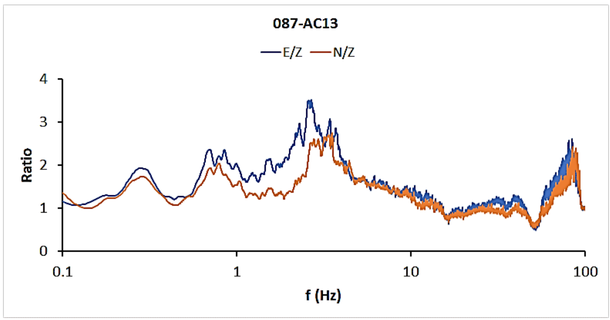
087-AC13
E/Z N/Z
Ratio
f (Hz)

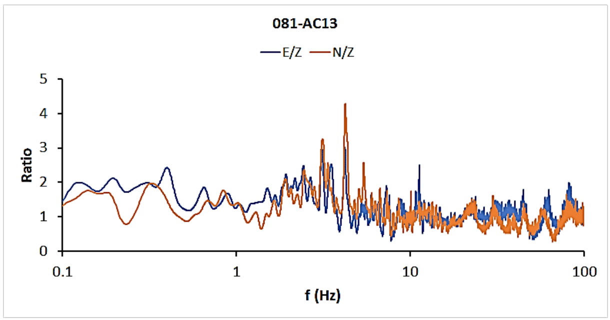
081-AC13
E/Z N/Z
Ratio
f (Hz)

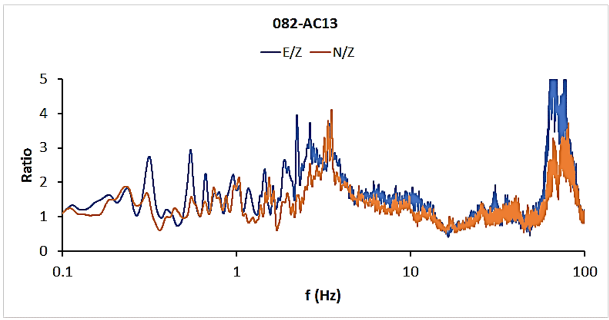
082-AC13
E/Z N/Z
Ratio
f (Hz)

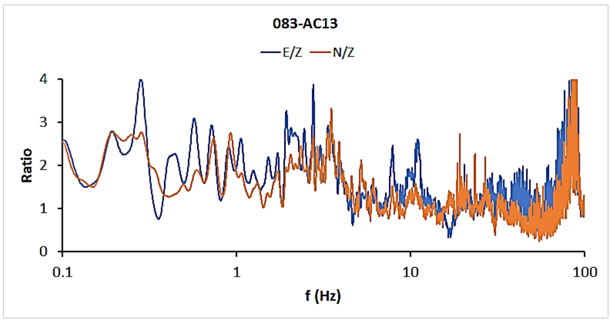
083-AC13
E/Z N/Z
Ratio
f (Hz)

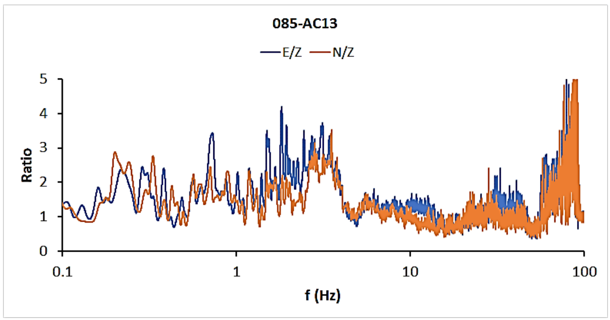
085-AC13
E/Z N/Z
Ratio
f (Hz)

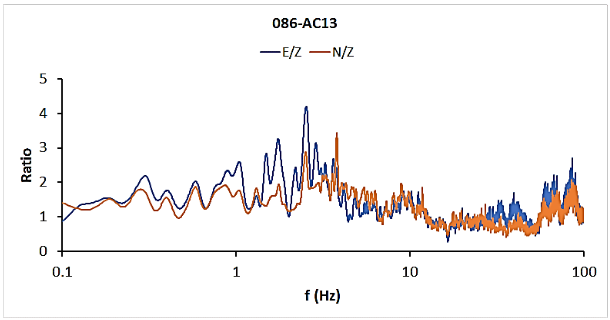
086-AC13
E/Z N/Z
Ratio
f (Hz)

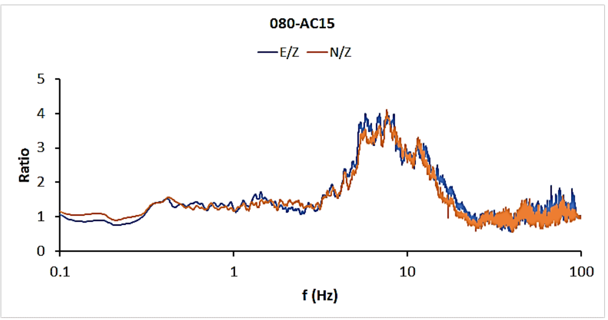
080-AC15
E/Z
N/Z
Ratio
f (Hz)

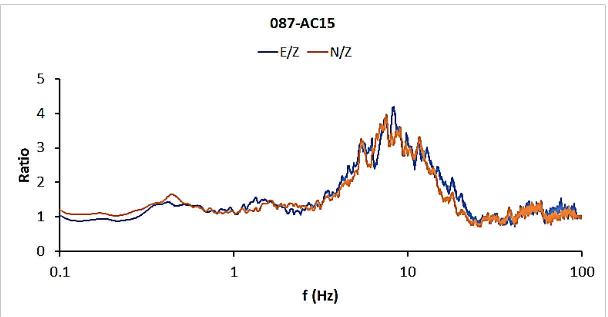
087-AC15
E/Z
N/Z
Ratio
f (Hz)

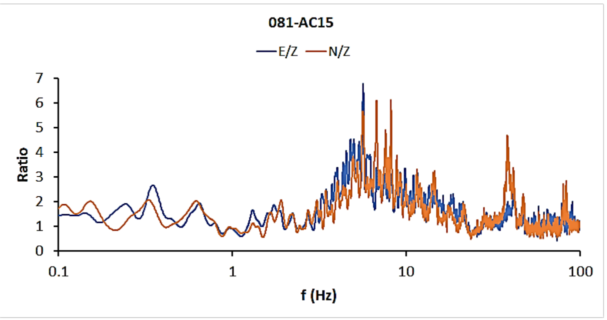
081-AC15
E/Z
N/Z
Ratio
f (Hz)

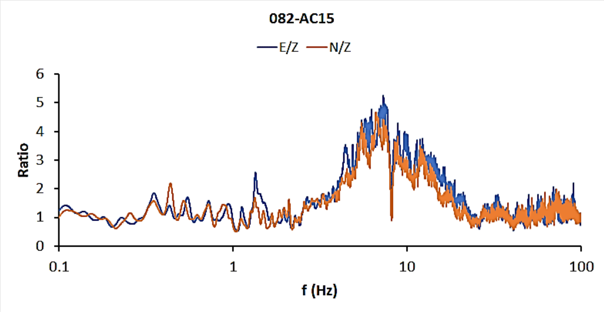
082-AC15
E/Z
N/Z
Ratio
f (Hz)

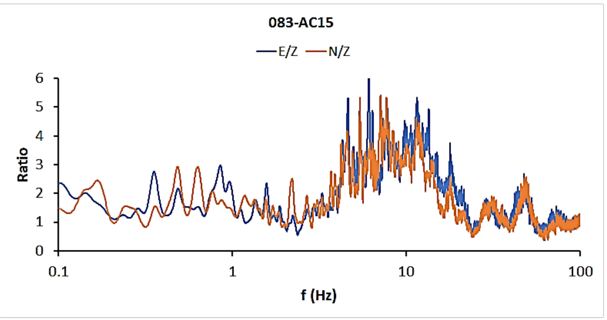
083-AC15
E/Z
N/Z
Ratio
f (Hz)

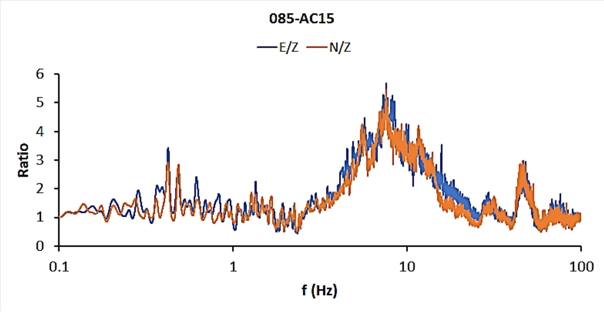
085-AC15
E/Z
N/Z
Ratio
f (Hz)

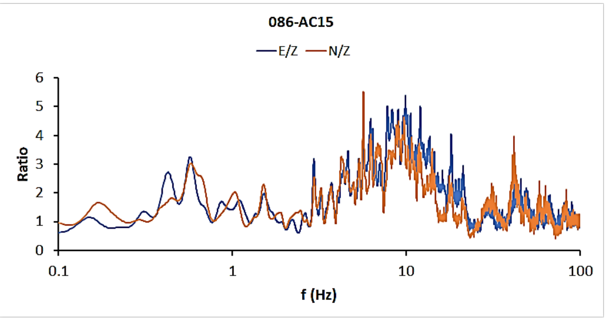
086-AC15
E/Z
N/Z
Ratio
f (Hz)

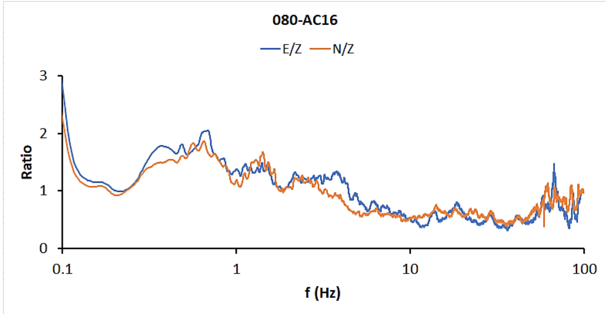
080-AC16
E/Z
N/Z
Ratio
f (Hz)
0 1 2 3
0.1 1 10 100

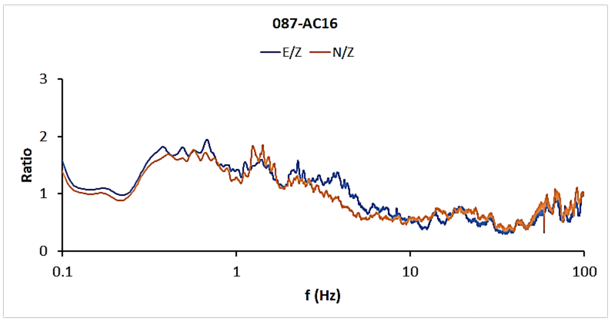
087-AC16
E/Z
N/Z
Ratio
f (Hz)
0 1 2 3
0.1 1 10 100

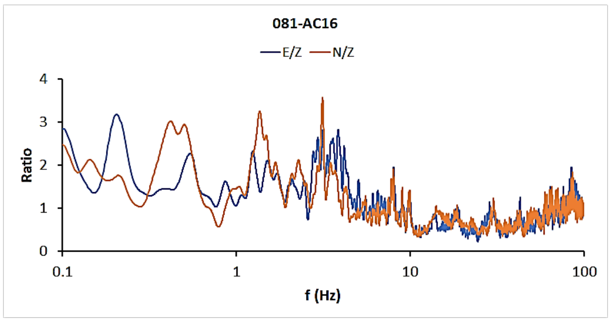
081-AC16
E/Z
N/Z
Ratio
f (Hz)
0 1 2 3 4
0.1 1 10 100

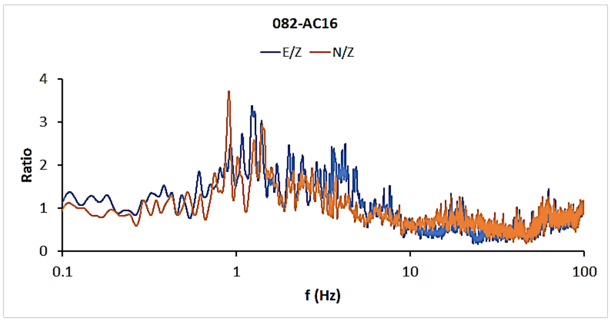
082-AC16
E/Z
N/Z
Ratio
f (Hz)
0 1 2 3 4
0.1 1 10 100

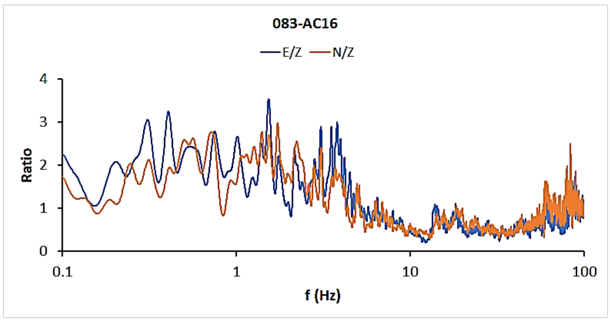
083-AC16
E/Z
N/Z
Ratio
f (Hz)
0 1 2 3 4
0.1 1 10 100

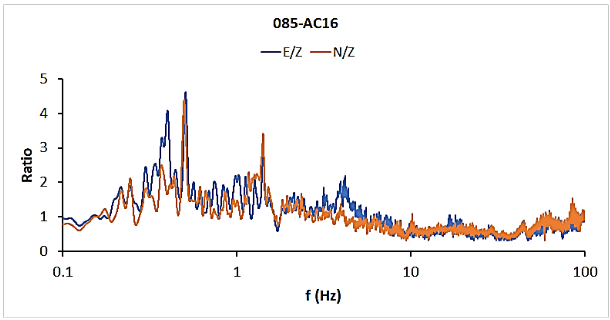
085-AC16
E/Z
N/Z
Ratio
f (Hz)
0 1 2 3 4 5
0.1 1 10 100

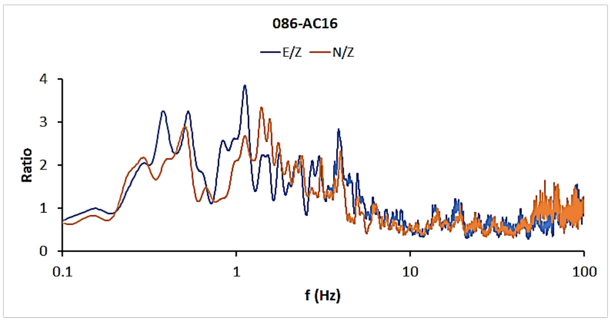
086-AC16
E/Z
N/Z
Ratio
f (Hz)
0 1 2 3 4
0.1 1 10 100

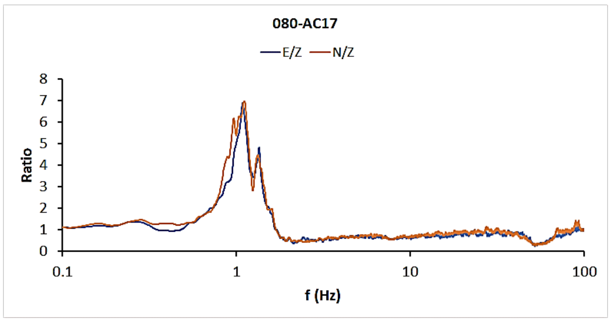
080-AC17
E/Z
N/Z
Ratio
0 1 2 3 4 5 6 7 8
0.1 1 10 100
f (Hz)

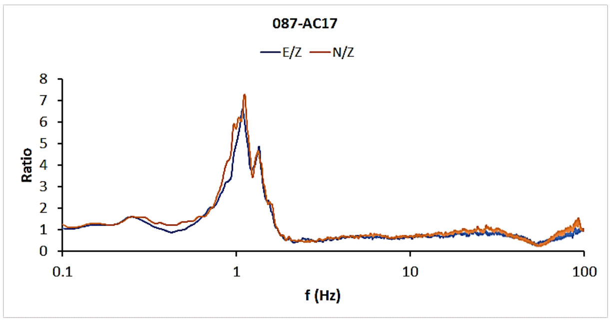
087-AC17
E/Z
N/Z
Ratio
0 1 2 3 4 5 6 7 8
0.1 1 10 100
f (Hz)

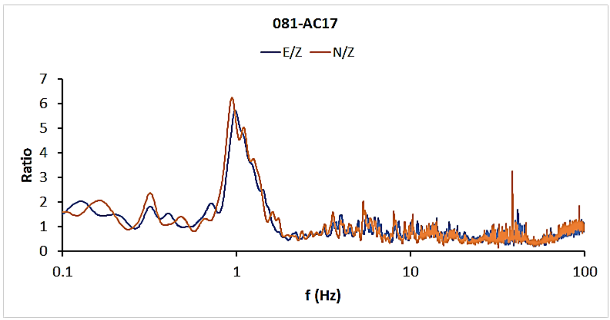
081-AC17
E/Z
N/Z
Ratio
0 1 2 3 4 5 6 7
0.1 1 10 100
f (Hz)

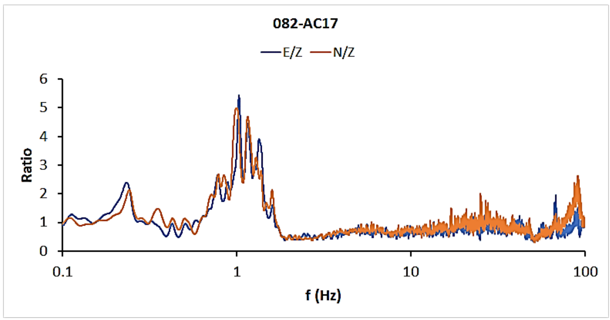
082-AC17
E/Z
N/Z
Ratio
0 1 2 3 4 5 6
0.1 1 10 100
f (Hz)

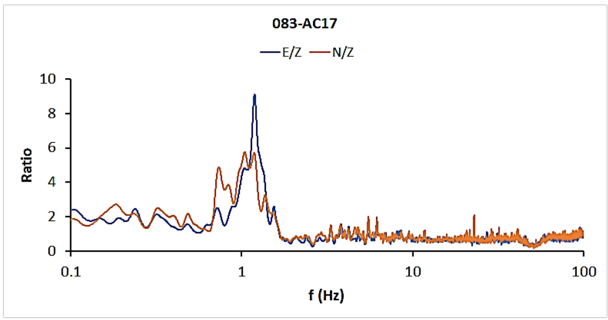
083-AC17
E/Z
N/Z
Ratio
0 2 4 6 8 10
0.1 1 10 100
f (Hz)

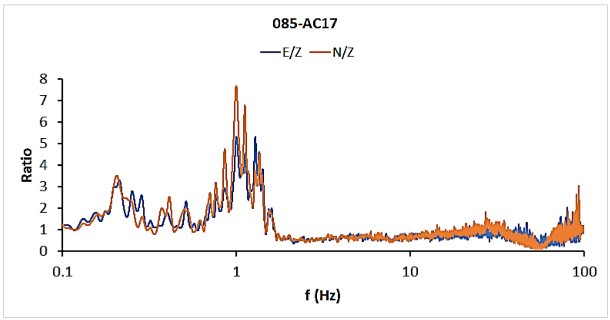
085-AC17
E/Z
N/Z
Ratio
0 1 2 3 4 5 6 7 8
0.1 1 10 100
f (Hz)

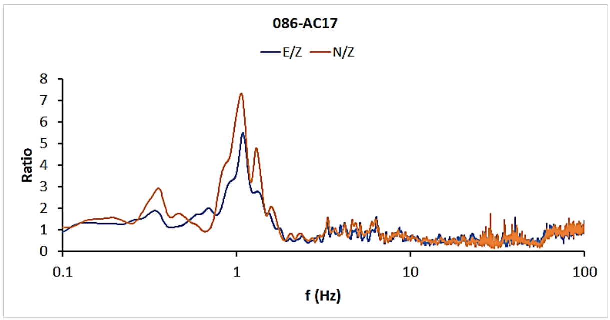
086-AC17
E/Z
N/Z
Ratio
0 1 2 3 4 5 6 7 8
0.1 1 10 100
f (Hz)

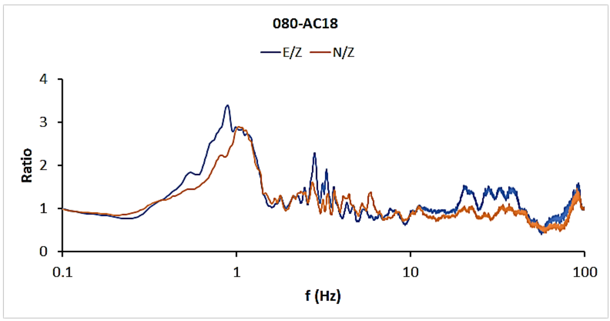
080-AC18
E/Z
N/Z
Ratio
0
1
2
3
4
0.1
1
10
100
f (Hz)

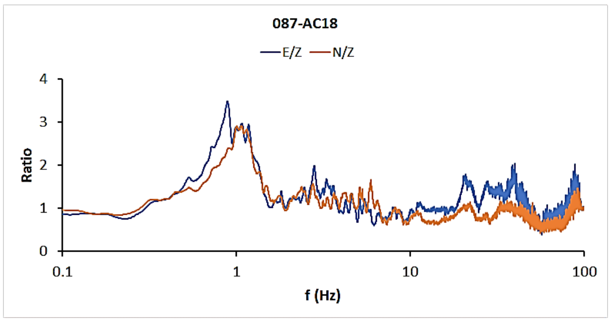
087-AC18
E/Z
N/Z
Ratio
0
1
2
3
4
0.1
1
10
100
f (Hz)

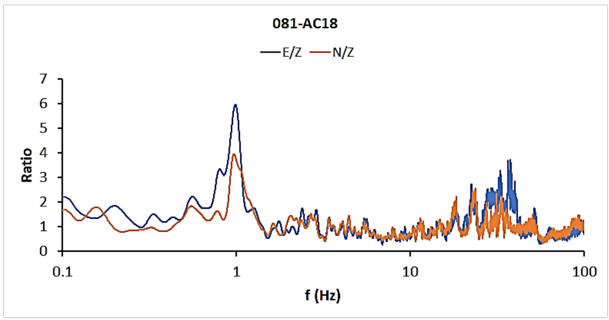
081-AC18
E/Z
N/Z
Ratio
0
1
2
3
4
5
6
7
0.1
1
10
100
f (Hz)

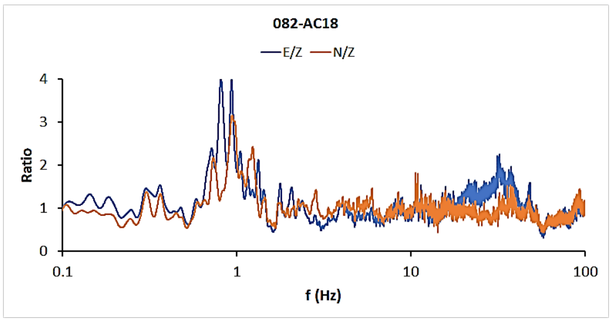
082-AC18
E/Z
N/Z
Ratio
0
1
2
3
4
0.1
1
10
100
f (Hz)

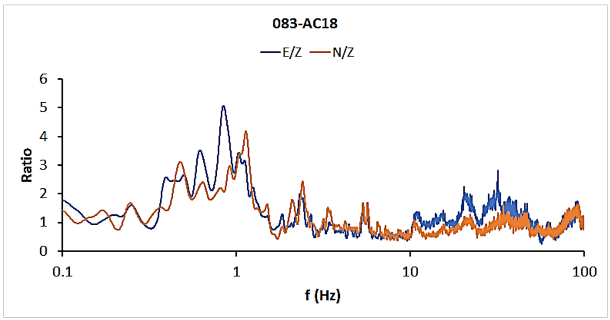
083-AC18
E/Z
N/Z
Ratio
0
1
2
3
4
5
6
0.1
1
10
100
f (Hz)

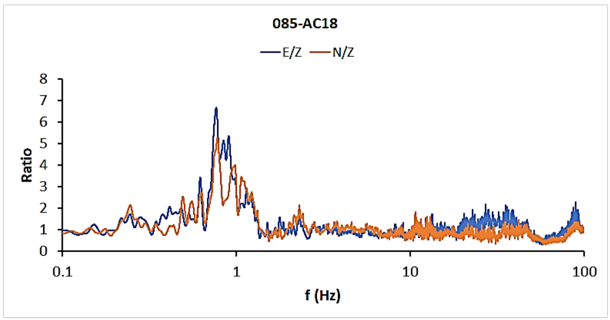
085-AC18
E/Z
N/Z
Ratio
0
1
2
3
4
5
6
7
8
0.1
1
10
100
f (Hz)

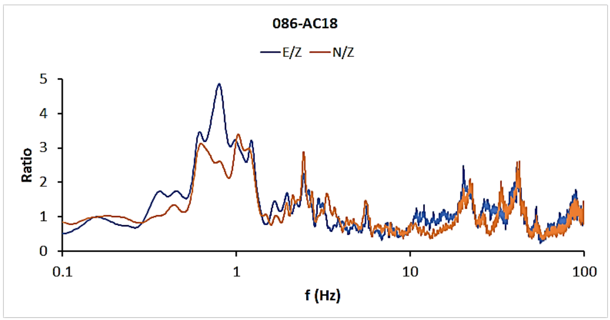
086-AC18
E/Z
N/Z
Ratio
0
1
2
3
4
5
0.1
1
10
100
f (Hz)

Coordination Office, GEMex project
Helmholtz-Zentrum Potsdam
Deutsches GeoForschungsZentrum
Telegrafenberg, 14473 Potsdam
Germany